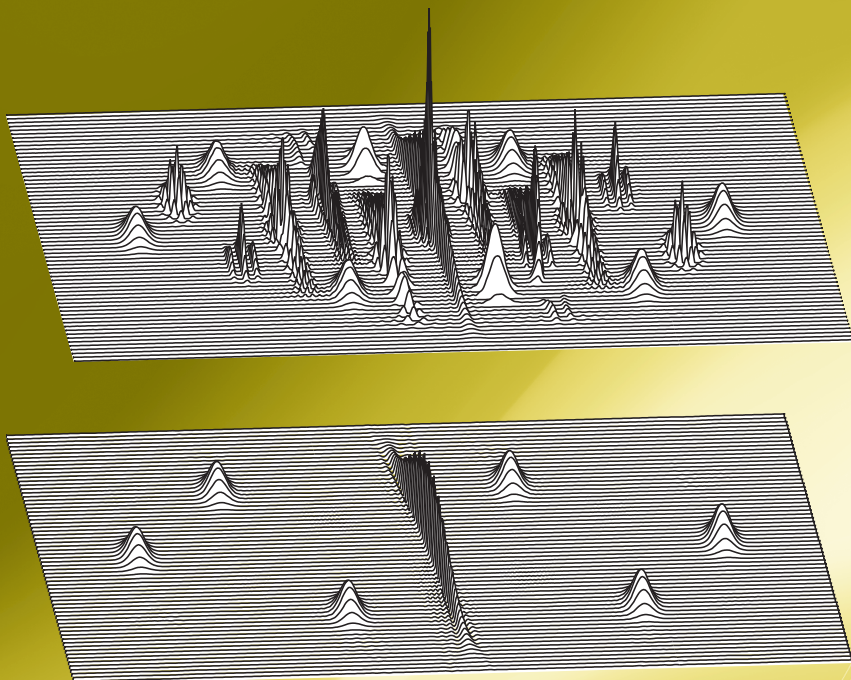


Time-Frequency Signal Analysis with Applications



**Ljubiša Stanković • Miloš Daković
Thayananthan Thayaparan**

Time-Frequency Signal Analysis with Applications

For a complete listing of titles in the
Artech House Radar Series,
turn to the back of this book.

Time-Frequency Signal Analysis with Applications

Ljubiša Stanković,

Miloš Daković,

Thayanathan Thayaparan



**A R T E C H
H O U S E**

BOSTON | LONDON
artechhouse.com

Library of Congress Cataloging-in-Publication Data

A catalog record for this book is available from the U.S. Library of Congress.

British Library Cataloguing in Publication Data

A catalogue record for this book is available from the British Library.

Cover design by Vicki Kane

ISBN 13: 978-1-60807-651-2

© 2013 ARTECH HOUSE

685 Canton Street

Norwood, MA 02062

All rights reserved. Printed and bound in the United States of America. No part of this book may be reproduced or utilized in any form or by any means, electronic or mechanical, including photocopying, recording, or by any information storage and retrieval system, without permission in writing from the publisher.

All terms mentioned in this book that are known to be trademarks or service marks have been appropriately capitalized. Artech House cannot attest to the accuracy of this information. Use of a term in this book should not be regarded as affecting the validity of any trademark or service mark.

10 9 8 7 6 5 4 3 2 1

Contents

Preface	xi
Chapter 1 Introduction to Fourier Analysis	1
1.1 Continuous-Time Signals	2
1.1.1 Periodic Signals and Fourier Series	5
1.1.2 Linear Systems	8
1.1.3 Fourier Transform	11
1.1.4 Relationship Between the Fourier Series and the Fourier Transform	21
1.2 Discrete-Time Signals and Systems	22
1.2.1 Fourier Transform of Discrete-Time Signals	26
1.2.2 Sampling Theorem in the Time Domain	29
1.2.3 Discrete Fourier Transform	33
1.2.4 Analysis of a Sinusoid by Using the DFT	39
1.2.5 Laplace and z-Transform	46
1.3 Discrete-Time Random Signals	49
1.3.1 First-Order Statistics	49
1.3.2 Second-Order Statistics	51
1.3.3 Noise	53
1.3.4 Linear Systems and Random Signals	56
1.3.5 Discrete Fourier Transform of Noisy Signals	57
1.4 Two-Dimensional Signals	60
1.5 Problems	63
1.6 Solutions	68

Chapter 2 Linear Time-Frequency Representations	81
2.1 Short-Time Fourier Transform	82
2.1.1 Windows	85
2.1.2 Continuous STFT Inversion	91
2.1.3 Spectrogram	94
2.1.4 STFT of Multicomponent Signals	95
2.2 Duration Measures and Uncertainty Principle	96
2.3 Discrete Form and Realizations of the STFT	99
2.3.1 Recursive STFT Implementation	100
2.3.2 Filter Bank STFT Implementation	102
2.3.3 Time-Frequency Plane Lattice	103
2.4 Gabor Transform	121
2.5 Stationary-Phase Method	123
2.6 Instantaneous Frequency	125
2.7 Local Polynomial Fourier Transform	130
2.8 Fractional Fourier Transform with Relation to the LPFT	135
2.9 Relation Between the STFT and the Continuous Wavelet Transform	136
2.9.1 Constant Q-Factor Transform	139
2.9.2 Affine Transforms	139
2.9.3 Filter Bank Formulation	140
2.9.4 Generalized Time-Frequency Varying Lattice	142
2.9.5 S-Transform	143
2.10 Chirplet Transform	144
2.11 Generalization	146
2.12 Parameter Optimization	148
2.12.1 Adaptive Analysis	151
2.13 Problems	153
2.14 Solutions	158
Chapter 3 Quadratic Time-Frequency Distributions	177
3.1 Rihaczek Distribution	179
3.2 Wigner Distribution	181
3.2.1 Introducing the Wigner Distribution Based on the IF Representation	185
3.2.2 Signal Reconstruction and Inversion	187
3.2.3 Properties of the Wigner Distribution	189
3.2.4 Linear Coordinate Transforms	194

3.3	Quantum Mechanics Wigner Distribution Review	201
3.3.1	Spreading Factor	204
3.3.2	Uncertainty Principle and the Wigner Distribution	204
3.3.3	Pseudo Quantum Signal Representation	206
3.3.4	Instantaneous Frequency, Bandwidth, and Moments	207
3.4	Implementation of the Wigner distribution	215
3.4.1	Pseudo Wigner Distribution	215
3.4.2	Smoothed Wigner Distribution	215
3.4.3	Discrete Pseudo Wigner Distribution	218
3.4.4	Wigner Distribution-Based Inversion and Synthesis	227
3.4.5	Auto-Terms and Cross-Terms	229
3.4.6	Inner Interferences in the Wigner Distribution	231
3.5	Ambiguity Function	232
3.6	Cohen Class of Distributions	238
3.6.1	Properties of the Cohen Class of Distributions	242
3.6.2	Reduced Interference Distributions	243
3.6.3	Optimal Kernel Design	247
3.6.4	Auto-Term Form in the Cohen Class of Distributions	251
3.7	Kernel Decomposition-Based Calculation	253
3.7.1	Spectrograms in the Cohen Class of Distributions	253
3.7.2	The Cohen Class of Distributions Decomposition	255
3.8	S-Method	256
3.8.1	Discrete Realization of the S-Method	260
3.8.2	Smoothed Spectrogram Versus S-Method as a Principle of Composition	268
3.8.3	Decomposition of Multicomponent Signals	270
3.8.4	Empirical Mode Decomposition	274
3.9	Reassignment in Time-Frequency Analysis	277
3.10	Affine Class of Time-Frequency Representations	285
3.11	Problems	287
3.12	Solutions	292
Chapter 4	Higher-Order Time-Frequency Representations	317
4.1	Third-Order Time-Frequency Representations	318
4.1.1	Second-Order Moment and Spectrum	318
4.1.2	Third-Order Moment and Bispectrum	320
4.1.3	The Wigner Bispectrum	324
4.2	Wigner Higher-Order Spectra	328

4.2.1	Instantaneous Frequency in the Wigner Higher-Order Spectra	329
4.2.2	Wigner Multitime Distribution	333
4.3	The L-Wigner Distribution	337
4.4	The Polynomial Wigner-Ville Distribution	341
4.5	Phase Derivative Estimation	342
4.5.1	Quadratic Distributions	343
4.5.2	Higher-Order Distributions	344
4.5.3	Real-Time Causal Distributions	347
4.5.4	Instantaneous Rate Estimation	348
4.6	Complex-Lag Distributions	348
4.7	S-Method-Based Realization	353
4.7.1	The L-Wigner Distribution Realization	354
4.7.2	Real-Time Causal Distribution Realization	356
4.7.3	Polynomial Wigner-Ville Distribution Realization	360
4.8	Local Polynomial Wigner Distribution	362
4.9	Higher-Order Ambiguity Functions	364
4.9.1	Monocomponent Polynomial Phase Signals	364
4.9.2	Multicomponent Polynomial Phase Signals	367
4.10	Problems	371
4.11	Solutions	375
Chapter 5	Analysis of Noisy Signals	391
5.1	Short-Time Fourier Transform of Noisy Signals	392
5.2	Wigner Distribution of Noisy Signals	394
5.2.1	Pseudo Wigner Distribution Bias	396
5.2.2	Pseudo Wigner Distribution Variance	397
5.2.3	On the Optimal Window Width	398
5.3	Wigner Distribution-Based Instantaneous Frequency Estimation	399
5.3.1	Estimation Error	401
5.3.2	Instantaneous Frequency Estimation Bias	407
5.3.3	Instantaneous Frequency Estimation Variance	408
5.4	Adaptive Algorithm	410
5.4.1	Parameters in the Adaptive Algorithm	413
5.5	Influence of High Noise on the Instantaneous Frequency	422
5.5.1	Estimation Error	423
5.5.2	Mean Square Error	427

5.6	Noise in Quadratic Time-Frequency Distributions	429
5.6.1	Complex Stationary and Nonstationary White Noise	431
5.6.2	Colored Stationary Noise	431
5.6.3	Analytic Noise	433
5.6.4	Real-Valued Noise	433
5.6.5	Noisy Signals	434
5.7	Robust Time-Frequency Analysis	442
5.7.1	Robust Short-Time Fourier Transform	443
5.7.2	Robust Wigner Distribution	450
5.7.3	L-Estimation	451
5.7.4	Resulting Noise Distribution in the Local Auto-Correlation Function	454
5.8	Sparse Signal Analysis in Time-Frequency	455
5.9	Compressive Sensing and Robust Time-Frequency Analysis	463
5.9.1	Compressive Sensing-Based Processing of the L-Estimated Time-Frequency Representations	465
5.9.2	CS-Based Separation of Signals in Time-Frequency Domain	469
5.9.3	Compressive Sensing and Signal Inversion in Overlapping STFT	472
5.9.4	Compressive Sensing Formulation with Frequency-Varying Windows (Wavelets)	477
5.10	Wigner Spectrum and Time-Varying Filtering	478
5.11	Problems	482
5.12	Solutions	487
Chapter 6	Applications of Time-Frequency Analysis	511
6.1	Radar Signal Processing	511
6.1.1	Analytic CW Radar Signal Model	512
6.1.2	Signal and Resolution in the Doppler Domain	517
6.1.3	Nonuniform Target Motion	518
6.1.4	ISAR Basic Definitions and Model	521
6.1.5	SAR Setup	529
6.1.6	Micro-Doppler Effects in ISAR/SAR Imaging	531
6.1.7	Micro-Doppler Description in SAR	535
6.1.8	Time-Frequency Analysis and L-Statistics	536
6.2	Interference Rejection in Spread Spectrum Communication Systems	553

6.2.1	Direct Sequence Spread Spectrum Model	554
6.2.2	Filtering and Reconstruction	555
6.3	Car Engine Signal Analysis	562
6.3.1	Car Engine Signal Models and Analysis	563
6.4	Estimation of Time-Varying Velocities in Video	572
6.5	Time-Frequency-Based Detection of Deterministic Signals	579
6.5.1	Signal Detection by Using the Fourier Transform	581
6.5.2	Parametric Extension of the Fourier Transform	583
6.5.3	Detection in the Time-Frequency Domain	585
6.5.4	Real Radar Data Analysis	591
6.6	Multidimensional Space-Spatial Frequency Analysis	594
6.6.1	Multidimensional Short-Time Fourier Transform	597
6.6.2	Multidimensional Wigner Distribution	598
6.6.3	Cohen Class of Distributions	598
6.6.4	Multicomponent n -Dimensional Signals	599
6.7	Array Processing Based on Time-Frequency Distributions	603
6.8	High-Resolution Time-Frequency Techniques	608
6.9	Watermarking in the Space/Spatial-Frequency Domain	614
6.10	Hardware Design for Time-Frequency Analysis	617
6.11	Seismic Signal Analysis	622
6.12	Biomedical Signal Analysis	623
6.13	Time-Frequency Analysis of Speech Signals	623
	Bibliography	625
	About the Authors	653
	Index	655

Preface

This book is a result of more than twenty years of research and education in the area of time-frequency signal analysis and signal theory, in general.

The book presents time-frequency analysis, which is of crucial interest to a variety of researchers, students, and engineers dealing with any aspects of signal processing in their work. It deals with the theory, concepts, and applications of time-frequency analysis being at the core of some new technologies used in most fields of engineering, science, and technology, like information technologies, radar and sonar signal processing, biomedicine, multimedia, telecommunications, seismology, car engine technology, and optics.

After publishing several research monographs the authors concluded that there was a need for a textbook that could be used by students, researchers, and engineers who want to apply time-frequency tools in their work. Time-frequency analysis has been regarded as a part of advanced graduate courses on signal processing.

This book begins with the basic concepts needed to understand time-frequency techniques. An overview of Fourier analysis, presenting relations among the Fourier transform, the Fourier transform of discrete-signals, the Fourier series, and the discrete Fourier transform, is given. The sampling theorem is discussed as well. Next the book focuses on advanced techniques and methods needed for the analysis and processing of signals with time-varying spectral content. Chapter 2 deals with time localization of the spectral content of signals. The short-time Fourier transform is presented as the basic linear tool for the time-frequency analysis. Other linear signal transformations used for localization of the signal content in the time-frequency domain, including the local polynomial Fourier transform, the fractional Fourier transform, and their generalizations are studied as well.

Quadratic time-frequency distributions is the topic of Chapter 3. The Wigner distribution, as the basic quadratic distribution, is presented in detail. The generalized form of quadratic distributions, known as the Cohen class of distributions, is studied. This chapter concludes with a short overview of other approaches used for signal localization, such as time-scale distributions, empirical mode decomposition, and the reassignment method. Higher-order distributions are presented in Chapter 4. Their properties are studied along with various methods for construction and realization of highly concentrated distributions. Methods used for higher-order non-stationary signal analysis, such as higher-order ambiguity function methods, are also presented here. The noise analysis and instantaneous frequency estimation are considered in Chapter 5. An efficient algorithm for the adaptive analysis of noisy signals is presented. Robust forms of time-frequency representations are analyzed. This chapter ends with a presentation of some methods in time-frequency analysis of sparse signals.

The book concludes with numerous applications, including but not limited to radar signal processing, communications, movement analysis in video sequences, car engine data analysis, multidimensional signal analysis, watermarking in the time-frequency domain, array signal processing, and high-resolution time-frequency methods. Special attention has been paid to the radar signal analysis, due to the authors' intensive research work in this area during the last several years. The presentation of material is supported by numerous examples in each chapter and problems at the end. Problems sometimes cover several areas within one chapter. MATLAB codes of the most important methods and examples are included as well. The initial versions of all chapters in the book were written by Ljubiša Stanković.

We would like to thank to all collaborators who helped to make the presentation clearer, especially, we would like to thank colleagues who have worked on the same topic for years: Professor Zdravko Uskoković, Professor Srdjan Stanković, Professor Igor Djurović, Professor Veselin Ivanović, Dr. Vesna Popović, Dr. Slobodan Djukanović, Dr. Ervin Sejdić, Dr. Irena Orović, Dr. Nikola Žarić, Predrag Raković, and Marko Simeunović. We also thank to Professor Viktor Sučić and his colleagues for their valuable comments on this text. We thank postgraduate students, Miloš Brajović, Filip Radenović, and Stefan Vujović for their careful reading of the draft of this book. We thank the reviewer of the book for a thorough reading of the manuscript and numerous comments that helped us to improve the presentation.

Chapter 1

Introduction to Fourier Analysis

Signal is a physical process, mathematical function, or any other physical or symbolic representation of information. Signal theory and processing are the areas dealing with efficient generation, description, transformation, transmission, reception, and interpretation of information. In the beginning, the most common physical processes used for these purposes were the electric signals, for example, varying current or electromagnetic waves. The signal theory is most commonly studied within electrical engineering. Tools of signal theory are strongly related to the applied mathematics and information theory. Examples of signals include: speech, music, image, video, medical, biological, geophysical, sonar, radar, biomedical, car engine, financial, and molecular data. In terms of signal generation, the main topics are in sensing, acquisition, synthesis, and reproduction of information. Various mathematical transforms, representations, and algorithms are used for describing signals. Signal transformations are a set of methods for decomposition, filtering, estimation, and detection. Modulation, demodulation, detection, coding, and compression are the most important aspects of signal transmission. In the process of interpretation, various approaches may be used, including adaptive and learning-based tools and analysis.

Mathematically, signals are presented by functions of one or more variables. Examples of one-dimensional signals are speech and music signals. A typical example of a two-dimensional signal is an image, while video sequence is a sample of a three-dimensional signal. Some signals, for example, geophysical, medical, biological, radar, or sonar, may be represented and interpreted as one-dimensional, two-dimensional, or multidimensional.

Signals may be continuous functions of independent variables, for example, functions of time and/or space. Independent variables may also be discrete, with the

signal values being defined only over an ordered set of discrete independent variable values. This is a discrete-time signal. The discrete-time signals, after being stored in a general computer or special-purpose hardware, are discretized (quantized) in amplitude as well, so that they can be memorized within the registers of a finite length. These kinds of signals are referred to as digital signals. Their processing is known as digital signal processing. However, in modern computers, the quantization errors are very small. The digital signals are usually mathematically treated as continuous (nondiscretized) in amplitude, while the quantization error is studied, if needed, as a small disturbance in processing, reduced to a noise in the input signal.

According to the nature of their behavior, all signals could be deterministic or stochastic. For the deterministic signals, the values are known in the past and future, while the stochastic signals are described by probabilistic methods. The deterministic signals are commonly used for theoretical description, analysis, and syntheses of the systems for signal processing.

1.1 CONTINUOUS-TIME SIGNALS

One-dimensional signals, represented by a function of time as a continuous independent variable, are referred to as continuous-time signals (continuous signals). Some simple forms of deterministic continuous-time signals are presented next.

The unit step signal (Heaviside function) is defined by

$$u(t) = \begin{cases} 1, & \text{for } t \geq 0 \\ 0, & \text{for } t < 0. \end{cases} \quad (1.1)$$

In the Heaviside function definition, the value of $u(0) = 1/2$ is also used. Note that the independent variable t is continuous, while the signal itself is not a continuous function. It has a discontinuity at $t = 0$.

The boxcar signal is formed as $b(t) = u(t + 1/2) - u(t - 1/2)$, that is, $b(t) = 1$ for $-1/2 \leq t < 1/2$ and $b(t) = 0$ elsewhere. A signal obtained by multiplying the unit step signal by t is called the ramp signal, with notation $R(t) = tu(t)$.

The impulse signal (or delta function) is defined as

$$\delta(t) = 0, \text{ for } t \neq 0 \quad \text{and} \quad \int_{-\infty}^{\infty} \delta(t) dt = 1. \quad (1.2)$$

The impulse signal is equal to 0 everywhere, except for $t = 0$, where it assumes an infinite value, so its area is 1. From the definition of the impulse signal, it follows

$\delta(at) = \delta(t)/|a|$. This function cannot be implemented in real systems due to its infinitely short duration and an infinitely large amplitude at $t = 0$.

In theory, any signal can be expressed by using the impulse signal, as

$$x(t) = \int_{-\infty}^{\infty} x(t-\tau) \delta(\tau) d\tau = \int_{-\infty}^{\infty} x(\tau) \delta(t-\tau) d\tau. \quad (1.3)$$

Using the previous relation, it is possible to relate the unit step signal and the impulse signal

$$u(t) = \int_{-\infty}^{\infty} \delta(\tau) u(t-\tau) d\tau = \int_{-\infty}^t \delta(\tau) d\tau$$

or

$$\frac{du(t)}{dt} = \delta(t). \quad (1.4)$$

A sinusoidal signal, with its amplitude A , its frequency equal to Ω_0 , and its initial phase given by φ , is a signal of the form

$$x(t) = A \sin(\Omega_0 t + \varphi). \quad (1.5)$$

This signal is periodic in time, since it satisfies the periodicity condition

$$x(t+T) = x(t). \quad (1.6)$$

In this case, the period is $T = 2\pi/\Omega_0$.

A signal periodic with a period T could also be considered periodic with periods kT , where k is an integer.

A complex sinusoidal signal

$$x(t) = Ae^{j(\Omega_0 t + \varphi)} = A \cos(\Omega_0 t + \varphi) + jA \sin(\Omega_0 t + \varphi) \quad (1.7)$$

is also periodic with period $T = 2\pi/\Omega_0$. Fig. 1.1 depicts sample continuous-time signals.

Example 1.1. Find the period of a signal

$$x(t) = \sum_{n=0}^N A_n e^{jn\Omega_0 t}.$$

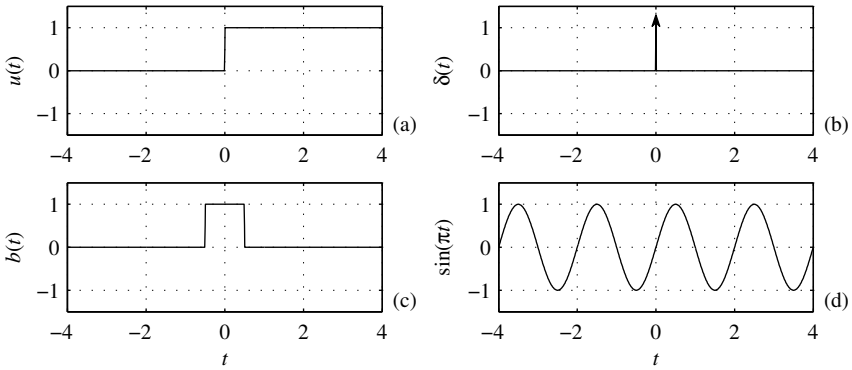


Figure 1.1 Sample continuous-time signals: (a) unit step signal, (b) impulse signal, (c) boxcar signal, and (d) sinusoidal signal.

★This signal consists of $N + 1$ components. The constant component A_0 could be considered as periodic with any period. The remaining components $A_1 e^{j\Omega_0 t}$, $A_2 e^{j2\Omega_0 t}$, $A_3 e^{j3\Omega_0 t}$, ..., $A_N e^{jN\Omega_0 t}$ are periodic with periods, $T_1 = 2\pi/\Omega_0$, $T_2 = 2\pi/(2\Omega_0)$, $T_3 = 2\pi/(3\Omega_0)$, ..., $T_N = 2\pi/(N\Omega_0)$. A sum of the periodic signals is periodic with the period being equal to the smallest time interval T containing all of periods $T_1, T_2, T_3, \dots, T_N$ an integer number of times. In this case, it is $T = 2\pi/\Omega_0$. □

Example 1.2. Find the periods of signals: $x_1(t) = \sin(2\pi t/36)$, $x_2(t) = \cos(4\pi t/15 + 2)$, $x_3(t) = \exp(j0.1t)$, $x_4(t) = x_1(t) + x_2(t)$, and $x_5(t) = x_1(t) + x_3(t)$.

★Periods are calculated according to (1.6). For $x_1(t)$ the period follows from $2\pi T_1/36 = 2\pi$, as $T_1 = 36$. Similarly, $T_2 = 15/2$ and $T_3 = 20\pi$. The period of $x_4(t)$ is the smallest interval containing T_1 and T_2 . It is $T_4 = 180$ (5 periods of $x_1(t)$ and 24 periods of $x_2(t)$). For the signal $x_5(t)$, when the periods of components are $T_1 = 36$ and $T_3 = 20\pi$, there is no common interval T_5 such that the periods T_1 and T_3 are contained an integer number of times. Thus, the signal $x_5(t)$ is not periodic. □

Some parameters that can be used to describe a signal are:

- Maximum absolute value (magnitude) of a signal

$$M_x = \max_{-\infty < t < \infty} |x(t)|, \quad (1.8)$$

- Signal energy

$$E_x = \int_{-\infty}^{\infty} |x(t)|^2 dt, \quad (1.9)$$

- Signal instantaneous power

$$P_x(t) = |x(t)|^2. \quad (1.10)$$

The average signal power is defined by

$$P_{AV} = \lim_{T \rightarrow \infty} \frac{1}{2T} \int_{-T}^{T} |x(t)|^2 dt.$$

The average power is a time average of energy. It is a useful parameter when the energy of the signal goes to infinity, for example, in cases of sinusoids of infinite duration. *Energy signals* are signals with a finite energy, while *power signals* have finite and nonzero power. Average signal power of energy signals is zero.

1.1.1 Periodic Signals and Fourier Series

Consider a periodic signal $x(t)$ with a period T . It can be expressed as a sum of weighted periodic complex sinusoidal functions $e^{j2\pi nt/T}$, $-\infty < n < \infty$,

$$\begin{aligned} x(t) &= \dots + X_{-1}e^{-j2\pi t/T} + X_0e^{-j0} + X_1e^{j2\pi t/T} + \dots \\ &= \sum_{n=-\infty}^{\infty} X_n e^{j2\pi nt/T} \end{aligned} \quad (1.11)$$

if the Dirichlet conditions are met: (1) the signal $x(t)$ has a finite number of discontinuities within the period T ; (2) it has a finite average value in the period T ; and (3) the signal has a finite number of maxima and minima. Since the signal analysis deals with real-world physical signals, rather than with mathematical generalizations, these conditions are almost always met.

The set of basis functions $\{e^{j2\pi nt/T}\}$, $-\infty < n < \infty$, is an orthonormal set of functions since their inner product is

$$\begin{aligned} \left\langle e^{j2\pi mt/T}, e^{j2\pi nt/T} \right\rangle &= \frac{1}{T} \int_{-T/2}^{T/2} e^{j2\pi mt/T} e^{-j2\pi nt/T} dt \\ &= \begin{cases} 1 & \text{for } m = n \\ \frac{\sin(\pi(m-n))}{\pi(m-n)} = 0 & \text{for } m \neq n \end{cases}. \end{aligned}$$

It means that the inner product of any two different basis functions is zero (orthogonal set), while the inner product of a function with itself is 1 (normal set). In the case of orthonormal set of basis functions, it is easy to show that the weighting coefficients X_n can be calculated as projections of $x(t)$ onto the basis functions $e^{j2\pi nt/T}$,

$$X_n = \left\langle x(t), e^{j2\pi nt/T} \right\rangle = \frac{1}{T} \int_{-T/2}^{T/2} x(t) e^{-j2\pi nt/T} dt. \quad (1.12)$$

This relation follows after a simple multiplication of the right and left sides of (1.11) by $e^{-j2\pi nt/T}$ and the integration within the period $\frac{1}{T} \int_{-T/2}^{T/2} (\cdot) dt$.

Since the signal and the basis functions are periodic with period T , in all previous integrals, we can use

$$\frac{1}{T} \int_{-T/2}^{T/2} x(t) e^{-j2\pi nt/T} dt = \frac{1}{T} \int_{-T/2+\Lambda}^{T/2+\Lambda} x(t) e^{-j2\pi nt/T} dt \quad (1.13)$$

where Λ is an arbitrary constant.

The signal expansion (1.11) is known as the Fourier series, and the coefficients X_n are the Fourier series coefficients.

Example 1.3. Show that the Fourier series coefficients X_n of a periodic signal $x(t)$ can be obtained by minimizing the mean square error between the signal and the sinusoid $X_n e^{j2\pi nt/T}$, within the period T , that is, by finding “a projection” of signal onto $e^{j2\pi nt/T}$.

★The mean square value of error

$$e(t) = x(t) - X_n e^{j2\pi nt/T},$$

within the period, is

$$\begin{aligned} I &= \frac{1}{T} \int_{-T/2}^{T/2} |x(t) - X_n e^{j2\pi nt/T}|^2 dt \\ &= \frac{1}{T} \int_{-T/2}^{T/2} |x(t)e^{-j2\pi nt/T} - X_n|^2 dt. \end{aligned}$$

From $\partial I / \partial X_n^* = 0$ follows

$$\begin{aligned} \frac{2}{T} \int_{-T/2}^{T/2} (x(t)e^{-j2\pi nt/T} - X_n) dt &= 0 \\ X_n &= \frac{1}{T} \int_{-T/2}^{T/2} x(t)e^{-j2\pi nt/T} dt. \end{aligned} \quad (1.14)$$

□

Example 1.4. Calculate the Fourier series coefficients of a periodic signal $x(t) = \cos^2(\pi t/4)$. What will be the coefficients values if period $T = 8$ is assumed?

★The signal $x(t)$ can be written as $x(t) = (1 + \cos(\pi t/2))/2$. The period is $T = 4$. Assuming that the Fourier series coefficients are calculated with $T = 4$, after transforming the signal into (1.11) form, we get

$$x(t) = \frac{1}{4}e^{-j\pi t/2} + \frac{1}{2} + \frac{1}{4}e^{j\pi t/2}.$$

The Fourier series coefficients are recognized as $X_{-1} = 1/4$, $X_0 = 1/2$ and $X_1 = 1/4$ (without the (1.12) calculation). Other coefficients are equal to zero. In the above transformation, the relation $\cos(\pi t/2) = (e^{j\pi t/2} + e^{-j\pi t/2})/2$ is used. If the period $T = 8$ is used, then the signal is decomposed into complex sinusoids $e^{-j2\pi nt/8} = e^{-j\pi nt/4}$. The signal can be written as

$$x(t) = \frac{1}{4}e^{-j2\pi t/4} + \frac{1}{2} + \frac{1}{4}e^{j2\pi t/4}. \quad (1.15)$$

Thus, comparing the signal definition with the basis functions $e^{-j\pi nt/4}$, we may write $X_{-2} = 1/4$, $X_0 = 1/2$, and $X_2 = 1/4$. Other coefficients are zero. □

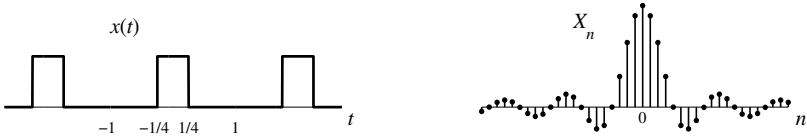


Figure 1.2 Periodic signal (left) and its Fourier series coefficients (right).

Example 1.5. Calculate the Fourier series coefficients of a periodic signal $x(t)$ defined as

$$x_0(t) = u(t + 1/4) - u(t - 1/4)$$

with

$$x(t) = \sum_{n=-\infty}^{\infty} x_0(t + 2n). \quad (1.16)$$

★The signal $x(t)$ is a periodic extension of $x_0(t)$, with period $T = 2$. This signal is equal to 1 for $-1/4 \leq t < 1/4$, within its basic period. Thus,

$$X_n = \frac{1}{2} \int_{-1/4}^{1/4} 1 e^{-j2\pi nt/2} dt = \frac{\sin(\pi n/4)}{\pi n}. \quad (1.17)$$

Values of X_n are presented in Fig. 1.2.

The signal $x(t)$ can be reconstructed by using the Fourier series (1.11). In calculations, a finite number of terms denoted by M should be used,

$$x_M(t) = \sum_{n=-M}^M X_n e^{j\pi nt}.$$

The reconstructed signal, with $M = 1, 2, 6$, and 30 , is shown in Fig. 1.3. □

1.1.2 Linear Systems

A system transforms one signal (input signal) into another signal (output signal). Assume that $x(t)$ is the input signal. The system transformation will be denoted by an operator $\mathbb{T}\{\circ\}$. The output signal can be written as

$$y(t) = \mathbb{T}\{x(t)\}. \quad (1.18)$$

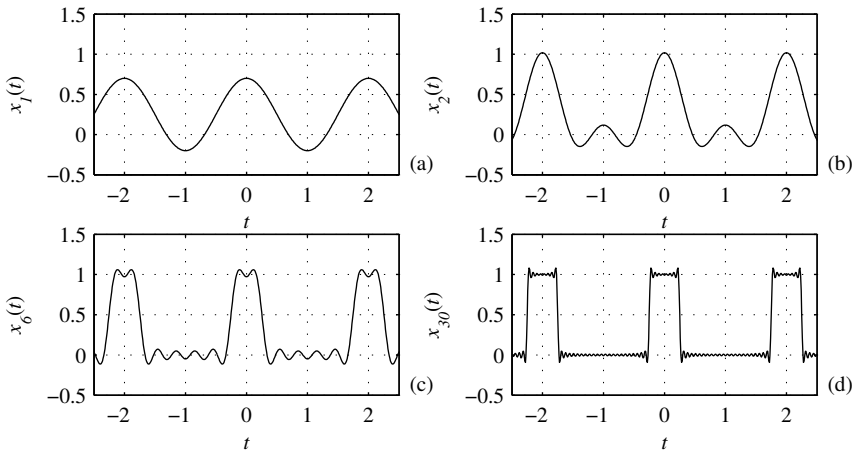


Figure 1.3 Illustration of the signal reconstruction by using the finite Fourier series with: (a) coefficients X_n within $-1 \leq n \leq 1$, (b) coefficients X_n within $-2 \leq n \leq 2$, (c) coefficients X_n within $-6 \leq n \leq 6$, and (d) coefficients X_n within $-30 \leq n \leq 30$.

A system is linear if, for any signals $x_1(t)$ and $x_2(t)$ and arbitrary constants a_1 and a_2 , it holds

$$y(t) = \mathbb{T}\{a_1x_1(t) + a_2x_2(t)\} = a_1\mathbb{T}\{x_1(t)\} + a_2\mathbb{T}\{x_2(t)\}. \quad (1.19)$$

We say that a system is time-invariant if its properties and parameters do not change in time. For the time-invariant system, it holds

$$\text{if } y(t) = \mathbb{T}\{x(t)\}, \text{ then } \mathbb{T}\{x(t-t_0)\} = y(t-t_0), \quad (1.20)$$

for any t_0 .

Systems which are linear and time-invariant (LTI systems) are fully described by their response to the impulse signal. If we know the impulse response of these systems,

$$y(t) = h(t) = \mathbb{T}\{\delta(t)\},$$

then for arbitrary signal $x(t)$ at the input, the output can be calculated, by using (1.3), as

$$\begin{aligned} y(t) = \mathbb{T}\{x(t)\} &= \mathbb{T}\left\{\int_{-\infty}^{\infty} x(\tau) \delta(t - \tau) d\tau\right\} \\ &\stackrel{\text{Linearity}}{=} \int_{-\infty}^{\infty} x(\tau) \mathbb{T}\{\delta(t - \tau)\} d\tau \stackrel{\text{Time-invariance}}{=} \int_{-\infty}^{\infty} x(\tau) h(t - \tau) d\tau. \end{aligned}$$

The last integral is of particular significance. It is called a convolution of $x(t)$ and $h(t)$, in time. Its notation is

$$y(t) = x(t) *_t h(t) = \int_{-\infty}^{\infty} x(\tau) h(t - \tau) d\tau. \quad (1.21)$$

The convolution is a commutative operation

$$x(t) *_t h(t) = h(t) *_t x(t). \quad (1.22)$$

Example 1.6. Find convolution of signals $x(t) = u(t + 1) - u(t - 1)$ and $h(t) = e^{-t}u(t)$.

★By using the convolution definition, we get

$$\begin{aligned} y(t) &= \int_{-\infty}^{\infty} x(\tau) h(t - \tau) d\tau = \int_{-1}^1 1 \cdot e^{-(t-\tau)} u(t - \tau) d\tau \\ &= - \int_{t+1}^{t-1} e^{-\lambda} u(\lambda) d\lambda = \begin{cases} \int_{t-1}^{t+1} e^{-\lambda} d\lambda = e^{-t}(e - 1/e), & \text{for } t \geq 1 \\ \int_0^{t+1} e^{-\lambda} d\lambda = 1 - e^{-(t+1)}, & \text{for } -1 \leq t < 1 \\ 0 & \text{for } t < -1 \end{cases}. \end{aligned} \quad (1.23)$$

□

Example 1.7. Consider two signals $x(t)$ and $h(t)$ of finite duration. Signal $x(t)$ is different from zero only within $|t| < M$, while $h(t)$ is different from zero only within $|t| < L$. Show that the duration of the signal obtained as a convolution of these two signals, in general, is equal to the sum of durations of both signals.

★The value of convolution of signals $x(t)$ and $h(t)$,

$$y(t) = \int_{-\infty}^{\infty} x(\tau)h(t - \tau)d\tau,$$

in general, will be different from zero when $x(\tau)$ and $h(t - \tau)$ are different than zero, that is, when

$$\begin{aligned} -M < \tau < M \quad &\text{and} \\ -L < t - \tau < L. \end{aligned}$$

Obviously, the limits for t are obtained from $-L + \tau < t < L + \tau$, by using the extreme values of τ . They are

$$-(M + L) < t < M + L. \quad (1.24)$$

Thus, in general, the signal $y(t)$ will assume nonzero values within $|t| < M + L$. \square

1.1.3 Fourier Transform

The Fourier series has been introduced and presented for periodic signals with a period T . Assume now that we extend the period to infinity, while not changing the signal. This case corresponds to the analysis of an aperiodic signal $x(t)$. Its transform, the Fourier series coefficients normalized by the period, is given by

$$\lim_{T \rightarrow \infty} X_n T = \lim_{T \rightarrow \infty} \int_{-T/2}^{T/2} x(t) e^{-j2\pi nt/T} dt = \int_{-\infty}^{\infty} x(t) e^{-j\Omega t} dt \quad (1.25)$$

with $2\pi/T = \Delta\Omega \rightarrow d\Omega$ (being infinitesimal) and $2\pi n/T \rightarrow \Omega$ becoming a continuous variable, as $T \rightarrow \infty$ and $-\infty < n < \infty$.

The function $X(\Omega)$, defined by

$$X(\Omega) = \int_{-\infty}^{\infty} x(t) e^{-j\Omega t} dt, \quad (1.26)$$

is called the Fourier transform (FT) of a signal $x(t)$. For the existence of the Fourier transform it is sufficient for a signal to be absolutely integrable. There are some signals, in theory, that do not satisfy this condition, whose Fourier transform exists in a form of generalized functions, such as delta function. There is never a question of existence for Fourier transforms of signals encountered in practice.

The inverse Fourier transform (IFT) can be obtained by multiplying both sides by $e^{j\Omega\tau}$ and integrating over Ω ,

$$\int_{-\infty}^{\infty} X(\Omega) e^{j\Omega\tau} d\Omega = \int_{-\infty}^{\infty} \int_{-\infty}^{\infty} x(t) e^{j\Omega(\tau-t)} dt d\Omega.$$

Using the fact that

$$\int_{-\infty}^{\infty} e^{j\Omega(\tau-t)} d\Omega = 2\pi\delta(\tau-t)$$

we get the inverse Fourier transform

$$x(t) = \frac{1}{2\pi} \int_{-\infty}^{\infty} X(\Omega) e^{j\Omega t} d\Omega. \quad (1.27)$$

Example 1.8. Calculate the Fourier transform of $x(t) = Ae^{-at}u(t)$, $a > 0$.

★According to the Fourier transform definition we get

$$X(\Omega) = \int_0^{\infty} Ae^{-at} e^{-j\Omega t} dt = \frac{A}{(a + j\Omega)}.$$

□

Example 1.9. Find the Fourier transform of

$$x(t) = \text{sign}(t) = \begin{cases} 1 & \text{for } t > 0 \\ 0 & \text{for } t = 0 \\ -1 & \text{for } t < 0 \end{cases}. \quad (1.28)$$

★Since a direct calculation of the Fourier transform for this signal is not possible, let us consider the signal

$$x_a(t) = \begin{cases} e^{-at} & \text{for } t > 0 \\ 0 & \text{for } t = 0 \\ -e^{at} & \text{for } t < 0 \end{cases}$$

where $a > 0$ is a real-valued constant. It is obvious that

$$\lim_{a \rightarrow 0} x_a(t) = x(t).$$

The Fourier transform of $x(t)$ can be obtained as

$$X(\Omega) = \lim_{a \rightarrow 0} X_a(\Omega),$$

where

$$X_a(\Omega) = \int_{-\infty}^0 -e^{at} e^{-j\Omega t} dt + \int_0^\infty e^{-at} e^{-j\Omega t} dt = \frac{2\Omega}{ja^2 + j\Omega^2}. \quad (1.29)$$

It results in

$$X(\Omega) = \frac{2}{j\Omega}. \quad (1.30)$$

□

Based on the definitions of the Fourier transform and the inverse Fourier transform, it is easy to conclude that the duality property holds. The duality property reads:

If $X(\Omega)$ is the Fourier transform of $x(t)$, then the Fourier transform of $X(t)$ is $2\pi x(-\Omega)$

$$\begin{aligned} X(\Omega) &= \text{FT}\{x(t)\} \\ 2\pi x(-\Omega) &= \text{FT}\{X(t)\}. \end{aligned} \quad (1.31)$$

Example 1.10. Find the Fourier transform of $\delta(t)$, $x(t) = 1$ and $u(t)$.

★The Fourier transform of $\delta(t)$ is

$$\text{FT}\{\delta(t)\} = \int_{-\infty}^\infty \delta(t) e^{-j\Omega t} dt = 1. \quad (1.32)$$

According to the duality property,

$$\text{FT}\{1\} = 2\pi\delta(\Omega).$$

Finally,

$$\text{FT}\{u(t)\} = \text{FT}\left\{\frac{\text{sign}(t) + 1}{2}\right\} = \frac{1}{j\Omega} + \pi\delta(\Omega). \quad (1.33)$$

□

1.1.3.1 Fourier Transform and Linear Time-Invariant Systems

Consider a linear, time-invariant system with an impulse response $h(t)$ and the input signal $x(t) = Ae^{j(\Omega_0 t + \varphi)}$. The output signal is

$$\begin{aligned} y(t) &= x(t) *_t h(t) = \int_{-\infty}^{\infty} Ae^{j(\Omega_0(t-\tau)+\varphi)} h(\tau) d\tau \\ &= Ae^{j(\Omega_0 t + \varphi)} \int_{-\infty}^{\infty} h(\tau) e^{-j\Omega_0 \tau} d\tau = H(\Omega_0)x(t), \end{aligned} \quad (1.34)$$

where

$$H(\Omega) = \int_{-\infty}^{\infty} h(t) e^{-j\Omega t} dt \quad (1.35)$$

is the Fourier transform of $h(t)$. The linear time-invariant system does not change the form of an input complex harmonic signal $Ae^{j(\Omega_0 t + \varphi)}$. It remains complex harmonic signal after passing through the system, with the same frequency Ω_0 . The amplitude of the input signal is changed for $|H(\Omega_0)|$ and the phase is changed for $\arg\{H(\Omega_0)\}$.

1.1.3.2 Properties of the Fourier Transform

The Fourier transform satisfies the following properties:

1. Linearity

$$\text{FT}\{a_1x_1(t) + a_2x_2(t)\} = a_1X_1(\Omega) + a_2X_2(\Omega), \quad (1.36)$$

where $\text{FT}\{\circ\}$ denotes the Fourier transform operator, while $X_1(\Omega)$ and $X_2(\Omega)$ are the Fourier transforms of signals $x_1(t)$ and $x_2(t)$, respectively.

2. Realness

The Fourier transform of a signal is real (i.e., $X^*(\Omega) = X(\Omega)$), if

$$x^*(-t) = x(t),$$

since

$$X^*(\Omega) = \int_{-\infty}^{\infty} x^*(t) e^{j\Omega t} dt \stackrel{t \rightarrow -t}{=} \int_{-\infty}^{\infty} x^*(-t) e^{-j\Omega t} dt = X(\Omega). \quad (1.37)$$

3. Modulation

$$\text{FT}\{x(t)e^{j\Omega_0 t}\} = \int_{-\infty}^{\infty} x(t)e^{j\Omega_0 t}e^{-j\Omega t}dt = X(\Omega - \Omega_0). \quad (1.38)$$

4. Shift in time

$$\text{FT}\{x(t - t_0)\} = \int_{-\infty}^{\infty} x(t - t_0)e^{-j\Omega t}dt = X(\Omega)e^{-jt_0\Omega}. \quad (1.39)$$

5. Time scaling

$$\text{FT}\{x(at)\} = \int_{-\infty}^{\infty} x(at)e^{-j\Omega t}dt = \frac{1}{|a|}X\left(\frac{\Omega}{a}\right). \quad (1.40)$$

6. Convolution

$$\begin{aligned} \text{FT}\{x(t) *_t h(t)\} &= \int_{-\infty}^{\infty} \int_{-\infty}^{\infty} x(\tau)h(t - \tau)e^{-j\Omega t}d\tau dt \\ &\stackrel{t - \tau \rightarrow u}{=} \int_{-\infty}^{\infty} \int_{-\infty}^{\infty} x(\tau)h(u)e^{-j\Omega(\tau+u)}d\tau du = X(\Omega)H(\Omega). \end{aligned} \quad (1.41)$$

7. Multiplication

$$\begin{aligned} \text{FT}\{x(t)h(t)\} &= \frac{1}{2\pi} \int_{-\infty}^{\infty} x(t) \int_{-\infty}^{\infty} H(\theta)e^{j\theta t}d\theta e^{-j\Omega t}dt \\ &= \frac{1}{2\pi} \int_{-\infty}^{\infty} H(\theta)X(\Omega - \theta)d\theta = X(\Omega) *_\Omega H(\Omega) = H(\Omega) *_\Omega X(\Omega). \end{aligned} \quad (1.42)$$

Convolution in frequency domain is denoted by $*_\Omega$ with a factor of $1/2\pi$ being included.

8. Parseval's theorem

$$\begin{aligned} \int_{-\infty}^{\infty} x(t)y^*(t)dt &= \frac{1}{2\pi} \int_{-\infty}^{\infty} X(\Omega)Y^*(\Omega)d\Omega \\ \int_{-\infty}^{\infty} |x(t)|^2 dt &= \frac{1}{2\pi} \int_{-\infty}^{\infty} |X(\Omega)|^2 d\Omega. \end{aligned} \quad (1.43)$$

9. Differentiation

$$\text{FT}\left\{\frac{dx(t)}{dt}\right\} = \text{FT}\left\{\frac{d}{dt}\left(\frac{1}{2\pi} \int_{-\infty}^{\infty} X(\Omega)e^{j\Omega t} d\Omega\right)\right\} = j\Omega X(\Omega). \quad (1.44)$$

10. Integration

The Fourier transform of

$$\int_{-\infty}^t x(\tau)d\tau$$

can be calculated as the Fourier transform of

$$x(t) *_t u(t) = \int_{-\infty}^{\infty} x(\tau)u(t-\tau)d\tau = \int_{-\infty}^t x(\tau)d\tau.$$

Then,

$$\begin{aligned} \text{FT}\left\{\int_{-\infty}^t x(\tau)d\tau\right\} &= \text{FT}\{x(t)\}\text{FT}\{u(t)\} = \\ X(\Omega) \left(\frac{1}{j\Omega} + \pi\delta(\Omega) \right) &= \frac{1}{j\Omega}X(\Omega) + \pi X(0)\delta(\Omega). \end{aligned} \quad (1.45)$$

11. An analytic part of a signal $x(t)$, whose Fourier transform is $X(\Omega)$, is a signal with the Fourier transform defined by

$$X_a(\Omega) = \begin{cases} 2X(\Omega) & \text{for } \Omega > 0 \\ X(0) & \text{for } \Omega = 0 \\ 0 & \text{for } \Omega < 0 \end{cases}. \quad (1.46)$$

It can be written as

$$X_a(\Omega) = X(\Omega) + X(\Omega)\text{sign}(\Omega) = X(\Omega) + jX_h(\Omega) \quad (1.47)$$

where $X_h(\Omega)$ is the Fourier transform of the Hilbert transform of the signal $x(t)$. From the example with signal $x(t) = \text{sign}(t)$ and the duality property of the Fourier transform pair, obviously the inverse Fourier transform of $\text{sign}(\Omega)$ is $j/(\pi t)$. Therefore, the analytic part of the signal, in the time domain, reads as

$$x_a(t) = x(t) + jx_h(t) = x(t) + x(t) *_t \frac{j}{\pi t} = x(t) + j \frac{1}{\pi} \int_{-\infty}^{\infty} \frac{x(\tau)}{t - \tau} d\tau \quad (1.48)$$

where *p.v.* stands for Cauchy principal value of the considered integral.

Example 1.11. For the signal $x(t) = A(t)\cos(\phi(t))$ show that its analytic part is

$$x_a(t) = A(t)e^{j\phi(t)}$$

if $X_+(\Omega) = \text{FT}\{A(t)e^{j\phi(t)}\} = 0$ for $\Omega < 0$. Functions $A(t)$ and $\phi(t)$ are real-valued. What is the Fourier transform of the analytic part of $x(t)$ if this is not the case?

★The Fourier transform, multiplied by 2, of

$$x(t) = A(t)e^{-j\phi(t)}/2 + A(t)e^{j\phi(t)}/2$$

is

$$\begin{aligned} 2X(\Omega) &= \int_{-\infty}^{\infty} A(t)e^{-j\phi(t)}e^{-j\Omega t} dt + \int_{-\infty}^{\infty} A(t)e^{j\phi(t)}e^{-j\Omega t} dt \\ &= X_+^*(-\Omega) + X_+(\Omega). \end{aligned}$$

If $X_+(\Omega) = 0$ for $\Omega < 0$, then $X_a(\Omega) = X_+(\Omega)$, that is, $x_a(t) = A(t)e^{j\phi(t)}$, according to (1.46). If the condition $X_+(\Omega) = 0$ for $\Omega < 0$ is not satisfied, then $X_a(\Omega) = X_+(\Omega) + X_+^*(-\Omega) \neq X_+(\Omega)$ for $\Omega > 0$. \square

Example 1.12. Find the Fourier transform of the following function

$$x(t) = \begin{cases} \cos^2(\pi t/T) & \text{for } |t| < T/2 \\ 0 & \text{elsewhere,} \end{cases} \quad (1.49)$$

representing the Hann window (also known as the Hanning window).

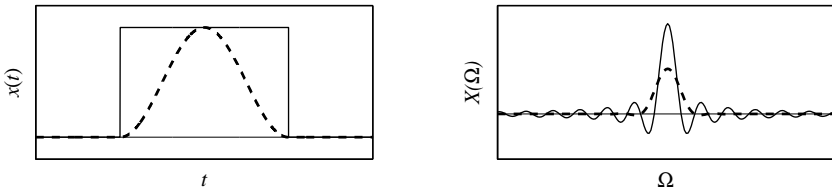


Figure 1.4 The rectangular window (solid line) and the Hann(ing) window (dashed line) (left) with their Fourier transforms (right).

★The Fourier transform of this function is

$$\begin{aligned} X(\Omega) &= \int_{-T/2}^{T/2} \frac{1 + \cos(2\pi t/T)}{2} e^{-j\Omega t} dt = \\ &= \frac{\sin(\Omega T/2)}{\Omega} + \frac{\sin((\Omega - 2\pi/T)T/2)}{2(\Omega - 2\pi/T)} + \frac{\sin((\Omega + 2\pi/T)T/2)}{2(\Omega + 2\pi/T)}. \end{aligned}$$

The final form is

$$X(\Omega) = \frac{\sin(\Omega T/2)}{\Omega \left(1 - \left(\frac{\Omega T}{2\pi} \right)^2 \right)}. \quad (1.50)$$

This Fourier transform behaves as $1/\Omega^3$, as $\Omega \rightarrow \infty$.

The Fourier transform of the rectangular window $x(t) = u(t + T/2) - u(t - T/2)$ would be $2 \sin(\Omega T/2)/\Omega$. This Fourier transform behaves as $1/\Omega$ as $\Omega \rightarrow \infty$. These two functions, with the corresponding Fourier transforms, are presented in Fig. 1.4. \square

Example 1.13. Find the Fourier transform of

$$x(t) = 2 \cos(\Omega_0 t) \cos^2(\pi t/T) [u(t + T/2) - u(t - T/2)].$$

★The Fourier transform of $2 \cos(\Omega_0 t)$ is

$$\text{FT}\{2 \cos(\Omega_0 t)\} = \int_{-\infty}^{\infty} (e^{j\Omega_0 t} + e^{-j\Omega_0 t}) e^{-j\Omega t} dt = 2\pi\delta(\Omega + \Omega_0) + 2\pi\delta(\Omega - \Omega_0).$$

Now we have

$$\begin{aligned}
 & \text{FT}\{2\cos(\Omega_0 t)\cos^2(\pi t/T)[u(t+T/2) - u(t-T/2)]\} \\
 &= \text{FT}\{2\cos(\Omega_0 t)\} *_{\Omega} \text{FT}\{\cos^2(\pi t/T)[u(t+T/2) - u(t-T/2)]\} \\
 &= \frac{\sin((\Omega + \Omega_0)T/2)}{(\Omega + \Omega_0) \left(1 - \left(\frac{(\Omega + \Omega_0)T}{2\pi}\right)^2\right)} + \frac{\sin((\Omega - \Omega_0)T/2)}{(\Omega - \Omega_0) \left(1 - \left(\frac{(\Omega - \Omega_0)T}{2\pi}\right)^2\right)}. \quad (1.51)
 \end{aligned}$$

In the case of a sinusoid, truncated by a rectangular window, the Fourier transform

$$\text{FT}\{2\cos(\Omega_0 t)[u(t+T/2) - u(t-T/2)]\}$$

would be of the form

$$2\sin((\Omega + \Omega_0)T/2)/(\Omega + \Omega_0) + 2\sin((\Omega - \Omega_0)T/2)/(\Omega - \Omega_0).$$

These two Fourier transforms are shown in Fig. 1.5 for four different window widths T , starting from the narrowest toward the widest window. \square

Example 1.14. Given the Fourier transformation pair

$$\begin{aligned}
 x(t) &= e^{-t^2/(2\sigma^2)} \\
 X(\Omega) &= \sigma\sqrt{2\pi}e^{-\Omega^2\sigma^2/2}. \quad (1.52)
 \end{aligned}$$

Show that

$$M^2 = \frac{1}{E_x} \int_{-\infty}^{\infty} t^2 x^2(t) dt \cdot \frac{1}{2\pi E_x} \int_{-\infty}^{\infty} \Omega^2 X^2(\Omega) d\Omega = \frac{1}{4}.$$

★The signal energy E_x is equal to

$$E_x = \int_{-\infty}^{\infty} x^2(t) dt = \int_{-\infty}^{\infty} e^{-t^2/\sigma^2} dt = \sigma\sqrt{\pi}, \quad (1.53)$$

since the Fourier transform of e^{-t^2/σ^2} is $\sigma\sqrt{\pi}e^{-\Omega^2\sigma^2/4}$, according to the given Fourier transformation pair

$$\int_{-\infty}^{\infty} e^{-t^2/(2\sigma^2)} e^{-j\Omega t} dt = \sigma\sqrt{2\pi}e^{-\Omega^2\sigma^2/2},$$

with $\sigma \rightarrow \sigma/\sqrt{2}$. The energy follows with $\Omega = 0$.

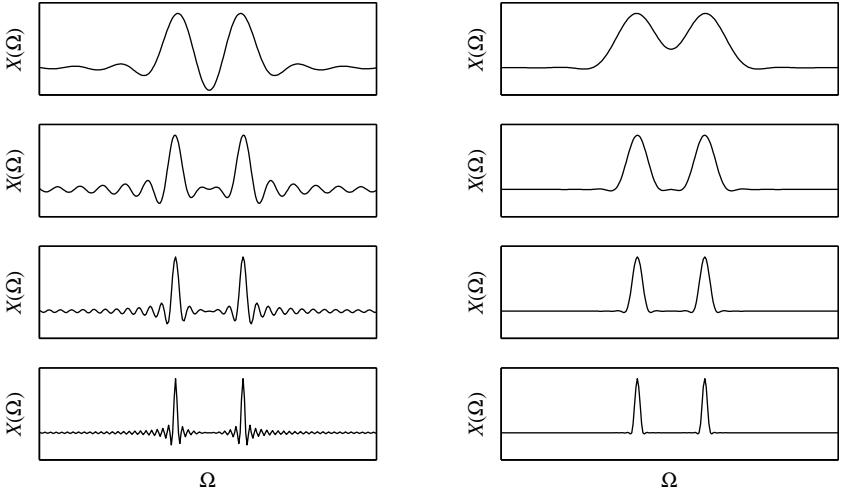


Figure 1.5 The Fourier transform of signal $2\cos(\Omega_0 t)$ multiplied by the rectangular window (left) and the Hann(ing) window (right), for $\Omega_0 = 3$ and various durations $T = 1/2$, $T = 1$, $T = 2$, and $T = 4$ from the top to the bottom, respectively.

The product of integrals could be calculated as

$$M^2 E_x^2 = \frac{1}{2\pi} \int_{-\infty}^{\infty} t^2 x^2(t) dt \int_{-\infty}^{\infty} \Omega^2 X^2(\Omega) d\Omega = \sigma^2 \int_{-\infty}^{\infty} \int_{-\infty}^{\infty} t^2 \Omega^2 e^{-t^2/\sigma^2 - \Omega^2 \sigma^2} dt d\Omega.$$

After the polar coordinate substitution $t = \rho \sigma \sin(\theta)$, $\Omega = \frac{1}{\sigma} \rho \cos(\theta)$ with $dt d\Omega = \rho d\rho d\theta$, we get

$$M^2 E_x^2 = \sigma^2 \int_0^{\infty} \int_0^{2\pi} \rho^4 \sin^2 \theta \cos^2 \theta e^{-\rho^2} \rho d\rho d\theta = \frac{\pi \sigma^2}{8} \int_0^{\infty} u^2 e^{-u} du = \frac{\pi \sigma^2}{4}.$$

Finally,

$$M^2 = \frac{\frac{\pi \sigma^2}{4}}{E_x^2} = \frac{1}{4}. \quad (1.54)$$

□

1.1.4 Relationship Between the Fourier Series and the Fourier Transform

Consider an aperiodic signal $x(t)$, with the Fourier transform $X(\Omega)$. Assume that the signal is of a limited duration (i.e., $x(t) = 0$ for $|t| > T_0/2$). Then,

$$X(\Omega) = \int_{-T_0/2}^{T_0/2} x(t) e^{-j\Omega t} dt. \quad (1.55)$$

If we make a periodic extension of $x(t)$, with a period T , we get a signal

$$x_p(t) = \sum_{n=-\infty}^{\infty} x(t + nT).$$

The periodic signal $x_p(t)$ can be expanded into Fourier series with the coefficients

$$X_n = \frac{1}{T} \int_{-T/2}^{T/2} x_p(t) e^{-j2\pi nt/T} dt. \quad (1.56)$$

If $T > T_0$ it is easy to conclude that

$$\int_{-T/2}^{T/2} x_p(t) e^{-j2\pi nt/T} dt = \int_{-T_0/2}^{T_0/2} x(t) e^{-j\Omega t} dt|_{\Omega=2\pi n/T}$$

or

$$X_n = \frac{1}{T} X(\Omega)|_{\Omega=2\pi n/T}. \quad (1.57)$$

It means that the Fourier series coefficients are the samples of the Fourier transform, divided by T . The only condition in the derivation of this relation is that the signal duration is shorter than the period of the periodic extension (i.e., $T > T_0$). The sampling interval in frequency is

$$\Delta\Omega = \frac{2\pi}{T}, \quad \Delta\Omega < \frac{2\pi}{T_0}.$$

It should be smaller than $2\pi/T_0$, where T_0 is the signal $x(t)$ duration. This is a form of the sampling theorem in the frequency domain. The sampling theorem in the time domain will be discussed later.

In order to write the Fourier series coefficients in the Fourier transform form, note that a periodic signal $x_p(t)$, formed by a periodic extension of $x(t)$ with period T , can be written as

$$x_p(t) = \sum_{n=-\infty}^{\infty} x(t + nT) = x(t) *_t \sum_{n=-\infty}^{\infty} \delta(t + nT). \quad (1.58)$$

The Fourier transform of this periodic signal is

$$\begin{aligned} X_p(\Omega) &= \text{FT} \left\{ x(t) *_t \sum_{n=-\infty}^{\infty} \delta(t + nT) \right\} \\ &= X(\Omega) \cdot \frac{2\pi}{T} \sum_{n=-\infty}^{\infty} \delta \left(\Omega - \frac{2\pi}{T} n \right) = \frac{2\pi}{T} \sum_{n=-\infty}^{\infty} X \left(\frac{2\pi}{T} n \right) \delta \left(\Omega - \frac{2\pi}{T} n \right) \end{aligned} \quad (1.59)$$

since

$$\begin{aligned} \text{FT} \left\{ \sum_{n=-\infty}^{\infty} \delta(t + nT) \right\} &= \sum_{n=-\infty}^{\infty} \int_{-\infty}^{\infty} \delta(t + nT) e^{-j\Omega t} dt \\ &= \sum_{n=-\infty}^{\infty} e^{j\Omega n T} = \frac{2\pi}{T} \sum_{n=-\infty}^{\infty} \delta \left(\Omega - \frac{2\pi}{T} n \right). \end{aligned} \quad (1.60)$$

The Fourier transform of a periodic signal is a series of generalized impulse signals at $\Omega = 2\pi n/T$ with weighting factors $X(\frac{2\pi}{T} n)/T$ being equal to the Fourier series coefficients X_n . The relation between periodic generalized impulse signals in time and frequency will be explained (derived) later, (see Example 1.16).

1.2 DISCRETE-TIME SIGNALS AND SYSTEMS

Discrete-time signals (discrete signals) are represented in the form of an ordered set of numbers $\{x(n)\}$. Commonly, they are obtained by sampling continuous-time signals. However, there are discrete-time signals whose independent variable is inherently discrete in nature.

In the case that a discrete-time signal is obtained by sampling a continuous-time signal, we can write (Fig. 1.6),

$$x(n) = x(t) \Big|_{t=n\Delta t} \Delta t. \quad (1.61)$$

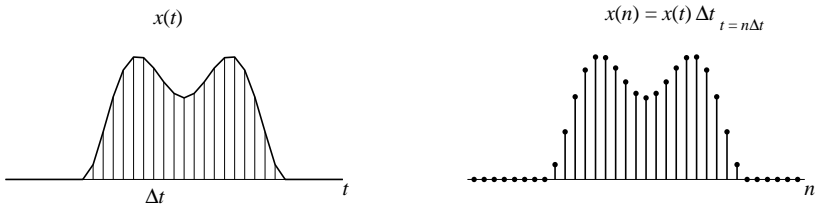


Figure 1.6 Signal discretization: continuous time signal (left) and corresponding discrete-time signal (right).

Discrete-time signals are defined for an integer value of the argument n . We will use the same notation for continuous-time and discrete-time signals, $x(t)$ and $x(n)$. However, we hope that this will not cause any confusion since we will use different sets of variables, for example, t and τ for continuous time and n and m for discrete time. Also, we hope that the context will be always clear, so that there is no doubt what kind of signal is considered.

Examples of discrete-time signals are presented next.

The discrete-time impulse signal is defined by

$$x(n) = \delta(n) = \begin{cases} 1, & \text{for } n = 0 \\ 0, & \text{for } n \neq 0 \end{cases}. \quad (1.62)$$

In contrast to the continuous time impulse signal, that can not be practically implemented and used, the discrete-time unit impulse is a signal that can easily be implemented and used in realizations. In mathematical notation, this signal corresponds to the Kronecker delta function

$$\delta_{m,n} = \begin{cases} 1, & \text{for } m = n \\ 0, & \text{for } m \neq n \end{cases}. \quad (1.63)$$

Any discrete-time signal can be written in the form of shifted and weighted discrete-time impulses,

$$x(n) = \sum_{k=-\infty}^{\infty} x(k)\delta(n-k). \quad (1.64)$$

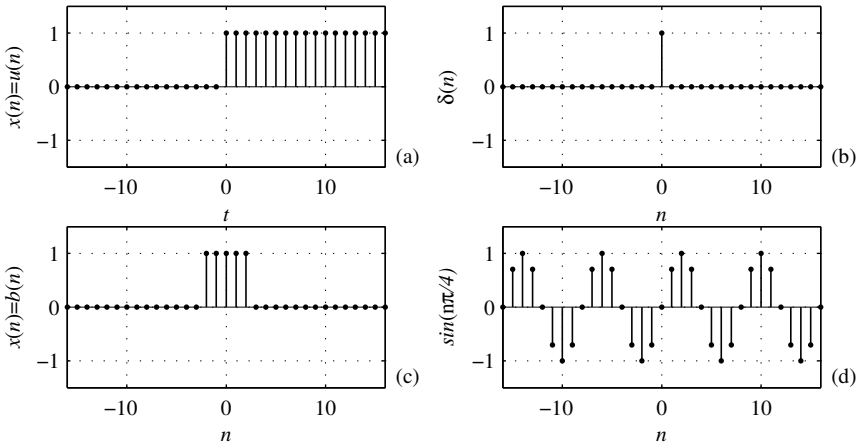


Figure 1.7 Illustration of simple discrete-time signals: (a) unity step function, (b) discrete-time impulse signal, (c) boxcar signal $b(n) = u(n+2) - u(n-3)$, and (d) discrete-time sinusoid.

The discrete unit step signal is defined by

$$x(n) = u(n) = \begin{cases} 1, & \text{for } n \geq 0 \\ 0, & \text{for } n < 0 \end{cases}. \quad (1.65)$$

The discrete complex sinusoidal signal definition is

$$x(n) = A e^{j(\omega_0 n + \varphi)} = A \cos(\omega_0 n + \varphi) + j A \sin(\omega_0 n + \varphi). \quad (1.66)$$

A discrete-time signal is periodic if there exists an integer N such that

$$x(n+N) = x(n). \quad (1.67)$$

Smallest positive integer N that satisfies this equation is called the period of the discrete-time signal $x(n)$. Note that a signal $x(n)$ with a period N is also periodic with any integer multiple of N . Some simple discrete-time signals are presented in Fig. 1.7.

Example 1.15. Check the periodicity of discrete-time signals $x_1(n) = \sin(2\pi n/36)$, $x_2(n) = \cos(4\pi n/15 + 2)$, $x_3(n) = \exp(j0.1n)$, $x_4(n) = x_1(n) + x_2(n)$, and $x_5(n) = x_1(n) + x_3(n)$.

★The period of the discrete-time signal $x_1(t)$ is obtained from $2\pi N_1/36 = 2\pi k$, where k is an integer. It is $N_1 = 36$, for $k = 1$. The period N_2 follows from $4\pi N_2/15 = 2\pi k$, as $N_2 = 15$ for $k = 2$. For signal $x_3(n)$ the period should be calculated from $0.1N_3 = 2\pi k$. Obviously, there is no integer k such that N_3 is an integer. This signal is not periodic. The same holds for $x_5(n)$. The period of $x_4(n)$ is the common period for $N_1 = 36$ and $N_2 = 15$. It is $N_4 = 180$. \square

Discrete system transforms one discrete-time signal (input) into the other (output signal)

$$y(n) = \mathbb{T}\{x(n)\}. \quad (1.68)$$

As in the continuous-time case, for a linear time-invariant discrete system we can calculate the output to any input signal $x(n)$ if we know the output to the impulse signal (i.e., if we know the impulse response $h(n) = \mathbb{T}\{\delta(n)\}$). Then, we have

$$y(n) = \mathbb{T}\{x(n)\} = \mathbb{T}\left\{\sum_{k=-\infty}^{\infty} x(k)\delta(n-k)\right\}.$$

For a linear time-invariant system we get

$$y(n) = \sum_{k=-\infty}^{\infty} x(k)h(n-k) = \sum_{k=-\infty}^{\infty} h(k)x(n-k). \quad (1.69)$$

This is a form of the discrete-time convolution. Its notation is

$$x(n) *_n h(n) = \sum_{k=-\infty}^{\infty} x(k)h(n-k). \quad (1.70)$$

Discrete time convolution is commutative operation,

$$x(n) *_n h(n) = h(n) *_n x(n). \quad (1.71)$$

Energy of discrete-time signals is defined by

$$E_x = \sum_{n=-\infty}^{\infty} |x(n)|^2. \quad (1.72)$$

The instantaneous power is $P_x(n) = |x(n)|^2$, while the average signal power is

$$P_{AV} = \lim_{N \rightarrow \infty} \frac{1}{2N+1} \sum_{n=-N}^N |x(n)|^2. \quad (1.73)$$

1.2.1 Fourier Transform of Discrete-Time Signals

The Fourier transform of a discrete-time signal is defined by

$$X(e^{j\omega}) = \sum_{n=-\infty}^{\infty} x(n)e^{-j\omega n}. \quad (1.74)$$

Notation $X(e^{j\omega})$ is used to emphasize the fact that it is a periodic function of the normalized frequency ω . The period is 2π .

In order to establish the relation between the Fourier transform of discrete-time signals and the Fourier transform of continuous signals,

$$X(\Omega) = \int_{-\infty}^{\infty} x(t)e^{-j\Omega t} dt,$$

we will write an approximation of the Fourier transform of continuous signal according to the rectangular rule of numerical integration,

$$X(\Omega) \cong \sum_{n=-\infty}^{\infty} x(n\Delta t)e^{-j\Omega n\Delta t}\Delta t. \quad (1.75)$$

By using the notation

$$\begin{aligned} x(n\Delta t)\Delta t &\longrightarrow x(n) \\ \Omega\Delta t &\longrightarrow \omega, \end{aligned} \quad (1.76)$$

the previous approximation can be written as

$$\sum_{n=-\infty}^{\infty} x(n)e^{-j\omega n} = X(e^{j\omega}). \quad (1.77)$$

This is the Fourier transform of the discrete-time signal $x(n)$.

Later we will show that, under some conditions, the Fourier transform of discrete-time signals, $X(e^{j\omega})$, is not just an approximation of the Fourier transform of continuous-time signal $X(\Omega)$, but the equality holds (i.e., $X(\Omega) = X(e^{j\omega})$) with $\Omega\Delta t = \omega$ and $-\pi \leq \omega < \pi$.

The inverse Fourier transform of discrete-time signals is obtained by multiplying both sides of (1.77) by $e^{j\omega m}$ and integrating them over a period of $X(e^{j\omega})$

$$\sum_{n=-\infty}^{\infty} x(n) \int_{-\pi}^{\pi} e^{-j\omega(n-m)} d\omega = \int_{-\pi}^{\pi} X(e^{j\omega})e^{j\omega m} d\omega.$$

Since

$$\int_{-\pi}^{\pi} e^{-j\omega(n-m)} d\omega = 2 \frac{\sin((n-m)\pi)}{(n-m)} = 2\pi\delta(n-m),$$

we get

$$x(n) = \frac{1}{2\pi} \int_{-\pi}^{\pi} X(e^{j\omega}) e^{jn\omega} d\omega. \quad (1.78)$$

Properties of this transform may be derived in the same way as in the case of continuous-time signals. The Fourier transform of discrete-time signals is linear. With respect to the shift and modulation it behaves like the Fourier transform,

$$FT\{x(n-n_0)\} = X(e^{jn_0\omega}) \quad (1.79)$$

and

$$FT\{x(n)e^{j\omega_0 n}\} = X(e^{j(\omega-\omega_0)}). \quad (1.80)$$

For a convolution of discrete-time signals,

$$FT\{x(n) *_n h(n)\} = \sum_{n=-\infty}^{\infty} \sum_{k=-\infty}^{\infty} x(k)h(n-k)e^{-jn\omega} = X(e^{j\omega})H(e^{j\omega}), \quad (1.81)$$

we get that its Fourier transform is equal to the product of the Fourier transforms of signals.

The Fourier transform of a product of discrete-time signals,

$$FT\{x(n)h(n)\} = \frac{1}{2\pi} \int_{-\pi}^{\pi} X(e^{j\theta})H(e^{j(\omega-\theta)}) d\theta = X(e^{j\omega}) *_\omega H(e^{j\omega}), \quad (1.82)$$

is equal to the convolution of the Fourier transforms in frequency. This convolution is periodic with period 2π (circular convolution).

The Parseval's theorem for discrete-time signals reads as

$$\begin{aligned} \sum_{n=-\infty}^{\infty} x(n)y^*(n) &= \sum_{n=-\infty}^{\infty} \frac{1}{2\pi} \int_{-\pi}^{\pi} X(e^{j\omega}) e^{jn\omega} y^*(n) d\omega \\ &= \frac{1}{2\pi} \int_{-\pi}^{\pi} X(e^{j\omega}) \left(\sum_{n=-\infty}^{\infty} (e^{-j\omega n} y(n))^* \right) d\omega = \frac{1}{2\pi} \int_{-\pi}^{\pi} X(e^{j\omega}) Y^*(e^{j\omega}) d\omega. \end{aligned} \quad (1.83)$$

Example 1.16. Find the inverse Fourier transform of a discrete-time signal if $X(e^{j\omega}) = 2\pi\delta(\omega)$ for $-\pi \leq \omega < \pi$ or $X(e^{j\omega}) = 2\pi \sum_{k=-\infty}^{\infty} \delta(\omega + 2k\pi)$ for any ω .

★By definition

$$x(n) = \frac{1}{2\pi} \int_{-\pi}^{\pi} 2\pi\delta(\omega)e^{j\omega n} d\omega = 1.$$

Therefore,

$$\sum_{n=-\infty}^{\infty} e^{-j\omega n} = 2\pi \sum_{k=-\infty}^{\infty} \delta(\omega + 2k\pi). \quad (1.84)$$

The equivalent form in the continuous domain is obtained, by knowing that $\delta(T\Omega) = \delta(\Omega)/T$ holds for the impulse signal, as

$$\sum_{n=-\infty}^{\infty} e^{j\Omega n T} = 2\pi \sum_{k=-\infty}^{\infty} \delta(\Omega T + 2k\pi) = \frac{2\pi}{T} \sum_{k=-\infty}^{\infty} \delta(\Omega + 2k\pi/T).$$

□

Example 1.17. Find the Fourier transform of the discrete-time signal

$$x(n) = Ae^{-\alpha|n|}$$

where $\alpha > 0$ is a real constant.

★The Fourier transform of this signal is

$$\begin{aligned} X(e^{j\omega}) &= A + \sum_{n=-\infty}^{-1} Ae^{\alpha n - j\omega n} + \sum_{n=1}^{\infty} Ae^{-\alpha n - j\omega n} \\ &= A \left(1 + \frac{e^{j\omega - \alpha}}{1 - e^{j\omega - \alpha}} + \frac{e^{-j\omega - \alpha}}{1 - e^{-j\omega - \alpha}} \right) = A \frac{1 - e^{-2\alpha}}{1 - 2e^{-\alpha} \cos(\omega) + e^{-2\alpha}}. \end{aligned} \quad (1.85)$$

□

Example 1.18. Calculate the Fourier transform of a discrete-time signal (rectangular window),

$$w_R(n) = u(N+n) - u(n-N-1). \quad (1.86)$$

Write the Fourier transform of the Hann(ing) window

$$w_H(n) = \frac{1}{2} [1 + \cos(n\pi/N)] [u(N+n) - u(n-N-1)].$$

★By definition

$$W_R(e^{j\omega}) = \sum_{n=-N}^N e^{-jn\omega n} = e^{j\omega N} \frac{1 - e^{-j\omega(2N+1)}}{1 - e^{-j\omega}} = \frac{\sin(\omega \frac{2N+1}{2})}{\sin(\omega/2)}. \quad (1.87)$$

The Fourier transform of the Hann(ing) window can easily be written as

$$\begin{aligned} W_H(e^{j\omega}) &= \frac{1}{2} \sum_{n=-N}^N \left(1 + \frac{1}{2} e^{jn\pi/N} + \frac{1}{2} e^{-jn\pi/N} \right) e^{-jn\omega n} = \\ &= \frac{\sin(\omega \frac{2N+1}{2})}{2 \sin(\omega/2)} + \frac{\sin((\omega - \frac{\pi}{N}) \frac{2N+1}{2})}{4 \sin((\omega - \frac{\pi}{N})/2)} + \frac{\sin((\omega + \frac{\pi}{N}) \frac{2N+1}{2})}{4 \sin((\omega + \frac{\pi}{N})/2)}. \end{aligned} \quad (1.88)$$

□

1.2.2 Sampling Theorem in the Time Domain

Continuous-time signal $x(t)$, whose Fourier transform $X(\Omega)$ is limited, that is,

$$X(\Omega) = 0 \text{ for } |\Omega| > \Omega_m, \quad (1.89)$$

can be reconstructed, for any t , based on the samples taken with a sampling interval Δt ,

$$x(n) = x(n\Delta t)\Delta t,$$

such that

$$\Delta t < \frac{\pi}{\Omega_m} = \frac{1}{2f_m},$$

with $\Omega_m = 2\pi f_m$, where f_m is a frequency in [Hz], while Ω_m is frequency in [rad/s].

Now we will prove this statement. Since we have assumed a limited frequency duration of $X(\Omega)$ we can make its periodic extension

$$X_p(\Omega) = \sum_{m=-\infty}^{\infty} X(\Omega + 2\Omega_0 m) \quad (1.90)$$

with a period $2\Omega_0$. It is very important to note that $X_p(\Omega) = X(\Omega)$ for $|\Omega| < \Omega_0$ if

$$\Omega_0 > \Omega_m.$$

In this case, it is possible to go from $X(\Omega)$ to $X_p(\Omega)$ and back without losing any information.

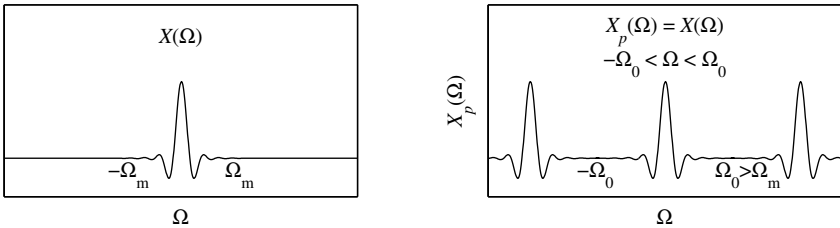


Figure 1.8 Fourier transform of a signal, with $X(\Omega) = 0$ for $|\Omega| > \Omega_m$ (left) and its periodically extended version, with period $2\Omega_0 > 2\Omega_m$ (right).

Of course, that would not be the case if $\Omega_0 > \Omega_m$ did not hold. By periodic extension of $X(\Omega)$, in that case, overlapping (aliasing) would have occurred in $X_p(\Omega)$. It would not be reversible. Then it would not be possible to recover $X(\Omega)$ from $X_p(\Omega)$. The periodic extension is illustrated in Fig. 1.8.

The periodic function $X_p(\Omega)$ can be expanded into Fourier series with coefficients

$$X_{-n} = \frac{1}{2\Omega_0} \int_{-\Omega_0}^{\Omega_0} X_p(\Omega) e^{j\pi\Omega n/\Omega_0} d\Omega = \frac{1}{2\Omega_0} \int_{-\infty}^{\infty} X(\Omega) e^{j\pi\Omega n/\Omega_0} d\Omega.$$

Since within the basic period $X(\Omega) = X_p(\Omega)$ and $X(\Omega) = 0$ outside this period, the integration limits are extended to the infinity.

The inverse Fourier transform of continuous-time signal is

$$x(t) = \frac{1}{2\pi} \int_{-\infty}^{\infty} X(\Omega) e^{j\Omega t} d\Omega. \quad (1.91)$$

By comparing the last two equations, we easily conclude that

$$\begin{aligned} X_{-n} &= \frac{\pi}{\Omega_0} x(t)|_{t=\pi n/\Omega_0} = x(n\Delta t)\Delta t \\ \Delta t &= \frac{\pi}{\Omega_0}, \end{aligned} \quad (1.92)$$

meaning that the Fourier series coefficients of the periodically extended Fourier transform of $X(\Omega)$ are the samples of the signal, taken with the sampling interval $\Delta t = \pi/\Omega_0$.

Therefore, the samples of a signal and the periodically extended Fourier transform are the Fourier series pair

$$X_{-n} = x(n\Delta t)\Delta t \Leftrightarrow X_p(\Omega) = \sum_{m=-\infty}^{\infty} X(\Omega + 2\Omega_0 m) \quad (1.93)$$

with $\Delta t = \pi/\Omega_0$.

The reconstruction formula for $x(t)$ then follows from

$$\begin{aligned} x(t) &= \frac{1}{2\pi} \int_{-\infty}^{\infty} X(\Omega) e^{j\Omega t} d\Omega = \frac{1}{2\pi} \int_{-\Omega_0}^{\Omega_0} X_p(\Omega) e^{j\Omega t} d\Omega \\ &= \frac{1}{2\pi} \int_{-\Omega_0}^{\Omega_0} \left(\sum_{n=-\infty}^{\infty} X_n e^{j\pi n \Omega / \Omega_0} \right) e^{j\Omega t} d\Omega \\ &= \frac{1}{2\pi} \int_{-\Omega_0}^{\Omega_0} \left(\sum_{n=-\infty}^{\infty} x(n\Delta t) \Delta t e^{-j\pi n \Omega / \Omega_0} \right) e^{j\Omega t} d\Omega \end{aligned} \quad (1.94)$$

as

$$x(t) = \sum_{n=-\infty}^{\infty} x(n\Delta t) \frac{\sin(\pi(t - n\Delta t)/\Delta t)}{\pi(t - n\Delta t)/\Delta t}. \quad (1.95)$$

Thus, the signal $x(t)$, for any t , is expressed in terms of its samples $x(n\Delta t)$.

Example 1.19. The last relation can be used to prove that $X(\Omega) = X(e^{j\omega})$ with $\Omega\Delta t = \omega$ and $|\omega| < \pi$ for the signals sampled at the rate satisfying the sampling theorem.

★Starting from

$$X(\Omega) = \int_{-\infty}^{\infty} x(t) e^{-j\Omega t} dt$$

the signal $x(t)$, satisfying the sampling theorem, can be written in terms of samples, according to the third row of (1.94), as

$$x(t) = \frac{1}{2\pi} \int_{-\Omega_0}^{\Omega_0} \left(\sum_{n=-\infty}^{\infty} x(n\Delta t) \Delta t e^{-j\Delta t n \theta} \right) e^{j\theta t} d\theta.$$

It follows

$$\begin{aligned}
 X(\Omega) &= \int_{-\infty}^{\infty} \frac{1}{2\pi} \int_{-\Omega_0}^{\Omega_0} \left(\sum_{n=-\infty}^{\infty} x(n\Delta t) \Delta t e^{-j\Delta t n \theta} \right) e^{j\theta t} d\theta e^{-j\Omega t} dt \\
 &= \sum_{n=-\infty}^{\infty} x(n\Delta t) \Delta t \int_{-\Omega_0}^{\Omega_0} \delta(\theta - \Omega) e^{-j\Delta t n \theta} d\theta \\
 &= \sum_{n=-\infty}^{\infty} x(n\Delta t) \Delta t e^{-j\Delta t n \Omega} \text{ for } |\Omega| < \Omega_0
 \end{aligned} \tag{1.96}$$

resulting in

$$X(\Omega) = \sum_{n=-\infty}^{\infty} x(n) e^{-j\omega n} \text{ for } |\omega| < \pi$$

with $\omega = \Omega \Delta t$ and $x(n) = x(n\Delta t) \Delta t$. \square

Example 1.20. If the highest frequency in a signal $x(t)$ is Ω_{m1} and the highest frequency in a signal $y(t)$ is Ω_{m2} what should be the sampling interval for: the signal $x(t)y(t)$ and for the signal $x(t-t_1)y^*(t-t_2)$? The highest frequency in $x(t)$ is used in the sense that $X(\Omega) = 0$ for $|\Omega| > \Omega_{m1}$.

★The Fourier transform of a product $x(t)y(t)$ is a convolution of the Fourier transforms $X(\Omega)$ and $Y(\Omega)$. Since these functions are of limited duration $|\Omega| < \Omega_{m1}$ and $|\Omega| < \Omega_{m2}$, respectively, we have shown that the duration of their convolution is limited to the interval $|\Omega| < \Omega_{m1} + \Omega_{m2}$. Therefore, the sampling interval for $y(t)$ should be

$$\Delta t < \frac{\pi}{\Omega_{m1} + \Omega_{m2}}.$$

Shifts in time and complex conjugate operation do not change the width of the Fourier transform, thus the conclusion remains the same for $x(t-t_1)y^*(t-t_2)$. \square

Example 1.21. If the signal

$$x(t) = e^{-|t|}$$

is sampled with $\Delta t = 0.1$, write the Fourier transform of the obtained discrete-time signal: (a) by periodical extension of the continuous Fourier transform and (b) by a direct calculation based on the discrete-time signal. Comment on the expected error due to the discretization.

★The Fourier transform of this signal is

$$\begin{aligned} X(\Omega) &= \int_{-\infty}^{\infty} x(t)e^{-j\Omega t} dt = \int_{-\infty}^0 e^t e^{-j\Omega t} dt + \int_0^{\infty} e^{-t} e^{-j\Omega t} dt \\ &= \frac{1}{1-j\Omega} + \frac{1}{1+j\Omega} = \frac{2}{1+\Omega^2}. \end{aligned} \quad (1.97)$$

After sampling with $\Delta t = 0.1$, the Fourier transform is periodically extended with period $2\Omega_0 = 2\pi/\Delta t = 20\pi$.

(a) The periodic Fourier transform is

$$X_p(\Omega) = \dots + \frac{2}{1+(\Omega+20\pi)^2} + \frac{2}{1+\Omega^2} + \frac{2}{1+(\Omega-20\pi)^2} + \dots$$

Thus, the value of $X_p(\Omega)$ at the period ending points $\pm 10\pi$ will approximately be $X_p(\pm 10\pi) = 2/(1+100\pi^2) \cong 0.002$. Comparing with the maximum value $X_p(0) = 2$, it means that the expected error due to the discretization of this signal, that does not strictly satisfy the sampling theorem, will be of a 0.1% order.

(b) The discrete signal obtained by sampling $x(t) = \exp(-|t|)$ with $\Delta t = 0.1$ is $x(n) = 0.1e^{-0.1|n|}$. Its Fourier transform is already calculated with $A = 0.1$ and $\alpha = 0.1$, eq.(1.85). The value is

$$X(e^{j\omega}) = 0.1 \frac{1-e^{-0.2}}{1-2e^{-0.1}\cos(\omega) + e^{-0.2}}. \quad (1.98)$$

Therefore, the exact value of the infinite sum in $X_p(\Omega)$ is $X(e^{j\omega})$ with $\omega = \Omega\Delta t = 0.1\Omega$

$$X_p(\Omega) = \sum_{k=-\infty}^{\infty} \frac{2}{1+(\Omega+20k\pi)^2} = 0.1 \frac{1-e^{-0.2}}{1-2e^{-0.1}\cos(0.1\Omega) + e^{-0.2}}.$$

Note that in this way we solve an interesting mathematical problem of finding a sum of infinite series.

For $\Omega = 0$, the original value of the Fourier transform is $X(0) = 2$. In the signal that could be reconstructed based on the discretized signal $X_p(0) = 0.1(1+e^{-0.1})/(1-e^{-0.1}) = 2.00167$. It corresponds to our previous conclusion of about a 0.1% error. \square

1.2.3 Discrete Fourier Transform

The discrete Fourier transform (DFT) is defined by

$$\text{DFT}\{x(n)\} = X(k) = \sum_{n=0}^{N-1} x(n)e^{-j2\pi kn/N} \quad (1.99)$$

for $k = 0, 1, 2, \dots, N - 1$. In order to establish a relation between the DFT with the Fourier transform of discrete-time signals, consider a discrete-time signal $x(n)$ of limited duration in time (i.e., signal $x(n)$ being different from zero only within $0 \leq n \leq N_0 - 1$). Its Fourier transform would be

$$X(e^{j\omega}) = \sum_{n=0}^{N_0-1} x(n)e^{-j\omega n}.$$

The DFT can be considered as samples of the Fourier transform of discrete-time signals in frequency, taken at $\Delta\omega = 2\pi/N$, corresponding to N frequency samples within the period $-\pi \leq \omega < \pi$, since we have

$$X(k) = X(e^{j2\pi k/N}) = X(e^{j\omega})|_{\omega=k\Delta\omega=2\pi k/N}. \quad (1.100)$$

In order to examine the influence of sampling the Fourier transform in the frequency domain to the signal in the time domain, let form a periodic extension of $x(n)$ with a period $N \geq N_0$.

With N being greater than the signal duration N_0 , we will be able to reconstruct the original signal $x(n)$ from its periodic extension $x_p(n)$. Furthermore, let assume that the periodic signal $x_p(n)$ is formed from the samples of periodic continuous signal $x_p(t)$ with a period T (corresponding to N signal samples, $T = N\Delta t$) then its Fourier series coefficients would be

$$X_k = \frac{1}{T} \int_0^T x_p(t) e^{-j2\pi kt/T} dt$$

assuming that the sampling theorem is satisfied, the integral could be replaced by a sum (in the sense of Example 1.19)

$$X_k = \frac{1}{T} \sum_{n=0}^{N-1} x(n\Delta t) e^{-j2\pi kn\Delta t/T} \Delta t$$

with $x_p(t) = x(t)$ within $0 \leq t < T$. With $T/\Delta t = N$, $x(n\Delta t)\Delta t = x(n)$ and $X(k) = TX_k$ this sum can be written as

$$X(k) = \sum_{n=0}^{N-1} x(n) e^{-j2\pi kn/N}. \quad (1.101)$$

Therefore, the relation between the DFT and the Fourier series coefficients is

$$X(k) = T X_k. \quad (1.102)$$

Sampling the Fourier transform of a discrete-time signal corresponds to the periodical extension of the original discrete-time signal in time by a period N . The period N is equal to the number of samples of the Fourier transform in one period. We can conclude that this periodic extension in time (discretization in frequency) will not affect the possibility to recover the original signal if the duration of the original discrete-time signal was shorter than N (the number of samples in the Fourier transform of discrete-time signal).

The inverse DFT is obtained by multiplying both sides of the DFT definition (1.99) by $e^{j2\pi km/N}$ and summing over k

$$\sum_{k=0}^{N-1} X(k) e^{j2\pi mk/N} = \sum_{n=0}^{N-1} x(n) \sum_{k=0}^{N-1} e^{j2\pi k(m-n)/N}$$

with

$$\sum_{k=0}^{N-1} e^{j2\pi k(m-n)/N} = N\delta(m-n).$$

The inverse discrete Fourier transform (IDFT) of signal $x(n)$ then reads as

$$x(n) = \frac{1}{N} \sum_{k=0}^{N-1} X(k) e^{j2\pi nk/N}. \quad (1.103)$$

In a matrix form, the DFT can be written as

$$\begin{bmatrix} X(0) \\ X(1) \\ \vdots \\ X(N-1) \end{bmatrix} = \begin{bmatrix} 1 & 1 & \cdots & 1 \\ 1 & e^{-j\frac{2\pi}{N}} & \cdots & e^{-j\frac{2\pi(N-1)}{N}} \\ \vdots & \vdots & \ddots & \vdots \\ 1 & e^{-j\frac{2\pi(N-1)}{N}} & \cdots & e^{-j\frac{2\pi(N-1)(N-1)}{N}} \end{bmatrix} \begin{bmatrix} x(0) \\ x(1) \\ \vdots \\ x(N-1) \end{bmatrix} \quad (1.104)$$

or

$$\mathbf{X} = \mathbf{W}\mathbf{x}, \quad (1.105)$$

where \mathbf{X} and \mathbf{x} are the vectors containing the signal and its DFT values

$$\begin{aligned} \mathbf{X} &= [X(0) \ X(1) \ \dots \ X(N-1)]^T \\ \mathbf{x} &= [x(0) \ x(1) \ \dots \ x(N-1)]^T, \end{aligned}$$

respectively, while \mathbf{W} is the discrete Fourier transform matrix with coefficients

$$\mathbf{W} = \begin{bmatrix} 1 & 1 & \cdots & 1 \\ 1 & e^{-j\frac{2\pi}{N}} & \cdots & e^{-j\frac{2\pi(N-1)}{N}} \\ \vdots & \vdots & \ddots & \vdots \\ 1 & e^{-j\frac{2\pi(N-1)}{N}} & \cdots & e^{-j\frac{2\pi(N-1)(N-1)}{N}} \end{bmatrix}. \quad (1.106)$$

Obviously, the order of the number of multiplications and additions for the DFT calculation is N^2 . The inverse DFT is

$$\mathbf{x} = \mathbf{W}^{-1}\mathbf{X}, \quad (1.107)$$

with

$$\mathbf{W}^{-1} = \frac{1}{N}\mathbf{W}^*, \quad (1.108)$$

where $*$ denotes here complex conjugate operation.

Algorithms that provide efficient calculation of the DFT, with a reduced number of arithmetic operations, are called the fast Fourier transform (FFT); see Problem 1.17. The inverse DFT, (1.103), can be calculated by using the same algorithms. The only differences are in the sign of the exponent and the division of the final result by N .

Example 1.22. Consider a signal $x(n)$ within $0 \leq n \leq N - 1$. Assume that N is an even number. Show that the DFT of $x(n)$ can be calculated as two DFTs, one using the even samples of $x(n)$ and the other using odd samples of $x(n)$.

★By definition

$$\begin{aligned} X(k) &= \sum_{n=0}^{N-1} x(n)e^{-j2\pi kn/N} \\ &= \sum_{m=0}^{N/2-1} x(2m)e^{-j2\pi k2m/N} + \sum_{m=0}^{N/2-1} x(2m+1)e^{-j2\pi k(2m+1)/N} \\ &= \sum_{m=0}^{N/2-1} x_e(m)e^{-j2\pi km/(N/2)} + e^{-j2\pi k/N} \sum_{m=0}^{N/2-1} x_o(m)e^{-j2\pi km/(N/2)}, \end{aligned} \quad (1.109)$$

where $x_e(m) = x(2m)$ and $x_o(m) = x(2m+1)$ are even and odd samples of the signal, respectively. Thus, a DFT of N elements is split into two DFTs of $N/2$ elements. Two DFTs of $N/2$ elements require an order of $2(N/2)^2 = N^2/2$ operations. It is less than

N^2 . In this way, if $N/2$ is an even number, we can continue and split two DFTs of $N/2$ elements into four DFTs of $N/4$ elements, and so on.

The reduction of a higher-order DFT to several lower-order DFTs is in the core of the FFT algorithms. The calculation complexity is significantly reduced in this way. \square

Most of the DFT properties could be derived in the same way as in the Fourier transform and Fourier transform of discrete-time signals.

For a signal shifted in time we have,

$$\begin{aligned} \text{DFT}\{x(n - n_0)\} &= \sum_{n=0}^{N-1} x(n - n_0) e^{-j\frac{2\pi}{N}kn} \\ &= \sum_{m=-n_0}^{N-1-n_0} x(m) e^{-j\frac{2\pi}{N}k(n_0+m)}. \end{aligned} \quad (1.110)$$

Since both the signal $x(n)$ and the function $\exp(-j\frac{2\pi}{N}km)$ are periodic in m with period N , the sum is the same for any N consecutive terms, so we can write

$$\sum_{m=-n_0}^{N-1-n_0} x(m) e^{-j\frac{2\pi}{N}km} = \sum_{m=0}^{N-1} x(m) e^{-j\frac{2\pi}{N}km}.$$

This kind of shift in periodic signals, used in the above relation, is also referred to as a circular shift. Thus,

$$\text{DFT}\{x(n - n_0)\} = X(k) e^{-j2\pi k n_0 / N}. \quad (1.111)$$

For $x(n)e^{j2\pi nk_0/N}$ we easily get

$$\text{DFT}\left\{x(n)e^{j2\pi nk_0/N}\right\} = X(k - k_0). \quad (1.112)$$

Convolution of two periodic signals $x(n)$ and $h(n)$, whose period is N , is defined by

$$y(n) = \sum_{m=0}^{N-1} x(m) h(n-m).$$

The DFT of this signal is

$$Y(k) = \text{DFT}\{y(n)\} = \sum_{n=0}^{N-1} \sum_{m=0}^{N-1} x(m) h(n-m) e^{-j2\pi nk/N} = X(k) H(k). \quad (1.113)$$

Thus, the DFT of the convolution of two periodic signals is equal to the product of DFTs of individual signals. Since the convolution is performed on periodic signals (the DFT inherently assumes signals periodicity), a circular shift of signals is assumed. This kind of convolution is called circular convolution.

This relation indicates that we can calculate convolution of two nonperiodic discrete-time signals of limited duration in the following way:

- Calculate DFTs of $x(n)$ and $h(n)$ and obtain $X(k)$ and $H(k)$. At this point, we inherently make a periodic extension of $x(n)$ and $h(n)$ with period N .
- Multiply these two DFTs to obtain the DFT of output signal $Y(k) = X(k)H(k)$.
- Calculate the inverse DFT to get the convolution $y(n) = \text{IDFT}\{Y(k)\}$.

This procedure looks more complex than the direct calculation of convolution by definition. However, due to very efficient FFT routines for the DFT and the IDFT calculation, this way of calculation could be more efficient than the direct one.

In using this procedure, we have to take care about the length of signals and their DFTs that assume periodic extension. If signal $x(n)$ is of length M , then we can calculate its DFT with any $N \geq M$, so that the signal will not overlap in periods, added in this way. If the signal $h(n)$ is of length L , then we can calculate its DFT with any $N \geq L$. However, if we want to use their DFTs for convolution calculation (to use circular convolution), then from one of earlier examples we see that the length of convolution, that is, length of signal $y(n)$, is $M + L - 1$. Therefore, for the DFT calculation of $y(n)$, we have to use at least $N \geq M + L - 1$. This means that both DFTs, $X(k)$ and $H(k)$, whose product results in $Y(k)$, must be at least of $N \geq M + L - 1$ duration. Otherwise, aliasing (overlapping of the periods) will appear. Then the circular convolution calculated in this way would not correspond (within the basic period) to the convolution of original discrete-time, aperiodic signals with limited durations.

1.2.3.1 Zero-Padding and Interpolation

We have seen that the DFT of a signal whose duration is limited to M samples can be calculated by using any $N \geq M$. In practice, this means that we can add (use) as many zeros, after the nonzero signal values, as we like. By doing this, we increase the calculation complexity, but we also increase the number of samples within the same frequency range of the Fourier transform of the discrete-time signal.

If we recall that

$$X(k) = X(e^{j\omega})_{|\omega=k\Delta\omega=2\pi k/N} = X(\Omega)_{|\Omega=k\Delta\Omega=2\pi k/(N\Delta t)}, \quad (1.114)$$

holds in the case when the sampling theorem is satisfied, then we see that by increasing N in the DFT calculation, the density of sampling (interpolation) the Fourier transform of the original signal increases.

The same holds for the frequency domain. If we calculate DFT with N samples and then add, for example, N zeros after the region corresponding to the highest frequencies, then if we calculate the IDFT of this $2N$ point DFT, we will interpolate the original signal in time. It is important to emphasize that the basic period of the DFT $X(k)$ should be considered as having two parts: one part for $0 \leq k \leq N/2 - 1$, that corresponds to the positive frequencies

$$\omega = \frac{2\pi}{N}k \text{ or } \Omega = \frac{2\pi}{N\Delta t}k, \text{ for } 0 \leq k \leq N/2 - 1, \quad (1.115)$$

and the other part being a shifted version of the negative frequencies (in the original nonperiodic signal)

$$\omega = \frac{2\pi}{N}(k - N) \text{ or } \Omega = \frac{2\pi}{N\Delta t}(k - N), \text{ for } N/2 \leq k \leq N - 1. \quad (1.116)$$

Thus, all added zero values should be inserted between these two parts (regions) of the original DFT. The DFT interpolation by zero padding is illustrated in Fig. 1.9.

Finally, we will conclude the presentation of the DFT with an illustration (Fig. 1.10) of the relation among four forms of the Fourier signal representation for the cases of:

1. Continuous-time aperiodic signal (Fourier transform);
2. Continuous-time periodic signal (Fourier series);
3. Discrete-time aperiodic signal (Fourier transform of discrete-time signals);
4. Discrete-time periodic signal (discrete Fourier transform).

1.2.4 Analysis of a Sinusoid by Using the DFT

Consider a simple sinusoidal signal

$$x(t) = e^{j\Omega_0 t} \quad (1.117)$$

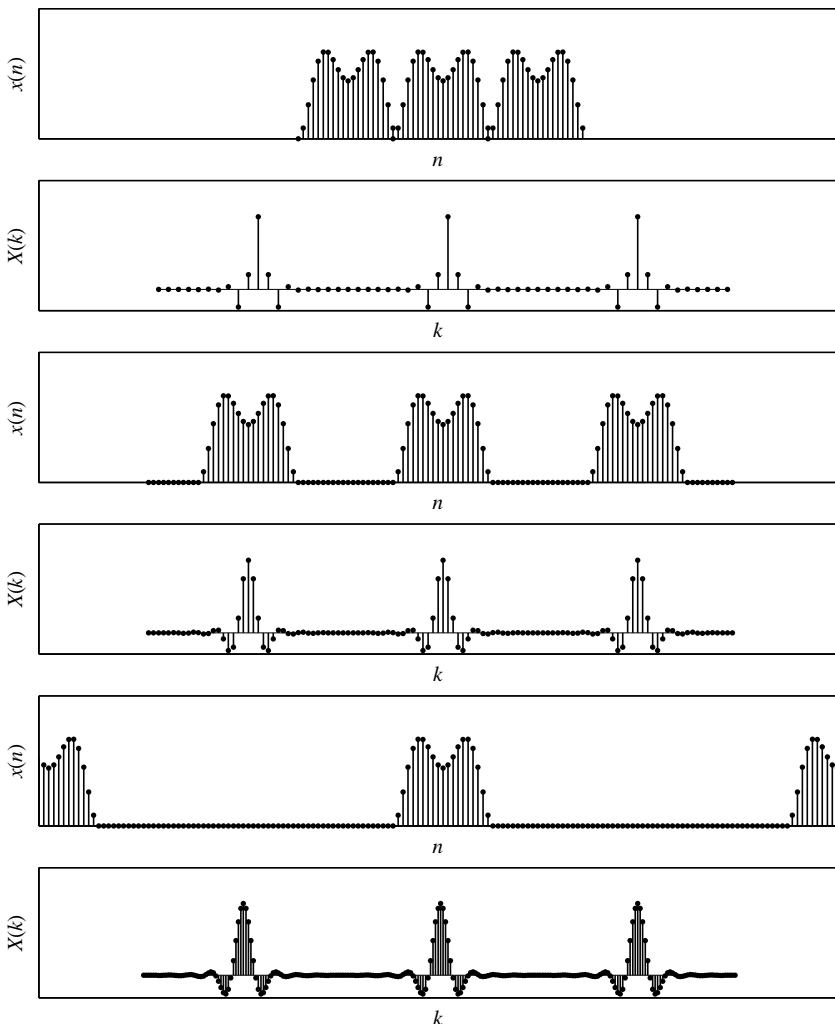


Figure 1.9 Discrete signal and its DFT (two top subplots); discrete signal zero-padded and its DFT interpolated (two subplots in the middle). Zero-padding (interpolation) factor was 2; discrete signal zero-padded and its DFT interpolated (two bottom subplots). Zero-padding (interpolation) factor was 4. According to the duality property, the same holds if $X(k)$ were signal in the discrete-time and $x(-n)$ was its Fourier transform.

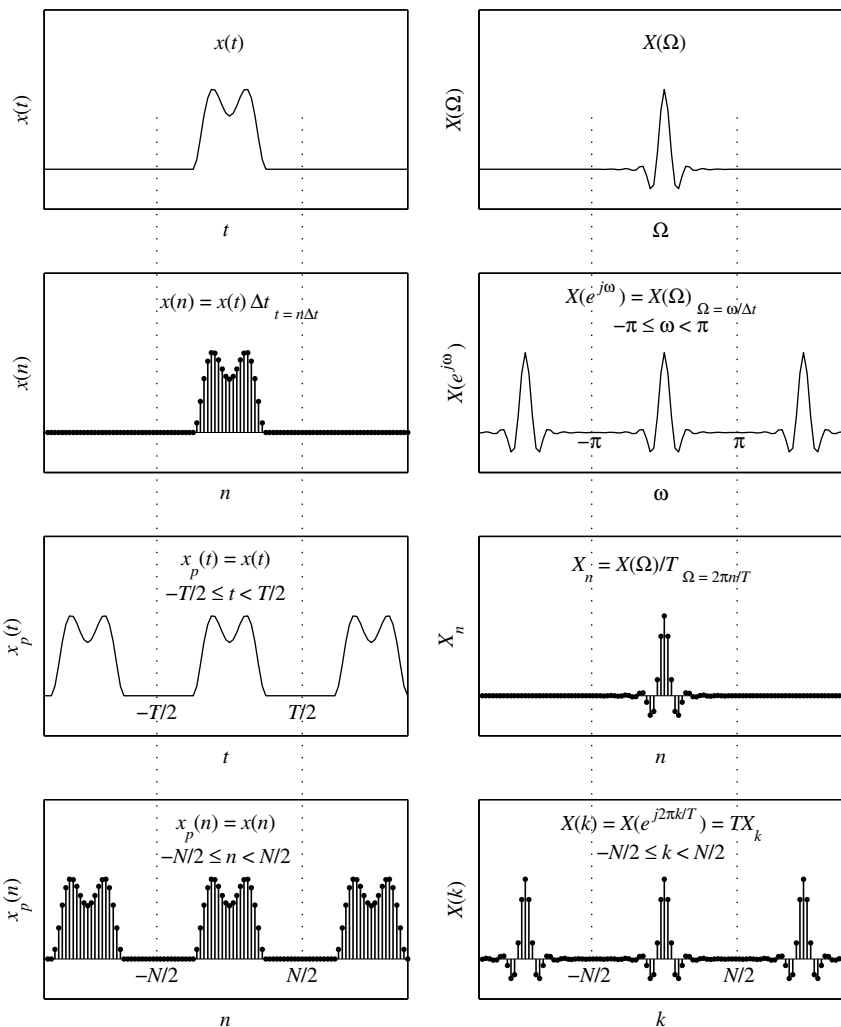


Figure 1.10 Aperiodic continuous signal and its Fourier transform (first row); discrete signal and the Fourier transform of discrete signals (second row); periodic continuous-time signal and its Fourier series coefficients (third row); and periodic discrete-time signal and its discrete Fourier transform (DFT), (fourth row).

whose Fourier transform is

$$X(\Omega) = 2\pi\delta(\Omega - \Omega_0).$$

The whole signal energy is concentrated just in one frequency point at $\Omega = \Omega_0$. Obviously, the position of maximum is equal to the signal's frequency. For this operation we will use the notation

$$\Omega_0 = \arg \left\{ \max_{-\infty < \Omega < \infty} |X(\Omega)| \right\}. \quad (1.118)$$

Assume that the signal is sampled with Δt . The discrete-time form of this signal is

$$x(n) = e^{j\omega_0 n} \Delta t,$$

with $\omega_0 = \Omega_0 \Delta t$.

In order to compute the DFT of this signal, we will assume a value of N and calculate

$$X(k) = \sum_{n=0}^{N-1} e^{j\omega_0 n} e^{-j2\pi n k / N} \Delta t.$$

Two cases may appear:

1. The discretization step Δt is such that it is contained an integer number of times within the signal's period T_0 . At the same time the total number of samples N for the DFT calculation contains an integer number k_0 of signal periods with k samples in each signal period, $T_0 = k\Delta t$. Here, k is an integer and $N = k_0 k$. It means that

$$T_0 = 2\pi/\Omega_0 = k\Delta t = N\Delta t/k_0$$

or $\Omega_0 = 2\pi k_0 / (N\Delta t)$ and $\omega_0 = 2\pi k_0 / N$. Then

$$X(k) = \sum_{n=0}^{N-1} e^{j2\pi k_0 n / N} e^{-j2\pi n k / N} \Delta t = N\delta(k - k_0)\Delta t. \quad (1.119)$$

Obviously we can find the signal's frequency from

$$k_0 = \arg \left\{ \max_{0 \leq k \leq N-1} |X(k)| \right\}. \quad (1.120)$$

Frequency is calculated as $\Omega_0 = 2\pi k_0 / (N\Delta t)$ for $0 \leq k_0 \leq N/2 - 1$ and $\Omega_0 = 2\pi(k_0 - N) / (N\Delta t)$ for $N/2 \leq k_0 \leq N - 1$.

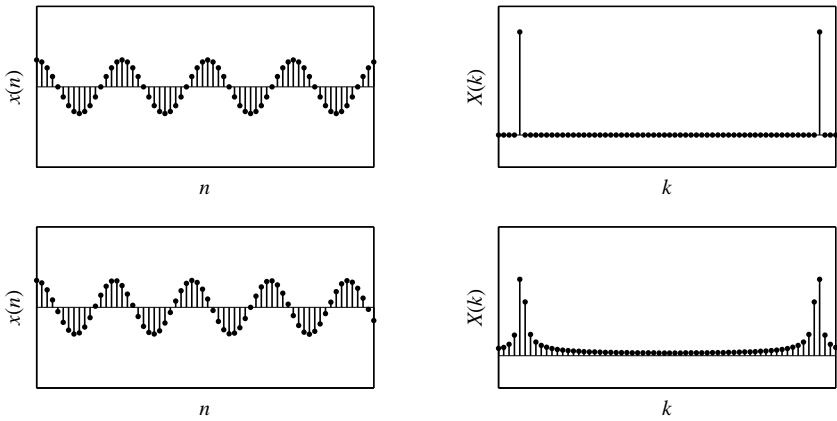


Figure 1.11 Sinusoid $x(n) = \cos(8\pi n/64)$ and its DFT with $N = 64$ (top row) and sinusoid $x(n) = \cos(8.8\pi n/64)$ and its DFT absolute value, with $N = 64$ (bottom row).

2. In reality, we never know the signal period (or Ω_0) in advance (if we knew it, then this analysis would not be needed). So, it is highly unlikely to have a case when $\Omega_0 = k_0 \frac{2\pi}{N\Delta t}$, as in Fig. 1.11, top row. In general, the DFT is of the form

$$X(k) = \sum_{n=0}^{N-1} e^{j\omega_0 n} e^{-j2\pi nk/N} \Delta t = \frac{1 - e^{j\omega_0 N} e^{-j2\pi k}}{1 - e^{j\omega_0} e^{-j2\pi k/N}} \Delta t$$

$$|X(k)| = \left| \frac{\sin(N(\omega_0 - 2\pi k/N)/2)}{\sin((\omega_0 - 2\pi k/N)/2)} \right| \Delta t, \quad (1.121)$$

as illustrated in Fig. 1.11, bottom row. The true frequency does not correspond to any DFT sample position.

Estimation of frequency, based on

$$\hat{k}_0 = \arg \left\{ \max_{0 \leq k \leq N-1} \left| \frac{\sin(N(\omega_0 - 2\pi k/N)/2)}{\sin((\omega_0 - 2\pi k/N)/2)} \right| \right\},$$

will produce an estimation error

$$e = \Omega_0 - \frac{2\pi}{N\Delta t} \hat{k}_0.$$

The estimation error could be up to a half of the discretization period in frequency, $\Delta\Omega = 2\pi/(N\Delta t)$,

$$\begin{aligned} -\frac{\pi}{N\Delta t} &\leq e < \frac{\pi}{N\Delta t} \\ \frac{2\pi}{N\Delta t}\hat{k}_0 - \frac{\pi}{N\Delta t} &\leq \Omega_0 < \frac{2\pi}{N\Delta t}\hat{k}_0 + \frac{\pi}{N\Delta t}. \end{aligned} \quad (1.122)$$

There are several ways to improve the estimation. We will describe two of them.

1. The simplest way to reduce the estimation error is to increase the number of samples and reduce the discretization interval in frequency $\Delta\Omega = 2\pi/(N\Delta t)$. This could be achieved by appropriate zero-padding in the time domain, before the DFT calculation (corresponding to the interpolation in the frequency domain). This way increases the calculation complexity.
2. The other way is based on a weighting (window) function application in the DFT calculation. Then the relation of the maximum value and few surrounding values of the window's DFT is used to calculate correction, the displacement bin of the estimated frequency. If we apply a window function $w(n)$ in the DFT calculation, we get

$$\begin{aligned} X(k) &= \sum_{n=0}^{N-1} w(n)e^{j\omega_0 n}e^{-j2\pi nk/N}\Delta t \\ &= W\left(e^{j(\frac{2\pi k}{N}-\omega_0)}\right)\Delta t, \end{aligned}$$

where $W(e^{j\omega})$ is the Fourier transform of the window function.

Displacement bin relation for the Hann(ing) window $w(n)$ is derived as

$$d = 1.5 \frac{|X(\hat{k}_0 + 1)| - |X(\hat{k}_0 - 1)|}{|X(\hat{k}_0 - 1)| \left(1 + \frac{|X(\hat{k}_0 + 1)|}{|X(\hat{k}_0)|}\right) + |X(\hat{k}_0)| + |X(\hat{k}_0 + 1)|}. \quad (1.123)$$

Thus, the best frequency estimation is

$$\Omega_0 = \frac{2\pi}{N\Delta t}(\hat{k}_0 + d) \quad (1.124)$$

for $0 \leq \hat{k}_0 \leq N/2 - 1$ and $\Omega_0 = \frac{2\pi}{N\Delta t}((\hat{k}_0 + d) - N)$ for $N/2 \leq \hat{k}_0 \leq N - 1$.

In general, we can combine these two approaches, for any window. We can interpolate the DFT, so that there are several samples within the main lobe, then for any symmetric window we can approximate the Fourier transform around the maximum by a quadratic function (in analog domain $X(\Omega) = a\Omega^2 + b\Omega + c$). Let us denote the largest sample, following from

$$\hat{k}_0 = \arg \left\{ \max_{0 \leq k \leq N-1} |X(k)| \right\},$$

by

$$X_0 = |X(\hat{k}_0)|$$

and the two neighboring samples by

$$\begin{aligned} X_{-1} &= |X(\hat{k}_0 - 1)| \\ X_1 &= |X(\hat{k}_0 + 1)|. \end{aligned}$$

By using the Lagrange polynomial interpolation of the second-order, at a point $x = d$, taking the bin index as independent variable $k_{-1} = -1$, $k_0 = 0$, $k_1 = 1$ with the function values at these points being denoted by X_{-1} , X_0 and X_1 , we have the Lagrange second-order polynomial

$$\begin{aligned} X(\hat{k}_0 + d) &= X_{-1} \frac{(d-0)(d-1)}{(-1-0)(-1-1)} + X_0 \frac{(d+1)(d-1)}{(0+1)(0-1)} + X_1 \frac{(d-0)(d+1)}{(1-0)(1+1)} \\ &= d^2[-X_0 + X_{-1}/2 + X_1/2] + d[X_1 - X_{-1}]/2 + X_0. \end{aligned} \quad (1.125)$$

This function reaches maximum at

$$\partial X(\hat{k}_0 + d) / \partial d = 0,$$

resulting in the displacement bin for the frequency correction

$$d = 0.5 \frac{|X(\hat{k}_0 + 1)| - |X(\hat{k}_0 - 1)|}{2|X(\hat{k}_0)| - |X(\hat{k}_0 + 1)| - |X(\hat{k}_0 - 1)|}, \quad (1.126)$$

with frequency as in (1.124). The displacement procedure is illustrated in Fig. 1.12.

Example 1.23. A sinusoidal signal $x(t) = A \exp(j\Omega_0 t)$ is sampled with a sampling interval $\Delta t = 1/128$ and $N_0 = 64$ samples are considered. Prior to the DFT calculation,

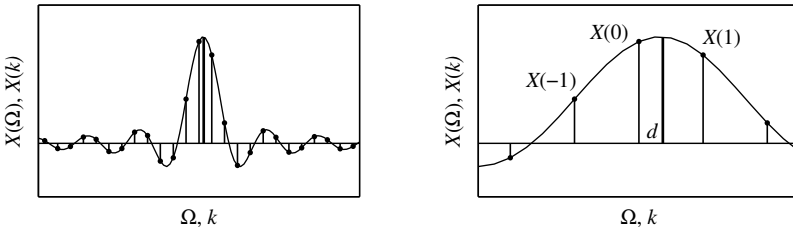


Figure 1.12 Illustration of the displacement bin correction for a true maximum position calculation based on three neighboring values (full range – left and zoomed graph – right).

the signal is zero padded four times. The DFT maximum is detected at $\hat{k}_0 = 95$. The maximum DFT value is $X(95) = 0.9$. Neighboring values are $X(96) = 0.7$ and $X(94) = 0.3$. Calculate the displacement bin d and estimate the value of Ω_0 .

★The displacement bin value is

$$d = 0.5 \frac{0.7 - 0.3}{1.8 - 0.7 - 0.3} = 0.25.$$

The total number of samples in the DFT calculation was $N = 4N_0 = 256$, meaning that the value $\hat{k}_0 = 95$ is within the first half of the samples (corresponding to positive frequency Ω_0). Therefore, we can use (1.124) for the frequency calculation

$$\Omega_0 = \frac{2\pi}{N\Delta t} (\hat{k}_0 + d) = 95.25\pi.$$

□

1.2.5 Laplace and z-Transform

The Fourier transform could be considered as a special case of the Laplace transform. At the beginning, the Fourier work was even not published since it was considered as a special case of the existing Laplace transform, defined by

$$X(s) = \int_{-\infty}^{\infty} x(t)e^{-st} dt, \quad (1.127)$$

where $s = \sigma + j\Omega$ is a complex number. It is obvious that the Fourier transform is the value of Laplace transform along the imaginary axis, $\sigma = 0$ or $s = j\Omega$. This

form of the Laplace transform is also known as the bilateral Laplace transform (in contrast to unilateral one, where the integration limits are from 0_- to ∞).

Example 1.24. Calculate the Laplace transform of $x(t) = e^{-at}u(t)$.

★According to the definition

$$X(s) = \int_0^\infty e^{-at} e^{-st} dt = -\frac{e^{-(s+a)t}}{s+a} \Big|_0^\infty = \frac{1}{s+a}$$

if

$$\lim_{t \rightarrow \infty} e^{-(s+a)t} = 0$$

or $\sigma + a > 0$, that is, $\sigma > -a$. Therefore, the region of convergence of this Laplace transform is the region where $\sigma > -a$. \square

The Laplace transform may be considered as a Fourier transform of a signal $x(t)$ multiplied by $\exp(-\sigma t)$, with varying parameter σ ,

$$\text{FT}\{x(t)e^{-\sigma t}\} = \int_{-\infty}^{\infty} x(t)e^{-\sigma t} e^{-j\Omega t} dt = \int_{-\infty}^{\infty} x(t)e^{-st} dt = X(s). \quad (1.128)$$

In this way, we may calculate the Laplace transform of functions that are not absolutely integrable (i.e., do not satisfy condition for the Fourier transform existence, $\int_{-\infty}^{\infty} |x(t)| dt < \infty$). In these cases, for some values of σ , the new signal $x(t)e^{-\sigma t}$ may be absolutely integrable and the Laplace transform could exist. In the previous example, the Fourier transform does not exist for $a < 0$, while for $a = 0$ it exists only in the generalized functions sense. The Laplace transform always exists, with the region of convergence $\sigma > -a$. If $a > 0$, then the region of convergence $\sigma > -a$ includes the line $\sigma = 0$, meaning that the Fourier transform exists.

The inverse Laplace transform is

$$x(t) = \frac{1}{2\pi j} \lim_{T \rightarrow \infty} \int_{\gamma-jT}^{\gamma+jT} X(s)e^{st} ds$$

where the integration is performed along a path in the region of convergence of $X(s)$.

Example 1.25. Consider a signal $x(t)$ such that $x(t) = 0$ for $|t| > T$ (time-limited signal).

Its Fourier transform is $X(\Omega)$. Derive the relation to calculate Laplace transform $X(s)$ for any σ within the region of convergence, based on the value of $X(\Omega)$.

★Based on $X(\Omega)$, the signal values are

$$x(t) = \frac{1}{2\pi} \int_{-\infty}^{\infty} X(\Omega) e^{j\Omega t} d\Omega.$$

The Laplace transform is

$$\begin{aligned} X(s) &= \int_{-T}^T \left(\frac{1}{2\pi} \int_{-\infty}^{\infty} X(\Omega) e^{j\Omega t} d\Omega \right) e^{-st} dt \\ &= \frac{1}{2\pi} \int_{-\infty}^{\infty} X(\Omega) \int_{-T}^T e^{-st+j\Omega t} dt d\Omega = \frac{1}{\pi} \int_{-\infty}^{\infty} X(\Omega) \frac{\sinh((j\Omega-s)T)}{j\Omega-s} d\Omega. \end{aligned} \quad (1.129)$$

□

The Fourier transform of discrete-time signals can be considered as special case of the z -transform defined by

$$X(z) = \sum_{n=-\infty}^{\infty} x(n) z^{-n}, \quad (1.130)$$

where $z = r \exp(j\omega)$ is a complex number. The value of the z -transform along the unit circle $r = 1$ or $z = \exp(j\omega)$ is equal to the Fourier transform of the discrete-time signals.

By discretization of a signal $x(t)$, the Laplace transform integral can be approximated by a sum

$$X(s) \cong \sum_{n=-\infty}^{\infty} x(n\Delta t) e^{-sn\Delta t} \Delta t = \sum_{n=-\infty}^{\infty} x(n) e^{-sn\Delta t}$$

with $x(n) = x(n\Delta t)\Delta t$. Comparing this relation with the z -transform definition we can conclude that the Laplace transform of $x(t)$ corresponds to the z -transform of its samples with $z = \exp(s\Delta t)$, that is,

$$X(s) \leftrightarrow X(z)|_{z=\exp(s\Delta t)}. \quad (1.131)$$

Example 1.26. Consider a discrete-time signal with N samples different than zero. Show that all values of $X(z)$, for any z , can be calculated based on its N samples on the unit circle in the z -plane.

★If the signal has N nonzero samples, then it can be expressed in term of its DFT as

$$X(k) = \sum_{n=0}^{N-1} x(n)e^{-j2\pi nk/N} \text{ and } x(n) = \frac{1}{N} \sum_{k=0}^{N-1} X(k)e^{j2\pi nk/N}.$$

Thus,

$$X(z) = \frac{1}{N} \sum_{k=0}^{N-1} \sum_{n=0}^{N-1} X(k)e^{j2\pi nk/N} z^{-n} = \frac{1}{N} \sum_{k=0}^{N-1} \frac{1 - z^{-N} e^{j2\pi k}}{1 - z^{-1} e^{j2\pi k/N}} X(k)$$

with $X(k) = X(z)$ for $z = \exp(j2\pi k/N), k = 0, 1, 2, \dots, N-1$. \square

1.3 DISCRETE-TIME RANDOM SIGNALS

Random signals can not be described by a simple mathematical function. Their values are not known in advance. They may be described by stochastic tools only. Here we will restrict the analysis to the discrete-time random signals, since they will be used in numerical implementations. In this section, the first-order and the second-order statistics will be considered.

1.3.1 First-Order Statistics

The first-order statistics, the mean value or expected value, is the starting point in describing the random signals. If we have a set of signal values,

$$\{x(n)\}, n = 1, 2, \dots, N, \quad (1.132)$$

the mean over this set is calculated as

$$\mu_x = \frac{1}{N} (x(1) + x(2) + \dots + x(N)).$$

In general, the mean for each signal sample could be different. For example, if the signal values represent the highest daily temperature, during the year and over the years, then the mean value is highly dependent on the considered sample. In

order to calculate a mean value of the temperature of the n -th day in a year, we have to have several realizations of this random signals (measurements over several years), denoted by $\{x_i(n)\}, n = 1, 2, \dots, N$ and $i = 1, 2, \dots, M$, where argument n is the cardinal number of the day and i is the number of realization. The mean value is calculated as

$$\mu_x(n) = \frac{1}{M}(x_1(n) + x_2(n) + \dots + x_M(n)) \quad (1.133)$$

for $n = 1, 2, \dots, N$. In this case we have a set of mean values $\{\mu_x(n)\}, n = 1, 2, \dots, N$.

If the probabilistic description of a random signal is known, then we can calculate the mean value and other parameters of random signals. For the first-order statistics calculation, it is sufficient to know the probability density function. The probability density function $p_{x(n)}(\xi)$ defines the probability that the n -th signal sample, $x(n)$, takes a value within a small interval around ξ

$$\text{Probability } \{\xi \leq x(n) < \xi + d\xi\} = p_{x(n)}(\xi)d\xi \quad (1.134)$$

where $d\xi$ is an infinitesimally small interval.

In this case, the expected value of random variable $x(n)$, in notation $E\{x(n)\}$, is

$$\mu_x(n) = E\{x(n)\} = \int_{-\infty}^{\infty} \xi p_{x(n)}(\xi)d\xi. \quad (1.135)$$

If a random signal assumes only discrete values in amplitude $\{\xi_1, \xi_2, \dots\}$, then we have probabilities,

$$\text{Probability } \{x(n) = \xi_i\} = P_{x(n)}(\xi_i), \quad (1.136)$$

rather than the probability density functions. An example of such a signal is the signal being equal to the numbers appearing in die tossing, when the signal may assume only one of the values from the set $\{1, 2, 3, 4, 5, 6\}$. In this case, the mean value is calculated as a sum over the set of possible amplitudes, instead of integral,

$$\mu_x(n) = E\{x(n)\} = \sum_{i=1}^{\infty} \xi_i P_{x(n)}(\xi_i). \quad (1.137)$$

If we are able to calculate the mean values based on probabilities, before the signal is measured, then these values are a priori values, while the values calculated from the already measured set of signal values are a posteriori values. The interpretation of (1.133), within the probability framework (1.137), is that all values $x_i(n), i = 1, 2, \dots, M$, since they already occurred, are of equal probability $P_{x(n)}(\xi_i) = 1/M$ for $\xi_i = x_i(n), i = 1, 2, \dots, M$.

In addition to the mean value, a median is used for the description of the set of random values. The median is a value in the middle of the set, after the members of the set are sorted. The median will not be influenced by a possible small number of big outliers, being significantly different from the values of the rest of data.

Example 1.27. Find the median of sets:

$$A = \{-1, 1, -2, 4, 6, -9, 0\}$$

and

$$B = \{-1, 1, -1367, 4, 35, -9, 0\}.$$

★ After sorting we get $A = \{-9, -2, -1, 0, 1, 4, 6\}$. Thus, $\text{median}(A) = 0$. In a similar way $\text{median}(B) = 0$. The means of these data would significantly differ. \square

1.3.2 Second-Order Statistics

Second-order statistics deals with two samples of a random signal. For a signal $\{x_i(n)\}, n = 1, 2, \dots, N$ and $i = 1, 2, \dots, M$, being the number of realizations, the auto-correlation function is defined by

$$r_{xx}(n, m) = \frac{1}{M} \sum_{i=1}^M x_i(n)x_i^*(m). \quad (1.138)$$

If the second-order probability functions (or probabilities) are known, then

$$r_{xx}(n, m) = E\{x(n)x^*(m)\} = \int_{-\infty}^{\infty} \xi_1 \xi_2^* p_{x(n), x(m)}(\xi_1, \xi_2) d\xi_1 d\xi_2, \quad (1.139)$$

or in the case of discrete amplitude values of random signals

$$r_{xx}(n, m) = E\{x(n)x^*(m)\} = \sum_{\xi_1} \sum_{\xi_2} \xi_1 \xi_2^* P_{x(n), x(m)}(\xi_1, \xi_2), \quad (1.140)$$

where $P_{x(n), x(m)}(\xi_1, \xi_2)$ is the probability that the random variable $x(n)$ takes value ξ_1 and at the same that the random variable $x(m)$ takes value ξ_2 .

If the random variables $x(n)$ and $x(m)$ are statistically independent, then $p_{x(n), x(m)}(\xi_1, \xi_2) = p_{x(n)}(\xi_1)p_{x(m)}(\xi_2)$ and $r_{xx}(n, m) = \mu_x(n)\mu_x^*(m)$.

Signals whose first-order and second-order statistics are invariant to a shift in time are called wide sense stationary (WSS) signals. For the WSS signals holds

$$\begin{aligned}\mu_x(n) &= \text{E}\{x(n)\} = \mu_x \\ r_{xx}(n, m) &= \text{E}\{x(n)x^*(m)\} = r_{xx}(m - n).\end{aligned}\quad (1.141)$$

The Fourier transform of the auto-correlation function of a WSS signal is the spectral power density

$$S_{xx}(e^{j\omega}) = \sum_{l=-\infty}^{\infty} r_{xx}(l)e^{-j\omega l} \quad (1.142)$$

$$r_{xx}(l) = \frac{1}{2\pi} \int_{-\pi}^{\pi} S_{xx}(e^{j\omega})e^{j\omega l} d\omega. \quad (1.143)$$

Integral of $S_{xx}(e^{j\omega})$ over frequency,

$$\frac{1}{2\pi} \int_{-\pi}^{\pi} S_{xx}(e^{j\omega})d\omega = r_{xx}(0) = \text{E}\{|x(n)|^2\}, \quad (1.144)$$

is equal to the average power of the random signal.

A signal is stationary in the strict sense (SSS) if not only first- and second-order statistics are independent from the initial value, but if all order statistics are shift invariant.

The auto-covariance function is defined by

$$c_{xx}(n, m) = \frac{1}{M} \sum_{i=1}^M (x_i(n) - \mu_x(n))(x_i(m) - \mu_x(m))^*. \quad (1.145)$$

It may be easily shown that

$$c_{xx}(n, m) = \text{E}\{(x(n) - \mu_x(n))(x(m) - \mu_x(m))^*\} = r_{xx}(n, m) - \mu_x(n)\mu_x^*(m).$$

The value of the auto-covariance for $m = n$ is called the variance. The variance is defined by

$$\sigma_{xx}^2(n) = \text{E}\{|x(n) - \mu_x(n)|^2\} = r_{xx}(n, n) - |\mu_x(n)|^2. \quad (1.146)$$

The standard deviation is a square root of the variance. For a set of stationary data, $\{x(n)\}, n = 1, 2, \dots, N$, the standard deviation can be estimated as a square root

of the mean of squares of the centered data. For stationary signals,

$$\sigma_x = \sqrt{\frac{1}{N} \left((x(1) - \mu)^2 + (x(2) - \mu)^2 + \dots + (x(N) - \mu)^2 \right)}. \quad (1.147)$$

For small number of samples, this estimate tends to produce lower values of the standard deviation thus, an adjusted version, the sample standard deviation, is also used. It reads

$$\sigma_x = \sqrt{\frac{1}{N-1} \left((x(1) - \mu)^2 + (x(2) - \mu)^2 + \dots + (x(N) - \mu)^2 \right)}.$$

This form confirms the fact that in the case when only one sample is available, $N = 1$, we should not be able estimate the standard deviation.

The cross-correlation and the cross-covariance of two signals $x(n)$ and $y(n)$ are defined as

$$r_{xy}(n, m) = E\{x(n)y^*(m)\}$$

and

$$\begin{aligned} c_{xy}(n, m) &= E\{(x(n) - \mu_x(n))(y(m) - \mu_y(m))^*\} \\ &= r_{xy}(n, m) - \mu_x(n)\mu_y^*(m). \end{aligned} \quad (1.148)$$

1.3.3 Noise

In many applications, the desired signal is disturbed by various forms of random signals, caused by numerous factors in the phases of the signal sensing, transmission, and/or processing. Often, a cumulative influence of these factors, disturbing useful signal, is described by an equivalent random signal, called noise. We will use the notation $\varepsilon(n)$ for these kinds of signals, in most cases, to model this random, multiple source, disturbance. A noise is said to be white if its values are noncorrelated

$$\begin{aligned} r_{\varepsilon\varepsilon}(n, m) &= \sigma_\varepsilon^2 \delta(n - m) \\ S_{\varepsilon\varepsilon}(e^{j\omega}) &= \sigma_\varepsilon^2. \end{aligned} \quad (1.149)$$

If this property is not satisfied, then the spectral power density is not constant (like it is in the white light) and such a noise is referred to as colored.

Regarding to the distribution of the values (amplitudes) of $\varepsilon(n)$, the most common types are:

- The uniform noise, with the probability density function (pdf)

$$p_{\varepsilon(n)}(\xi) = \frac{1}{\Delta} \text{ for } -\Delta/2 \leq \xi < \Delta/2 \quad (1.150)$$

and $p_{\varepsilon(n)}(\xi) = 0$ elsewhere, $\sigma_\varepsilon^2 = \Delta^2/12$. This kind of noise is used for modeling rounding error in the amplitude quantization of a signal. It indicates that all errors within $-\Delta/2 \leq \xi < \Delta/2$ are equally probable.

- The Gaussian zero-mean noise with probability density function

$$p_{\varepsilon(n)}(\xi) = \frac{1}{\sigma_\varepsilon \sqrt{2\pi}} e^{-\xi^2/(2\sigma_\varepsilon^2)}. \quad (1.151)$$

Variance of this noise is σ_ε^2 . The Gaussian noise is used to model a disturbance caused by many small independent factors. Namely, the central limit theorem states that a sum of a large number of statistically independent random variables with any distribution, obeys to the Gaussian distribution.

The probability that the amplitude of a Gaussian random variable takes a value smaller than λ is

$$\text{Probability}\{|\varepsilon(n)| < \lambda\} = \frac{1}{\sigma_\varepsilon \sqrt{2\pi}} \int_{-\lambda}^{\lambda} e^{-\xi^2/(2\sigma_\varepsilon^2)} d\xi = \text{erf}(\lambda/(\sqrt{2}\sigma_\varepsilon)) \quad (1.152)$$

where

$$\text{erf}(\lambda) = \frac{2}{\sqrt{\pi}} \int_0^{\lambda} e^{-\xi^2} d\xi$$

is the error function.

Commonly used probabilities that the absolute value of the noise is within the standard deviation, two standard deviations (two sigma rule), or three standard deviations are:

$$\text{Probability}\{-\sigma_\varepsilon < \varepsilon(n) < \sigma_\varepsilon\} = \text{erf}(1/\sqrt{2}) = 0.6827, \quad (1.153)$$

$$\text{Probability}\{-2\sigma_\varepsilon < \varepsilon(n) < 2\sigma_\varepsilon\} = \text{erf}(\sqrt{2}) = 0.9545,$$

$$\text{Probability}\{-3\sigma_\varepsilon < \varepsilon(n) < 3\sigma_\varepsilon\} = \text{erf}(3/\sqrt{2}) = 0.9973.$$

Example 1.28. Given 12 measurements of a Gaussian zero mean noise $\{-0.7519, 1.5163, -0.0326, -0.4251, 0.5894, -0.0628, -2.0220, -0.9821, 0.6125, -0.0549,$

$-1.1187, 1.6360\}$, estimate the probability that an absolute value of this noise will be smaller than 2.5.

★The standard deviation of this noise could be estimated by using (1.147) with $\mu = 0$ and $N = 12$. It is $\sigma = 1.031$. Thus, an absolute value will be smaller than 2.5 with probability

$$P = \frac{1}{1.031\sqrt{2\pi}} \int_{-2.5}^{2.5} e^{-\xi^2/(2 \cdot 1.031^2)} d\xi = \text{erf}(2.5/(\sqrt{2} \cdot 1.031)) = 0.9847.$$

□

Example 1.29. Consider a signal $s(n) = A\delta(n - n_0)$ and zero-mean Gaussian noise $\varepsilon(n)$ with variance σ_ε^2 within the interval $0 \leq n \leq N - 1$, where n_0 is a constant integer within $0 \leq n_0 \leq N - 1$. Find the probability of the event A that a maximum value of $x(n) = s(n) + \varepsilon(n)$ is obtained at $n = n_0$ and not at any other $n \neq n_0$.

★Probability density function for any sample $x(n)$, $n \neq n_0$, is

$$p_{x(n), n \neq n_0}(\xi) = \frac{1}{\sigma_\varepsilon\sqrt{2\pi}} e^{-\xi^2/(2\sigma_\varepsilon^2)}.$$

The probability that any of these samples is smaller than a value of λ could be defined by using (1.152)

$$\begin{aligned} P^-(\lambda) &= \text{Probability}\{x(n) < \lambda, n \neq n_0\} \\ &= \text{Probability}\{x(n) < 0, n \neq n_0\} + \text{Probability}\{0 \leq x(n) < \lambda, n \neq n_0\} \\ &= [0.5 + 0.5 \text{erf}(\lambda/(\sqrt{2}\sigma_\varepsilon))]. \end{aligned}$$

Since the random variables $x(n)$, $0 \leq n \leq N - 1, n \neq n_0$, are statistically independent, then the probability that all of them are smaller than a value of λ is

$$\begin{aligned} P_{N-1}^-(\lambda) &= \text{Probability}\{\text{All } N-1 \text{ values of } x(n) < \lambda, n \neq n_0\} \\ &= [0.5 + 0.5 \text{erf}(\lambda/(\sqrt{2}\sigma_\varepsilon))]^{N-1}. \end{aligned}$$

The probability density function of the sample $x(n_0)$ is a Gaussian function with the mean value A ,

$$p_{x(n_0)}(\xi) = \frac{1}{\sigma_\varepsilon\sqrt{2\pi}} e^{-(\xi-A)^2/(2\sigma_\varepsilon^2)}.$$

The probability that random variable $x(n_0)$ takes a value around λ , $\lambda \leq x(n_0) < \lambda + d\lambda$, is

$$P_{n_0}^+(\lambda) = \text{Probability}\{\lambda \leq x(n_0) < \lambda + d\lambda\} = \frac{1}{\sigma_\varepsilon\sqrt{2\pi}} e^{-(\xi-A)^2/(2\sigma_\varepsilon^2)} d\lambda \quad (1.154)$$

The probability that all values of $x(n), 0 \leq n \leq N-1, n \neq n_0$ are smaller than λ and that, at the same time, $\lambda \leq x(n_0) < \lambda + d\lambda$ is

$$P_A(\lambda) = P_{N-1}^-(\lambda)P_{n_0}^+(\lambda) = \left[0.5 + 0.5\operatorname{erf}\left(\frac{\lambda}{\sqrt{2}\sigma_\varepsilon}\right)\right]^{N-1} \frac{1}{\sigma_\varepsilon\sqrt{2\pi}} e^{-(\xi-A)^2/(2\sigma_\varepsilon^2)} d\lambda,$$

while the total probability is an integral over all possible values of λ

$$P_A = \int_{-\infty}^{\infty} P_A(\lambda) d\lambda. \quad (1.155)$$

□

- The Laplacian (heavy tailed) noise has the probability density function

$$p_{\varepsilon(n)}(\xi) = \frac{1}{2\alpha} e^{-|\xi|/\alpha}.$$

It decays much slower as $|\xi|$ increases. This noise is used to model disturbances when impulses occur more often (repeat the previous example with the Laplacian noise). The impulse noise could be distributed in other ways, like, for example, Cauchy distributed noise. In a mathematical sense, noises of this kind could appear as a result of multiplication or raising to a power greater than one of the Gaussian noises.

In many cases, we will assume that the noise is added to the signal $s(n)$, that is, that we have $x(n) = s(n) + \varepsilon(n)$. Then, we say that the noise is additive. Noise can also be multiplicative, when $x(n) = (1 + \varepsilon(n))s(n)$.

1.3.4 Linear Systems and Random Signals

If a random signal $x(n)$ passes through a linear time-invariant system, then the mean of output signal $y(n)$ is

$$\mu_y(n) = E\{y(n)\} = \sum_{k=-\infty}^{\infty} h(k)E\{x(n-k)\} \quad (1.156)$$

$$= \sum_{k=-\infty}^{\infty} h(k)\mu_x(n-k) = h(n) *_n \mu_x(n). \quad (1.157)$$

For a stationary signal

$$\mu_y = \mu_x \sum_{k=-\infty}^{\infty} h(k) = \mu_x H(e^{j0}). \quad (1.158)$$

The cross-correlation of input and output signal is

$$\begin{aligned} r_{xy}(n, m) &= E\{x(n)y^*(m)\} = \sum_{k=-\infty}^{\infty} E\{x(n)x^*(k)\}h^*(m-k) \\ &= \sum_{k=-\infty}^{\infty} r_{xx}(n, k)h^*(m-k). \end{aligned} \quad (1.159)$$

For a stationary signal, with $n - m = l$ and $n - k = p$, we get

$$r_{xy}(l) = \sum_{p=-\infty}^{\infty} r_{xx}(p)h^*(p-l).$$

If we calculate the Fourier transform of both sides, we get

$$S_{xy}(e^{j\omega}) = S_{xx}(e^{j\omega})H^*(e^{-j\omega}). \quad (1.160)$$

Similarly, starting from

$$\begin{aligned} r_{yy}(n, m) &= E\{y(n)y^*(m)\} \\ &= \sum_{k=-\infty}^{\infty} \sum_{l=-\infty}^{\infty} E\{x(l)x^*(k)\}h(n-l)h^*(m-k), \end{aligned} \quad (1.161)$$

after some straightforward calculations, we get the Fourier transform of the output signal auto-correlation function,

$$S_{yy}(e^{j\omega}) = S_{xx}(e^{j\omega}) |H(e^{j\omega})|^2, \quad (1.162)$$

proving that $S_{xx}(e^{j\omega})$ is indeed a power density function, since by taking a narrow-pass filter with unit amplitude $|H(e^{j\omega})|^2 = 1$ for $\omega_0 \leq \omega < \omega_0 + d\omega$, we will get the spectral density for that small frequency range.

1.3.5 Discrete Fourier Transform of Noisy Signals

Consider a noisy signal

$$x(n) = s(n) + \varepsilon(n) \quad (1.163)$$

where $s(n)$ is a deterministic useful signal and $\varepsilon(n)$ is an additive noise. The DFT of this signal is

$$X(k) = \sum_{n=0}^{N-1} (s(n) + \varepsilon(n))e^{-j2\pi kn/N} = S(k) + \Xi(k). \quad (1.164)$$

The mean value of $X(k)$ is

$$\mathbb{E}\{X(k)\} = \sum_{n=0}^{N-1} s(n)e^{-j2\pi kn/N} + \sum_{n=0}^{N-1} \mathbb{E}\{\varepsilon(n)\}e^{-j2\pi kn/N} = S(k) + \text{DFT}\{\mu_\varepsilon(n)\}.$$

In the case of zero mean noise $\varepsilon(n)$, $\mu_\varepsilon(n) = 0$, follows

$$\mu_X(k) = \mathbb{E}\{X(k)\} = S(k). \quad (1.165)$$

The variance of $X(k)$, for the zero-mean noise, is

$$\begin{aligned} \sigma_{XX}^2(k) &= \mathbb{E}\{|X(k) - \mu_X(k)|^2\} = \mathbb{E}\{X(k)X^*(k) - S(k)S^*(k)\} \\ &= \sum_{n_1=0}^{N-1} \sum_{n_2=0}^{N-1} \mathbb{E}\{(s(n_1) + \varepsilon(n_1))(s^*(n_2) + \varepsilon^*(n_2))\} e^{-j2\pi k(n_1-n_2)/N} \\ &\quad - \sum_{n_1=0}^{N-1} \sum_{n_2=0}^{N-1} s(n_1)s^*(n_2)e^{-j2\pi k(n_1-n_2)/N} \\ &= \sum_{n_1=0}^{N-1} \sum_{n_2=0}^{N-1} \mathbb{E}\{\varepsilon(n_1)\varepsilon^*(n_2)\} e^{-j2\pi k(n_1-n_2)/N}. \end{aligned} \quad (1.166)$$

For a white noise, with auto-correlation

$$r_{\varepsilon\varepsilon}(n_1, n_2) = \mathbb{E}\{\varepsilon(n_1)\varepsilon^*(n_2)\} = \sigma_\varepsilon^2 \delta(n_1 - n_2),$$

we get

$$\sigma_{XX}^2(k) = \sigma_\varepsilon^2 N. \quad (1.167)$$

If the deterministic signal was a complex sinusoid, $s(n) = Ae^{j2\pi k_0 n/N}$, with a frequency adjusted to the grid $\Omega_0 = 2\pi k_0/(N\Delta t)$, then its DFT will have the value

$$S(k) = AN \delta(k - k_0).$$

Peak signal-to-noise ratio, being relevant for the frequency estimation based on the DFT, is

$$SNR_{out} = \frac{\max_k |S(k)|^2}{\sigma_{XX}^2} = \frac{A^2 N^2}{\sigma_\varepsilon^2 N} = \frac{A^2}{\sigma_\varepsilon^2} N. \quad (1.168)$$

It increases as N increases. We have expected this result since the signal values are added in phase, increasing amplitude of the DFT N times (its power N^2 times),

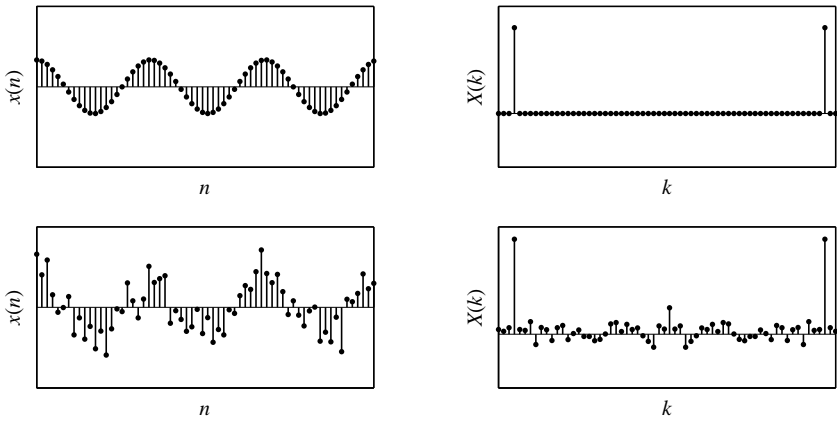


Figure 1.13 Illustration of a signal $x(n) = \cos(6\pi n/64)$ and its DFT (top row); the same signal corrupted with additive zero mean real-valued Gaussian noise of variance $\sigma_n^2 = 1/4$, with its DFT (bottom row).

while the noise values are added in power, increasing SNR N times in the DFT. Noise influence to DFT of real valued sinusoid is illustrated in Fig. 1.13.

Just to note that the input signal to noise ratio (SNR) is

$$SNR_{in} = \frac{\max_n |s(n)|^2}{\sigma_\epsilon^2} = \frac{A^2}{\sigma_\epsilon^2} \quad (1.169)$$

or

$$SNR_{out} = N \cdot SNR_{in},$$

taking $10\log(\circ)$ of both sides we get the SNR improvement in dB,

$$SNR_{out}[\text{dB}] = 10\log N + SNR_{in}[\text{dB}]. \quad (1.170)$$

Example 1.30. If the DFT is calculated by using a window function $w(n)$, find its mean and variance.

★Here,

$$X(k) = \sum_{n=0}^{N-1} w(n) [s(n) + \epsilon(n)] e^{-j2\pi kn/N}.$$

We get

$$\mu_X(k) = \mathbb{E}\{X(k)\} = \sum_{n=0}^{N-1} w(n)s(n)e^{-j2\pi kn/N} = W(k) *_k S(k)$$

and

$$\begin{aligned} \sigma_{XX}^2(k) &= \sum_{n_1=0}^{N-1} \sum_{n_2=0}^{N-1} w(n_1)w^*(n_2)\sigma_\varepsilon^2 \delta(n_1 - n_2)e^{-j2\pi k(n_1 - n_2)/N} \\ &= \sigma_\varepsilon^2 \sum_{n=0}^{N-1} |w(n)|^2 = \sigma_\varepsilon^2 E_w. \end{aligned} \quad (1.171)$$

□

1.4 TWO-DIMENSIONAL SIGNALS

A two-dimensional signal can be presented by a two-dimensional function $f(x, y)$. A short presentation of these signals will be restricted to the cases that easily follow one-dimensional analysis. In a general case, analysis of two-dimensional signals is quite complex and cannot be reduced to one-dimensional cases.

A two-dimensional separable complex sinusoidal signal is defined by

$$f(x, y) = Ae^{j(\Omega_x x + \Omega_y y)}$$

with periods in x and y directions $T_x = 2\pi/\Omega_x$ and $T_y = 2\pi/\Omega_y$, respectively.

The two-dimensional Fourier transform is

$$F(u, v) = \int_{-\infty}^{\infty} \int_{-\infty}^{\infty} f(x, y) e^{-j(ux+vy)} dx dy, \quad (1.172)$$

with the inverse Fourier transform

$$f(x, y) = \frac{1}{4\pi^2} \int_{-\infty}^{\infty} \int_{-\infty}^{\infty} F(u, v) e^{j(ux+vy)} du dv. \quad (1.173)$$

Most of the properties of these transforms can be derived by a direct generalization of the ones derived for the one-dimensional case. For example, the derivative

of $f(x, y)$ over x corresponds to

$$\frac{\partial f(x, y)}{\partial x} = \frac{1}{4\pi^2} \int_{-\infty}^{\infty} \int_{-\infty}^{\infty} juF(u, v)e^{j(ux+vy)} du dv$$

meaning that $\partial f(x, y)/\partial x$ and $juF(u, v)$ are the two-dimensional Fourier transformation pair. Similarly,

$$\frac{\partial^2 f(x, y)}{\partial x \partial y} \leftrightarrow -uvF(u, v). \quad (1.174)$$

The Parseval's theorem for two-dimensional signals is

$$\int_{-\infty}^{\infty} \int_{-\infty}^{\infty} f(x, y)f^*(x, y) dx dy = \frac{1}{4\pi^2} \int_{-\infty}^{\infty} \int_{-\infty}^{\infty} F(u, v)F^*(u, v) du dv. \quad (1.175)$$

If the signal is limited in frequency u direction by u_m , then it can be sampled in the direction of the x -axis by

$$\Delta x \leq \frac{\pi}{u_m}.$$

The same holds for sampling interval in y direction,

$$\Delta y \leq \frac{\pi}{v_m},$$

where v_m is the maximal frequency in v frequency direction.

The discrete form of the two-dimensional Fourier transform is

$$F(e^{j\omega_x}, e^{j\omega_y}) = \sum_{m=-\infty}^{\infty} \sum_{n=-\infty}^{\infty} f(m, n) e^{-j(m\omega_x + n\omega_y)},$$

with $f(m, n) = f(m\Delta x, n\Delta y)\Delta x \Delta y$ and $\omega_x = u\Delta x$, $\omega_y = v\Delta y$. For limited duration signals, the discrete two-dimensional Fourier transform is given by

$$F(k, l) = \sum_{m=-N/2}^{N/2-1} \sum_{n=-N/2}^{N/2-1} f(m, n) e^{-j2\pi(mk+nl)/N}.$$

A projection of a two-dimensional function $f(x, y)$ onto the x -axis is

$$R_f(x) = \int_{-\infty}^{\infty} f(x, y) dy. \quad (1.176)$$

The Fourier transform of the projection onto x is equal to the slice of the two-dimensional Fourier transform along the corresponding u -axis, since

$$\int_{-\infty}^{\infty} R_f(x) e^{-jxu} dx = \int_{-\infty}^{\infty} \left(\int_{-\infty}^{\infty} f(x,y) dy \right) e^{-jxu} dx = F(u,0). \quad (1.177)$$

The same holds for the projection onto the y -axis.

A rotated version of a two-dimensional signal may be described in a new, rotated coordinate system, by a coordinate rotation transform. For an angle α , it reads

$$\begin{bmatrix} x \\ y \end{bmatrix} = \begin{bmatrix} \cos(\alpha) & -\sin(\alpha) \\ \sin(\alpha) & \cos(\alpha) \end{bmatrix} \begin{bmatrix} \xi \\ \zeta \end{bmatrix}$$

$$\begin{bmatrix} \xi \\ \zeta \end{bmatrix} = \begin{bmatrix} \cos(\alpha) & \sin(\alpha) \\ -\sin(\alpha) & \cos(\alpha) \end{bmatrix} \begin{bmatrix} x \\ y \end{bmatrix}.$$

Sometimes, a simple rotation is enough to transform a coordinate nonseparable function into a separable function.

The projection of a function $f(x,y)$ onto ξ , with a varying rotation angle α , is called the Radon transform of the signal $f(x,y)$

$$R_f(\xi, \alpha) = \int_{-\infty}^{\infty} f(\xi, \zeta) d\zeta = \int_{-\infty}^{\infty} \int_{-\infty}^{\infty} f(\lambda, \zeta) \delta(\lambda - \xi) d\lambda d\zeta. \quad (1.178)$$

Example 1.31. Find the Radon transform of a signal $f(x,y) = \delta(x - x_0)\delta(y - y_0)$ in x, y domain.

★Projection of $f(x,y)$ onto x axis is

$$R_f(x, 0) = \int_{-\infty}^{\infty} f(x, y) dy = \delta(x - x_0).$$

For an arbitrary direction $\xi_0 = x_0 \cos(\alpha) + y_0 \sin(\alpha)$, $\zeta_0 = -x_0 \sin(\alpha) + y_0 \cos(\alpha)$, the function

$$f(\xi, \zeta) = \delta(\xi - \xi_0)\delta(\zeta - \zeta_0)$$

results in the Radon transform

$$R_f(\xi, \alpha) = \int_{-\infty}^{\infty} f(\xi, \zeta) d\zeta = \delta(\xi - \xi_0)$$

$$= \delta(\xi - (x_0 \cos(\alpha) + y_0 \sin(\alpha))). \quad (1.179)$$

Note that this is a sinusoidal pattern in a two-dimensional (ξ, α) domain, with the amplitude $\sqrt{x_0^2 + y_0^2}$ and the phase $\psi = \arctan(y_0/x_0)$. Of course, the Radon transform is periodic in α with 2π . Projections for $0 \leq \alpha < \pi$ are sufficient to calculate all transform values. Thus, a point in the (x, y) domain transforms to a sinusoidal pattern in Radon transform domain. This relation can be used to transform a sinusoidal pattern into a point via inverse Radon transform. \square

It may be shown that the Fourier transform of the Radon transform, along direction $\xi = x\cos(\alpha) + y\sin(\alpha)$, is the two-dimensional Fourier transform of the original signal $f(x, y)$ along the same direction in transform domain. Thus, by knowing all the projections, for $0 \leq \alpha < \pi$, we can calculate the two-dimensional Fourier transform of $f(x, y)$. It means that we can reconstruct a two-dimensional function $f(x, y)$ from its projections or integrals (basic theorem for computed tomography).

In the chapters that follow, we will often use a specific form of the two-dimensional function $P(t, \Omega)$, with time and frequency as independent variables. Then, for the two-dimensional Fourier transform we will use the notation

$$A(\theta, \tau) = \frac{1}{2\pi} \int_{-\infty}^{\infty} \int_{-\infty}^{\infty} P(t, \Omega) e^{-j\theta t + j\Omega \tau} dt d\Omega. \quad (1.180)$$

Note that this is indeed the inverse Fourier transform over Ω and the Fourier transform over t . However, we can still use all the discrete calculation routines, for the standard two-dimensional Fourier transform, since $2\pi A(-\theta, \tau)$ is the standard two-dimensional transform. Thus, in the discrete domain, one axis should be reversed and the result multiplied by the number of samples N .

The inverse two-dimensional Fourier transform, in this notation, reads

$$P(t, \Omega) = \frac{1}{2\pi} \int_{-\infty}^{\infty} \int_{-\infty}^{\infty} A(\theta, \tau) e^{j\theta t - j\Omega \tau} d\theta d\tau. \quad (1.181)$$

It can be calculated by using the standard two-dimensional Fourier transform routines, by appropriate reversal and multiplication, as well.

1.5 PROBLEMS

Problem 1.1. If a signal $x(t)$ is periodic with period T , find the period of signal $y(t) = x(3t/4)x(t/3 - T)$.

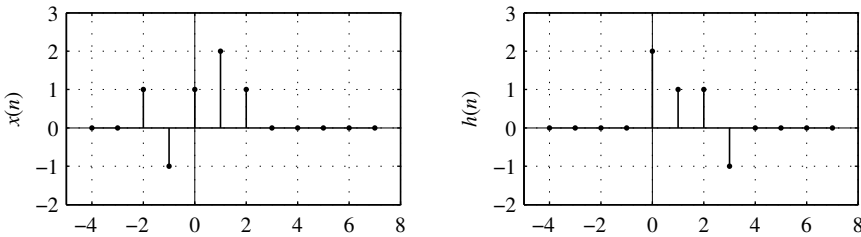


Figure 1.14 Signals for Problem 1.6.

Problem 1.2. Signal $x(t)$ is periodic with period 2. Its nonzero Fourier series coefficients are $X_0 = 5$, $X_1 = 3j$, $X_2 = 2$. Signal $h(t)$ is periodic with period 4. Its nonzero coefficients are $H_0 = 4$, $H_1 = 1 + j$, $H_{-1} = 1 - j$. Check the periodicity and find the Fourier series coefficients of signal $y(t) = x(t) + h(t)$.

Problem 1.3. Find the output signal of an LTI system, with the impulse response $h(t) = te^{-t}u(t)$, to the input signal $x(t) = u(t)$.

Problem 1.4. Find the Fourier transform of a signal $x(t)$ defined by

$$x(t) = \begin{cases} \sin(\pi t) & \text{for } |t| < 1 \\ 0 & \text{for } |t| \geq 1 \end{cases}.$$

Problem 1.5. The Fourier transform of a time-limited signal $x(t)$ ($x(t) = 0$ for $|t| > 4$) is

$$X(\Omega) = 4\pi j \frac{\sin(2\Omega)}{4\Omega^2 - \pi^2}.$$

Find the Fourier series coefficients for signals $y(t)$ and $z(t)$ obtained as periodic extensions of $x(t)$ with periods $T = 4$ and $T = 8$, respectively.

Problem 1.6. Calculate discrete-time convolution of signals $x(n)$ and $h(n)$ shown in Fig. 1.14.

Problem 1.7. Consider three causal linear time-invariant systems in cascade. Impulse responses of these systems are $h_1(n)$, $h_2(n)$, and $h_3(n)$, respectively. The impulse response of the second and the third system is $h_2(n) = u(n) - u(n-2)$, while the impulse response of the whole system,

$$h(n) = h_1(n) *_n h_2(n) *_n h_3(n),$$

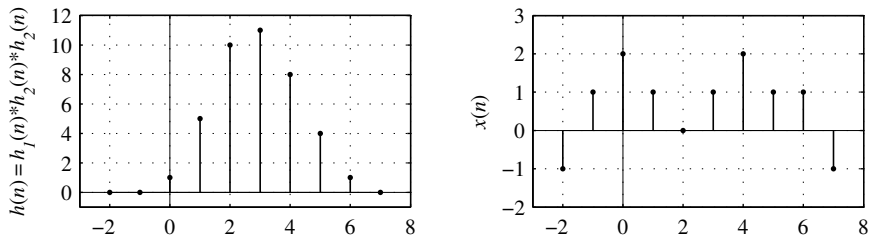


Figure 1.15 Problem 1.7, impulse response $h(n)$ (left) and Problem 1.9, discrete signal $x(n)$ (right).

is shown in Fig. 1.15 (left).

Find $h_1(n)$ and $y(n) = h(n) *_n x(n)$, with $x(n) = \delta(n) - \delta(n-1)$.

Problem 1.8. Find the Fourier transform of the following discrete-time signal (triangular window)

$$w_T(n) = \left(1 - \frac{|n|}{N+1}\right) [u(n+N) - u(n-N-1)].$$

with N being an even number.

Problem 1.9. The discrete-time signal $x(n)$ is given in Fig. 1.15 (right). Without calculating its Fourier transform $X(e^{j\omega})$ find

$$X(e^{j0}), \quad X(e^{j\pi}), \quad \int_{-\pi}^{\pi} X(e^{j\omega}) d\omega, \quad \int_{-\pi}^{\pi} |X(e^{j\omega})|^2 d\omega,$$

and a signal whose Fourier transform is the real part of $X(e^{j\omega})$, denoted by $\text{Re}\{X(e^{j\omega})\}$.

Problem 1.10. Impulse response of a discrete system is given as:

- (a) $h(n) = \frac{\sin(n\pi/3)}{n\pi},$
- (b) $h(n) = \frac{\sin^2(n\pi/3)}{(n\pi)^2},$
- (c) $h(n) = \frac{\sin((n-2)\pi/4)}{(n-2)\pi}.$

Find the responses to $x(n) = \sin(n\pi/6)$.

Problem 1.11. Find the value of integral

$$I = \frac{1}{2\pi} \int_{-\pi}^{\pi} \frac{\sin^2((N+1)\omega/2)}{\sin^2(\omega/2)} d\omega.$$

Problem 1.12. The Fourier transform of a continuous signal $x(t)$ is different from 0 only within $3\Omega_1 < \Omega < 5\Omega_1$. Find the maximum possible sampling interval Δt such that the signal can be reconstructed based on the samples $x(n\Delta t)$.

Problem 1.13. Sampling of a signal is done twice, with the sampling interval $\Delta t = 2\pi/\Omega_m$ that is twice larger than the sampling interval required by the sampling theorem ($\Delta t = \pi/\Omega_m$ is required). After first sampling process, the discrete-time signal $x_1(n) = \Delta t x(n\Delta t)$ is formed, while after the second sampling process $x_2(n) = \Delta t x(n\Delta t + a)$ is formed. Show that we can reconstruct continuous signal $x(t)$ based on $x_1(n)$ and $x_2(n)$ if $a \neq k\Delta t$, that is, if samples $x_1(n)$ and $x_2(n)$ do not overlap in continuous-time.

Problem 1.14. In general, a sinusoidal signal $x(t) = A \sin(\Omega_0 t + \varphi)$ is described with three parameters A, Ω_0 and φ . Thus, generally speaking, three points of $x(t)$ would be sufficient to find three signal parameters. If we know the signal $x(t)$ at $t = t_0$, $t = t_0 + \Delta t$ and $t = t_0 - \Delta t$ what is the relation to reconstruct, for example, Ω_0 , which is usually the most important parameter of a sinusoid?

Problem 1.15. What is the relation between $X(k)$ and $X(N - k)$ for real-valued signals? If $X(k)$ is real-valued, what should the relation be between $x(n)$ and $x(N - n)$?

Problem 1.16. The relationship between the argument in the DFT and the continuous signal frequency is given by

$$\Omega = \begin{cases} \frac{2\pi k}{N\Delta t} & \text{for } 0 \leq k \leq N/2 - 1 \\ \frac{2\pi(k-N)}{N\Delta t} & \text{for } N/2 \leq k \leq N - 1. \end{cases}$$

This is achieved by using shift functions in programs. Show that the shift will not be necessary if we use the signal $x(n)(-1)^n$. The order of DFT values will be starting from the lowest negative frequency, toward the highest positive frequency.

Problem 1.17. In order to illustrate the algorithms for the fast DFT calculation (the FFT algorithms), show that a DFT of N elements can be split into two DFTs of $N/2$ elements, by a simple splitting of the original signal of N samples into two parts of $N/2$ samples. Use this property to prove that the calculation savings can be achieved in the DFT calculation.

Problem 1.18. Find the DFT of signal $x(n) = \exp(j4\pi\sqrt{3}n/N)$, with $N = 16$. If the signal is interpolated four times, find the displacement bin and compare it with the true frequency value. What is the displacement bin if the general formula is applied without interpolation?

Problem 1.19. The random variable $\varepsilon(n)$ is stationary and Cauchy distributed with probability density function

$$p_{\varepsilon(n)}(\xi) = \frac{a}{1 + \xi^2}.$$

Find the coefficient a , mean, and variance.

Problem 1.20. Consider a linear time-invariant system whose input is

$$x(n) = w(n)u(n)$$

and the impulse response is

$$h(n) = a^n u(n),$$

where $w(n)$ is a stationary real-valued noise with mean μ_w and auto-correlation $r_{ww}(n, m) = \sigma_w^2 \delta(n - m) + \mu_w^2$. Find the mean and the variance of the output signal.

Problem 1.21. Find the mean, auto-correlation, and spectral power density of the random signal

$$x(n) = w(n) + \sum_{k=1}^N a_k e^{j(\omega_k n + \theta_k)},$$

where $w(n)$ is a stationary real-valued noise with mean μ_w and auto-correlation $r_{ww}(n, m) = \sigma_w^2 \delta(n - m) + \mu_w^2$ and θ_k are random variables uniformly distributed over $-\pi < \theta_k \leq \pi$. All random variables are statistically independent.

1.6 SOLUTIONS

Solution 1.1. From the definition of signal periodicity, we have to find T_y so that $y(t)$ satisfies

$$y(t + T_y) = y(t).$$

For a given $y(t)$, this relation reads as

$$\begin{aligned} x(3(t + T_y)/4)x((t + T_y)/3 - T) &= x(3t/4)x(t/3 - T) \\ x(3t/4 + 3T_y/4)x(t/3 - T + T_y/3) &= x(3t/4)x(t/3 - T). \end{aligned}$$

Since $x(t)$ is periodic with T , then $x(3t/4 + 3T_y/4) = x(3t/4)$ for $3T_y/4 = k_1 T$ and $x(t/3 - T + T_y/3) = x(t/3 - T)$ for $T_y/3 = k_2 T$, where k_1 and k_2 are integers. It follows $T_y = 4k_1 T/3$ and $T_y = 3k_2 T$. The smallest common value of T_y for these two equations is the period of $y(t)$. It is $T_y = 12T$ for $k_1 = 9$ and $k_2 = 4$.

Solution 1.2. Since the signal $y(t)$ is a sum of two periodic signals with periods $T = 2$ and $T = 4$, the period of $y(t)$ is 4. From the definition of Fourier series coefficients, we have that

$$\begin{aligned} X_n &= \frac{1}{2} \int_{-1}^1 x(t)e^{-j2\pi nt/2} dt, \\ H_n &= \frac{1}{4} \int_{-2}^2 h(t)e^{-j2\pi nt/4} dt, \\ Y_n &= \frac{1}{4} \int_{-2}^2 y(t)e^{-j2\pi nt/4} dt = \frac{1}{4} \int_{-2}^2 x(t)e^{-j2\pi nt/4} dt + \frac{1}{4} \int_{-2}^2 h(t)e^{-j2\pi nt/4} dt. \end{aligned}$$

The last integral in Y_n is equal to H_n . The first integral should be calculated separately for even and odd n . For an even n , $n = 2m$, having in mind that the integrand is periodic with a period of 2 and that we perform integration over two periods of the integrand, we will get

$$\frac{1}{4} \int_{-2}^2 x(t)e^{-j2\pi(2m)t/4} dt = \frac{1}{4} 2 \int_{-1}^1 x(t)e^{-j2\pi mt/2} dt = X_m.$$

For an odd n , $n = 2m + 1$, we will get

$$\begin{aligned} & \frac{1}{4} \int_{-2}^2 x(t) e^{-j2\pi(2m+1)t/4} dt \\ &= \frac{1}{4} \int_{-2}^0 x(t) e^{-j2\pi(2m+1)t/4} dt + \frac{1}{4} \int_0^2 x(t) e^{-j2\pi(2m+1)t/4} dt \\ &= \frac{1}{4} \int_0^2 x(t-2) e^{-j2\pi(2m+1)(t-2)/4} dt + \frac{1}{4} \int_0^2 x(t) e^{-j2\pi(2m+1)t/4} dt \\ &= \frac{1}{4} \int_0^2 (x(t) - x(t-2)) e^{-j2\pi(2m+1)t/4} dt = 0, \end{aligned}$$

since $x(t) = x(t-2)$, due to this signal periodicity. Finally, we have

$$Y_n = \begin{cases} X_{n/2} + H_n & \text{for even } n \\ H_n & \text{for odd } n \end{cases},$$

resulting in nonzero coefficients $Y_{-1} = 1 - j$, $Y_0 = 9$, $Y_1 = 1 + j$, $Y_2 = 3j$, and $Y_4 = 2$.

Solution 1.3. The output signal $y(t)$ can be calculated by a convolution $x(t) *_t h(t)$,

$$y(t) = \int_{-\infty}^{\infty} x(\tau) h(t - \tau) d\tau = \int_{-\infty}^{\infty} u(\tau) (t - \tau) e^{-(t-\tau)} u(t - \tau) d\tau.$$

It is obvious that $y(t) = 0$ for $t < 0$. For $t \geq 0$ we have

$$y(t) = \int_0^t (t - \tau) e^{-(t-\tau)} d\tau = 1 - e^{-t} - te^{-t}.$$

Solution 1.4. By definition, we have

$$X(\Omega) = \int_{-\infty}^{\infty} x(t) e^{-j\Omega t} dt = \int_{-1}^1 \sin(\pi t) e^{-j\Omega t} dt = 2\pi j \frac{\sin \Omega}{\Omega^2 - \pi^2}.$$

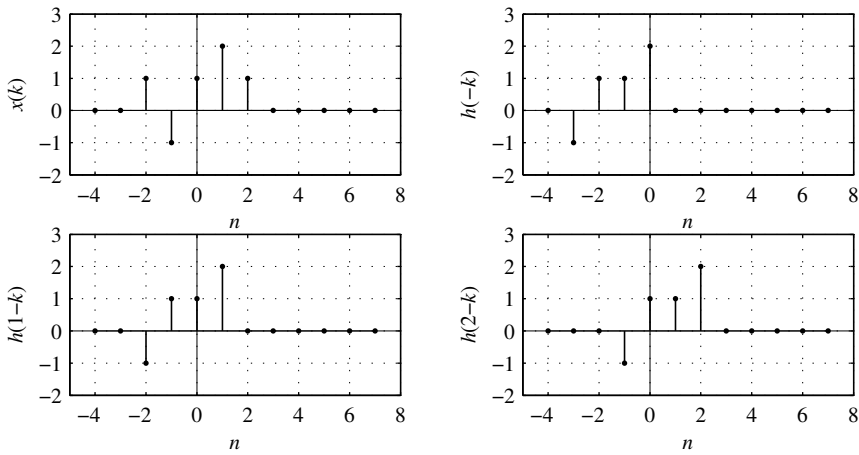


Figure 1.16 Problem 1.6: signals for $y(0)$, $y(1)$, and $y(2)$ calculation.

Solution 1.5. According to (1.57), we get

$$Y_n = \frac{1}{4}X(\Omega)|_{\Omega=2\pi n/4} = j \frac{\sin(n\pi)}{\pi(n^2-1)} = 0 \quad \text{for } n \neq \pm 1$$

and $Y_1 = -j/2$, $Y_{-1} = j/2$, meaning that the obtained periodic extension $y(t)$ is a pure sinusoidal signal, $y(t) = \sin(\frac{\pi}{2}t)$.

In the second case, we get

$$Z_n = \frac{1}{8}X(\Omega)|_{\Omega=2\pi n/8} = 2j \frac{\sin(\frac{n\pi}{2})}{\pi(n^2-4)}.$$

For even values of n , we have that $Z_n = 0$ for $n \neq \pm 2$, $Z_2 = -j/4$ and $Z_{-2} = j/4$. For odd values of n

$$Z_n = 2j \frac{(-1)^{(n-1)/2}}{\pi(n^2-4)}.$$

Solution 1.6. By definition, according to Fig. 1.16, we have

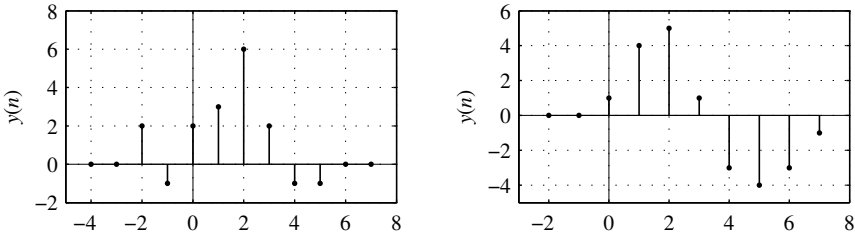


Figure 1.17 Problem 1.6: resulting signal $y(n)$ (left) and Problem 1.7, output signal $y(n)$ (right).

$$\begin{aligned}y(0) &= \sum_{k=-\infty}^{\infty} x(k)h(-k) = 1 - 1 + 2 = 2, \\y(1) &= \sum_{k=-\infty}^{\infty} x(k)h(1-k) = -1 - 1 + 1 + 4 = 3.\end{aligned}$$

In a similar way $y(-2) = 2$, $y(-1) = -1$, $y(2) = 6$, $y(3) = 2$, $y(4) = -1$, $y(5) = -1$, and $y(n) = 0$, for all other n . The convolution $y(n)$ is shown in Fig. 1.17 (left).

Solution 1.7. Since we know $h_2(n)$, we can calculate

$$h_2(n) *_n h_2(n) = \delta(n) + 2\delta(n-1) + \delta(n-2).$$

Therefore, the total impulse response

$$\begin{aligned}h(n) &= h_1(n) *_n [h_2(n) *_n h_2(n)] \\&= h_1(n) + 2h_1(n-1) + h_1(n-2) \\h_1(n) &= h(n) - 2h_1(n-1) - h_1(n-2).\end{aligned}$$

From the last relation it follows $h_1(n) = 0$ for $n < 0$, $h_1(0) = h(0) = 1$, $h_1(1) = h(1) - 2h_1(0) = 3$, $h_1(2) = h(2) - 2h_1(1) - h_1(0) = 3$, $h_1(3) = 2$, $h_1(4) = 1$, $h_1(5) = 0$, and $h_1(n) = 0$ for $n > 5$.

Output to $x(n) = \delta(n) - \delta(n-1)$ can be easily calculated as

$$y(n) = h(n) - h(n-1).$$

It is presented in Fig. 1.17 (right).

Solution 1.8. Note that $w_T(n) = \frac{1}{N+1} w_R(n) *_n w_R(n)$ where $w_R(n) = u(n+N/2) - u(n-N/2-1)$ is the rectangular window. Since

$$W_R(e^{j\omega}) = \frac{\sin(\omega \frac{N+1}{2})}{\sin(\omega/2)},$$

we have

$$W_T(e^{j\omega}) = \frac{1}{N+1} W_R(e^{j\omega}) W_R(e^{j\omega}) = \frac{1}{N+1} \frac{\sin^2(\omega \frac{N+1}{2})}{\sin^2(\omega/2)}.$$

Solution 1.9. Based on the definition of the Fourier transform of discrete-time signals,

$$\begin{aligned} X(e^{j0}) &= \sum_{n=-\infty}^{\infty} x(n) = 7, \\ X(e^{j\pi}) &= \sum_{n=-\infty}^{\infty} x(n)(-1)^n = 1, \\ \int_{-\pi}^{\pi} X(e^{j\omega}) d\omega &= 2\pi x(0) = 4\pi, \\ \int_{-\pi}^{\pi} |X(e^{j\omega})|^2 d\omega &= 2\pi \sum_{n=-\infty}^{\infty} |x(n)|^2 = 30\pi. \end{aligned}$$

Finally, $X(e^{j\omega}) = \operatorname{Re}\{X(e^{j\omega})\} + j\operatorname{Im}\{X(e^{j\omega})\}$ and $X^*(e^{j\omega}) = \operatorname{Re}\{X(e^{j\omega})\} - j\operatorname{Im}\{X(e^{j\omega})\}$. Thus,

$$\operatorname{Re}\{X(e^{j\omega})\} = \frac{1}{2} (X(e^{j\omega}) + X^*(e^{j\omega})).$$

The inverse Fourier transform of $\operatorname{Re}\{X(e^{j\omega})\}$ is

$$y(n) = \frac{1}{2}(x(n) + x^*(-n)).$$

Solution 1.10. (a) The Fourier transform of $h(n)$ is

$$H(e^{j\omega}) = \begin{cases} 1 & \text{for } |\omega| \leq \pi/3 \\ 0 & \text{for } \pi/3 < |\omega| < \pi \end{cases}$$

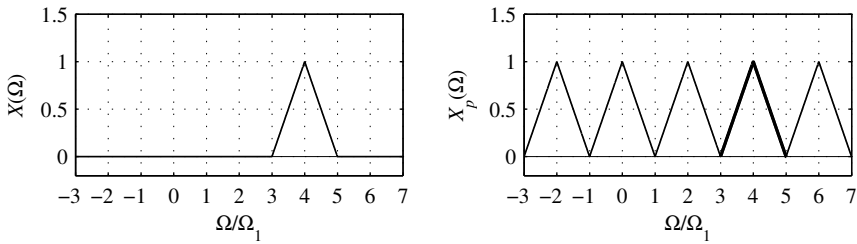


Figure 1.18 Problem 1.12: illustration of the Fourier transform periodic extension.

with $H(e^{\pm j\pi/6}) = 1$ thus, $y(n) = \sin(n\pi/6)$.

(b) Frequency response, in this case, is $H(e^{j\omega}) *_{\omega} H(e^{j\omega})$, resulting in $y(n) = 0.25 \sin(n\pi/6)$.

(c) Output signal in this case is $y(n) = \sin(n\pi/6 - \pi/3)$.

Solution 1.11. The integral represents the energy of a discrete-time signal with Fourier transform $X(e^{j\omega}) = \sin(\omega \frac{N+1}{2}) / \sin(\omega/2)$. This signal is the rectangular window, $x(n) = u(n+N/2) - u(n-N/2-1)$. Its energy is

$$I = \frac{1}{2\pi} \int_{-\pi}^{\pi} \frac{\sin^2((N+1)\omega/2)}{\sin^2(\omega/2)} d\omega = \sum_{n=-N/2}^{N/2} x^2(n) = \sum_{n=-N/2}^{N/2} 1 = N + 1.$$

Solution 1.12. By a direct application of the sampling theorem, we could conclude that the sampling interval should be related to the maximum frequency $5\Omega_1$ as $\Delta t = \pi/(5\Omega_1)$, corresponding to the periodical extension of the Fourier transform $X(\Omega)$ with period $10\Omega_1$. However, in this case, there is no need to use such a large period in order to achieve that two periods do not overlap. It is sufficient to use the period of $2\Omega_1$, as shown in Fig. 1.18, and we will be able to reconstruct the signal, with some additional processing.

It is obvious that after signal sampling with $\Delta t = \pi/\Omega_1$ (periodic extension of Fourier transform with $2\Omega_1$) the basic period $-\Omega_1 < \Omega < \Omega_1$ will contain the original Fourier transform shifted by $4\Omega_1$. The reconstructed signal is

$$x(t) = e^{j4\Omega_1 t} \sum_{n=-\infty}^{\infty} x(n\Delta t) \frac{\sin(\pi(t-n\Delta t)/\Delta t)}{\pi(t-n\Delta t)/\Delta t} \text{ with } \Delta t = \pi/\Omega_1.$$

Solution 1.13. The Fourier transforms of discrete-time signals, in continuous frequency notation, are periodically extended versions of $X(\Omega)$ with a period $2\pi/\Delta t$,

$$X_1(\Omega) = \sum_{n=-\infty}^{\infty} X(\Omega + 2\pi n/\Delta t),$$

$$X_2(\Omega) = \sum_{n=-\infty}^{\infty} X(\Omega + 2\pi n/\Delta t) e^{j(\Omega + 2\pi n/\Delta t)a}.$$

Within the basic period (considering only positive frequencies $0 \leq \Omega < \Omega_m$), only two periods overlap

$$X_1(\Omega) = X(\Omega) + X(\Omega - 2\pi/\Delta t),$$

$$X_2(\Omega) = X(\Omega) e^{j\Omega a} + X(\Omega - 2\pi/\Delta t) e^{j(\Omega - 2\pi/\Delta t)a}.$$

The second term $X(\Omega - 2\pi/\Delta t)$ in these relations is overlapped period (aliasing) that should be eliminated based on these two equations. The original signal's Fourier transform $X(\Omega)$ follows as

$$X(\Omega) = \frac{X_1(\Omega) e^{-j2\pi a/\Delta t} - X_2(\Omega) e^{-j\Omega a}}{e^{-j2\pi a/\Delta t} - 1} \text{ for } a \neq k\Delta t.$$

Similarly for negative frequencies, within the basic period $-\Omega_m < \Omega < 0$, follows

$$X(\Omega) = \frac{X_1(\Omega) e^{j2\pi a/\Delta t} - X_2(\Omega) e^{-j\Omega a}}{e^{j2\pi a/\Delta t} - 1} \text{ for } a \neq k\Delta t.$$

Therefore, the signal can be reconstructed from two independent signals undersampled with factor of two. A similar result could be derived for N independently sampled, N times undersampled signals.

Solution 1.14. It is easy to show that

$$\begin{aligned} & \frac{x(t_0 + \Delta t) + x(t_0 - \Delta t)}{2x(t_0)} \\ &= \frac{A \sin(\Omega_0 t_0 + \varphi + \Omega_0 \Delta t) + A \sin(\Omega_0 t_0 + \varphi - \Omega_0 \Delta t)}{2A \sin(\Omega_0 t_0 + \varphi)} \\ &= \frac{2 \sin(\Omega_0 t_0 + \varphi) \cos(\Omega_0 \Delta t)}{2 \sin(\Omega_0 t_0 + \varphi)} = \cos(\Omega_0 \Delta t), \end{aligned}$$

with

$$\Omega_0 = \frac{1}{\Delta t} \arccos \left(\frac{x(t_0 + \Delta t) + x(t_0 - \Delta t)}{2x(t_0)} \right).$$

The condition for a unique solution is that the argument of cosine is $0 \leq \Omega_0 \Delta t \leq \pi$, limiting the approach to small values of Δt .

In addition, here we will discuss the discrete complex-valued signal. For a complex sinusoid $x(n) = A \exp(j2\pi k_0 n/N + \phi_0)$, with available two samples $x(n_1) = A \exp(j\varphi(n_1))$ and $x(n_2) = A \exp(j\varphi(n_2))$, from

$$\frac{x(n_1)}{x(n_2)} = \exp(j2\pi k_0(n_1 - n_2)/N)$$

follows

$$2\pi k_0(n_1 - n_2)/N = \varphi(n_1) - \varphi(n_2) + 2k\pi,$$

where k is an arbitrary integer. Then

$$k_0 = \frac{\varphi(n_1) - \varphi(n_2)}{2\pi(n_1 - n_2)} N + \frac{k}{n_1 - n_2} N. \quad (1.182)$$

Let us analyze the ambiguous term $kN/(n_1 - n_2)$ role in the determination of k_0 . For $n_1 - n_2 = 1$, this term is kN , meaning that any frequency k_0 would be ambiguous with kN . Any value $k_0 + kN$ for $k \neq 0$, in this case, will be outside the basic period $0 \leq k \leq N - 1$. Thus, we may find k_0 in a unique way, within $0 \leq k_0 \leq N - 1$. However, for $n_1 - n_2 = L > 1$, the terms $kN/(n_1 - n_2) = kN/L$ produce shifts within the frequency basic period. Then several possible solutions for the frequency k_0 are obtained. For example, for $N = 16$ and $k_0 = 3$ if we use $n_1 = 1$ and $n_2 = 5$, a possible solution of (1.182) is $k_0 = 5$, but also

$$k_0 = 5 + 16k/4,$$

or $k_0 = 9$, $k_0 = 13$, and $k_0 = 1$, for k_0 within $0 \leq k_0 \leq 15$, are possible solutions for frequency.

Solution 1.15. For real-valued signals

$$\begin{aligned} x(n) &= x^*(n) \\ \sum_{k=0}^{N-1} X(k) e^{j2\pi nk/N} &= \sum_{k=0}^{N-1} X^*(k) e^{-j2\pi nk/N}. \end{aligned}$$

Since $e^{-j2\pi nk/N} = e^{j2\pi n(N-k)/N}$ it follows that

$$X^*(k) = X(N - k).$$

In the same way, using the duality principle, for real-valued DFT the signal should satisfy

$$x^*(n) = x(N - n).$$

Solution 1.16. The DFT of $x(n)(-1)^n$ is

$$X'(k) = \sum_{n=0}^{N-1} x(n)(-1)^n e^{-j2\pi nk/N}.$$

For $0 \leq k \leq N/2 - 1$

$$\begin{aligned} X'(k) &= \sum_{n=0}^{N-1} x(n)e^{-j\pi n} e^{-j2\pi nk/N} = \sum_{n=0}^{N-1} x(n)e^{-j2\pi n(k+N/2)/N} \\ &= X(k+N/2). \end{aligned}$$

For $N/2 \leq k \leq N - 1$

$$\begin{aligned} X'(k) &= \sum_{n=0}^{N-1} x(n)e^{j\pi n} e^{-j2\pi nk/N} = \sum_{n=0}^{N-1} x(n)e^{-j2\pi n(k-N/2)/N} \\ &= X(k-N/2). \end{aligned}$$

Solution 1.17. By definition,

$$\begin{aligned} \text{DFT}_N \rightarrow X(k) &= \sum_{n=0}^{N-1} x(n)e^{-j2\pi nk/N} = \\ &= \sum_{n=0}^{N/2-1} x(n)e^{-j2\pi nk/N} + \sum_{n=N/2}^{N-1} x(n)e^{-j2\pi nk/N} = \\ &= \sum_{n=0}^{N/2-1} [x(n) + x(n+N/2)(-1)^k] e^{-j2\pi nk/N}. \end{aligned}$$

For $k = 2r$ being an even number, we have

$$\text{DFT}_{N/2} \rightarrow X(2r) = \sum_{n=0}^{N/2-1} g(n)e^{-j2\pi nr/(N/2)}$$

with $g(n) = x(n) + x(n+N/2)$.

For an odd number $k = 2r + 1$, we have

$$\text{DFT}_{N/2} \rightarrow X(2r+1) = \sum_{n=0}^{N/2-1} h(n)e^{-j2\pi nr/(N/2)}$$

with $h(n) = (x(n) - x(n+N/2))e^{-j2\pi n/N}$.

In this way, we split one DFT of N elements into two DFTs of $N/2$ elements. Having in mind that the direct calculation of a DFT with N elements requires an order of N^2 operations, it means that we will reduce the calculation complexity, since $N^2 > (N/2)^2 + (N/2)^2$. An illustration of this calculation, with $N = 8$, is shown in Fig. 1.19. We can continue and split $N/2$ DFTs into $N/4$ DFTs, and so on. A complete calculation scheme is shown in Fig. 1.20.

We can conclude that in the FFT algorithms an order of $N \log_2 N$ of operations is required.

Solution 1.18. The DFT is

$$X(k) = \sum_{n=0}^{15} e^{j2\pi(2\sqrt{3}-k)n/16} = \frac{1 - e^{j2\pi(2\sqrt{3}-k)}}{1 - e^{j2\pi(2\sqrt{3}-k)/16}},$$

$$|X(k)| = \left| \frac{\sin(\pi(2\sqrt{3}-k))}{\sin(\pi(2\sqrt{3}-k)/16)} \right|,$$

$$|\mathbf{X}| = [1.5799, 2.1361, 3.5045, 10.9192, 9.4607, 3.3454, 2.0805, 1.5530, 1.2781, 1.1225, 1.0362, 0.99781, 0.9992, 1.0406, 1.1310, 1.2929],$$

where $|\mathbf{X}|$ is the vector whose elements are the DFT values $|X(k)|$, $k = 0, 1, \dots, 15$. For the zero-padded signal (interpolated DFT), with a factor of 4, the DFT is

$$X(k) = \sum_{n=0}^{15} e^{j4\pi\sqrt{3}n/16} e^{-j2\pi nk/64} = \sum_{n=0}^{15} e^{j2\pi(8\sqrt{3}-k)n/64},$$

$$|X(k)| = \left| \frac{\sin(\pi(8\sqrt{3}-k)/4)}{\sin(\pi(8\sqrt{3}-k)/64)} \right|.$$

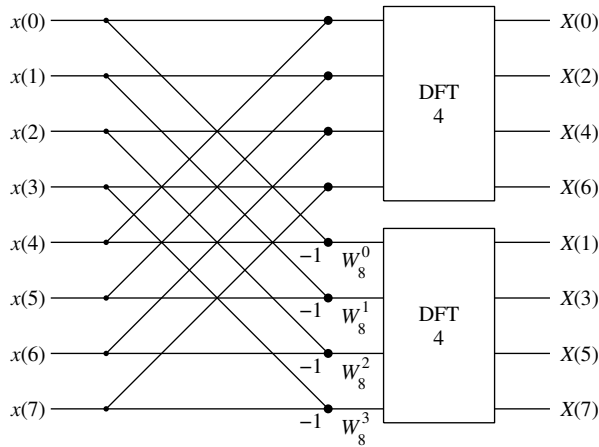


Figure 1.19 DFT of length 8 calculation from two DFTs of length 4.

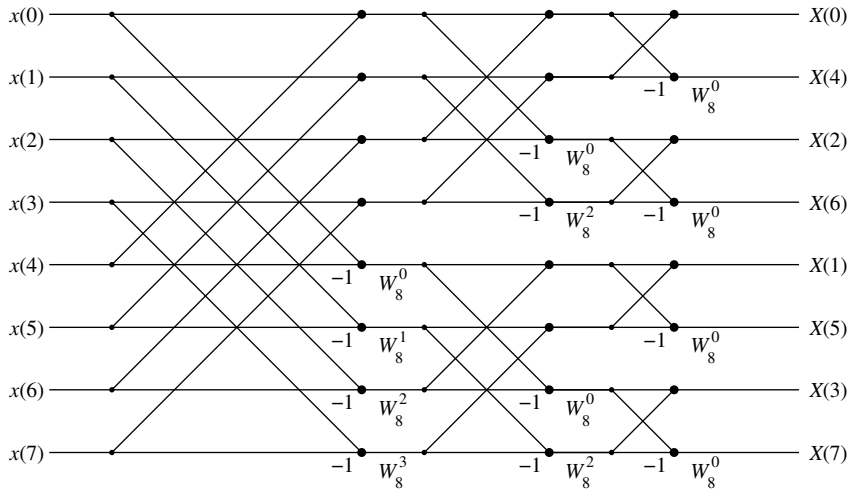


Figure 1.20 FFT calculation scheme obtained by decimation in frequency for $N = 8$.

Maximal value is obtained for $k = \lceil 8\sqrt{3} \rceil = 14$, where $\lceil 8\sqrt{3} \rceil$ denotes the nearest integer value. Then

$$\begin{aligned}|X(14)| &= \left| \frac{\sin(\pi(8\sqrt{3}-14)/4)}{\sin(\pi(8\sqrt{3}-14)/64)} \right| = 15.9662, \\ |X(15)| &= \left| \frac{\sin(\pi(8\sqrt{3}-15)/4)}{\sin(\pi(8\sqrt{3}-15)/64)} \right| = 13.9412, \\ |X(13)| &= \left| \frac{\sin(\pi(8\sqrt{3}-13)/4)}{\sin(\pi(8\sqrt{3}-13)/64)} \right| = 14.8249,\end{aligned}$$

with

$$d = 0.5 \frac{|X(15)| - |X(13)|}{2|X(14)| - |X(15)| - |X(13)|} = -0.1395.$$

The true frequency value is shifted from the nearest integer (grid) for -0.1436 , since $8\sqrt{3} = 13.8564$, when the interpolation is done. Thus, the obtained value -0.1395 is close to the true value -0.1436 . If the displacement formula is applied on the DFT values, without interpolation, we would get $d = 0.3356$, while $2\sqrt{3} = 3.4641$ is displaced from the nearest integer for 0.4641 .

Solution 1.19. Probability that random variable is $-\infty < \xi < \infty$ is

$$1 = \int_{-\infty}^{\infty} p_{\varepsilon(n)}(\xi) d\xi = \int_{-\infty}^{\infty} \frac{a}{1+\xi^2} d\xi = a \arctan(\xi) \Big|_{-\infty}^{\infty} = a\pi,$$

resulting in $a = 1/\pi$. The mean value is

$$\mu_{\varepsilon} = \frac{1}{\pi} \int_{-\infty}^{\infty} \frac{\xi}{1+\xi^2} d\xi = 0,$$

while the variance

$$\sigma_{\varepsilon} = \frac{1}{\pi} \int_{-\infty}^{\infty} \frac{\xi^2}{1+\xi^2} d\xi \rightarrow \infty$$

does not exist. This noise belongs to the class of impulse noises.

Solution 1.20. The mean of $y(n)$ is

$$\begin{aligned}\mu_y(n) &= E \left\{ \sum_{k=-\infty}^{\infty} h(k)x(n-k) \right\} = \sum_{k=0}^{\infty} a^k E\{w(n-k)\}u(n-k) \\ &= \sum_{k=0}^n a^k \mu_w = \mu_w \frac{1-a^{n+1}}{1-a} u(n).\end{aligned}$$

The variance is

$$\begin{aligned}\sigma_y^2(n) &= E \left\{ (y(n) - \mu_y(n))^2 \right\} = E\{y^2(n)\} - \mu_y^2(n) \\ &= \sum_{k_1=0}^n \sum_{k_2=0}^n a^{k_1} a^{k_2} E\{w(n-k_1)w(n-k_2)\}u(n) - \left(\mu_w \frac{1-a^{n+1}}{1-a} \right)^2 u(n).\end{aligned}$$

Since $E\{w(n-k_1)w(n-k_2)\} = \sigma_w^2 \delta(k_1 - k_2) + \mu_w^2$, we get

$$\sigma_y^2(n) = \sigma_w^2 \frac{1-a^{2(n+1)}}{1-a^2} u(n)$$

Solution 1.21. The mean value is

$$\mu_x = \mu_w + \sum_{k=1}^N a_k E\{e^{j(\omega_k n + \theta_k)}\} = \mu_w,$$

since

$$E\{e^{j(\omega_k n + \theta_k)}\} = \frac{1}{2\pi} \int_{-\pi}^{\pi} e^{j(\omega_k n + \theta_k)} d\theta_k = 0.$$

The auto-correlation is

$$r_{xx}(n) = \sigma_w^2 \delta(n) + \mu_w^2 + \sum_{k=1}^N a_k^2 e^{j\omega_k n},$$

while the spectral power density for $-\pi < \omega \leq \pi$ is

$$S_{xx}(e^{j\omega}) = \text{FT}\{r_{xx}(n)\} = \sigma_w^2 + 2\pi \mu_w^2 \delta(\omega) + 2\pi \sum_{k=1}^N a_k^2 \delta(\omega - \omega_k).$$

Chapter 2

Linear Time-Frequency Representations

The Fourier transform provides a unique mapping of a signal from the time domain to the frequency domain. The frequency domain representation provides the signal's spectral content. Although the phase characteristic of the Fourier transform contains information about the time distribution of the spectral content, it is very difficult to use this information. Therefore, one may say that the Fourier transform is practically useless for this purpose, that is, that the Fourier transform does not provide a time distribution of the spectral components.

Depending on problems encountered in practice, various representations have been proposed to analyze signals whose spectral content changes in time ("nonstationary" signals) in order to provide time-varying spectral descriptions of signals. The field of time-frequency signal analysis deals with these representations and their properties.

Time-frequency representations may roughly be classified as linear, quadratic, or higher-order representations.

Linear time-frequency representations exhibit linearity, that is, the representation of a linear combination of signals equals the linear combination of the individual representations. From this class, the most important one is the short-time Fourier transform (STFT) and its variations. A specific form of the STFT was originally introduced by Gabor in the mid-1940s. The energetic version of the STFT is a spectrogram. It is the most frequently used tool in time-frequency signal analysis.

A time-frequency transform is linear if a linear combination of signals produces the linear combination of the transforms. For a signal

$$x(t) = \sum_{m=1}^M c_m x_m(t) \quad (2.1)$$

a linear time-frequency transform, denoted by $\Upsilon\{x(t)\}$, may be written as

$$\Upsilon\{x(t)\} = \sum_{m=1}^M c_m \Upsilon\{x_m(t)\}. \quad (2.2)$$

Various forms of signal representations satisfy this property, starting from the short-time Fourier transform, via local polynomial Fourier transforms and wavelet transforms, up to quite general signal decomposition forms, including chirplet transforms. Although energetic versions of the linear transforms, calculated as their squared moduli, $|\Upsilon\{x(t)\}|^2$, do not preserve the linearity, they will be considered within this Chapter as well.

2.1 SHORT-TIME FOURIER TRANSFORM

The Fourier transform of a signal $x(t)$ and its inverse are defined by

$$X(\Omega) = \int_{-\infty}^{\infty} x(t) e^{-j\Omega t} dt \quad \text{and} \quad x(t) = \frac{1}{2\pi} \int_{-\infty}^{\infty} X(\Omega) e^{j\Omega t} d\Omega. \quad (2.3)$$

The information about the time distribution of the spectral content is contained in the phase of the Fourier transform. However, it is very difficult to use this information. Therefore, one may say that the Fourier transform does not provide a time distribution of the spectral components.

Example 2.1. Consider a signal $x(t)$ and its form shifted in time for t_0 , that is, $x(t - t_0)$. Show that the Fourier transform amplitudes of these two signals are equal.

★ The Fourier transform of $x(t - t_0)$ is equal to $X(\Omega)e^{-j\Omega t_0}$. The Fourier transform amplitudes of $x(t)$ and $x(t - t_0)$ are, therefore, the same. They are equal to $|X(\Omega)|$. The phase of the Fourier transform of $x(t - t_0)$ contains the information about t_0 .

The same holds, for example, for a real-valued signal $x(t)$ and its shifted and reversed version $x(t_0 - t)$. □

This fact will be additionally illustrated on two different signals (distributed over time in a different manner) producing the same amplitude of the Fourier transform (see Fig. 2.1).

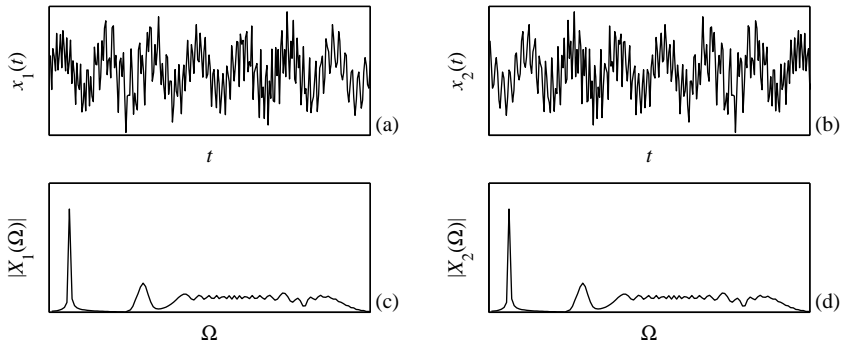


Figure 2.1 (a, b) Two different signals $x_1(t) \neq x_2(t)$ with (c, d) the same amplitudes of their Fourier transforms, that is, $|X_1(\Omega)| = |X_2(\Omega)|$.

Example 2.2. Signals

$$\begin{aligned} x_1(t) = & \sin(9\pi t/16 - (t-128)^2\pi/1280 - \pi/2) + \sin(\pi t/18) \\ & + 1.2 \sin(15\pi t/16 - (t-128)^2\pi/1024 - \pi/2) \exp(-((t-180)/40)^2) \\ & + 1.2 \sin(4\pi t/16 - (t-128)^2\pi/4096 - \pi/2) \exp(-((t-64)/40)^2) \end{aligned}$$

and $x_2(t) = x_1(255-t)$ are considered within $0 \leq t < 256$. Calculate and plot their Fourier transforms. For the numerical Fourier transform calculation, the signals are sampled at $\Delta t = 1$.

★The DFT is calculated based on the samples $x_1(n\Delta t)$ and $x_2(n\Delta t)$, at $\Delta t = 1$ for $n = 0, 1, 2, \dots, 255$. The positive frequencies part of the absolute DFT value is shown in Fig. 2.1.

□

The basic idea behind the short-time Fourier transform (STFT) is to apply the Fourier transform to a portion of the original signal, obtained by introducing a sliding window function $w(t)$ that will localize, truncate (and weight), the analyzed signal $x(t)$. The Fourier transform is calculated for the localized part of the signal. It produces the spectral content of the portion of the analyzed signal within the time interval defined by the width of the window function. The STFT (a time-frequency representation of the signal) is then obtained by sliding the window along the signal. The illustration of the STFT calculation is presented in Fig. 2.2.

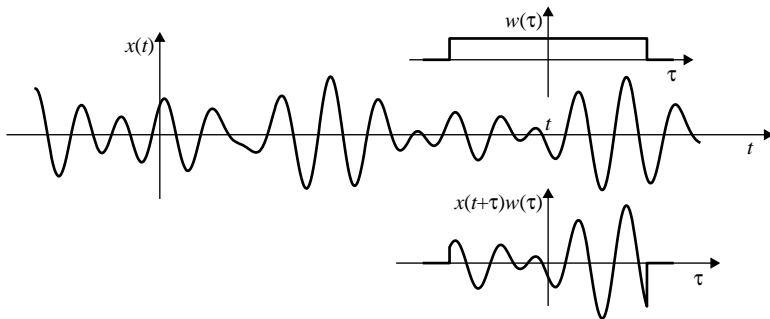


Figure 2.2 Illustration of the signal localization in the STFT calculation.

The analytic formulation of the STFT is

$$STFT(t, \Omega) = \int_{-\infty}^{\infty} x(t + \tau)w(\tau)e^{-j\Omega\tau}d\tau. \quad (2.4)$$

From (2.4) it is apparent that the STFT actually represents the Fourier transform of a signal \$x(t)\$, truncated by the window \$w(\tau)\$, centered at instant \$t\$ (see Fig. 2.2). From the definition, it is clear that the STFT satisfies properties inherited from the Fourier transform (e.g., linearity, modulation, shift).

By denoting \$x_t(\tau) = x(t + \tau)\$, we can conclude that the STFT is the Fourier transform of the windowed signal \$x_t(\tau)w(\tau)\$,

$$STFT(t, \Omega) = \text{FT}_\tau\{x_t(\tau)w(\tau)\}.$$

Another form of the STFT, with the same time-frequency performance, is

$$STFT_{II}(t, \Omega) = \int_{-\infty}^{\infty} x(\tau)w^*(\tau - t)e^{-j\Omega\tau}d\tau \quad (2.5)$$

where \$w^*(\tau)\$ denotes the conjugated window function.

It is obvious that definitions (2.4) and (2.5) differ only in phase, that is,

$$STFT_{II}(t, \Omega) = e^{-j\Omega t}STFT(t, \Omega) \quad (2.6)$$

for real-valued windows $w(\tau)$. Thus, their amplitudes are the same. The second form is more appropriate for the signal decomposition formulation of the STFT, which will be explained at the end of this Chapter. We will mainly use the first definition of the STFT.

Example 2.3. Find the STFT of signal

$$x(t) = \delta(t - t_1) + \delta(t - t_2) + e^{j\Omega_1 t} + e^{j\Omega_2 t}. \quad (2.7)$$

★The STFT-based time-frequency representation of this signal is

$$\begin{aligned} STFT(t, \Omega) &= w(t_1 - t)e^{-j\Omega(t_1 - t)} + w(t_2 - t)e^{-j\Omega(t_2 - t)} \\ &\quad + W(\Omega - \Omega_1)e^{j\Omega_1 t} + W(\Omega - \Omega_2)e^{j\Omega_2 t}, \end{aligned} \quad (2.8)$$

where $W(\Omega)$ is the Fourier transform of the used lag window $w(\tau)$. It is depicted in Fig. 2.3 for various window widths, along with the ideal representation.

The ideal time-frequency representation $ITF(t, \Omega)$, in this case, would be a line along the frequency for a delta pulse (representing the signal energy at the considered instant, for all frequencies) and a line along time for a pure harmonic signal (representing the signal energy at the considered frequency, for all time),

$$ITF(t, \Omega) = \delta(t - t_1) + \delta(t - t_2) + 2\pi\delta(\Omega - \Omega_1) + 2\pi\delta(\Omega - \Omega_2).$$

□

The STFT can be expressed in terms of the signal's Fourier transform

$$\begin{aligned} STFT(t, \Omega) &= \frac{1}{2\pi} \int_{-\infty}^{\infty} \int_{-\infty}^{\infty} X(\theta) e^{j(t+\tau)\theta} w(\tau) e^{-j\Omega\tau} d\theta d\tau \\ &= \frac{1}{2\pi} \int_{-\infty}^{\infty} X(\theta) W(\Omega - \theta) e^{j\theta} d\theta = \left(X(\Omega) e^{jt\Omega} \right) *_{\Omega} W(\Omega). \end{aligned} \quad (2.9)$$

It may be interpreted as an inverse Fourier transform of the localized version of $X(\Omega)$, with localization window $W(\Omega) = \text{FT}\{w(\tau)\}$.

2.1.1 Windows

It is obvious that the window function plays a crucial role in the localization of the signal in the time-frequency plane. Thus, we will briefly review windows commonly used for time localization of signal analysis.

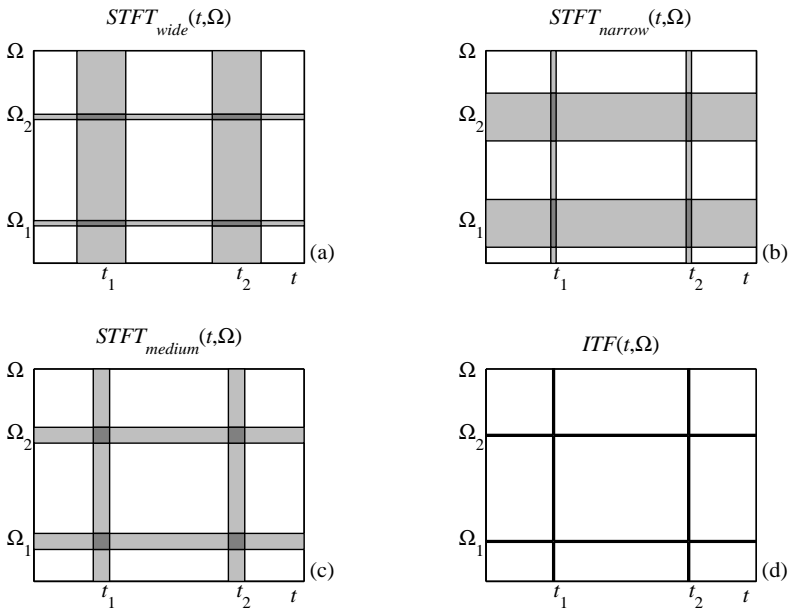


Figure 2.3 Time-frequency representation of the sum of two delta pulses and two sinusoids obtained by using: (a) a wide window, (b) a narrow window, (c) a medium width window, and (d) an ideal time-frequency representation.

2.1.1.1 Rectangular Window

The simplest window is the rectangular one, defined by

$$w(\tau) = \begin{cases} 1 & \text{for } |\tau| < T \\ 0 & \text{elsewhere} \end{cases} \quad (2.10)$$

whose Fourier transform is

$$W_R(\Omega) = \int_{-T}^T e^{-j\Omega\tau} d\tau = \frac{2\sin(\Omega T)}{\Omega}. \quad (2.11)$$

The rectangular window function has very strong and oscillatory sidelobes in the frequency domain, since the function $\sin(\Omega T)/\Omega$ converges very slowly, toward zero, in Ω as $\Omega \rightarrow \pm\infty$. Slow convergence in the Fourier domain is caused by a significant discontinuity in time domain, at $t = \pm T$. The mainlobe width of $W_R(\Omega)$ is $d_\Omega = 2\pi/T$. In order to enhance signal localization in the frequency domain, other window functions have been introduced.

2.1.1.2 Triangular (Bartlett) Window

It is defined by

$$w(\tau) = \begin{cases} 1 - |\tau/T| & \text{for } |\tau| < T \\ 0 & \text{elsewhere.} \end{cases} \quad (2.12)$$

It could be considered as a convolution of the rectangular window of duration T with itself, since

$$\begin{aligned} & [u(t + T/2) - u(t - T/2)] *_t [u(t + T/2) - u(t - T/2)] \\ &= (1 - |\tau/T|)[u(t + T) - u(t - T)]. \end{aligned}$$

The Fourier transform of the triangular window is a product of two Fourier transforms of the rectangular window of the width T ,

$$W_T(\Omega) = \frac{4 \sin^2(\Omega T/2)}{\Omega^2}. \quad (2.13)$$

Convergence of this function toward zero as $\Omega \rightarrow \pm\infty$ is of the $1/\Omega^2$ order. It is a continuous function of time, with discontinuities in the first derivative at $t = 0$ and $t = \pm T$. The mainlobe of this window function is twice wider in the frequency domain than in the rectangular window case. Its width follows from $\Omega T/2 = \pi$ as $d_\Omega = 4\pi/T$.

2.1.1.3 Hann(ing) Window

This window is of the form

$$w(\tau) = \begin{cases} 0.5(1 + \cos(\pi\tau/T)) & \text{for } |\tau| < T \\ 0 & \text{elsewhere.} \end{cases} \quad (2.14)$$

Since $\cos(\pi\tau/T) = [\exp(j\pi\tau/T) + \exp(-j\pi\tau/T)]/2$, the Fourier transform of this window is related to the Fourier transform of the rectangular window of the

same width as

$$\begin{aligned} W_H(\Omega) &= \frac{1}{2}W_R(\Omega) + \frac{1}{4}W_R(\Omega - \pi/T) + \frac{1}{4}W_R(\Omega + \pi/T) \\ &= \frac{\pi^2 \sin(\Omega T)}{\Omega(\pi^2 - \Omega^2 T^2)}. \end{aligned} \quad (2.15)$$

The function $W_H(\Omega)$ decays in frequency as Ω^3 , much faster than $W_R(\Omega)$.

The previous relation also implies the relationship between the STFTs of the signal $x(t)$ calculated using the rectangular and Hann(ing) windows, $STFT_R(t, \Omega)$ and $STFT_H(t, \Omega)$, respectively.

Example 2.4. Find the relation to calculate the STFT with a Hann(ing) window, if the STFT calculated with a rectangular window is known.

★From the frequency domain STFT definition

$$STFT(t, \Omega) = \frac{1}{2\pi} \int_{-\infty}^{\infty} X(\theta)W(\Omega - \theta)e^{j\theta t} d\theta$$

easily follows that, if we use the window, $W_H(\Omega) = \frac{1}{2}W_R(\Omega) + \frac{1}{4}W_R(\Omega - \pi/T) + \frac{1}{4}W_R(\Omega + \pi/T)$, then

$$STFT_H(t, \Omega) = \frac{1}{2}STFT_R(t, \Omega) + \frac{1}{4}STFT_R\left(t, \Omega - \frac{\pi}{T}\right) + \frac{1}{4}STFT_R\left(t, \Omega + \frac{\pi}{T}\right). \quad (2.16)$$

□

For the Hann(ing) window $w(\tau)$ of the width $2T$, we may roughly assume that its Fourier transform $W_H(\Omega)$ is nonzero within the main lattice $|\Omega| < 2\pi/T$ only, since the sidelobes decay very fast. Then we may write $d_\Omega = 4\pi/T$. It means that the STFT is nonzero valued in the shaded regions in Fig. 2.3.

We see that the duration in time of the STFT of a delta pulse is equal to the widow width $d_t = 2T$. The STFTs of two delta pulses (very short duration signals) do not overlap in time-frequency domain if their distance is greater than the window duration $|t_1 - t_2| > d_t$. Then, these two pulses can be resolved. Thus, the window width is here a measure of time resolution. Since the Fourier transform of the Hann(ing) window converges fast, we can roughly assume that a measure of duration in frequency is the width of its mainlobe, $d_\Omega = 4\pi/T$. Then we may say that the Fourier transforms of two sinusoidal signals do not overlap in frequency if the condition $|\Omega_1 - \Omega_2| > d_\Omega$ holds. It is important to observe that the product of the

window durations in time and frequency is a constant. In this example, considering time domain duration of the Hann(ing) window and the width of its mainlobe in the frequency domain, this product is $d_t d_\Omega = 8\pi$. Therefore, if we improve the resolution in the time domain d_t , by decreasing T , we inherently increase the value of d_Ω in the frequency domain. This essentially prevents us from achieving the ideal resolution ($d_t = 0$ and $d_\Omega = 0$) in both domains. A general formulation of this principle, stating that the product of effective window durations in time and in frequency cannot be arbitrarily small, will be presented later.

2.1.1.4 Hamming Window

This window has the form

$$w(\tau) = \begin{cases} 0.54 + 0.46 \cos(\pi\tau/T) & \text{for } |\tau| < T \\ 0 & \text{elsewhere.} \end{cases} \quad (2.17)$$

A similar relation between the Hamming and the rectangular window transforms holds, as in the case of Hann(ing) window.

The Hamming window was derived starting from

$$w(\tau) = a + (1 - a) \cos(\pi\tau/T)$$

within $|\tau| < T$, with

$$W(\Omega) = a \frac{2 \sin(\Omega T)}{\Omega} + (1 - a) \left(\frac{\sin((\Omega - \pi/T)T)}{\Omega - \pi/T} + \frac{\sin((\Omega + \pi/T)T)}{\Omega + \pi/T} \right).$$

If we choose such a value of a to cancel out the second sidelobe at its maximum (i.e., at $\Omega T \cong 2.5\pi$) then we get

$$0 = \frac{2aT}{2.5\pi} - (1 - a) \left(\frac{T}{1.5\pi} + \frac{T}{3.5\pi} \right)$$

resulting in

$$a = 25/46 \cong 0.54. \quad (2.18)$$

This window has several sidelobes, next to the mainlobe, lower than the previous two windows. However, since it is not continuous at $t = \pm T$, its decay in frequency, as $\Omega \rightarrow \pm\infty$, is not fast. Note that we let the mainlobe to be twice wider than in the rectangular window case, so we cancel out not the first but the second sidelobe, at its maximum.

2.1.1.5 Gaussian Window

This window localizes signal in time, although it is not time-limited. Its form is

$$w(\tau) = e^{-\tau^2/\alpha^2}.$$

Example 2.5. Calculate the area under the Gaussian window

$$I = \int_{-\infty}^{\infty} e^{-\tau^2/\alpha^2} d\tau. \quad (2.19)$$

★Let us form the function

$$\begin{aligned} I^2 &= \int_{-\infty}^{\infty} \int_{-\infty}^{\infty} e^{-\tau_1^2/\alpha^2} e^{-\tau_2^2/\alpha^2} d\tau_1 d\tau_2 \\ &= \int_0^{2\pi} \int_0^{\infty} e^{-\rho^2/\alpha^2} \rho d\rho d\varphi = \pi\alpha^2, \end{aligned}$$

with $\tau_1 = \rho \cos \varphi$ and $\tau_2 = \rho \sin \varphi$, when $\tau_1^2 + \tau_2^2 = \rho^2$ and $d\tau_1 d\tau_2 = |\rho| d\rho d\varphi$. Then,

$$\int_{-\infty}^{\infty} e^{-\tau^2/\alpha^2} d\tau = |\alpha| \sqrt{\pi}.$$

□

The Fourier transform of the Gaussian window is

$$W(\Omega) = |\alpha| \sqrt{\pi} e^{-\Omega^2 \alpha^2 / 4}. \quad (2.20)$$

It follows from

$$W(\Omega) = \int_{-\infty}^{\infty} e^{-\tau^2/\alpha^2} e^{-j\Omega\tau} d\tau$$

and

$$\begin{aligned} \int_{-\infty}^{\infty} e^{-\tau^2/\alpha^2} e^{-j\Omega\tau} d\tau &= \int_{-\infty}^{\infty} e^{-(\tau/\alpha + j\Omega\alpha/2)^2 - \Omega^2 \alpha^2 / 4} d\tau \\ &= e^{-\Omega^2 \alpha^2 / 4} |\alpha| \sqrt{\pi}, \end{aligned} \quad (2.21)$$

with $\int_{-\infty}^{\infty} e^{-(\tau + j\Omega\alpha^2/2)^2/\alpha^2} d\tau = \int_{-\infty}^{\infty} e^{-s^2/\alpha^2} ds = |\alpha| \sqrt{\pi}$.

2.1.1.6 Blackman and Kaiser Windows

In some applications it is crucial that the sidelobes are suppressed, as much as possible. This is achieved by using windows of more complicated forms, like the Blackman window. It is defined by

$$w(\tau) = \begin{cases} 0.42 + 0.5 \cos(\pi\tau/T) + 0.08 \cos(2\pi\tau/T) & \text{for } |\tau| < T \\ 0 & \text{elsewhere.} \end{cases} \quad (2.22)$$

This window is derived from

$$w(\tau) = a_0 + a_1 \cos(\pi\tau/T) + a_2 \cos(2\pi\tau/T)$$

with $a_0 + a_1 + a_2 = 1$ and canceling out the Fourier transform values $W(\Omega)$ at the positions of the third and the fourth sidelobe maxima (i.e., at $\Omega T \cong 3.5\pi$ and $\Omega T \cong 4.5\pi$). Here, we let the mainlobe to be three times wider than in the rectangular window case, so we cancel out not the first nor the second but the third and fourth sidelobes, at their maxima.

Further reduction of the sidelobes can be achieved by, for example, the Kaiser (Kaiser-Bessel) window. It is an approximation to a restricted time duration function with minimum energy outside the mainlobe. This window is defined by using the zero-order Bessel functions, with a localization parameter. It has the ability to keep the maximum energy within the mainlobe, while minimizing the sidelobe energy. The sidelobe level can be as low -70 dB, as compared to the mainlobe, and even lower. This kind of window is used in the analysis of signals with significantly different amplitudes, when the sidelobe of one component can be much higher than the amplitude of the mainlobe of other components.

These are just a few of the windows used in signal processing. Some windows, along with the corresponding Fourier transforms, are presented in Fig. 2.4. They will be sufficient for the analysis in this book.

2.1.2 Continuous STFT Inversion

The original signal $x(t)$ may be easily reconstructed from its STFT, (2.4), as the inverse Fourier transform

$$x(t + \tau) = \frac{1}{2\pi w(\tau)} \int_{-\infty}^{\infty} STFT(t, \Omega) e^{j\Omega\tau} d\Omega. \quad (2.23)$$

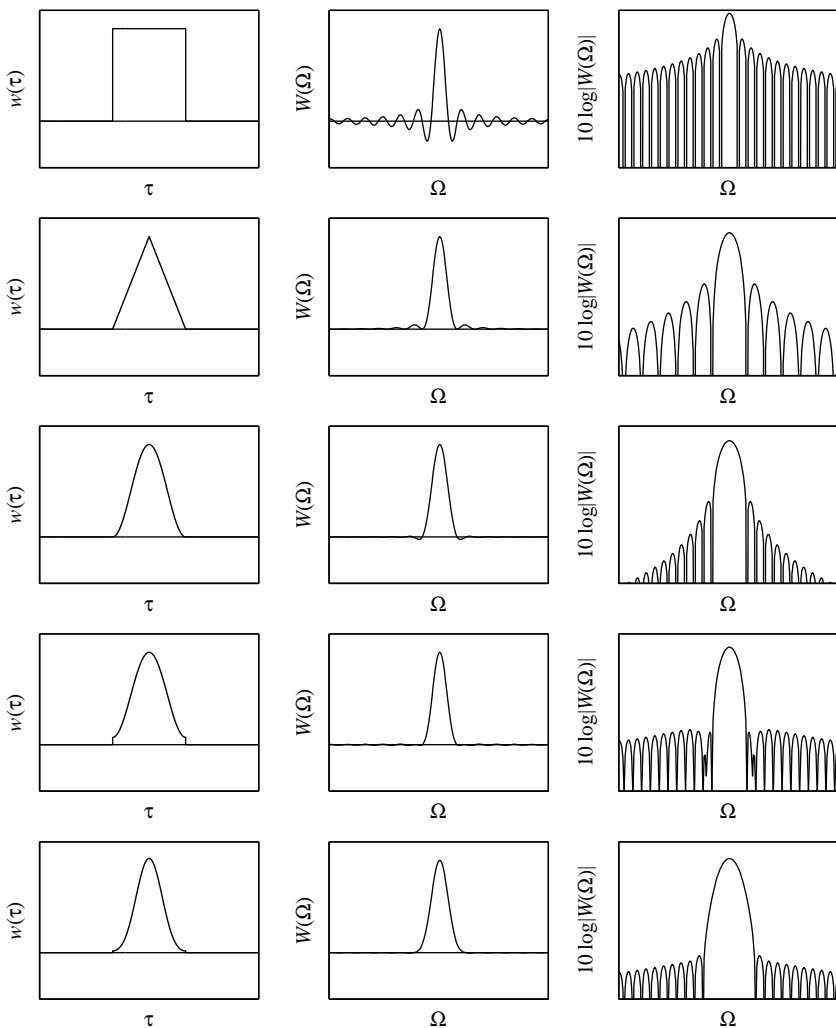


Figure 2.4 Windows in the time and frequency domains: rectangular window (first row), triangular (Bartlett) window (second row), Hann(ing) window (third row), Hamming window (fourth row), and Blackman window (fifth row).

In this way, we can calculate the values of $x(t + \tau)$ for a given instant t and for the values of τ where $w(\tau)$ is nonzero. Then we may skip the window width, take the time instant $t + 2T$, and calculate the inverse of $STFT(t + 2T, \Omega)$, and so on.

Theoretically, for a window of the width $2T$, it is sufficient to know the STFT calculated at $t = 2kR$, $k = 0, \pm 1, \pm 2, \dots$, with $R \leq T$, in order to reconstruct the signal for any t .

Example 2.6. Time-frequency analysis is performed with a window of the width $2T$. The STFT is calculated at $t = kT$, $k = 0, \pm 1, \pm 2, \dots$, that is, with an overlap of half of the window width, by using the rectangular window, the triangular window, the Hann(ing) window, and the Hamming window. What is the reconstruction relation in each of these cases.

★ The windowed reconstruction, at an instant $t = kT$, is

$$x(kT + \tau)w(\tau) = \frac{1}{2\pi} \int_{-\infty}^{\infty} STFT(kT, \Omega)e^{j\Omega\tau} d\Omega$$

or with substitution $kT + \tau \rightarrow \tau$

$$x(\tau)w(\tau - kT) = \frac{1}{2\pi} e^{-j\Omega kT} \int_{-\infty}^{\infty} STFT(kT, \Omega)e^{j\Omega\tau} d\Omega.$$

By summing the values for all instants kT , corresponding to all k , we get

$$x(\tau) \sum_{k=-\infty}^{\infty} w(\tau - kT) = \frac{1}{2\pi} \sum_{k=-\infty}^{\infty} e^{-j\Omega kT} \int_{-\infty}^{\infty} STFT(kT, \Omega)e^{j\Omega\tau} d\Omega. \quad (2.24)$$

In general, the signal is multiplied by a window-dependent function,

$$c(\tau) = \sum_{k=-\infty}^{\infty} w(\tau - kT). \quad (2.25)$$

For the rectangular window of the width $2T$, $\sum_{k=-\infty}^{\infty} w(\tau - kT) = 2$, while for the triangular window of the same with $\sum_{k=-\infty}^{\infty} w(\tau - kT) = 1$. The same holds for the Hann(ing) window, $\sum_{k=-\infty}^{\infty} w(\tau - kT) = 1$, while $\sum_{k=-\infty}^{\infty} w(\tau - kT) = 1.08$ for the Hamming window. Repeat the analysis, when the STFT is calculated at $t = kT/2$ or $t = kT/4$, $k = 0, \pm 1, \pm 2, \dots$ In general, for any step R , use $c(\tau) = w(\tau) *_{\tau} \sum_{k=-\infty}^{\infty} \delta(t - kR)$ and find the Fourier transform of $c(\tau)$. □

A special case of the inversion formula, for $\tau = 0$, gives

$$x(t) = \frac{1}{2\pi w(0)} \int_{-\infty}^{\infty} STFT(t, \Omega) d\Omega. \quad (2.26)$$

For the STFT defined by (2.5), the signal can be obtained as

$$x(\tau) = \frac{1}{2\pi w^*(\tau-t)} \int_{-\infty}^{\infty} STFT_{II}(t, \Omega) e^{j\Omega\tau} d\Omega.$$

The last equation can be used for $w(\tau-t) \neq 0$. If we calculate $STFT(t, \Omega)$ for all values of t (which is a common case in the analysis of highly nonstationary signals), the inversion results in multiple values of signal for one instant, which all can be used for better signal reconstruction, as follows

$$x(\tau) = \frac{1}{2\pi W^*(0)} \int_{-\infty}^{\infty} \int_{-\infty}^{\infty} STFT_{II}(\Omega, t) e^{j\Omega\tau} dt d\Omega.$$

In the case that we are interested only in a part of the time-frequency plane, relation (2.26) can be used for the time-varying signal filtering. The STFT, for a given t , can be filtered by a filter transfer function $B(t, \Omega)$, for a given t . The filtered signal is obtained as

$$y(t) = \frac{1}{2\pi w(0)} \int_{-\infty}^{\infty} B(t, \Omega) STFT(t, \Omega) d\Omega.$$

For example, we can use $B(t, \Omega) = 1$ within the frequency region of interest, for given t , and $B(t, \Omega) = 0$ elsewhere.

2.1.3 Spectrogram

The energetic version of the STFT, called a spectrogram, is defined by

$$\begin{aligned} SPEC(t, \Omega) &= |STFT(t, \Omega)|^2 \\ &= \left| \int_{-\infty}^{\infty} x(\tau) w^*(\tau-t) e^{-j\Omega\tau} d\tau \right|^2 = \left| \int_{-\infty}^{\infty} x(t+\tau) w(\tau) e^{-j\Omega\tau} d\tau \right|^2. \end{aligned} \quad (2.27)$$

Obviously, the linearity property is lost in the spectrogram.

Example 2.7. Calculate the integral of spectrogram over time and over frequency.

★The integral of the spectrogram over frequency is

$$\begin{aligned}
 & \frac{1}{2\pi} \int_{-\infty}^{\infty} SPEC(t, \Omega) d\Omega \\
 &= \frac{1}{2\pi} \int_{-\infty}^{\infty} \int_{-\infty}^{\infty} \int_{-\infty}^{\infty} x(t + \tau_1) x^*(t + \tau_2) w(\tau_1) w(\tau_2) e^{-j\Omega(\tau_1 - \tau_2)} d\tau_1 d\tau_2 d\Omega \\
 &= \int_{-\infty}^{\infty} |x(t + \tau)|^2 w^2(\tau) d\tau = \int_{-\infty}^{\infty} |x(\tau)|^2 w^2(\tau - t) d\tau \\
 &= |x(t)|^2 *_t w^2(t)
 \end{aligned} \tag{2.28}$$

where an even, real-valued window is assumed.

In a similar way, by using the frequency domain STFT form, we get

$$\int_{-\infty}^{\infty} SPEC(t, \Omega) dt = |X(\Omega)|^2 *_{\Omega} W^2(\Omega).$$

Note that

$$\frac{1}{2\pi} \int_{-\infty}^{\infty} \int_{-\infty}^{\infty} SPEC(t, \Omega) d\Omega dt = E_x E_w$$

where E_x and E_w are the energies of the signal and window, respectively. Note also that the convolution of two functions results in a function whose width is, in general, equal to the sum of the widths of individual functions. \square

2.1.4 STFT of Multicomponent Signals

Let us introduce the multicomponent signal $x(t)$ as the sum of M components $x_m(t)$,

$$x(t) = \sum_{m=1}^M x_m(t) = \sum_{m=1}^M A_m(t) e^{j\phi_m(t)}. \tag{2.29}$$

The STFT of this signal is equal to the sum of the STFTs of individual components,

$$STFT(t, \Omega) = \sum_{m=1}^M STFT_m(t, \Omega), \tag{2.30}$$

that will be referred to as the auto-terms. This is one of very appealing properties of the STFT, which will be lost in the quadratic and higher-order distributions.

2.1.4.1 Cross-Terms in the Spectrogram

The spectrogram of multicomponent signal (2.29) is of the form

$$SPEC(t, \Omega) = |STFT(t, \Omega)|^2 = \sum_{m=1}^M |STFT_m(t, \Omega)|^2,$$

if the STFTs of signal components, $STFT_m(t, \Omega)$, $m = 1, 2, \dots, M$, do not overlap in the time-frequency plane, that is, if

$$STFT_m(t, \Omega)STFT_n^*(t, \Omega) = 0 \text{ for all } (t, \Omega) \text{ if } m \neq n.$$

In general

$$SPEC(t, \Omega) = \sum_{m=1}^M |STFT_m(t, \Omega)|^2 + \sum_{m=1}^M \sum_{\substack{n=1 \\ n \neq m}}^M STFT_m(t, \Omega)STFT_n^*(t, \Omega), \quad (2.31)$$

where the second term on the right side represents the terms resulting from the interaction between two signal components. They are called cross-terms. The cross-terms are usually undesirable components, arising due to nonlinear structure of the spectrogram. Here they appear only at the time-frequency points where the auto-terms overlap. In other quadratic time-frequency representations, the cross-terms may appear even if the components do not overlap.

2.2 DURATION MEASURES AND UNCERTAINTY PRINCIPLE

We started the discussion about signal concentration (window duration) and resolution in the Hann(ing) window case, with the illustration in Fig. 2.3. In general, window duration in time or/and in frequency is not obvious from its definition or form. Then the effective duration is used as a measure of signal (window) duration. In the time domain the effective duration measure is defined by

$$\sigma_t^2 = \frac{\int_{-\infty}^{\infty} \tau^2 |w(\tau)|^2 d\tau}{\int_{-\infty}^{\infty} |w(\tau)|^2 d\tau}. \quad (2.32)$$

Similarly, the measure of effective duration in frequency is

$$\sigma_{\Omega}^2 = \frac{\int_{-\infty}^{\infty} \Omega^2 |W(\Omega)|^2 d\Omega}{\int_{-\infty}^{\infty} |W(\Omega)|^2 d\Omega}. \quad (2.33)$$

The uncertainty principle in signal processing states that the product of measures of effective duration in time and frequency, for any function satisfying $w(\tau)\sqrt{|\tau|} \rightarrow 0$ as $\tau \rightarrow \pm\infty$, is

$$\sigma_t^2 \sigma_{\Omega}^2 \geq 1/4. \quad (2.34)$$

Since this principle will be used in the further analysis, we will present its short proof.

Consider the time derivative of $w(\tau)$ denoted by $w'(\tau)$. Since $w'(\tau)$ is the inverse Fourier transform of $j\Omega W(\Omega)$, then according to Parseval's theorem, we have

$$\frac{1}{2\pi} \int_{-\infty}^{\infty} |j\Omega W(\Omega)|^2 d\Omega = \int_{-\infty}^{\infty} |w'(\tau)|^2 d\tau.$$

The product of effective durations in time and frequency may be written as

$$\sigma_t^2 \sigma_{\Omega}^2 = \frac{1}{E_w^2} \int_{-\infty}^{\infty} \tau^2 |w(\tau)|^2 d\tau \int_{-\infty}^{\infty} |w'(\tau)|^2 d\tau,$$

where E_w is the energy of window (function),

$$E_w = \int_{-\infty}^{\infty} |w(\tau)|^2 d\tau = \frac{1}{2\pi} \int_{-\infty}^{\infty} |W(\Omega)|^2 d\Omega. \quad (2.35)$$

For any two integrable functions $x_1(\tau)$ and $x_2(\tau)$, the Cauchy-Schwartz inequality

$$\left| \int_{-\infty}^{\infty} x_1(\tau) x_2^*(\tau) d\tau \right|^2 \leq \int_{-\infty}^{\infty} |x_1(\tau)|^2 d\tau \int_{-\infty}^{\infty} |x_2(\tau)|^2 d\tau \quad (2.36)$$

holds. The equality holds for $x_1(\tau) = \pm \gamma x_2^*(\tau)$, where γ is a positive constant.

In our case, the equality holds for

$$\tau w(\tau) = \pm \gamma w'(\tau).$$

This differential equation may be written as

$$\tau d\tau/\gamma = \pm \frac{dw(\tau)}{w(\tau)}.$$

Its solution is $\ln(w(\tau)) = \pm \tau^2/(2\gamma) + C$, resulting into the Gaussian function

$$w(\tau) = \exp(-\tau^2/(2\gamma)), \quad (2.37)$$

as the finite energy solution, with $w(0) = 1$.

For the Gaussian window (function), it has been shown that this product is equal to $\sigma_t^2 \sigma_\Omega^2 = 1/4$, eq.(1.54), meaning that the Gaussian window (function) is the best localized window (function) in this sense. In the sense of illustration in Fig. 2.3, this fact also means that, for a given width of the STFT of a pulse $\delta(t)$ in the time direction, the narrowest presentation of a sinusoid in the frequency direction is achieved by using the Gaussian window. However, this window is neither time nor frequency limited, so it cannot be used in numerical implementations without additional truncation that spoils its theoretical efficiency.

Example 2.8. Calculate the effective duration measures for the rectangular window of the width $2T$ and for the triangular window of the same width, $w(\tau) = (1 - |\tau|/T)[u(\tau + T) - u(\tau - T)]$.

★The effective duration measure in time for the rectangular window is

$$\sigma_t^2 = \frac{T^2}{3}.$$

The effective duration in frequency, for the rectangular window does not exist, since the integral $\int_{-\infty}^{\infty} |\sin(\Omega T)|^2 d\Omega$ does not have a finite value.

For the triangular window, the effective duration measure in time is

$$\sigma_t^2 = \frac{2 \int_0^T \tau^2 (1 - \tau/T)^2 d\tau}{2 \int_0^T (1 - \tau/T)^2 d\tau} = \frac{T^2}{10}$$

with $E_w = 2T/3$.

The effective duration measure in the frequency domain is

$$\begin{aligned} \sigma_\Omega^2 &= \frac{\frac{1}{2\pi} \int_{-\infty}^{\infty} \Omega^2 |W(\Omega)|^2 d\Omega}{E_w} \\ &= \frac{2 \int_0^T |w'(\tau)|^2 d\tau}{E_w} = \frac{2/T}{2T/3} = \frac{3}{T^2}, \end{aligned}$$

with $\sigma_t^2 \sigma_\Omega^2 = 3/10$. □

2.3 DISCRETE FORM AND REALIZATIONS OF THE STFT

In numerical calculations the continuous-time form of the STFT should be discretized. By sampling the signal with sampling interval Δt , we get

$$\begin{aligned} STFT(t, \Omega) &= \int_{-\infty}^{\infty} x(t + \tau)w(\tau)e^{-j\Omega\tau}d\tau \\ &\simeq \sum_{m=-\infty}^{\infty} x((n+m)\Delta t)w(m\Delta t)e^{-jm\Delta t\Omega}\Delta t. \end{aligned} \quad (2.38)$$

Denoting $x(n) = x(n\Delta t)\Delta t$ and normalizing the frequency Ω by Δt , $\omega = \Omega\Delta t$, we get a discrete-time form of the STFT as

$$STFT(n, \omega) = \sum_{m=-\infty}^{\infty} w(m)x(n+m)e^{-jm\omega}. \quad (2.39)$$

It is important to note that the discrete-time form $STFT(n, \omega)$ is periodic in frequency with period 2π in contrast to the continuous-time STFT form $STFT(t, \Omega)$. Again, these two forms should be distinguished by the independent variable notation.

The relation between the continuous-time and the discrete-time forms is

$$STFT(n, \omega) = \sum_{k=-\infty}^{\infty} STFT(n\Delta t, \Omega + 2k\Omega_0), \text{ with } \Omega = \omega/\Delta t.$$

The sampling interval Δt is related to the period in frequency as $\Delta t = \pi/\Omega_0$. According to the sampling theorem, in order to avoid the overlapping of the STFT periods (aliasing), we should take

$$\Delta t = \frac{\pi}{\Omega_0} < \frac{\pi}{\Omega_m}$$

where Ω_m is the maximal frequency in the STFT. Strictly speaking, the windowed signal $x(t + \tau)w(\tau)$ is time limited thus, it is not frequency limited. Theoretically, there is no maximal frequency since the width of the window's Fourier transform is infinite. However, in practice we can always assume that the value of spectral content of $x(t + \tau)w(\tau)$ above frequency Ω_m , that is, for $|\Omega| > \Omega_m$, can be neglected, and that overlapping of the frequency content above Ω_m does not degrade the signal in the basic frequency period.

The discretization in frequency should be done with a number of samples greater than or equal to the window length N . If we assume that the number of discrete frequency points is equal to the window length, then

$$STFT(n, k) = STFT(n, \omega)_{|\omega=\frac{2\pi}{N}k} = \sum_{m=-N/2}^{N/2-1} w(m)x(n+m)e^{-j2\pi mk/N}. \quad (2.40)$$

It can be efficiently calculated using the fast DFT routines

$$STFT(n, k) = \text{DFT}_m\{w(m)x(n+m)\}, \quad (2.41)$$

over m , for a given instant n .

When the DFT routines, with indices from 0 to $N - 1$, are used, a shifted version of $w(m)x(n+m)$ should be formed for the calculation for $N/2 \leq m \leq N - 1$. It is obtained as $w(m-N)x(n+m-N)$, since in the DFT calculation, periodicity of the signal $w(m)x(n+m)$ with period N is inherently assumed.

Example 2.9. Consider a signal from Example 2.2, presented in Fig. 2.1. Calculate its STFT with a Hamming window of the width $N = 64$.

★The STFT is calculated as the DFT of samples $x_1(n\Delta t)$ and $x_2(n\Delta t)$, at $\Delta t = 1$ for $n = 0, 1, 2, \dots, 255$. The Hamming window of the width $N = 64$ is used. For the instant $n = 0$ the Hamming window covers the interval $-N/2 \leq m \leq N/2 - 1$ thus, the signal interval from $t = -32\Delta t$ is used. Since the same is done for the ending point, the last signal point used in calculation was $t = 31\Delta t$. The squared absolute value of the STFT (spectrogram), calculated for each instant n , is shown in Fig. 2.5. □

2.3.1 Recursive STFT Implementation

For the rectangular window, the STFT values at an instant n can be calculated recursively from the STFT values at instant $n - 1$, as

$$\begin{aligned} STFT_R(n, k) &= [x(n+N/2-1) - x(n-N/2-1)](-1)^k e^{j2\pi k/N} \\ &\quad + STFT_R(n-1, k) e^{j2\pi k/N}. \end{aligned} \quad (2.42)$$

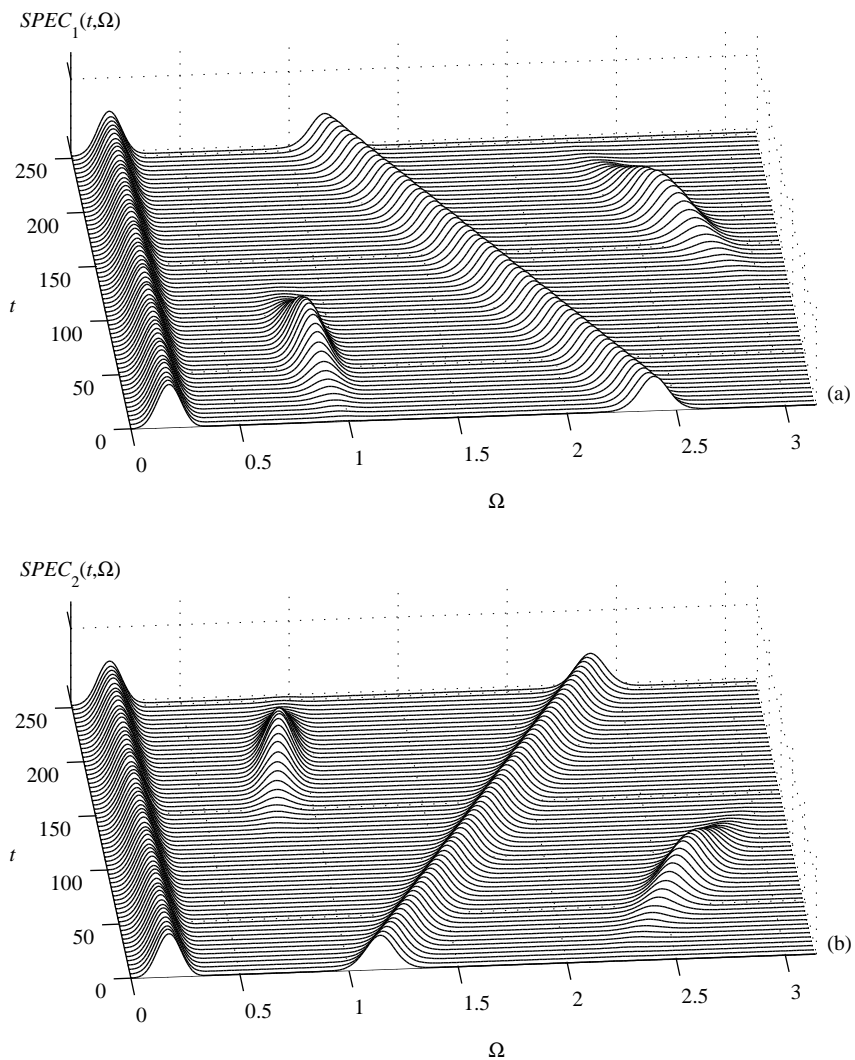


Figure 2.5 (a, b) Spectrograms of the signals presented in Figure 2.1.

This recursive formula follows easily from the STFT definition (2.40), as

$$\begin{aligned} STFT_R(n, k) &= \sum_{m=-N/2}^{N/2-1} x(n+m)e^{-j2\pi mk/N} \\ &= \sum_{m=-N/2-1}^{N/2-2} x(n+m)e^{-j\frac{2\pi}{N}mk} + x\left(n+\frac{N}{2}-1\right)e^{-j\frac{2\pi}{N}\left(\frac{N}{2}-1\right)k} - x\left(n-\frac{N}{2}-1\right)e^{j\frac{2\pi}{N}\left(\frac{N}{2}+1\right)k} \end{aligned}$$

with

$$\begin{aligned} \sum_{m=-N/2-1}^{N/2-2} x(n+m)e^{-j2\pi mk/N} &= \sum_{m=-N/2}^{N/2-1} x(n+m-1)e^{-j2\pi(m-1)k/N} \\ &= STFT_R(n-1, k)e^{j2\pi k/N}. \end{aligned}$$

For other window forms, the STFT can be obtained from the STFT calculated using the rectangular window. For example, according to (2.16), the STFT with Hann(ing) window is related to the STFT with rectangular window as

$$STFT_H(n, k) = \frac{1}{2}STFT_R(n, k) + \frac{1}{4}STFT_R(n, k-1) + \frac{1}{4}STFT_R(n, k+1). \quad (2.43)$$

The recursive calculation is important for hardware online implementations of the STFT and other related time-frequency representations (e.g., the higher-order representations implementations based on the STFT).

A system for the recursive implementation of the STFT is shown in Fig. 2.6. The STFT obtained by using the rectangular window is denoted by $STFT_R(n, k)$, Fig. 2.6, while the values of coefficients are

$$\begin{aligned} (a_{-1}, a_0, a_1) &= (0.25, 0.5, 0.25), \\ (a_{-1}, a_0, a_1) &= (0.23, 0.54, 0.23), \\ (a_{-2}, a_{-1}, a_0, a_1, a_2) &= (0.04, 0.25, 0.42, 0.25, 0.04) \end{aligned}$$

for the Hann(ing), Hamming, and Blackman windows, respectively.

2.3.2 Filter Bank STFT Implementation

According to (2.4), the STFT can be written as a convolution

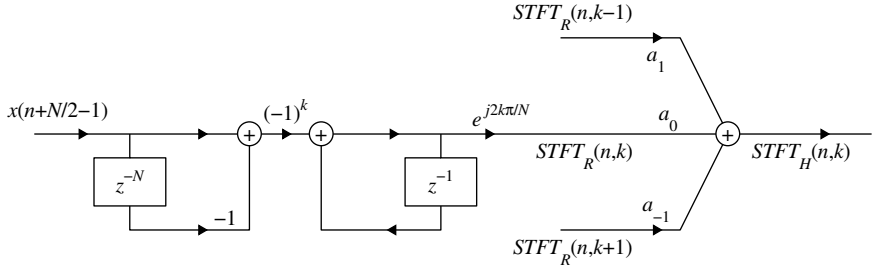


Figure 2.6 Recursive implementation of the STFT for the rectangular and other windows.

$$STFT(t, \Omega) = \int_{-\infty}^{\infty} x(t - \tau) w(-\tau) e^{j\Omega\tau} d\tau = x(t) *_t [w(t) e^{j\Omega t}] \quad (2.44)$$

where an even, real-valued, window function is assumed, $w(\tau) = w(-\tau)$. For a discrete set of frequencies $\Omega_k = k\Delta\Omega = 2\pi k/(N\Delta t)$, $k = 0, 1, 2, \dots, N - 1$, and discrete values of signal $x(n)$, we get that the discrete STFT, (2.40), is an output of the filter bank with impulse responses

$$\begin{aligned} h_k(n) &= w(n) e^{j2\pi kn/N} \\ k &= 0, 1, \dots, N - 1 \end{aligned}$$

which is illustrated in Fig. 2.7. Note that a bandpass filtering can be implemented by using the following relation

$$x(n) *_n [w(n) e^{j2\pi kn/N}] = \left([x(n) e^{-j2\pi kn/N}] *_n w(n) \right) e^{j2\pi kn/N}.$$

A possible STFT downsampling in time, at the output, will be discussed later.

2.3.3 Time-Frequency Plane Lattice

In order to additionally explain this form of realization, as well as to introduce various possibilities of splitting the whole time-frequency plane, let us assume that

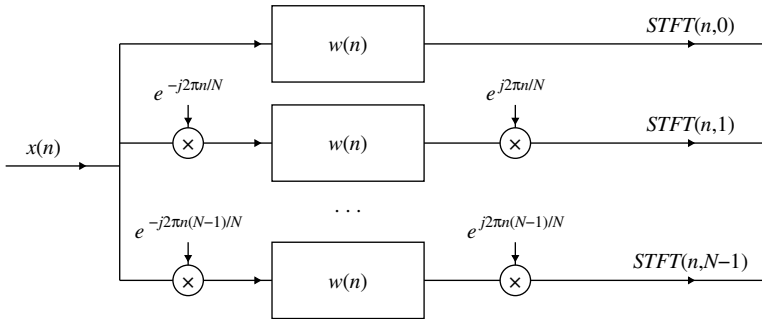


Figure 2.7 Filter bank realization of the STFT.

the total length of discrete signal $x(n)$ is M , while N is the length of the window used for the STFT analysis. If the signal was sampled by Δt , then the time-frequency region of interest in the continuous domain is $t \in [0, (M-1)\Delta t]$ and $\Omega \in [-\Omega_m, \Omega_m]$, with $\Omega_m = \pi/\Delta t$, or $\omega \in [-\pi, \pi]$. Note that $\omega \in [0, 2\pi]$ could also be used. Using all signal samples in the discrete-time, we would have M discrete-time signal values in time, $n = 0, 1, \dots, M-1$, while the Fourier transform of the whole signal would have $k = 0, 1, \dots, M-1$ values in the discrete frequency domain.

An index will be introduced in the STFT notation, showing the window width being used in the STFT calculation, since it will be changing in this analysis. Thus, $STFT_N(n, k)$ denotes the k th frequency sample, calculated at an time instant n , by using the rectangular window, whose width is N . Rectangular windows of the form $w_2(m) = \delta(m) + \delta(m+1)$, $w_4(m) = \delta(m) + \delta(m+1) + \delta(m+2) + \delta(m+3) \dots$ with the STFT notation

$$STFT_N(n, k) = \sum_{m=-(N-1)}^0 x(n+m) e^{-j2\pi mk/N} = \sum_{m=0}^{N-1} x(n-m) e^{j2\pi mk/N} \quad (2.45)$$

is used. The value of $STFT_N(n, k)$ is calculated using only the current and the past signal samples, $x(n)$ and $x(n-1)$, $x(n-2), \dots, x(n-N+1)$. This discrete form follows from the continuous-time form (2.4) with the window $w(\tau) = u(\tau+2T) - u(\tau)$. It differs from a symmetric window definition in the phase factor only.

For the illustration, we will assume $M = 16$. The first special case is the window of width $N = 1$, $w_1(m) = \delta(m)$, when the STFT is the signal itself,

$$STFT_1(n, 0) = x(n).$$

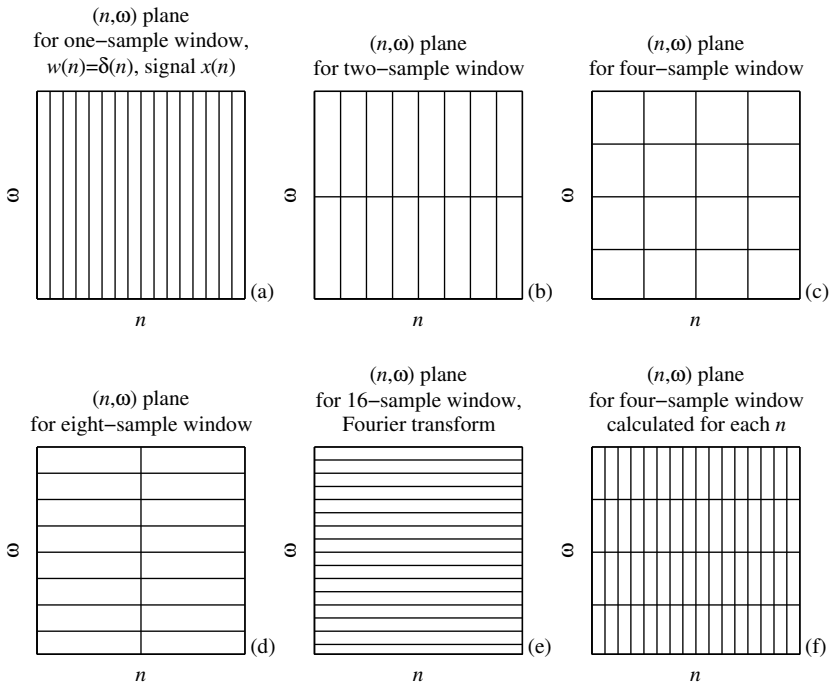


Figure 2.8 Time-frequency plane for a signal $x(n)$ having 16 samples. (a) The STFT of signal $x(n)$ using a one-sample window (note that $STFT(n, k) = x(n)$, for $w(n) = \delta(n)$). (b) The STFT of a signal obtained by using a two-sample window $w(n)$, without overlapping. (c) The STFT of a signal obtained by using a four-sample window $w(n)$, without overlapping. (d) The STFT of a signal obtained by using an eight-sample window $w(n)$, without overlapping. (e) The STFT of signal obtained by using a 16-sample window $w(n)$, without overlapping (note that $STFT(n, k) = X(k)$ for $w(n) = 1$ for all n). (f) The STFT of a signal obtained by using a four-sample window $w(n)$, calculated for each n . Overlapping is present in this case.

There is no information about the frequency content, since the STFT is equal to the signal in the time domain $x(n)$, for the whole frequency range. The whole considered time-frequency plane is divided as in Fig. 2.8(a). Of course, the signal resolution in time is preserved, since the time domain is not transformed.

Let us now consider a two-sample rectangular window, $w_2(m) = \delta(m) + \delta(m+1)$, with $N = 2$. The corresponding two-sample STFT is

$$STFT_2(n, 0) = x(n) + x(n - 1),$$

for $k = 0$ (corresponding to $\omega = 0$) and

$$STFT_2(n, 1) = x(n) - x(n - 1),$$

for $k = 1$ (corresponding to $\omega = \pm\pi$).

The whole frequency interval, in the two-sample window case, is represented by the low-frequency value $STFT_2(n, 0)$ and the high-frequency value $STFT_2(n, 1)$. From the signal reconstruction point of view, we can skip one sample in the STFT calculation and calculate $STFT_2(n + 2, 0) = x(n + 2) + x(n + 1)$ and $STFT_2(n + 2, 1) = x(n + 2) - x(n + 1)$, and so on. It means that $STFT_2(n, k)$ could be downsampled in discrete time n by a factor of 2.

In a matrix form

$$\begin{bmatrix} STFT_2(n, 0) \\ STFT_2(n, 1) \end{bmatrix} = \begin{bmatrix} C_2(n, 0) \\ C_2(n, 1) \end{bmatrix} = \begin{bmatrix} 1 & 1 \\ 1 & -1 \end{bmatrix} \begin{bmatrix} x(n) \\ x(n - 1) \end{bmatrix}, \quad (2.46)$$

where we introduced the notation $C_2(n, k) = STFT_2(n, k)$. The reason to introduce the notation $C_N(n, k)$ will be explained later, since starting with the proper two-sample STFT, the final result, after we continue to split the time-frequency plane in this way, will not correspond to a proper STFT.

If we assume that the signal samples $[x(0), x(1), x(2), x(3), \dots, x(N - 1)]$ at N instants are available, then, according to (2.46), the values $[C_2(1, k), C_2(3, k), \dots, C_2(N - 1, k)]$, for $k \in \{0, 1\}$, can be calculated, at instants $n = 1, 3, \dots, N - 1$. The transformation matrix is

$$\mathbf{T}_2 = \begin{bmatrix} 1 & 1 \\ 1 & -1 \end{bmatrix}. \quad (2.47)$$

The signal reconstruction, in this case, is based on

$$\begin{bmatrix} x(n) \\ x(n - 1) \end{bmatrix} = \frac{1}{2} \begin{bmatrix} C_2(n, 0) + C_2(n, 1) \\ C_2(n, 0) - C_2(n, 1) \end{bmatrix} = \mathbf{T}_2^{-1} \begin{bmatrix} C_2(n, 0) \\ C_2(n, 1) \end{bmatrix},$$

where $C_2(n, k) = STFT_2(n, k)$ is calculated for every other n . In the time-frequency plane, the time resolution is now $2\Delta t$ corresponding to two samples, and the whole frequency interval is divided into two parts (lowpass and highpass), corresponding to Fig. 2.8(b).

In this way, we can proceed and divide the lowpass part of the two-sample STFT into two frequency regions. In the first step, we divide the whole frequency

range into the lower and higher part, by summing and subtracting two adjacent samples, respectively. In order to split

$$C_2(n,0) = STFT_2(n,0) = x(n) + x(n-1), \quad (2.48)$$

into its low-frequency and high-frequency part, we will use its neighboring sample

$$C_2(n-2,0) = STFT_2(n-2,0) = x(n-2) + x(n-3).$$

The lowpass part of $C_2(n,0)$ and $C_2(n-2,0)$ will be calculated by summing their values,

$$C_2(n,0) + C_2(n-2,0) = x(n) + x(n-1) + x(n-2) + x(n-3),$$

while the highpass part of $C_2(n,0)$ and $C_2(n-2,0)$ is obtained by calculating its difference

$$C_2(n,0) - C_2(n-2,0) = x(n) + x(n-1) - (x(n-2) + x(n-3)).$$

Here, four samples of a signal are used in the calculation, so the window width index will be 4,

$$\begin{aligned} C_4(n,0) &= C_2(n,0) + C_2(n-2,0) \\ C_4(n,1) &= C_2(n,0) - C_2(n-2,0), \end{aligned}$$

or in matrix form

$$\begin{bmatrix} C_4(n,0) \\ C_4(n,1) \end{bmatrix} = \begin{bmatrix} 1 & 1 \\ 1 & -1 \end{bmatrix} \begin{bmatrix} C_2(n,0) \\ C_2(n-2,0) \end{bmatrix}. \quad (2.49)$$

For the four-sample transform coefficients, we will not use the STFT notation, since they are not equal to the four-sample STFT values.

The same procedure is applied for the highpass part of the two-sample-based transform

$$C_2(n,1) = STFT_2(n,1) = x(n) - x(n-1) \quad (2.50)$$

and its neighboring sample

$$C_2(n-2,1) = STFT_2(n-2,1) = x(n-2) - x(n-3)$$

to obtain its lowpass and highpass part, as

$$\begin{aligned} C_4(n,2) &= C_2(n,1) + C_2(n-2,1) \\ C_4(n,3) &= C_2(n,1) - C_2(n-2,1) \end{aligned}$$

or

$$\begin{bmatrix} C_4(n,2) \\ C_4(n,3) \end{bmatrix} = \begin{bmatrix} 1 & 1 \\ 1 & -1 \end{bmatrix} \begin{bmatrix} C_2(n,1) \\ C_2(n-2,1) \end{bmatrix}. \quad (2.51)$$

Let us summarize the notation for the four-sample transform. Here $C_4(n,0)$ is used for the lowpass part of the lowpass region of two-sample transforms, while $C_4(n,1)$ denotes the highpass part of the lowpass region of two-sample transforms. By $C_4(n,2)$ and $C_4(n,3)$ low and high parts of the highpass region of two-sample transforms are denoted, respectively. In this way, we divide the frequency range into four parts and the transform C_4 can be downsampled in time by 4 (time resolution corresponding to four sampling intervals). The order of regions in frequency is low-low, low-high, high-low, and high-high. The illustration is given in Fig. 2.8(c).

The transformation matrix, for the case of four-sample transform, is obtained by joining the matrix forms (2.49) and (2.51) into the notation

$$\begin{bmatrix} C_4(n,0) \\ C_4(n,1) \\ C_4(n,2) \\ C_4(n,3) \end{bmatrix} = \left[\begin{array}{c|c} \begin{bmatrix} 1 & 1 \\ 1 & -1 \end{bmatrix} \begin{bmatrix} C_2(n,0) \\ C_2(n-2,0) \end{bmatrix} & \\ \hline \cdots & \\ \begin{bmatrix} 1 & 1 \\ 1 & -1 \end{bmatrix} \begin{bmatrix} C_2(n,1) \\ C_2(n-2,1) \end{bmatrix} & \end{array} \right]. \quad (2.52)$$

By replacing the values of transforms C_2 with signal values, we get the transformation equation

$$\begin{bmatrix} C_4(n,0) \\ C_4(n,1) \\ C_4(n,2) \\ C_4(n,3) \end{bmatrix} = \begin{bmatrix} 1 & 1 & 1 & 1 \\ 1 & 1 & -1 & -1 \\ 1 & -1 & 1 & -1 \\ 1 & -1 & -1 & 1 \end{bmatrix} \begin{bmatrix} x(n) \\ x(n-1) \\ x(n-2) \\ x(n-3) \end{bmatrix} = \mathbf{T}_4 \begin{bmatrix} x(n) \\ x(n-1) \\ x(n-2) \\ x(n-3) \end{bmatrix}, \quad (2.53)$$

with the transformation matrix \mathbf{T}_4 .

This analysis may be continued, until we split the frequency region into M intervals, and downsample the STFT in time by a factor of M , that is, until the spectral content with resolution 1 is produced, without any time-resolution (time resolution is equal to the whole considered time interval, Fig. 2.8(d-e)).

For example, the next step would be in grouping two four-sample transforms into an eight-sample-based analysis. The transformation equation in the case of eight samples is

$$\begin{bmatrix} C_8(n,0) \\ C_8(n,1) \\ C_8(n,2) \\ C_8(n,3) \\ C_8(n,4) \\ C_8(n,5) \\ C_8(n,6) \\ C_8(n,7) \end{bmatrix} = \begin{bmatrix} 1 & 1 & 1 & 1 & 1 & 1 & 1 & 1 \\ 1 & 1 & 1 & 1 & -1 & -1 & -1 & -1 \\ 1 & 1 & -1 & -1 & 1 & 1 & -1 & -1 \\ 1 & 1 & -1 & -1 & -1 & -1 & 1 & 1 \\ 1 & -1 & 1 & -1 & 1 & -1 & 1 & -1 \\ 1 & -1 & 1 & -1 & -1 & 1 & -1 & 1 \\ 1 & -1 & -1 & 1 & 1 & -1 & -1 & 1 \\ 1 & -1 & -1 & 1 & -1 & 1 & 1 & -1 \end{bmatrix} \begin{bmatrix} x(n) \\ x(n-1) \\ x(n-2) \\ x(n-3) \\ x(n-4) \\ x(n-5) \\ x(n-6) \\ x(n-7) \end{bmatrix} = \mathbf{T}_8 \begin{bmatrix} x(n) \\ x(n-1) \\ x(n-2) \\ x(n-3) \\ x(n-4) \\ x(n-5) \\ x(n-6) \\ x(n-7) \end{bmatrix}, \quad (2.54)$$

with the transformation matrix \mathbf{T}_8 .

In this way, although we started from a two-point DFT, in splitting the time-frequency plane, at the end, we did not obtain the Fourier transform of a signal, but a form of the Hadamard transform. That is why we stopped using the standard STFT notation after the two-sample case. However, in ordering the coefficients (matrix rows) in our example, we followed here the frequency region order from the Fourier domain (for example, in the four-sample case, low-low, low-high, high-low, and high-high region). In the Hadamard transformation case, the order of coefficients (order or transformation matrix rows) is different. In our notation, the Hadamard transform would correspond to the following coefficient order

$$[C_4(n,0), C_4(n,2), C_4(n,1), C_4(n,3)]^T$$

in the four-sample case and

$$[C_8(n,0), C_8(n,4), C_8(n,2), C_8(n,6), C_8(n,1), C_8(n,5), C_8(n,3), C_8(n,7)]^T$$

in the eight-sample case.

Example 2.10. Consider a signal of $N = 8$ samples. Its various transforms are calculated, according to the previous scheme, for different time and frequency ranges. It has been found that the signal could be represented by $C_2(1,0) = 1$, $C_4(7,1) = 2$, $C_8(7,6) = 1/2$, and 0 elsewhere in the time-frequency domain (Fig. 2.9). Calculate the signal values.

★Given transform values, written by using the signal values, are

$$C_2(1,0) = x(1) + x(0) = 1$$

$$C_4(7,1) = x(7) + x(6) - x(5) - x(4) = 2$$

$$C_8(7,6) = x(7) - x(6) - x(5) + x(4) + x(3) - x(2) - x(1) + x(0) = 1/2.$$

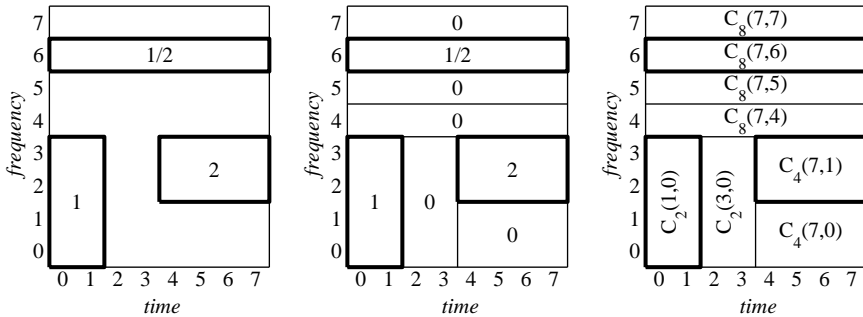


Figure 2.9 Values of the signal transform in the time-frequency plane.

Now we have to add condition that the signal transform is 0 in the remaining regions of the time-frequency plane. We have to cover the rest of the time frequency plane in an appropriate way,

$$\begin{aligned}
 C_8(7,7) &= x(7) - x(6) - x(5) + x(4) - x(3) + x(2) + x(1) - x(0) = 0 \\
 C_8(7,5) &= x(7) - x(6) + x(5) - x(4) - x(3) + x(2) - x(1) + x(0) = 0 \\
 C_8(7,4) &= x(7) - x(6) + x(5) - x(4) + x(3) - x(2) + x(1) - x(0) = 0 \\
 C_2(3,0) &= x(3) + x(2) = 0 \\
 C_4(7,0) &= x(7) + x(6) + x(5) + x(4) = 0.
 \end{aligned}$$

The transform matrix \mathbf{T} , for this case, and the matrix of free coefficients \mathbf{B} are

$$\mathbf{T} = \begin{bmatrix} 1 & 1 & 0 & 0 & 0 & 0 & 0 & 0 \\ 0 & 0 & 0 & 0 & -1 & -1 & 1 & 1 \\ 1 & -1 & -1 & 1 & 1 & -1 & -1 & 1 \\ -1 & 1 & 1 & -1 & 1 & -1 & -1 & 1 \\ 1 & -1 & 1 & -1 & -1 & 1 & -1 & 1 \\ -1 & 1 & -1 & 1 & -1 & 1 & -1 & 1 \\ 0 & 0 & 1 & 1 & 0 & 0 & 0 & 0 \\ 0 & 0 & 0 & 0 & 1 & 1 & 1 & 1 \end{bmatrix}, \quad \mathbf{B} = \begin{bmatrix} 1 \\ 2 \\ 0.5 \\ 0 \\ 0 \\ 0 \\ 0 \\ 0 \end{bmatrix}.$$

The signal is calculated as $\mathbf{x} = \mathbf{T}^{-1}\mathbf{B}$. The signal values are

$$\begin{aligned}
 & [x(0) \quad x(1) \quad x(2) \quad x(3) \quad x(4) \quad x(5) \quad x(6) \quad x(7)]^T \\
 & = \frac{1}{8} [4 \quad 4 \quad 0 \quad 0 \quad -3 \quad -5 \quad 3 \quad 5]^T.
 \end{aligned}$$

□

Example 2.11. Consider a signal of $N = 8$ samples. We know that its various STFT transforms are calculated by using the STFT definition, for different nonoverlapping time and frequency ranges, by using the rectangular window. It has been found that $STFT_2(3, 1) = 1$, $STFT_4(7, 3) = 2$, $STFT_1(0, 0) = 1/2$, and 0 elsewhere in the time-frequency domain. Calculate the signal values. Note that the STFT definition is used here and not the previously derived coefficients, corresponding to a modified Hadamard form.

★Given the STFT values (2.45), as functions of the signal samples, are

$$\begin{aligned} STFT_2(3, 1) &= \sum_{m=0}^1 x(n-m)e^{j2\pi m/2} = x(3) - x(2) = 1 \\ STFT_4(7, 3) &= \sum_{m=0}^3 x(n-m)e^{j2\pi m3/4} = x(7) - jx(6) - x(5) + jx(4) = 2 \\ STFT_1(0, 0) &= \sum_{m=0}^0 x(n-m)e^{j2\pi 0/1} = x(0) = 1/2. \end{aligned}$$

Now we have to add the condition that the transform values, in other parts of the time-frequency plane, are 0. Thus, the rest of the time frequency plane should be covered by 0 values, in an appropriate way,

$$\begin{aligned} STFT_1(1, 0) &= x(1) = 0 \\ STFT_2(3, 0) &= \sum_{m=0}^1 x(n-m)e^{j2\pi m/2} = x(3) + x(2) = 0 \\ STFT_4(7, 0) &= \sum_{m=0}^3 x(n-m)e^{j2\pi m0/4} = x(7) + x(6) + x(5) + x(4) = 0 \\ STFT_4(7, 1) &= \sum_{m=0}^3 x(n-m)e^{j2\pi m1/4} = x(7) + jx(6) - x(5) - jx(4) = 0 \\ STFT_4(7, 2) &= \sum_{m=0}^3 x(n-m)e^{j2\pi m2/4} = x(7) - x(6) + x(5) - x(4) = 0. \end{aligned}$$

The transform matrix, for this case, is

$$\mathbf{T} = \begin{bmatrix} 0 & 0 & -1 & 1 & 0 & 0 & 0 & 0 \\ 0 & 0 & 0 & 0 & j & -1 & -j & 1 \\ 1 & 0 & 0 & 0 & 0 & 0 & 0 & 0 \\ 0 & 1 & 0 & 0 & 0 & 0 & 0 & 0 \\ 0 & 0 & 1 & 1 & 0 & 0 & 0 & 0 \\ 0 & 0 & 0 & 0 & 1 & 1 & 1 & 1 \\ 0 & 0 & 0 & 0 & -j & -1 & j & 1 \\ 0 & 0 & 0 & 0 & -1 & 1 & -1 & 1 \end{bmatrix}. \quad (2.55)$$

For easier inversion, it can be rearranged into

$$\mathbf{T} = \begin{bmatrix} 1 & 0 & 0 & 0 & 0 & 0 & 0 & 0 \\ 0 & 1 & 0 & 0 & 0 & 0 & 0 & 0 \\ 0 & 0 & 1 & 1 & 0 & 0 & 0 & 0 \\ 0 & 0 & -1 & 1 & 0 & 0 & 0 & 0 \\ 0 & 0 & 0 & 0 & 1 & 1 & 1 & 1 \\ 0 & 0 & 0 & 0 & j & -1 & -j & 1 \\ 0 & 0 & 0 & 0 & -j & -1 & j & 1 \\ 0 & 0 & 0 & 0 & -1 & 1 & -1 & 1 \end{bmatrix}, \quad \mathbf{B} = \begin{bmatrix} 0.5 \\ 0 \\ 0 \\ 1 \\ 0 \\ 2 \\ 0 \\ 0 \end{bmatrix}.$$

The signal values are calculated as $\mathbf{x} = \mathbf{T}^{-1}\mathbf{B}$, with \mathbf{B} as in the previous example,

$$\begin{aligned} & [x(0) \quad x(1) \quad x(2) \quad x(3) \quad x(4) \quad x(5) \quad x(6) \quad x(7)]^T \\ &= [1/2 \quad 0 \quad -1/2 \quad 1/2 \quad -j/2 \quad -1/2 \quad j/2 \quad 1/2]^T. \end{aligned}$$

□

In general, we may split the original signal into K signals of duration N : $x_1(n)$ for $n = 0, 1, 2, \dots, N-1$, $x_2(n)$ for $n = N, N+1, \dots, 2N-1$, and so on until $x_K(n)$ for $n = (K-1)N, (K-1)N+1, \dots, KN-1$. Obviously by each signal $x_i(n)$ we cover N samples in time, with corresponding STFT covering N samples of the whole frequency interval.

This case corresponds to the STFT calculation with a filter bank (Fig. 2.7). It may be followed by the STFT downsampling by a factor of N , that is, after $STFT(n, k)$ is calculated for each k , the next time instant for the STFT calculation is $n+N$, and so on.

The second special case is the Fourier transform of the whole signal, $X(k)$, $k = 0, 1, 2, \dots, M$. It contains M frequency points, but there is no time resolution, since it is calculated over the entire time interval (Fig. 2.8(e)). Now we can do the same analysis by using the signal's Fourier transform $X(k)$, $k = 0, 1, 2, \dots, M$, and using the STFT definition in the frequency domain. We may group its two values and calculate the low-time and high-time part of the time-frequency plane, with a two-sample window in the frequency direction. It would correspond to splitting the signal into two parts, $x_1(n)$ for $n = 0, 1, 2, \dots, M/2-1$ and $x_2(n)$ for $n = M/2, M/2+1, \dots, M-1$ (low-time and high-time intervals). By calculating the Fourier transform of $x_1(n)$ we get half of the frequency samples within the whole frequency interval. In the time domain, these samples correspond to the half of the original signal duration, that is, to the lower time interval $n = 0, 1, 2, \dots, M/2-1$. The same holds for signal $x_2(n)$ (Fig. 2.8(d)). In this way, we may continue and split the signal into four parts (Fig. 2.8(c)).

2.3.3.1 Time-Varying Window Case

In the time-frequency analysis we can use windows of different widths for different time instants. In this case window width changes in time, but for one time instant the same window is used for all frequency ranges. Assume that we use the window width N_0 for the instant $n = N_0 - 1$ and calculate the STFT (in notation (2.45)),

$$\begin{aligned} STFT_{N_0}(N_0 - 1, k) &= \sum_{m=0}^{N_0-1} x(N_0 - 1 - m) e^{j2\pi mk/N_0} \\ \mathbf{STFT}_{N_0}(N_0 - 1) &= \mathbf{W}_{N_0} \mathbf{x}_{N_0}(N_0 - 1). \end{aligned} \quad (2.56)$$

where $\mathbf{STFT}_{N_0}(N_0 - 1)$ and $\mathbf{x}_{N_0}(N_0 - 1)$ are the vectors

$$\begin{aligned} \mathbf{STFT}_{N_0}(N_0 - 1) &= [STFT_{N_0}(N_0 - 1, 0), \dots, STFT_{N_0}(N_0 - 1, N_0 - 1)]^T \\ \mathbf{x}_{N_0}(N_0 - 1) &= [x(N_0 - 1), x(N_0 - 2), \dots, x(0)]^T \end{aligned}$$

and \mathbf{W}_{N_0} is the conjugated $N_0 \times N_0$ DFT matrix. Then, in nonoverlapping case, we skip N_1 signal samples and use next window of N_1 width to calculate

$$\begin{aligned} \mathbf{STFT}_{N_1}(N_0 + N_1 - 1) &= \mathbf{W}_{N_1} \mathbf{x}_{N_1}(N_0 + N_1 - 1), \\ \mathbf{x}_{N_1}(N_0 + N_1 - 1) &= [x(N_0 + N_1 - 1), x(N_0 + N_1 - 2), \dots, x(N_0)]^T \end{aligned} \quad (2.57)$$

and so on, until the last one

$$\mathbf{STFT}_{N_K}(M - 1) = \mathbf{W}_{N_K} \mathbf{x}_{N_K}(M - 1)$$

is calculated. In full matrix form, we can write

$$\begin{bmatrix} \mathbf{STFT}_{N_0}(N_0 - 1) \\ \mathbf{STFT}_{N_1}(N_0 + N_1 - 1) \\ \vdots \\ \mathbf{STFT}_{N_K}(M - 1) \end{bmatrix} = \begin{bmatrix} \mathbf{W}_{N_0} & \mathbf{0} & \cdots & \mathbf{0} \\ \mathbf{0} & \mathbf{W}_{N_1} & \cdots & \mathbf{0} \\ \vdots & \vdots & \ddots & \vdots \\ \mathbf{0} & \mathbf{0} & \cdots & \mathbf{W}_{N_K} \end{bmatrix} \begin{bmatrix} x(0) \\ x(1) \\ \vdots \\ x(M - 1) \end{bmatrix}. \quad (2.58)$$

Example 2.12. The STFT of a signal with 16 samples is calculated by a four-sample window at the beginning (covering the first four time samples, $x(0), x(1), x(2), x(3)$). Then two one-sample windows STFTs (covering the next two time samples, $x(4)$ and

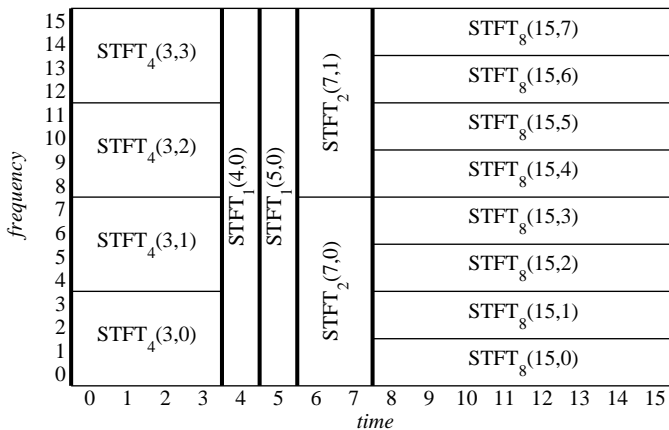


Figure 2.10 An example of time-frequency grid with a time-varying window

$x(5)$) are calculated, followed by one two-sample window STFT, and with an eight-sample window-based STFT, at the end. Show the time-frequency plane structure in this case.

★The STFT calculation, with a time-varying window width ($N = 4$, for $n = 0, 1, 2, 3$, followed by $N = 1$ for $n = 4$ and $n = 5$, then $N = 2$ for $n = 6, 7$, and finally $N = 8$ for $n = 8, 9, 10, 11, 12, 13, 14, 15$) is presented in Fig. 2.10. □

In this way we have covered the whole time-frequency plane. Since the STFT are calculated only at $n = 3, 4, 5, 7$, and 15 , if we want to estimate a signal parameter, at each time instant n , based on the STFT, the remaining instants should be interpolated. The natural interpolation way would be to calculate the STFT for the rest of instants, as well with an appropriate window (overlapped windows, as in the analysis that follows). If we want to keep all STFTs with same number of samples in frequency, then we could zero pad all windows up the widest window width.

2.3.3.2 Frequency-Varying Window Case

The simplest way to explain the frequency-varying window-based STFT calculation scheme is to calculate the Fourier transform of the signal $X(k) = \text{DFT}\{x(n)\}$ and

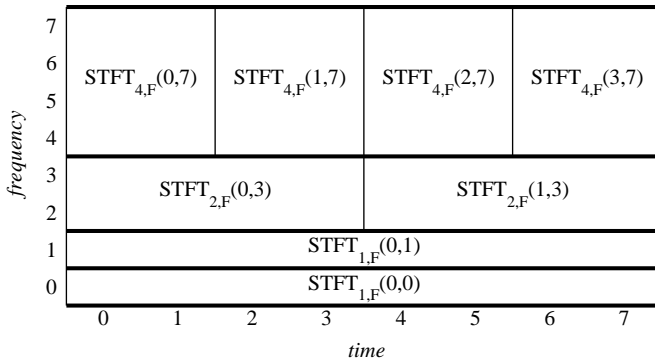


Figure 2.11 An example of a time-frequency grid with a frequency-varying window.

to use the frequency-domain STFT definition, with a frequency-domain window, (2.9),

$$\begin{aligned} STFT_{N,F}(n,k) &= \frac{1}{N} \sum_{i=k-N+1}^k X(i) W_N(k-i) e^{j2\pi i n/N} \\ &= \frac{1}{N} \sum_{i=0}^{N-1} X(k-i) W_N(i) e^{j2\pi(k-i)n/N}. \end{aligned}$$

It is important to note that here, for the localization in the frequency domain, we use window forms similar to those in the time domain, not the Fourier transforms of the lag windows. In this case, for a given frequency point, all time ranges are calculated with the same frequency-domain window (Fig. 2.11).

For example, with a signal with $M = 8$ samples, we may calculate the Fourier transform $X(k)$ and then calculate the STFT along the frequency axis.

We will illustrate this calculation by an example with two one-sample frequency-domain windows in the STFTs first, then by using one two-sample frequency-domain window, followed by a four-sample window-based STFT calculation. Such a calculation scheme is presented in Fig. 2.11.

We added the subscript F to the window width to indicate and emphasize again that a frequency-domain window is used in the STFT calculation.

The STFT values in this case are

$$\begin{aligned}
 STFT_{1,F}(0,0) &= X(0) \\
 STFT_{1,F}(0,1) &= X(1) \\
 STFT_{2,F}(0,3) &= X(2)/2 + X(3)/2 \\
 STFT_{2,F}(1,3) &= X(2)/2 - X(3)/2 \\
 STFT_{4,F}(0,7) &= X(4)/4 + X(5)/4 + X(6)/4 + X(7)/4 \\
 STFT_{4,F}(1,7) &= X(4)/4 + jX(5)/4 - X(6)/4 - jX(7)/4 \\
 STFT_{4,F}(2,7) &= X(4)/4 - X(5)/4 + X(6)/4 - X(7)/4 \\
 STFT_{4,F}(3,7) &= X(4)/4 - jX(5)/4 - X(6)/4 + jX(7)/4
 \end{aligned}$$

Example 2.13. Consider a signal of $N = 8$ samples. We know that its various STFT transforms are calculated by using the STFT definition in the frequency domain, for different nonoverlapping time and frequency ranges, by using the rectangular frequency-domain window, $W_N(i) = 1$ for $i = 0, 1, \dots, N - 1$. It has been found that $STFT_{4,F}(3,7) = 1$, $STFT_{2,F}(1,3) = 2$ and $STFT_{1,F}(0,1) = 1/2$. Calculate the signal values.

Hint: Since the STFT definition in the frequency domain is used (its version (2.5)), calculate the signal's Fourier transform values $X(k)$ first.

★Given the STFT values, as functions of signal's Fourier transform samples, the transformation matrix is

$$\begin{bmatrix} STFT_{1,F}(0,0) \\ STFT_{1,F}(0,1) \\ STFT_{2,F}(0,3) \\ STFT_{2,F}(1,3) \\ STFT_{4,F}(0,7) \\ STFT_{4,F}(1,7) \\ STFT_{4,F}(2,7) \\ STFT_{4,F}(3,7) \end{bmatrix} = \frac{1}{4} \begin{bmatrix} 4 & 0 & 0 & 0 & 0 & 0 \\ 0 & 4 & 0 & 0 & 0 & 0 \\ 0 & 0 & 2 & 2 & 0 & 0 \\ 0 & 0 & 0 & 2 & -2 & 0 \\ 0 & 0 & 0 & 0 & 1 & 1 \\ 0 & 0 & 0 & 0 & 1 & j \\ 0 & 0 & 0 & 0 & 1 & -1 \\ 0 & 0 & 0 & 0 & 1 & -j \end{bmatrix} \begin{bmatrix} X(0) \\ X(1) \\ X(2) \\ X(3) \\ X(4) \\ X(5) \\ X(6) \\ X(7) \end{bmatrix} = \begin{bmatrix} 0 \\ 1/2 \\ 0 \\ 2 \\ 0 \\ 0 \\ 0 \\ 1 \end{bmatrix}.$$

The Fourier transform values are

$$\begin{aligned}
 & [X(0) \quad X(1) \quad X(2) \quad X(3) \quad X(4) \quad X(5) \quad X(6) \quad X(7)]^T \\
 & = [0 \quad 0.5 \quad 2 \quad -2 \quad 1 \quad j \quad -1 \quad -j]^T,
 \end{aligned}$$

with the signal $x(n)$ being its inverse Fourier transform,

$$\begin{aligned}
 & [x(0) \quad x(1) \quad x(2) \quad x(3) \quad x(4) \quad x(5) \quad x(6) \quad x(7)]^T \\
 & = [0.0625 \quad 0.096 \quad -0.25 \quad -0.346 \quad 0.4375 \quad -0.346 \quad 0.25 \quad 0.096]^T \\
 & + j [0 \quad 0.0656 \quad 0.3125 \quad -0.3308 \quad 0 \quad 0.6844 \quad -0.3125 \quad -0.4192]^T.
 \end{aligned}$$

□

We may easily write a matrix form for the frequency varying windows, corresponding to (2.58) in the frequency domain.

2.3.3.3 General Hybrid Time-Frequency Grid

A time-frequency representation may combine time-varying and frequency-varying windows, for some time-frequency regions. Then this is a hybrid time-frequency grid. We still consider the nonoverlapping cases, only. We used this scheme in the first example illustrating lattice structure of the time-frequency plane. If we consider a signal with M samples, then its time-frequency plane can be split in a large number of different grids for the nonoverlapping STFT calculation. All possible variations of time-varying or frequency-varying windows are just special cases of general hybrid time-frequency varying grid. Covering a time-frequency $M \times M$ plane, by any combination of nonoverlapping rectangular areas, whose individual area is M , corresponds to a valid nonoverlapping STFT calculation scheme. The total number of ways $F(M)$, how an $M \times M$ plane can be split (into nonoverlapping STFTs of area M), is

M	1	4	6	8	12	14	16	...
$F(M)$	1	6	18	56	542	1690	5272	

The approximative formula for $F(M)$ can be written in the form, (see Problem 2.17)

$$F(M) \approx \lfloor 1.0366(1.7664)^{M-1} \rfloor, \quad (2.59)$$

where $\lfloor \cdot \rfloor$ stands for an integer part of the argument. It holds with relative error smaller than 0.4% for $1 \leq M \leq 1024$. For example, for $M = 16$ we have 5272 different ways to split the time-frequency plane into nonoverlapping time-frequency regions. Of course, most of them cannot be considered within the either time-varying or frequency-varying-only case, since they are time-frequency varying (hybrid) in general.

2.3.3.4 Overlapping in Time-Frequency Plane

Signal can be reconstructed from the STFT calculated with N signal samples, if the calculated STFT is downsampled in time by $R \leq N$. If the window used in the STFT is the Hamming window (or similar), then the signal values close to the ending

points of window are multiplied by small window values. They may be unreliable for the reconstruction. When $R = N/2$, we may use the reconstructed signal values from two adjacent windows (and combine them).

Here the signal general reconstruction scheme from the STFT values, overlapped in time, will be presented. Consider the STFT, (2.40), written in a vector form, as

$$\begin{aligned} STFT(n, k) &= \sum_{m=-N/2}^{N/2-1} w(m)x(n+m)e^{-j2\pi mk/N} \\ \mathbf{STFT}(n) &= \mathbf{W}_N \mathbf{H}_w \mathbf{x}(n) \end{aligned} \quad (2.60)$$

where the vector $\mathbf{STFT}(n)$ contains all frequency values of the STFT, for a given n ,

$$\mathbf{STFT}(n) = [STFT(n, 0), STFT(n, 1), \dots, STFT(n, N-1)]^T.$$

The signal vector is

$$\mathbf{x}(n) = [x(n-N/2), x(n-N/2+1), \dots, x(n+N/2-1)]^T,$$

while \mathbf{W}_N is the DFT matrix with coefficients $W(n, k) = e^{-j2\pi nk/N}$. A diagonal matrix \mathbf{H}_w is the window matrix $H_w(m, m) = w(m)$ and $H(m, l) = 0$ for $m \neq l$.

It has been assumed that the STFTs are calculated with a step $1 \leq R \leq N$ in time. So they are overlapped for $R < N$. Available STFT values are

$$STFT(n + iR, k) = \sum_{m=-N/2}^{N/2-1} w(m)x(n + iR + m)e^{-j2\pi mk/N}$$

or in vector form

$$\begin{aligned} &\dots \\ \mathbf{STFT}(n - 2R), \\ \mathbf{STFT}(n - R), \\ \mathbf{STFT}(n), \\ \mathbf{STFT}(n + R), \\ \mathbf{STFT}(n + 2R), \\ &\dots \end{aligned}$$

Based on the available STFT values (2.60), the windowed signal values can be reconstructed as

$$w(m)x(n+iR+m) = \frac{1}{N} \sum_{k=-N/2}^{N/2-1} STFT(n+iR, k) e^{j2\pi mk/N}$$

for $m = -N/2, -N/2 + 1, \dots, N/2 - 1$, or in vector form

$$\mathbf{H}_w \mathbf{x}(n+iR) = \mathbf{W}_N^{-1} \mathbf{STFT}(n+iR), \quad i = \dots -2, -1, 0, 1, 2, \dots$$

Let first reindex the reconstructed signal values by substitution $m = l - iR$

$$w(l-iR)x(n+l) = \frac{1}{N} \sum_{k=-N/2}^{N/2-1} STFT(n+iR, k) e^{j2\pi lk/N} e^{-j2\pi iRk/N}$$

$$-N/2 \leq l - iR \leq N/2 - 1.$$

By summing over i satisfying $-N/2 \leq l - iR \leq N/2 - 1$ we get that the signal is undistorted if

$$\begin{aligned} \sum_i w(l-iR)x(n+l) &= \text{const} \cdot x(n+l) \\ c(l) &= \sum_i w(l-iR) = \text{const} \\ -N/2 &\leq l - iR \leq N/2 - 1. \end{aligned} \tag{2.61}$$

Special cases:

1. For $R = N$ (nonoverlapping), relation (2.61) is satisfied for the rectangular window only.
2. For a half of the overlapping period, $R = N/2$, condition (2.61) is met for the rectangular, Hann(ing), Hamming, and triangular windows.
3. The same holds for $R = N/2, N/4, N/8$, if the values of R are integers.
4. For $R = 1$ (the STFT calculation in each available time instant), any window satisfies the inversion relation.

The illustration of overlapping windows is presented in Fig. 2.12, for a half of the window width (top) and for a fourth of the window width (bottom).

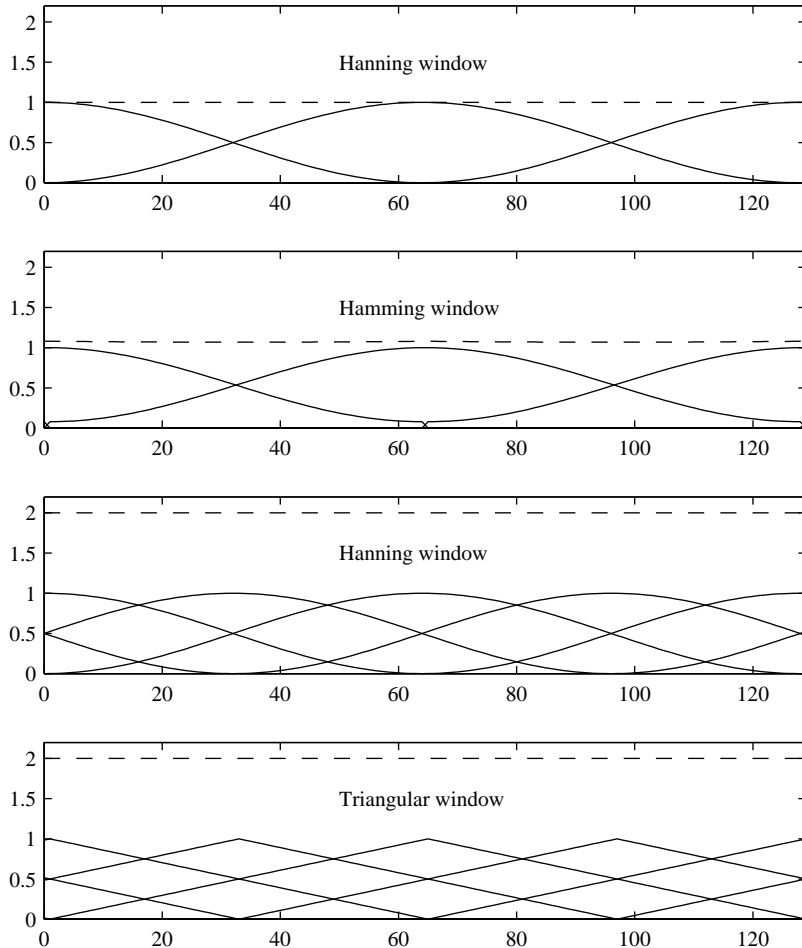


Figure 2.12 Equivalent inversion window $c(l)$ in the cases of the Hann(ing), Hamming, and triangular windows, overlapping for half of the width (top two) and a fourth of the width (bottom two). The dotted line is the value of $c(l)$.

In analysis of nonstationary signals, our primary interest is not in signal reconstruction with the fewest number of calculation points. We are interested in tracking signals' nonstationary parameters, for example, instantaneous frequency. These parameters may significantly vary between neighboring time instants n and $n + 1$. Quasi-stationarity of signal within R samples (implicitly assumed when downsampling by factor of R is done) in this case is not a good starting point for the analysis. Here we have to use the time-frequency analysis of signal at each instant n without any downsampling. Very efficient realizations, for this case, are the recursive ones.

2.4 GABOR TRANSFORM

The Gabor transform is the oldest time-frequency form applied in the signal processing field (since the Wigner distribution remained for a long time within quantum mechanics only). It has been introduced with the aim to expand a signal $x(t)$ into a series of time-frequency-shifted elementary functions $w(t - nT)e^{jk\Delta\Omega t}$ (logons)

$$x(t) = \sum_{k=-K}^K \sum_{n=-N}^N a(n, k) w(t - nT) e^{jk\Delta\Omega t}. \quad (2.62)$$

The function $w(t)$ is shifted in time as $w(t - nT)$ and in frequency by multiplication with $e^{jk\Delta\Omega t}$. If the original function $w(t)$ is well localized in time and frequency, around $t = 0$ and $\Omega = 0$, the functions $w(t - nT)e^{jk\Delta\Omega t}$ are localized around $t = nT$ and $\Omega = k\Delta\Omega$. The coefficients in (2.62) should follow from the minimization of the mean square error, over time and frequency,

$$I = \int_{-\infty}^{\infty} \left| x(\tau) - \sum_{k=-K}^K \sum_{n=-N}^N a(n, k) w(\tau - nT) e^{jk\Delta\Omega\tau} \right|^2 d\tau$$

as

$$\begin{aligned} \frac{\partial I}{\partial a^*(n, k)} &= 0 \\ \int_{-\infty}^{\infty} \left(x(\tau) - \sum_{l=-K}^K \sum_{m=-N}^N a(m, l) w(\tau - mT) e^{jl\Delta\Omega\tau} \right) w^*(\tau - nT) e^{-jk\Delta\Omega\tau} d\tau &= 0, \end{aligned}$$

resulting in

$$\sum_{l=-K}^K \sum_{m=-M}^M a(m, l) b(n, m, k, l) = c(n, k), \quad (2.63)$$

for $n = -N, \dots, N-1, N$, and $k = -K, \dots, K-1, K$,

with

$$b(n, m, k, l) = \int_{-\infty}^{\infty} w(\tau - mT) e^{jl\Delta\Omega\tau} w^*(\tau - nT) e^{-jk\Delta\Omega\tau} d\tau$$

$$c(n, k) = \int_{-\infty}^{\infty} x(\tau) w^*(\tau - nT) e^{-jk\Delta\Omega\tau} d\tau.$$

The Gabor's original choice was the Gaussian localization function (window)

$$w(\tau) = \exp\left(-\pi \frac{\tau^2}{2T^2}\right),$$

due to its best concentration in the time-frequency plane. Gabor also used $\Delta\Omega = 2\pi/T$.

For the analysis of signal, Gabor has divided the whole information (time-frequency) plane by a grid at $t = nT$ and $\Omega = k\Delta\Omega$, with area of elementary cell $T\Delta\Omega/2\pi = 1$. Then the signal is expanded at the central points of the grid $(nT, k\Delta\Omega)$ by using the elementary atoms $\exp(-\pi(t - nT)^2/(2T^2)) \exp(jk\Delta\Omega t)$.

If the elementary functions $w(\tau - nT) e^{jk\Delta\Omega\tau}$ were orthogonal to each other, that is, if

$$\int_{-\infty}^{\infty} w(\tau - nT) e^{jk\Delta\Omega\tau} w^*(\tau - mT) e^{-jl\Delta\Omega\tau} d\tau = \delta(n-m)\delta(k-l),$$

then we would easily get

$$a(n, k) = \int_{-\infty}^{\infty} x(\tau) w^*(\tau - nT) e^{-jk\Delta\Omega\tau} d\tau, \quad (2.64)$$

which would correspond to the STFT at $t = nT$. However, the elementary logons do not satisfy the orthogonality property. Gabor originally proposed an iterative

procedure for the calculation of $a(n, k)$, having in mind that the inner product in $b(n, m, k, l)$ is small for values of m and n that are not close to each other, as well as, for k and l that are not close.

Interest for the Gabor transform, in its original formulation, had been lost for decades, until a simplified procedure for the calculation of coefficients has been developed. This procedure is based on introducing elementary signal $\gamma(\tau)$ dual to $w(\tau)$ such that

$$\int_{-\infty}^{\infty} w(\tau - nT) e^{jk\Delta\Omega\tau} \gamma^*(\tau - mT) e^{-jl\Delta\Omega\tau} d\tau = \delta(n - m)\delta(k - l) \quad (2.65)$$

holds (Bastiaans logons). Then

$$a(n, k) = \int_{-\infty}^{\infty} x(\tau) \gamma^*(\tau - nT) e^{-jk\Delta\Omega\tau} d\tau. \quad (2.66)$$

However, the dual function $\gamma(\tau)$ has a poor time-frequency localization. In addition, there is no stable algorithm to reconstruct the signal with the critical sampling condition $\Delta\Omega T = 2\pi$. One solution is to use an oversampled set of functions with $\Delta\Omega T < 2\pi$.

2.5 STATIONARY-PHASE METHOD

When a signal

$$x(t) = A(t) e^{j\phi(t)} \quad (2.67)$$

is not of a simple analytic form, it may be possible, in some cases, to obtain an approximative expression for its Fourier transform and the short-time Fourier transform, by using the method of stationary phase.

The method of stationary phase states that if the phase function $\phi(t)$ is monotonous and the amplitude $A(t)$ is sufficiently smooth function, then

$$\int_{-\infty}^{\infty} A(t) e^{j\phi(t)} e^{-j\Omega t} dt \simeq A(t_0) e^{j\phi(t_0)} e^{-j\Omega t_0} \sqrt{\frac{2\pi j}{\phi''(t_0)}}, \quad (2.68)$$

where t_0 is the solution of

$$\phi'(t_0) = \Omega.$$

The most significant contribution to the integral on the left side of (2.68) comes from the region where the phase of the exponential function $\exp(j(\phi(t) - \Omega t))$ is stationary in time, since the contribution of the intervals with fast varying $\phi(t) - \Omega t$ tends to zero. In other words, in the considered time region, the signal's phase $\phi(t)$ behaves as Ωt . Thus, we may say that the rate of the phase change $\phi'(t)$, for that particular instant is its instantaneous frequency corresponding to frequency Ω . The stationary point t_0 of phase $\phi(t) - \Omega t$ (phase of signal $A(t)e^{j\phi(t)}$ demodulated by $e^{-j\Omega t}$) is obtained as a solution of

$$\frac{d(\phi(t) - \Omega t)}{dt} \Big|_{t=t_0} = 0. \quad (2.69)$$

By expanding $\phi(t) - \Omega t$ into a Taylor series up to the second-order term, around the stationary point t_0 , we have

$$\phi(t) - \Omega t \simeq \phi(t_0) - \Omega t_0 + \frac{1}{2} \frac{d^2\phi(t)}{dt^2} \Big|_{t=t_0} (t - t_0)^2.$$

The integral in (2.68) can be written as

$$\int_{-\infty}^{\infty} A(t)e^{j\phi(t)}e^{-j\Omega t} dt \simeq \int_{-\infty}^{\infty} A(t)e^{j(\phi(t_0) - \Omega t_0 + \frac{1}{2}\phi''(t_0)(t - t_0)^2)} dt. \quad (2.70)$$

Using the Fourier transform pair

$$\exp(j\alpha t^2/2) \leftrightarrow \sqrt{\frac{2\pi j}{\alpha}} \exp(-j\Omega^2/(2\alpha)), \quad (2.71)$$

for large $\alpha = \phi''(t_0)$ follows $\text{FT}\{\sqrt{\alpha/(2\pi j)} \exp(j\alpha t^2/2)\} \rightarrow 1$, that is,

$$\lim_{\alpha \rightarrow \infty} \sqrt{\frac{\alpha}{2\pi j}} \exp(j\alpha t^2/2) = \delta(t). \quad (2.72)$$

Relation (2.68) is now easily obtained from (2.70) with (2.72), for large $\phi''(t_0)$.

If the equation $\phi'(t_0) = \Omega$ has two (or more) solutions t_0^+ and t_0^- , then the integral on the left side of (2.68) is equal to the sum of functions at both (or more) stationary phase points. Finally, this relation holds for $\phi''(t_0) \neq 0$. If $\phi''(t_0) = 0$, then similar analysis may be performed, using the lowest nonzero phase derivative at the stationary-phase point.

Example 2.14. Consider a frequency-modulated signal

$$x(t) = \exp(jat^{2N}).$$

Find its Fourier transform approximation by using the stationary-phase method.

★According to the stationary-phase method, we get that the stationary-phase point is $2Nat_0^{2N-1} = \Omega$ with

$$t_0 = \left(\frac{\Omega}{2Na} \right)^{1/(2N-1)}$$

and

$$\phi''(t_0) = 2N(2N-1)a \left(\frac{\Omega}{2Na} \right)^{(2N-2)/(2N-1)}. \quad (2.73)$$

The amplitude and phase of $X(\Omega)$, according to (2.68), are

$$\begin{aligned} |X(\Omega)|^2 &\simeq \left| \frac{2\pi}{\phi''(t_0)} \right| = \left| \frac{2\pi}{(2N-1)\Omega} \left(\frac{\Omega}{2aN} \right)^{1/(2N-1)} \right| \\ \arg \{X(\Omega)\} &\simeq \phi(t_0) - \Omega t_0 + \pi/4 = \frac{(1-2N)}{2N} \Omega \left(\frac{\Omega}{2aN} \right)^{1/(2N-1)} + \pi/4 \end{aligned} \quad (2.74)$$

for a large value of a . The integrand in (2.68) is illustrated in Fig. 2.13, for $N = 1$, when $|X(\Omega)|^2 = |\pi/a|$ and $\arg \{X(\Omega)\} = -\Omega^2/(4a) + \pi/4$. \square

2.6 INSTANTANEOUS FREQUENCY

Here we present a simple instantaneous frequency (IF) interpretation when a signal may be considered as stationary within the localization window (quasi-stationary signal). Consider a signal $x(t) = A(t)e^{j\phi(t)}$ within the window $w(\tau)$ of the width $2T$. If we can assume that the amplitude variations are small and the phase variations are almost linear within $w(\tau)$, that is,

$$\begin{aligned} A(t+\tau) &\simeq A(t) \\ \phi(t+\tau) &\simeq \phi(t) + \phi'(t)\tau, \end{aligned}$$

then

$$x(t+\tau) \simeq A(t)e^{j\phi(t)}e^{j\phi'(t)\tau}.$$

Thus, for a given instant t , the signal behaves as a sinusoid in the τ domain with amplitude $A(t)$, phase $\phi(t)$, and frequency $\phi'(t)$. The first derivative of phase, $\phi'(t)$,

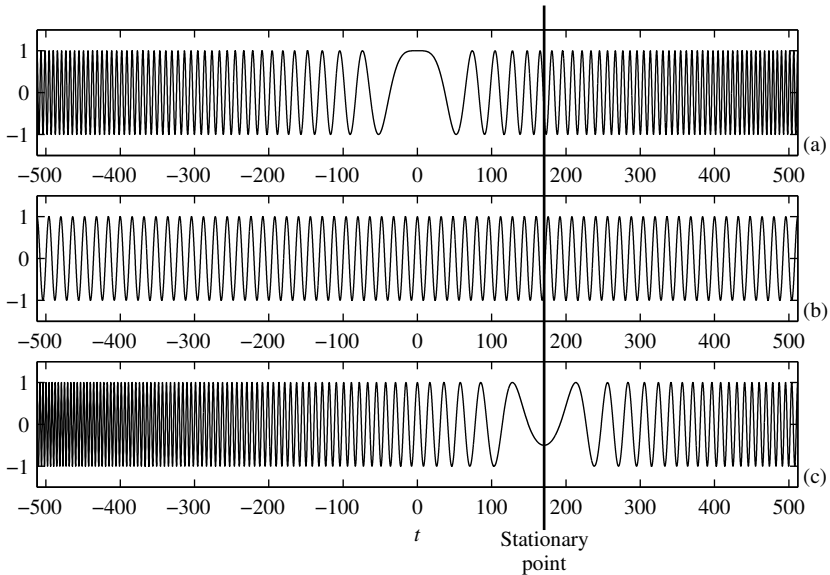


Figure 2.13 Stationary-phase method illustration: (a) real part of linear frequency modulated signal, (b) real part of demodulation signal, and (c) real part of the integrand.

plays the role of frequency within the considered lag interval around t . This is the case when a simple correspondence may be established.

The stationary-phase method relates the signal in the time domain and the spectral content at a frequency Ω in a more sophisticated way. It states that the spectral content at frequency Ω in the Fourier transform of the signal is related to signal's value at time instant t , such that $\phi'(t) = \Omega$. A signal in the time domain that satisfies stationary-phase method conditions, contributes at the considered instant t to the Fourier transform at the corresponding frequency

$$\Omega(t) = \phi'(t). \quad (2.75)$$

It establishes the Fourier transformation pair as

$$A(t)e^{j\phi(t)} \leftrightarrow A(t_0)e^{j\phi(t_0)}e^{-j\Omega t_0} \sqrt{\frac{2\pi j}{\phi''(t_0)}}, \quad \text{with } \phi'(t_0) = \Omega.$$

Additional comments on this relation are given within the above stationary phase method presentation.

In general, the instantaneous frequency is not so clearly defined as the frequency in the Fourier transform. For example, the frequency in the Fourier transform has the physical interpretation as the number of signal periods within the considered time interval, while this interpretation is not possible if a single time instant is considered. Thus, a significant caution has to be taken in using this notion. Various definitions and interpretations of the instantaneous frequency are given in the literature.

Example 2.15. The STFT of the signal

$$x(t) = e^{jat^2} \quad (2.76)$$

can be approximately calculated for a large a , by using the method of stationary phase. Find its form and the relation for the optimal window width.

★ Applying the stationary-phase method, we get

$$\begin{aligned} STFT(t, \Omega) &= \int_{-\infty}^{\infty} e^{ja(t+\tau)^2} w(\tau) e^{-j\Omega\tau} d\tau \simeq e^{jat^2} e^{j(2at-\Omega)\tau_0} e^{ja\tau_0^2} w(\tau_0) \sqrt{\frac{2\pi j}{2a}} \\ &= e^{jat^2} e^{-j(2at-\Omega)^2/4a} w\left(\frac{\Omega-2at}{2a}\right) \sqrt{\frac{\pi j}{a}} \end{aligned} \quad (2.77)$$

since

$$2a(t + \tau_0) = \Omega.$$

Note that the absolute value of the STFT reduces to

$$|STFT(t, \Omega)| \simeq \left| w\left(\frac{\Omega-2at}{2a}\right) \right| \sqrt{\frac{\pi}{a}}. \quad (2.78)$$

In this case, the width of $|STFT(t, \Omega)|$ in frequency does not decrease with the increase of the window $w(\tau)$ width. The width of $|STFT(\Omega, t)|$ around the central frequency $\Omega = 2at$ is

$$D = 4aT,$$

where $2T$ is the window width in the time domain. Note that this relation holds for a wide window $w(\tau)$ such that the stationary-phase method may be applied. If the window is narrow with respect to the phase variations of the signal, the STFT width is defined by the width of the Fourier transform of window, being proportional to $1/T$. Thus, the overall STFT width is equal to the sum of the frequency variation caused width and the window's Fourier transform width, that is,

$$D_o = 4aT + \frac{2c}{T}, \quad (2.79)$$

where c is a constant defined by the window shape. Therefore, there is a window width T producing the narrowest possible STFT for this signal. It is obtained by equating the derivative of the overall width to zero, $2a - c/T^2 = 0$, which results in

$$T_o = \sqrt{\frac{c}{2a}}. \quad (2.80)$$

As expected, for a sinusoid, $a \rightarrow 0$, $T_o \rightarrow \infty$. This is just an approximation of the optimal window, since for narrow windows we may not apply the stationary-phase method. \square

Example 2.16. Consider a signal

$$x(t) = e^{-t^2} e^{-j6\pi t^2 - j32\pi t} + e^{-4(t-1)^2} e^{j16\pi t^2 + j160\pi t}.$$

Assuming that the values of the signal with amplitudes below $1/e^4$ could be neglected, find the sampling rate for the STFT-based analysis of this signal. Write the approximate spectrogram expression for the Hann(ing) window of $N = 32$ samples in the analysis. What signal will be presented in the time-frequency plane, within the basic frequency period, if the signal is sampled at $\Delta t = 1/128$?

★The time interval, with significant signal content, for the first signal component is $-2 \leq t \leq 2$, with the frequency content within $-56\pi \leq \Omega \leq -8\pi$, since the instantaneous frequency is $\Omega(t) = -12\pi t - 32\pi$. For the second component these intervals are $0 \leq t \leq 2$ and $160\pi \leq \Omega \leq 224\pi$. The maximal frequency in the signal is $\Omega_m = 224\pi$. Here we have to take into account possible spreading of the spectrum caused by the lag window. Its width in the time domain is $2T = N\Delta t = 32\Delta t$. The width of the mainlobe in frequency domain is defined by $32\Omega_w\Delta t = 4\pi$, or $\Omega_w = \pi/(8\Delta t)$. Thus, taking the sampling interval $\Delta t = 1/256$, we will satisfy the sampling theorem condition in the worst instant case, since $\pi/(\Omega_m + \Omega_w) = 1/256$.

In the case of the Hann(ing) window with $N = 32$ and $\Delta t = 1/256$, the lag interval is $N\Delta t = 1/8$. We will assume that the amplitude variations within the window are small, that is, $w(\tau)e^{-(t+\tau)^2} \cong w(\tau)e^{-t^2}$ for $-1/16 < \tau < 1/16$. Then according to the stationary-phase method, we can write the STFT approximation,

$$|STFT(t, \Omega)|^2 = \frac{1}{6} e^{-2t^2} w^2 \left(\frac{\Omega+12\pi t+32\pi}{12\pi} \right) + \frac{1}{32} e^{-8(t-1)^2} w^2 \left(\frac{\Omega-32\pi t-160\pi}{32\pi} \right)$$

with $t = n/256$ and $\Omega = 256\omega$ within $-\pi \leq \omega < \pi$. It has been assumed that the spectrogram is cross-terms free.

In the case of $\Delta t = 1/128$, the signal will be periodically extended with period $2\Omega_0 = 256\pi$. The basic period will be for $-128\pi \leq \Omega < 128\pi$. It means that the first component will remain unchanged within the basic period, while the second component is outside the basic period. However, its replica shifted for one period to

the left, that is, for -256π , will be within the basic period. It will be located within $160\pi - 256\pi \leq \Omega \leq 224\pi - 256\pi$, that is, within $-96\pi \leq \Omega \leq -32\pi$. Thus, the signal represented by the STFT in this case will correspond to

$$x_r(t) = e^{-t^2} e^{-j6\pi t^2 - j32\pi t} + e^{-4(t-1)^2} e^{j16\pi t^2 + j(160-256)\pi t},$$

with approximation,

$$|STFT(t, \Omega)|^2 = \frac{1}{6} e^{-2t^2} w^2 \left(\frac{\Omega + 12\pi t + 32\pi}{12\pi} \right) + \frac{1}{32} e^{-8(t-1)^2} w^2 \left(\frac{\Omega - 32\pi t - 96\pi}{32\pi} \right), \quad (2.81)$$

with $t = n/128$ and $\Omega = 128\omega$ within $-\pi \leq \omega < \pi$ or $-128\pi \leq \Omega < 128\pi$. \square

Consider now a general form of an FM signal

$$x(t) = A e^{j\phi(t)},$$

where $\phi(t)$ is a differentiable function. Its STFT is of the form

$$\begin{aligned} STFT(t, \Omega) &= \int_{-\infty}^{\infty} A e^{j\phi(t+\tau)} w(\tau) e^{-j\Omega\tau} d\tau \\ &= \int_{-\infty}^{\infty} A e^{j(\phi(t) + \phi'(t)\tau + \phi''(t)\tau^2/2 + \dots)} w(\tau) e^{-j\Omega\tau} d\tau \\ &= A e^{j\phi(t)} FT\{e^{j\phi'(t)\tau}\} *_{\Omega} FT\{w(\tau)\} *_{\Omega} FT\left\{\sum_{k=2}^{\infty} e^{j\phi^{(k)}(t)\tau^k/k!}\right\} \end{aligned} \quad (2.82)$$

where $\phi(t+\tau)$ is expanded into the Taylor series around t as

$$\phi(t+\tau) = \phi(t) + \phi'(t)\tau + \phi''(t)\tau^2/2 + \dots + \phi^{(k)}(t)\tau^k/k! + \dots \quad (2.83)$$

Neglecting the higher-order terms in the Taylor series, we can write

$$\begin{aligned} STFT(t, \Omega) &= A e^{j\phi(t)} FT\{e^{j\phi'(t)\tau}\} *_{\Omega} FT\{w(\tau)\} *_{\Omega} FT\{e^{j\phi''(t)\tau^2/2}\} \\ &= 2\pi A e^{j\phi(t)} \delta(\Omega - \phi'(t)) *_{\Omega} W(\Omega) *_{\Omega} e^{-j\Omega^2/(2\phi''(t))} \sqrt{\frac{2\pi j}{\phi''(t)}} \end{aligned}$$

where $*_{\Omega}$ denotes the convolution in frequency. As expected, the influence of the window is manifested as a spread of ideal concentration $\delta(\Omega - \phi'(t))$. In addition, the term due to the frequency nonstationarity $\phi''(t)$ causes an additional spread. This relation confirms our previous conclusion that the overall STFT width can be approximated by the sum of the width of $W(\Omega)$ and the width caused by the signal's nonstationarity.

2.7 LOCAL POLYNOMIAL FOURIER TRANSFORM

There are signals whose form is known up to an unknown set of parameters. For example, many signals could be expressed as polynomial-phase signals

$$x(t) = A e^{j(\Omega_0 t + a_1 t^2 + a_2 t^3 + \dots + a_N t^{N+1})}$$

where the parameters $\Omega_0, a_1, a_2, \dots, a_N$ are unknown. A high concentration of such signals in the frequency domain is achieved by the polynomial Fourier transform defined by

$$PFT_{\Omega_1, \Omega_2, \dots, \Omega_N}(\Omega) = \int_{-\infty}^{\infty} x(t) e^{-j(\Omega t + \Omega_1 t^2 + \Omega_2 t^3 + \dots + \Omega_N t^{N+1})} dt \quad (2.84)$$

when parameters $\Omega_1, \Omega_2, \dots, \Omega_N$ are equal to the signal parameters a_1, a_2, \dots, a_N . Finding values of unknown parameters $\Omega_1, \Omega_2, \dots, \Omega_N$ that match signal parameters can be done by a simple search over a possible set of values for $\Omega_1, \Omega_2, \dots, \Omega_N$ and stopping the search when the maximally concentrated distribution is achieved (in an ideal case, the delta function at $\Omega = \Omega_0$, for $\Omega_1 = a_1, \Omega_2 = a_2, \dots$ is obtained). This procedure may be time-consuming.

For nonstationary signals, this approach may be used if the nonstationary signal could be considered as a polynomial phase signal within the analysis window. In that case, the local polynomial Fourier transform (LPFT), proposed by Katkovnik, may be used. It is defined as

$$LPFT_{\Omega_1, \Omega_2, \dots, \Omega_N}(t, \Omega) = \int_{-\infty}^{\infty} x(t + \tau) w(\tau) e^{-j(\Omega\tau + \Omega_1 \tau^2 + \Omega_2 \tau^3 + \dots + \Omega_N \tau^{N+1})} d\tau. \quad (2.85)$$

In general, parameters $\Omega_1, \Omega_2, \dots, \Omega_N$ could be time dependent, that is, for each time instant t , the set of optimal parameters could be different.

Example 2.17. Consider the second-order polynomial-phase signal

$$x(t) = e^{j(\Omega_0 t + a_1 t^2)}.$$

Show that its LPFT could be completely concentrated along the instantaneous frequency.

★Its LPFT has the form

$$\begin{aligned} LPFT_{\Omega_1}(t, \Omega) &= \int_{-\infty}^{\infty} x(t+\tau)w(\tau)e^{-j(\Omega\tau+\Omega_1\tau^2)}d\tau \\ &= e^{j(\Omega_0 t + a_1 t^2)} \int_{-\infty}^{\infty} w(\tau)e^{-j(\Omega - \Omega_0 - 2a_1 t)\tau}e^{j(\Omega_1 - a_1)\tau^2}d\tau. \end{aligned} \quad (2.86)$$

For $\Omega_1 = a_1$, the second-order phase term does not introduce any distortion to the local polynomial spectrogram,

$$|LPFT_{\Omega_1=a_1}(t, \Omega)|^2 = |W(\Omega - \Omega_0 - 2a_1 t)|^2,$$

with respect to the spectrogram of a sinusoid with constant frequency. For a wide window $w(\tau)$, like in the case of the STFT of a pure sinusoid, we achieve high concentration. \square

Next we will illustrate the LPFT application on a signal with sinusoidal frequency modulation (nonpolynomial phase signal). The LPFTs of the first and second-order, along with the STFT, is presented in Fig. 2.14. The first-order LPFT is presented in Fig. 2.14(c) and it achieves good concentration with small oscillations at points where frequency reaches maximum (or minimum). These oscillations are almost completely removed by the second-order LPFT Fig. 2.14(d). Here the optimal parameters Ω_1 and Ω_2 are time-dependent.

The LPFT could be considered as the Fourier transform of windowed signal demodulated with $\exp(-j(\Omega_1\tau^2 + \Omega_2\tau^3 + \dots + \Omega_N\tau^{N+1}))$. Thus, if we are interested in signal filtering, we can find the coefficients $\Omega_1, \Omega_2, \dots, \Omega_N$, demodulate the signal by multiplying it with $\exp(-j(\Omega_1\tau^2 + \Omega_2\tau^3 + \dots + \Omega_N\tau^{N+1}))$ and use a standard filter for almost a pure sinusoid. In general, we can extend this approach to any signal $x(t) = e^{j\phi(t)}$ by estimating its phase $\phi(t)$ with $\hat{\phi}(t)$ (using the instantaneous frequency estimation that will be discussed later) and filtering demodulated signal $x(t)\exp(-j\hat{\phi}(t))$ by a lowpass filter. The resulting signal is obtained when the filtered signal is returned back to the original frequencies, by modulation with $\exp(j\hat{\phi}(t))$.

The filtering of signal can be modeled by the following expression

$$x_f(t) = \frac{1}{2\pi} \int_{-\infty}^{+\infty} B_t(t, \Omega)LPFT(t, \Omega)d\Omega, \quad (2.87)$$

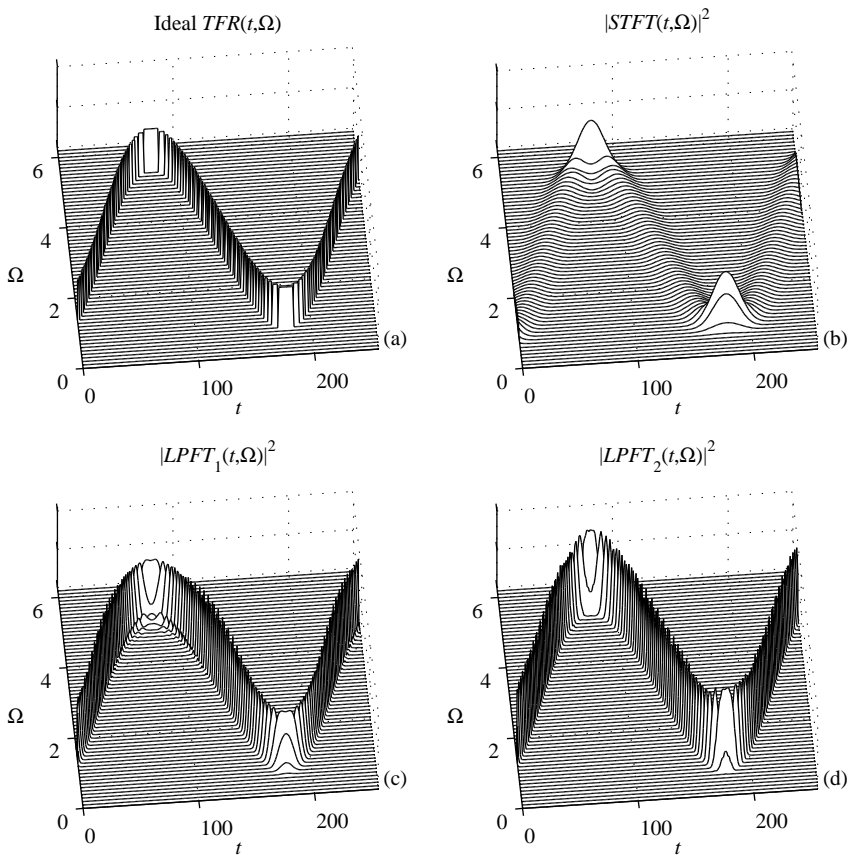


Figure 2.14 (a) Ideal time-frequency representation, (b) squared magnitude of the STFT, (c) the first-order LPFT, and (d) the second-order LPFT of the sinusoidally modulated signal.

where $LPFT(t, \Omega)$ is the LPFT of $x(t)$, $x_f(t)$ is the filtered signal, $B_t(t, \Omega)$ is a support function used for filtering. It could be 1 for the region where we assume that the signal of interest exists and 0 elsewhere.

Note that the sufficient order of the LPFT can be obtained recursively. We start from the STFT and check whether its auto-term's width is equal to the width of the Fourier transform of the used window. If true, it means that a signal is a

pure sinusoid and the STFT provides its best possible concentration. We should not calculate the LPFT. If the auto-term is wider than the width of the Fourier transform of the used window, it means that there are signal nonstationarities within the window and the first-order LPFT should be calculated. The auto-term's width is again compared to the width of the window's Fourier transform and if they do not coincide we should increase the LPFT order.

In the case of multicomponent signals, the distribution will be optimized to the strongest component first. Then the strongest component is filtered out and the procedure is repeated for the next component in the same manner, until the energy of the remaining signal is negligible, that is, until all the components are processed.

Example 2.18. Consider the first-order LPFT of a signal $x(t)$. Show that the second-order moments of the LPFT could be calculated based on the windowed signal moment, windowed signal's Fourier transform moment and one more LPFT moment for any Ω_1 in (2.85), for example, for $\Omega_1 = 1$.

★The second-order moment of the first-order LPFT,

$$LPFT_{\Omega_1}(t, \Omega) = \int_{-\infty}^{\infty} x_t(\tau) e^{-j(\Omega\tau + \Omega_1\tau^2)} d\tau,$$

defined by

$$M_{\Omega_1} = \frac{1}{2\pi} \int_{-\infty}^{\infty} \Omega^2 |LPFT_{\Omega_1}(t, \Omega)|^2 d\Omega \quad (2.88)$$

is equal to

$$M_{\Omega_1} = \int_{-\infty}^{\infty} \left| \frac{d(x_t(\tau) e^{-j\Omega_1\tau^2})}{d\tau} \right|^2 d\tau,$$

since the LPFT could be considered as the Fourier transform of $x_t(\tau) e^{-j\Omega_1\tau^2}$, that is, $LPFT_{\Omega_1}(t, \Omega) = \text{FT}\{x_t(\tau) e^{-j\Omega_1\tau^2}\}$, and the Parseval's theorem is used. After the derivative calculation

$$\begin{aligned} M_{\Omega_1} &= \int_{-\infty}^{\infty} \left| \frac{d[x_t(\tau)]}{d\tau} - j2\Omega_1 \tau x_t(\tau) \right|^2 d\tau \\ &= \int_{-\infty}^{\infty} \left(\left| \frac{d[x_t(\tau)]}{d\tau} \right|^2 + j2\Omega_1 \tau x_t^*(\tau) \frac{d[x_t(\tau)]}{d\tau} - j2\Omega_1 \tau x_t(\tau) \frac{d[x_t^*(\tau)]}{d\tau} + |2\Omega_1 \tau x_t(\tau)|^2 \right) d\tau. \end{aligned}$$

We can recognize some of the terms in the last line, as

$$M_0 = \int_{-\infty}^{\infty} \left| \frac{d[x_t(\tau)]}{d\tau} \right|^2 d\tau = \frac{1}{2\pi} \int_{-\infty}^{\infty} \Omega^2 |LPFT_{\Omega_1=0}(t, \Omega)|^2 d\Omega.$$

This is the moment of $X_t(\Omega) = \text{FT}\{x_t(\tau)\}$, since the integral of $|dx_t(\tau)/d\tau|^2$ over τ is equal to the integral of $|j\Omega X_t(\Omega)|^2$ over Ω , according to Parseval's theorem. Also, we can see that the last term in M_{Ω_1} contains the signal moment,

$$m_x = \int_{-\infty}^{\infty} \tau^2 |x_t(\tau)|^2 d\tau, \quad (2.89)$$

multiplied by $4\Omega_1^2$. Then, it is easy to conclude that

$$M_{\Omega_1} - M_0 - 4m_x\Omega_1^2 = \Omega_1 \int_{-\infty}^{\infty} \left(j2\tau x_t^*(\tau) \frac{d[x_t(\tau)]}{d\tau} - j2\tau x_t(\tau) \frac{d[x_t^*(\tau)]}{d\tau} \right) d\tau.$$

Note that the last integral does not depend on parameter Ω_1 . Thus, the relation among the LPFT moments at any two Ω_1 , for example, $\Omega_1 = a$ and an arbitrary Ω_1 , easily follows as the ratio

$$\frac{M_{\Omega_1=a} - M_0 - 4a^2 m_x}{M_{\Omega_1} - M_0 - 4\Omega_1^2 m_x} = \frac{a}{\Omega_1}. \quad (2.90)$$

With $a = 1$, by leaving the notation for an arbitrary Ω_1 unchanged, we get

$$\frac{M_1 - M_0 - 4m_x}{M_{\Omega_1} - M_0 - 4\Omega_1^2 m_x} = \frac{1}{\Omega_1}, \quad (2.91)$$

with $M_1 = M_{\Omega_1=1}$.

Obviously, the second-order moment, for any Ω_1 , can be expressed as a function of other three moments. In this case the relation reads

$$M_{\Omega_1} = 4\Omega_1^2 m_x + \Omega_1(M_1 - M_0 - 4m_x) + M_0.$$

□

Example 2.19. Find the position and the value of the second-order moment minimum of the LPFT, based on the windowed signal moment, the windowed signal's Fourier transform moment, and the LPFT moment for $\Omega_1 = 1$.

★The minimal value of the second-order moment (meaning the best concentrated LPFT in the sense of the duration measures) could be calculated from

$$\frac{dM_{\Omega_1}}{d\Omega_1} = 0$$

as

$$\Omega_1 = -\frac{M_1 - M_0 - 4m_x}{8m_x}.$$

Since $m_x > 0$ this is a minimum of the function M_{Ω_1} . Thus, in general, there is no need for a direct search for the best concentrated LPFT over all possible values of Ω_1 . It can be found based on three moments.

The value of M_{Ω_1} is

$$M_{\Omega_1} = M_0 - \frac{(M_1 - M_0 - 4m_x)^2}{16m_x}. \quad (2.92)$$

Note that any two moments, instead of M_0 and M_1 , could be used in the derivation. \square

2.8 FRACTIONAL FOURIER TRANSFORM WITH RELATION TO THE LPFT

The fractional Fourier transform (FRFT) was reintroduced in the signal processing by Almeida. For an angle α ($\alpha \neq k\pi$), the FRFT is defined as

$$X_\alpha(u) = \int_{-\infty}^{\infty} x(\tau) K_\alpha(u, \tau) d\tau, \quad (2.93)$$

where

$$K_\alpha(u, \tau) = \sqrt{\frac{1-j\cot\alpha}{2\pi}} e^{j(u^2/2)\cot\alpha} e^{j(\tau^2/2)\cot\alpha} e^{-ju\tau\csc\alpha}. \quad (2.94)$$

It can be considered as a rotation of signal in the time-frequency plane for an angle α (what will be shown in Chapter 3 within the quadratic time-frequency representations analysis). Its inverse can be considered as a rotation for angle $-\alpha$

$$x(t) = \int_{-\infty}^{\infty} X_\alpha(u) K_{-\alpha}(u, t) du.$$

Special cases of the FRFT reduce to: $X_0(u) = x(u)$ and $X_{\pi/2}(u) = X(u)/\sqrt{2\pi}$, that is, the signal and its Fourier transform.

The windowed FRFT is

$$X_{w,\alpha}(t, u) = \sqrt{\frac{1-j\cot\alpha}{2\pi}} e^{j(u^2/2)\cot\alpha} \int_{-\infty}^{\infty} x(t + \tau) w(\tau) e^{j(\tau^2/2)\cot\alpha} e^{-ju\tau\csc\alpha} d\tau. \quad (2.95)$$

Relation between the windowed FRFT and the first-order LPFT is

$$X_{w,\alpha}(t, u) = \sqrt{\frac{1 - j \cot \alpha}{2\pi}} e^{j(u^2/2)\cot \alpha} LPFT_{\Omega_1}(t, \Omega) \quad (2.96)$$

where $\Omega_1 = \cot(\alpha)/2$ and $\Omega = u \csc(\alpha)$. Thus, all results can be easily converted from the first-order LPFT to the windowed FRFT, and vice versa. That is the reason why we will not present a detailed analysis for this transform after the LPFT has been presented.

By using a window, local forms of the FRFT are introduced as:

$$STFT_\alpha(u, v) = \int_{-\infty}^{\infty} X_\alpha(u + \tau) w(\tau) e^{-jv\tau} d\tau \quad (2.97)$$

$$STFT_\alpha(u, v) = \int_{-\infty}^{\infty} x(t + \tau) w(\tau) K_\alpha(u, \tau) d\tau \quad (2.98)$$

meaning that the lag truncation could be applied after signal rotation or prior to the rotation. Results are similar. A similar relation for the moments, like (2.91) in the case of LPFT, could be derived here. It states that any FRFT moment can be calculated if we know just any three of its moments. This derivation for the FRFT is simpler by using the ambiguity function that will be introduced later.

2.9 RELATION BETWEEN THE STFT AND THE CONTINUOUS WAVELET TRANSFORM

The first form of functions having the basic property of wavelets was used by Haar at the beginning of the twentieth century. At the beginning of the 1980s, Morlet introduced a form of basis functions for analysis of seismic signals, naming them wavelets. The theory of wavelets was linked to the image processing by Mallat in the following years. In late the 1980s Daubechies presented a whole new class of wavelets that, in addition to the orthogonality property, can be implemented in a simple way by using simple digital filtering ideas. The most important applications of the wavelets are found in image processing and compression, pattern recognition, and signal denoising. Since their application to the time-frequency analysis is of limited interest, we will only link the continuous wavelet transform to the time-frequency analysis and present the discrete wavelet transform within the generalized time-frequency theory framework.

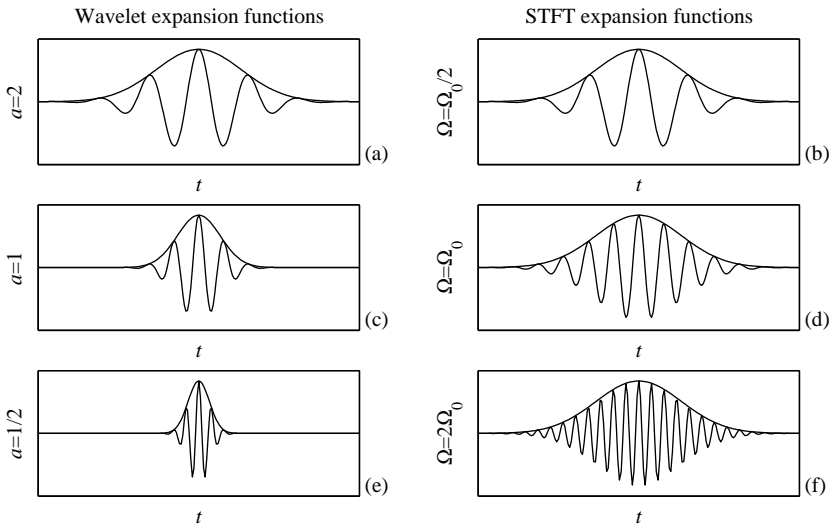


Figure 2.15 Expansion functions for the wavelet transform (a, c, e) and the short-time Fourier transform (b, d, f). The top row (a, b) presents high scale (low frequency), the middle row (c, d) is for medium scale (medium frequency), and the bottom row (e, f) is for low scale (high frequency).

The STFT is characterized by constant time and frequency resolutions for both low and high frequencies. The basic idea behind the wavelet transform is to vary the resolutions with scale (being related to frequency), so that a high frequency resolution is obtained for low frequencies, whereas a high time resolution is obtained for high frequencies, which could be relevant for some practical applications. It is achieved by introducing a variable window width, such that it is decreased for higher frequencies. The basic idea of the wavelet transform and its comparison with the STFT is illustrated in Fig. 2.15. Time-frequency grids (lattices) are schematically illustrated in Fig. 2.16.

When the above idea is translated into the mathematical form, one gets the definition of a continuous wavelet transform

$$WT(t, a) = \frac{1}{\sqrt{|a|}} \int_{-\infty}^{\infty} x(\tau) h^* \left(\frac{\tau - t}{a} \right) d\tau \quad (2.99)$$

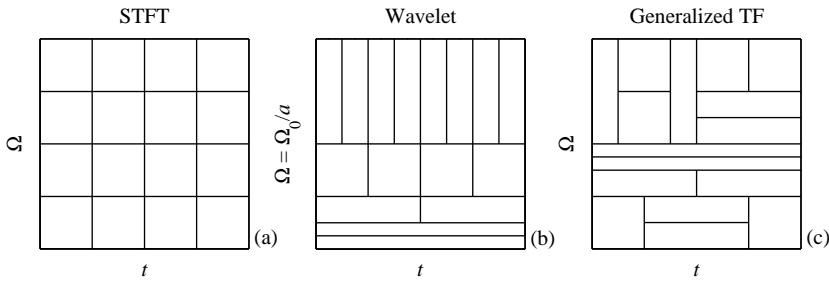


Figure 2.16 Time-frequency grid illustration for (a) the STFT with a constant window, (b) the wavelet transform, and (c) the generalized STFT representation with a time and frequency varying window.

where $h(t)$ is a bandpass signal and the parameter a is the scale. This transform produces a time-scale, rather than the time-frequency signal representation. For the Morlet wavelet (which will be used for illustrations in this short presentation), the relation between the scale and the frequency is $a = \Omega_0/\Omega$. In order to establish a strong formal relationship between the wavelet transform and the STFT, we will choose the basic wavelet $h(t)$ in the form

$$h(t) = w(t)e^{j\Omega_0 t} \quad (2.100)$$

where $w(t)$ is a window function and Ω_0 is a constant frequency. For example, for the Morlet wavelet we have a modulated Gaussian function

$$h(t) = \sqrt{\frac{1}{2\pi}} e^{-\alpha t^2} e^{j\Omega_0 t}$$

where the values of α and Ω_0 are chosen such that the ratio of $h(0)$ and the first maximum is $1/2$, $\Omega_0 = 2\pi\sqrt{\alpha/\ln 2}$. From the definition of $h(t)$ it is obvious that small Ω (that is, large a) corresponds to a wide wavelet, that is, a wide window, and vice versa.

Substitution of (2.100) into (2.99) leads to a continuous wavelet transform form suitable for a direct comparison with the STFT

$$WT(t, a) = \frac{1}{\sqrt{|a|}} \int_{-\infty}^{\infty} x(\tau) w^* \left(\frac{\tau - t}{a} \right) e^{-j\Omega_0 \frac{\tau - t}{a}} d\tau. \quad (2.101)$$

From the filter theory point of view, the wavelet transform, for a given scale a , could be considered as the output of system with impulse response $h^*(-t/a)\sqrt{|a|}$, that is, $WT(t, a) = x(t) *_t h^*(-t/a)\sqrt{|a|}$, where $*_t$ denotes a convolution in time. Similarly the STFT, for a given Ω , may be considered as $STFT_{II}(t, \Omega) = x(t) *_t [w^*(-t)e^{j\Omega t}]$. If we consider these two bandpass filters from the bandwidth point of view we can see that, in the case of STFT, the filtering is done by a system whose impulse response $w^*(-t)e^{j\Omega t}$ has a constant bandwidth, being equal to the width of the Fourier transform of $w(t)$.

2.9.1 Constant Q-Factor Transform

The quality filter factor Q for a bandpass filter, as a measure of the filter selectivity, is defined as

$$Q = \frac{\text{Central Frequency}}{\text{Bandwidth}}$$

In the STFT the bandwidth is constant, equal to the window Fourier transform width, B_w . Thus, the factor Q is proportional to the considered frequency,

$$Q = \frac{\Omega}{B_w}.$$

In the case of the wavelet transform, the bandwidth of impulse response is the width of the Fourier transform of $w(t/a)$. It is equal to B_0/a , where B_0 is the constant bandwidth corresponding to the mother wavelet. Thus, for the wavelet transform

$$Q = \frac{\Omega}{B_0/a} = \frac{\Omega_0}{B_0} = \text{const.} \quad (2.102)$$

Therefore, the continuous wavelet transform corresponds to the passing a signal through a series of bandpass filters centered at Ω , with constant factor Q . Again we can conclude that the filtering, which produces wavelet transform, results in a small bandwidth (high frequency resolution and low time resolution) at low frequencies and wide bandwidth (low frequency and high time resolution) at high frequencies.

2.9.2 Affine Transforms

A whole class of signal representations, including the quadratic ones, is defined with the aim to preserve the constant Q property. They belong to the area of the time-scale signal analysis or affine time-frequency representations. The basic property of

an affine time-frequency representation is that the representation of time shifted and scaled version of signal

$$y(t) = \frac{1}{\sqrt{\gamma}} x\left(\frac{t-t_0}{\gamma}\right), \quad (2.103)$$

whose Fourier transform is $Y(\Omega) = \sqrt{\gamma}X(\gamma\Omega)e^{-j\Omega t_0}$, results in a time-frequency representation

$$TFR_y(t, \Omega) = TFR_x\left(\frac{t-t_0}{\gamma}, \gamma\Omega\right). \quad (2.104)$$

The name affine comes from the affine transformation of time, that is, in general a transformation of the form $t \rightarrow \alpha t + \beta$. It is easy to verify that continuous wavelet transform satisfies this property.

Example 2.20. Find the wavelet transform of signal (2.7)

$$x(t) = \delta(t - t_1) + \delta(t - t_2) + e^{j\Omega_1 t} + e^{j\Omega_2 t}. \quad (2.105)$$

★ Its continuous wavelet transform is

$$\begin{aligned} WT(t, a) &= \frac{1}{\sqrt{|a|}} \left[w((t_1 - t)/a) e^{-j\Omega_0(t_1 - t)/a} + w((t_2 - t)/a) e^{-j\Omega_0(t_2 - t)/a} \right] \\ &\quad + \sqrt{|a|} \left[e^{j\Omega_1 t} W[a(\Omega_0/a - \Omega_1)] + e^{j\Omega_2 t} W[a(\Omega_0/a - \Omega_2)] \right]. \end{aligned} \quad (2.106)$$

where $w(t)$ is a real-valued function. The transform (2.106) has nonzero values in the region depicted in Fig. 2.17(a). \square

In analogy with spectrogram, the scalogram is defined as the squared magnitude of a wavelet transform

$$SCAL(t, a) = |WT(t, a)|^2. \quad (2.107)$$

The scalogram obviously loses the linearity property, and fits into the category of quadratic transforms. The scalogram and spectrogram of linearly frequency modulated signal are presented in Fig. 2.18.

2.9.3 Filter Bank Formulation

The time-frequency lattice for wavelet transform is presented in Fig. 2.16(b). Within the filter bank framework, it means that the original signal is processed in the

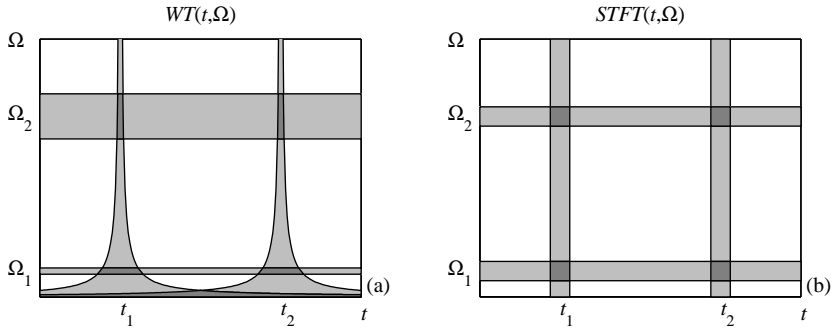


Figure 2.17 Illustration of the wavelet transform of (a) a sum of two delta pulses and two sinusoids compared with (b) the STFT.

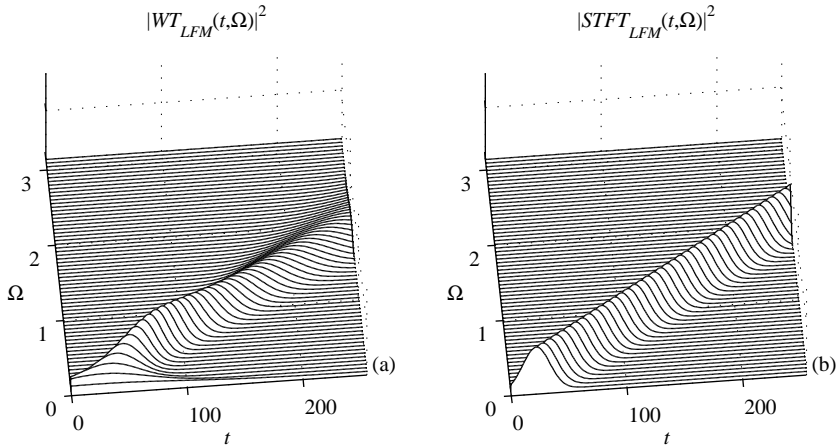


Figure 2.18 (a) Scalogram and (b) spectrogram of the linear frequency modulated signal. The spectrogram is calculated with the optimal window width.

following way. The signal's spectral content is divided into the high-frequency and low-frequency part.

An example, how to achieve this lattice is presented in the STFT analysis by using a two-sample rectangular window $w(n) = \delta(n) + \delta(n - 1)$, with $N = 2$. Then its two-sample WT is $WT_L(n, 0) = x(n) + x(n - 1)$, for $k = 0$, corresponding to low-frequency part, $\omega = 0$, and $WT_H(n, 1) = x(n) - x(n - 1)$ for $k = 1$ corresponding to the high-frequency part, $\omega = \pi$. The high-frequency part, $WT_H(n, 1)$, having a high resolution in time, is not processed any more. It is kept with this high resolution in time, expecting that this kind of resolution will be needed for a signal analysis. The lowpass part $WT_L(n, 0) = x(n) + x(n - 1)$ is further processed, by dividing it into its low-frequency part, $WT_{LL}(n, 0, 0) = WT_L(n, 0) + WT_L(n - 2, 0)$ and its high-frequency part $WT_{LH}(n, 0, 1) = WT_L(n, 0) - WT_L(n - 2, 0)$. The highpass of this part, with resolution four in time, is not processed anymore, while the lowpass part is further processed, by dividing it into its low and high-frequency part until the full length of signal is achieved (Fig. 2.16(b)).

The transformation matrix in the case of signal with eight samples is

$$\begin{bmatrix} C(7) \\ C(6) \\ C(5) \\ C(4) \\ C(3) \\ C(2) \\ C(1) \\ C(0) \end{bmatrix} = \begin{bmatrix} WT_H(n, 1) \\ WT_H(n - 2, 1) \\ WT_H(n - 4, 1) \\ WT_H(n - 6, 1) \\ WT_{LH}(n, 0, 1) \\ WT_{LH}(n - 4, 0, 1) \\ WT_{LLH}(n, 0, 0, 1) \\ WT_{LLL}(n, 0, 0, 0) \end{bmatrix} = \begin{bmatrix} 1 & -1 & 0 & 0 & 0 & 0 & 0 & 0 \\ 0 & 0 & 1 & -1 & 0 & 0 & 0 & 0 \\ 0 & 0 & 0 & 0 & 1 & -1 & 0 & 0 \\ 0 & 0 & 0 & 0 & 0 & 0 & 1 & -1 \\ 1 & 1 & -1 & -1 & 0 & 0 & 0 & 0 \\ 0 & 0 & 0 & 0 & 1 & 1 & -1 & -1 \\ 1 & 1 & 1 & 1 & -1 & -1 & -1 & -1 \\ 1 & 1 & 1 & 1 & 1 & 1 & 1 & 1 \end{bmatrix} \begin{bmatrix} x(n) \\ x(n - 1) \\ x(n - 2) \\ x(n - 3) \\ x(n - 4) \\ x(n - 5) \\ x(n - 6) \\ x(n - 7) \end{bmatrix}.$$

This is a form of the Haar transform. The inverse transformation is

$$\begin{bmatrix} x(n) \\ x(n - 1) \\ x(n - 2) \\ x(n - 3) \\ x(n - 4) \\ x(n - 5) \\ x(n - 6) \\ x(n - 7) \end{bmatrix} = \frac{1}{8} \begin{bmatrix} 4 & 0 & 0 & 0 & 2 & 0 & 1 & 1 \\ -4 & 0 & 0 & 0 & 2 & 0 & 1 & 1 \\ 0 & 4 & 0 & 0 & -2 & 0 & 1 & 1 \\ 0 & -4 & 0 & 0 & -2 & 0 & 1 & 1 \\ 0 & 0 & 4 & 0 & 0 & 2 & -1 & 1 \\ 0 & 0 & -4 & 0 & 0 & 2 & -1 & 1 \\ 0 & 0 & 0 & 4 & 0 & -2 & -1 & 1 \\ 0 & 0 & 0 & -4 & 0 & -2 & -1 & 1 \end{bmatrix} \begin{bmatrix} C(7) \\ C(6) \\ C(5) \\ C(4) \\ C(3) \\ C(2) \\ C(1) \\ C(0) \end{bmatrix}.$$

2.9.4 Generalized Time-Frequency Varying Lattice

In general, the spectral content of signal changes in time and frequency in an arbitrary manner. There are several methods in the literature that adapt windows or

basis functions to the signal form for each time instant or even for every considered time and frequency point in the time-frequency plane (e.g., as in Fig. 2.16(c)). Selection of the most appropriate form of the basis functions (windows) for each time-frequency point includes a criterion for selecting the optimal basis function scale (optimal window width) for each point (time-frequency region). One method that belongs to the class of signal adaptive methods for the time-frequency denoising, with varying windows, will be presented later in the book.

2.9.5 S-Transform

The S-transform (the Stockwell transform) is conceptually a combination of short-time Fourier analysis and wavelet analysis (a form of continuous wavelet transform in the time-frequency notations and framework). It employs a variable window length but preserves the phase information by using the STFT form in the signal decomposition. As a result, the phase spectrum is absolute in the sense that it is always referred to a fixed time reference. The real and imaginary spectrum can be localized independently with resolution in time, in terms of basis functions. The changes in the absolute phase of a certain frequency can be tracked along the time axis and useful information can be extracted. The frequency-dependent window function produces a higher frequency resolution at lower frequencies, while at higher frequencies sharper time localization can be achieved, the same as in the continuous wavelet case.

For a signal $x(t)$ it reads as

$$S_c(t, \Omega) = \frac{|\Omega|}{(2\pi)^{3/2}} \int_{-\infty}^{+\infty} x(\tau) e^{-\frac{(\tau-t)^2 \Omega^2}{8\pi^2}} e^{-j\Omega\tau} d\tau, \quad (2.108)$$

with substitutions $\tau - t \rightarrow \tau$, the above equation can be rewritten as follows

$$S_c(t, \omega) = \frac{|\Omega| e^{-j\Omega t}}{(2\pi)^{3/2}} \int_{-\infty}^{+\infty} x(t + \tau) e^{-\frac{\tau^2 \Omega^2}{8\pi^2}} e^{-j\Omega\tau} d\tau. \quad (2.109)$$

For the window function of form

$$w(\tau, \Omega) = \frac{|\Omega|}{(2\pi)^{3/2}} e^{-\frac{\tau^2 \Omega^2}{8\pi^2}}, \quad (2.110)$$

the definition of the continuous S-transform can be rewritten as follows

$$S_c(t, \Omega) = e^{-j\Omega t} \int_{-\infty}^{+\infty} x(t + \tau) w(\tau, \Omega) e^{-j\Omega\tau} d\tau. \quad (2.111)$$

A discretization over τ of (2.111) results in

$$S_d(t, \Omega) = e^{-j\Omega t} \sum_n x(t + n\Delta t) w(n\Delta t, \Omega) e^{-j\Omega n\Delta t} \Delta t. \quad (2.112)$$

An energetic version of the S-transform is the square of amplitude of (2.112)

$$S(t, \Omega) = |S_d(t, \Omega)|^2. \quad (2.113)$$

Example 2.21. Consider a signal in the form

$$x(t) = \exp(-j2\pi a \log(-bt + 1)) \exp(j2\pi a \log(bt + 1)),$$

with $a = 5$, $b = 5$, and the time interval is $-512 \leq t < 512$ with sampling interval $\Delta t = 1$. Its instantaneous frequencies are shown in Fig. 2.19(a). Calculate its S-transform.

★The spectrogram with a narrow and a wide window is shown in Fig. 2.19(b), and (c), while the energetic version of the S-transform is shown in Fig. 2.19(d). As can be seen, the signal is quite stationary at low frequencies, with a fast transition close to $t = 0$, thus being a good example of signal that can be efficiently analyzed with the S-transform. Note that this kind of signals has the instantaneous frequency function of $1/f$ form. They could be very efficiently processed by the wavelet and other affine transforms as well, since they fit very well to the wavelet-based partition of the time-frequency plane. □

2.10 CHIRPLET TRANSFORM

An extension of the wavelet transform, for time-frequency analysis, is the chirplet transform. By using linear frequency-modulated forms instead of the constant frequency ones, the chirplet is formed.

Here we will present a Gaussian chirplet atom that is a four-parameter function,

$$\varphi(\tau; [t, \Omega, \Omega_1, \sigma]) = \frac{1}{\sqrt{\sqrt{\pi}\sigma}} \exp\left(-\frac{1}{2} \left(\frac{\tau-t}{\sigma}\right)^2 + j\Omega_1(\tau-t)^2 + j\Omega(\tau-t)\right), \quad (2.114)$$

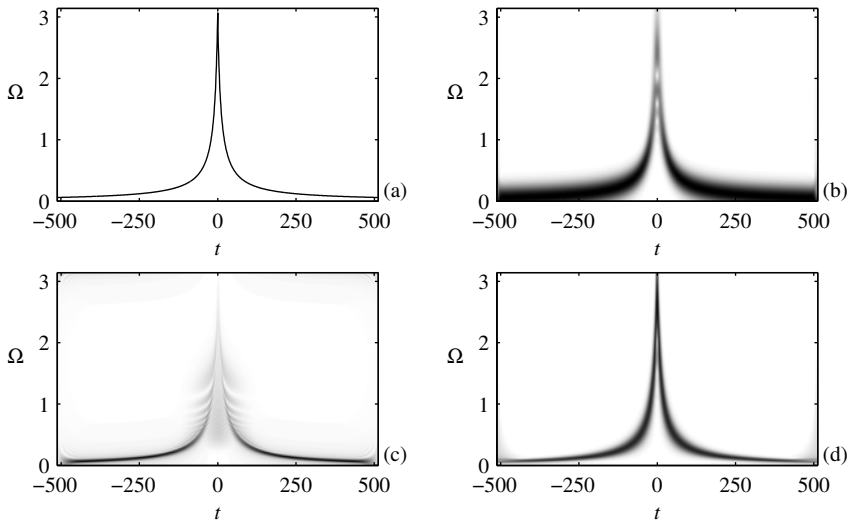


Figure 2.19 Analysis of a signal by using the S-transform: (a) instantaneous frequency of the analyzed signal, (b) spectrogram with a narrow window, (c) spectrogram with a wide window, and (d) squared modulus of the S-transform.

where the parameter σ controls the width of the chirplet in time, parameter Ω_1 stands for the chirplet rate in time-frequency plane, while t and Ω are the coordinates of the central time and frequency point in the time-frequency plane. In this way, for a given set of parameters $[t, \Omega, \Omega_1, \sigma]$, we project signal onto a Gaussian chirp, centered at t, Ω whose width is defined by σ and rate is Ω_1 ,

$$c(t, \Omega, \Omega_1, \sigma) = \int_{-\infty}^{\infty} x(\tau) \varphi^*(\tau; [t, \Omega, \Omega_1, \sigma]) d\tau. \quad (2.115)$$

In general, the projection procedure should be performed for each point in the time-frequency plane, for all possible parameter values. Interest in using a Gaussian chirplet atom stems from the fact that it provides the highest joint time-frequency concentration. In practice, all four parameters should be discretized. The set of the parameter discretized atoms is called a dictionary. In contrast to the second-order local polynomial Fourier transform, here the window width is parametrized and varies

as well. Since we have a multiparameter problem, computational requirements for this transform are very high.

In order to improve efficiency of the chirplet transform calculation, various adaptive forms of the chirplet transform were proposed. The matching pursuit procedure is a typical example. The first step of this procedure is to choose a chirplet atom from the dictionary yielding the largest amplitude of the inner product between the atom and the signal. Then the residual signal, obtained after extracting the first atom, is decomposed in the same way. Consequently, the signal is decomposed into a sum of chirplet atoms.

2.11 GENERALIZATION

In general, any set of well-localized functions in time and frequency can be used for the time-frequency analysis of a signal. Let us denote the signal as $x(\tau)$ and the set of such functions with $\varphi(\tau; [\text{Parameters}])$, then the projection of the signal $x(\tau)$ onto such functions,

$$c([\text{Parameters}]) = \int_{-\infty}^{\infty} x(\tau) \varphi^*(\tau; [\text{Parameters}]) d\tau \quad (2.116)$$

represents similarity between $x(t)$ and $\varphi(t; [\text{Parameters}])$, at a given point with parameter values defined by an ordered set of values, denoted by $[\text{Parameters}]$.

We may have the following cases:

- Frequency as the only parameter. Then, we have projection onto complex sinusoids with changing frequency, and $c([\Omega])$ is the Fourier transform of signal $x(\tau)$ with

$$\varphi(\tau; [\Omega]) = e^{j\Omega\tau}.$$

- Time and frequency as parameters. By varying t and Ω and calculating projections of the signal $x(\tau)$ we get the STFT. In this case we use $w(\tau - t)e^{j\Omega\tau}$ as a localization function around parameter t and

$$\varphi(\tau; [t, \Omega]) = w(\tau - t)e^{j\Omega\tau}.$$

- Time and frequency as parameters with a frequency-dependent localization in time, $h^*((\tau - t)/(\Omega_0/\Omega)) = w((\tau - t)/(\Omega_0/\Omega))e^{j\Omega(\tau-t)}$, we get wavelet transform. It is more often expressed as function of scale parameter $a =$

Ω_0/Ω , than the frequency. The S-transform belongs to this class. For the continuous wavelet transform with mother wavelet $w(t)$, we have

$$\varphi(\tau; [t, a]) = w((\tau - t)/a) e^{j\Omega_0(\tau-t)/a}.$$

- Frequency and signal phase rate as parameters. Then we get the polynomial Fourier transform of the second-order, with

$$\varphi(\tau; [\Omega, \Omega_1]) = e^{j(\Omega\tau + \Omega_1\tau^2)}.$$

- Time, frequency, and signal phase rate as parameters results in a form of the local polynomial Fourier transform with

$$\varphi(\tau; [t, \Omega, \Omega_1]) = w(\tau - t) e^{j(\Omega\tau + \Omega_1\tau^2)}.$$

- Time, frequency, and signal phase rate as parameters, with a varying time localization, as parameters, result in the chirplets with the localization function

$$\varphi(\tau; [t, \Omega, \Omega_1, \sigma]) = w((\tau - t)/\sigma) e^{j\Omega_1(\tau-t)^2 + j\Omega(\tau-t)}.$$

- Frequency, signal phase rate, and other higher-order coefficients as parameters. We get the polynomial Fourier transform of the N th order, with

$$\varphi(\tau; [\Omega, \Omega_1, \Omega_2, \dots, \Omega_N]) = e^{j(\Omega\tau + \Omega_1\tau^2 + \Omega_2\tau^3 + \dots + \Omega_N\tau^N)}.$$

- Time, frequency, signal phase rate, and other higher-order coefficients as parameters. Then, we get the local polynomial Fourier transform of the N th order, with

$$\varphi(\tau; [t, \Omega, \Omega_1, \Omega_2, \dots, \Omega_N]) = w(\tau - t) e^{j(\Omega\tau + \Omega_1\tau^2 + \Omega_2\tau^3 + \dots + \Omega_N\tau^N)}.$$

- Time, frequency, signal phase rate, and other higher-order coefficients as parameters, with a variable window width, we get the N th order-lets, with

$$\varphi(\tau; [t, \Omega, \Omega_1, \Omega_2, \dots, \Omega_N, \sigma]) = w((\tau - t)/\sigma) e^{j(\Omega\tau + \Omega_1\tau^2 + \Omega_2\tau^3 + \dots + \Omega_N\tau^N)}.$$

- Time, frequency, and any other parametrized phase function form, like sinusoidal ones, with constant or variable window width.

2.12 PARAMETER OPTIMIZATION

The optimization of time-frequency presentations is closely related to criteria for measurement of their quality. One possible criterion is in measuring and improving time-frequency representation concentration. Intuitively we can assume that better concentration in the time-frequency domain means that the signal energy is focused within a smaller region, having higher values. In this way detections and estimations, based on time-frequency signal representation, are expected to be more reliable. Concentration measure can provide a quantitative criterion for the evaluation of various representation performances. It can be used for adaptive and automatic parameter selection in time-frequency analysis, without the supervision of a user.

In most cases, some quantities from statistics and information theory were the inspiration for defining concentration measures of time-frequency representations.

The basic idea for measuring time-frequency representation concentration can be explained on a simplified example motivated by the probability theory. Consider a set of N nonnegative numbers $\{p_1, p_2, \dots, p_N\}$, such that

$$p_1 + p_2 + \dots + p_N = 1. \quad (2.117)$$

Form a simple test function

$$\mathcal{M}(p_1, p_2, \dots, p_N) = p_1^2 + p_2^2 + \dots + p_N^2.$$

It is easy to conclude that $\mathcal{M}(p_1, p_2, \dots, p_N)$, under the constraint $p_1 + p_2 + \dots + p_N = 1$, has the minimal value for $p_1 = p_2 = \dots = p_N = 1/N$, that is, for maximally spread values of p_1, p_2, \dots, p_N . The highest value of $\mathcal{M}(p_1, p_2, \dots, p_N)$, under the same constraint, is achieved when only one p_i is different from zero, $p_i = \delta(i - i_0)$, where i_0 is an arbitrary integer $1 \leq i_0 \leq N$. This case corresponds to the maximally concentrated values of p_1, p_2, \dots, p_N , at a single $p_{i_0} = 1$. Therefore, the function $\mathcal{M}(p_1, p_2, \dots, p_N)$ can be used as a measure of concentration of the set of numbers p_1, p_2, \dots, p_N , under the unity sum constraint. In general, the constraint (2.117) can be included in the function itself by using the form

$$\mathcal{M}(p_1, p_2, \dots, p_N) = \frac{p_1^2 + p_2^2 + \dots + p_N^2}{(p_1 + p_2 + \dots + p_N)^2}.$$

For nonnegative p_1, p_2, \dots, p_N this function has the minimum for $p_1 = p_2 = \dots = p_N$, and reaches its maximal value when only one p_i is different from zero.

In time-frequency analysis this idea has been used in order to measure the concentration. Several forms of the concentration measure, based on this fundamental idea, are introduced.

Applying the previous reasoning to the spectrogram, we may write a function for measuring the concentration of the time-frequency representation $STFT(n, k)$ as

$$\mathcal{M}[SPEC(n, k)] = \frac{\sum_n \sum_k |SPEC(n, k)|^2}{(\sum_n \sum_k |SPEC(n, k)|)^2} = \frac{\sum_n \sum_k |STFT(n, k)|^4}{\left(\sum_n \sum_k |STFT(n, k)|^2\right)^2}. \quad (2.118)$$

This form is just the fourth power of the ratio of the fourth- and second-order norms of $STFT(n, k)$. High values of \mathcal{M} indicate that the representation $STFT(n, k)$ is highly concentrated, and vice versa. In general, it has been shown (by Jones, Parks, Baraniuk, Flandrin, Williams, *et al.*) that any other ratio of norms L_p and L_q , $p > q > 1$, can also be used for measuring the concentration of $STFT(n, k)$.

When there are two or more components (or regions in time-frequency plane of a single component) of approximately equal energies (importance), whose concentrations are very different, the norm-based measures will favor the distribution with a “peaky” component, due to raising of distribution values to a high power. It means that if one component (region) is extremely highly concentrated, and all the others are very poorly concentrated, then the measure will not look for a trade-off, when all components are well concentrated. In order to deal with this kind of problems, common in time-frequency analysis, a concentration measure could be applied to smaller, local time-frequency regions

$$\mathcal{M}_{(n, k)} = \frac{\sum_n \sum_k Q^2(m - n, l - k) |STFT(n, k)|^4}{\left(\sum_n \sum_k Q(m - n, l - k) |STFT(n, k)|^2\right)^2}. \quad (2.119)$$

The localization weighting function $Q(n, k)$ determines the region where the concentration is measured. A Gaussian form of this function is used in literature.

Another direction to measure time-frequency representation concentration (by Stanković) comes from a classical definition of the time-limited signal duration, rather than measuring signal peakedness. If a signal $x(n)$ is time-limited to the interval $n \in [n_1, n_2 - 1]$, that is, $x(n) \neq 0$ only for $n \in [n_1, n_2 - 1]$, then the duration of $x(n)$ is $d = n_2 - n_1$. It can be written as

$$d = \lim_{p \rightarrow \infty} \sum_n |x(n)|^{1/p} = \|x(n)\|_0, \quad (2.120)$$

where $\|x(n)\|_0$ denotes the norm zero of signal. The same definition applied to a two-dimensional function $|P(n, k)|^2 \neq 0$ only for $(n, k) \in D_x$ gives

$$N_D = \lim_{p \rightarrow \infty} \sum_n \sum_k |P(n, k)|^{1/p} \quad (2.121)$$

where N_D is the number of points within D_x . In reality, there is no a sharp edge between $|P(n, k)|^2 \neq 0$ and $|P(n, k)|^2 = 0$, so the value of (2.121) could, for very large p , be sensitive to small values of $|P(n, k)|^2$. The robustness may be achieved by using lower-order forms, with $p \geq 1$ in contrast to (2.119) where, in this notation, $p = 1/2$.

Therefore, the spectrogram concentration can be measured with the function of the form

$$\mu[SPEC(n, k)] = \sum_n \sum_k |STFT(n, k)|^{2/p}, \quad (2.122)$$

with $p > 1$. Here lower value of the concentration measure μ indicates better concentrated distribution. For example, with $p = 2$, it is of the norm one form

$$\mu[SPEC(n, k)] = \sum_n \sum_k |STFT(n, k)| = \|STFT(n, k)\|_1.$$

In the case that variations of amplitude may be expected, an energy normalized version of measure

$$\mu[SPEC(n, k)] = \left(\sum_n \sum_k |STFT(n, k)| \right)^2 / \sum_n \sum_k |STFT(n, k)|^2$$

should be used.

In the probability theory all results are derived for the probability values p_i , assuming that $\sum_i p_i = 1$ and $p_i \geq 0$. The same assumptions are made in classical signal analysis for the signal power. Since a general time-frequency representation, as we will see later, commonly does not satisfy nonnegativity condition, the concentration measures should be carefully used in those cases.

Example 2.22. Consider the signal

$$\begin{aligned} x(t) = & \cos(50\cos(\pi t) + 10\pi t^2 + 70\pi t) \\ & + \cos(25\pi t^2 + 180\pi t) \end{aligned} \quad (2.123)$$

sampled at $\Delta t = 1/256$, within $-1 \leq t < 1$. The Hann(ing) window $w(m)$ with different lengths is used in the spectrogram calculation for each instant. Here we used the measure (2.122) with $p = 2$, although for this signal all presented measures

would produce similar results. The spectrogram is calculated with different window widths.

The best window width, according to the measure $\mu[SPEC_N(n,k)]$, will be that which minimizes (or maximizes if measure $\mathcal{M}[SPEC_N(n,k)]$ is used)

$$N_{opt} = \min_N \{\mu[SPEC_N(n,k)]\}, \quad (2.124)$$

where the index for the window width is added. For wide lag windows, signal non-stationarity makes the spectrogram spread in the time-frequency plane, having a relatively large measure $\mu[SPEC_N(n,k)]$ (Fig. 2.20(a, b)). For narrow lag windows its Fourier transform is very wide, causing spread distributions and large measure $\mu[SPEC_N(n,k)]$ (Fig. 2.20(d, e)). Obviously, between these two extreme situations there is a window that produces an acceptable trade-off between the signal nonstationarity and small window length effects. The measure $\mu[SPEC_N(n,k)]$ is calculated for a set of spectrograms with $N = 32$ up to $N = 256$ window length (Fig. 2.20(f)). The minimal measure value, meaning the best concentrated spectrogram according to this measure, is achieved for $N = 88$ (Fig. 2.20(f)). The spectrogram with $N = 88$ is shown in Fig. 2.20(c). \square

2.12.1 Adaptive Analysis

Parameter optimization may be done by a straightforward computation of a distribution measure $\mu[SPEC(n,k)]$ for various parameter values. The best choice according to this criterion (optimal distribution with respect to this measure) is the distribution which produces the minimal value of $\mu[SPEC(n,k)]$. In the cases when one has to consider a wide region of possible parameter values for the distribution calculation (like for example window lengths in spectrogram), this approach can be numerically inefficient. Then some more sophisticated optimization procedures should be considered, like the one using the steepest descent approach, used in adaptive signal processing.

The gradient of a measure $\mu[SPEC(n,k)]$, with respect to a distribution's generalized optimization parameter (for example, window width N), in general denoted by ξ , is

$$\frac{\partial \mu[SPEC(n,k)]}{\partial \xi} = \frac{\partial \mu[SPEC(n,k)]}{\partial SPEC(n,k)} \frac{\partial SPEC(n,k)}{\partial \xi}.$$

Iterations, starting from a very low concentrated distribution toward the maximally concentrated one, that is, toward the measure minimum, can be done according to

$$\xi_{m+1} = \xi_m - \lambda \frac{\partial \mu[SPEC(n,k)]}{\partial \xi} \quad (2.125)$$

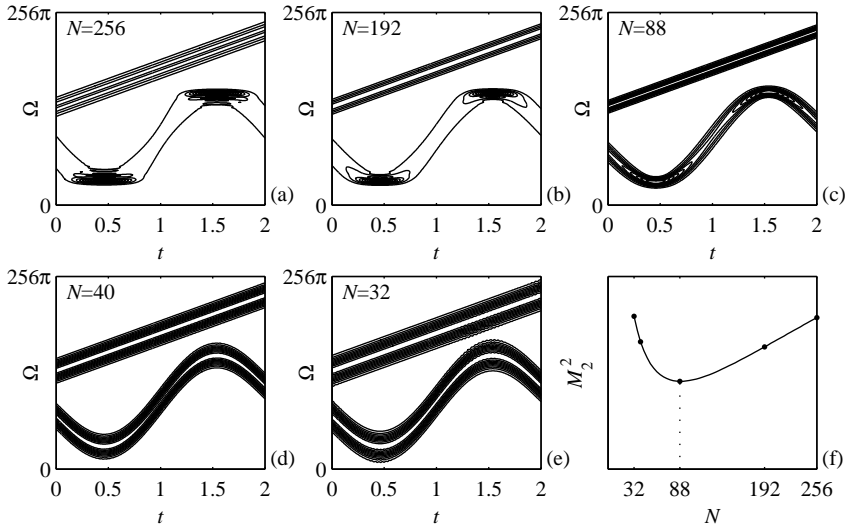


Figure 2.20 (a - e) Spectrogram for various window lengths, and (f) its measure $M_2 = \mu[SPEC(n, k)]$, $p = 2$. The lowest $\mu[SPEC(n, k)]$ is achieved for $N = 88$, being the best window length choice according to this measure.

where λ is the step that should be chosen in the same way as the step in the other adaptive algorithms. The step should not be too small (since the convergence would be too slow) and not too large (to miss the minimum or cause the divergence).

In discrete implementations, the gradient $\partial\mu[SPEC(n, k)]/\partial\xi$ can be approximated based on $\mu[SPEC(n, k; \xi_m)]$ calculated with ξ_m and its previous value ξ_{m-1}

$$\xi_{m+1} = \xi_m - \lambda \frac{\mu[SPEC(n, k; \xi_m)] - \mu[SPEC(n, k; \xi_{m-1})]}{\xi_m - \xi_{m-1}}. \quad (2.126)$$

Example 2.23. The optimization procedure will be illustrated on the signal $x(t)$, its spectrogram, and the measure from the previous Example. The optimal window width is obtained in few iterations by using (2.126), starting from the very narrow window. Values of $\xi_0 = N = 16$ and $\xi_1 = N = 20$ in the initial and first iteration are assumed. The next value of $\xi_{m+1} \equiv N$ is calculated according to (2.126). During the iterations we get $\xi_m = 16, 20, 76$, and 90 . The algorithm is stopped at $\xi_m = 90$, when $|\xi_{m+1} - \xi_m| < 2$, since even number of samples are used in the realization. Note that

the obtained optimal value is within ± 2 of the value obtained by direct calculation. The value of parameter $\lambda = 1/3$ was used. \square

Generalization of the parameter optimization could be done by applying measure concentration and parameters optimization for each instant or each frequency or combined for some time-frequency regions.

2.13 PROBLEMS

Problem 2.1. For a signal $x(t) = 3 \exp(j64 \sin(\pi t) - j8\pi t)$ calculate the instantaneous frequency. What is the maximal frequency that we may expect in the Fourier transform, according to the stationary-phase method? What is a minimal sampling interval? Repeat the same for $x(t) = \exp(j128\pi t^2)$ within $-2 \leq t \leq 2$ and $x(t) = 0$ elsewhere.

Problem 2.2. For the Hann(ing) window calculate the effective widths in the frequency and time domains. Compare it with the mainlobe width and the window width.

Hint: Use Parseval's theorem.

Problem 2.3. For a signal limited in time within $-T < t < T$, show that the effective width is always lower than a half of the signal duration, that is, $\sigma_t < T$.

Problem 2.4. Show that the Fourier transform of Gaussian window

$$w(\tau) = e^{-\tau^2/2}$$

satisfies the differential equation

$$\frac{dW(\Omega)}{d\Omega} = -\Omega W(\Omega) \text{ with } W(0) = \sqrt{2\pi},$$

resulting in the fact that, in this case, the signal equals its Fourier transform, $W(\Omega) = \sqrt{2\pi}w(\Omega)$.

Problem 2.5. Time-frequency analysis is performed with a window of the width $2T$. The STFT is calculated at $t = 2kR$, $k = 0, \pm 1, \pm 2$, with overlap, $R < T$. Derive the reconstruction formula for these STFTs, by using all available signal samples for one time instant.

Problem 2.6. What is the optimal Hann(ing) window width for the STFT calculation of the signal $x(t) = \exp(j64\pi t^2 + j8\pi t + j\pi/3)$ for $-1 \leq t \leq 1$.

Problem 2.7. Signal

$$x(t) = e^{-t^2} e^{j8\pi t^2 + j64\pi t}$$

is sampled at $\Delta t = 1/32$. If we may assume that the signal is zero outside $-1 \leq t \leq 1$ what will be the region of support for the time-frequency representation? What sampling interval should be used for this signal?

Problem 2.8. Find the sampling interval for

$$x(t) = e^{-t^2} e^{j8\pi t^2 + j64\pi t}$$

assuming now that the signal values smaller than $e^{-4} = 0.018$ could be neglected. What is the maximal possible sampling interval that the time-frequency representation of this signal could be recovered (allowing a possible additional frequency shift)? Comment on the results in the sense of processing with lower rates than the sampling theorem required ones (sparse processing).

Problem 2.9. Two second-order moments of the first-order LPFT at $\Omega_1 = 0$ and $\Omega_1 = 0.5$ are $M_0 = 25$ and $M_{0.5} = 15$, for a given instant t . The windowed signal moment is $m_x = 20$. Find the parameter Ω_1 in the LPFT when the LPFT is the best concentrated.

Problem 2.10. Signal has 16 samples in total. The first four samples are used with a window $w(m) = \delta(m) + \delta(m-1) + \delta(m-2) + \delta(m-3)$ and the STFT of the windowed signal is calculated

$$\begin{aligned} STFT_4(n, k) &= \sum_{i=0}^3 x(n+i) \exp(-j2\pi ik/4) \\ STFT_4(0, 0) &= x_{LL}(n) = x(0) + x(1) + x(2) + x(3) \\ STFT_4(0, 1) &= x_{LM}(n) = x(0) - jx(1) - x(2) + jx(3) \\ STFT_4(0, 2) &= x_{HM}(n) = x(0) - x(1) + x(2) - x(3) \\ STFT_4(0, 3) &= x_{HH}(n) = x(0) + jx(1) - x(2) - jx(3). \end{aligned}$$

Then four samples are skipped, and the same procedure is repeated.

- (a) Plot the time-frequency plane lattice in this case (nonoverlapping STFT with four-sample window).

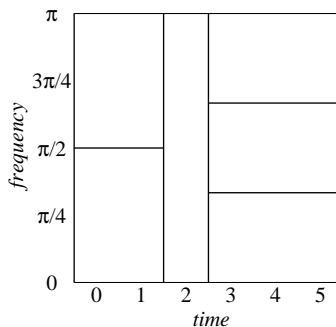


Figure 2.21 Time-frequency plane division for Problem 2.13.

(b) The LL and HH regions are additionally divided into two regions, while the remaining two regions from (a) are not divided. Plot the time-frequency plane lattice. Hint: The LL and HH regions are divided in frequency and doubled in time so they last now eight samples each with two frequency samples inside.

(c) Only the HH region is additionally divided into four parts, while the other regions are kept with the same resolution. Plot the time-frequency plane lattice in this case.

Problem 2.11. The STFT is realized in the recursive manner, assuming the rectangular lag window of the width N . The STFT values are not updated after each sample, but after each other sample, since only every other STFT is needed in an analysis. Write the updating relation for such STFT calculation. Comment the calculation complexity, as compared to the FFT calculation for each considered time instant. What would be the calculation complexity if K samples are skipped in the recursive realization?

Problem 2.12. Show that the transformation matrices in (2.53) and (2.54) could be calculated in a recursive manner. Generalize.

Problem 2.13. Discrete signal $x(n)$ for $n = 0, 1, 2, 3, 4, 5$ is considered. Time-frequency plane is divided as presented in Fig. 2.21.

(a) Denote each region in the figure by appropriate coefficient $STFT_N(n, k)$, defined by (2.45), where N is window length, n is the time index, and k is the frequency index.

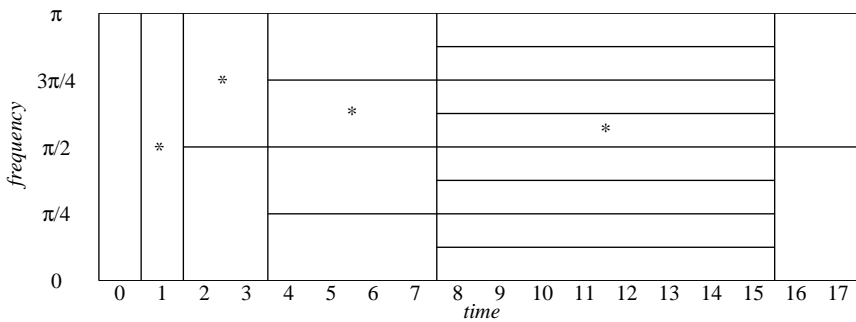


Figure 2.22 Time-frequency plane division for Problem 2.14.

- (b) Write relations for coefficients calculation and write transformation matrix \mathbf{T} .
- (c) By using the transformation matrix, find STFT values if signal samples are $x(0) = 2, x(1) = -2, x(2) = 4, x(3) = \sqrt{3}, x(4) = -\sqrt{3}, x(5) = 0$.
- (d) If STFT coefficients for signal $y(n)$ are

$$\begin{aligned} STFT_2(1,0) &= 4, & STFT_2(1,0) &= 0 \\ STFT_1(2,0) &= 1, & STFT_3(5,0) &= 0 \\ STFT_3(5,1) &= 3, & STFT_3(5,2) &= 3 \end{aligned}$$

find signal samples $y(n)$.

Problem 2.14. Consider time-frequency plane divided with lowpass highpass division as presented in Fig. 2.22.

- (a) Denote each region in the division by appropriate coefficient $C_N(n,k)$.
- (b) Find formulae for coefficients calculation for regions marked with a star.
- (c) Find the transformation matrix \mathbf{T} having in mind that coefficients are ordered first in a descending order in time and in an ascending order in frequency.
- (d) If coefficient values for regions marked with a star are 12 and 0 in unmarked regions, find signal samples $x(n)$ for $n = 0, 1, \dots, 17$.

Problem 2.15. Consider a signal $x(n)$ with $M = 8$ samples. Its values are

$$\begin{bmatrix} x(0) & x(1) & x(2) & x(3) & x(4) & x(5) & x(6) & x(7) \end{bmatrix} = \begin{bmatrix} 0 & 1 & 1/2 & -1/2 & 1/4 & j/4 & -1/4 & -j/4 \end{bmatrix}.$$

(a) Calculate the nonoverlapping STFTs of this signal with the rectangular window of the widths $N = 1$, $N = 2$, and $N = 4$. Plot the regions and indicate the values of $STFT_1(n, k)$ for $n = 0, 1, 2, 3, 4, 5, 6, 7$, then $STFT_2(n, k)$ for $n = 1, 2, 3, 5, 7$ and $STFT_4(n, k)$ for $n = 3, 7$ in three figures. Use (2.45) as the $STFT_N(n, k)$ definition.

(b) Assuming that the time-varying approach is used in the STFT calculation (for one instant, one window is used for all frequency bins), find the total number of possible representations using only the regions from (a).

(c) Calculate the concentration measure for each of the cases in (b) and find the representation (nonoverlapping combination of previous STFTs) when the signal is represented with the smallest number of coefficients.

Problem 2.16. Consider a signal $x(n)$ with $M = 8$ samples. Its values are

$$\begin{bmatrix} x(0) & x(1) & x(2) & x(3) & x(4) & x(5) & x(6) & x(7) \end{bmatrix} \\ = \begin{bmatrix} 1 & 1/2 & -1/2 & -1/4 & 1/4 & -1/4 & 1/4 & 0 \end{bmatrix}.$$

(a) Calculate the STFTs of this signal with rectangular window of the widths $N = 1$, $N = 2$, $N = 4$, and $N = 8$. Calculate $STFT_1(n, k)$ for $n = 0, 1, 2, 3, 4, 5, 6, 7$, then $STFT_2(n, k)$ for $n = 1, 2, 3, 4, 6, 7$, then $STFT_4(n, k)$ for $n = 3, 4, 5, 6, 7$ and $STFT_8(n, k)$ for $n = 7$. Use (2.45) as the $STFT_N(n, k)$ definition.

(b) Assuming that time-varying approach is used in the nonoverlapping STFT calculation (for one instant, one window is used for all frequency bins), find the total number of possible representations. What is the difference from the previous problem?

(c) Calculate the concentration measure for each of the cases in (b) and find the representation (nonoverlapping combination of previous STFTs) when the signal is represented with the smallest number of coefficients.

Problem 2.17. A discrete signal $x(n)$ is considered for $0 \leq n < N$. Find the number of the STFTs of this signal with time-varying windows.

(a) Consider arbitrary window widths from 1 to N .

(b) Consider diadic windows, that is, windows whose width is 2^m , where m is an integer, such that $2^m \leq N$. In this case find the number of time-varying window STFTs for $N = 1, 2, 3, \dots, 15, 16$.

Problem 2.18. Write a function that will calculate the STFT. The input arguments are: a signal in vector x , a window in vector w , and a time step T_s . The function

should return the STFT as a matrix S . Assume that x and w are column vectors and T_s is a nonnegative integer.

Problem 2.19. By using the function defined in Problem 2.18, write a code for calculation of the spectrogram described in Example 2.9 and for displaying results as in Fig. 2.5(a). Use `imagesc` function instead of `waterfall` for data visualization.

Problem 2.20. By using the function defined in Problem 2.18, write a code for the spectrogram calculation with the best window width, determined by using the concentration measure according to (2.118). A set W of possible window widths is given. The Hann(ing) window form is assumed. All spectrograms are zero-padded up to the widest window from the set of window widths W . Use the measure with $p = 2$ as a default value.

Problem 2.21. Calculate the best concentrated spectrogram for the signal described in Example 2.22. Assume that the time step is 1, while the set of window widths is from 32 to 256 with step 8. Plot the spectrogram obtained with the best window, as well as the concentration measure versus window width.

2.14 SOLUTIONS

Solution 2.1. The instantaneous frequency is

$$\Omega_i(t) = \frac{d(64\sin(\pi t) - 8\pi t)}{dt} = 64\pi\cos(\pi t) - 8\pi.$$

Extreme values of the instantaneous frequency are $\Omega_i(\pm(2k + 1)) = -72\pi$ and $\Omega_i(2k) = 56\pi$, where k is an integer. Thus, the sampling interval is defined by using the maximal absolute value $|\Omega_i(\pm(2k + 1))| = 72\pi$ with

$$\Delta t < \frac{\pi}{72\pi} = \frac{1}{72}.$$

For the signal $x(t) = \exp(j128\pi t^2)$ within $-2 \leq t \leq 2$ and $x(t) = 0$ elsewhere, the instantaneous frequency is

$$\Omega_i(t) = 256\pi t \text{ within } -2 \leq t \leq 2.$$

Thus, the sampling interval is

$$\Delta t < \frac{\pi}{512\pi} = \frac{1}{512}.$$

Since the stationary phase is just an approximation, the values of sampling interval close to this limit should be avoided, in real applications.

Solution 2.2. The effective window width in the frequency domain is

$$\begin{aligned}\sigma_{\Omega}^2 &= \frac{\frac{1}{2\pi} \int_{-\infty}^{\infty} \Omega^2 |W(\Omega)|^2 d\Omega}{\frac{1}{2\pi} \int_{-\infty}^{\infty} |W(\Omega)|^2 d\Omega} = \frac{\int_{-\infty}^{\infty} |w'(t)|^2 dt}{\int_{-\infty}^{\infty} |w(t)|^2 dt} \\ &= \frac{\pi^2}{T^2} \frac{\int_{-T}^T \sin^2(t\pi/T) dt}{\int_{-T}^T (1 + \cos(t\pi/T))^2 dt} = \frac{\pi^2}{T^2} \frac{T}{2T + T} = \frac{\pi^2}{3T^2}.\end{aligned}$$

The Fourier transform of the Hann(ing) window is

$$W(\Omega) = \frac{\pi^2 \sin(\Omega T)}{\Omega(\pi^2 - \Omega^2 T^2)}$$

with the mainlobe width following from $\Omega T = 2\pi$ as $d_{\Omega} = 4\pi/T$. Obviously the effective width, in this case, is smaller than the mainlobe width.

The effective window width in the time domain is

$$\begin{aligned}\sigma_t^2 &= \frac{\int_{-\infty}^{\infty} t^2 |w(t)|^2 dt}{\int_{-\infty}^{\infty} |w(t)|^2 dt} = \frac{\int_{-T}^T t^2 (1 + \cos(t\pi/T))^2 dt}{\int_{-T}^T (1 + \cos(t\pi/T))^2 dt} \\ &= \frac{T^3(1 - \frac{15}{2\pi^2})}{2T + T} = T^2 \left(\frac{1}{3} - \frac{5}{2\pi^2} \right).\end{aligned}$$

The width of the Hann(ing) window in the time domain is $d_t = 2T$. Again, the effective width, in this case, is lower than the window width, whose measure is $d_t/2 = T$.

The product of the widths in time and frequency is constant in both cases. For effective durations it is $\sigma_{\Omega} \sigma_t = \sqrt{\frac{\pi^2}{9} - \frac{5}{6}} = 0.5131$, while the product of the window width and mainlobe measures is $d_{\Omega}/2 \cdot d_t/2 = 2\pi$.

Solution 2.3. For a signal limited within $-T < t < T$, the difference between the effective duration measure and the squared half of the duration in time is

$$\sigma_t^2 - T^2 = \frac{\int_{-T}^T t^2 |w(t)|^2 dt}{\int_{-T}^T |w(t)|^2 dt} - T^2 < 0.$$

To prove this, let us rewrite the previous inequality as

$$\begin{aligned} \int_{-T}^T t^2 |w(t)|^2 dt - T^2 \int_{-T}^T |w(t)|^2 dt &< 0 \\ \int_{-T}^T (t^2 - T^2) |w(t)|^2 dt &< 0. \end{aligned}$$

The last integral is negative since $(t^2 - T^2) < 0$ for any $|t| < T$.

Solution 2.4. For this Gaussian window $w(\tau) = e^{-\tau^2/2}$ the Fourier transform is

$$W(\Omega) = \int_{-\infty}^{\infty} e^{-\tau^2/2} e^{-j\Omega\tau} d\tau,$$

with

$$\frac{dW(\Omega)}{d\Omega} = -j \int_{-\infty}^{\infty} \tau e^{-\tau^2/2} e^{-j\Omega\tau} d\tau.$$

Applying the integration by parts $du = \tau e^{-\tau^2/2} d\tau$ and $v = e^{-j\Omega\tau}$, we get

$$\frac{dW(\Omega)}{d\Omega} = -\Omega W(\Omega) \text{ with } W(0) = \sqrt{2\pi}.$$

The solution of the differential equation

$$\frac{dW(\Omega)}{W(\Omega)} = -\Omega d\Omega$$

is

$$\ln W(\Omega) = -\Omega^2/2 + \text{const},$$

with $W(\Omega) = \sqrt{2\pi} \exp(-\Omega^2/2) = \sqrt{2\pi} w(\Omega)$.

Solution 2.5. Windowed reconstruction, at an instant $t + 2kR$, is

$$x(t + 2kR + \tau)w(\tau) = \frac{1}{2\pi} \int_{-\infty}^{\infty} STFT(t + 2kR, \Omega) e^{j\Omega\tau} d\Omega.$$

Obviously for $R < T$ some of these regions overlap. In order to reduce the windowed signal to the same range in τ we will make the substitution $2kR + \tau \rightarrow \tau$, resulting in

$$x(t + \tau)w(\tau - 2kR) = \frac{1}{2\pi} \int_{-\infty}^{\infty} STFT(t + 2kR, \Omega) e^{j\Omega(\tau - 2kR)} d\Omega.$$

Summing these values over k , we get

$$x(t + \tau) = \frac{1}{\sum_{k=-\infty}^{\infty} w(\tau - 2kR)} \sum_{k=-\infty}^{\infty} \frac{1}{2\pi} \int_{-\infty}^{\infty} STFT(t + 2kR, \Omega) e^{j\Omega(\tau - 2kR)} d\Omega,$$

for a given t and $-T \leq \tau \leq T$.

Hint: Plot $q(\tau) = \sum_{k=-\infty}^{\infty} w(\tau - 2kR)$ within $-T \leq \tau \leq T$ for various R and windows. Consider step T equal to a half of the window width and: (a) Hann(ing), (b) Hamming, (c) triangular, and (d) rectangular window. Consider the cases when the steps are equal to $T/2$ and $T/4$, as well.

Solution 2.6. The overall STFT width is equal to the sum of the frequency variation caused width and the window's Fourier transform width. For Hann(ing) window, assuming that the Fourier transform width is the width of the mainlobe, it is

$$D_o = 4aT + \frac{4\pi}{T},$$

with $a = 64\pi$. From $dD_o/dT = 0$ follows the optimal window width

$$T = \frac{1}{8}.$$

Solution 2.7. For this signal the instantaneous frequency is $\Omega_i(t) = 16\pi t + 64\pi$. Since the phase variations are significantly faster than the amplitude variations, then we may approximate the frequency range by using the stationary-phase method, for $-1 \leq t \leq 1$, as $48\pi \leq \Omega \leq 80\pi$. Since the signal is sampled with $\Delta t = 1/32$ then the maximal frequency is $\Omega_m = \pi/\Delta t = 32\pi$ with periodical extension period $2\Omega_0 = 2\Omega_m = 64\pi$. Thus, the original frequency range is outside the maximal frequency. In the time-frequency plane we will have its periodically extended replica within $48\pi - 64\pi \leq \Omega \leq 80\pi - 64\pi$ or in the time-frequency domain

$$\begin{aligned} -16\pi &\leq \Omega \leq 16\pi \\ -1 &\leq t \leq 1, \end{aligned}$$

presenting the signal

$$x_r(t) = e^{-t^2} e^{j8\pi t^2}.$$

The Nyquist rate for the original signal should be

$$\Delta t < \frac{\pi}{80\pi} = \frac{1}{80}.$$

Obviously, the interval $\Delta t = 1/32$ does not satisfy this condition. However, the time-frequency representation form is preserved (with frequency shift only).

Solution 2.8. The sampling interval for this signal, assuming that values smaller than e^{-4} , that is, outside $-2 \leq t \leq 2$ could be neglected, is

$$\Delta t < \frac{1}{96}$$

since the frequency range is $32\pi \leq \Omega \leq 96\pi$. The maximal possible sampling interval that allows the time-frequency representation recovering (with an additional shift in frequency of -64π) is obtained from $-32\pi \leq \Omega \leq 32\pi$ as

$$\Delta t < \frac{1}{32}.$$

The comment is left to the reader.

Solution 2.9. The moment relation, by using the third moment for Ω_1 , reads

$$\frac{M_{0.5} - M_0 - m_x}{M_{\Omega_1} - M_0 - 4\Omega_1^2 m_x} = \frac{0.5}{\Omega_1}$$

with

$$\begin{aligned} M_{\Omega_1} &= 4\Omega_1^2 m_x + M_0 + 2\Omega_1(M_{0.5} - M_0 - m_x) \\ &= 80\Omega_1^2 - 60\Omega_1 + 25. \end{aligned}$$

The minimum is achieved at

$$160\Omega_1 - 60 = 0$$

or $\Omega_1 = 0.375$.

Thus, the best concentrated second-order LPFT of this signal is

$$\begin{aligned} LPFT_{\Omega_1}(t, \Omega) &= \int_{-\infty}^{\infty} x(t+\tau) e^{-j0.375\tau^2} w(\tau) e^{-j\Omega\tau} d\tau \\ &= STFT \left\{ x(t+\tau) e^{-j0.375\tau^2} \right\}, \end{aligned}$$

with the second-order moment being quite small $M_{\Omega_1=0.375} = 13.75$, meaning a highly concentrated representation with $\Omega_1 = 0.375$.

Solution 2.10. (a) In this case the time-frequency plane will be divided into two parts in time with four regions resolution in frequency. It will look like

$$\begin{array}{cccc} STFT_4(0, 3) & STFT_4(4, 3) & STFT_4(8, 3) & STFT_4(12, 3) \\ STFT_4(0, 2) & STFT_4(4, 2) & STFT_4(8, 2) & STFT_4(12, 2) \\ STFT_4(0, 1) & STFT_4(4, 1) & STFT_4(8, 1) & STFT_4(12, 1) \\ STFT_4(0, 0) & STFT_4(4, 0) & STFT_4(8, 0) & STFT_4(12, 0) \end{array}$$

(b) This case corresponds to the scheme,

$$\begin{array}{cccc} \dots \dots \dots STFT_8(0, 7) \dots \dots \dots & \dots \dots \dots STFT_8(8, 7) \dots \dots \dots \\ \dots \dots \dots STFT_8(0, 6) \dots \dots \dots & \dots \dots \dots STFT_8(8, 6) \dots \dots \dots \\ STFT_4(0, 2) & STFT_4(4, 2) & STFT_4(8, 2) & STFT_4(12, 2) \\ STFT_4(0, 1) & STFT_4(4, 1) & STFT_4(8, 1) & STFT_4(12, 1) \\ \dots \dots \dots STFT_8(0, 1) \dots \dots \dots & \dots \dots \dots STFT_8(8, 1) \dots \dots \dots \\ \dots \dots \dots STFT_8(0, 0) \dots \dots \dots & \dots \dots \dots STFT_8(8, 0) \dots \dots \dots \end{array}$$

(c) In this case we have the scheme

$$\begin{array}{cccc} \dots \dots \dots STFT_{16}(0, 15) \dots \dots \dots \\ \dots \dots \dots STFT_{16}(0, 14) \dots \dots \dots \\ \dots \dots \dots STFT_{16}(0, 13) \dots \dots \dots \\ \dots \dots \dots STFT_{16}(0, 12) \dots \dots \dots \\ STFT_4(0, 2) & STFT_4(4, 2) & STFT_4(8, 2) & STFT_4(12, 2) \\ STFT_4(0, 1) & STFT_4(4, 1) & STFT_4(8, 1) & STFT_4(12, 1) \\ STFT_4(0, 0) & STFT_4(4, 0) & STFT_4(8, 0) & STFT_4(12, 0) \end{array}$$

Solution 2.11. If we skip two signal samples, then the STFT with a rectangular window is

$$\begin{aligned}
 STFT(n+2, k) &= \sum_{m=0}^{N-1} x(n+2+m)e^{-j2\pi mk/N} \\
 &= \sum_{m=2}^{N+2-1} x(n+m)e^{-j2\pi(m-2)k/N} \\
 &= e^{j4\pi k/N} \left[\sum_{m=0}^{N-1} x(n+m)e^{-j2\pi mk/N} + x(n+N)e^{-j2\pi Nk/N} \right. \\
 &\quad \left. + x(n+N+1)e^{-j2\pi(N+1)k/N} - x(n) - x(n+1)e^{-j2\pi k/N} \right] = e^{j4\pi k/N} \times \\
 &\quad \times [STFT(n, k) + x(n+N) + x(n+N+1)e^{-j2\pi k/N} - x(n) - x(n+1)e^{-j2\pi k/N}].
 \end{aligned}$$

The calculation complexity is three complex multiplications for each k , meaning in total $3N$ complex multiplications. In the FFT-based calculation the order of multiplications is $N/2 \log_2 N$. Thus, the recursive calculation is more efficient, regarding the multiplications, as far as $3 < 0.5 \log_2 N$. In this case $N > 64$. In a similar way we can analyze the number of additions.

The STFT for Hann(ing) and Hamming may be easily obtained by combining $STFT(n, k)$ and $STFT(n, k \pm 1)$ with appropriate coefficients.

Solution 2.12. The four-sample transform matrix for $C_4(n, k)$ coefficients could be written as

$$\begin{aligned}
 \mathbf{T}_4 &= \begin{bmatrix} 1 & 1 & 1 & 1 \\ 1 & 1 & -1 & -1 \\ 1 & -1 & 1 & -1 \\ 1 & -1 & -1 & 1 \end{bmatrix} \\
 &= \begin{bmatrix} \mathbf{T}_2 \otimes \begin{bmatrix} 1 & 1 \end{bmatrix} \\ \mathbf{T}_2 \otimes \begin{bmatrix} 1 & -1 \end{bmatrix} \end{bmatrix} \\
 &= \begin{bmatrix} \mathbf{T}_2 \otimes [\mathbf{T}_2(1, :)] \\ \mathbf{T}_2 \otimes [\mathbf{T}_2(2, :)] \end{bmatrix}
 \end{aligned}$$

where \otimes denotes Kronecker multiplication of two row submatrices in \mathbf{T}_2 with \mathbf{T}_2 . The notation $\mathbf{T}_2(i, :)$, means the i th row of matrix \mathbf{T}_2 .

The transformation matrix for $N = 8$ case is of the form

$$\begin{aligned} \mathbf{T}_8 &= \begin{bmatrix} 1 & 1 & 1 & 1 & 1 & 1 & 1 & 1 \\ 1 & 1 & 1 & 1 & -1 & -1 & -1 & -1 \\ 1 & 1 & -1 & -1 & 1 & 1 & -1 & -1 \\ 1 & 1 & -1 & -1 & -1 & -1 & 1 & 1 \\ 1 & -1 & 1 & -1 & 1 & -1 & 1 & -1 \\ 1 & -1 & 1 & -1 & -1 & 1 & -1 & 1 \\ 1 & -1 & -1 & 1 & 1 & -1 & -1 & 1 \\ 1 & -1 & -1 & 1 & -1 & 1 & 1 & -1 \end{bmatrix} \\ &= \begin{bmatrix} \mathbf{T}_2 \otimes [\mathbf{T}_4(1,:)] \\ \mathbf{T}_2 \otimes [\mathbf{T}_4(2,:)] \\ \mathbf{T}_2 \otimes [\mathbf{T}_4(3,:)] \\ \mathbf{T}_2 \otimes [\mathbf{T}_4(4,:)] \end{bmatrix}. \end{aligned}$$

Obviously the next order transformation matrix is obtained by a Kronecker product of the lower-order matrix rows and \mathbf{T}_2 . Therefore, the transformation matrix of $C_{16}(n,k)$, for $N = 16$, could be written as

$$\mathbf{T}_{16} = \begin{bmatrix} \mathbf{T}_2 \otimes [\mathbf{T}_8(1,:)] \\ \mathbf{T}_2 \otimes [\mathbf{T}_8(2,:)] \\ \mathbf{T}_2 \otimes [\mathbf{T}_8(3,:)] \\ \mathbf{T}_2 \otimes [\mathbf{T}_8(4,:)] \\ \mathbf{T}_2 \otimes [\mathbf{T}_8(5,:)] \\ \mathbf{T}_2 \otimes [\mathbf{T}_8(6,:)] \\ \mathbf{T}_2 \otimes [\mathbf{T}_8(7,:)] \\ \mathbf{T}_2 \otimes [\mathbf{T}_8(8,:)] \end{bmatrix} = \begin{bmatrix} 1 & 1 & 1 & 1 & 1 & 1 & 1 & 1 & 1 & 1 & 1 & 1 & 1 & 1 & 1 & 1 \\ 1 & 1 & 1 & 1 & 1 & 1 & 1 & 1 & -1 & -1 & -1 & -1 & -1 & -1 & -1 & -1 \\ 1 & 1 & 1 & 1 & -1 & -1 & -1 & -1 & 1 & 1 & 1 & 1 & -1 & -1 & -1 & -1 \\ 1 & 1 & 1 & 1 & -1 & -1 & -1 & -1 & -1 & -1 & -1 & -1 & 1 & 1 & 1 & 1 \\ 1 & 1 & -1 & -1 & 1 & 1 & -1 & -1 & 1 & 1 & -1 & -1 & 1 & 1 & -1 & -1 \\ 1 & 1 & -1 & -1 & 1 & 1 & -1 & -1 & -1 & 1 & 1 & -1 & 1 & 1 & -1 & -1 \\ 1 & 1 & -1 & -1 & -1 & 1 & 1 & 1 & 1 & -1 & -1 & -1 & 1 & 1 & 1 & 1 \\ 1 & 1 & -1 & -1 & -1 & 1 & 1 & 1 & -1 & 1 & 1 & -1 & -1 & 1 & 1 & 1 \\ 1 & -1 & 1 & -1 & 1 & -1 & 1 & -1 & 1 & -1 & 1 & -1 & 1 & -1 & 1 & -1 \\ 1 & -1 & 1 & -1 & 1 & -1 & 1 & -1 & -1 & 1 & -1 & 1 & -1 & 1 & -1 & 1 \\ 1 & -1 & 1 & -1 & -1 & 1 & -1 & 1 & 1 & -1 & 1 & -1 & -1 & 1 & -1 & 1 \\ 1 & -1 & 1 & -1 & -1 & 1 & -1 & -1 & 1 & 1 & -1 & 1 & -1 & -1 & 1 & -1 \\ 1 & -1 & -1 & 1 & 1 & -1 & -1 & 1 & 1 & 1 & -1 & -1 & 1 & 1 & -1 & -1 \\ 1 & -1 & -1 & 1 & 1 & -1 & -1 & -1 & 1 & 1 & -1 & -1 & 1 & 1 & -1 & -1 \\ 1 & -1 & -1 & -1 & 1 & 1 & -1 & -1 & -1 & 1 & 1 & -1 & 1 & -1 & 1 & -1 \\ 1 & -1 & -1 & -1 & 1 & 1 & -1 & -1 & -1 & -1 & 1 & 1 & -1 & 1 & -1 & 1 \end{bmatrix}.$$

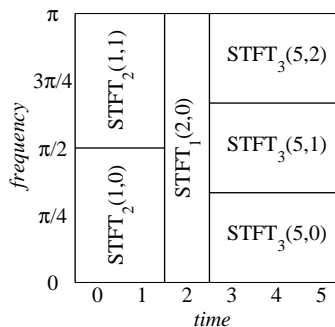


Figure 2.23 Denoted areas in the time-frequency plane.

Solution 2.13. (a) Denoted areas are presented in Fig. 2.23.

(b) Relations for the STFT calculations are

$$\begin{aligned}STFT_2(1,0) &= x(1) + x(0) \\STFT_2(1,1) &= x(1) - x(0) \\STFT_1(2,0) &= x(2) \\STFT_3(5,0) &= x(5) + x(4) + x(3)\end{aligned}$$

$$\begin{aligned}STFT_3(5,1) &= x(5) - \frac{1-j\sqrt{3}}{2}x(4) - \frac{1+j\sqrt{3}}{2}x(3) \\STFT_3(5,2) &= x(5) - \frac{1+j\sqrt{3}}{2}x(4) - \frac{1-j\sqrt{3}}{2}x(3)\end{aligned}$$

and the transformation matrix (where the STFT coefficients are arranged into column vector \mathbf{S}) is

$$\mathbf{T} = \begin{bmatrix} 1 & 1 & 0 & 0 & 0 & 0 \\ -1 & 1 & 0 & 0 & 0 & 0 \\ 0 & 0 & 1 & 0 & 0 & 0 \\ 0 & 0 & 0 & 1 & 1 & 1 \\ 0 & 0 & 0 & -\frac{1+j\sqrt{3}}{2} & -\frac{1-j\sqrt{3}}{2} & 1 \\ 0 & 0 & 0 & -\frac{1-j\sqrt{3}}{2} & -\frac{1+j\sqrt{3}}{2} & 1 \end{bmatrix}.$$

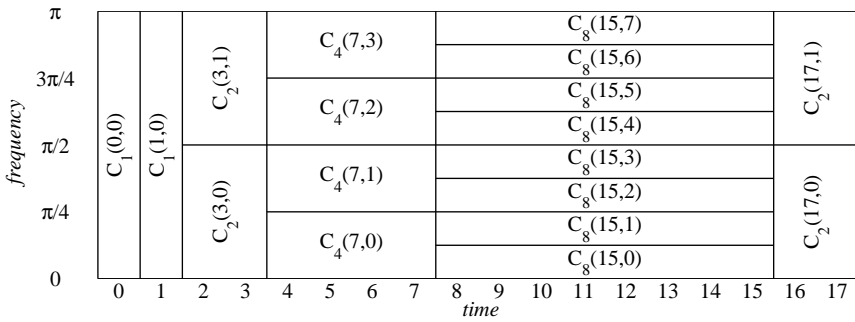


Figure 2.24 Denoted regions in the time-frequency plane.

(c) The STFT coefficients are

$$\mathbf{S} = \begin{bmatrix} 1 & 1 & 0 & 0 & 0 & 0 \\ -1 & 1 & 0 & 0 & 0 & 0 \\ 0 & 0 & 1 & 0 & 0 & 0 \\ 0 & 0 & 0 & 1 & 1 & 1 \\ 0 & 0 & 0 & -\frac{1+j\sqrt{3}}{2} & -\frac{1-j\sqrt{3}}{2} & 1 \\ 0 & 0 & 0 & -\frac{1-j\sqrt{3}}{2} & -\frac{1+j\sqrt{3}}{2} & 1 \end{bmatrix} \begin{bmatrix} 2 \\ -2 \\ 4 \\ \sqrt{3} \\ -\sqrt{3} \\ 0 \end{bmatrix} = \begin{bmatrix} 0 \\ -4 \\ 4 \\ 0 \\ -j3 \\ j3 \end{bmatrix}.$$

(d) The signal samples $y(n)$ are obtained as $\mathbf{T}^{-1}\mathbf{S}$ resulting in

$$\begin{bmatrix} y(5) & y(4) & y(3) & y(2) & y(1) & y(0) \end{bmatrix}^T = \begin{bmatrix} 2 & 2 & 1 & -1 & -1 & 2 \end{bmatrix}^T.$$

Solution 2.14. (a) Denoted regions are given in Fig. 2.24.

(b) According to the notation presented in Fig. 2.24, we have

$$C_1(1,0) = x(1)$$

$$C_2(3,1) = x(3) - x(2)$$

$$C_4(7,2) = x(7) - x(6) + x(5) - x(4)$$

$$C_8(15,4) = x(15) - x(14) + x(13) - x(12) + x(11) - x(10) + x(9) - x(8).$$

(c) The transformation matrix \mathbf{T} can be presented in a block form as

$$\mathbf{T} = \begin{bmatrix} \mathbf{T}_2 & \mathbf{0} & \mathbf{0} & \mathbf{0} & \mathbf{0} & \mathbf{0} \\ \mathbf{0} & \mathbf{T}_8 & \mathbf{0} & \mathbf{0} & \mathbf{0} & \mathbf{0} \\ \mathbf{0} & \mathbf{0} & \mathbf{T}_4 & \mathbf{0} & \mathbf{0} & \mathbf{0} \\ \mathbf{0} & \mathbf{0} & \mathbf{0} & \mathbf{T}_2 & \mathbf{0} & \mathbf{0} \\ \mathbf{0} & \mathbf{0} & \mathbf{0} & \mathbf{0} & \mathbf{T}_1 & \mathbf{0} \\ \mathbf{0} & \mathbf{0} & \mathbf{0} & \mathbf{0} & \mathbf{0} & \mathbf{T}_1 \end{bmatrix}$$

where the elements outside main diagonal are zero matrices. Note that here, the signal vector is formed by arranging samples $x(17)$ to $x(0)$ into a descending order

$$[x(17) \quad x(16) \quad x(15) \quad \dots \quad x(1) \quad x(0)]^T.$$

Finally, we get 18×18 matrix

$$\mathbf{T} = \begin{bmatrix} + & + & \cdot \\ + & - & \cdot \\ \cdot & + & + & + & + & + & + & + & + & + & + & + & + & + & + & + & + & + \\ \cdot & + & + & + & + & - & - & - & - & - & - & - & - & - & - & - & - & - \\ \cdot & + & + & - & - & + & + & - & - & + & + & - & - & + & + & - & - & + \\ \cdot & + & + & - & - & - & - & - & + & + & + & + & + & + & + & + & + & + \\ \cdot & + & - & + & - & + & - & + & - & + & - & + & - & + & - & + & - & + \\ \cdot & + & - & + & - & + & - & + & - & + & - & + & - & + & - & + & - & + \\ \cdot & + & - & - & + & + & - & - & + & + & - & - & + & + & - & - & + & + \\ \cdot & + & - & - & + & - & + & - & + & - & + & - & + & - & + & - & + & - \\ \cdot & \cdot \\ \cdot & \cdot \\ \cdot & \cdot \\ \cdot & \cdot \\ \cdot & \cdot \\ \cdot & \cdot \end{bmatrix}$$

where “+” denotes $+1$, “-” denotes -1 and “.” stands for 0 .

(d) We can find the signal samples as $\mathbf{T}^{-1}\mathbf{C}$, where \mathbf{T} is the transformation matrix and \mathbf{C} is the coefficients vector. Resulting vector, containing signal samples, is

$$\frac{n}{x(n)} \left| \begin{array}{cccccccccccccccccc} 17 & 16 & 15 & 14 & 13 & 12 & 11 & 10 & 9 & 8 & 7 & 6 & 5 & 4 & 3 & 2 & 1 & 0 \\ 0 & 0 & 1 & -1 & 1 & -1 & 2 & -2 & 2 & -2 & 3 & -3 & 3 & -3 & 6 & -6 & 12 & 0 \end{array} \right.$$

Solution 2.15. (a) The signal $x(0) = 0$, $x(1) = 1$, $x(2) = 1/2$, $x(3) = -1/2$, $x(4) = 1/4$, $x(5) = -j/4$, $x(6) = -1/4$, and $x(7) = j/4$, has the STFTs as:
 $STFT_N(n, k) = \sum_{m=0}^{N-1} x(n-m) e^{j2\pi mk/N}$
– for $N = 1$

$$STFT_1(n, 0) = x(n), \quad \text{for all } n = 0, 1, 2, 3, 4, 5, 6, 7;$$

– for $N = 2$

$$\begin{aligned} STFT_2(n, 0) &= x(n) + x(n-1) \\ STFT_2(1, 0) &= 1, \\ STFT_2(3, 0) &= 0, \\ STFT_2(5, 0) &= (1+j)/4, \\ STFT_2(7, 0) &= (-1-j)/4 \\ STFT_2(n, 1) &= x(n) - x(n-1) \\ STFT_2(1, 1) &= 1, \\ STFT_2(3, 1) &= -1, \\ STFT_2(5, 1) &= (-1-j)/4, \\ STFT_2(7, 1) &= (1+j)/4 \end{aligned}$$

– for $N = 4$

$$\begin{aligned} STFT_4(n, 0) &= x(n) + x(n-1) + x(n-2) + x(n-3) \\ STFT_4(3, 0) &= 1, \\ STFT_4(7, 0) &= 0 \\ STFT_4(n, 1) &= x(n) + jx(n-1) - x(n-2) - jx(n-3) \\ STFT_4(3, 1) &= (-3+j)/2, \\ STFT_4(7, 1) &= 0 \\ STFT_4(n, 2) &= x(n) - x(n-1) + x(n-2) - x(n-3) \\ STFT_4(3, 2) &= 0, \\ STFT_4(7, 2) &= 0, \\ STFT_4(n, 3) &= x(n) - jx(n-1) - x(n-2) + jx(n-3) \\ STFT_4(3, 3) &= -(3+j)/2, \\ STFT_4(7, 3) &= j \end{aligned}$$

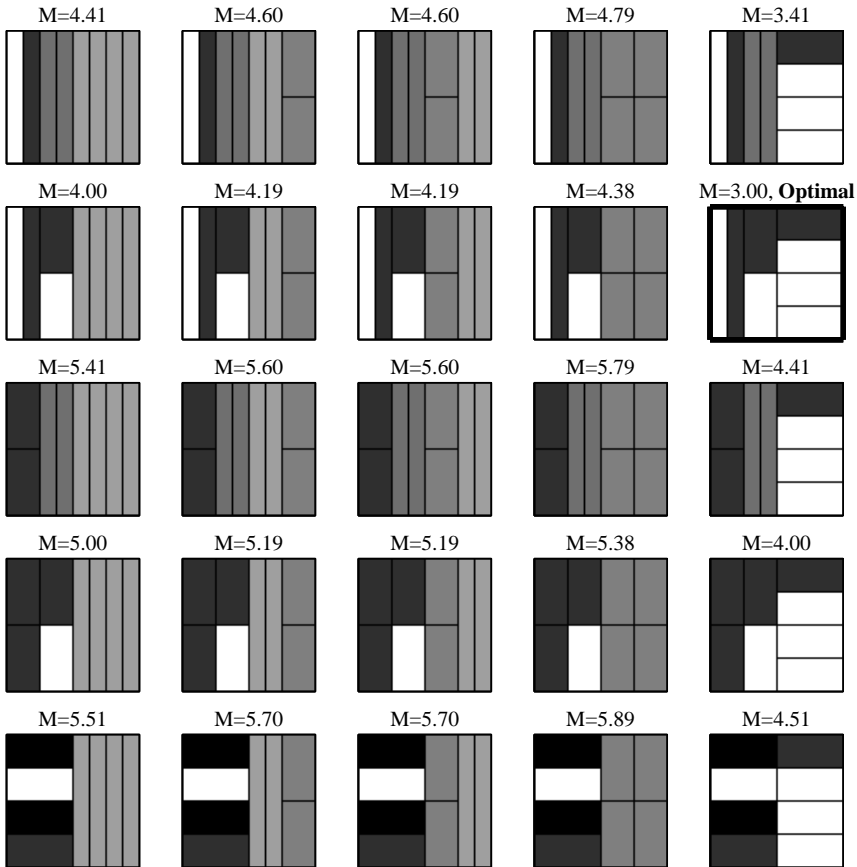


Figure 2.25 Time-frequency representation in various lattices (grid-lines are shown), with concentration measure $M = \mu[\text{SPEC}(n,k)]$ value. The optimal representation, with respect to this measure, is presented with thicker gridlines.

(b) Now we have to make all possible nonoverlapping combinations of these transforms and to calculate the concentration measure for each of them. The absolute STFT values are shown in Fig. 2.25, along with measure $\mu[\text{SPEC}(n,k)] = \sum_n \sum_k |\text{STFT}(n,k)|^{1/2}$ for each case.

(c) By measuring the concentration for all of them, we will get that the optimal combination, to cover the time-frequency plane, is

$$\begin{aligned} STFT_1(1,0) &= x(1) = 1 \\ STFT_2(3,1) &= x(3) - x(2) = -1 \\ STFT_4(7,3) &= x(7) - jx(6) - x(5) + jx(4) = j \\ STFT_1(0,0) &= x(0) = 0 \\ STFT_2(3,0) &= x(3) + x(2) = 0 \\ STFT_4(7,0) &= x(7) + x(6) + x(5) + x(4) = 0 \\ STFT_4(7,1) &= x(7) + jx(6) - x(5) - jx(4) = 0 \\ STFT_4(7,2) &= x(7) - x(6) + x(5) - x(4) = 0, \end{aligned}$$

with just three nonzero transformation coefficients and $\mu[SPEC(n,k)] = 3$.

In this case there is an algorithm for efficient optimal lattice determination, based on two regions consideration, starting from lattices 1, 19, and 25 from the Fig. 2.25, corresponding to the constant window widths of $N = 1$, $N = 2$, and $N = 4$ samples.

Solution 2.16. The possible cases, that are not included in the previous problem analysis, are $STFT_1(n,k)$ followed by $STFT_2(n,k)$, and so on. Also here we may have $STFT_1(n,k)$ followed by $STFT_4(n,k)$ and similar combinations, not included in the previous problem, analysis. All possible lattices with corresponding measures are presented in Fig. 2.26 .

Solution 2.17. (a) Let us analyze the problem recursively. Denote by $F(N)$ the number of STFTs for a signal with N samples. It is obvious that $F(1) = 1$, that is, for one-sample signal there is only one STFT (signal sample itself). If $N > 1$, we can use window with widths $k = 1, 2, \dots, N$, as the first analysis window. Now let us analyze remaining $(N - k)$ samples in all possible ways, so we can write a recursive relation for the total number of the STFTs. If the first window is one-sample window, then the number of the STFTs is $F(N - 1)$. When the first window is a two-sample window, then the total number of the STFTs is $F(N - 2)$, and so on, until the first window is the N -sample window, when $F(N - N) = 1$. Thus, the total number of the STFTs for all cases is

$$F(N) = F(N - 1) + F(N - 2) + \dots + F(1) + 1$$

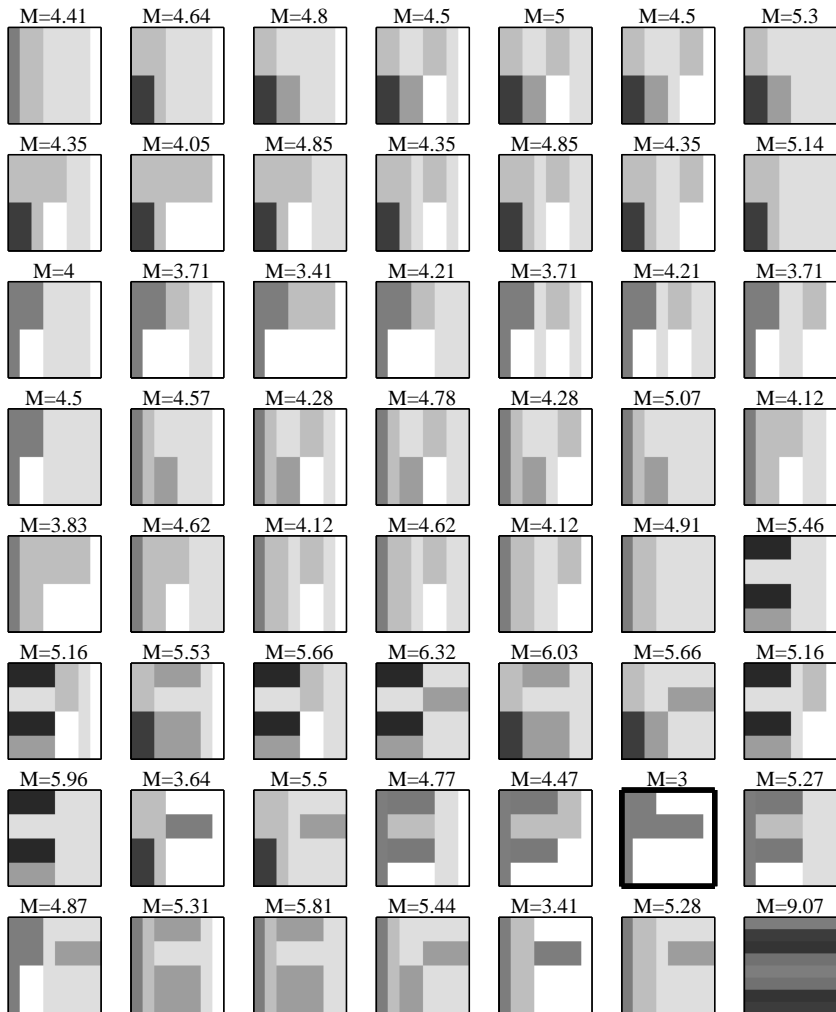


Figure 2.26 All possible time-frequency representations (lattices) for an eight-sample signal with the time-varying window only. Concentration measure $M = \mu[\text{SPEC}(n, k)]$ value for each representation is given.

We can introduce $F(0) = 1$ (meaning that if there are no signal samples we have only one way to calculate time-varying window STFT) and obtain

$$F(N) = F(N-1) + F(N-2) + \dots + F(1) + F(0) = \sum_{k=1}^N F(N-k)$$

Now, for $N > 1$ we can write

$$F(N-1) = \sum_{k=1}^{N-1} F(N-1-k) = \sum_{k=2}^N F(N-k)$$

and

$$\begin{aligned} F(N) - F(N-1) &= \sum_{k=1}^N F(N-k) - \sum_{k=2}^N F(N-k) = F(N-1) \\ F(N) &= 2F(N-1) \end{aligned}$$

resulting in

$$F(N) = 2^{N-1}.$$

(b) In a similar way, following the previous analysis, we can write

$$\begin{aligned} F(N) &= F(N-2^0) + F(N-2^1) + F(N-2^2) + \dots + F(N-2^m) \\ &= \sum_{m=0}^{\lfloor \log_2 N \rfloor} F(N-2^m) \end{aligned}$$

where $\lfloor \log_2 N \rfloor$ is an integer part of $\log_2 N$. Here we cannot write a simple recurrent relation as in the previous case. It is obvious that $F(1) = 1$. We can also assume that $F(0) = 1$. By unfolding recurrence we will get

$$\begin{aligned} F(2) &= F(1) + F(0) = 2 \\ F(3) &= F(2) + F(1) = 3 \\ F(4) &= F(3) + F(2) + F(0) = 6 \\ &\vdots \end{aligned}$$

The results are presented in the table

N	1	2	3	4	5	6	7	8
$F(N)$	1	2	3	6	10	18	31	56
N	9	10	11	12	13	14	15	16
$F(N)$	98	174	306	542	956	1690	2983	5272

Note that the approximative formula

$$F(N) \approx [1.0366 \cdot (1.7664)^{N-1}]$$

where $[.]$ is an integer part of the argument, holds, with relative error smaller than 0.4% for $1 \leq N \leq 1024$. Check it numerically.

Solution 2.18. The function STFT_calc.m for an STFT calculation is

```
function S=STFT_calc(x,w,Ts)
M=length(x);
N=length(w);
t=1:Ts:M-N;
S=zeros(N,length(t));
tau=(0:N-1);
for k=1:length(t)
    S(:,k)=x(t(k)+tau).*w;
end
S=fftshift(fft(S),1);
```

Solution 2.19. The code is given in the sequel.

```
t=(-32:(255+32))';
x1=sin(9*pi/16*t-pi/10/128*(t-128).^2-pi/2)+...
    sin(pi/18*t)+...
    1.2*sin(15*pi/16*t-pi/8/128*(t-128).^2-pi/2)...
    .*exp(-((t-180)/40).^2)+...
    1.2*sin(4*pi/16*t-pi/32/128*(t-128).^2-pi/2)...
    .*exp(-((t-64)/40).^2);
S=STFT_calc(x1,hamming(64),1);
SP=abs(S).^2;
imagesc(SP)
```

In the considered problem the time axis is expanded in both directions by a half of the window width (32 samples) in order to obtain full forms of the STFT and the spectrogram for ending time points, 0 and 255.

The obtained image contains positive and negative frequencies. Since the analyzed signal is real-valued, it is enough to show positive frequencies only. The frequency axis is discretized with 64 samples (window width). In order to obtain a more detailed image, the frequency interpolation should be performed. The simplest way for this interpolation is to calculate the FFT with zero padding, up to, for example, 512 frequency samples, with $S=\text{fftshift}(\text{fft}(S, 512), 1)$; in the `STFT_calc` function. Another approach would be to zero pad the lag window (both sides) up to 512 samples.

Solution 2.20. The required code can be implemented as

```
function [STFTopt,M]=Opt_Conc(x,W,p)
if nargin==2, p=2; end
M=zeros(size(W));
for k=1:length(W);
    Win=padarray(hanning(W(k)), (max(W)-W(k))/2);
    S=abs(STFT_calc(x,Win,1)).^2;
    M(k)=sum(sum(S.^((1/2))))^2/sum(sum(S));
end
[d,k]=min(M);
Win=padarray(hanning(W(k)), (max(W)-W(k))/2);
STFTopt=STFT_calc(x,Win,1);
```

The windows are zero padded up to $\max(W)$ samples with `padarray` function. We also assumed that the window widths in `W` are even numbers.

Solution 2.21. This code can be written as

```
% Signal definition
dt=1/256;
t=[-2:dt:2]';
x=cos(50*cos(pi*t)+10*pi*t.^2+70*pi*t)...
+cos(25*pi*t.^2+180*pi*t);
% Optimal window calculation, for signal x,
% for windows W and measure with p=2
W=32:8:256;
[STFTopt,M]=Opt_Conc(x,W,2);
```

```
S=abs(STFTopt).^2;
% Displaying results
figure(1), plot(W,M)
figure(2), imagesc(S)
```

Chapter 3

Quadratic Time-Frequency Distributions

In order to provide additional insight into the field of joint time-frequency analysis, as well as to improve concentration of time-frequency representation, quadratic distributions of signals were introduced. We have already mentioned the spectrogram, a straightforward extension of the STFT, which belongs to this class of representations. Here, we will discuss other distributions and their generalizations.

The starting point for the definition of time-frequency energy distributions is that a two-dimensional function of time and frequency $P(t, \Omega)$ represents the energy density of a signal in the time-frequency plane. Thus, the signal energy associated with small time and frequency intervals Δt and $\Delta\Omega$, respectively, would be

$$\text{Signal energy within } [\Omega + \Delta\Omega, t + \Delta t] = P(t, \Omega) \Delta\Omega \Delta t.$$

However, point-by-point definition of time-frequency energy densities in the time-frequency plane is not possible, since the uncertainty principle prevents us from defining concept of energy at a specific instant and frequency. This is the reason why some more general conditions are being considered to derive time-frequency distributions of a signal. Namely, one requires that the integral of $P(t, \Omega)$ over Ω , for a particular instant of time, should be equal to the signal power $|x(t)|^2$, while the integral over time for a particular frequency should be equal to the spectral energy density $|X(\Omega)|^2$. These conditions are known as marginal conditions or marginal properties of time-frequency distributions.

Therefore, it is desirable that a quadratic energy time-frequency distribution of a signal $x(t)$ satisfies:

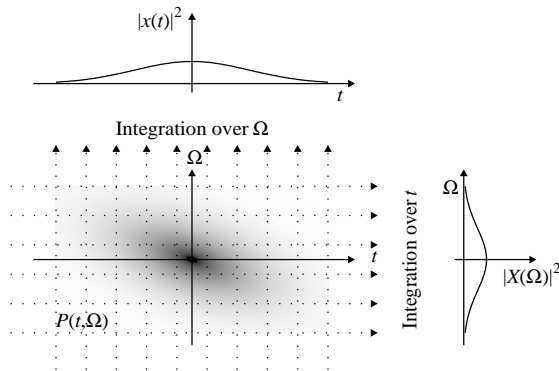


Figure 3.1 Illustration of the marginal properties.

1. Energy property

$$\frac{1}{2\pi} \int_{-\infty}^{\infty} \int_{-\infty}^{\infty} P(t, \Omega) d\Omega dt = E_x, \quad (3.1)$$

2. Time marginal property

$$\frac{1}{2\pi} \int_{-\infty}^{\infty} P(t, \Omega) d\Omega = |x(t)|^2, \quad (3.2)$$

3. Frequency marginal property

$$\int_{-\infty}^{\infty} P(t, \Omega) dt = |X(\Omega)|^2, \quad (3.3)$$

where E_x denotes the energy of $x(t)$. It is obvious that if either one of marginal properties (3.2) or (3.3) is fulfilled, so is the energy property. Note that relations (3.1), (3.2), and (3.3), do not reveal any information about the local distribution of energy at a point (t, Ω) . The marginal properties are illustrated in Fig. 3.1.

Next we will introduce some distributions satisfying these properties.

3.1 RIHACZEK DISTRIBUTION

Presentation of the quadratic distributions will start with a simple electrical engineering example. Consider a simple electrical circuit analysis. Assume that a voltage $v(t)$ is applied on a resistor whose resistance is $R = 1$ Ohm, but only within a very narrow frequency band (filter is used) $[\Omega, \Omega + \Delta\Omega]$

$$R(\theta) = \begin{cases} 1 & \text{for } \Omega \leq \theta < \Omega + \Delta\Omega \\ \infty & \text{elsewhere.} \end{cases} \quad (3.4)$$

The spectral content of the applied voltage is defined by its Fourier transform

$$V(\Omega) = \int_{-\infty}^{\infty} v(t) e^{-j\Omega t} dt.$$

The spectral content of current, through this circuit, at a frequency θ is

$$I(\theta) = \frac{V(\theta)}{R(\theta)} \quad (3.5)$$

or in the time domain

$$i(t) = \frac{1}{2\pi} \int_{-\infty}^{\infty} I(\theta) e^{j\theta t} d\theta = \frac{1}{2\pi} \int_{\Omega}^{\Omega + \Delta\Omega} V(\theta) e^{j\theta t} d\theta. \quad (3.6)$$

The energy dissipated at the resistor, within a short time interval $[t, t + \Delta t]$, is defined by

$$E(t, \Omega) = \int_t^{t + \Delta t} v(\tau) i^*(\tau) d\tau. \quad (3.7)$$

The substitution of (3.6) into (3.7) produces

$$E(t, \Omega) = \frac{1}{2\pi} \int_t^{t + \Delta t} \int_{\Omega}^{\Omega + \Delta\Omega} v(\tau) V^*(\theta) e^{-j\theta\tau} d\theta d\tau. \quad (3.8)$$

Based on the above considerations, one may define a time-frequency energy distribution as

$$P(t, \Omega) = \lim_{\substack{\Delta\Omega \rightarrow 0 \\ \Delta t \rightarrow 0}} \frac{E(t, \Omega)}{\Delta t \Delta\Omega / 2\pi} = v(t) V^*(\Omega) e^{-j\Omega t}. \quad (3.9)$$

The previous analysis may be generalized for an arbitrary signal $x(t)$ with the associated Fourier transform $X(\Omega)$.

Time-frequency distribution derived in this way is the Rihaczek distribution,

$$\begin{aligned} RD(t, \Omega) &= x(t)X^*(\Omega)e^{-j\Omega t} \\ &= \int_{-\infty}^{\infty} x(t)x^*(t-\tau)e^{-j\Omega\tau}d\tau = \frac{1}{2\pi} \int_{-\infty}^{\infty} X(\Omega+\theta)X^*(\Omega)e^{j\theta t}d\theta. \end{aligned} \quad (3.10)$$

This distribution satisfies marginal properties, since

$$\begin{aligned} \frac{1}{2\pi} \int_{-\infty}^{\infty} RD(t, \Omega)d\Omega &= \frac{1}{2\pi} \int_{-\infty}^{\infty} \int_{-\infty}^{\infty} [x(t)x^*(t-\tau)e^{-j\Omega\tau}]d\Omega d\tau = |x(t)|^2 \\ \int_{-\infty}^{\infty} RD(t, \Omega)dt &= \frac{1}{2\pi} \int_{-\infty}^{\infty} \int_{-\infty}^{\infty} [X(\Omega+\theta)X^*(\Omega)e^{j\theta t}]d\theta dt = |X(\Omega)|^2. \end{aligned}$$

The Rihaczek distribution form may also be introduced from the signal energy definition, as

$$\begin{aligned} E_x &= \int_{-\infty}^{\infty} x(t)x^*(t)dt = \frac{1}{2\pi} \int_{-\infty}^{\infty} \int_{-\infty}^{\infty} x(t)X^*(\Omega)e^{-j\Omega t}d\Omega dt \\ &= \frac{1}{2\pi} \int_{-\infty}^{\infty} \int_{-\infty}^{\infty} RD(t, \Omega)d\Omega dt, \end{aligned} \quad (3.11)$$

where the signal $x^*(t)$ is replaced by its inverse Fourier transform.

It seems that the Rihaczek distribution is the ideal distribution of signal energy, we have been looking for. However, energy is calculated over the intervals $[t, t + \Delta t]$ and $[\Omega, \Omega + \Delta\Omega]$, while $V(\Omega)$ was calculated over the entire time interval $(-\infty, \infty)$. This introduces an influence of other time intervals onto the interval $[t, t + \Delta t]$. Therefore, it is not as local as it may seem from the derivation. This distribution exhibits significant drawbacks for possible time-frequency analysis, as well. The most important one is its complex-valuedness, despite the fact that it has been derived with the aim of representing signal energy density. In addition, its time-frequency concentration of time-varying signals is quite low, as will be shown later. This distribution is of limited practical importance, yet some recent

contributions show that it could be interesting in the phase synchrony and stochastic signal analysis.

The Rihaczek distribution may be easily generalized. Namely, the marginal properties of the Rihaczek distribution (as a two-dimensional function of time and frequency) may be considered as its projections (Radon transforms) onto the time and frequency axis. The Fourier transform of the projection of a two-dimensional function, onto a given line, is equal to the value of the two-dimensional Fourier transform of this two-dimensional function, along the same line (inverse Radon transform property). Thus, any two-dimensional function having the same two-dimensional Fourier transform as the Rihaczek distribution, along the coordinate axes only, will satisfy the marginal properties. This kind of generalization will be presented later in this Chapter.

3.2 WIGNER DISTRIBUTION

The other quadratic distributions can not be easily derived, from a similar physical experiment, like the Rihaczek distribution. In order to introduce some other quadratic time-frequency distributions, observe that the Rihaczek distribution may be interpreted as the Fourier transform of the function

$$R(t, \tau) = x(t)x^*(t - \tau), \quad (3.12)$$

that will be referred to as the local auto-correlation function, since it corresponds to the auto-correlation function $R(t, t - \tau) = E\{x(t)x^*(t - \tau)\}$, for the case of deterministic signals. Its Fourier transform in τ

$$RD(t, \Omega) = \int_{-\infty}^{\infty} R(t, \tau)e^{-j\Omega\tau}d\tau, \quad (3.13)$$

results in the Rihaczek distribution. A general form of the local auto-correlation function, for an instant t , with the difference of arguments equal to τ , may be written as

$$R(t, \tau) = x(t + (\alpha + 1/2)\tau)x^*(t + (\alpha - 1/2)\tau) \quad (3.14)$$

where α is an arbitrary constant. Value of $\alpha = -1/2$ produces the Rihaczek distribution. The value $\alpha = 1/2$ could be also used as a variant of the Rihaczek distribution.

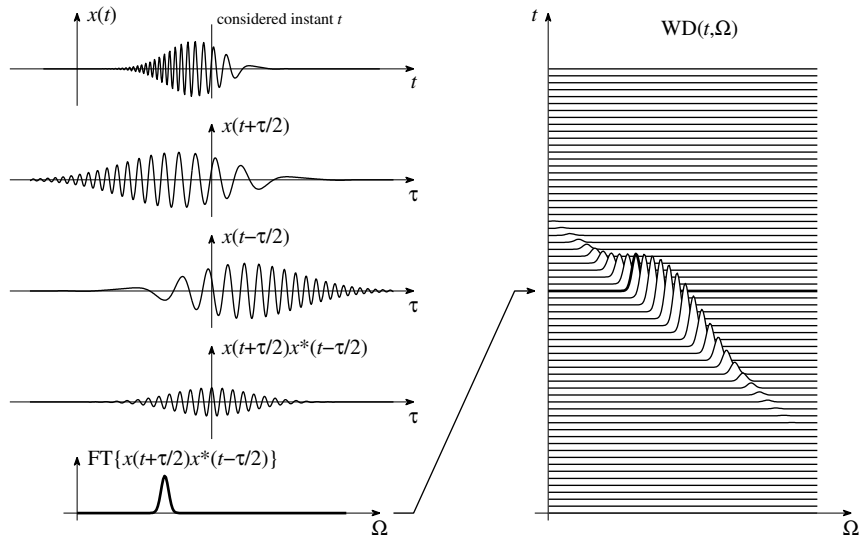


Figure 3.2 Illustration of the Wigner distribution calculation, for a considered time instant t . Real values of a linear frequency modulated signal (linear chirp) are presented.

For $\alpha = 0$, the local auto-correlation function $R(t, \tau)$ is Hermitian with respect to τ ,

$$R(t, \tau) = R^*(t, -\tau), \quad (3.15)$$

and its Fourier transform is real-valued. The distribution that satisfies this property is called the Wigner distribution (or the Wigner-Ville distribution). It is defined as

$$WD(t, \Omega) = \int_{-\infty}^{\infty} x(t + \tau/2)x^*(t - \tau/2)e^{-j\Omega\tau} d\tau. \quad (3.16)$$

The Wigner distribution is originally introduced in quantum mechanics. A review of the quantum mechanics interpretation of the Wigner distribution will be given after some of its basic properties are illustrated. In signal processing, it was introduced by Ville (Wigner-Ville distribution). The illustration of the Wigner distribution calculation is presented in Fig. 3.2.

Expressing $x(t)$ in terms of $X(\Omega)$ and substituting it into (3.16), we get

$$WD(t, \Omega) = \frac{1}{2\pi} \int_{-\infty}^{\infty} X(\Omega + \theta/2) X^*(\Omega - \theta/2) e^{j\theta t} d\theta, \quad (3.17)$$

which represents a definition of the Wigner distribution in terms of the signal's Fourier transform $X(\Omega)$.

A distribution defined as the Fourier transform of (3.14) is called the generalized Wigner distribution (GWD),

$$GWD(t, \Omega) = \int_{-\infty}^{\infty} x(t + (\alpha + 1/2)\tau) x^*(t + (\alpha - 1/2)\tau) e^{-j\Omega\tau} d\tau. \quad (3.18)$$

The name generalized Wigner distribution stems from the fact that this distribution is based on the Wigner distribution (for $\alpha = 0$), as its most important special case.

It is easy to show that the Wigner distribution and all the other distributions from the generalized Wigner distributions class satisfy the marginal properties. From the Wigner distribution definition, we may easily conclude that its inverse Fourier transform is the local auto-correlation,

$$x(t + \tau/2)x^*(t - \tau/2) = \text{IFT}\{WD(t, \Omega)\} = \frac{1}{2\pi} \int_{-\infty}^{\infty} WD(t, \Omega) e^{j\Omega\tau} d\Omega. \quad (3.19)$$

For $\tau = 0$ it produces time marginal property (3.2),

$$|x(t)|^2 = \frac{1}{2\pi} \int_{-\infty}^{\infty} WD(t, \Omega) d\Omega. \quad (3.20)$$

Based on the definition of the Wigner distribution in the frequency domain, (3.17), one may easily prove the fulfillment of the frequency marginal.

The marginal properties are satisfied for the whole class of the generalized Wigner distributions (3.18).

Example 3.1. Find the Wigner distribution of signals: (a) $x(t) = \delta(t - t_1)$ and (b) $x(t) = \exp(j\Omega_1 t)$.

★ The Wigner distribution of signal $x(t) = \delta(t - t_1)$ is

$$\begin{aligned} WD(t, \Omega) &= \int_{-\infty}^{\infty} \delta(t - t_1 + \tau/2) \delta(t - t_1 - \tau/2) e^{-j\Omega\tau} d\tau \\ &= 2\delta(2(t - t_1)) e^{-j2\Omega(t-t_1)} = \delta(t - t_1), \end{aligned}$$

since $|a|\delta(at)x(t) = \delta(t)x(0)$. From the Wigner distribution definition in terms of the Fourier transform, for $x(t) = \exp(j\Omega_1 t)$ with $X(\Omega) = 2\pi\delta(\Omega - \Omega_1)$, follows

$$WD(t, \Omega) = 2\pi\delta(\Omega - \Omega_1).$$

A high concentration of time-frequency representation for both of these signals is achieved. Note that this fact does not mean that we will be able to achieve an arbitrary high concentration simultaneously, in a point, in the time-frequency domain. □

Example 3.2. Consider a linear frequency modulated signal, $x(t) = Ae^{jbt^2/2}$. Find its Wigner distribution.

★ In this case we have

$$x(t + \tau/2)x^*(t - \tau/2) = |A|^2 e^{jb\tau\tau}$$

with

$$WD(t, \Omega) = 2\pi|A|^2 \delta(\Omega - bt).$$

Again, a high concentration along the instantaneous frequency in the time-frequency plane may be achieved for the linear frequency modulated signals. □

These two examples demonstrate that the Wigner distribution can provide superior time-frequency representation of one-component signal, in comparison to the STFT.

Example 3.3. Calculate the Wigner distribution for a linear frequency modulated signal, with Gaussian amplitude (Gaussian chirp signal)

$$x(t) = Ae^{-at^2/2} e^{j(bt^2/2+ct)}.$$

★ For the chirp signal, the local auto-correlation function reads as

$$R(t, \tau) = x(t + \tau/2)x^*(t - \tau/2) = |A|^2 e^{-at^2} e^{-a\tau^2/4} e^{jb\tau\tau + jc\tau}.$$

The Wigner distribution is obtained as the Fourier transform of $R(t, \tau)$,

$$WD(t, \Omega) = 2|A|^2 e^{-at^2} \sqrt{\frac{\pi}{a}} e^{-\frac{(\Omega-bt-c)^2}{a}}. \quad (3.21)$$

The Wigner distribution from Example 3.2 is obtained with $c = 0$ and $a \rightarrow 0$, since $2\sqrt{\pi/a}e^{-\Omega^2/a} \rightarrow 2\pi\delta(\Omega)$ as $a \rightarrow 0$.

The Wigner distribution of the Gaussian chirp signal is always positive, as it could be expected from a distribution introduced with the aim to represent local density of signal energy. Unfortunately, this is the only signal when the Wigner distribution is always positive, for any point in the time-frequency plane (t, Ω) . This drawback is not the only reason why the study of time-frequency distributions does not end with the Wigner distribution. \square

Example 3.4. Find the Wigner distribution of a rectangular window

$$x(t) = u(t+T) - u(t-T).$$

★ For this signal, the local auto-correlation function reads

$$R(t, \tau) = \left[u\left(t + \frac{\tau}{2} + T\right) - u\left(t + \frac{\tau}{2} - T\right) \right] \left[u\left(t - \frac{\tau}{2} + T\right) - u\left(t - \frac{\tau}{2} - T\right) \right].$$

It is equal to 1 within the region defined by inequalities

$$-T \leq t + \frac{\tau}{2} < T \quad \text{and} \quad -T \leq t - \frac{\tau}{2} < T.$$

For a given time instant t , we get

$$-2T - 2t \leq \tau < 2T - 2t \quad \text{and} \quad -2T + 2t < \tau \leq 2T + 2t.$$

The intersection of these two intervals is for $|t| < T$

$$-2T + 2|t| < \tau < 2T - 2|t|,$$

while there is no intersection for $|t| \geq T$. Thus, the Wigner distribution is the Fourier transform of a rectangular window function, whose time-varying width is 0 for $|t| \geq T$ and $4T - 4|t|$ for $|t| < T$. It reads

$$WD(t, \Omega) = \begin{cases} 2 \frac{\sin(2\Omega(T-|t|))}{\Omega} & \text{for } -T < t < T \\ 0 & \text{elsewhere.} \end{cases}$$

It is easy to see that the Wigner distribution is limited to the same time interval as the signal itself, as well as that here it assumes significant negative values. \square

3.2.1 Introducing the Wigner Distribution Based on the IF Representation

For a general monocomponent signal of the form

$$x(t) = A(t)e^{j\phi(t)}, \tag{3.22}$$

with a slow varying amplitude, as compared to the signal phase variations $|A'(t)| \ll |\phi'(t)|$, the instantaneous frequency is defined in Chapter 2 by

$$\Omega(t) = \phi'(t).$$

If a signal is real-valued, then its analytic part, which can be written in form (3.22), is assumed.

In the sense of the instantaneous frequency estimation, the aim of an ideal time-frequency representation (ITF) is to fully concentrate the whole signal (signal component) energy along its instantaneous frequency. Thus, this kind of representation may be described as

$$ITF(t, \Omega) = 2\pi|A(t)|^2\delta(\Omega - \phi'(t)). \quad (3.23)$$

The corresponding local auto-correlation function that will produce $ITF(t, \Omega)$ as its Fourier transform is

$$R(t, \tau) = |A(t)|^2 e^{j\phi'(t)\tau}. \quad (3.24)$$

Example 3.5. Show that the ideal distribution, defined by (3.23), satisfies the energy and time marginal properties for a wide class of frequency-modulated signals, with monotonous phase derivative function $\phi'(t)$.

★ The time marginal is satisfied since

$$\frac{1}{2\pi} \int_{-\infty}^{\infty} ITF(t, \Omega) d\Omega = |A(t)|^2,$$

where a monotonous function $\phi'(t)$ is assumed. Since the time marginal property is satisfied, so is the energy property.

If the signal satisfies the stationary-phase method conditions, it can be shown that the frequency marginal is satisfied by (3.23) as well. □

From a similar analysis in the frequency domain, one may define a distribution fully concentrated along the group delay. For a signal whose Fourier transform is

$$X(\Omega) = |X(\Omega)| \exp(j\Phi(\Omega)), \quad (3.25)$$

its ITF is

$$ITF(t, \Omega) = |X(\Omega)|^2 \delta(t + \Phi'(\Omega)), \quad (3.26)$$

where

$$t_g(\Omega) = -\Phi'(\Omega)$$

is the group delay.

We can define the Wigner distribution starting from the ideal time-frequency representation of the signal

$$x(t) = A e^{j\phi(t)} = A e^{j(at^2/2 + bt + c)}. \quad (3.27)$$

The question that we are going to address now is: What form of the quadratic signal representation should be used to produce (3.23) for (3.27)?

Since we assume that $A(t) = A$ is constant, our problem is reduced to finding the auto-correlation form (3.24) based on the given signal, that is, to calculate $\phi'(t)\tau$ from the signal exponent $\phi(t)$, for arbitrary values of lag τ . In this way we have reduced our problem to the first derivative calculation for a quadratic function. We know that

$$\phi\left(t + \frac{\tau}{2}\right) - \phi\left(t - \frac{\tau}{2}\right) = \phi'(t)\tau \quad (3.28)$$

for quadratic functions $\phi(t) = at^2/2 + bt + c$.

For any other function $\phi(t)$, this is an approximation only. The error term in this derivative relation is then proportional to $\phi'''(\tau_1)$ where τ_1 is a value between $(t - \tau/2)$ and $(t + \tau/2)$. Any other nonsymmetric approximation of the first derivative has a larger approximation error (we will be back to this derivatives approximation topic in the higher-order representation analysis in Chapter 4).

Therefore, the auto-correlation function $R(t, \tau)$, producing (3.24) for quadratic phase (linear frequency-modulated) signals, according to (3.28), is of the form

$$R(t, \tau) = x\left(t + \frac{\tau}{2}\right)x^*\left(t - \frac{\tau}{2}\right).$$

The Fourier transform of this auto-correlation function, producing (3.23), is the Wigner distribution.

The Rihaczek distribution, in this sense, corresponds to the first derivative estimator of the form $\phi(t) - \phi(t - \tau) = \phi'(t)\tau$. It produces an ideal representation (correct first derivative) for a linear phase (constant frequency) signals only.

3.2.2 Signal Reconstruction and Inversion

The signal can be reconstructed from the Wigner distribution, (3.19) with $\tau/2 = t$ and $2t \rightarrow t$, as

$$x(t) = \frac{1}{2\pi x^*(0)} \int_{-\infty}^{\infty} WD(t/2, \Omega) e^{j\Omega t} d\Omega.$$

Due to the term $x^*(0)$, ambiguity in the signal phase remains. This is a consequence of losing information about a constant in the signal's phase after the product $x(t + \tau/2)x^*(t - \tau/2)$ in the Wigner distribution is calculated.

Since the Wigner distribution is a two-dimensional representation of a one-dimensional signal, obviously an arbitrary real-valued two-dimensional function will not be a valid Wigner distribution. A two-dimensional real function $P(t, \Omega)$ is the Wigner distribution of a signal if

$$\frac{\partial^2 \ln [\rho(t_1, t_2)]}{\partial t_1 \partial t_2} = 0, \quad (3.29)$$

where

$$\rho(t_1, t_2) = \frac{1}{2\pi} \int_{-\infty}^{\infty} P\left(\frac{t_1 + t_2}{2}, \Omega\right) e^{j\Omega(t_1 - t_2)} d\Omega.$$

To prove this statement, find the solution of partial differential equation (3.29). It is

$$\ln [\rho(t_1, t_2)] = \varphi_1(t_1) + \varphi_2(t_2),$$

where $\varphi_1(t_1)$ and $\varphi_2(t_2)$ are arbitrary functions of t_1 and t_2 . Therefore,

$$\rho(t_1, t_2) = e^{\varphi_1(t_1)} e^{\varphi_2(t_2)} = f_1(t_1) f_2(t_2).$$

With $t_1 = t + \frac{\tau}{2}$ and $t_2 = t - \frac{\tau}{2}$, we get

$$f_1\left(t + \frac{\tau}{2}\right) f_2\left(t - \frac{\tau}{2}\right) = \frac{1}{2\pi} \int_{-\infty}^{\infty} P(t, \Omega) e^{j\Omega\tau} d\Omega.$$

Since $P(t, \Omega)$ is a real function, it follows that

$$f_1(t) = f_2^*(t) = x(t). \quad (3.30)$$

Thus, for $P(t, \Omega)$ satisfying (3.29), there exists function $x(t)$ such that $P(t, \Omega)$ and $x(t + \frac{\tau}{2})x^*(t - \frac{\tau}{2})$ are the Fourier transform pair.

A mean squared approximation of an arbitrary two-dimensional function by a valid Wigner distribution, or a sum of the Wigner distributions, will be discussed later.

3.2.3 Properties of the Wigner Distribution

A list of the properties satisfied by the Wigner distribution follows. The obvious ones will be just stated, while the proofs will be given for more complex ones. In the case when the Wigner distributions of more than one signal are considered, the signal will be added as an index in the Wigner distribution notation. Otherwise, signal $x(t)$ is assumed, as a default signal in the notation.

P₁ – Realness

For any signal holds,

$$WD^*(t, \Omega) = WD(t, \Omega).$$

P₂ – Time-shift property

The Wigner distribution of a signal shifted in time

$$y(t) = x(t - t_0),$$

is

$$WD_y(t, \Omega) = WD_x(t - t_0, \Omega).$$

P₃ – Frequency shift property

For a modulated signal

$$y(t) = x(t)e^{j\Omega_0 t},$$

we have

$$WD_y(t, \Omega) = WD_x(t, \Omega - \Omega_0).$$

P₄ – Time marginal property

$$\frac{1}{2\pi} \int_{-\infty}^{\infty} WD(t, \Omega) d\Omega = |x(t)|^2.$$

P₅ – Frequency marginal property

$$\int_{-\infty}^{\infty} WD(t, \Omega) dt = |X(\Omega)|^2.$$

P₆ – Time moments property

$$\frac{1}{2\pi} \int_{-\infty}^{\infty} \int_{-\infty}^{\infty} t^n WD(t, \Omega) dt d\Omega = \int_{-\infty}^{\infty} t^n |x(t)|^2 dt.$$

★ This property follows from $\frac{1}{2\pi} \int_{-\infty}^{\infty} WD(t, \Omega) d\Omega = |x(t)|^2$. □

P₇ -Frequency moments property

$$\int_{-\infty}^{\infty} \int_{-\infty}^{\infty} \Omega^n WD(t, \Omega) d\Omega dt = \int_{-\infty}^{\infty} \Omega^n |X(\Omega)|^2 d\Omega.$$

P₈ – Scaling

For a scaled version of the signal

$$y(t) = \sqrt{|a|} x(at), \quad a \neq 0,$$

the Wigner distribution reads

$$WD_y(t, \Omega) = WD_x(at, \Omega/a).$$

P₉ – Instantaneous frequency property

For $x(t) = A(t)e^{j\phi(t)}$

$$\frac{\int_{-\infty}^{\infty} \Omega WD(t, \Omega) d\Omega}{\int_{-\infty}^{\infty} WD(t, \Omega) d\Omega} = \Omega_i(t) = \frac{d}{dt} \arg[x(t)] = \phi'(t). \quad (3.31)$$

★ In order to prove this property, we will use the derivative of the inverse Fourier transform of the Wigner distribution

$$\frac{d[x(t + \tau/2)x^*(t - \tau/2)]}{d\tau} = \frac{1}{2\pi} \int_{-\infty}^{\infty} j\Omega WD(t, \Omega) e^{j\Omega\tau} d\Omega$$

with $x(t) = A(t)e^{j\phi(t)}$, calculated at $\tau = 0$. It results in

$$\frac{j}{2\pi} \int_{-\infty}^{\infty} \Omega WD(t, \Omega) d\Omega = \frac{1}{2} [x'(t)x^*(t) - x(t)x^{*\prime}(t)] = j\phi'(t)A^2(t).$$

With the frequency marginal property $\int_{-\infty}^{\infty} WD(t, \Omega) d\Omega = 2\pi A^2(t)$, this property follows. \square

P₁₀ – Group delay

For signal whose Fourier transform is of the form $X(\Omega) = |X(\Omega)| e^{j\Phi(\Omega)}$, the group delay $t_g(\Omega) = -\Phi'(\Omega)$ is

$$\frac{\int_{-\infty}^{\infty} t WD(t, \Omega) dt}{\int_{-\infty}^{\infty} WD(t, \Omega) dt} = t_g(\Omega) = -\frac{d}{d\Omega} \arg[X(\Omega)] = -\Phi'(\Omega).$$

The proof is the same as in the instantaneous frequency case, using the frequency domain relations.

P₁₁ – Time constraint

If $x(t) = 0$ for t outside $[t_1, t_2]$, then $WD(t, \Omega) = 0$ for t outside $[t_1, t_2]$.

★ The Wigner distribution is a function of $x(t + \tau/2)x^*(t - \tau/2)$. If $x(t) = 0$ for t outside $[t_1, t_2]$ then $x(t + \tau/2)x^*(t - \tau/2)$ is different from zero within

$$t_1 \leq t + \tau/2 \leq t_2 \quad \text{and} \quad t_1 \leq t - \tau/2 \leq t_2.$$

The range of values of t defined by the previous inequalities is $t_1 \leq t \leq t_2$. \square

P₁₂ – Frequency constraint

If $X(\Omega) = 0$ for Ω outside $[\Omega_1, \Omega_2]$, then, also $WD(t, \Omega) = 0$ for Ω outside $[\Omega_1, \Omega_2]$.

P₁₃ – Convolution

$$WD_y(t, \Omega) = \int_{-\infty}^{\infty} WD_h(t - \tau, \Omega) WD_x(\tau, \Omega) d\tau.$$

for

$$y(t) = \int_{-\infty}^{\infty} h(t - \tau) x(\tau) d\tau,$$

P₁₄ – Product

$$WD_y(t, \Omega) = \frac{1}{2\pi} \int_{-\infty}^{\infty} WD_h(t, \Omega - v) WD_x(t, v) dv$$

for

$$y(t) = h(t)x(t).$$

★ The local auto-correlation of $y(t)$ is $h(t + \tau/2)h^*(t - \tau/2)x(t + \tau/2)x^*(t - \tau/2)$. Thus, the Wigner distribution of $y(t)$ is the Fourier transform of the product of local auto-correlations $h(t + \tau/2)h^*(t - \tau/2)$ and $x(t + \tau/2)x^*(t - \tau/2)$. It is a convolution in frequency of the corresponding Wigner distributions of $h(t)$ and $x(t)$. Property P₁₃ could be proven in the same way using the Fourier transforms of signals $h(t)$ and $x(t)$. □

P₁₅ – Fourier transform property

$$WD_y(t, \Omega) = WD_x(-\Omega/c, ct) \quad (3.32)$$

for

$$y(t) = \sqrt{|c|/(2\pi)}X(ct), \quad c \neq 0.$$

★ Here the signal $y(t)$ is equal to the scaled version of the Fourier transform of signal $x(t)$,

$$\begin{aligned} WD_y(t, \Omega) &= \frac{|c|}{2\pi} \int_{-\infty}^{\infty} X\left(ct + \frac{c\tau}{2}\right) X^*\left(ct - \frac{c\tau}{2}\right) e^{-j\Omega\tau} d\tau \\ &= \frac{1}{2\pi} \int_{-\infty}^{\infty} X\left(ct + \frac{\theta}{2}\right) X^*\left(ct - \frac{\theta}{2}\right) e^{j(-\Omega/c)\theta} d\theta. \end{aligned} \quad (3.33)$$

Comparing (3.17) to (3.16), with $ct \rightarrow \Omega$ and $(-\Omega/c) \rightarrow t$, we get

$$WD_y(t, \Omega) = \int_{-\infty}^{\infty} x\left(-\frac{\Omega}{c} + \frac{\tau}{2}\right) x^*\left(-\frac{\Omega}{c} - \frac{\tau}{2}\right) e^{-jct\tau} d\tau = WD_x\left(-\frac{\Omega}{c}, ct\right).$$

□

P₁₆ – Chirp convolution

$$WD_y(t, \Omega) = WD_x\left(t - \frac{\Omega}{c}, \Omega\right) \quad (3.34)$$

for

$$y(t) = x(t) * \sqrt{|c|}e^{jct^2/2}.$$

★ With $Y(\Omega) = \text{FT}\{x(t) *_t \sqrt{|c|} e^{jct^2/2}\} = \sqrt{2\pi j} X(\Omega) e^{-j\Omega^2/(2c)}$ and the signal's Fourier transform-based definition of the Wigner distribution, proof of this property reduces to the next one. \square

P₁₇ – Chirp product

$$WD_y(t, \Omega) = WD_x(t, \Omega - ct)$$

for

$$y(t) = x(t) e^{jct^2/2}.$$

★ The Wigner distribution of $y(t)$ is

$$\begin{aligned} & \int_{-\infty}^{\infty} x\left(t + \frac{\tau}{2}\right) e^{jc(t+\tau/2)^2/2} x^*\left(t - \frac{\tau}{2}\right) e^{-jc(t-\tau/2)^2/2} e^{-j\Omega\tau} d\tau \\ &= \int_{-\infty}^{\infty} x\left(t + \frac{\tau}{2}\right) x^*\left(t - \frac{\tau}{2}\right) e^{jct\tau} e^{-j\Omega\tau} d\tau = WD_x(t, \Omega - ct). \end{aligned} \quad (3.35)$$

\square

P₁₈ – Moyal property

$$\frac{1}{2\pi} \int_{-\infty}^{\infty} \int_{-\infty}^{\infty} WD_x(t, \Omega) WD_y(t, \Omega) dt d\Omega = \left| \int_{-\infty}^{\infty} x(t) y(t) dt \right|^2. \quad (3.36)$$

★ This property follows from

$$\begin{aligned} & \frac{1}{2\pi} \int_{-\infty}^{\infty} \int_{-\infty}^{\infty} \int_{-\infty}^{\infty} x\left(t + \frac{\tau_1}{2}\right) x^*\left(t - \frac{\tau_1}{2}\right) y\left(t + \frac{\tau_2}{2}\right) y^*\left(t - \frac{\tau_2}{2}\right) \\ & \quad \times \int_{-\infty}^{\infty} e^{-j\Omega\tau_1} e^{-j\Omega\tau_2} d\Omega d\tau_1 d\tau_2 dt \\ &= \int_{-\infty}^{\infty} \int_{-\infty}^{\infty} x\left(t + \frac{\tau}{2}\right) x^*\left(t - \frac{\tau}{2}\right) y\left(t - \frac{\tau}{2}\right) y^*\left(t + \frac{\tau}{2}\right) d\tau dt. \end{aligned}$$

With $t + \tau/2 = u$ and $t - \tau/2 = v$, we get

$$= \int_{-\infty}^{\infty} x(u) y^*(u) du \int_{-\infty}^{\infty} x^*(v) y(v) dv = \left| \int_{-\infty}^{\infty} x(t) y(t) dt \right|^2.$$

3.2.4 Linear Coordinate Transforms

Linear coordinate transformation of the Wigner distribution, with a coordinate rotation as a special case, is an important topic in optics. In signal processing it has been used in a direct and indirect way. For example, the Wigner distribution of a linear frequency-modulated signal is located along a line in the time-frequency plane. By appropriate coordinate transformation, there is a coordinate system in which this line will correspond to a complex sinusoid. Then it is much easier to analyze this simple signal form and to apply classic analysis tools, having in mind that the essence of the result is not changed, since the Wigner distribution is just presented in a linearly transformed (or rotated) coordinate system. The same would hold for a signal with small deviations around a linear frequency-modulated signal, having one dominant direction in the time-frequency plane. By transforming such a signal into a simpler one, in an appropriate domain, various other benefits may be achieved, including a lower sampling rate.

A general form of the linear coordinate transformation of the Wigner distribution is derived here, with the coordinate rotation as a special case. From the property P₁₇, it is easy to conclude that multiplication of signal by a chirp,

$$y(t) = x(t)e^{jct^2/2},$$

leads to

$$WD_y(t, \Omega) = WD_x(t, \Omega - ct).$$

It may be understood as the coordinate transformation of the original time-frequency plane. The new coordinates are $u = t$ and $v = \Omega - ct$. In a matrix form, we have

$$\begin{bmatrix} u \\ v \end{bmatrix} = \begin{bmatrix} 1 & 0 \\ -c & 1 \end{bmatrix} \begin{bmatrix} t \\ \Omega \end{bmatrix}, \quad (3.37)$$

where the Wigner distribution coordinate transformation matrix is

$$\mathbf{L}_1 = \begin{bmatrix} 1 & 0 \\ -c & 1 \end{bmatrix}. \quad (3.38)$$

Similarly, for the convolution of signal with a linear frequency-modulated signal,

$$z(t) = y(t) *_t \sqrt{|b|} e^{jb t^2/2}, \quad (3.39)$$

according to P₁₆,

$$WD_z(t, \Omega) = WD_y\left(t - \frac{\Omega}{b}, \Omega\right)$$

The corresponding coordinate transformation matrix is

$$\mathbf{L}_2 = \begin{bmatrix} 1 & -1/b \\ 0 & 1 \end{bmatrix}. \quad (3.40)$$

The transformation matrix for $x(t) \rightarrow y(t) \rightarrow z(t)$ would be obtained from

$$WD_z(t, \Omega) = WD_y(t - \Omega/b, \Omega) = WD_x(t - \Omega/b, \Omega - ct + \Omega c/b),$$

as $\mathbf{L}_{12} = \mathbf{L}_1 \mathbf{L}_2$.

Now, we can easily conclude that for the signal

$$x_L(t) = \left[\left(x(t) e^{jct^2/2} \right) *_t \left(\sqrt{|b|} e^{jbt^2/2} \right) \right] e^{jat^2/2} \quad (3.41)$$

the transformation matrix is

$$\begin{aligned} \mathbf{L} &= \begin{bmatrix} 1 & 0 \\ -c & 1 \end{bmatrix} \begin{bmatrix} 1 & -1/b \\ 0 & 1 \end{bmatrix} \begin{bmatrix} 1 & 0 \\ -a & 1 \end{bmatrix} \\ &= \begin{bmatrix} 1+a/b & -1/b \\ -c-a(c/b+1) & c/b+1 \end{bmatrix} \end{aligned} \quad (3.42)$$

with $b \neq 0$. The transformation is unitary $\det(\mathbf{L}) = 1$, since the determinants of matrices \mathbf{L}_1 and \mathbf{L}_2 are equal to 1. Since we work with matrices, remember that their order is important. Thus, a signal transformation defined by (3.41) results in the linear coordinate transformation of the Wigner distribution

$$WD_{x_L}(t, \Omega) = WD_x(At + B\Omega, Ct + D\Omega), \quad (3.43)$$

where $WD_x(t, \Omega)$ is the Wigner distribution of $x(t)$, $WD_{x_L}(t, \Omega)$ is the Wigner distribution of $x_L(t)$, defined by (3.41), and the transformation matrix \mathbf{L} has the form

$$\mathbf{L} = \begin{bmatrix} A & B \\ C & D \end{bmatrix}. \quad (3.44)$$

The values of A, B, C , and D are defined by (3.42).

3.2.4.1 Rotation of the Time-Frequency Plane

We may easily conclude that the fractional Fourier transform directly follows as a special case of linear coordinate transformation of the Wigner distribution, with the

transformation matrix

$$\mathbf{L} = \begin{bmatrix} \cos \alpha & -\sin \alpha \\ \sin \alpha & \cos \alpha \end{bmatrix} \quad (3.45)$$

which corresponds to the coordinate rotation of the time-frequency plane. By comparing (3.42) and (3.45), we easily get

$$-1/b = -\sin(\alpha) = -1/\csc(\alpha)$$

producing

$$a = c = -\tan(\alpha/2).$$

Substituting these values into (3.41), we get

$$\begin{aligned} x_L(t) &= \{[x(t)e^{-j\tan(\alpha/2)t^2/2}] *_t \sqrt{\csc(\alpha)} e^{j\csc(\alpha)t^2/2}\} e^{-j\tan(\alpha/2)t^2/2} \\ &= \sqrt{\csc(\alpha)} e^{-j\tan(\alpha/2)t^2/2} \int_{-\infty}^{\infty} x(\tau) e^{-j\tan(\alpha/2)\tau^2/2} e^{j\csc(\alpha)(t-\tau)^2/2} d\tau \\ &= \sqrt{2j\pi e^{-j\alpha}} \sqrt{\frac{1-j\cot\alpha}{2\pi}} e^{j\cot(\alpha)t^2/2} \int_{-\infty}^{\infty} x(\tau) e^{j\cot(\alpha)\tau^2/2} e^{-jt\tau\csc(\alpha)} d\tau, \end{aligned}$$

which is the fractional Fourier transform, in the form commonly used in literature, up to the constant factor $\sqrt{2j\pi e^{-j\alpha}}$,

$$\begin{aligned} X_\alpha(t) &= \sqrt{\frac{1-j\cot\alpha}{2\pi}} e^{j\cot(\alpha)t^2/2} \int_{-\infty}^{\infty} x(\tau) e^{j\cot(\alpha)\tau^2/2} e^{-jt\tau\csc(\alpha)} d\tau \\ x_L(t) &= \sqrt{2j\pi e^{-j\alpha}} X_\alpha(t), \end{aligned}$$

with the same limits as $\alpha \rightarrow 2k\pi$ or $\alpha \rightarrow (2k+1)\pi$. It is easy to verify that for $\alpha = \pi/2$, when $\csc(\alpha) = 1$ and $\cot(\alpha) = 0$,

$$\begin{aligned} x_L(t) &= \int_{-\infty}^{\infty} x(\tau) e^{-jt\tau} d\tau = X(t) \\ X_{\pi/2}(t) &= \frac{1}{\sqrt{2\pi}} \int_{-\infty}^{\infty} x(\tau) e^{-jt\tau} d\tau = \frac{1}{\sqrt{2\pi}} X(t) \end{aligned} \quad (3.46)$$

where $X(t)$ is the Fourier transform of $x(t)$ written in an unusual way, by using t as the argument. In this notation, the fractional Fourier transform can be distinguished from the Fourier transform by the index, indicating the angle. For $\alpha = 0$, when $\csc(\alpha) \rightarrow \infty$ and $\cot(\alpha) \rightarrow \infty$, with $\lim_{\gamma \rightarrow \infty} \sqrt{\gamma/(2\pi j)} \exp(-j\gamma t^2/2) = \delta(t)$, follows

$$x_L(t) = \sqrt{2\pi j} x(t)$$

and

$$X_0(t) = x(t).$$

Note that the energy of signal would be obtained as

$$\begin{aligned} E_x &= \int_{-\infty}^{\infty} |X_0(t)|^2 dt = \int_{-\infty}^{\infty} |x(t)|^2 dt \\ &= \int_{-\infty}^{\infty} |X_{\pi/2}(t)|^2 dt = \frac{1}{2\pi} \int_{-\infty}^{\infty} |X(t)|^2 dt \end{aligned}$$

justifying the additional factor $1/\sqrt{2j\pi e^{-j\alpha}}$ in the fractional Fourier transform $X_\alpha(t)$ with respect to $x_L(t)$.

Therefore, the fractional Fourier transform is a special form of the signal transform that produces a linear coordinate transformation of the Wigner distribution.

Here we will present some examples to demonstrate the application of these forms to the time-frequency signal analysis.

The Radon transform of the Wigner distribution (RTWD) has been used in literature in order to establish the direction of the linear frequency-modulated signal in the time-frequency plane. The Radon transform of a two-dimensional function, at an angle θ , is defined by a projection onto (integrals along the lines normal to) the line with an angle θ . Angle θ is defined with respect to the time axis. Recall that two projections of the Wigner distribution are already used. For $\theta = 0$ the Radon transform of the Wigner distribution is

$$RTWD(\theta, u)_{|\theta=0, u=t} = \int_{-\infty}^{\infty} WD(t, \Omega) d\Omega = 2\pi |x(t)|^2,$$

while for $\theta = \pi/2$ it is

$$RTWD(\theta, u)_{|\theta=\pi/2, u=\Omega} = \int_{-\infty}^{\infty} WD(t, \Omega) dt = |X(\Omega)|^2.$$

We may easily conclude that the frequencies of complex sinusoidal signals

$$x(t) = \sum_{m=1}^M A_m \exp(j\Omega_m t)$$

may efficiently be estimated by detecting maxima of

$$RTWD(\theta, u)_{|\theta=\pi/2, u=\Omega} = |X(\Omega)|^2 = \left| 2\pi \sum_{m=1}^M A_m \delta(\Omega - \Omega_m) \right|^2. \quad (3.47)$$

The same would hold for a sum of linear frequency-modulated signals

$$x(t) = \sum_{m=1}^M A_m \exp(ja_m t^2/2 + j\Omega_m t).$$

The maximal values of the projections in the Radon Wigner transform will obviously be obtained for an angle when the integration lines coincide with a signal component direction. Thus, by varying the value of angle θ and calculating the Radon transform of the Wigner distribution, the local maxima will be at

$$\theta_1 = \pi/2 + \arctan(a_1), \theta_2 = \pi/2 + \arctan(a_2), \dots, \theta_M = \pi/2 + \arctan(a_M).$$

By detecting these local maxima, the values of signal rate follows. The position of the maximal Radon transform value, for a single θ_m is equal to the signal frequency Ω_m . The Radon transform of the Wigner distribution of signal from Fig. 2.1(a) is shown in Fig. 3.3. Based on the picks, it is possible to conclude that signal contains two linear frequency-modulated signals. One of them is at $\theta = 90^\circ$, being a pure sinusoid.

Of course, instead of calculating the Wigner distribution and then its Radon transform, we may just calculate the absolute squared value of the fractional Fourier transform, knowing that the Wigner distribution projection, according to the marginal property, is equal to the squared modulus of the signal that produces this rotated Wigner distribution.

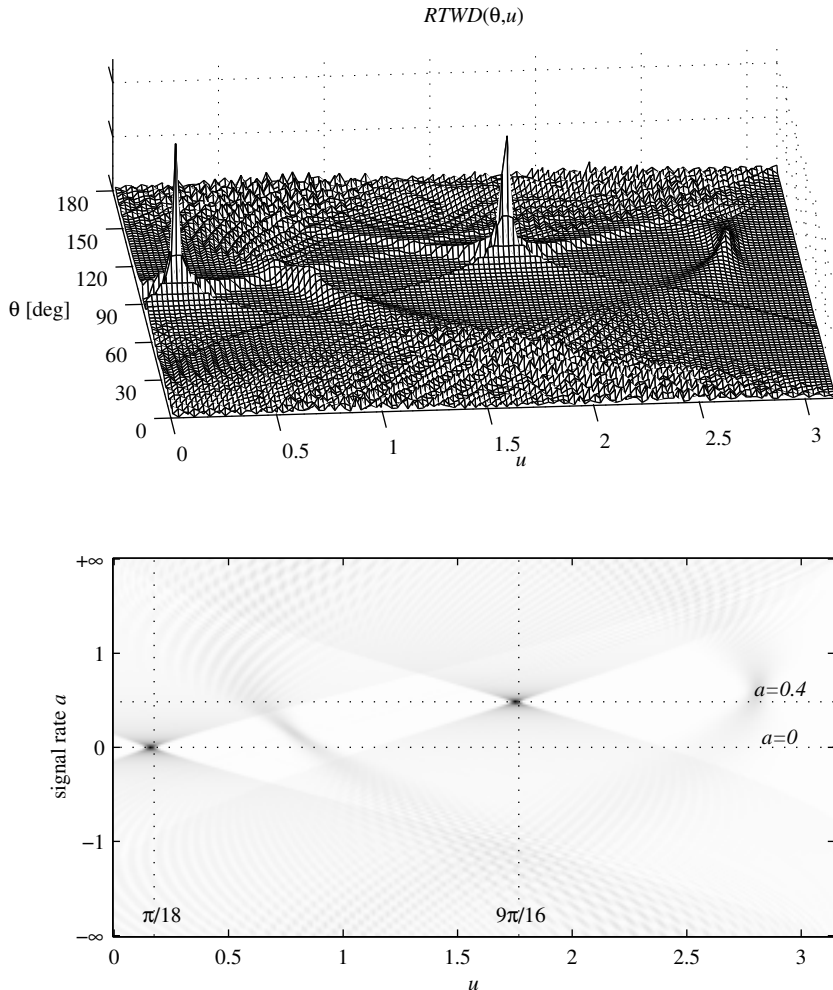


Figure 3.3 The Radon Wigner distribution of the signal presented in Fig. 2.1(a), with two visible picks indicating two linear frequency-modulated signals (mesh graphics in the upper subplot). The normalized signal rates are shown instead of θ in the lower subplot image. The normalization is done in such a way that the linear frequency-modulated signal along the time-frequency plane diagonal (passing through $(t, \Omega) = (0, 0)$ and $(t, \Omega) = (t_m, \Omega_m)$) has the rate $a = 1$.

To efficiently determine the direction of a linear frequency-modulated signal (signal frequency rate) we may use a transformation matrix

$$L = \begin{bmatrix} 1 & 0 \\ -a & 1 \end{bmatrix}, \quad (3.48)$$

as well. This form corresponds to the second-order polynomial Fourier transform,

$$X_L(\Omega, a) = \int_{-\infty}^{\infty} x_L(t) e^{-j\Omega t} dt = \int_{-\infty}^{\infty} x(t) e^{jat^2/2} e^{-j\Omega t} dt.$$

It is the Fourier transform of $x_L(t) = x(t)e^{jat^2/2}$. It reaches maximum when the parameter a is equal to the signal frequency rate.

Example 3.6. Time-scaled signals $y(t) = x(t/\gamma)$, where γ has an arbitrary value, may be needed in some applications. Such signals can be used, for example, to scale the frequency range in time-frequency distributions, since $WD_y(t, \Omega) = WD_x(t/\gamma, \gamma\Omega)$. The corresponding coordinate transformation matrix is

$$L = \begin{bmatrix} 1/\gamma & 0 \\ 0 & \gamma \end{bmatrix}.$$

Show that a scaled version of signal may be obtained, in the continuous time domain, based on the original signal, as

$$\begin{aligned} y(t) &= \left(\left(\left[x(t) e^{-j\alpha t^2/2} \right] *_t \sqrt{|1-\gamma|/\alpha} e^{j\alpha t^2/(2(1-\gamma))} \right) e^{j\alpha t^2/(2\gamma)} \right) \\ &\quad *_t \sqrt{|\gamma^2 - \gamma|/\alpha} e^{j\alpha t^2/(2(\gamma^2 - \gamma))}, \end{aligned}$$

where α is an arbitrary constant.

★ A linear coordinate transformation matrix for the Wigner distribution of $y(t)$ is

$$\begin{aligned} L &= \begin{bmatrix} 1 & 0 \\ \alpha & 1 \end{bmatrix} \begin{bmatrix} 1 & \frac{\gamma-1}{\alpha} \\ 0 & 1 \end{bmatrix} \begin{bmatrix} 1 & 0 \\ -\frac{\alpha}{\gamma} & 1 \end{bmatrix} \begin{bmatrix} 1 & -\frac{\gamma^2-\gamma}{\alpha} \\ 0 & 1 \end{bmatrix} \\ &= \begin{bmatrix} 1 & \frac{\gamma-1}{\alpha} \\ \alpha & \gamma \end{bmatrix} \begin{bmatrix} 1 & -\frac{\gamma^2-\gamma}{\alpha} \\ -\frac{\alpha}{\gamma} & \gamma \end{bmatrix} = \begin{bmatrix} 1/\gamma & 0 \\ 0 & \gamma \end{bmatrix}. \end{aligned}$$

□

One more special case follows from (3.42) with

$$\mathbf{L} = \begin{bmatrix} 1+a/b & -1/b \\ -c-a(c/b+1) & c/b+1 \end{bmatrix} = \begin{bmatrix} 0 & -1 \\ 1 & 0 \end{bmatrix} \quad (3.49)$$

for $b = 1, a = c = -1$ when $WD_y(t, \Omega) = WD_x(-\Omega, t)$ meaning that

$$x_L(t) = \left[\left(x(t) e^{-jt^2/2} \right) *_t e^{jt^2/2} \right] e^{-jt^2/2} = X(t)/\sqrt{2\pi}. \quad (3.50)$$

We can calculate the continuous Fourier transform function $X(t)$, with continuous time t as independent variable instead of Ω , of signal $x(t)$ by using multiplications and convolution with linear frequency modulated signals (using the quadratic phase filter for analog domain implementations).

3.3 QUANTUM MECHANICS WIGNER DISTRIBUTION REVIEW

Since the Wigner distribution is originally defined in the quantum mechanics, here we present a short overview of its definition. Although this part relates some interesting concepts in quantum mechanics and signal processing, for example, the signal spreading factor and the quantum correction factor, as well as the uncertainty principle in these two conceptually different areas, this part is presented just for information to signal processing specialists.

The classical mechanics equations, describing a particle motion, are given by

$$dx/dt = p/m$$

and

$$dp/dt = -\nabla V(x) = -V'(x),$$

where x is the position, m is the mass, $p = mv$ is the momentum of a particle, and $V(x)$ is the potential. If the initial conditions are not given by $x(0)$ and $p(0)$, but rather by their probability distribution $W(p, x, t = 0)$, then the particle dynamics is described by the Liouville's equation

$$\frac{\partial W}{\partial t} + \frac{p}{m} \frac{\partial W}{\partial x} = V'(x) \frac{\partial W}{\partial p}. \quad (3.51)$$

The quantum mechanics generalization of the Liouville's equation was introduced by Wigner (a Nobel prize laureate) in the form

$$\frac{\partial W}{\partial t} + \frac{p}{m} \frac{\partial W}{\partial x} = \frac{1}{j\hbar} \left[V \left(x + \frac{j\hbar}{2} \frac{\partial}{\partial p} \right) - V \left(x - \frac{j\hbar}{2} \frac{\partial}{\partial p} \right) \right] W \quad (3.52)$$

where $\hbar = h/(2\pi)$, with h being the Planck's constant. A momentum operator is denoted by \hat{p} and its form is $\hat{p} = -j\hbar\nabla$ (for a one-dimensional case $\hat{p} = -j\hbar\frac{\partial}{\partial x}$) in the space of x ($\hat{x} = x$). Expanding $V(x \pm \frac{j\hbar}{2} \frac{\partial}{\partial p})$ into a Taylor series around x , we get

$$\frac{\partial W}{\partial t} + \frac{p}{m} \frac{\partial W}{\partial x} = V'(x) \frac{\partial W}{\partial p} - \frac{\hbar^2}{24} V^{(3)}(x) \frac{\partial^3 W}{\partial p^3} + \dots \quad (3.53)$$

From (3.53) one may easily conclude that the classical Liouville equation (3.51) follows as a limit of its quantum mechanics extension. This limit appears if the potential is of the form

$$V(x) = V_0 + V_1 x + V_2 x^2$$

(potential in the linear oscillator) or if the terms in (3.53) of order \hbar^n , for $n \geq 2$, are negligible. Expression

$$\begin{aligned} Q &= \frac{1}{j\hbar} \left[V \left(x + \frac{j\hbar}{2} \frac{\partial}{\partial p} \right) - V \left(x - \frac{j\hbar}{2} \frac{\partial}{\partial p} \right) \right] W - V'(x) \frac{\partial W}{\partial p} \\ &= -\frac{\hbar^2}{24} V^{(3)}(x) \frac{\partial^3 W}{\partial p^3} + \dots \end{aligned} \quad (3.54)$$

may be considered as a quantum correction of the classical Liouville's form. This is a significant property of the quantum Wigner representation, since it may be used to transform the solutions from the classical to the quantum forms or to deal with problems with mixed (quantum and classical) variables. We will show that it has an interesting signal processing interpretation as well. It will define the Wigner distribution spread from the instantaneous frequency.

The Wigner distribution, for stationary problems, is defined by

$$W(x, p) = \frac{1}{2\pi} \int_{-\infty}^{\infty} \psi \left(x + \frac{\hbar\xi}{2} \right) \psi^* \left(x - \frac{\hbar\xi}{2} \right) e^{-jp\xi} d\xi \quad (3.55)$$

where

$$\psi(x, t) = F(x, t) e^{j\Phi(t)/\hbar}$$

is the wave function ψ that satisfies the Schrödinger equation

$$\frac{\hbar^2}{2m} \frac{\partial^2 \psi}{\partial x^2} + j\hbar \frac{\partial \psi}{\partial t} = V(x)\psi \quad (3.56)$$

if $W(x, p, t)$ satisfies the Wigner quantum equation (3.52). It may be shown that the Wigner representation and the Schrödinger's one are equivalent, that is, they uniquely follow from each other. Any function of the form

$$\psi(x) = A(x)e^{j\phi(x)/\hbar} = \psi_0^{[1/\hbar]}(x)$$

with

$$\psi_0(x) = A(x)e^{j\phi(x)}$$

being \hbar -independent, under certain conditions, is the solution of the Schrödinger's equation. The uncertainty principle for the Wigner distribution in (x, p) is

$$\sigma_x^2 \sigma_p^2 \geq \frac{\hbar^2}{4}.$$

In signal analysis, the variables of frequency (Ω) and time (t) are used instead of momentum (p) and position (x). In time domain the operators are given by $\hat{\Omega} = -j\frac{\partial}{\partial t}$ and $\hat{t} = t$. The Wigner distribution of signal $x(t)$ is derived as

$$WD(t, \Omega) = \int_{-\infty}^{\infty} x\left(t + \frac{\tau}{2}\right)x^*\left(t - \frac{\tau}{2}\right)e^{-j\Omega\tau}d\tau. \quad (3.57)$$

The formal mathematical correspondence between quantum mechanics definition (3.55) and signal analysis definition (3.57) is obvious with: $\psi(x) \rightarrow x(t)$, $x \rightarrow t$, $p \rightarrow \Omega$ and $\hbar \rightarrow 1$. The presence of factor $\frac{1}{2\pi}$ is due to different forms of the Fourier transform commonly used in quantum mechanics and signal analysis (we intentionally did not want to modify any of them). This is a natural analogy that was used in the extension of quantum mechanics concepts and definitions to the signal analysis by Cohen, Claassen, Mecklenbrauker, Escudie, Flandrin, Boashash, et al. Of course, in signal analysis, a signal does not need to satisfy the Schrödinger equation (3.56). The signal is rather obtained as a result of some physical processes or theoretical analysis. Note also that the quantum mechanics is an inherently probabilistic theory in contrast to signal analysis.

3.3.1 Spreading Factor

For a frequency modulated signal $x(t) = A \exp(j\phi(t))$, the Wigner distribution (3.57) assumes the form

$$\begin{aligned} WD(t, \Omega) &= A^2 \int_{-\infty}^{\infty} e^{j[\phi(t+\tau/2)-\phi(t-\tau/2)]} e^{-j\Omega\tau} d\tau \\ &= A^2 \int_{-\infty}^{\infty} e^{j[\phi(t+\tau/2)-\phi(t-\tau/2)]-j\phi'(t)\tau} e^{j\phi'(t)\tau} e^{-j\Omega\tau} d\tau. \end{aligned}$$

The factor

$$A^2 \int_{-\infty}^{\infty} e^{j\phi'(t)\tau} e^{-j\Omega\tau} d\tau = 2\pi A^2 \delta(\Omega - \phi'(t))$$

produces the ideal distribution concentration, while the term (whose phase is of the form which formally corresponds to the quantum correction factor (3.54))

$$Q(t, \tau) = j \left[\phi \left(t + \frac{\tau}{2} \right) - \phi \left(t - \frac{\tau}{2} \right) \right] - j\phi'(t)\tau = j \frac{1}{24} \phi^{(3)}(t) \tau^3 + \dots \quad (3.58)$$

causes distribution spread around the instantaneous frequency. This factor may be used to measure the distribution concentration (spread) along (from) the instantaneous frequency. For a fully concentrated distribution, defined by (3.23), the spreading factor would be zero, $Q(t, \tau) \equiv 0$.

For the Wigner distribution the factor Q is equal to zero if instantaneous frequency $\phi'(t)$ is a linear function, that is, if $\phi^{(n)}(t) \equiv 0$, for $n \geq 3$. In quantum mechanics, the quantum correction term Q was equal to zero for the potential function such that the terms with \hbar^{n-1} , $V^{(n)}(x)$, $n \geq 3$ are negligible. This is in accordance with (3.54), where linear function $\phi'(t)$ corresponds to quadratic function $V(x)$.

3.3.2 Uncertainty Principle and the Wigner Distribution

The uncertainty principle, discussed in Chapter 2, can be reinterpreted within the Wigner distribution definition framework. Recall that this principle states that the product of effective durations of a signal $x(t)$ in time σ_t and in frequency σ_Ω cannot

be arbitrarily small. It satisfies the inequality

$$\sigma_t^2 \sigma_\Omega^2 \geq \frac{1}{4}$$

were σ_t^2 and σ_Ω^2 are defined by

$$\sigma_t^2 = \frac{1}{E_x} \int_{-\infty}^{\infty} (t - t_c)^2 |x(t)|^2 dt = \frac{1}{2\pi E_x} \int_{-\infty}^{\infty} \int_{-\infty}^{\infty} (t - t_c)^2 WD(t, \Omega) dt d\Omega \quad (3.59)$$

with

$$t_c = \frac{1}{E_x} \int_{-\infty}^{\infty} t |x(t)|^2 dt$$

and

$$\sigma_\Omega^2 = \frac{1}{2\pi E_x} \int_{-\infty}^{\infty} (\Omega - \Omega_c)^2 |X(\Omega)|^2 d\Omega = \frac{1}{2\pi E_x} \int_{-\infty}^{\infty} \int_{-\infty}^{\infty} (\Omega - \Omega_c)^2 WD(t, \Omega) dt d\Omega \quad (3.60)$$

with

$$\Omega_c = \frac{1}{2\pi E_x} \int_{-\infty}^{\infty} \Omega |X(\Omega)|^2 d\Omega.$$

The signal energy is denoted by E_x , while notation t_c and Ω_c is used to denote the central points of $|x(t)|^2$ and $|X(\Omega)|^2$.

The equality holds for the Gaussian signal (as it has been shown earlier). Thus, it is not possible to achieve arbitrary high concentration in both directions, simultaneously. The product of effective durations is higher than 1/4 for any other than Gaussian signal.

Note that the product $\sigma_t^2 \sigma_\Omega^2$ has a lower limit 1/4, but there is no upper limit. It can be very large. Signals whose product of durations in time and frequency is large,

$$\sigma_t^2 \sigma_\Omega^2 \gg 1,$$

are called asymptotic signals.

Example 3.7. Consider signal $x(t) = A(t)e^{j\phi(t)}$. Show that

$$\sigma_\Omega^2 = \frac{1}{E_x} \int_{-\infty}^{\infty} \left((A'(t))^2 + (A(t)\phi'(t))^2 \right) dt \quad (3.61)$$

for $\Omega_c = 0$.

★ Using the Parseval's theorem, we may write

$$\begin{aligned}\sigma_{\Omega}^2 &= \frac{1}{2\pi E_x} \int_{-\infty}^{\infty} \Omega^2 |X(\Omega)|^2 d\Omega = \frac{1}{E_x} \int_{-\infty}^{\infty} |x'(t)|^2 dt \\ &= \frac{1}{E_x} \int_{-\infty}^{\infty} \left| A'(t) e^{j\phi(t)} + jA(t) \phi'(t) e^{j\phi(t)} \right|^2 dt \\ &= \frac{1}{E_x} \int_{-\infty}^{\infty} |A'(t) + jA(t) \phi'(t)|^2 dt\end{aligned}$$

resulting in (3.61). \square

The fact that the signal $x(t)$ is located within $[t_g - \sigma_t, t_g + \sigma_t]$ in time and within $[\Omega_i - \sigma_{\Omega}, \Omega_i + \sigma_{\Omega}]$ in frequency does not provide any information about the local concentration of the signal within this time-frequency region. It can be spread all over the region or highly concentrated along a line within that region. Thus, the conclusion that the Wigner distribution is highly concentrated along a line (that we made earlier for a linear frequency-modulated signal) does not contradict the uncertainty principle. Local concentration measures are used to grade signal's concentration in the time-frequency domain.

3.3.3 Pseudo Quantum Signal Representation

A distribution that parametrizes the uncertainty, keeping the marginal properties and the location of the instantaneous frequency, is defined as a pseudo quantum signal representation

$$SD_L(t, \wp) = \int_{-\infty}^{\infty} x^{[L]} \left(t + \frac{\tau}{2L} \right) x^{[L]*} \left(t - \frac{\tau}{2L} \right) e^{-j\wp\tau} d\tau \quad (3.62)$$

with

$$x^{[L]}(t) = A(t) e^{jL\phi(t)}.$$

The spreading factor in this representation is

$$Q(t, \tau) = j \left[L\phi \left(t + \frac{\tau}{2L} \right) - L\phi \left(t - \frac{\tau}{2L} \right) \right] - j\phi'(t)\tau = j \frac{1}{24L^2} \phi^{(3)}(t) \tau^3 + \dots$$

For the Gaussian chirp signal

$$x(t) = Ae^{-at^2/2}e^{j(bt^2/2+ct)} \quad (3.63)$$

we get

$$SD_L(t, \phi) = 2|A|^2 e^{-at^2} \sqrt{\frac{\pi}{a}} L e^{-\frac{(\phi - bt - c)^2}{a/L^2}}.$$

For a large parameter L , when $L\sqrt{\frac{\pi}{a}} e^{-L^2\phi^2/a} \rightarrow \pi\delta(\phi)$, we get

$$SD_L(t, \phi) = |A|^2 e^{-at^2} 2\pi\delta(\phi - bt - c),$$

being highly concentrated, simultaneously in time and in frequency ϕ at $(0, c)$ for a large a , if $a/L^2 \rightarrow 0$. The uncertainty principle for (3.62) is

$$\sigma_t^2 \sigma_\phi^2 \geq \frac{1}{4L^2}. \quad (3.64)$$

It follows from the quantum mechanics form $\sigma_x^2 \sigma_p^2 \geq \hbar^2/4$.

Note that the distribution $SD_L(t, \phi) = |A|^2 e^{-at^2} 2\pi\delta(\phi - bt - c)$ satisfies the energy and the time marginal property for any set of parameters.

The pseudo quantum signal representation of signal (3.63) with $a = 1$, $b = 1/2$ and $c = 0$ for $L = 1$ (Wigner distribution), $L = 4$ and $L = 16$ is given in Fig. 3.4 (see also Problem 3.17).

3.3.4 Instantaneous Frequency, Bandwidth, and Moments

From the definition of the signal width in frequency (3.60) we can conclude that, at a given instant t , we may define similar local value

$$\sigma_\Omega^2(t) = \frac{1}{2\pi|x(t)|^2} \int_{-\infty}^{\infty} (\Omega - \Omega_i(t))^2 WD(t, \Omega) d\Omega$$

with $\Omega_i(t) = \phi'(t)$ defined in terms of $WD(t, \Omega)$ according to property P₉ of the Wigner distribution.

The instantaneous bandwidth is defined with the aim to be a measure of the Wigner distribution deviation from the instantaneous frequency, at a given instant t .

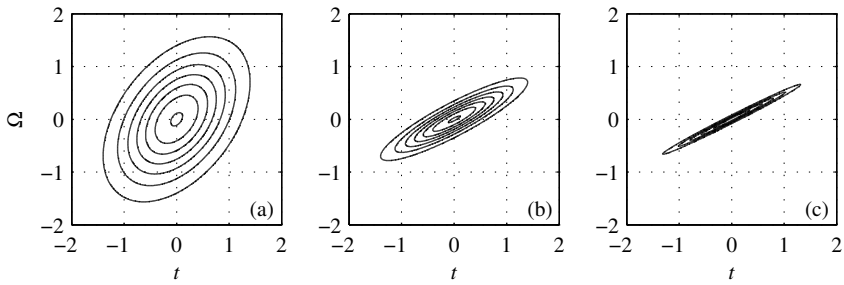


Figure 3.4 The pseudo quantum signal representation of a Gaussian chirp for (a) the Wigner distribution, $L = 1$, (b) $L = 4$, and (c) $L = 16$.

It can be calculated as

$$\begin{aligned}\sigma_{\Omega}^2(t) &= \frac{1}{2\pi|x(t)|^2} \int_{-\infty}^{\infty} \Omega^2 WD(t, \Omega) d\Omega - \Omega_i^2(t) \\ &= \frac{-\frac{d^2}{d\tau^2} [x(t + \frac{\tau}{2}) x^*(t - \frac{\tau}{2})]|_{\tau=0}}{|x(t)|^2} - \Omega_i^2(t)\end{aligned}$$

since $-\Omega^2 WD(t, \Omega)$ and the second derivative of $x(t + \frac{\tau}{2}) x^*(t - \frac{\tau}{2})$ over τ are the Fourier transformation pair. After the second derivative evaluation, we can write

$$\sigma_{\Omega}^2(t) = -\frac{x''(t)x^*(t) - 2x'(t)x^{*'}(t) + x(t)x^{*''}(t)}{4|x(t)|^2} - \Omega_i^2(t). \quad (3.65)$$

For $x(t) = A(t) \exp(j\phi(t))$ we get

$$\sigma_{\Omega}^2(t) = \frac{1}{2} \left[\left(\frac{A'(t)}{A(t)} \right)^2 - \frac{A''(t)}{A(t)} \right]. \quad (3.66)$$

The instantaneous bandwidth is obtained with the Wigner distribution as a weighting function, that can assume negative values. It may result in small values of $\sigma_{\Omega}^2(t)$ even in the cases when the Wigner distribution is quite spread. Thus, we should be cautious in using the instantaneous bandwidth as a measure of the

distribution spread around the instantaneous frequency, in contrast to the global parameters σ_t^2 and σ_Ω^2 , which indicate a global region of the distribution spread with always positive weighting functions $|x(t)|^2$ and $|X(\Omega)|$.

Note that this form can be generalized to the instantaneous (conditional) moments. The n th instantaneous moment of the Wigner distribution, at an instant t , is defined as

$$m_i^n(t) = \frac{1}{2\pi|x(t)|^2} \int_{-\infty}^{\infty} \Omega^n WD(t, \Omega) d\Omega. \quad (3.67)$$

Using the fact that the Wigner distribution and the local auto-correlation function are the Fourier transform pair,

$$WD(t, \Omega) \xleftarrow[\Omega, \tau]{} x(t + \tau/2)x^*(t - \tau/2),$$

results in

$$(j\Omega)^n WD(t, \Omega) \xleftarrow[\Omega, \tau]{} \frac{d^n}{d\tau^n} (x(t + \tau/2)x^*(t - \tau/2)).$$

The instantaneous moments are calculated as

$$\begin{aligned} m_i^n(t) &= \frac{(-j)^n \frac{d^n}{d\tau^n} (x(t + \tau/2)x^*(t - \tau/2)) \Big|_{\tau=0}}{|x(t)|^2}, \\ &= \frac{(-j/2)^n \sum_{l=0}^n \binom{n}{l} (-1)^l x^{*(l)}(t) x^{(n-l)}(t)}{|x(t)|^2}. \end{aligned} \quad (3.68)$$

In a similar way we can define moments for other distributions from the generalized Wigner distribution form, including the Rihaczek distribution.

Example 3.8. Find the global duration measures and the instantaneous bandwidth of the linear frequency modulated Gaussian function. What is the minimal product of global duration measures, as phase rate changes?

★ For a linear frequency modulated signal

$$x(t) = e^{-\frac{1}{2}t^2/\alpha^2} e^{jat^2}$$

the Wigner distribution is

$$WD(t, \Omega) = 2\alpha\sqrt{\pi} e^{-t^2/\alpha^2} e^{-\alpha^2(\Omega-2at)^2}.$$

The Fourier transform of this signal is

$$\begin{aligned} X(\Omega) &= \int_{-\infty}^{\infty} e^{-(1/(2\alpha^2)+ja)t^2} e^{-j\Omega t} dt \\ &= \sqrt{\frac{\pi}{1/(2\alpha^2)+ja}} \exp\left(\frac{-\Omega^2}{4(1/(2\alpha^2)+ja)}\right) \\ &= \sqrt{\frac{2\pi\alpha^2}{1+j2\alpha^2a}} \exp\left(\frac{-\Omega^2\alpha^2}{2(1+4\alpha^4a^2)}\right) \exp\left(j\frac{\Omega^2aa^4}{(1+4\alpha^4a^2)}\right). \end{aligned} \quad (3.69)$$

The global effective durations in time and frequency are

$$\begin{aligned} \sigma_t^2 &= \frac{1}{E_x} \int_{-\infty}^{\infty} t^2 |x(t)|^2 dt = \frac{\int_{-\infty}^{\infty} t^2 e^{-(t/\alpha)^2} dt}{\int_{-\infty}^{\infty} e^{-(t/\alpha)^2} dt} = \alpha^2/2 \\ \sigma_{\Omega}^2 &= \frac{\int_{-\infty}^{\infty} \Omega^2 |X(\Omega)|^2 d\Omega}{\int_{-\infty}^{\infty} |X(\Omega)|^2 d\Omega} = (1+4\alpha^4a^2)/(2\alpha^2), \end{aligned}$$

since signal and its Fourier transform are even functions with $t_g = 0$ and $\Omega_i = 0$.

Their product is

$$\sigma_t^2 \sigma_{\Omega}^2 = (1+4\alpha^4a^2)/4 \geq 1/4. \quad (3.70)$$

The minimum $\sigma_t^2 \sigma_{\Omega}^2 = 1/4$ is achieved for pure (nonmodulated) Gaussian chirp with $a = 0$.

For large α , when the considered signal tends to a pure linear frequency-modulated signal $x(t) = \exp(jat^2)$, the duration measures tend to

$$\sigma_t^2 = \alpha^2/2 \text{ and } \sigma_{\Omega}^2 \rightarrow 2\alpha^2a^2.$$

With $a \neq 0$, the product $\sigma_t^2 \sigma_{\Omega}^2 \rightarrow a^2\alpha^4$ is large for large α . Then, this signal behaves as an asymptotic signal. However, a large product of duration measures and large global values σ_t^2 and σ_{Ω}^2 do not mean that signal cannot be highly concentrated in frequency for one time instant, or in time for one frequency value.

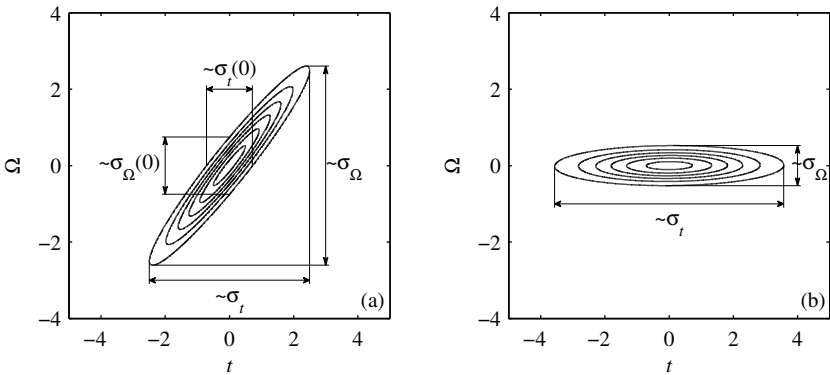


Figure 3.5 Illustration of the global and local effective duration measures on the Wigner distribution of a Gaussian chirp (left) and on the rotated Wigner distribution (right), that is, on the Wigner distribution of a pure Gaussian signal. The presented durations are proportional to the effective duration so the symbol \sim is used.

The local effective duration in frequency (instantaneous bandwidth) value, that measures the distribution width in frequency for a given instant t , follows from

$$\begin{aligned}\sigma_\Omega^2(t) &= \frac{1}{2\pi|x(t)|^2} \int_{-\infty}^{\infty} (\Omega - \Omega_i(t))^2 WD(t, \Omega) d\Omega \\ &= \frac{1}{2\pi e^{-(t/\alpha)^2}} \int_{-\infty}^{\infty} (\Omega - 2at)^2 2\alpha\sqrt{\pi}e^{-(t/\alpha)^2} e^{-(\alpha(\Omega-2at))^2} d\Omega \\ &= \frac{\alpha}{\sqrt{\pi}} \int_{-\infty}^{\infty} \theta^2 e^{-\alpha^2\theta^2} d\theta = \frac{1}{2\alpha^2}\end{aligned}$$

with $\Omega_i(t) = 2at$. The same value follows also from (3.66) with $A(t) = e^{-\frac{1}{2}(t/\alpha)^2}$, as $\sigma_\Omega^2(t) = 1/(2\alpha^2)$.

For a large value of α , as compared to a (slow-varying amplitude with respect to phase variations), we get a very concentrated distribution along the instantaneous frequency $\Omega_i(t) = 2at$, with $\sigma_\Omega^2(t) \rightarrow 0$. It is compliant with the instantaneous bandwidth definition. Illustration of duration measures is presented in Fig. 3.5. \square

Example 3.9. What is the linear coordinate transformation matrix of the Wigner distribution which will transform the signal from the previous example into the one with minimal product of effective durations, $\sigma_t^2 \sigma_\Omega^2 = 1/4$?

★ A signal with minimal product is a pure (nonmodulated) Gaussian chirp. It may be obtained, without any change in the Wigner distribution form, by a pure rotation of the time-frequency plane, from

$$WD(t, \Omega) = 2\alpha\sqrt{\pi}e^{-t^2/\alpha^2}e^{-\alpha^2(\Omega-2at)^2} = 2\alpha\sqrt{\pi}e^{-t^2(1/\alpha^2+\alpha^24a^2)}e^{-\alpha^2\Omega^2}e^{4\alpha^2a\Omega t}$$

for an angle β , with

$$\begin{bmatrix} u \\ v \end{bmatrix} = \begin{bmatrix} \cos\beta & -\sin\beta \\ \sin\beta & \cos\beta \end{bmatrix} \begin{bmatrix} t \\ \Omega \end{bmatrix}$$

$$\begin{bmatrix} t \\ \Omega \end{bmatrix} = \begin{bmatrix} \cos\beta & \sin\beta \\ -\sin\beta & \cos\beta \end{bmatrix} \begin{bmatrix} u \\ v \end{bmatrix}.$$

By replacing t and Ω with u and v

$$WD(u, v) = 2\alpha\sqrt{\pi}e^{-(u\cos\beta+v\sin\beta)^2(1/\alpha^2+\alpha^24a^2)}e^{-\alpha^2(-u\sin\beta+v\cos\beta)^2} \\ \times e^{4\alpha^2a(u\cos\beta+v\sin\beta)(-u\sin\beta+v\cos\beta)}$$

and equating the coefficient with product uv , in the obtained rotated Wigner distribution, with zero,

$$-2\cos\beta\sin\beta(1/\alpha^2 + \alpha^24a^2) + 2\alpha^2\sin\beta\cos\beta + 4\alpha^2a\cos^2\beta - 4\alpha^2a\sin^2\beta = 0, \\ \sin(2\beta)(1/\alpha^2 + \alpha^24a^2 - \alpha^2) = 4\alpha^2a\cos(2\beta)$$

follows

$$\tan(2\beta) = \frac{4\alpha^2a}{(1/\alpha^2 + \alpha^24a^2) - \alpha^2}. \quad (3.71)$$

Then, a separable Wigner distribution is obtained, Fig. 3.5. Simple check is for $\alpha \rightarrow \infty$, when a pure linear frequency-modulated signal is obtained along $\Omega = 2a$. Thus, the rotation should provide angle β such that $\tan(\beta) = -2a$. Indeed, then

$$\lim_{\alpha \rightarrow \infty} \tan(2\beta) = \frac{4a}{4a^2 - 1},$$

with the well-known trigonometric relation $\tan(2\beta) = 2\tan(\beta)/[1 - \tan^2(\beta)]$, gives $\tan(\beta) = -2a$. It is interesting to note that for a finite α ,

$$\tan(\beta) \neq -2a,$$

as it can be spotted in Fig. 3.4.

The rotation of coordinates is achieved by the fractional Fourier transformation for the angle β ,

$$x_L(t) = \{[x(t)e^{-j\tan(\beta/2)t^2/2}]*\sqrt{\csc(\beta)}e^{j\csc(\beta)t^2/2}\}e^{-j\tan(\beta/2)t^2/2},$$

$$X_\beta(t) = x_L(t)/\sqrt{2j\pi e^{-j\beta}}.$$

If the original signal is just multiplied by $\exp(-jat^2)$, then

$$x_L(t) = x(t)e^{-jat^2} = e^{-\frac{1}{2}t^2/\alpha^2}, \quad (3.72)$$

will correspond to the linear transformation $WD(t, \Omega + 2at)$ with the transformation matrix

$$\mathbf{L}_1 = \begin{bmatrix} 1 & 0 \\ 2a & 1 \end{bmatrix}.$$

However, scaling in addition to the rotation is performed here, so the shape of the obtained Wigner distribution would not be equal to the rotated only original distribution. \square

Example 3.10. Consider the instantaneous bandwidth of a quadratic frequency modulated Gaussian function.

★ For a cubic phase signal (quadratic frequency modulated)

$$x(t) = e^{-\frac{1}{2}(t/\alpha)^2} e^{jat^3} \quad (3.73)$$

the relation for the instantaneous bandwidth, given by (3.66), is not phase dependent, producing again small instantaneous bandwidth $\sigma_\Omega^2(0) = 1/(2\alpha^2)$ for large α . In order to check whether a small $\sigma_\Omega^2(0)$ mean that the Wigner distribution is not spread around the instantaneous frequency, at $t = 0$, we will calculate and plot the Wigner distribution for this signal. The Wigner distribution is

$$WD(t, \Omega) = e^{-t^2/\alpha^2} \int_{-\infty}^{\infty} e^{-\tau^2/(2\alpha)^2} e^{jat^3/4} e^{-j(\Omega - 3at^2)\tau} d\tau.$$

The stationary-phase points are

$$3a\tau_0^2/4 = \Omega - 3at^2$$

or

$$\tau_{0+} = \sqrt{4(\Omega - 3at^2)/(3a)}$$

and

$$\tau_{0-} = -\sqrt{4(\Omega - 3at^2)/(3a)}$$

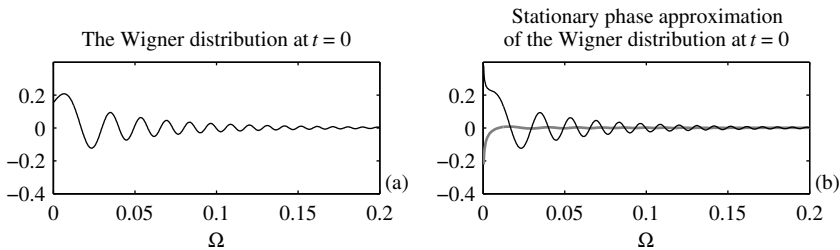


Figure 3.6 Stationary-phase approximation of the Wigner distribution for cubic-phase signal. The approximation error is presented with thick gray line.

for $(\Omega - 3at^2) \geq 0$, and

$$\phi''(\tau_0) = 3a\tau_0/2. \quad (3.74)$$

The resulting stationary-phase approximation of the Wigner distribution is obtained by summing contribution from both stationary-phase points, τ_{0+} and τ_{0-} , as

$$\begin{aligned} WD(t, \Omega) &= \sqrt{\frac{2\pi}{\sqrt{3a(\Omega - 3at^2)}}} \exp(-t^2/\alpha^2) \\ &\times \exp\left(-(\Omega - 3at^2)/(3a\alpha^2)\right) \cos\left(\frac{4}{3\sqrt{3a}} \left[(\Omega - 3at^2)\right]^{3/2} - \pi/4\right) \end{aligned} \quad (3.75)$$

for $\Omega - 3at^2 \geq 0$ and $WD(t, \Omega) = 0$ for $\Omega - 3at^2 < 0$.

For $t = 0$, significant oscillations appear, since the attenuation in frequency is $\exp(-(\Omega - 3at^2)/(3a\alpha^2))$. Note that this is not in accordance with the expectation that the instantaneous bandwidth $\sigma_\Omega^2(0) = 1/\alpha^2$ is small for a large α . This kind of unexpected behavior is due to the fact that the Wigner distribution assumes negative values.

Note that the stationary phase is an approximation, producing accurate results for large arguments. In this case, exact Wigner distribution almost coincides with this approximation, already for $\Omega - 3at^2 > \pi/4$ as presented in Fig. 3.6(b). This example will be very illustrative for the analysis of the Wigner distribution inner interferences, as well. \square

3.4 IMPLEMENTATION OF THE WIGNER DISTRIBUTION

The Wigner distribution is implemented with finite integration interval. In numerical realization discrete time signal is also used. These forms are studied within this section.

3.4.1 Pseudo Wigner Distribution

In the STFT calculation the localization window plays a crucial role in time-frequency analysis. Without a window, the STFT does not have any time-frequency property. It reduces to the Fourier transform. In the Wigner distribution, time-frequency representation may be achieved without any window. Thus, the role of a window is not crucially important in the Wigner distribution, as it is in the short time Fourier transform. However, in practical realizations of the Wigner distribution, a finite time interval should be used, for any numerical calculation. Thus, here we are constrained with a finite time lag τ for practical (numerical complexity), not substantial reasons. The Wigner distribution, with a finite lag window, is referred to as the pseudo Wigner distribution. It is defined as

$$PWD(t, \Omega) = \int_{-\infty}^{\infty} w\left(\frac{\tau}{2}\right) w^*\left(-\frac{\tau}{2}\right) x\left(t + \frac{\tau}{2}\right) x^*\left(t - \frac{\tau}{2}\right) e^{-j\Omega\tau} d\tau \quad (3.76)$$

where window $w(\tau)$ localizes the considered time interval. If $w(0) = 1$, the pseudo Wigner distribution satisfies the time marginal property. The pseudo Wigner distribution is smoothed in the frequency direction with respect to the Wigner distribution

$$PWD(t, \Omega) = \frac{1}{2\pi} \int_{-\infty}^{\infty} WD(t, v) W_e(\Omega - v) dv$$

where $W_e(\Omega)$ is the Fourier transform of $w_e(\tau) = w(\tau/2)w^*(-\tau/2)$. The pseudo Wigner distribution example with Hann(ing) window is shown in Fig. 3.7.

3.4.2 Smoothed Wigner Distribution

In order to reduce the interferences in the Wigner distribution, the distribution is sometimes smoothed not only in the frequency axis direction, achieved by the pseudo Wigner distribution, but also in time, by using a time-smoothing window

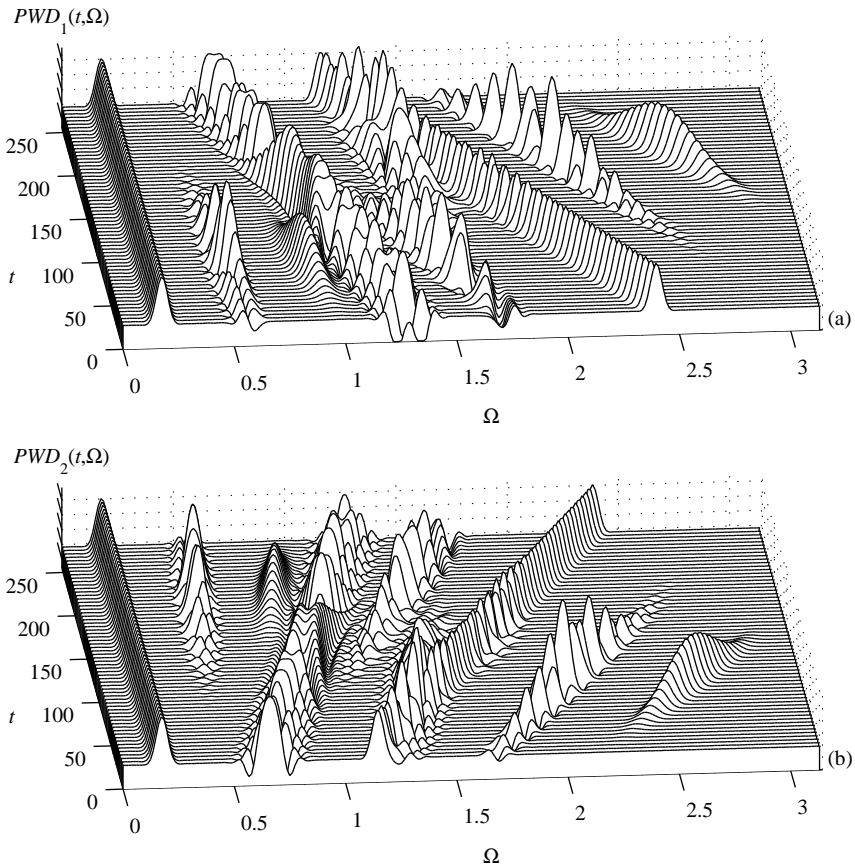


Figure 3.7 (a, b) The pseudo Wigner distribution of the signals from Figure 2.1.

$G(t)$. This form is called the smoothed Wigner distribution

$$SWD(t, \Omega) = \frac{1}{2\pi} \int_{-\infty}^{\infty} \int_{-\infty}^{\infty} G(t-u) W_e(\Omega-v) WD(u, v) du dv. \quad (3.77)$$

Example 3.11. The most commonly used smoothing function is of the form

$$G(t)W_e(\Omega) = \alpha e^{-\gamma t^2} e^{-\beta \Omega^2} = \alpha e^{-(\gamma t^2 + \beta \Omega^2)}.$$

What condition should α , β , and γ satisfy so that the smoothed Wigner distribution is equal to a spectrogram?

★ The smoothed Wigner distribution is

$$SWD(t, \Omega) = \frac{1}{2\pi} \int_{-\infty}^{\infty} \int_{-\infty}^{\infty} \int_{-\infty}^{\infty} \alpha e^{-\gamma u^2 - \beta v^2} x(t-u+\frac{\tau}{2}) x^*(t-u-\frac{\tau}{2}) e^{-j(\Omega-v)\tau} du dv d\tau$$

with change of variables $-u + \frac{\tau}{2} = v_1$ and $-u - \frac{\tau}{2} = v_2$, we get

$$\frac{1}{2\pi} \int_{-\infty}^{\infty} \int_{-\infty}^{\infty} \int_{-\infty}^{\infty} \alpha e^{-\gamma(v_1+v_2)^2/4} e^{-\beta v^2} x(t+v_1) x^*(t+v_2) e^{-j(v_1-v_2)(\Omega-v)} dv_1 dv_2.$$

After integration over v , follows

$$\frac{1}{2\sqrt{\pi\beta}} \int_{-\infty}^{\infty} \int_{-\infty}^{\infty} \alpha e^{-\gamma(v_1+v_2)^2/4} e^{-(v_1-v_2)^2/(4\beta)} x(t+v_1) x^*(t+v_2) e^{-j(v_1-v_2)\Omega} dv_1 dv_2.$$

The spectrogram is obtained for

$$\frac{\alpha}{2\sqrt{\pi\beta}} e^{-\gamma(v_1+v_2)^2/4} e^{-(v_1-v_2)^2/(4\beta)} = w(v_1)w(v_2).$$

For $\gamma = 1/\beta$ and $\alpha = 2\sqrt{\pi\beta} = 2\sqrt{\pi/\gamma}$, we get

$$e^{-\gamma(v_1+v_2)^2/4} e^{-\gamma(v_1-v_2)^2/4} = e^{-\gamma v_1^2/2} e^{-\gamma v_2^2/2}$$

or

$$w(\tau) = e^{-\gamma\tau^2/2} \quad (3.78)$$

and

$$G(t)W_e(\Omega) = 2\sqrt{\pi/\gamma} e^{-(\gamma t^2 + \Omega^2/\gamma)}. \quad (3.79)$$

It is interesting to note that, this form of the smoothed Wigner distribution is always positive, for any signal. □

3.4.3 Discrete Pseudo Wigner Distribution

If the signal in (3.76) is discretized in τ with a sampling interval Δt , then a sum instead of an integral is formed. The pseudo Wigner distribution of a discrete-lag signal, for a given time instant t , is given by

$$PWD(t, \Omega) = \sum_{m=-\infty}^{\infty} w\left(m \frac{\Delta t}{2}\right) w^*\left(-m \frac{\Delta t}{2}\right) x\left(t + m \frac{\Delta t}{2}\right) x^*\left(t - m \frac{\Delta t}{2}\right) e^{-jm\Omega\Delta t} \Delta t. \quad (3.80)$$

Sampling in τ with $\Delta t = \pi/\Omega_0$, $\Omega_0 > \Omega_m$ corresponds to the sampling of signal $x(t + \tau/2)$ in $\tau/2$ with $\Delta t/2 = \pi/(2\Omega_0)$.

The discrete-lag pseudo Wigner distribution is the Fourier transform of signal

$$R(t, m) = w\left(m \frac{\Delta t}{2}\right) w^*\left(-m \frac{\Delta t}{2}\right) x\left(t + m \frac{\Delta t}{2}\right) x^*\left(t - m \frac{\Delta t}{2}\right) \Delta t.$$

For a given instant t , it can be written as

$$PWD(t, \omega) = \sum_{m=-\infty}^{\infty} R(t, m) e^{-jm\omega}$$

with $\omega = \Omega\Delta t$. If the sampling interval satisfies the sampling theorem, then the sum in (3.80) is equal to the integral form (3.76).

A discrete form of the pseudo Wigner distribution, with $N + 1$ samples and $\omega = 2\pi k/(N + 1)$, for a given time instant t , is

$$PWD(t, k) = \sum_{m=-N/2}^{N/2} R(t, m) e^{-j2\pi mk/(N+1)}.$$

Here, $N/2$ is an integer. This distribution could be calculated by using the standard DFT routines.

For discrete-time instants $t = n\Delta t$, introducing the notation

$$\begin{aligned} & R(n\Delta t, m\Delta t) \\ &= w\left(m \frac{\Delta t}{2}\right) w^*\left(-m \frac{\Delta t}{2}\right) x\left(n\Delta t + m \frac{\Delta t}{2}\right) x^*\left(n\Delta t - m \frac{\Delta t}{2}\right) \Delta t \\ & R(n, m) = w\left(\frac{m}{2}\right) w^*\left(-\frac{m}{2}\right) x\left(n + \frac{m}{2}\right) x^*\left(n - \frac{m}{2}\right), \end{aligned}$$

the discrete-time and discrete-lag pseudo Wigner distribution can be written as

$$PWD(n, \omega) = \sum_{m=-\infty}^{\infty} w\left(\frac{m}{2}\right) w^*\left(-\frac{m}{2}\right) x\left(n + \frac{m}{2}\right) x^*\left(n - \frac{m}{2}\right) e^{-j m \omega}. \quad (3.81)$$

Notation $x(n + m/2)$, for given n and m , should be understood as the signal value at the instant $x((n + m/2)\Delta t)$. In this notation, the discrete-time pseudo Wigner distribution is periodic in ω with period 2π .

Since various discretization steps are used (here and in open literature), we will provide a relation of discrete indexes to the continuous time and frequency, for each definition, as

$$PWD(t, \Omega)|_{t=n\Delta t, \Omega=\frac{2\pi k}{(N+1)\Delta t}} = PWD\left(n\Delta t, \frac{2\pi k}{(N+1)\Delta t}\right) \rightarrow PWD(n, k).$$

The sign \rightarrow could be understood as the equality sign in the sense of sampling theorem (Example 1.19). Otherwise, it should be considered as a correspondence sign. The discrete form of (3.76), with $N+1$ samples, is

$$\begin{aligned} PWD\left(n\Delta t, \frac{2\pi k}{(N+1)\Delta t}\right) &\rightarrow PWD(n, k) \\ PWD(n, k) = \sum_{m=-N/2}^{N/2} w\left(\frac{m}{2}\right) w^*\left(-\frac{m}{2}\right) x\left(n + \frac{m}{2}\right) x^*\left(n - \frac{m}{2}\right) e^{-j 2\pi km/(N+1)}, \end{aligned}$$

where $N/2$ is an integer, $-N/2 \leq k \leq N/2$ and $\omega = \Omega\Delta t = 2\pi k/(N+1)$ or $\Omega = 2\pi k/((N+1)\Delta t)$.

In order to avoid different sampling intervals in time and lag in the discrete Wigner distribution definition, the discrete Wigner distribution can be oversampled in time, as it has been done in lag. It means that the same sampling interval $\Delta t/2$, for both time and lag axes, can be used. Then, we can write

$$\begin{aligned} R\left(n \frac{\Delta t}{2}, m \Delta t\right) &\rightarrow R(n, m) \\ R\left(n \frac{\Delta t}{2}, m \Delta t\right) = w\left(m \frac{\Delta t}{2}\right) w^*\left(-m \frac{\Delta t}{2}\right) x\left(n \frac{\Delta t}{2} + m \frac{\Delta t}{2}\right) x^*\left(n \frac{\Delta t}{2} - m \frac{\Delta t}{2}\right) \Delta t \\ R(n, m) = w(m) w^*(-m) x(n+m) x^*(n-m) \end{aligned} \quad (3.82)$$

The discrete-time and discrete-lag pseudo Wigner distribution, in this case, is of the form

$$PWD(n, \omega) = \sum_{m=-\infty}^{\infty} w(m)w^*(-m)x(n+m)x^*(n-m)e^{-j2m\omega}. \quad (3.83)$$

It corresponds to the continuous-time pseudo Wigner distribution (3.76) with substitution $\tau/2 \rightarrow \tau$

$$PWD(t, \Omega) = 2 \int_{-\infty}^{\infty} w(\tau)w^*(-\tau)x(t+\tau)x^*(t-\tau)e^{-j2\Omega\tau}d\tau.$$

The discrete pseudo Wigner distribution is given here by

$$\begin{aligned} PWD\left(\frac{n\Delta t}{2}, \frac{4\pi k}{(N+1)\Delta t}\right) &\rightarrow PWD(n, k) \\ PWD(n, k) &= \sum_{m=-N/2}^{N/2} w(m)w^*(-m)x(n+m)x^*(n-m)e^{-j4\pi mk/(N+1)} \end{aligned} \quad (3.84)$$

for $-N/2 \leq 2k \leq N/2$. Since, the standard DFT routines are commonly used for the pseudo Wigner distribution calculation, we may use every other ($2k$) sample in (3.84) or oversample the pseudo Wigner distribution in frequency (as it has been done in time). Then,

$$\begin{aligned} PWD\left(\frac{n\Delta t}{2}, \frac{2\pi k}{(N+1)\Delta t}\right) &\rightarrow PWD(n, k) \\ PWD(n, k) &= \sum_{m=-N/2}^{N/2} w(m)w^*(-m)x(n+m)x^*(n-m)e^{-j2\pi mk/(N+1)}. \end{aligned} \quad (3.85)$$

This discrete pseudo Wigner distribution, oversampled in both time and in frequency by factor of 2, has finer time-frequency grid, producing smaller time-frequency estimation errors at the expense of the calculation complexity.

Example 3.12. Signal $x(t) = \exp(j31\pi t^2)$ is considered within $-1 \leq t \leq 1$. Find the sampling interval of signal for discrete pseudo Wigner distribution calculation. If the rectangular window of the width $N+1 = 31$ is used in analysis, find the pseudo Wigner distribution values and estimate the instantaneous frequency at $t = 0.5$ based on the discrete pseudo Wigner distribution.

★ For this signal the instantaneous frequency is $\Omega_i(t) = 62\pi t$. It is within the range $-62\pi \leq \Omega_i(t) \leq 62\pi$. Thus, we may approximately assume that the maximal frequency is $\Omega_m = 62\pi$. The sampling interval for the Fourier transform would be $\Delta t \leq 1/62$. For the direct pseudo Wigner distribution calculation, it should be twice smaller, $\Delta t/2 \leq 1/124$. Therefore, the discrete version of the pseudo Wigner distribution (3.82), normalized with Δt , at $t = 0.5$ or $n = 62$, is (3.84)

$$\begin{aligned} PWD(n, k) &= \sum_{m=-15}^{15} e^{j31\pi((n+m)/124)^2} e^{-j31\pi((n-m)/124)^2} e^{-j4\pi mk/31} \\ &= \sum_{m=-15}^{15} e^{j\pi mn/124} e^{-j4\pi mk/31} = \frac{\sin(\frac{\pi}{8}(n-16k))}{\sin(\frac{\pi}{248}(n-16k))}. \end{aligned}$$

The argument k , when the pseudo Wigner distribution reaches maximum for $n = 62$, follows from $62 - 16k = 0$ as

$$\hat{k} = \arg \left\{ \max_k PWD(n, k) \right\} = \left[\frac{62}{16} \right] = 4,$$

where $[\cdot]$ stands for the nearest integer. Obviously, the exact instantaneous frequency is not on the discrete frequency grid. The estimated value of the instantaneous frequency at $t = 1/2$ is $\hat{\Omega} = 4\pi\hat{k}/((N+1)\Delta t) = 16\pi/(31/62) = 32\pi$. The true value is $\Omega_i(1/2) = 31\pi$. When the true frequency is not on the grid, the estimation can be improved by using the interpolation or displacement bin, as explained in Chapter 1. The frequency sampling interval is $\Delta\Omega = 4\pi/((N+1)\Delta t) = 8\pi$, with maximal estimation absolute error $\Delta\Omega/2 = 4\pi$.

If we used the standard DFT routine (3.85) with $N + 1 = 31$ and all available frequency samples, we would get

$$\begin{aligned} PWD(n, k) &= \text{DFT}_{31} \left\{ e^{j31\pi((n+m)/124)^2} e^{-j31\pi((n-m)/124)^2} \right\} \\ &= \sum_{m=-15}^{15} e^{j31\pi((n+m)/124)^2} e^{-j31\pi((n-m)/124)^2} e^{-j2\pi mk/31} = \frac{\sin(\frac{\pi}{8}(n-8k))}{\sin(\frac{\pi}{248}(n-8k))}. \end{aligned}$$

The maximum would be at $\hat{k} = 8$, with the estimated frequency $\hat{\Omega} = 2\pi\hat{k}/((N+1)\Delta t)$. Thus, $\hat{\Omega} = 32\pi$, as expected. By this calculation, the frequency sampling interval is $\Delta\Omega = 2\pi/((N+1)\Delta t) = 4\pi$, with the maximal estimation absolute error $\Delta\Omega/2 = 2\pi$. □

By using an odd number of samples $N + 1$ in the previous definitions, the symmetry of the product $x(n+m)x^*(n-m)$ is preserved in the summation. However, when an even number of samples is used, that is not the case. To illustrate this effect, consider a simple example of signal, for $n = 0$, with $N = 4$ samples.

Then, four values of the signal $x(m)$, used in calculation, are

$x(m)$	$x(-2)$	$x(-1)$	$x(0)$	$x(1)$	
$x(-m)$		$x(1)$	$x(0)$	$x(-1)$	$x(-2)$

So, in forming the local auto-correlation function, there are several possibilities. One is to omit sample $x(-2)$ and to use an odd number of samples, in this case as well. Also, it is possible to periodically extend the signal and to form the product based on

$x(m)$	\dots	$x(1)$	$x(-2)$	$x(-1)$	$x(0)$	$x(1)$	$x(-2)$	$x(-1)$	\dots
$x(-m)$	\dots	$x(-1)$	$x(-2)$	$x(1)$	$x(0)$	$x(-1)$	$x(-2)$	$x(1)$	\dots
$w_e(m)$	\dots	0	0	$w_e(1)$	$w_e(0)$	$w_e(1)$	0	0	\dots

Here we can use four product terms, but with the first one formed as $x(-2)x^*(-2)$, that is, as $x(-N/2)x^*(-N/2)$. When a lag window with zero ending value is used (for example, a Hann(ing) window), this term does not make any influence to the result. The used lag window must also follow the symmetry, for example $w_e(m) = \cos^2(\pi m/N)$, when,

$$\begin{aligned} PWD\left(\frac{n\Delta t}{2}, \frac{2\pi k}{N\Delta t}\right) &\rightarrow PWD(n, k) \\ PWD(n, k) &= \sum_{m=-N/2}^{N/2-1} w_e(m) x(n+m) x^*(n-m) e^{-j2\pi mk/N} \\ &= \sum_{m=-N/2+1}^{N/2-1} w_e(m) x(n+m) x^*(n-m) e^{-j2\pi mk/N}, \end{aligned}$$

since $w_e(-N/2) = 0$. However, if the window is nonzero at the ending point $m = -N/2$, this term will result in a kind of aliased distribution.

In order to introduce another way of the discrete Wigner distribution calculation, with an even number of samples, consider again the continuous form of the Wigner distribution of a signal with a limited duration. Assume that the signal is sampled in such a way that the sampling theorem can be applied and the equality

sign used (Example 1.19). Then, the integral may be replaced by a sum

$$\begin{aligned}
 WD(t, \Omega) &= \sum_{m=-N}^N x(t + m\frac{\Delta t}{2})x^*(t - m\frac{\Delta t}{2})e^{-jm\Omega\Delta t}\Delta t \\
 &= \sum_{m=-N/2}^{N/2} x(t + 2m\frac{\Delta t}{2})x^*(t - 2m\frac{\Delta t}{2})e^{-j2m\Omega\Delta t}\Delta t \\
 &+ \sum_{m=-N/2}^{N/2-1} x(t + (2m+1)\frac{\Delta t}{2})x^*(t - (2m+1)\frac{\Delta t}{2})e^{-j(2m+1)\Omega\Delta t}\Delta t. \tag{3.86}
 \end{aligned}$$

The initial sum is split into its even and odd terms part. Now, let us assume that the signal is sampled in such a way that twice wider sampling interval Δt is also sufficient to obtain the Wigner distribution (by using every other signal sample). Then, for the first sum (with an odd number of samples) holds,

$$\sum_{m=-N/2}^{N/2} x(t + m\Delta t)x^*(t - m\Delta t)e^{-j2m\Omega\Delta t}\Delta t = \frac{1}{2}WD(t, \Omega).$$

The factor 1/2 comes from the sampling interval. Now, from (3.86) follows

$$\sum_{m=-N/2}^{N/2-1} x(t + (2m+1)\frac{\Delta t}{2})x^*(t - (2m+1)\frac{\Delta t}{2})e^{-j(2m+1)\Omega\Delta t}\Delta t = \frac{1}{2}WD(t, \Omega). \tag{3.87}$$

This is just the discrete Wigner distribution with an even number of samples. If we denote

$$\begin{aligned}
 x(t + (2m+1)\frac{\Delta t}{2}) &= x(t + m\Delta t + \frac{\Delta t}{2}) = x_e(t + m\Delta t) \\
 x(n\Delta t + m\Delta t + \frac{\Delta t}{2})\sqrt{2\Delta t} &= x_e(n+m)
 \end{aligned}$$

then

$$\begin{aligned}
 x(t - m\Delta t - \frac{\Delta t}{2}) &= x(t - m\Delta t + \frac{\Delta t}{2} - \Delta t) \\
 x(n\Delta t - m\Delta t + \frac{\Delta t}{2} - \Delta t)\sqrt{2\Delta t} &= x_e(n-m-1).
 \end{aligned}$$

The summation terms, for example for $n = 0$, are of the form

$x_e(m)$	\dots	$x_e(-2)$	$x_e(-1)$	$x_e(0)$	$x_e(1)$	\dots
$x_e(-m-1)$	\dots	$x_e(1)$	$x_e(0)$	$x_e(-1)$	$x_e(-2)$	\dots

They would produce a modulated version of the pseudo Wigner distribution, due to the shift of a half of the sampling interval. However, this shift can be corrected as (3.87)

$$WD(t, \Omega) = e^{-j\Omega\Delta t} \sum_{m=-N/2}^{N/2-1} x_e(t + m\Delta t)x_e^*(t - m\Delta t - \Delta t)e^{-j2m\Omega\Delta t}(2\Delta t)$$

for any t and Ω (having in mind the sampling theorem). Thus, we may also write

$$\begin{aligned} WD\left(n\Delta t, \frac{\pi k}{N\Delta t}\right) &\rightarrow WD(n, k) \\ WD(n, k) &= e^{-j\pi k/N} \sum_{m=-N/2}^{N/2-1} x_e(n+m)x_e^*(n-m-1)e^{-j2\pi mk/N}. \end{aligned} \quad (3.88)$$

In MATLAB notation, relation (3.4.3) can be implemented, as follows. The signal values are $\mathbf{x}_n^+ = [x_e(n-N/2), x_e(n-N/2+1), \dots, x_e(n+N/2-1)]$, $\mathbf{x}_n^- = [x_e^*(n+N/2-1), x_e^*(n+N/2-2), \dots, x_e^*(n-N/2)]$. The vector of Wigner distribution values, for a given n and k , is $WD(n, k) = e^{-j\pi k/N} \left\{ \mathbf{x}_n^+ * (\mathbf{x}_n^- .* e^{-j\pi k\mathbf{m}/N})^T \right\}$, where $e^{-j\pi k\mathbf{m}/N}$ is the vector with elements $e^{-j\pi km/N}$, for $-N/2 \leq m \leq N/2-1$, $*$ is the matrix multiplication and $.*$ denotes the vector multiplication term by term.

Thus, in the case of an even number of samples, the discrete Wigner distribution of a signal $x_e(n)$, calculated according to (3.4.3), corresponds to the original signal $x(t)$ related to $x_e(n)$ as $x_e(n) \leftrightarrow x(n\Delta t + \Delta t/2)\sqrt{2\Delta t}$. To check this statement, consider the time marginal property of this distribution. It is

$$\begin{aligned} \frac{1}{N} \sum_{k=-N/2}^{N/2-1} WD(n, k) &= \sum_{m=-N/2}^{N/2-1} \left(x_e(n+m)x_e^*(n-m-1) \frac{1}{N} \sum_{k=-N/2}^{N/2-1} e^{-j(2m+1)\pi k/N} \right) \\ &= \sum_{m=-N/2}^{N/2-1} \left(x_e(n+m)x_e^*(n-m-1) \frac{1}{N} e^{j(2m+1)\pi/2} \frac{1 - e^{-j(2m+1)\pi}}{1 - e^{-j(2m+1)\pi/N}} \right) \\ &= \sum_{m=-N/2}^{N/2-1} (x_e(n+m)x_e^*(n-m-1)\delta(2m+1)) = \left| x_e(n - \frac{1}{2}) \right|^2 = |x(n\Delta t)|^2 (2\Delta t), \end{aligned}$$

for $|2m+1| < N$.

Since for any signal $y(n)$ and its DFT holds $DFT_{N/2}\{y(n) + y(n+N/2)\} = Y(2k)$, where $Y(k) = DFT_N\{y(n)\}$, the pseudo Wigner distribution (3.4.3), without

frequency oversampling, in the case of an even N , can be calculated as

$$WD\left(n\Delta t, \frac{2\pi k}{N\Delta t}\right) \rightarrow WD(n, k)$$

$$WD(n, k) = e^{-j\pi k/(N/2)} \sum_{m=-N/4}^{N/4-1} (R(n, m) + R(n, m + N/2)) e^{-j2\pi mk/(N/2)}$$

where $R(n, m) = x_e(n+m)x_e^*(n-m-1)$. Periodicity in m , for a given n , with period N is assumed in $R(n, m)$, that is, $R(n, m+N) = R(n, m) = R(n, m-N)$. It is needed to calculate $R(n, m+N/2)$ for $-N/4 \leq m \leq N/4 - 1$ using $R(n, m)$ for $-N/2 \leq m \leq N/2 - 1$ only.

In the case of real-valued signals, in order to avoid the need for oversampling, as well as to eliminate cross-terms (that will be discussed later) between positive and negative frequency components, their analytic part is used in calculations. The analytic part of signal is defined in Chapter 1, (1.46).

Some of the Discrete Wigner distribution Forms: The discrete Wigner distribution has attracted significant research interest, since there is obviously no unique simple way to express it (Claasen, Mecklenbräuker, Boashash, Nuttal, Peyrin, Prost, O'Neill, Richman, Flandrin, Williams, Richard, Amin, Bouderax-Bartels, Matz, Hlawatsch,...). In addition, some of the desirable properties of the continuous-time Wigner distribution, are lost in the discrete formulation. Here, we will list some of the discrete Wigner distribution forms. For a signal $x(n)$ of finite duration $-N/2 \leq n \leq N/2$, the basic standard form, that will be repeated here, is

$$WD\left(\frac{n\Delta t}{2}, \frac{2\pi k}{(N+1)\Delta t}\right) \rightarrow WD(n, k)$$

$$WD(n, k) = \sum_{m=-M(n)}^{M(n)} x(n+m)x^*(n-m)e^{-j2\pi mk/(N+1)}.$$

It is oversampled in time and in frequency. The summation limits $M(n)$ are defined by the smallest value of m when one of the following inequalities is not satisfied,

$$\begin{aligned} -N/2 &\leq n+m \leq N/2 \\ -N/2 &\leq n-m \leq N/2, \end{aligned}$$

for odd $N+1$, (i.e., integer $N/2$). The same form can be used for even total number of samples if we restrict the summation to the symmetric interval $-M(n) \leq m \leq M(n)$, for available signal values.

Peyrin and Prost have defined the pseudo Wigner distribution in the form

$$WD(n, k) = \sum_{m=0}^{N-1} x(m)x^*(n-m)e^{-j2\pi k(m-n/2)/N}.$$

It could be related to the continuous-time Wigner distribution form that follows, with $t/2 + \tau/2 = \lambda$, as

$$\begin{aligned} WD\left(\frac{t}{2}, \frac{\Omega}{2}\right) &= 2 \int_{-\infty}^{\infty} x(\lambda)x^*\left(\frac{t}{2} - (\lambda - \frac{t}{2})\right)e^{-j\Omega(2\lambda-t)/2}d\lambda \\ &= 2 \int_{-\infty}^{\infty} x(\lambda)x^*(t-\lambda)e^{-j\Omega(\lambda-t/2)}d\lambda, \end{aligned}$$

sampled in t with $n\Delta t$ and in Ω with $2\pi k/(N\Delta t)$.

The idea of duplicating the signal samples, instead of oversampling, introduced by Claassen and Mecklenbräuker

$$\begin{aligned} WD\left(n\Delta t, \frac{2\pi k}{2N\Delta t}\right) &\rightarrow WD(n, k) \\ WD(n, k) &= \sum_{m=-M(n)}^{M(n)} x(n + \left\lfloor \frac{m}{2} \right\rfloor)x^*(n - \left\lceil \frac{m}{2} \right\rceil)e^{-j2\pi mk/(2N)} \end{aligned}$$

was recently used to in relation to the unitarity property. Symbol $\lfloor m/2 \rfloor$ is used to denote the greatest integer less than or equal to $m/2$, while $\lceil \frac{m}{2} \rceil$ stands for the smallest integer larger than or equal to $m/2$. The limit $M(n)$ follows from $-N \leq n + \lfloor \frac{m}{2} \rfloor \leq N - 1$ and $-N \leq n - \lceil \frac{m}{2} \rceil \leq N - 1$.

All previous discrete Wigner distribution forms can be rewritten in the frequency domain, using a Fourier transform of the signal $X(k) = \text{DFT}\{x(n)\}$ within $-N \leq k \leq N - 1$. For example, a form oversampled in time and frequency, could be written as

$$\begin{aligned} WD(n, k) &= \frac{1}{2N} \sum_{i=-I(k)}^{I(k)} X(k+i)X^*(k-i)e^{-j2\pi in/(2N)} \\ &-N \leq n \leq N - 1, \quad -N \leq k \leq N - 1, \end{aligned}$$

where $I(k)$ is defined by $-N \leq i+k \leq N - 1$ and $N \leq k-i \leq N - 1$.

3.4.4 Wigner Distribution-Based Inversion and Synthesis

In order to define an efficient algorithm for the synthesis of a signal with specified time-frequency distribution, we will restate the Wigner distribution inversion within the eigenvalue and eigenvectors decomposition framework. A discrete form of the Wigner distribution (3.85) is defined by

$$WD(n, k) = \sum_{m=-N/2}^{N/2} x(n+m)x^*(n-m)e^{-j\frac{2\pi}{N+1}mk}, \quad (3.89)$$

where we assume that the signal $x(n)$ is time limited within $|n| \leq N/2$. The inversion relation for the Wigner distribution reads as

$$x(n+m)x^*(n-m) = \frac{1}{N+1} \sum_{k=-N/2}^{N/2} WD(n, k)e^{j\frac{2\pi}{N+1}mk}.$$

After substitutions $n_1 = n+m$ and $n_2 = n-m$, we get

$$x(n_1)x^*(n_2) = \frac{1}{N+1} \sum_{k=-N/2}^{N/2} WD\left(\frac{n_1+n_2}{2}, k\right) e^{j\frac{\pi}{N+1}k(n_1-n_2)}. \quad (3.90)$$

For cases when $(n_1+n_2)/2$ is not an integer, an appropriate interpolation is performed in order to calculate $WD((n_1+n_2)/2, k)$.

Note that relation (3.90) is a discrete counterpart of the Wigner distribution inversion in analog domain, that reads

$$x(t_1)x^*(t_2) = \frac{1}{2\pi} \int_{-\infty}^{\infty} WD\left(\frac{t_1+t_2}{2}, \Omega\right) e^{j\Omega(t_1-t_2)} d\Omega.$$

By discretizing angular frequency $\Omega = k\Delta\Omega$ and time $t_1 = n_1\Delta t$, $t_2 = n_2\Delta t$, with appropriate definition of discrete values, we easily obtain (3.90).

Introducing the notation,

$$R(n_1, n_2) = \frac{1}{N+1} \sum_{k=-N/2}^{N/2} WD\left(\frac{n_1+n_2}{2}, k\right) e^{j\frac{\pi}{N+1}k(n_1-n_2)}, \quad (3.91)$$

we get

$$R(n_1, n_2) = x(n_1)x^*(n_2). \quad (3.92)$$

Matrix form of (3.92) reads

$$\mathbf{R} = \mathbf{x}(n)\mathbf{x}^*(n), \quad (3.93)$$

where $\mathbf{x}(n)$ is a column vector whose elements are the signal values, $\mathbf{x}^*(n)$ is a row vector (Hermitian transpose of $\mathbf{x}(n)$), and \mathbf{R} is a matrix with the elements $R(n_1, n_2)$, defined by (3.91).

As for any square matrix, the eigenvalue decomposition of \mathbf{R} reads

$$\mathbf{R} = \mathbf{Q}\Lambda\mathbf{Q}^T = \sum_{i=1}^{N+1} \lambda_i \mathbf{q}_i(n) \mathbf{q}_i^*(n), \quad (3.94)$$

where λ_i are eigenvalues and $\mathbf{q}_i(n)$ are eigenvectors of \mathbf{R} . By comparing (3.93) and (3.94), it follows that the matrix with elements of form (3.91) can be decomposed by using only one nonzero eigenvalue. Note that the energy of the corresponding eigenvector is equal to 1, by definition

$$\|\mathbf{q}_1(n)\|^2 = 1. \quad (3.95)$$

By comparing (3.93) and (3.94), having in mind that there is only one nonzero eigenvalue, we have

$$\mathbf{x}(n)\mathbf{x}^*(n) = \lambda_1 \mathbf{q}_1(n) \mathbf{q}_1^*(n) = \left(\sqrt{\lambda_1} \mathbf{q}_1(n) \right) \left(\sqrt{\lambda_1} \mathbf{q}_1(n) \right)^*$$

and

$$\lambda_1 = \left\| \sqrt{\lambda_1} \mathbf{q}_1(n) \right\|^2 = \|\mathbf{x}(n)\|^2 = \sum_{n=-N/2}^{N/2} x^2(n) = E_x,$$

resulting in

$$\lambda_i = E_x \delta(i - 1), \quad (3.96)$$

where $\delta(i)$ denotes the Kronecker symbol. The eigenvector $\mathbf{q}_1(n)$ is equal to the signal vector $\mathbf{x}(n)$, up to the constant amplitude and phase factor. Therefore, an eigenvalue decomposition of the matrix, formed according to (3.91), can be used to check if an arbitrary two-dimensional function $D(n, k)$ is a valid Wigner distribution.

These relations can be used in signal synthesis. Assume that we have a given function $D(n, k)$, calculate (3.91) and perform eigenvalue decomposition (3.94). If

the given function is the Wigner distribution of a signal, it will result in one nonzero eigenvalue and corresponding eigenvector.

If that is not the case then the first (largest) eigenvalue and the corresponding eigenvector produce a signal such that its Wigner distribution will be the closest possible Wigner distribution (in the LMS sense) to the given arbitrary function $D(n, k)$. This conclusion follows from the eigenvalue/eigenvectors decomposition properties. As an example, a desired time-frequency distribution is defined as a function having unity values in a time-frequency region shown in Fig. 3.8(a). Its decomposition is performed and the Wigner distribution of the largest eigenvector is shown in Fig. 3.8(b), as its best approximation. We see that the difference in shape is significant, as we expected, since the Wigner distributions are two-dimensional functions of quite specific form.

3.4.5 Auto-Terms and Cross-Terms

A drawback of the Wigner distribution is the presence of cross-terms when the multicomponent signals are analyzed. For a multicomponent signal

$$x(t) = \sum_{m=1}^M x_m(t) \quad (3.97)$$

the Wigner distribution has the form

$$WD(t, \Omega) = \sum_{m=1}^M \sum_{n=1}^M \int_{-\infty}^{\infty} x_m\left(t + \frac{\tau}{2}\right) x_n^*\left(t - \frac{\tau}{2}\right) e^{-j\Omega\tau} d\tau. \quad (3.98)$$

Besides the auto-terms

$$WD_{at}(t, \Omega) = \sum_{m=1}^M \int_{-\infty}^{\infty} x_m\left(t + \frac{\tau}{2}\right) x_m^*\left(t - \frac{\tau}{2}\right) e^{-j\Omega\tau} d\tau$$

the Wigner distribution contains a significant number of cross-terms,

$$WD_{ct}(t, \Omega) = \sum_{m=1}^M \sum_{\substack{n=1 \\ n \neq m}}^M \int_{-\infty}^{\infty} x_m\left(t + \frac{\tau}{2}\right) x_n^*\left(t - \frac{\tau}{2}\right) e^{-j\Omega\tau} d\tau. \quad (3.99)$$

Usually, they are not desirable in the time-frequency signal analysis. Cross-terms can mask the presence of auto-terms, which makes the Wigner distribution unsuitable for the time-frequency analysis of signals.

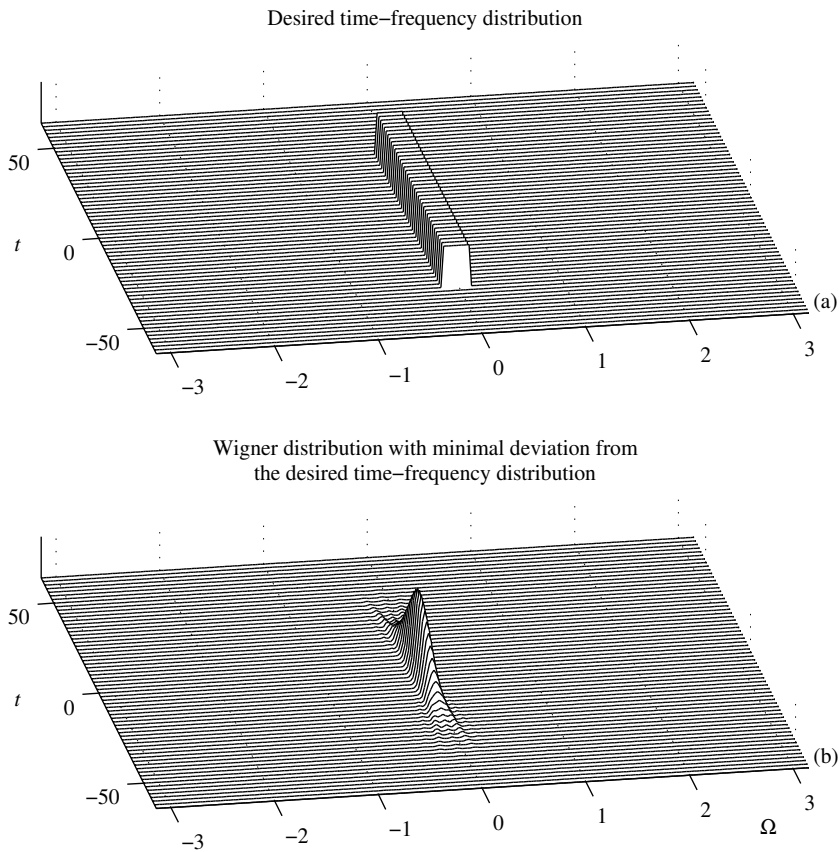


Figure 3.8 (a) A desired time-frequency distribution (TFD), defined as a function having unity values in a time-frequency region. (b) The Wigner distribution of the largest eigenvector, after desired time-frequency distribution is decomposed, as its best Wigner distribution approximation.

Here we will not go deeper into the discussion about the very definition of a multicomponent signal. We will assume that a signal is multicomponent, with M components, if there are M clearly separate time-frequency regions corresponding to M components, including their possible intersection in some points of the time-frequency plane.

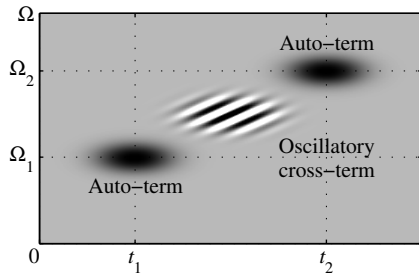


Figure 3.9 The Wigner distribution of a two-component signal.

Example 3.13. Analyze auto-terms and cross-terms for two-component signal of the form

$$x(t) = e^{-\frac{1}{2}(t-t_1)^2}e^{j\Omega_1 t} + e^{-\frac{1}{2}(t+t_1)^2}e^{-j\Omega_1 t}$$

★ In this case we have

$$\begin{aligned} WD(t, \Omega) = & 2\sqrt{\pi}e^{-(t-t_1)^2 - (\Omega-\Omega_1)^2} + 2\sqrt{\pi}e^{-(t+t_1)^2 - (\Omega+\Omega_1)^2} \\ & + 4\sqrt{\pi}e^{-t^2 - \Omega^2} \cos(2t_1\Omega - 2\Omega_1 t) \end{aligned}$$

where the first and second terms represent auto-terms while the third term is a cross-term. Note that the cross-term is oscillatory in both directions. The oscillation rate along the time axis is proportional to the frequency distance between components $2\Omega_1$, while the oscillation rate along frequency axis is proportional to the distance in time of components, $2t_1$. The oscillatory nature of cross-terms will be used for their suppression. □

For a two-component signal with auto-terms located around (t_1, Ω_1) and (t_2, Ω_2) the oscillatory cross-term is located at $((t_1+t_2)/2, (\Omega_1+\Omega_2)/2)$ (see Fig. 3.9 with depicted frequencies of oscillations along the specific directions). The auto-term and cross-term behavior will be additionally studied within the ambiguity function.

3.4.6 Inner Interferences in the Wigner Distribution

Another serious drawback of the Wigner distribution is in the presence of inner interferences for nonlinear frequency-modulated signals. In addition to the cross-terms between two separate components, a kind of inner cross-terms within a

component appear if the instantaneous frequency variations are nonlinear. Let us consider a one-component signal $x(t) = A \exp(j\phi(t))$ of constant amplitude. By using the Taylor series expansion, the Wigner distribution can be written as

$$\begin{aligned} WD(t, \Omega) &= \int_{-\infty}^{\infty} A^2 e^{j\phi(t+\tau/2)} e^{-j\phi(t-\tau/2)} e^{-j\Omega\tau} d\tau \\ &= A^2 \int_{-\infty}^{\infty} \exp\left(j\phi'(t)\tau + 2j \sum_{k=1}^{\infty} \frac{\phi^{(2k+1)}(t)}{(2k+1)!} \left(\frac{\tau}{2}\right)^{2k+1} - j\Omega\tau\right) d\tau \\ &= 2\pi A^2 \delta(\Omega - \phi'(t)) *_{\Omega} \text{FT} \left\{ \exp\left(2j \sum_{k=1}^{\infty} \frac{\phi^{(2k+1)}(t)}{(2k+1)!} \left(\frac{\tau}{2}\right)^{2k+1}\right) \right\} \end{aligned}$$

where

$$\text{FT} \left\{ \exp\left(2j \sum_{k=1}^{\infty} \frac{\phi^{(2k+1)}(t)}{(2k+1)!} \left(\frac{\tau}{2}\right)^{2k+1}\right) \right\}$$

is the term introducing interferences within single component, that is, its deviation from an ideal representation $2\pi A^2 \delta(\Omega - \phi'(t))$. The exact form of this term can be obtained by using the stationary phase approximation. The pseudo Wigner distribution of a cubic phase signal is presented in Fig. 3.10. The inner interference terms are significant.

If these interferences (inner cross-terms) are not reduced, they can reduce the accuracy of the time-frequency representation of a signal.

3.5 AMBIGUITY FUNCTION

The well-known ambiguity function can be used for an efficient analysis and processing of the auto-terms and cross-terms. It is defined as

$$AF(\theta, \tau) = \int_{-\infty}^{\infty} x\left(t + \frac{\tau}{2}\right) x^*\left(t - \frac{\tau}{2}\right) e^{-j\theta t} dt. \quad (3.100)$$

It is already a classical tool in optics, as well as in radar and sonar signal analysis.

The ambiguity function and the Wigner distribution form a two-dimensional Fourier transform pair (two-dimensional Fourier transform here means the Fourier transform in t and the inverse Fourier transform in Ω)

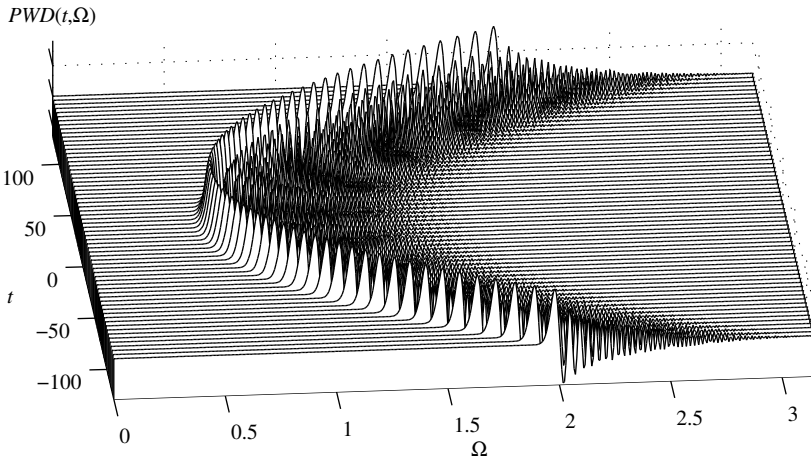


Figure 3.10 Inner interference in the pseudo Wigner distribution of a cubic phase signal.

$$\begin{aligned}
 AF(\theta, \tau) &= \text{FT}_{t, \Omega}^{2D}\{WD(t, \Omega)\} \\
 &= \frac{1}{2\pi} \int_{-\infty}^{\infty} \int_{-\infty}^{\infty} \left(\int_{-\infty}^{\infty} x\left(t + \frac{u}{2}\right) x^*\left(t - \frac{u}{2}\right) e^{-j\Omega u} du \right) e^{-j\theta t} e^{j\Omega \tau} d\Omega dt.
 \end{aligned}$$

Consider a signal

$$x(t) = \sum_{m=1}^M x_m(t)$$

whose components are limited in time to

$$x_m(t) \neq 0 \text{ only for } |t - t_m| < T_m.$$

In the ambiguity (θ, τ) domain, we have $x_m(t + \tau/2)x_m^*(t - \tau/2) \neq 0$ only for

$$-T_m < t - t_m + \frac{\tau}{2} < T_m \quad \text{and} \quad -T_m < t - t_m - \frac{\tau}{2} < T_m.$$

It means that auto-term $x_m(t + \tau/2)x_m^*(t - \tau/2)$ is located within

$$|\tau| < 2T_m,$$

that is, around the θ -axis independently of the signal's position t_m . The cross-term between signal's m th and n th component is located within

$$|\tau + t_n - t_m| < T_m + T_n. \quad (3.101)$$

It is dislocated from the θ -axis ($\tau = 0$) for two components that do not occur simultaneously, that is, when $t_m \neq t_n$. The cross-terms are centered around the difference of their locations $\tau_{mn} = t_m - t_n$. Thus, the cross-terms distance from the θ -axis is equal to the distance of terms to each other. Since the ambiguity domain is the two-dimensional domain for the Wigner distribution, with $\tau \leftrightarrow \Omega$, it also means that the cross-terms in the Wigner distribution are oscillatory in frequency direction Ω , with frequency of oscillations being proportional to the distance between terms.

From the frequency domain definition of the Wigner distribution, a corresponding ambiguity function form follows

$$AF(\theta, \tau) = \frac{1}{2\pi} \int_{-\infty}^{\infty} X\left(\Omega + \frac{\theta}{2}\right) X^*\left(\Omega - \frac{\theta}{2}\right) e^{j\Omega\tau} d\Omega. \quad (3.102)$$

From this form we can conclude that the auto-terms, limited in frequency to $X_m(\Omega) \neq 0$ to $|\Omega - \Omega_m| < W_m$, are located in the ambiguity domain around τ -axis within the region

$$|\theta| < 2W_m.$$

The cross-terms are within

$$|\theta + \Omega_n - \Omega_m| < W_m + W_n, \quad (3.103)$$

where Ω_m and Ω_n are the frequencies around which the Fourier transform of each component lies. Again, the cross-terms are oscillatory in the Wigner distribution, in time direction, with frequency of oscillations being proportional to the distance between corresponding terms.

Therefore, all auto-terms are located along and around the ambiguity domain axes. The cross-terms for the components which do not overlap in the time and frequency, simultaneously, are dislocated from the ambiguity axes (Fig. 3.11). This

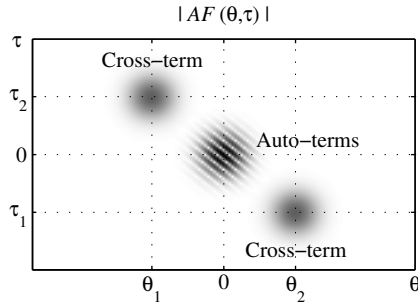


Figure 3.11 Auto-terms and cross-terms for a two-component signal in the ambiguity domain.

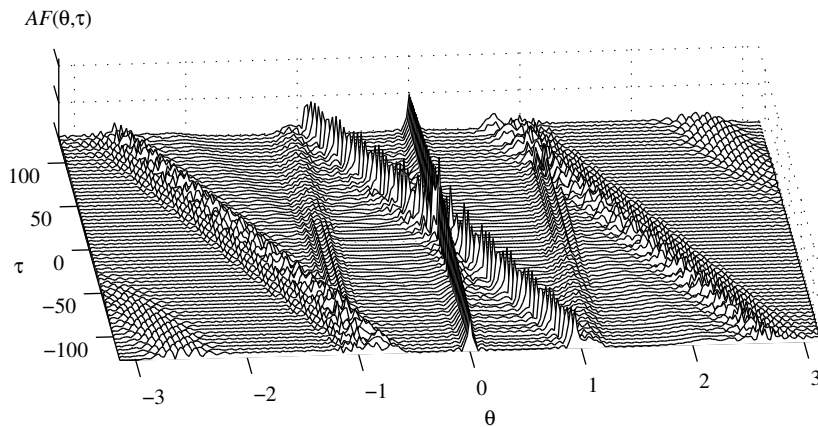


Figure 3.12 Ambiguity function of the signal from Figure 2.1.

property will be used in the definition of the reduced interference time-frequency distributions.

The ambiguity function of a four-component signal consisting of two Gaussian pulses, one sinusoidal and one LFM component is presented in Fig. 3.12.

Example 3.14. Let us consider signals of the form

$$\begin{aligned}x_1(t) &= e^{-\frac{1}{2}t^2} \\x_2(t) &= e^{-\frac{1}{2}(t-t_1)^2}e^{j\Omega_1 t} + e^{-\frac{1}{2}(t+t_1)^2}e^{-j\Omega_1 t}.\end{aligned}$$

★ The ambiguity function of $x_1(t)$ is

$$AF_{x_1}(\theta, \tau) = \sqrt{\pi}e^{-\frac{1}{4}\tau^2 - \frac{1}{4}\theta^2}$$

while the ambiguity function of two-component signal $x_2(t)$ is

$$\begin{aligned}AF_{x_2}(\theta, \tau) &= \sqrt{\pi}e^{-\frac{1}{4}\tau^2 - \frac{1}{4}\theta^2}e^{j\Omega_1 \tau}e^{-jt_1 \theta} + \sqrt{\pi}e^{-\frac{1}{4}\tau^2 - \frac{1}{4}\theta^2}e^{-j\Omega_1 \tau}e^{jt_1 \theta} \\&\quad + \sqrt{\pi}e^{-\frac{1}{4}(\tau-2t_1)^2 - \frac{1}{4}(\theta-2\Omega_1)^2} + \sqrt{\pi}e^{-\frac{1}{4}(\tau+2t_1)^2 - \frac{1}{4}(\theta+2\Omega_1)^2}.\end{aligned}$$

In the ambiguity domain (θ, τ) auto-terms are located around $(0, 0)$ while cross-terms are located around $(2\Omega_1, 2t_1)$ and $(-2\Omega_1, -2t_1)$. \square

Example 3.15. Find the joint moments of the Wigner distribution

$$\mu_{nm} = \frac{1}{2\pi} \int_{-\infty}^{\infty} \int_{-\infty}^{\infty} t^n \Omega^m WD(t, \Omega) dt d\Omega$$

in terms of the ambiguity function derivatives.

★ The relation between the Wigner distribution and the ambiguity function is

$$AF(\theta, \tau) = \frac{1}{2\pi} \int_{-\infty}^{\infty} \int_{-\infty}^{\infty} WD(t, \Omega) e^{-j\theta t} e^{j\Omega \tau} d\Omega dt$$

Taking partial derivatives n times over θ and m times over τ , we get

$$\frac{\partial^{n+m} A(\theta, \tau)}{\partial \theta^n \partial \tau^m} = \frac{1}{2\pi} \int_{-\infty}^{\infty} \int_{-\infty}^{\infty} (-jt)^n (j\Omega)^m WD(t, \Omega) e^{-j\theta t} e^{j\Omega \tau} d\Omega dt$$

The joint moments of the Wigner distribution are

$$\frac{1}{2\pi} \int_{-\infty}^{\infty} \int_{-\infty}^{\infty} t^n \Omega^m WD(t, \Omega) dt d\Omega = j^{n-m} \left. \frac{\partial^{n+m} A(\theta, \tau)}{\partial \theta^n \partial \tau^m} \right|_{\theta=0, \tau=0}. \quad (3.104)$$

For example, for $n = 1$ and $m = 1$ we have

$$\begin{aligned}\mu_{11} &= \frac{1}{2\pi} \int_{-\infty}^{\infty} \int_{-\infty}^{\infty} t\Omega WD(t, \Omega) dt d\Omega = \left. \frac{\partial^2 A(\theta, \tau)}{\partial \theta \partial \tau} \right|_{\theta=0, \tau=0} \\ &= \left. \frac{\partial^2}{\partial \theta \partial \tau} \int_{-\infty}^{\infty} x(t + \tau/2)x^*(t - \tau/2)e^{-j\theta t} dt \right|_{\theta=0, \tau=0} \\ &= \int_{-\infty}^{\infty} \frac{-jt}{2} (x'(t)x^*(t) - x(t)x^{*'}(t)) dt.\end{aligned}$$

For signal $x(t) = A(t)e^{j\phi(t)}$, we get

$$\begin{aligned}\mu_{11} &= \frac{1}{2\pi} \int_{-\infty}^{\infty} \int_{-\infty}^{\infty} t\Omega WD(t, \Omega) dt d\Omega \\ &= \int_{-\infty}^{\infty} t\phi'(t)A^2(t) dt.\end{aligned}\tag{3.105}$$

□

Example 3.16. Show that the second-order moment of the signal

$$x_L(t) = \left((x(t)e^{jct^2/2}) * \sqrt{|b|}e^{jbt^2/2} \right) e^{jat^2/2}$$

which produces a linear coordinate transformation for the Wigner distribution, may be calculated based on the signal's and the Fourier transform's second-order moments and the joint first-order moment.

★ For signal $x_L(t)$, the Wigner distribution is obtained by linear coordinate transformation of the Wigner distribution of a signal $x(t)$,

$$WD_{x_L}(t, \Omega) = WD_x(u, v) = WD_x(At + B\Omega, Ct + D\Omega),\tag{3.106}$$

The coordinate transformation matrix has the form

$$\begin{bmatrix} u \\ v \end{bmatrix} = \begin{bmatrix} 1+a/b & -1/b \\ -c-a(c/b+1) & c/b+1 \end{bmatrix} \begin{bmatrix} t \\ \Omega \end{bmatrix},$$

with A, B, C , and D being related to a, b, c by the expressions in the transformation matrix.

The second-order moment of $x_L(t)$ is

$$\begin{aligned} m_2(a, b, c) &= \frac{1}{2\pi} \int_{-\infty}^{\infty} \int_{-\infty}^{\infty} t^2 W D_{x_L}(t, \Omega) dt d\Omega \\ &= \frac{1}{2\pi} \int_{-\infty}^{\infty} \int_{-\infty}^{\infty} t^2 W D_x(At + B\Omega, Ct + D\Omega) dt d\Omega. \end{aligned}$$

With a change of variables $At + B\Omega = u$ and $Ct + D\Omega = v$, $t = Du - Bv$, having in mind that the transformation is unitary, $(AD - BC) = 1$,

$$\begin{aligned} m_2(a, b, c) &= \frac{1}{2\pi} \int_{-\infty}^{\infty} \int_{-\infty}^{\infty} (D^2 u^2 - 2BDuv + B^2 v^2) W D_x(u, v) du dv \\ &= D^2 \int_{-\infty}^{\infty} t^2 |x(t)|^2 dt - 2BD\mu_{11} + B^2 \frac{1}{2\pi} \int_{-\infty}^{\infty} \Omega^2 |X(\Omega)|^2 d\Omega \\ &= D^2 m_2 - 2BD\mu_{11} + B^2 M_2, \end{aligned} \quad (3.107)$$

where M_2 could be calculated as $M_2 = \int_{-\infty}^{\infty} |x'(t)|^2 dt$ and a simple expression for μ_{11} is derived in the previous example. This relation is useful for multiparameter optimization in order to find time-frequency representation (with distribution coordinate transformation) that would produce the best concentrated signal, with minimal moment $m_2(a, b, c)$. A similar relation was obtained in the local polynomial Fourier transform analysis. A special case that reduces to the time-frequency plane rotation with $-1/b = \sin(\alpha) = 1/\csc(\alpha)$ and $a = c = -\tan(\alpha/2)$ is used in practice by fractional Fourier transforms, when $D = \cos(\alpha)$ and $B = \sin(\alpha)$. \square

3.6 COHEN CLASS OF DISTRIBUTIONS

Time and frequency marginal properties (3.2) and (3.3) may be considered as the projections of a time-frequency distribution $P(t, \Omega)$ along the time and frequency axes, that is, as the Radon transform of $P(t, \Omega)$ along these two directions. It is known that the Fourier transform of the projection of a two-dimensional function on a given line is equal to the value of the two-dimensional Fourier transform of $P(t, \Omega)$, denoted by $A_P(\theta, \tau)$, along the same direction (inverse Radon transform property). Therefore, if $P(t, \Omega)$ satisfies marginal properties, then any other function having a two-dimensional Fourier transform equals to $A_P(\theta, \tau)$, along the axes lines

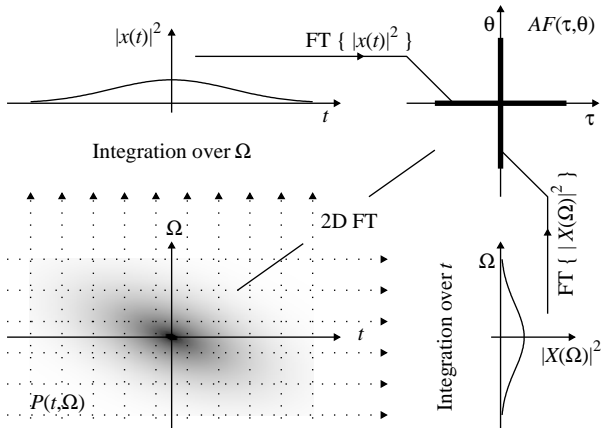


Figure 3.13 Marginal properties and their relation to the ambiguity function.

$\theta = 0$ and $\tau = 0$, and arbitrary values elsewhere, will satisfy the marginal properties (Fig. 3.13).

Assuming that the Wigner distribution is a basic distribution (i.e., $P(t, \Omega) = WD(t, \Omega)$ and $A_P(\theta, \tau) = AF(\theta, \tau)$) that satisfies the marginal properties (any other distribution satisfying the marginals can be used as the basic one), then any other distribution with two-dimensional Fourier transform

$$AF_g(\theta, \tau) = c(\theta, \tau) \text{FT}_{t, \Omega}^{2D}\{WD(t, \Omega)\} = c(\theta, \tau)AF(\theta, \tau) \quad (3.108)$$

where $c(0, \tau) = c(\theta, 0) = 1$, satisfies marginal properties as well.

The inverse two-dimensional Fourier transform (in the sense defined within the ambiguity function analysis) of the generalized ambiguity function $AF_g(\theta, \tau)$

$$CD(t, \Omega) = \frac{1}{2\pi} \int_{-\infty}^{\infty} \int_{-\infty}^{\infty} AF_g(\theta, \tau) e^{j\theta t} e^{-j\Omega \tau} d\tau d\theta \quad (3.109)$$

produces the Cohen class of distributions, introduced from quantum mechanics into the time-frequency analysis by Claasen and Mecklenbäcker, in the form

$$CD(t, \Omega) = \frac{1}{2\pi} \int_{-\infty}^{\infty} \int_{-\infty}^{\infty} \int_{-\infty}^{\infty} c(\theta, \tau) x(u + \tau/2) x^*(u - \tau/2) e^{j\theta t - j\Omega\tau - j\theta u} du d\tau d\theta \quad (3.110)$$

where $c(\theta, \tau)$ is called the kernel of a time-frequency distribution.

Alternatively, the frequency domain definition of the Cohen class of distributions is

$$CD(t, \Omega) = \frac{1}{4\pi^2} \int_{-\infty}^{\infty} \int_{-\infty}^{\infty} \int_{-\infty}^{\infty} c(\theta, \tau) X(u - \theta/2) X^*(u + \theta/2) e^{j\theta t - j\Omega\tau + j\tau u} du d\tau d\theta. \quad (3.111)$$

Various distributions can be obtained by altering the kernel function $c(\theta, \tau)$. For example, $c(\theta, \tau) = 1$ produces the Wigner distribution, while for $c(\theta, \tau) = e^{-j\theta\tau/2}$ the Rihaczek distribution follows.

The Cohen class of distributions can be defined with kernel in different domains:

1. Kernel $c(\theta, \tau)$ in the ambiguity domain, (3.110) or

$$CD(t, \Omega) = \frac{1}{2\pi} \int_{-\infty}^{\infty} \int_{-\infty}^{\infty} c(\theta, \tau) AF(\theta, \tau) e^{j\theta t - j\Omega\tau} d\tau d\theta. \quad (3.112)$$

2. Kernel $c_T(t, \tau)$ in the time-lag domain

$$CD(t, \Omega) = \int_{-\infty}^{\infty} \int_{-\infty}^{\infty} c_T(t - u, \tau) x(u + \tau/2) x^*(u - \tau/2) e^{-j\Omega\tau} d\tau du. \quad (3.113)$$

This relation follows from (3.110) after the integration over θ is performed, with

$$c_T(t, \tau) = \frac{1}{2\pi} \int_{-\infty}^{\infty} c(\theta, \tau) e^{j\theta t} d\theta. \quad (3.114)$$

3. Kernel $C_\Omega(\theta, \Omega)$ in the Doppler-frequency domain

$$CD(t, \Omega) = \frac{1}{4\pi^2} \int_{-\infty}^{\infty} \int_{-\infty}^{\infty} C_\Omega(\theta, \Omega - u) X(u + \theta/2) X^*(u - \theta/2) e^{j\theta t} d\theta du \quad (3.115)$$

with

$$C_\Omega(\theta, \Omega) = \int_{-\infty}^{\infty} c(\theta, \tau) e^{-j\Omega\tau} d\tau. \quad (3.116)$$

Here we use the name Doppler for the variable θ . The reason is that the ambiguity function is a classical tool for analysis of radar signals, where this variable is proportional to the Doppler shift in frequency, due to the target movement.

4. Kernel $\Pi(t, \Omega)$ in the time-frequency domain

$$CD(t, \Omega) = \frac{1}{2\pi} \int_{-\infty}^{\infty} \int_{-\infty}^{\infty} \Pi(t-u, \Omega-v) WD(u, v) du dv. \quad (3.117)$$

This form follows from the fact that (3.112) is a two-dimensional Fourier transform of the product $c(\theta, \tau)$ and $AF(\theta, \tau)$. Thus, it is equal to a two-dimensional convolution of the two-dimensional Fourier transforms of $c(\theta, \tau)$ and $AF(\theta, \tau)$. Therefore,

$$\Pi(t, \Omega) = \frac{1}{2\pi} \int_{-\infty}^{\infty} \int_{-\infty}^{\infty} c(\theta, \tau) e^{j\theta t - j\Omega\tau} d\tau d\theta. \quad (3.118)$$

The Cohen class of distribution may be viewed as a Fourier transform of the generalized auto-correlation function

$$CD(t, \Omega) = \int_{-\infty}^{\infty} R_{CD}(t, \tau) e^{-j\Omega\tau} d\tau = FT\{R_{CD}(t, \tau)\} = FT\{c_T(t, \tau) *_t R(t, \tau)\}$$

since

$$\begin{aligned} R_{CD}(t, \tau) &= \frac{1}{2\pi} \int_{-\infty}^{\infty} \int_{-\infty}^{\infty} c(\theta, \tau) x(u + \tau/2) x^*(u - \tau/2) e^{j\theta t - j\theta u} du d\theta \\ &= \int_{-\infty}^{\infty} c_T(t-u, \tau) x(u + \tau/2) x^*(u - \tau/2) du = c_T(t, \tau) *_t R(t, \tau), \end{aligned}$$

where the local auto-correlation function $R(t, \tau) = x(t + \tau/2)x^*(t - \tau/2)$ is convolved in time with $c_T(t, \tau)$.

According to (3.117) all distributions from the Cohen class may be considered as two-dimensional filtered versions of the Wigner distribution. Although any

distribution could be taken as a basis for the Cohen class derivation, the form with the Wigner distribution is used because it is the best concentrated distribution from the Cohen class with the signal independent kernels. Note that the Cohen class of distributions is more general than the class of distributions, in the literature referred to as the smoothed Wigner distributions (3.77), since generally $\Pi(t, \Omega)$ is not a separable function. The name smoothed Wigner distribution is usually reserved for the separable kernels, $\Pi(t, \Omega) = G(t)W_e(\Omega)$.

3.6.1 Properties of the Cohen Class of Distributions

Desired properties of the time-frequency representations presented in the case of the Wigner distribution are satisfied for distribution from the Cohen class under the following kernel constraints:

- P₁ – Realness for $c(\theta, \tau) = c^*(-\theta, -\tau)$.
- P₂ – Time-shift property for any $c(\theta, \tau)$.
- P₃ – Frequency shift property for any $c(\theta, \tau)$.
- P₄ – Time marginal property for $c(\theta, 0) = 1$.
- P₅ – Frequency marginal property for $c(0, \tau) = 1$.
- P₆ – Time moments for $c(\theta, 0) = 1$.
- P₇ – Frequency moments for $c(0, \tau) = 1$.
- P₈ – Scaling for $c(\theta, \tau) = c(a\theta, \tau/a)$.
- P₉ – Instantaneous frequency for

$$c(\theta, 0) = 1 \text{ and } \left. \frac{\partial c(\theta, \tau)}{\partial \tau} \right|_{\tau=0} = 0.$$

- P₁₀ – Group delay for

$$c(0, \tau) = 1 \text{ and } \left. \frac{\partial c(\theta, \tau)}{\partial \theta} \right|_{\theta=0} = 0.$$

- P₁₁ – Time constraint is satisfied if $c_T(t, \tau) = 0$ for $|t/\tau| > 1/2$.
- P₁₂ – Frequency constraint is satisfied if $C_\Omega(\theta, \Omega) = 0$ for $|\Omega/\theta| > 1/2$.
- P₁₃ – Convolution for $c(\theta, \tau_1)c(\theta, \tau_2) = c(\theta, \tau_1 + \tau_2)$.
- P₁₄ – Product for $c(\theta_1, \tau)c(\theta_2, \tau) = c(\theta_1 + \theta_2, \tau)$.
- P₁₅ – Fourier transform for $c(\theta, \tau) = c(a\tau, -\theta/a)$.
- P₁₆ – Chirp convolution for $c(\theta, \tau) = c(\theta, \tau - \theta/a)$.
- P₁₇ – Chirp product for $c(\theta, \tau) = c(\theta + a\tau, \tau)$.
- P₁₈ – Moyal property for $|c(\theta, \tau)|^2 = 1$.

Some of the properties will be proven within the problems.

3.6.2 Reduced Interference Distributions

The analysis performed on ambiguity function and Cohen class of time-frequency distributions leads to the conclusion that the cross-terms may be suppressed or eliminated, if a kernel $c(\theta, \tau)$ is a function of a two-dimensional lowpass type. In order to preserve the marginal properties, its values along the axis should be

$$c(\theta, 0) = c(0, \tau) = 1. \quad (3.119)$$

Choi and Williams exploited one of the possibilities defining the distribution with the kernel of the form

$$c(\theta, \tau) = e^{-\theta^2 \tau^2 / \sigma^2}. \quad (3.120)$$

The parameter σ controls the slope of the kernel function which affects the influence of cross-terms. Small σ causes the elimination of cross-terms, but it should not be too small because, for the finite width of the auto-terms around θ and τ coordinates, the kernel will cause their distortion, as well. Thus, there should be a trade-off in the selection of σ .

Here we will mention some other interesting kernel functions, producing corresponding distributions (Fig. 3.14):

Born-Jordan distribution

$$c(\theta, \tau) = \frac{\sin(\frac{\theta\tau}{2})}{\frac{\theta\tau}{2}}, \quad (3.121)$$

Sinc distribution

$$c(\theta, \tau) = b(\frac{\theta\tau}{\alpha}) = \begin{cases} 1 & \text{for } |\theta\tau/\alpha| < 1/2 \\ 0 & \text{otherwise} \end{cases}, \quad (3.122)$$

Zao-Atlas-Marks distribution

$$c(\theta, \tau) = w(\tau) |\tau| \frac{\sin(\frac{\theta\tau}{2})}{\frac{\theta\tau}{2}},$$

Butterworth distribution

$$c(\theta, \tau) = \frac{1}{1 + \left(\frac{\theta\tau}{\theta_c \tau_c}\right)^{2N}}, \quad (3.123)$$

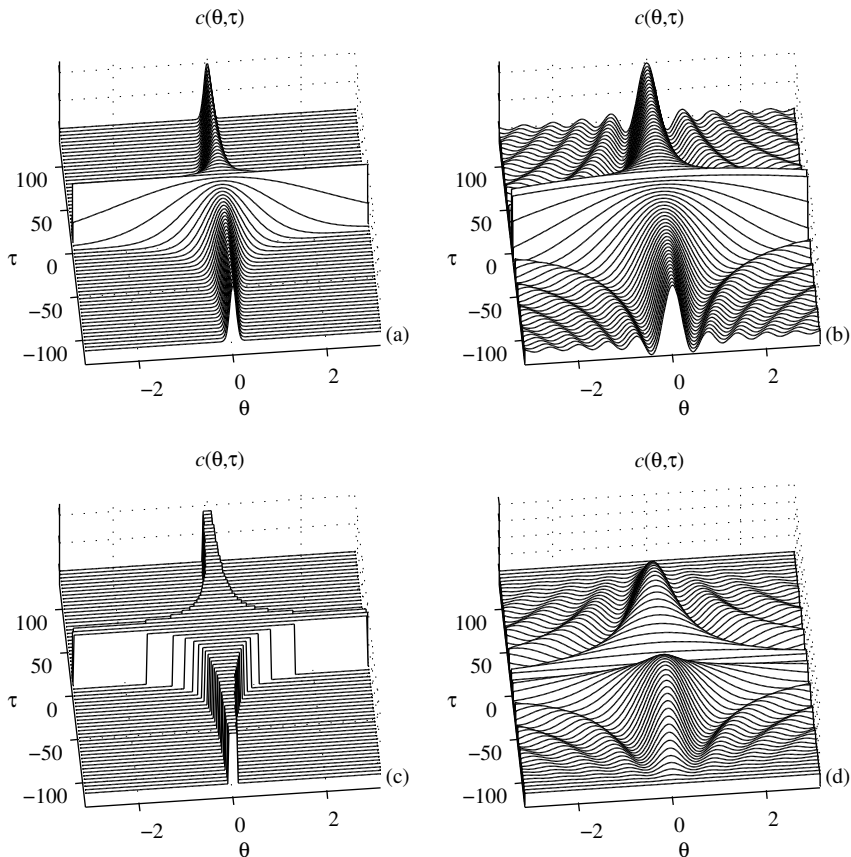


Figure 3.14 Kernel functions for: (a) the Choi-Williams distribution, (b) the Born-Jordan distribution, (c) the sinc distribution, and (d) the Zao-Atlas-Marks distribution.

where $w(\tau)$ is a function corresponding to a lag window and α , N , θ_c , and τ_c are constants in the above kernel definitions. The Zao-Atlas-Marks distribution is an example of a distribution which does not satisfy marginal properties.

Numerous other forms of the kernel function, for reduced interference distributions, have been defined in literature. Spectrogram belongs to this class of distributions. As will be shown later, its kernel in the (θ, τ) domain is the ambiguity function of the window

$$c(\theta, \tau) = \int_{-\infty}^{\infty} w(t + \tau/2)w(t - \tau/2)e^{-j\theta t} dt. \quad (3.124)$$

The kernel of the spectrogram in (t, Ω) domain is the Wigner distribution of the window function.

For the discrete-time signals, there are several ways to calculate a reduced interference distributions from the Cohen class, based on (3.112), (3.113), (3.115), or (3.117).

The kernel functions are usually defined in the Doppler-lag domain (θ, τ) . Thus, here we should use (3.112) with the ambiguity function of a discrete-time signal

$$AF(\theta, m\Delta t) = \sum_{p=-\infty}^{\infty} x\left(p\Delta t + m\frac{\Delta t}{2}\right)x^*\left(p\Delta t - m\frac{\Delta t}{2}\right)e^{-jp\theta\Delta t}\Delta t.$$

The signal should be sampled as in the Wigner distribution case. For a given lag instant m , the ambiguity function can be calculated by using the standard DFT routines. Another way to calculate the ambiguity function is just to take the inverse two-dimensional transform of the Wigner distribution. Note that the corresponding transformation pairs are *time* \leftrightarrow *Doppler* and *lag* \leftrightarrow *frequency*, that is, $t \leftrightarrow \theta$ and $\tau \leftrightarrow \Omega$. The relation between discretization values in the Fourier transform pairs (considered interval, sampling interval in time Δt , number of samples N , sampling interval in frequency $\Delta\Omega = 2\pi/(N\Delta t)$) is discussed in Chapter 1.

The generalized ambiguity function is obtained as

$$\begin{aligned} AF_g(l\Delta\theta, m\Delta t) &= c(l\Delta\theta, m\Delta t)AF(l\Delta\theta, m\Delta t) \\ &= c(l\Delta\theta, m\Delta t)\sum_{p=-\infty}^{\infty} x\left(p\Delta t + m\frac{\Delta t}{2}\right)x^*\left(p\Delta t - m\frac{\Delta t}{2}\right)e^{-jl\Delta\theta p\Delta t}\Delta t, \end{aligned} \quad (3.125)$$

while a distribution, with kernel $c(\theta, \tau)$ is the two-dimensional inverse Fourier transform in the form

$$CD(n\Delta t, k\Delta\Omega) = \frac{1}{2\pi} \sum_{l=-\infty}^{\infty} \sum_{m=-\infty}^{\infty} AF_g(l\Delta\theta, m\Delta t)e^{-jkm\Delta t\Delta\Omega}e^{jnl\Delta\theta\Delta t}\Delta t\Delta\theta.$$

In this notation we can calculate

$$CD(n, k) = \text{IDFT}_{l,m}^{2D} \{ AF_g(l, m) \}$$

where the values of $AF_g(l, m)$ are calculated according to (3.125).

In the time-lag domain, the discrete-time form reads

$$\begin{aligned} CD(n\Delta t, k\Delta\Omega) = \\ \sum_{p=-\infty}^{\infty} \sum_{m=-\infty}^{\infty} c_T(n\Delta t - p\Delta t, m\Delta t) x\left(p\Delta t + m\frac{\Delta t}{2}\right) x^*\left(p\Delta t - m\frac{\Delta t}{2}\right) e^{-jkm\Delta t\Delta\Omega} \Delta t \Delta\Omega \end{aligned} \quad (3.126)$$

with

$$c_T(n\Delta t - p\Delta t, m\Delta t) = \frac{1}{2\pi} \sum_{l=-\infty}^{\infty} c(l\Delta\theta, m\Delta t) e^{jnl\Delta\theta\Delta t} e^{-jlp\Delta\theta\Delta t} \Delta\theta.$$

For the discrete-time signals, it is common to write and use the Cohen class of distributions in the form

$$CD(n, \omega) = \sum_{p=-\infty}^{\infty} \sum_{m=-\infty}^{\infty} c_T(n-p, m) x(p+m) x^*(p-m) e^{-j2m\omega}, \quad (3.127)$$

where

$$\begin{aligned} x(p+m)x^*(p-m) &= x\left((p+m)\frac{\Delta t}{2}\right) x^*\left((p-m)\frac{\Delta t}{2}\right) \Delta t \\ c_T(n-p, m) &= c_T\left((n-p)\frac{\Delta t}{2}, m\Delta t\right) \frac{\Delta t}{2} \\ CD(n, \omega) &\rightarrow CD\left(n\frac{\Delta t}{2}, \Omega\Delta t\right). \end{aligned}$$

Here we should mention that the presented kernel functions are of infinite duration along the coordinate axis in (θ, τ) thus, they should be limited in calculations. Their transforms exist in a generalized sense only. For example, the time-lag form of the Choi-Williams kernel is

$$c_T(t, \tau) = \sqrt{\sigma^2/(\tau^2\pi)} e^{-\sigma^2t^2/\tau^2}.$$

The reduced interference distribution may also be calculated by using (3.113) or (3.117) with appropriate kernel transformations defined by (3.114) and (3.118). All these methods assume signal oversampling in order to avoid aliasing effects. Fig. 3.15 presents the ambiguity function, the kernel of Choi-Williams distribution and the product of the ambiguity function and the kernel, from Fig. 3.15(a) to Fig. 3.15(c), respectively. Fig. 3.16(a) presents Choi-Williams distribution calculated according to the presented procedure. In order to reduce high side lobes of the rectangular window, the Choi-Williams distribution is also calculated with the Hann(ing) window in the kernel definition $c(\theta, \tau)w(\tau)$ and presented in Fig. 3.16(b). The pseudo Wigner distribution of the same signal with the Hann(ing) window is shown in Fig. 3.7(a). The cross-terms are located in the ambiguity domain away from the origin. Thus, by using a two-dimensional lowpass kernel, as the one in Fig. 3.15(b), the cross-terms are attenuated (but not eliminated). The Choi-Williams distribution contains reduced cross-terms. Note that the auto-terms along the ambiguity domain coordinate axes are not distorted. However, the kernel function has changed the auto-term of the linear frequency-modulated signal, causing modification of its form with respect to that in the Wigner distribution. The same results are presented for the Born-Jordan distribution (Fig. 3.15(d - f) and Fig. 3.16(c)).

3.6.3 Optimal Kernel Design

The optimal kernel form, introduced by Baraniuk and Jones, is based on the ambiguity function and the kernel form optimization in the ambiguity domain. For a given signal and its ambiguity function, the optimal kernel is obtained as a real, nonnegative solution of the following optimization problem

$$\max \int_{-\infty}^{\infty} \int_{-\infty}^{\infty} |A(\theta, \tau)c(\theta, \tau)|^2 d\theta d\tau \quad \text{subject to} \quad c(0, 0) = 1, \quad (3.128)$$

where $c(\theta, \tau)$ is a radially nonincreasing function, with the kernel energy constraint

$$\frac{1}{2\pi} \int_{-\infty}^{\infty} \int_{-\infty}^{\infty} |c(\theta, \tau)|^2 d\theta d\tau < \alpha, \quad \text{where} \quad \alpha > 0.$$

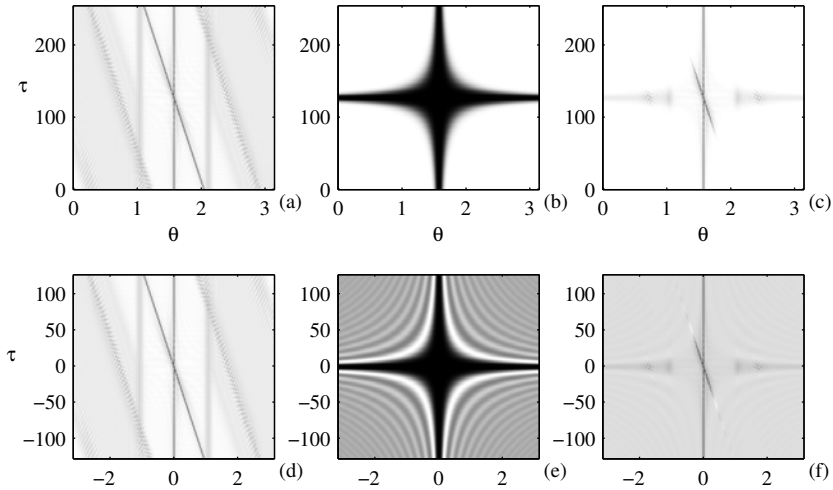


Figure 3.15 (a) Ambiguity function for the signal from Fig. 2.1(a), (b) the Choi-Williams kernel in the ambiguity domain, (c) product of the ambiguity function and the Choi-Williams kernel, (e) the Born-Jordan kernel in the ambiguity domain, (f) product of the ambiguity function and the Born-Jordan kernel.

In the derivation and the analysis these constraints were also expressed in the polar coordinate system with $\theta = \rho \cos \psi$ and $\tau = \rho \sin \psi$ as

$$\begin{aligned}
 & \max \int_0^\infty \int_0^{2\pi} |A(\rho, \psi) c(\rho, \psi)|^2 \rho d\rho d\psi \\
 & \text{subject to } c(0,0) = 1 \\
 & c(\rho_1, \psi) \leq c(\rho_2, \psi), \quad \text{for } \rho_1 \geq \rho_2 \\
 & \frac{1}{2\pi} \int_0^\infty \int_0^{2\pi} |c(\rho, \psi)|^2 \rho d\rho d\psi < \alpha, \quad \text{where } \alpha > 0. \tag{3.129}
 \end{aligned}$$

We can understand this optimization as the procedure to find the kernel that passes auto-terms and suppresses cross-terms. Since the auto-terms are centered about the ambiguity domain origin, while the cross-terms are dislocated from the origin, lowpass kernels are used. The constraints force the kernel to be a lowpass filter of fixed energy lower than α .

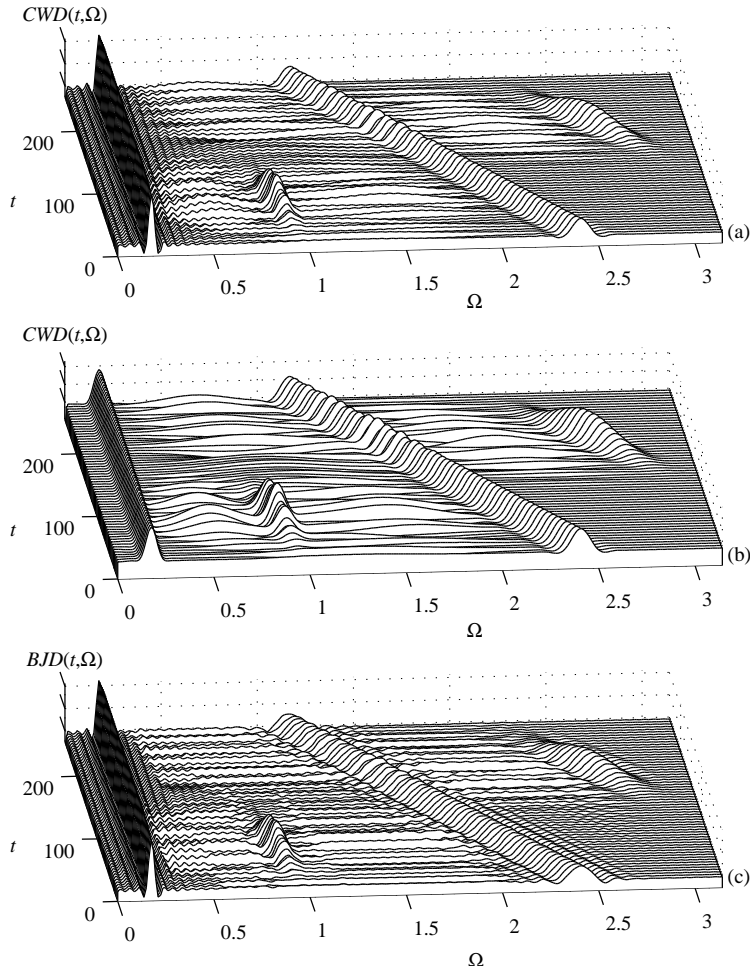


Figure 3.16 Time-frequency representation of the signal from Fig. 2.1(a). (a) The Choi-Williams distribution with a direct calculation. (b) Calculation of the Choi-Williams distribution with the kernel multiplied by a Hann(ing) lag window. (c) The Born-Jordan distribution.

These constraints are quite general and do not dictate the exact shape of the kernel. It is determined by maximizing the performance measure. Without the monotonicity constraint, the optimal kernel would be large, regardless of whether the peaks correspond to auto-terms or cross-terms. However, assuming that the auto-terms and cross-terms are separated in the ambiguity plane, the monotonicity constraint imposes a penalty on kernels whose passbands extend over cross-terms.

Note that the performance of this kernel design technique deteriorates for signals whose auto-terms and cross-terms considerably overlap in the ambiguity domain.

Other constraints that impose additional kernel properties (marginal properties, support properties) are considered in literature as well.

After the optimal kernel is obtained, as the result of the presented procedure, the signal's ambiguity function is multiplied by this kernel and the time-frequency distribution is calculated.

By controlling the volume under the optimal kernel, the parameter α controls the trade-off between cross-term suppression and smearing of the auto-terms. To minimize auto-terms distortion due to smearing, we must maximize the energy transferred by the optimal kernel. However, as α increases, a point of diminishing returns is reached: for large α , further increasing requires an exponential increase in kernel volume, making it more likely that significant cross-term energy will be passed into the optimal kernel and resulting distribution.

A specific kernel was proposed by Jones and Baraniuk for an efficient time-frequency analysis, known as optimal radially Gaussian kernel

$$c(\theta, \tau) = \exp(-(\theta^2 + \tau^2)/(2\sigma(\psi)))$$

with $\psi = \arctan(\tau/\theta)$ being a direction of the kernel, or in the polar coordinate system

$$c(\rho, \psi) = \exp((-\rho^2)/(2\sigma(\psi))). \quad (3.130)$$

The constraints are the same as for the general optimization procedure. An advantage of this formulation is that the constraints are insensitive to both the time scale and orientation of the signal in time-frequency. The radially Gaussian constraint favors kernels that pass components concentrated at the origin, which are the auto-terms.

By controlling the volume under the optimal kernel, the parameter α controls the trade-off between cross-term suppression and auto-terms smearing. If α is too small, then the kernel will induce excessive smearing of the auto-terms. If α is too large, then extra kernel volume will include cross-terms. While the kernel volume is

application-specific, the previous research has shown that $1 < \alpha < 5$ is reasonable bound for most applications.

The shape of a radially Gaussian kernel is completely parameterized by the spread function $\sigma(\psi)$. Algorithms for efficient minimization realization may be found in literature.

3.6.4 Auto-Term Form in the Cohen Class of Distributions

An ideally concentrated distribution of a signal $x(t) = Ae^{j\phi(t)}$, having the form $ITF(\Omega, t) = 2\pi A^2 \delta(\Omega - \phi'(t))$, may be easily translated into the general form (taking an inverse two-dimensional Fourier transform of $ITF(\Omega, t)$) as

$$ITF(\Omega, t) = \frac{A^2}{2\pi} \int_{-\infty}^{\infty} \int_{-\infty}^{\infty} \int_{-\infty}^{\infty} e^{j\phi'(u)\tau} e^{j\theta t - j\Omega\tau - j\theta u} du d\theta d\tau. \quad (3.131)$$

Comparing (3.131) with the Cohen class definition, while having in mind the uniqueness of the Fourier transform, we get that signal $x(t) = Ae^{j\phi(t)}$ has the distribution equal to the ideal one if

$$c(\theta, \tau) e^{j\phi(u+\tau/2) - j\phi(u-\tau/2)} = e^{j\phi'(u)\tau}.$$

From the last equation one may conclude that for any signal $x(t)$ there exists a signal-dependent kernel, such that the Cohen distribution is equal to the ideal one. With the assumption of a signal-independent kernel (which is of practical importance) we get that the ideal distribution may be obtained only if $\phi^{(3)}(u) \equiv 0$ (i.e., $c(\theta, \tau) \equiv 1$). The previous requirement ($\phi^{(3)}(u) \equiv 0$) is met only if the signal is linearly frequency modulated $x(t) = Ae^{j(at^2/2+bt)}$. The kernel $c(\theta, \tau) \equiv 1$ corresponds to the Wigner distribution. Any other distribution will have auto-terms that are more or less distorted when compared with the ideal representation.

Let us consider how other members of the Cohen distribution behave for $x(t) = Ae^{j(at^2/2+bt)}$

$$\begin{aligned} CD(\Omega, t) &= A^2 \int_{-\infty}^{\infty} c(a\tau, \tau) e^{j(at+b-\Omega)\tau} d\tau \\ &= A^2 C(\Omega - at - b) \end{aligned}$$

with

$$C(\Omega) = \text{FT}\{c(a\tau, \tau)\}. \quad (3.132)$$

The auto-term shape is determined by the function $C(\Omega)$ which will be referred to as the auto-term function. According to (3.132), one is able to derive the auto-term function for any distribution from the Cohen class. In addition, based on (3.132), one may construct a distribution with the desired auto-term shape, in the following way: If $C(\Omega)$ is a given auto-term function, for the linear frequency modulated signal with an instantaneous frequency rate a , then the product kernel, $c(\theta, \tau) = c(\theta\tau)$, which will produce this auto-term form, can be determined as

$$c(\theta\tau) = \frac{1}{2\pi} \int_{-\infty}^{\infty} C(\Omega) e^{j\Omega\tau} d\Omega \Big|_{a\tau^2 \rightarrow \theta\tau} \quad (3.133)$$

where a is the instantaneous frequency rate coefficient, $x(t) = Ae^{jat^2/2+bt}$.

Example 3.17. Let us determine the kernel function that will, for $a = 1$, produce the Hann(ing) auto-term function $C(\Omega) = \frac{k}{2}[1 + \cos(\Omega\pi)]$ for $|\Omega| < 1$ and $C(\Omega) = 0$ elsewhere (coefficient k will follow from the condition that $c(0, 0) = 1$).

★ According to (3.133) we get

$$c(\theta, \tau) = c(\theta\tau) = \frac{\pi^2 \sin(\sqrt{|\theta\tau|})}{\sqrt{|\theta\tau|}(\pi^2 - |\theta\tau|)}. \quad (3.134)$$

This kernel decreases in (θ, τ) plane as $1/|\theta\tau|^{3/2}$. Thus, kernel (3.134) will have better cross-term reduction than the ones decreasing as $1/(\theta\tau)$.

We have seen that the width of $c(\tau, \tau)$ (i.e., the width of $c(a\tau, \tau)$ for $a = 1$) should be as small as possible in order to have high cross-term suppression. However, at the same time, the width of auto-term function $C(\Omega) = \text{FT}\{c(\tau, \tau)\}$ should be small (i.e., $c(\tau, \tau)$ wide) in order to produce a concentrated and sharp distribution in the time-frequency plane. Product of the measures of widths of $c(\tau, \tau)$ (denoted by σ_τ) and its Fourier transform $C(\Omega)$ (denoted by σ_Ω) is constant for a given kernel. It satisfies the uncertainty principle relation $\sigma_\tau \sigma_\Omega \geq 1/2$. Thus, if one fixes the value of σ_Ω (the measure of the auto-term width), then the remaining value σ_τ (being the measure of cross-terms suppression) will be minimal if $\sigma_\tau \sigma_\Omega$ is minimal (i.e., equal to $1/2$). The same is valid if one fixes σ_τ . A kernel defined by $\sigma_\tau \sigma_\Omega = 1/2$ (optimal in the described way) is

$$c(\theta\tau) = e^{-|\theta\tau|/\sigma} \quad (3.135)$$

since its auto-term function is of the Gaussian form. □

3.7 KERNEL DECOMPOSITION-BASED CALCULATION

Distributions from the Cohen class can be calculated by using decomposition of the kernel function in the time-lag domain, introduced by Amin, Cunningham, and Williams. Since this decomposition is based on the spectrograms, we will first establish important relation of the spectrogram and a sum of spectrograms with the general form of quadratic distributions.

3.7.1 Spectrograms in the Cohen Class of Distributions

Distribution $CD(t, \Omega)$ from the Cohen class with kernel $c_T(t, \tau)$ in time-lag domain is defined as (3.113)

$$CD(t, \Omega) = \int_{-\infty}^{\infty} \int_{-\infty}^{\infty} c_T(t-u, \tau) x(u + \tau/2) x^*(u - \tau/2) e^{-j\Omega\tau} d\tau du$$

with substitutions $u + \tau/2 = t + v_1$ and $u - \tau/2 = t + v_2$ we get $t - u = -(v_1 + v_2)/2$ and $\tau = v_1 - v_2$, we get

$$CD(t, \Omega) = \int_{-\infty}^{\infty} \int_{-\infty}^{\infty} c_T \left(-\frac{v_1 + v_2}{2}, v_1 - v_2 \right) x(t + v_1) x^*(t + v_2) e^{-j\Omega(v_1 - v_2)} dv_1 dv_2. \quad (3.136)$$

Here it will be shown that the spectrogram belongs to Cohen class of distributions.

The spectrogram is defined by

$$SPEC(t, \Omega) = \left| \int_{-\infty}^{\infty} w(\tau) x(t + \tau) e^{-j\Omega\tau} d\tau \right|^2,$$

where $w(\tau)$ is the window function. The spectrogram can be written in the form

$$SPEC(t, \Omega) = \int_{-\infty}^{\infty} \int_{-\infty}^{\infty} w(v_1) w^*(v_2) x(t + v_1) x^*(t + v_2) e^{-j\Omega(v_1 - v_2)} dv_1 dv_2. \quad (3.137)$$

By comparing (3.136) and (3.137), the kernel of spectrogram in the time-lag domain is

$$c_T\left(-\frac{v_1 + v_2}{2}, v_1 - v_2\right) = w(v_1)w^*(v_2)$$

with $\frac{v_1 + v_2}{2} = t, v_2 - v_1 = \tau,$

$$c_T(-t, -\tau) = w\left(t - \frac{\tau}{2}\right)w^*\left(t + \frac{\tau}{2}\right)$$

for real-valued even window function (this condition is not needed if we used $w(-\tau)$ in the STFT definition)

$$c_T(t, \tau) = w\left(t - \frac{\tau}{2}\right)w\left(t + \frac{\tau}{2}\right). \quad (3.138)$$

Relation between kernels in the time-lag and the ambiguity domain is, (3.114),

$$c(\theta, \tau) = \int_{-\infty}^{\infty} c_T(t, \tau) e^{-j\theta t} dt,$$

resulting in the kernel of the spectrogram being equal to the ambiguity function of the window

$$c(\theta, \tau) = \int_{-\infty}^{\infty} w\left(t - \frac{\tau}{2}\right)w\left(t + \frac{\tau}{2}\right)e^{-j\theta t} dt = AF_w(\theta, \tau).$$

Example 3.18. A distribution is obtained as a weighted sum of two spectrograms

$$CD(t, \Omega) = a_1 SPEC_1(t, \Omega) + a_2 SPEC_2(t, \Omega) \quad (3.139)$$

with real-valued even windows $w_1(\tau)$ and $w_2(\tau)$. Find the kernel of this distribution.

★The kernel of a linear combination of distributions from the Cohen class is equal to the linear combination of the kernels thus, in the time-lag domain

$$c_T\left(-\frac{v_1 + v_2}{2}, v_1 - v_2\right) = a_1 w_1(v_1)w_1(v_2) + a_2 w_2(v_1)w_2(v_2)$$

or in the ambiguity domain

$$c(\theta, \tau) = a_1 AF_{w_1}(\theta, \tau) + a_2 AF_{w_2}(\theta, \tau).$$

□

In general, the kernel of

$$CD(t, \Omega) = \sum_{i=1}^M a_i SPEC_i(t, \Omega) \quad (3.140)$$

is

$$c_T \left(-\frac{v_1 + v_2}{2}, v_1 - v_2 \right) = \sum_{i=1}^M a_i w_i(v_1) w_i(v_2)$$

and

$$c(\theta, \tau) = \sum_{i=1}^M a_i AF_{w_i}(\theta, \tau). \quad (3.141)$$

If the constants a_i , $i = 1, 2, \dots, M$ are positive, then the general distribution is also positive, since the spectrograms are always nonnegative. It has been proven that the condition (3.141) is not only sufficient but also necessary for a distribution to be nonnegative. Interesting distributions of form (3.140) have been derived in theory allowing negative coefficients values.

3.7.2 The Cohen Class of Distributions Decomposition

The discrete-time version of the Cohen class of distributions (3.136) can be written, as

$$CD(n, \omega) = \sum_{n_1} \sum_{n_2} c_T \left(-\frac{n_1 + n_2}{2}, n_1 - n_2 \right) [x(n + n_1) e^{-j\omega n_1}] [x(n + n_2) e^{-j\omega n_2}]^*.$$

Assuming that \mathbf{C} is a square matrix of finite dimension, with elements

$$C(n_1, n_2) = c_T \left(-\frac{n_1 + n_2}{2}, n_1 - n_2 \right) \quad (3.142)$$

we can write

$$CD(n, \omega) = \mathbf{x}_n \mathbf{C} \mathbf{x}_n^*$$

where \mathbf{x}_n is a vector with elements $x(n + n_1) e^{-j\omega n_1}$. We can now perform the eigenvalue decomposition, finding solutions of

$$\det(\mathbf{C} - \lambda \mathbf{I}) = 0$$

and determining eigenvectors matrix \mathbf{Q} that satisfies

$$\mathbf{Q}\mathbf{Q}^* = \mathbf{I}$$

and

$$\mathbf{C} = \mathbf{Q}\Lambda\mathbf{Q}^*,$$

where Λ is a diagonal matrix containing the eigenvalues. It results in

$$CD(n, \omega) = (\mathbf{x}_n \mathbf{Q}) \Lambda (\mathbf{x}_n \mathbf{Q})^*. \quad (3.143)$$

Then it is easy to conclude that the Cohen class of distribution can be written as a sum of spectrograms

$$CD(n, \omega) = \sum_i \lambda_i |STFT_{\mathbf{q}_i}(n, \omega)|^2 \quad (3.144)$$

where λ_i represents eigenvalues, while \mathbf{q}_i are corresponding eigenvectors of \mathbf{C} , that is, columns of \mathbf{Q} , used as windows in the STFT calculations. The eigenvalues and corresponding eigenvectors in the case of Choi-Williams kernel are presented in Fig. 3.17.

Alternative decomposition matrix scheme, singular value decomposition, can be applied to the matrix of arbitrary shape.

3.8 S-METHOD

The reduced interference distributions are derived in order to suppress cross-terms, while preserving the marginal properties. Another method is based on the idea of preserving the auto-terms as in the Wigner distribution, with elimination or significant reduction of the cross-terms. This method has been derived from the relationship between the STFT and the pseudo Wigner distribution.

The pseudo Wigner distribution can be calculated as

$$PWD(t, \Omega) = \frac{1}{\pi} \int_{-\infty}^{\infty} STFT(t, \Omega + \theta) STFT^*(t, \Omega - \theta) d\theta, \quad (3.145)$$

where the STFT is defined as

$$STFT(t, \Omega) = \int_{-\infty}^{\infty} x(t + \tau) w(\tau) e^{-j\Omega\tau} d\tau. \quad (3.146)$$

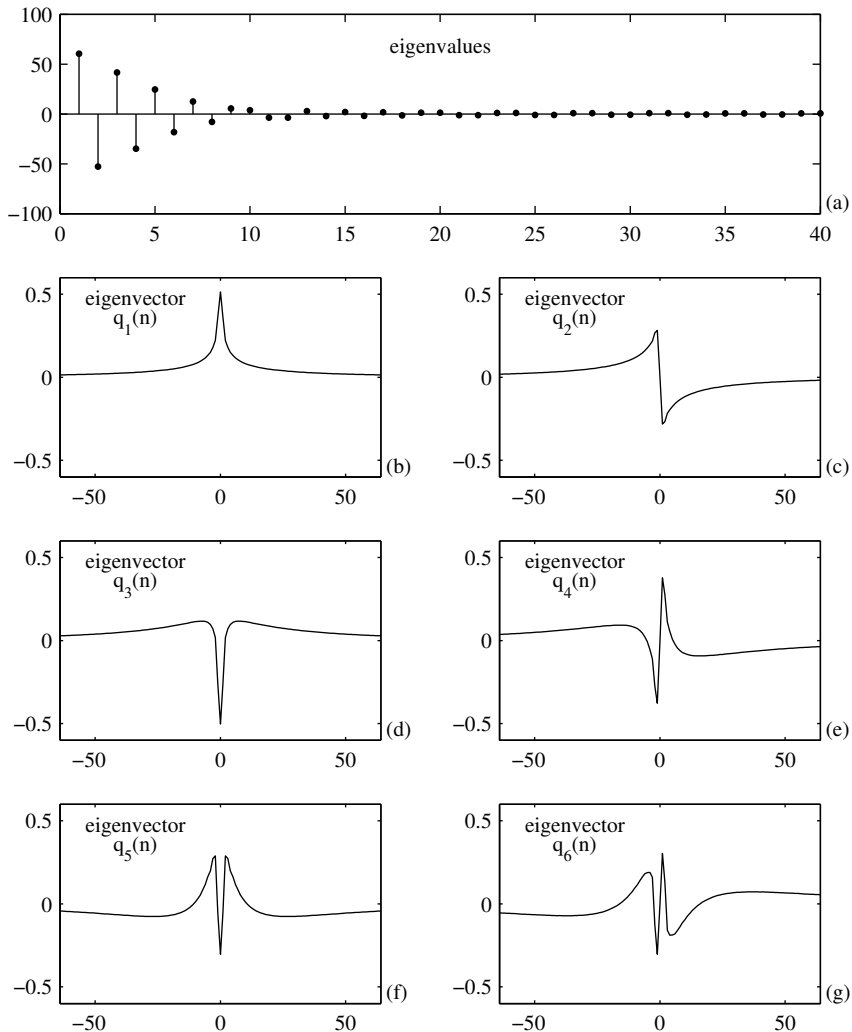


Figure 3.17 Kernel decomposition example for Choi-Williams kernel: (a) eigenvalues and (b - g) six eigenvectors $q_i(n)$ corresponding to the highest magnitude eigenvalues.

This can be proven by substituting (3.146) into (3.145),

$$\begin{aligned}
 PWD(t, \Omega) &= \frac{1}{\pi} \int_{-\infty}^{\infty} \int_{-\infty}^{\infty} w(\tau_1) w^*(\tau_2) x(t + \tau_1) x^*(t + \tau_2) \\
 &\quad \times e^{-j\Omega(\tau_1 - \tau_2)} \int_{-\infty}^{\infty} e^{j\theta(\tau_1 + \tau_2)} d\theta d\tau_1 d\tau_2 \\
 &= 2 \int_{-\infty}^{\infty} w(\tau) w^*(-\tau) x(t + \tau) x^*(t - \tau) e^{-j2\Omega\tau} d\tau \\
 &= \int_{-\infty}^{\infty} w\left(\frac{\tau}{2}\right) w^*\left(-\frac{\tau}{2}\right) x\left(t + \frac{\tau}{2}\right) x^*\left(t - \frac{\tau}{2}\right) e^{-j\Omega\tau} d\tau.
 \end{aligned} \tag{3.147}$$

Relation (3.145) has led to the definition of a time-frequency distribution

$$SM(t, \Omega) = \frac{1}{\pi} \int_{-\infty}^{+\infty} P(\theta) STFT(t, \Omega + \theta) STFT^*(t, \Omega - \theta) d\theta, \tag{3.148}$$

where $P(\theta)$ is a finite window (usually we also assume its rectangular form), $P(\theta) = 0$ for $|\theta| > L_P$, with L_P being its width,

$$SM(t, \Omega) = \frac{1}{\pi} \int_{-L_P}^{L_P} P(\theta) STFT(t, \Omega + \theta) STFT^*(t, \Omega - \theta) d\theta.$$

Distribution obtained in this way is referred to as the S-method. Two special cases are:

- the spectrogram with $P(\theta) = \pi\delta(\theta)$ and
- the pseudo Wigner distribution with $P(\theta) = 1$.

The S-method can produce a representation of a multicomponent signal such that the distribution of each component is its pseudo Wigner distribution, avoiding cross-terms, if the STFTs of the components do not overlap in time-frequency plane.

Consider a signal

$$x(t) = \sum_{m=1}^M x_m(t)$$

where $x_m(t)$ are monocomponent signals. Assume that the STFT of each component lies inside the region $D_m(t, \Omega)$, $m = 1, 2, \dots, M$ and assume that regions $D_m(t, \Omega)$ do not overlap. Denote the length of the m th region along Ω , for a given t , by $2B_m(t)$, and its central frequency by $\Omega_{0m}(t)$. Under this assumptions the S-method of $x(t)$ produces the sum of the pseudo Wigner distributions of each signal component

$$SM_x(t, \Omega) = \sum_{m=1}^M PWD_{x_m}(t, \Omega), \quad (3.149)$$

if the width of the rectangular window $P(\theta)$, for a point (t, Ω) , is defined by

$$L_P(t, \Omega) = \begin{cases} B_m(t) - |\Omega - \Omega_{0m}(t)| & \text{for } (t, \Omega) \in D_m(t, \Omega) \\ 0 & \text{elsewhere.} \end{cases} \quad (3.150)$$

To prove this consider a point (t, Ω) inside a region $D_m(t, \Omega)$. The integration interval in (3.148), for the m th signal component is symmetrical with respect to $\theta = 0$. It is defined by the smallest absolute value of θ for which $\Omega + \theta$ or $\Omega - \theta$ falls outside $D_m(t, \Omega)$,

$$|\Omega \pm \theta - \Omega_{0m}(t)| \geq B_m(t).$$

For $\Omega > \Omega_{0m}(t)$ and positive θ , the integration limit is reached for $\theta = B_m(t) - (\Omega - \Omega_{0m}(t))$. For $\Omega < \Omega_{0m}(t)$ and positive θ , the limit is reached for $\theta = B_m(t) + (\Omega - \Omega_{0m}(t))$. Thus, having in mind the interval symmetry, an integration limit which produces the same value of integral (3.148) as the value of (3.145), over the region $D_m(t, \Omega)$, is given by (3.150). Therefore, for $(t, \Omega) \in D_m(t, \Omega)$, we have

$$SM_x(t, \Omega) = PWD_{x_m}(t, \Omega).$$

Since the regions $D_m(t, \Omega)$ do not overlap, we conclude that (3.149) holds.

Note that any window $P(\theta)$ with constant width

$$L_P \geq \max_{(t, \Omega)} \{L_P(t, \Omega)\}$$

produces (3.149), if the regions $D_m(t, \Omega)$, $m = 1, 2, \dots, M$, are at least $2L_P$ apart along the frequency axis, that is, $|\Omega_{0p}(t) - \Omega_{0q}(t)| > B_p(t) + B_q(t) + 2L_P$, for each p, q , and t . This is the S-method with constant window width.

The best choice of L_P is the value when $P(\theta)$ is wide enough to enable complete integration over the auto-terms, but narrower than the distance between the auto-terms, in order to avoid the cross-terms. If two components overlap for some time instant t , then the cross-term will appear but only between these two components and for that time instant.

3.8.1 Discrete Realization of the S-Method

The discrete form of the S-method reads

$$SM(n, k) = \sum_{i=-L_d}^{L_d} P(i) STFT(n, k+i) STFT^*(n, k-i) \quad (3.151)$$

$$SM(n, k) = |STFT(n, k)|^2 + 2 \operatorname{Re} \left[\sum_{i=1}^{L_d} STFT(n, k+i) STFT^*(n, k-i) \right] \quad (3.152)$$

where

$$STFT(n, k) = \sum_{m=-N/2}^{N/2-1} x(n+m) w(m) e^{-j\frac{2\pi}{N}mk}$$

$$k = -N/2, -N/2+1, \dots, N/2-1,$$

and $P(i) = 1$ for $-L_d \leq i \leq L_d$ is assumed. The terms in summation improve the quality of spectrogram $|STFT(n, k)|^2$ toward the Wigner distribution quality. This relation could be used for an illustrative transition from the spectrogram to the pseudo Wigner distribution. In order to establish a direct relation to the discretization parameters of the STFT and the discrete pseudo Wigner distribution, rewrite (3.151), as

$$\begin{aligned} SM(n, k) &= \sum_i STFT(n, k+i) STFT^*(n, k-i) \\ &= \sum_i \sum_{m_1=-N/2}^{N/2-1} \sum_{m_2=-N/2}^{N/2-1} w(m_1) x(n+m_1) w^*(m_2) x^*(n+m_2) \\ &\quad \times e^{-j2\pi(m_1-m_2)k/N} e^{j2\pi(m_1+m_2)i/N}. \end{aligned}$$

Obviously, if the summation is done over all i , then

$$SM(n, k) = N \sum_{m=-N/2}^{N/2-1} w(m) w^*(-m) x(n+m) x^*(n-m) e^{-j2\pi(2m)k/N}.$$

Summation in (3.151) should be done over i such that $STFT(n, k+i) STFT^*(n, k-i) \neq 0$ or in multicomponent case, such that $STFT_{x_n}(n, k+i) STFT_{x_n}^*(n, k-i) \neq 0$,

for each component. Other terms do not contribute to the overall sum. It remains the same with or without these terms.

A recursive relation for the S-method calculation, with rectangular window $P(i)$ is

$$SM(n, k; L_d) = SM(n, k; L_d - 1) + 2 \operatorname{Re}[STFT(n, k + L_d) STFT^*(n, k - L_d)] \quad (3.153)$$

where

$$SM(n, k; 0) = |STFT(n, k)|^2,$$

and $SM(n, k; L_d)$ denotes $SM(n, k)$ in (3.152) calculated with L_d terms in the sum. In this way, we start from the spectrogram, and gradually make the transition toward the pseudo Wigner distribution, with $P(i) = 1/(2L_d + 1)$. The S-method calculation is illustrated in Fig. 3.18 for a 16-point linear frequency-modulated signal and $L_d = 0, 1, 2, 3$.

We suggest that reader calculate the signal's STFT, and then make a sequence of images starting with the S-method with $L_d = 0$ (the spectrogram) matrix, denoted as the starting video frame $SM(n, k; 0)$, and continue making images (video frames) $SM(n, k; 1)$, $SM(n, k; 2)$, ..., $SM(n, k; N/2)$, with $L_d = 1, 2, 3, \dots, N/2$. Finally, it is possible to play these images as a transition video from the spectrogram to the Wigner distribution.

For the S-method realization, we have to implement the STFT first, based either on the FFT routines or recursive approaches suitable for hardware realizations (as described in Chapter 2),

$$\begin{aligned} STFT_R(n, k) &= [x(n + N/2 - 1) - x(n - N/2 - 1)] (-1)^k e^{j2\pi k/N} \\ &\quad + STFT_R(n - 1, k) e^{j2\pi k/N}, \end{aligned}$$

where the subscript R implies rectangular window. The STFT with Hann(ing) window is related to the STFT with rectangular window as

$$STFT_H(n, k) = \frac{1}{2} STFT_R(n, k) + \frac{1}{4} STFT_R(n, k - 1) + \frac{1}{4} STFT_R(n, k + 1).$$

After we get the STFT, we have to “correct” the obtained values, according to (3.152), by adding few “correction” terms to the spectrogram values. Note that the S-method is one of the rare quadratic time-frequency distributions allowing easy hardware realization, based on the hardware realization of the STFT, presented in the first part, and its “correction” according to (3.152).

In the S-method calculation:

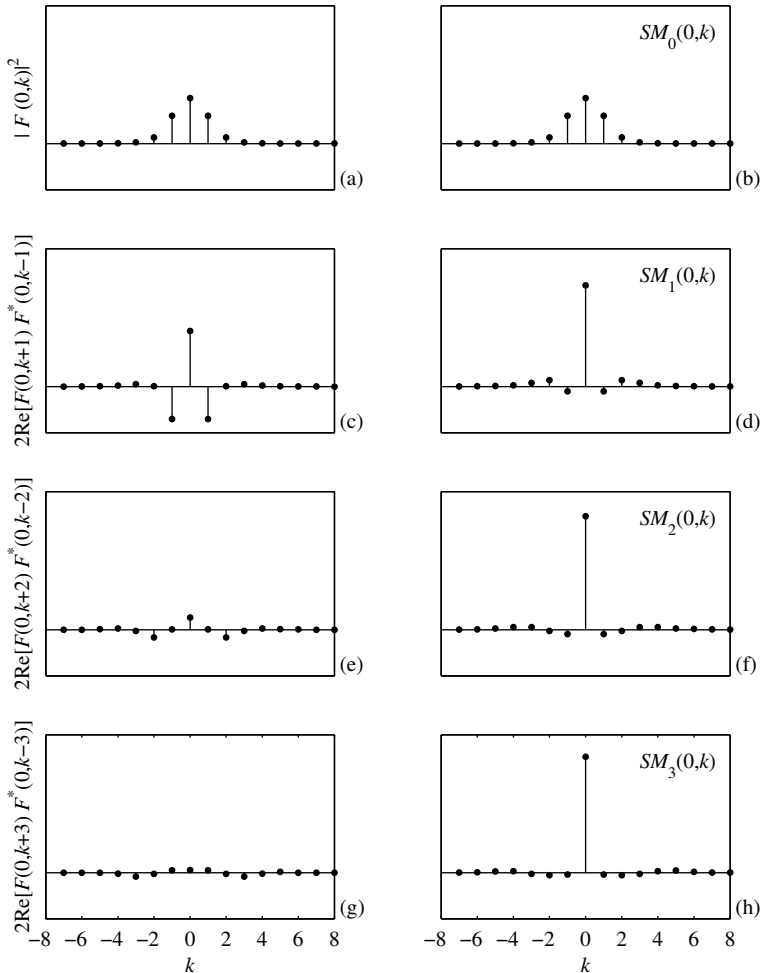


Figure 3.18 An illustration of the S-method calculation in the case of a 16-point linear frequency-modulated signal (a - h). Notation $F(n, k) = STFT(n, k)$ is used here for the graphical simplicity.

1. There is no need for analytic signal calculation since the cross-terms between negative and positive frequency components are removed in the same way as the other cross-terms.
2. If we set $STFT(n, k) = 0$ outside the basic period, that is, when $k < -N/2$ or $k > N/2 - 1$, then there is no aliasing when the STFT is alias-free. This way we can calculate the alias-free pseudo Wigner distribution $PWD_{af}(n, k)$ as

$$PWD_{af}(n, k) = |STFT(n, k)|^2 + 2 \operatorname{Re} \left[\sum_{i=1}^{L_d(k)} STFT(n, k+i) STFT^*(n, k-i) \right]$$

by taking $L_d = N/2$ and $P(i) = 1$ in (3.152). In order to avoid summation over the assumed zero-values of the STFT for $k < -N/2$ or $k > N/2 - 1$, the variable limit $L_d(k)$ is used, meaning that the summation should stop when $k+i > N/2 - 1$ or $k-i < -N/2$ for a given k is reached.

There are two possibilities to implement the summation in (3.152):

1. With a signal independent L_d . Theoretically, in order to get the pseudo Wigner distribution for each individual component, we should use a rectangular window with a length $2L_d + 1$ such that $2L_d$ is equal to the width of the widest auto-term. This will guarantee cross-terms free distribution for all components that are at least $2L_d$ samples apart. For components and time instants where this condition is not satisfied, the cross-terms will appear, but still in a reduced form. In this case, the calculation in (3.152) and (3.153) need not be done for each point (n, k) separately. It can be performed for the whole matrix of the S-method and the STFT. This can significantly save time in some matrix based calculation tools, like MATLAB (see the program in problem section). Assume that the STFT values are stored in a matrix, when the rows stand for constant time index, while the columns stand for constant frequency index. The spectrogram is obtained by calculating squared modulus of this matrix. The first correction term for the S-method is obtained by forming one matrix with the STFT columns shifted right for one index, and zeros inserted in the first column, and the other matrix with the STFT values shifted left and the zeros inserted into the last column. The first correction term for the whole spectrogram matrix is then a real value of the product of these two shifted matrices multiplied by 2. The matrix shifted right is complex conjugated as well. The next term is obtained by shifting left and right the previously shifted matrices for one more column, and so on.

Let us denote the matrix with the STFT elements as $[\text{STFT}]_{1:N,1:N}$, where the first index corresponds to time and the second index corresponds to the frequency. Then the spectrogram is a matrix

$$[\text{SPEC}]_{1:N,1:N} = [\text{STFT}]_{1:N,1:N} \cdot * [\text{STFT}]_{1:N,1:N}^*, \quad (3.154)$$

where $\cdot *$ stands for element-by-element matrix multiplication and $*$ denotes the conjugation. The S-method matrix, with one correction term, is

$$\begin{aligned} [\text{SM}]_{1:N,1:N} &= [\text{SPEC}]_{1:N,1:N} \\ &+ 2\text{Re} \left\{ \left[\begin{array}{cc} \text{STFT}_{1:N,2:N} & \mathbf{0}_{1:N,1} \end{array} \right] \cdot * \left[\begin{array}{cc} \mathbf{0}_{1:N,1} & \text{STFT}_{1:N,1:N-1} \end{array} \right]^* \right\} \end{aligned}$$

where $\mathbf{0}_{1:N,1}$ is the vector column with zero values. The two correction terms form is

$$\begin{aligned} [\text{SM}]_{1:N,1:N} &= [\text{SM}]_{1:N,1:N} \\ &+ 2\text{Re} \left\{ \left[\begin{array}{cc} \text{STFT}_{1:N,3:N} & \mathbf{0}_{1:N,2} \end{array} \right] \cdot * \left[\begin{array}{cc} \mathbf{0}_{1:N,2} & \text{STFT}_{1:N,1:N-2} \end{array} \right]^* \right\} \end{aligned}$$

with $\mathbf{0}_{1:N,2}$ being a matrix with two columns and N rows, with all 0 values. We continue in this way up to L_d terms. In case of using the rotated STFT values (circular shifts), that is, if instead of $[\text{STFT}_{1:N,2:N} \quad \mathbf{0}_{1:N,1}]$ we use $[\text{STFT}_{1:N,2:N} \quad \text{STFT}_{1:N,1}]$, then the original (aliased) form of the pseudo Wigner distribution will be obtained for $L_d = N/2$.

2. With a signal dependent $L_d = L_d(n, k)$ where the summation, for each point (n, k) , stops when the absolute square value of $\text{STFT}(n, k+i)$ or $\text{STFT}(n, k-i)$ is smaller than the assumed reference level R . If a small values may be expected within a single auto-term, then the summation lasts until the two subsequent values below the reference level are detected. The reference level is defined as a few percent of the spectrogram's maximal value at the considered instant n

$$R_n = \frac{1}{Q^2} \max_k \{ |\text{STFT}(n, k)|^2 \},$$

where Q is a constant. Index n is added to show that the reference level R is time dependent. Note that if $Q^2 \rightarrow \infty$, the Wigner distribution will be obtained, while $Q^2 = 1$ results in the spectrogram. A choice of an appropriate value for design parameter Q^2 will be discussed in Example 3.20. This is also known as the adaptive S-method.

Example 3.19. Consider real-valued multicomponent signals presented in Fig. 2.1. The S-method for $L_d = 4$ is presented in Fig. 3.19, and for $L_d = 3, 5$, and 7 in Fig. 3.20. Based on these two figures it is possible to conclude that the value of $L_d = 4$ was enough to fully concentrate all the auto-terms, so that they have a form as in the pseudo Wigner distribution. The value of L_d corresponds to the maximal auto-term width of about nine samples in the spectrogram. Also, it is easy to see that this presentation is not too sensitive on L_d . For $L_d = 3$ similar form of the auto-terms is obtained, with a hardly notable lower auto-terms concentration. In the case with $L_d = 5$, a full concentration, as in the case with $L_d = 4$, is achieved, meaning that any further increase of L_d does not produce improvement in the auto-terms form for this signal. However, by increasing the value of L_d , taking wider and wider intervals, products of two different components will start appearing. They are already notable in the case with $L_d = 7$ (Fig. 3.20(c)). If the value of L_d is increased toward $N/2$, the pseudo Wigner distribution, with all of its cross-terms, would be obtained. One of the methods for selecting the value of L_d could be as follows. Start with the spectrogram, $L_d = 0$. Add one term by calculating the S-method with $L_d = 1$. Check the concentration, by using, for example, the normalized sum of the absolute distribution values, for the considered time instant n . If the concentration improves, add one more term, use $L_d = 2$, check the concentration, if it improves, add the next term, and so on. When the pseudo Wigner distribution form of the auto-terms is achieved, then usually the S-method form will not change for few values of L_d . The values of added terms $STFT(n, k + L_d)STFT^*(n, k - L_d)$ will be then negligible, as compared to the distribution value. By further increase of L_d , the value of added terms $STFT(n, k + L_d)STFT^*(n, k - L_d)$ will start increasing, being the indicator that we start picking up the cross-terms, as in Fig. 3.20(c). By then, the concentration measure will start showing the worsening of the concentration. \square

Example 3.20. The adaptive S-method realization will be illustrated on a three-component real signal, with a nonlinear frequency-modulated component,

$$x(t) = e^{-t^2} \cos(25\pi t) + \cos(120t^3 + 45\pi t) + 1.5e^{-25t^2} \cos(40\pi t^2 + 150\pi t)$$

with the sampling interval $\Delta t = 1/256$. The signal is considered within the time interval $[-1, 1]$. The Hann(ing) window of the width $T = 1$ is used. The spectrogram is presented in Fig. 3.21(a), while the S-method with the constant $L_d = 3$ is shown in Fig. 3.21(b). The concentration improvement with respect to the case $L_d = 0$, Fig. 3.21(a), is evident. Further increase of L_d would improve the concentration, but the cross-terms would also appear. Small changes are already noticeable between the components with quadratic and constant instantaneous frequency. An improved concentration, without cross-terms, can be achieved by using the variable window width L_d . The regions $D_m(n, k)$, determining the summation limit $L_d(n, k)$ for each point (n, k) , are obtained by imposing the reference level R_n corresponding to

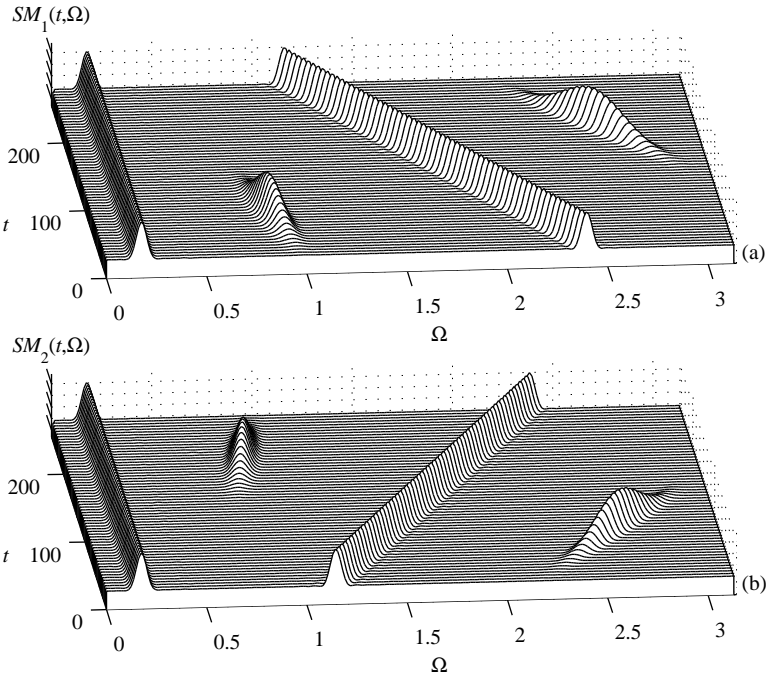


Figure 3.19 (a, b) The S-method (with $L_d = 4$) of the signals from Figure 2.1.

$Q^2 = 50$. They are defined as

$$D_m(n, k) = \begin{cases} 1 & \text{when } |STFT_{x_m}(n, k)|^2 \geq R_n \\ 0 & \text{elsewhere} \end{cases} \quad (3.155)$$

and presented in Fig. 3.21(c). White regions mean that the value of spectrogram is below 2% of its maximal value at that time instant n , meaning that the concentration improvement is not performed at these points. The signal-dependent S-method is given in Fig. 3.21(d). The method's sensitivity, with respect to the value of Q^2 , is low. A similar discussion for the value of Q^2 selection, as the one in the previous example for the value of L_d , holds. \square

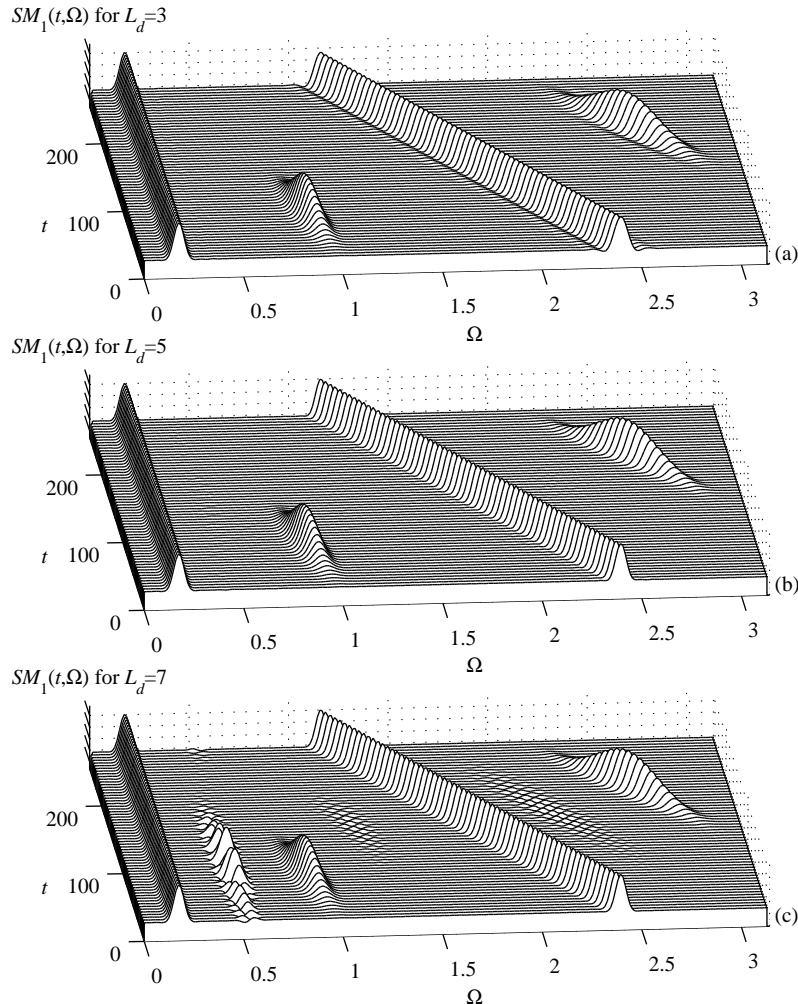


Figure 3.20 The S-method of the signal presented in Figure 2.1(a) for: (a) $L_d = 3$, (b) $L_d = 5$, and (c) $L_d = 7$.

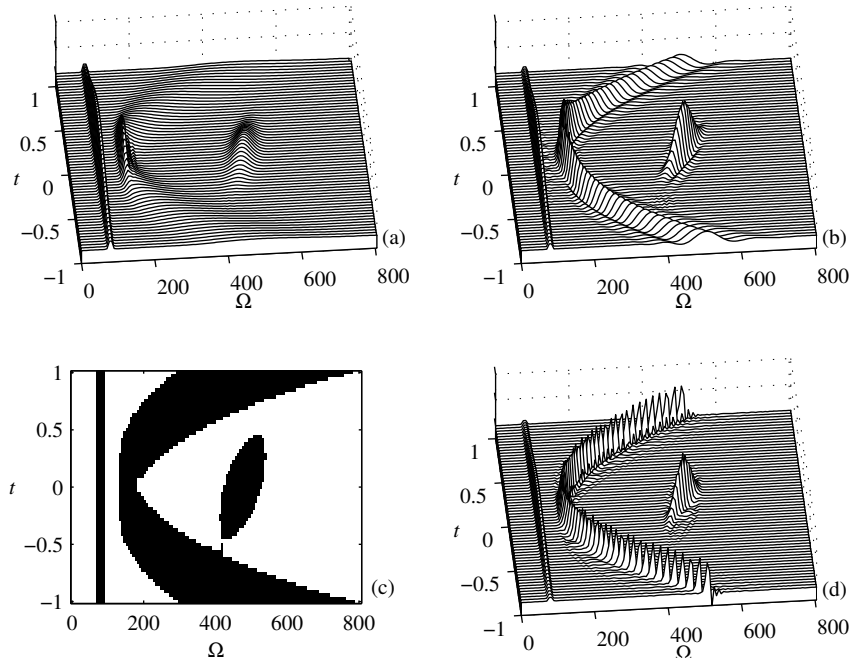


Figure 3.21 Time-frequency analysis of a multicomponent signal: (a) the spectrogram, (b) the S-method with a constant window, $L_d = 3$, (c) the regions of support for the S-method with a variable window width calculation, corresponding to $Q^2 = 50$, and (d) the S-method with the variable window width calculated by using regions given in (c).

3.8.2 Smoothed Spectrogram Versus S-Method as a Principle of Composition

The S-method belongs to the general class of quadratic TF distributions.

The kernel function of the S-method is given by

$$c(\theta, \tau) = P(\theta/2) *_{\theta} AF_{ww}(\theta, \tau)/2\pi, \quad (3.156)$$

where $AF_{ww}(\theta, \tau)$ is the ambiguity function of window $w(\tau)$ and $*_{\theta}$ is convolution over θ . In general, it is a nonseparable function in ambiguity or time-frequency domain. The kernel follows from the S-method form of (3.147) with a window

$P(\theta)$ included in the last integral over θ . In the time-lag domain we have

$$c_T \left(-\frac{v_1 + v_2}{2}, v_1 - v_2 \right) = 2w(\tau_1)w(\tau_2)p(\tau_1 + \tau_2)$$

with $p(t)$ being the inverse Fourier transform of $P(\theta)$. Further transformations are as in the example with the kernel of the spectrogram.

Note that the general form of quadratic distributions

$$CD(t, \Omega) = \int_{-\infty}^{\infty} \int_{-\infty}^{\infty} c_T \left(-\frac{v_1 + v_2}{2}, v_1 - v_2 \right) x(t + v_1)x^*(t + v_2)e^{-j\Omega(v_1 - v_2)}dv_1 dv_2$$

with the inner product kernel $G_T(v_1, v_2) = c_T \left(-\frac{v_1 + v_2}{2}, v_1 - v_2 \right)$ can be written as

$$CD(t, \Omega) = \int_{-\infty}^{\infty} \int_{-\infty}^{\infty} [x(t + v_1)e^{-j\Omega v_1}]G_T(v_1, v_2)[x(t + v_2)e^{-j\Omega v_2}]^*dv_1 dv_2.$$

If the inner product kernel is factorized in the Hankel form

$$G_T(v_1, v_2) = 2w(v_1)p(v_1 - v_2)w(v_2), \quad (3.157)$$

then the S-method follows.

The Toeplitz factorization of the inner product kernel

$$G_T(v_1, v_2) = 2w(v_1)p(v_1 - v_2)w(v_2) \quad (3.158)$$

results in the smoothed spectrogram. The smoothed spectrogram composes two STFTs in the same direction,

$$SSPEC(n, k) = \sum_{i=-L_d}^{L_d} P(i)STFT(n, k+i)STFT^*(n, k+i),$$

resulting in the distribution spread, in contrast to the S-method, where two STFTs are composed in a counter-direction,

$$SM(n, k) = \sum_{i=-L_d}^{L_d} P(i)STFT(n, k+i)STFT^*(n, k-i).$$

These forms led Scharf and Friedlander to divide all the estimators of discrete time-varying processes into two classes, one based on the smoothed spectrogram and the other based on the Stanković class of the Wigner distribution estimators (S-method).

In this sense we may conclude that it is possible to define various forms of the S-method and use it for various applications. For example, for:

- The time-direction form of the S-method,

$$SM_t(n, k) = \sum_{i=-L_d}^{L_d} STFT(n+i, k) STFT^*(n-i, k) e^{-j2\pi(2i)k/N}.$$

- The S-method composed in both time and frequency (two-dimensional S-method).
- Composing the windowed fractional Fourier transforms $XW_\alpha(n)$ (fractional form of the S-method),

$$SM_\alpha(n, k) = \sum_{i=-L_d}^{L_d} XW_\alpha(n, k+i) XW_\alpha^*(n, k-i) \quad (3.159)$$

where $XW_\alpha(n, k)$ is the windowed form of the fractional Fourier transform, defined by $XW_\alpha(n, k) = DFT\{X_\alpha(n+m)w^*(m)\}$ and $X_\alpha(n)$ is the fractional Fourier transform for an angle α . This approach was used in combination with the minimum moment, to process a signal in the domain where it is the best concentrated.

- Composing wavelets and other time-scale transforms (affine form of the S-method, will be given later).

All of these forms have been introduced, presented, and studied in the literature.

3.8.3 Decomposition of Multicomponent Signals

Let us consider a multicomponent signal

$$x(n) = \sum_{i=1}^M x_i(n)$$

where components $x_i(n)$ are mutually orthogonal, that is, the components do not overlap in the time-frequency plane.

For each signal component $x_i(n)$, we can write its inversion formula, corresponding to (3.90), as

$$x_i(n_1)x_i^*(n_2) = \frac{1}{N+1} \sum_{k=-N/2}^{N/2} WD_i\left(\frac{n_1+n_2}{2}, k\right) e^{j\frac{\pi}{N+1}k(n_1-n_2)} \quad \text{for } i = 1, 2, \dots, M,$$

if the Wigner distribution $WD_i(n, k)$ of this component were known. The total number of samples is an odd number $N + 1$. By summing the above relations for $i = 1, 2, \dots, M$, we get

$$\sum_{i=1}^M x_i(n_1) x_i^*(n_2) = \frac{1}{N+1} \sum_{k=-N/2}^{N/2} \sum_{i=1}^M WD_i\left(\frac{n_1+n_2}{2}, k\right) e^{j\frac{\pi}{N+1}k(n_1-n_2)}.$$

Having in mind (3.149), for the signals that satisfy the condition that S-method is equal to the sum of pseudo Wigner distributions of individual components, this relation reduces to

$$\sum_{i=1}^M x_i(n_1) x_i^*(n_2) = \frac{1}{N+1} \sum_{k=-N/2}^{N/2} SM\left(\frac{n_1+n_2}{2}, \frac{k}{2}\right) e^{j\frac{\pi}{N+1}k(n_1-n_2)}. \quad (3.160)$$

Note that for a rectangular window wider than a component duration the pseudo Wigner distribution is equal to the Wigner distribution, for the considered component.

By denoting

$$R_{SM}(n_1, n_2) = \frac{1}{N+1} \sum_{k=-N/2}^{N/2} SM\left(\frac{n_1+n_2}{2}, \frac{k}{2}\right) e^{j\frac{\pi}{N+1}k(n_1-n_2)} \quad (3.161)$$

and using the eigenvalue decomposition of matrix \mathbf{R}_{SM} , with the elements defined by (3.161), we get

$$\mathbf{R}_{SM} = \sum_{i=1}^{N+1} \lambda_i \mathbf{q}_i(n) \mathbf{q}_i^*(n).$$

As in the case of the Wigner distribution, we can conclude that $\lambda_i = E_{x_i}$, $i = 1, 2, \dots, M$ and $\lambda_i = 0$ for $i = M+1, \dots, N$.

The eigenvectors $\mathbf{q}_i(n)$ will be equal to the signal components $\mathbf{x}_i(n)$, up to the phase and amplitude constants, since the components orthogonality is assumed. Amplitude constants are again contained in the eigenvalues λ_i . Thus, the reconstructed signal can be written as

$$x_{rec}(n) = \sum_{i=1}^M \sqrt{\lambda_i} q_i(n).$$

It is equal to the original signal, up to the phase constants in each component. When we have several components of different energies $\mathbf{x}_1(n), \mathbf{x}_2(n), \dots, \mathbf{x}_M(n)$ and

when they are of equal importance in analysis, we can use normalized values of the signal components and calculate the time-frequency representation of

$$\mathbf{x}_{nor}(n) = \sum_{i=1}^M k(\lambda_i) \mathbf{q}_i(n) \quad (3.162)$$

by using the weights $k(\lambda_i) = 1$ in the signal, that is, when $i = 1, 2, \dots, M$.

Example 3.21. Consider a signal whose analog form reads

$$x(t) = e^{j\frac{\pi}{6400}t^2} e^{-(\frac{t}{96})^2} + \sum_{k=2}^7 \sqrt{\frac{27-k}{10}} e^{j\Omega_k t} e^{-(\frac{t-d_k}{16})^2}$$

within the interval $-128 \leq t \leq 127$, where $\Omega_2 = -\frac{3\pi}{4}$, $\Omega_3 = -\frac{\pi}{2}$, $\Omega_4 = -\frac{\pi}{4}$, $\Omega_5 = \frac{\pi}{4}$, $\Omega_6 = \frac{\pi}{2}$, $\Omega_7 = \frac{3\pi}{4}$, $d_2 = d_7 = 0$, $d_3 = d_5 = -64$ and $d_4 = d_6 = 64$. The sampling interval is $\Delta t = 1$.

★ The Wigner distribution is presented in Fig. 3.22(a). Based on the Wigner distribution, the elements of matrix \mathbf{R} are calculated by using (3.91). Eigenvalue decomposition (3.94) of this matrix produces exactly one nonzero eigenvalue, $\lambda_1 = 390.92$ ($\lambda_2 = 0.00$, $\lambda_3 = 0.00, \dots$), being equal to the total signal energy $E_x = 390.14$ (within the numerical calculation error), as expected from (3.91) to (3.96).

The S-method of the same signal is calculated by using (3.151) with $L = 12$. The obtained results are depicted in Fig. 3.23. Matrix \mathbf{R}_{SM} is formed according to (3.161). Its eigenvalue decomposition results in the same number of nonzero eigenvalues as the number of signal components. Eigenvalues correspond to the components energies, while the eigenvectors correspond to the normalized signal components, up to the phase constants. The first seven components correspond to the signal, while the remaining ones are with very small eigenvalues. Energies of discrete signal components are: $E_1 = 119.40$, $E_2 = 50.13$, $E_3 = 48.13$, $E_4 = 46.12$, $E_5 = 44.12$, $E_6 = 42.11$, and $E_7 = 40.11$, while the obtained eigenvalues by using the S-method with $L = 12$ are: $\lambda_1 = 119.40$, $\lambda_2 = 50.18$, $\lambda_3 = 48.19$, $\lambda_4 = 46.19$, $\lambda_5 = 44.18$, $\lambda_6 = 42.17$, $\lambda_7 = 40.15$, $\lambda_8 = 0.68, \dots$

Sensitivity of the results with respect to L is quite low within a wide region. We have repeated calculations with values of L from $L = 10$ up to $L = 20$ and obtained almost the same results. The error in components energy, estimated by corresponding eigenvalues, was within $\pm 0.25\%$. A modification for narrow window cases is studied in literature □

A similar procedure can be used for signal synthesis from a given function $D(n, k)$. We should calculate \mathbf{R}_D matrix by substituting $D(n, k)$ instead of $SM(n, k)$ in (3.161) and calculate corresponding eigenvalues. If we obtain a single nonzero

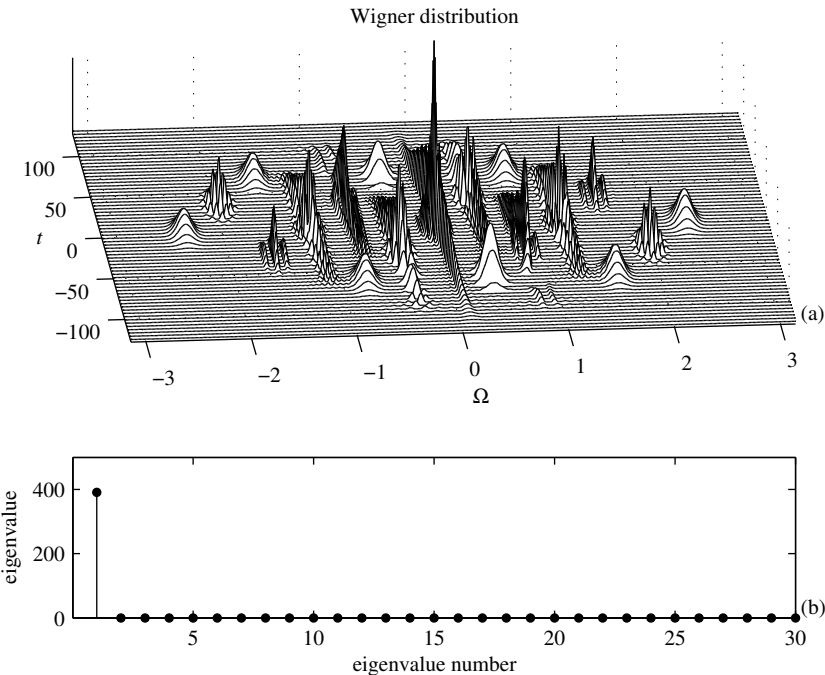


Figure 3.22 (a, b) Decomposition of the Wigner distribution. Only one nonzero eigenvalue is obtained.

eigenvalue, then there exists a signal $x(n)$ such that $D(n, k)$ is its Wigner distribution. In the case when M nonzero eigenvalues are present ($M > 1$), the function $D(n, k)$ can be approximated as a sum of Wigner distributions of several components. The approximation error can be estimated as a sum of the remaining eigenvalues ($\lambda_{M+1} + \lambda_{M+2} + \dots$).

Example 3.22. A two-dimensional function, representing the desired time-frequency distributions of signal energy, is given in Fig. 3.24(a). It consists of seven time-frequency regions. We will now find a seven-component signal, such that the Wigner distribution of each component is the mean squared estimation of each desired region. Performing the decomposition approach, by using the S-method as an approximation of the Wigner distributions of individual components, we get the eigenvalues

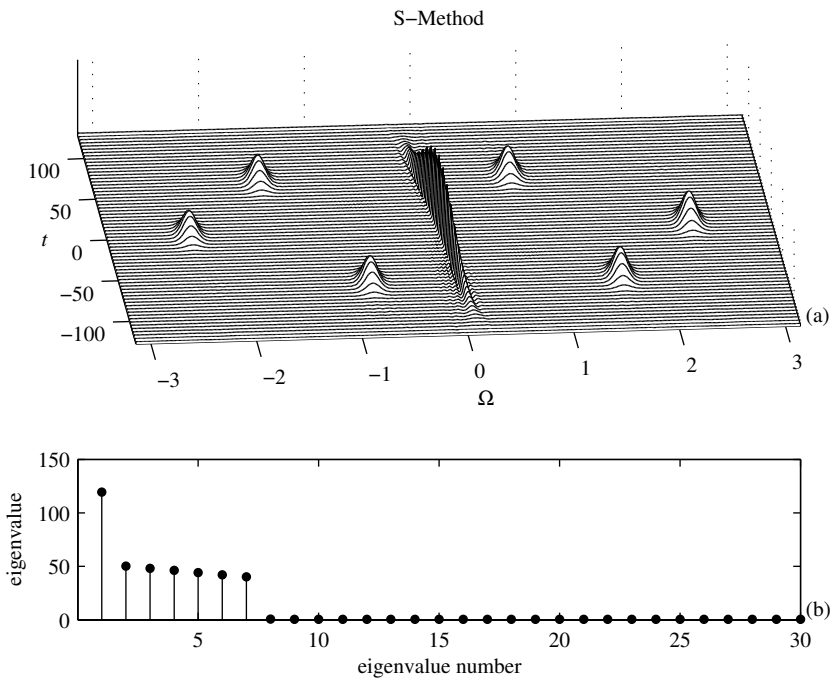


Figure 3.23 Decomposition of the S-method. Number of nonzero eigenvalues coincide with number of the signal components.

(Fig. 3.24(b)) with corresponding eigenvectors. Keeping the largest seven eigenvalues, with corresponding eigenvectors, we form a signal that is best time-frequency approximation of the desired arbitrary function form Fig. 3.24. The S-method, as a time-frequency representation, of the synthesized signal is shown in Fig. 3.25. \square

3.8.4 Empirical Mode Decomposition

One more empirical method for signal decomposition will be presented here. It belongs to other time-frequency analysis tools, rather than to the quadratic time-frequency distributions. The empirical mode decomposition (EMD) is originally proposed by Huang et al. It is introduced in signal processing to separate the signal

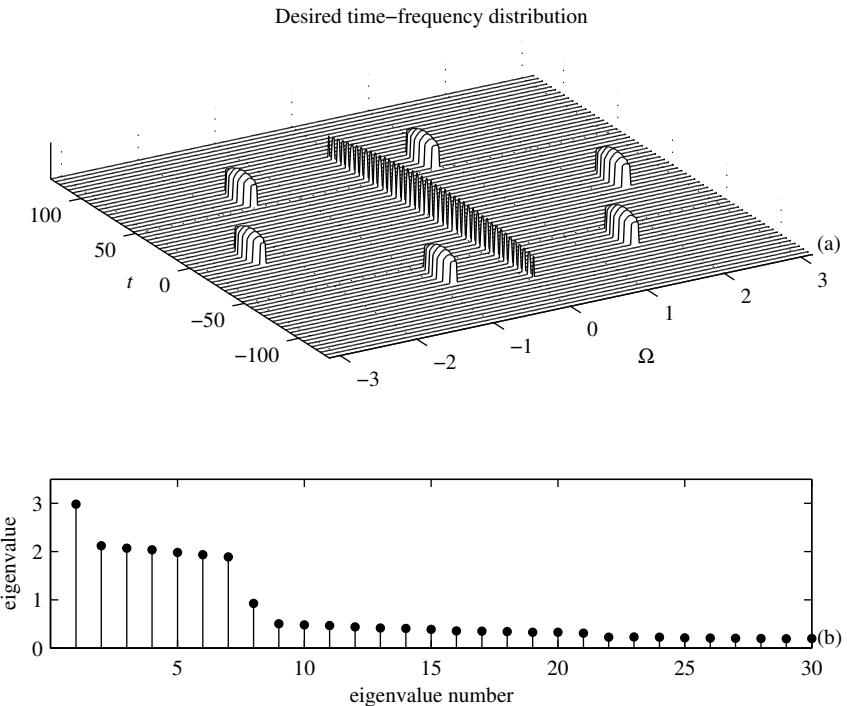


Figure 3.24 The desired time-frequency distribution and the corresponding eigenvalues

into components in a simple and efficient manner. The main reason for its inclusion, at this point, was that it deals with similar multicomponent signals, as we just considered. Its wide application and popularity in signal processing, led us to the conclusion that any consideration of signal decomposition, without presenting the empirical mode decomposition, would not be complete.

Let us consider a real-valued signal $x(t)$. In the EMD process we decompose signal into intrinsic mode functions (IMF) $x_k(t)$

$$x(t) = \sum_k x_k(t) \quad (3.163)$$

where IMF $x_k(t)$ is a function with the following properties:

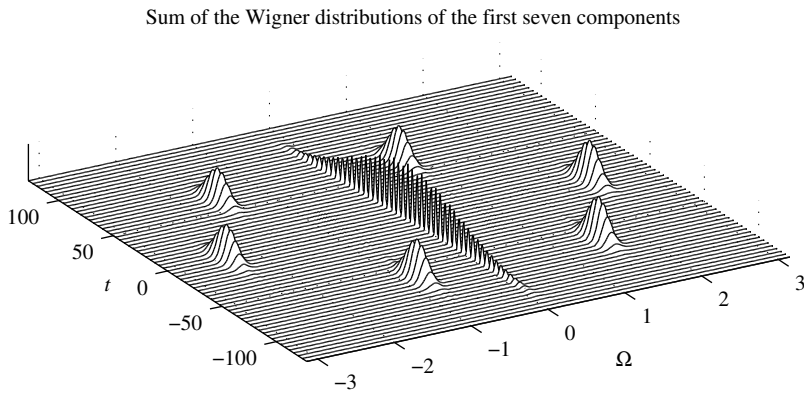


Figure 3.25 The resulting time-frequency distribution after signal synthesis from the most significant components.

1. The number of extrema and number of zero-crossing are equal or differ by 1.
2. The function is symmetric with respect to time axis.

The IMF presents the basic oscillatory process where the function's value moves from the minimal value toward the maximal (through zero) and then from the maximal to the minimal (again through zero) and so on. This oscillatory process does not introduce period or frequency of the oscillations in contrast to the standard harmonic analysis where basic oscillatory functions are periodic. An additional property of the IMF is that all the local maxima have positive value and all the local minima have negative values.

The condition that the IMF is a function symmetric with respect to the time axis means that the upper and the lower signal envelopes are symmetric functions. We can obtain the signal envelope by identifying local maxima (minima) points and interpolate the obtained points with a smooth function. The cubic spline interpolation is used in the most EMD applications.

The EMD algorithm is performed through sifting process. In each sift we extract a single IMF $x_k(t)$, then we subtract the estimated IMF $\hat{x}_k(t)$ from the analyzed signal and repeat sifting procedure for the next IMF.

- In the first step we identify the local maxima points as discrete points t where

$$x(t-1) \leq x(t) \geq x(t+1)$$

and local minima obtained as points t where

$$x(t-1) \geq x(t) \leq x(t+1).$$

- In the next step, the upper envelope $e_+(t)$ and the lower $e_-(t)$ envelope are obtained by cubic interpolation of local maxima (minima). Note that at the start and at the end of the considered interval, the envelope is obtained by extrapolation, introducing extrapolation error. The envelope mean is calculated as

$$m(t) = (e_+(t) + e_-(t))/2 \quad (3.164)$$

and subtracted from the original signal. We obtain the residual signal

$$h(t) = x(t) - m(t). \quad (3.165)$$

If the signal $h(t)$ is not the IMF, we should repeat the procedure with $h(t)$ instead of $x(t)$. If $h(t)$ is the IMF, then $x_k(t) = h(t)$ and we start searching for the other IMFs in the residue

$$r(t) = x(t) - h(t). \quad (3.166)$$

Example 3.23. Demonstrate the sifting process by considering the two-component signal

$$x(t) = 2 \sin\left(\frac{\pi}{30}t - \frac{\pi}{30000}t^2\right) + \frac{1}{2} \cos\left(\frac{2\pi}{15}t + \frac{\pi}{1500}t^2\right).$$

★ The sifting process of the first IMF is illustrated in Fig. 3.26. □

3.9 REASSIGNMENT IN TIME-FREQUENCY ANALYSIS

The reassignment method is an approach for postprocessing of the time-frequency representations. It was originally introduced by Kodera et al. to improve the readability of the spectrogram by using the phase information in the STFT to relocate (reassign) the distribution values closer to the instantaneous frequency or group delay.

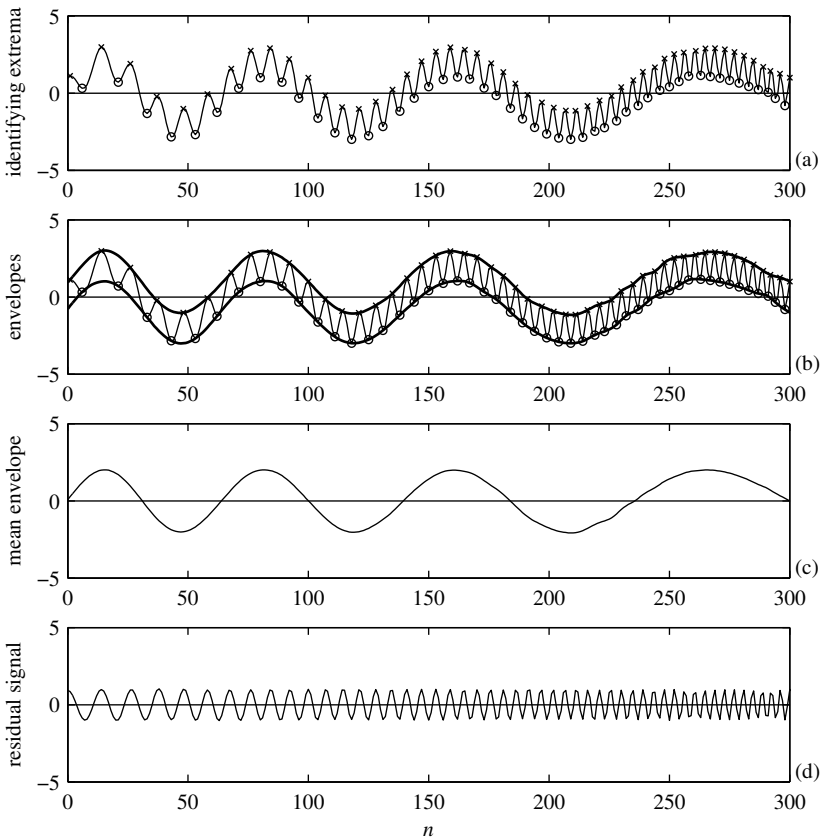


Figure 3.26 The empirical mode decomposition algorithm illustration: (a) the analyzed signal with marked local minima (o) and local maxima (x), (b) the upper and the lower signal envelope, (c) the mean envelope, and (d) the resulting signal.

In order to explain the principle of reassignment, let us consider the STFT definition that we used in this book

$$\begin{aligned}
 STFT_w(t, \Omega) &= \int_{-\infty}^{\infty} w(\tau)x(t + \tau)e^{-j\Omega\tau}d\tau = e^{j\Omega t} \int_{-\infty}^{\infty} w(\tau - t)x(\tau)e^{-j\Omega\tau}d\tau \\
 &= |STFT(t, \Omega)| e^{j\Psi(t, \Omega)}.
 \end{aligned}$$

It may be understood as decomposing a localized signal $x_t(\tau) = w(\tau)x(t + \tau)$ into the periodic functions $e^{-j\Omega\tau}$. Here index w in the $STFT_w(t, \Omega)$ indicates that a window $w(\tau)$ is used for the STFT calculation.

The signal can be reconstructed by

$$x(t) = \frac{1}{2\pi E_w} \int_{-\infty}^{\infty} \int_{-\infty}^{\infty} STFT_w(v, \Omega) w(t - v) e^{-j\Omega(v-t)} d\Omega dv, \quad (3.167)$$

where E_w is energy of the lag window $w(\tau)$, since

$$\begin{aligned} & \frac{1}{2\pi E_w} \int_{-\infty}^{\infty} \int_{-\infty}^{\infty} \int_{-\infty}^{\infty} e^{j\Omega v} w(u - v) x(u) e^{-j\Omega u} w(t - v) e^{-j\Omega(v-t)} du d\Omega dv \\ &= \frac{1}{E_w} \int_{-\infty}^{\infty} w(t - v) x(t) w(t - v) dv = x(t). \end{aligned}$$

Relation (3.167) can be written as

$$x(t) = \frac{1}{2\pi E_w} \int_{-\infty}^{\infty} \int_{-\infty}^{\infty} |STFT_w(v, \Omega)| w(t - v) e^{j(\Psi(v, \Omega) - \Omega v + \Omega t)} d\Omega dv. \quad (3.168)$$

According to the stationary-phase method, the most significant contribution to the reconstructed value of $x(t)$ is from the stationary point of the phase $\Psi(v, \Omega) - \Omega v + \Omega t$, in time and in frequency. The stationary phase point is obtained from the phase derivatives in the corresponding directions,

$$\begin{aligned} \frac{\partial \Psi(v, \Omega)}{\partial \Omega} - (v - t) &= 0 \\ \frac{\partial \Psi(v, \Omega)}{\partial v} - \Omega &= 0. \end{aligned} \quad (3.169)$$

It means that the calculated distribution value (in this case the spectrogram value) should be assigned not to the point (t, Ω) where it is calculated, but to the point where it contributes the most to the signal reconstruction, according to the

stationary-phase principle. The shifts of the calculated values are

$$\begin{aligned}\hat{t}(t, \Omega) &= t - \frac{\partial \Psi(t, \Omega)}{\partial \Omega} \\ \hat{\Omega}(t, \Omega) &= \Omega - \frac{\partial \Psi(t, \Omega)}{\partial t}.\end{aligned}\quad (3.170)$$

Note that the crucial role here is played by the STFT phase function, that is ignored in the spectrogram calculation and presentation.

In the case of the spectrogram, the reassigning shifts, are obtained as

$$\hat{t}(t, \Omega) = t + \operatorname{Re} \left\{ \frac{\operatorname{STFT}_{\tau w}(t, \Omega) \operatorname{STFT}_w^*(t, \Omega)}{|\operatorname{STFT}_w(t, \Omega)|^2} \right\} \quad (3.171)$$

$$\hat{\Omega}(t, \Omega) = \Omega - \operatorname{Im} \left\{ \frac{\operatorname{STFT}_{Dw}(t, \Omega) \operatorname{STFT}_w^*(t, \Omega)}{|\operatorname{STFT}_w(t, \Omega)|^2} \right\}, \quad (3.172)$$

where $\operatorname{STFT}_{\tau w}(t, \Omega)$ and $\operatorname{STFT}_{Dw}(t, \Omega)$ are the STFTs calculated with windows $\tau w(\tau)$ and $d w(\tau)/d\tau$, respectively. For $|\operatorname{STFT}_w(t, \Omega)|^2 = 0$, there is nothing to reassign, so the expressions (3.171) are not used.

To prove this, rewrite

$$|\operatorname{STFT}_w(t, \Omega)| e^{j\Psi(t, \Omega)} = \int_{-\infty}^{\infty} w(\tau) x(t + \tau) e^{-j\Omega\tau} d\tau.$$

The calculation of the $\operatorname{STFT}_{\tau w}(t, \Omega)$, with $\tau w(\tau)$ as the window function, corresponds to the derivative over Ω of both sides of the previous equation. It results in

$$\begin{aligned}& \int_{-\infty}^{\infty} \tau w(\tau) x(t + \tau) e^{-j\Omega\tau} d\tau \\ &= j \frac{\partial |\operatorname{STFT}_w(t, \Omega)|}{\partial \Omega} e^{j\Psi(t, \Omega)} - \frac{\partial \Psi(t, \Omega)}{\partial \Omega} |\operatorname{STFT}_w(t, \Omega)| e^{j\Psi(t, \Omega)}.\end{aligned}$$

Thus,

$$\begin{aligned}& \operatorname{STFT}_{\tau w}(t, \Omega) \operatorname{STFT}_w^*(t, \Omega) \\ &= j \frac{\partial |\operatorname{STFT}_w(t, \Omega)|}{\partial \Omega} |\operatorname{STFT}_w(t, \Omega)| - \frac{\partial \Psi(t, \Omega)}{\partial \Omega} |\operatorname{STFT}_w(t, \Omega)|^2\end{aligned}$$

with

$$\operatorname{Re} \{STFT_{\tau w}(t, \Omega) STFT_w^*(t, \Omega)\} = -\frac{\partial \Psi(v, \Omega)}{\partial \Omega} |STFT_w(t, \Omega)|^2, \quad (3.173)$$

producing the reassignment shift in time in (3.171).

In a similar way, using the frequency domain definitions of the STFT we obtain the reassignment shift in frequency.

The previous procedure, stating that a value of the spectrogram $SPEC(t, \Omega)$ should not be placed at (t, Ω) in the time-frequency plane but should be reassigned to the new positions $\hat{t}(t, \Omega)$ and $\hat{\Omega}(t, \Omega)$, results in the reassigned spectrogram

$$SPEC_{\text{reassign}}(t, \Omega) = \int_{-\infty}^{\infty} \int_{-\infty}^{\infty} SPEC(u, v) \delta(t - \hat{t}(u, v)) \delta(\Omega - \hat{\Omega}(u, v)) dudv. \quad (3.174)$$

The reassigned form of a distribution from the Cohen class $CD(t, \Omega)$, introduced by Flandrin et al. is defined by

$$RTF(t, \Omega) = \int_{-\infty}^{\infty} \int_{-\infty}^{\infty} CD(u, v) \delta(t - \hat{t}(u, v)) \delta(\Omega - \hat{\Omega}(u, v)) dudv, \quad (3.175)$$

where $\hat{t}(u, v)$ and $\hat{\Omega}(u, v)$ are time and frequency displacements defined, respectively, as:

$$\begin{aligned} \hat{t}(t, \Omega) &= t - \frac{\int_{-\infty}^{\infty} \int_{-\infty}^{\infty} u \Pi(u, v) WD(t-u, \Omega-v) dudv}{\int_{-\infty}^{\infty} \int_{-\infty}^{\infty} \Pi(u, v) WD(t-u, \Omega-v) dudv}, \\ \hat{\Omega}(t, \Omega) &= \Omega - \frac{\int_{-\infty}^{\infty} \int_{-\infty}^{\infty} v \Pi(u, v) WD(t-u, \Omega-v) dudv}{\int_{-\infty}^{\infty} \int_{-\infty}^{\infty} \Pi(u, v) WD(t-u, \Omega-v) dudv}, \end{aligned} \quad (3.176)$$

where $\Pi(t, \Omega)$ is the distribution kernel in the time-frequency domain, while $WD(t, \Omega)$ and $CD(t, \Omega)$ denote the Wigner distribution and a distribution from the Cohen class, respectively.

Here a reassigned distribution can also be understood as the one with the assigned values of the basic time-frequency representation to a center of gravity in the considered region.

The reassigned Cohen class based representations satisfy the following important properties.

1. **Time-frequency shift.** For a signal shifted in time and frequency $y(t) = x(t - t_0)e^{j\Omega_0 t}$, the reassigned representation is shifted version of the reassigned distribution of the original signal $x(t)$

$$RTF(t, \Omega) = RTF_x(t - t_0, \Omega - \Omega_0).$$

2. **Energy marginal.** For basic time-frequency representation satisfying

$$\frac{1}{2\pi} \int_{-\infty}^{\infty} \int_{-\infty}^{\infty} \Pi(t, \Omega) d\Omega = 1,$$

the reassigned distribution satisfies the energy property

$$\frac{1}{2\pi} \int_{-\infty}^{\infty} \int_{-\infty}^{\infty} RTF(t, \Omega) dt d\Omega = \int_{-\infty}^{\infty} |x(t)|^2 dt.$$

3. The reassigned representation is ideally concentrated for a linear frequency-modulated signal and a delta pulse. For a linear frequency-modulated signal $x(t) = A \exp(jat^2/2 + jbt)$ the frequency displacement is $\hat{\Omega}(t, \Omega) = b + \hat{a}(t, \Omega)$. Then the reassigned representation is

$$\begin{aligned} RTF(t, \Omega) &= \left(\frac{1}{2\pi} \int_{-\infty}^{\infty} \int_{-\infty}^{\infty} CD(u, v) \delta(t - \hat{t}(u, v)) du dv \right) \delta(\Omega - at - b) \\ &= G(t, \Omega) \delta(\Omega - at - b). \end{aligned}$$

For the delta impulse $x(t) = A\delta(t - t_0)$ the time displacement is $\hat{t}(t, \Omega) = t_0$. The reassigned representation is

$$RTF(t, \Omega) = \left(\frac{1}{2\pi} \int_{-\infty}^{\infty} \int_{-\infty}^{\infty} CD(u, v) \delta(t - \hat{\Omega}(u, v)) du dv \right) \delta(t - t_0).$$

4. **Reassigned Wigner distribution is the Wigner distribution itself.** For the Wigner distribution the time-frequency kernel is $\Pi(t, \Omega) = 2\pi\delta(t)\delta(\Omega)$. Then the displacements are:

$$\hat{t}(t, \Omega) = t - \frac{\int_{-\infty}^{\infty} \int_{-\infty}^{\infty} u \Pi(u, v) WD(t - u, \Omega - v) du dv}{2\pi WD(t, \Omega)} = t,$$

$$\hat{\Omega}(t, \Omega) = \Omega.$$

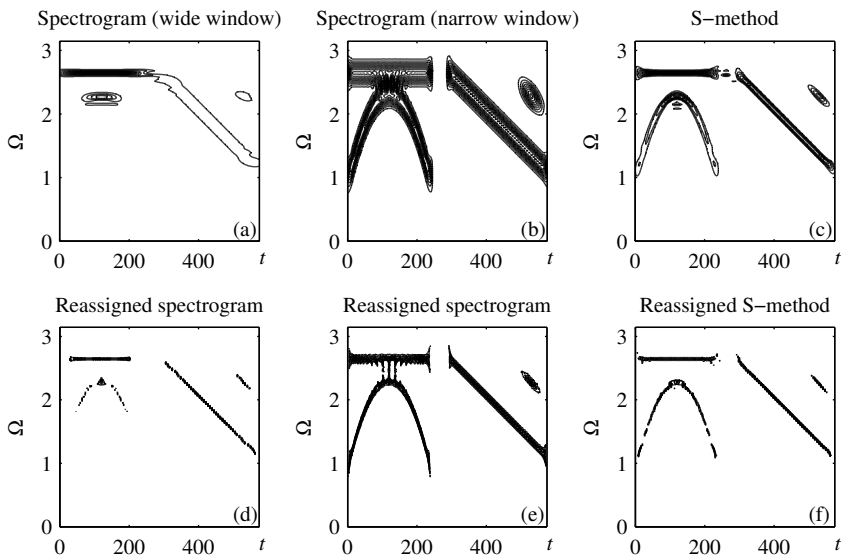


Figure 3.27 (a) The spectrogram with a wide window, (b) the spectrogram with a narrow window, (c) the S-method, (d) the reassigned spectrogram with a wide window (e) the reassigned spectrogram with a narrow window, and (f) the reassigned S-method .

Substituting these displacements into the reassignment method, the definition of the Wigner distribution easily follows.

The reassigned versions of the spectrogram for a wide and a narrow analysis window along with the reassigned S-method (see Problems 3.14) are presented in Fig. 3.27.

Example 3.24. Calculate the reassigned spectrogram of a signal

$$x(t) = e^{-4t^2} e^{j20t^2}$$

by using the Gaussian window $w(t) = e^{-20t^2}$. Find the spectrogram and the reassigned spectrogram for $t = 0$.

★ The spectrogram kernel in (t, Ω) domain is equal to the Wigner distribution of the analysis window $w(t)$

$$\Pi(t, \Omega) = \int_{-\infty}^{\infty} w(t + \tau/2)w(t - \tau/2)e^{-j\Omega\tau}d\tau = 2\sqrt{\frac{\pi}{40}}e^{-40t^2}e^{-\frac{\Omega^2}{40}}.$$

The Wigner distribution of $x(t)$, according to (3.21), is

$$WD(t, \Omega) = 2e^{-8t^2}\sqrt{\frac{\pi}{8}}e^{-\frac{(\Omega-40t)^2}{8}},$$

and the spectrogram follows as

$$\begin{aligned} SPEC(t, \Omega) &= \frac{1}{2\pi} \int_{-\infty}^{\infty} \int_{-\infty}^{\infty} \Pi(u, v) WD(t-u, \Omega-v) du dv \\ &= \frac{\pi}{4\sqrt{61}} e^{-\frac{1}{61}(1240t^2 + \frac{3}{4}\Omega^2 - 50\Omega t)}. \end{aligned}$$

Time and frequency displacements are

$$\begin{aligned} \hat{t}(t, \Omega) &= \frac{30}{61}t + \frac{5}{488}\Omega \\ \hat{\Omega}(t, \Omega) &= \frac{31}{61}\Omega + \frac{1000}{61}t. \end{aligned}$$

The reassigned spectrogram of the considered signal is obtained as

$$\begin{aligned} RTF(t, \Omega) &= \int_{-\infty}^{\infty} \int_{-\infty}^{\infty} SPEC(u, v) \delta(t - \hat{t}(u, v)) \delta(\Omega - \hat{\Omega}(u, v)) du dv \\ &= \frac{\pi}{4\sqrt{61}} e^{-(\frac{11448}{5}t^2 + \frac{11}{8}\Omega^2 - 112\Omega t)}. \end{aligned} \quad (3.177)$$

The spectrogram and its reassigned version are presented in Fig. 3.28. For $t = 0$ we have

$$SPEC(0, \Omega) = \frac{\pi}{4\sqrt{61}} e^{-\frac{3}{244}\Omega^2}, \quad RTF(0, \Omega) = \frac{\pi}{4\sqrt{61}} e^{-\frac{11}{8}\Omega^2}.$$

The same result can be obtained by using (3.171). □

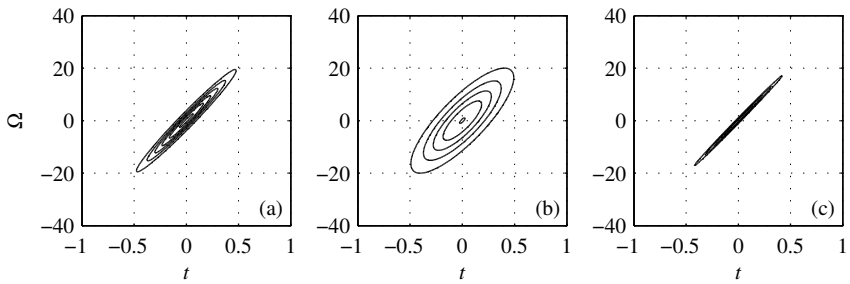


Figure 3.28 (a) The Wigner distribution, (b) the spectrogram, and (c) the reassigned spectrogram of a Gaussian chirp.

3.10 AFFINE CLASS OF TIME-FREQUENCY REPRESENTATIONS

Time-scale distributions or time-frequency representations that are covariant to scale changes and time translations,

$$\begin{aligned} y(t) &= \frac{1}{\sqrt{|a|}} x\left(\frac{\tau-t}{a}\right) \\ TFD_y(t, \Omega) &= TFD_x\left(\frac{\tau-t}{a}, \Omega a\right) \end{aligned} \quad (3.178)$$

belong to the affine class of distributions. Representations from the affine class may be written in the forms similar to the Cohen class of distributions. The simplest time-scale representation is the continuous wavelet transform. It is a linear expansion of the signal onto a set of analyzing functions. However, as it was explained, in time-frequency analysis applications the resolution of this transform limits its applications. We presented the wavelet transform of a linear frequency-modulated signal in Fig. 2.18.

In order to improve concentration and to satisfy some other desirable properties of a time-frequency representation, the quadratic affine distributions are introduced. They can be expressed as a function of any time-frequency distribution (as in the Cohen class of time-frequency distributions). Taking the Wigner distribution

as the central one, we can write

$$\begin{aligned}
 AD(t, \Omega) &= \frac{1}{2\pi} \int_{-\infty}^{\infty} \int_{-\infty}^{\infty} AF(\tau, \theta) c(\Omega\tau, \theta/\Omega) e^{-j\theta t} d\theta d\tau \\
 &= \frac{1}{2\pi} \int_{-\infty}^{\infty} \int_{-\infty}^{\infty} \int_{-\infty}^{\infty} x\left(u + \frac{\tau}{2}\right) x^*\left(u - \frac{\tau}{2}\right) c(\Omega\tau, \theta/\Omega) e^{ju\theta} e^{-j\theta t} du d\theta d\tau \\
 &= \frac{1}{2\pi} \int_{-\infty}^{\infty} \int_{-\infty}^{\infty} WD(\lambda, \mu) \Pi(\Omega(\lambda - t), \mu/\Omega) d\lambda d\mu
 \end{aligned} \tag{3.179}$$

The scalogram and the affine Wigner distributions belong to the affine class. Note that the scalogram in this sense is the Wigner distribution smoothed by the Wigner distribution of the basis function ψ

$$AD(t, \Omega) = \frac{1}{2\pi} \int_{-\infty}^{\infty} \int_{-\infty}^{\infty} WD(\lambda, \mu) WD_\psi(\Omega(\lambda - t), \mu/\Omega) d\lambda d\mu. \tag{3.180}$$

Because of the scale covariance property, many time-frequency representations in the affine class exhibit constant-Q behavior, permitting multiresolution analysis.

The time-scale pseudo Wigner distribution is defined by

$$WDT(t, a) = \int_{-\infty}^{\infty} w_0(\tau/a) x\left(t + \frac{\tau}{2}\right) x^*\left(t - \frac{\tau}{2}\right) e^{-j\Omega_0\tau/a} d\tau, \tag{3.181}$$

where $a = \Omega_0/\Omega$. The presented Wigner distribution definition means that the local auto-correlation function $x(t + \tau/2)x^*(t - \tau/2)$ is expanded onto the basis functions

$$h\left(\frac{\tau}{a}\right) = w\left(\frac{\tau}{a}\right) e^{j\Omega_0\tau/a}.$$

Pseudo affine Wigner distribution can be calculated by using the S-method with reduced interferences. The pseudo affine Wigner distribution may be written as

$$WDT(t, \Omega) = \int_{-\infty}^{\infty} w\left(\frac{\tau}{2\Omega_0}\Omega\right) w\left(-\frac{\tau}{2\Omega_0}\Omega\right) x\left(t + \frac{\tau}{2}\right) x^*\left(t - \frac{\tau}{2}\right) e^{-j\Omega\tau} d\tau. \tag{3.182}$$

The affine S-method form reads

$$SM(t, \Omega) = 2 \int_{-\infty}^{\infty} P(\theta) WT(t, \Omega; \Omega_0 + \theta) WT^*(t, \Omega; \Omega_0 - \theta) d\theta, \quad (3.183)$$

where $WT(t, \Omega; \Omega_0)$ is the wavelet transform calculated with

$$\begin{aligned} h(t) &= w(t) \exp(j2\pi(\Omega_0)t). \\ WT(t, \Omega) &= \int_{-\infty}^{\infty} x(\tau) h^*((\tau - t)\Omega/\Omega_0) d\tau / \sqrt{|\Omega_0/\Omega|}. \end{aligned}$$

with frequency being used instead of scale $a = \Omega_0/\Omega$.

If $P(\theta) = \delta(\theta)/2$, then $SM(t, \Omega)$ is equal to the scalogram of $x(t)$, while for $P(\theta) = 1$ it produces $WDT(t, \Omega)$ defined by (3.182). This form of the S-method has been extended to other time-scale representations.

3.11 PROBLEMS

Problem 3.1. Prove the time and frequency constraint properties for the Wigner distribution, stating that if $x(t) = 0$ for $|t| > T$, then also $WD_x(t, \Omega) = 0$ for $|t| > T$, and if $X(\Omega) = 0$ for $|\Omega| > \Omega_0$, then also $WD_x(t, \Omega) = 0$ for $|\Omega| > \Omega_0$. Show that these properties are satisfied for Cohen class of distributions if $c_T(t, \tau) = 0$ for $|t/\tau| > 1/2$ and $C_\Omega(\theta, \Omega) = 0$ for $|\Omega/\theta| > 1/2$.

Problem 3.2. Calculate the Wigner distribution of signal $x(t) = e^{j32\pi t^2} [u(t + 1/2) - u(t - 1/2)]$.

Problem 3.3. Calculate the Wigner distribution of signal $x(t) = e^{j3t^2 + jt} + e^{j3t^2 + j5t}$. Indicate the location of the auto-terms and cross-terms in the ambiguity domain. What would be an ideal form of the kernel that would preserve the marginal properties and the auto-term shape? Use the Choi-Williams kernel as a starting form. Repeat the same for the signal $x(t) = e^{j3t^2 + jt} + e^{j5t}$. Are the ambiguity axes cross-terms free?

Problem 3.4. Given a linear time-invariant system with impulse response $h(t) = \exp(j\alpha t^2/2)$. Find the Wigner distribution of the impulse response. If the input signal is $x(t) = \exp(-at^2/2)$, find the Wigner distribution of the input and output signal.

Problem 3.5. The Wigner distribution of a real-valued signal is usually calculated based on its analytic part. For a linear frequency-modulated signal

$$x(t) = e^{-\frac{1}{2}t^2/\alpha^2} e^{j(at^2+bt)}$$

find the condition which the positive real-valued constants α , a , and b must satisfy so that the absolute values of its Fourier transform does not differ from the absolute value of the positive frequency part of the Fourier transform, multiplied by 2 of the signal

$$x_r(t) = e^{-\frac{1}{2}t^2/\alpha^2} \cos(at^2 + bt)$$

for less than 0.67% (neglect values lower than e^{-5}).

Problem 3.6. Assume that the Rihaczek distribution is used as the basic one in the general class of quadratic distributions. Write the Wigner and Choi-Williams distribution kernels in the considered class. What would be the problem in expressing the Wigner distribution kernel if the Choi-Williams distribution is assumed as the basic one?

Problem 3.7. According to the Section 3.2.1 write the distribution that corresponds to the forward difference phase derivative estimator $\phi'(t) = (\phi(t + \tau) - \phi(t))/\tau$. Compare the obtained distribution with the Rihaczek distribution. Show that the mean of these two distributions satisfies the marginal properties and that it is real valued (this is the Margenau-Hill distribution). Find its kernel in the ambiguity domain.

Problem 3.8. Consider the two-dimensional function

$$P(t, \Omega) = ae^{-(at)^2} be^{-(b\Omega)^2}$$

where a and b are real positive constants. Check when $P(t, \Omega)$ is a valid Wigner distribution. Find $x(t)$ for real positive $x(0)$.

Problem 3.9. The Wigner distribution of a signal $x(t)$ is

$$WD(t, \Omega) = e^{-17t^2 - 8t\Omega - \Omega^2}.$$

Signal $y(t)$ is defined as $y(t) = [(x(t)e^{jt^2}) * (2e^{j2t^2})] e^{jt^2}$ where $*$ denotes convolution. Write the coordinate transform matrix \mathbf{L} and the Wigner distribution of the signal $y(t)$.

Problem 3.10. Show that the instantaneous frequency property for the Cohen class of distributions

$$\Omega(t) = \frac{\int_{-\infty}^{\infty} \Omega CD(t, \Omega) d\Omega}{\int_{-\infty}^{\infty} CD(t, \Omega) d\Omega}$$

of a signal $x(t) = A(t) \exp(j\phi(t))$, with $\Omega(t) = \phi'(t)$, is satisfied if

$$c(\theta, 0) = 1 \text{ and } \left. \frac{\partial c(\theta, \tau)}{\partial \tau} \right|_{\tau=0} = 0.$$

Problem 3.11. Show that the chirp product property in the Cohen class of distributions

$$CD_y(t, \Omega) = CD_x(t, \Omega - ct)$$

for

$$y(t) = x(t) e^{jct^2/2},$$

is satisfied if $c(\theta, \tau) = c(\theta + c\tau, \tau)$.

Problem 3.12. Define the distribution product kernel if we want the auto-term of the linear frequency-modulated signal to be of the triangular form.

Problem 3.13. Write the eigenvalue decomposition for the S-method and the smoothed spectrogram. What is the relation between the absolute values of the eigenvalues in these two cases?

Problem 3.14. Derive the formula for the S-method

$$SM_{w,w}(t, \omega) = \frac{1}{\pi} \int_{-\infty}^{\infty} P(\theta) STFT_w(t, \omega + \theta) STFT_w^*(t, \omega - \theta) d\theta,$$

reassignment in the time direction for a rectangular window $P(\theta)$. The indexes in $SM_{w,w}(t, \omega)$ denote the windows used in the corresponding STFT calculation.

Problem 3.15. Show that the instantaneous frequency of a signal could be reconstructed from the squared modulus of the fractional Fourier transform derivative (in numerical implementation, derivative means difference of two close projections of the fractional Fourier transform). When the instantaneous frequency and amplitude are reconstructed, then the solution of this problem is equivalent to reconstructing the Wigner distribution from two of its close projections.

Problem 3.16. Consider a multicomponent signal

$$x(t) = \exp(j680(t-0.1)^2) + 4\exp(-(150(t-0.8))^2 + j187.5t^2) + \exp(j1400t)$$

within $0.125 \leq t \leq 1$ with step $\Delta t = 0.02$ and window width $T = 0.25$. A new signal, without any amplitude variation, is formed by using an amplitude limiter as

$$x_0(t) = \exp(j\Phi(t))$$

where $\Phi(t)$ is the phase of the original signal $x(t) = |A(t)|\exp(j\Phi(t))$. Show the spectrogram and the S-method of these two signals. Discuss the result.

Problem 3.17. In an experiment, consider a pendulum, whose angular motion $\theta(t) = \theta_0 \cos(t\sqrt{g/l} + \phi_0)$ can be described in complex form as $s(t) = \theta_0 \exp(jt\sqrt{g/l} + j\phi_0)$. The pendulum is boxed in such way that we are able to observe its angle for a given instant(s) during a short time (lag) interval. The observed values, for given t , within $-T \leq \tau - t \leq T$, could be weighted by a function $w(\tau)$ before analysis.

(a) What is the uncertainty principle relation for time and oscillation frequency $\Omega_0 = \sqrt{g/l}$ localization? What is the uncertainty principle relation for time and the pendulum inverse squared root length $1/\sqrt{l}$ determination? What would be the uncertainty principle relation for time and inverse squared root length determination if the same pendulum system is observed, within the same lag intervals, in a room moving with a total acceleration $a = L^2 g$, $L > 1$? Write the corresponding observation relations and compare it with the S-distribution form.

(b) Assume now that the pendulum length changes in time as

$$l(t) = l_0 + kt,$$

when the angular motion is described by

$$\theta(t) = \frac{\theta_0}{\sqrt{l(t)}} J_1 \left(\frac{2\sqrt{gl(t)}}{k} \right) \cong \theta_0 \sqrt{\frac{k}{\pi l(t) \sqrt{gl(t)}}} \cos \left(\frac{2\sqrt{gl(t)}}{k} - 3\pi/4 \right)$$

for a large $2\sqrt{gl(t)}/k \gg 1$, where $J_1(t)$ is the Bessel function, or by

$$\theta(t) \cong \theta_0(t) \cos \left(\frac{2\sqrt{g}}{k} \left(\sqrt{l_0} + \frac{k}{2\sqrt{l_0}} t - \frac{1}{4} \frac{k^2}{\sqrt{l_0^3}} t^2 / 2 + \dots \right) - 3\pi/4 \right),$$

since

$$\sqrt{l_0 + kt} = \sqrt{l_0} + \frac{1}{2\sqrt{l_0}}kt - \frac{1}{4\sqrt{l_0^3}}(kt)^2/2 + \dots$$

How will the acceleration $a = L^2g$, $L > 1$, influence the instantaneous frequency analysis of the pendulum, in this case?

Problem 3.18. Write the function for the pseudo Wigner distribution calculation of a given signal x and window w . Assume that the window length is odd.

Problem 3.19. Using the function from Problem 3.18, calculate the pseudo Wigner distribution of the analytic part of the signal $x_1(t)$ defined in Example 2.2 by using the Hann(ing) window with 129 samples. Check the realness of the pseudo Wigner distribution. Identify the auto-terms and the cross-terms.

Problem 3.20. For a given STFT matrix ST and a given number of correction terms L write the function for the S-method calculation.

Problem 3.21. Write code for the S-method calculation, using $L = 2$, of the signal $x_1(t)$ defined in Example 2.2. Assume that the STFT is calculated with a 128 points Hann(ing) window with time step of 1.

Problem 3.22. Write code for the calculation of the Choi-Williams distribution using kernel decomposition approach. Use the analytic signal obtained from $x_1(t)$ defined in Example 2.2. Define the kernel in a function file so that it can easily be changed for any other distribution calculation.

Problem 3.23. Calculate the Choi-Williams distribution as a convolution of Wigner distribution and kernel in the time-frequency domain. Assume that the kernel is given in the θ - τ domain. Use the analytic signal derived from the signal $x_1(t)$ defined in Example 2.2.

Problem 3.24. Write code for multicomponent signal decomposition described in Section 3.8.3. Consider a seven-component signal defined in Example 3.21. Plot component eigenvalues and the reconstructed third component.

Problem 3.25. Given a two-dimensional function

$$WD_0(t, \Omega) = \exp\left(-\left(\frac{1}{4}t - \frac{32}{\pi}\Omega\right)^4 - \left(\frac{1}{32}t\right)^4\right)$$

write a code to calculate a signal whose Wigner distribution will correspond to the given two-dimensional function with a minimal mean square error.

3.12 SOLUTIONS

Solution 3.1. For the Wigner distribution

$$WD(t, \Omega) = \int_{-\infty}^{\infty} x(t + \tau/2)x^*(t - \tau/2)e^{-j\Omega\tau}d\tau$$

its value is different from zero if $x(t) = 0$ for $|t| > T$, when

$$-T \leq t + \tau/2 \leq T \quad \text{and} \quad -T \leq t - \tau/2 \leq T$$

resulting in

$$-2T \leq 2t \leq 2T.$$

The same holds for the frequency-domain relation

$$WD(t, \Omega) = \int_{-\infty}^{\infty} X(\Omega + \theta/2)X^*(\Omega - \theta/2)e^{j\theta t}d\theta.$$

For the Cohen class of distributions in the time-lag domain

$$CD(t, \Omega) = \int_{-\infty}^{\infty} \int_{-\infty}^{\infty} c_T(t - u, \tau)x(u + \tau/2)x^*(u - \tau/2)e^{-j\Omega\tau}d\tau du$$

if $x(t) = 0$ for $|t| > T$, then we can consider the above relation as a convolution of $c_T(t, \tau)$ and $x(t + \tau/2)x^*(t - \tau/2)$ in t thus, the sum of durations of term $x(t + \tau/2)x^*(t - \tau/2)$

$$-T \leq t + \tau/2 \leq T \quad \text{and} \quad -T \leq t - \tau/2 \leq T.$$

and term $c_T(t, \tau)$, for a given τ . Since the duration of $x(t + \tau/2)x^*(t - \tau/2)$ is $|t| \leq T - |\tau/2|$ the duration of, $c_T(t, \tau)$ could be $|t| \leq |\tau|/2$. Therefore, $c_T(t, \tau) = 0$ for $|t/\tau| > 1/2$.

A similar conclusion follows from the frequency-domain analysis.

Solution 3.2. The Wigner distribution of this signal is

$$WD(t, \Omega) = \int_{-\infty}^{\infty} e^{j64\pi t\tau} R_u(t, \tau) e^{-j\Omega\tau} d\tau$$

where

$$R_u(t, \tau) = [u(t + \tau/2 + \frac{1}{2}) - u(t + \tau/2 - \frac{1}{2})][u(t - \tau/2 + \frac{1}{2}) - u(t - \tau/2 - \frac{1}{2})].$$

The Fourier transform of $e^{j64\pi t\tau}$ is $2\pi\delta(\Omega - 64\pi t)$ while the Fourier transform of $R_u(t, \tau)$ is already calculated. It is

$$WD_u(t, \Omega) = \begin{cases} \frac{2\sin(2\Omega(1/2 - |t|))}{\Omega} & \text{for } -1/2 < t < 1/2 \\ 0 & \text{elsewhere.} \end{cases}.$$

Thus, the Wigner distribution is

$$\begin{aligned} WD(t, \Omega) &= 2\pi\delta(\Omega - 64\pi t) *_{\Omega} WD_u(\Omega, t) \\ WD(t, \Omega) &= \begin{cases} \frac{2\sin(2(\Omega - 64\pi t)(1/2 - |t|))}{\Omega - 64\pi t} & \text{for } -1/2 < t < 1/2 \\ 0 & \text{elsewhere} \end{cases}. \end{aligned}$$

It is located around $\Omega = 64\pi t$. It is best concentrated at $t = 0$ and spreads as the absolute value of t increases toward $t = \pm 1/2$.

Solution 3.3. The Wigner distribution of signal $x(t) = e^{j3t^2 + jt} + e^{j3t^2 + j5t}$ is

$$\begin{aligned} WD(t, \Omega) &= \int_{-\infty}^{\infty} x(t + \tau/2)x^*(t - \tau/2)e^{-j\Omega\tau}d\tau \\ &= \int_{-\infty}^{\infty} [e^{j3(t+\tau/2)^2 + j(t+\tau/2)} + e^{j3(t+\tau/2)^2 + j5(t+\tau/2)}] \\ &\quad \times [e^{-j3(t-\tau/2)^2 - j(t-\tau/2)} + e^{-j3(t-\tau/2)^2 - j5(t-\tau/2)}]e^{-j\Omega\tau}d\tau. \end{aligned}$$

The auto-terms are

$$WD_{at}(t, \Omega) = 2\pi\delta(\Omega - 6t - 1) + 2\pi\delta(\Omega - 6t - 5).$$

The cross-terms are

$$WD_{ct}(t, \Omega) = 2\pi\delta(\Omega - 6t - 3)2\cos(4t).$$

The ambiguity function of this signal is

$$\begin{aligned} AF(\theta, \tau) &= \int_{-\infty}^{\infty} x(t + \tau/2)x^*(t - \tau/2)e^{-j\theta t} dt \\ &= \int_{-\infty}^{\infty} [e^{j3(t+\tau/2)^2+j(t+\tau/2)} + e^{j3(t+\tau/2)^2+j5(t+\tau/2)}] \\ &\quad \times [e^{-j3(t-\tau/2)^2-j(t-\tau/2)} + e^{-j3(t-\tau/2)^2-j5(t-\tau/2)}]e^{-j\theta t} dt. \end{aligned}$$

The auto-terms in the ambiguity domain are

$$AF_{at}(\theta, \tau) = 2\pi\delta(\theta - 6\tau)e^{j\tau} + 2\pi\delta(\theta - 6\tau)e^{j5\tau}.$$

The cross-terms in this domain are

$$AF_{ct}(\theta, \tau) = 2\pi\delta(\theta - 6\tau - 4)e^{j3\tau} + 2\pi\delta(\theta - 6\tau + 4)e^{j3\tau}.$$

In order to satisfy the marginal property the kernel has to be 1 along the θ and τ axis. In the Choi-Williams distribution this is achieved by

$$c(\theta, \tau) = e^{-\theta^2\tau^2/\sigma^2}.$$

In order to preserve the auto-terms, that are in this case located along $\theta = 6\tau$ we should modify the kernel as

$$c(\theta, \tau) = e^{-\theta^2\tau^2(\theta-6\tau)^2/\sigma^2}.$$

This kernel, in addition to the marginal properties, will satisfy the condition that

$$c(\theta, \tau)AF_{at}(\theta, \tau) = AF_{at}(\theta, \tau).$$

Since the cross-terms are dislocated from the axis $\theta = 0$, $\tau = 0$, and $\theta = 6$, if we assume a large value of σ , then

$$c(\theta, \tau)AF_{ct}(\theta, \tau) \cong 0.$$

The new, signal-dependent, time-frequency distribution is

$$C(t, \Omega) \cong 2\pi\delta(\Omega - 6t - 1) + 2\pi\delta(\Omega - 6t - 5).$$

The ambiguity axes are approximately cross-terms free. They contain a small amount of cross-terms that can be easily obtained from $AF_{ct}(\theta, 0) = 2\pi\delta(\theta - 4) + 2\pi\delta(\theta + 4)$ and $AF_{ct}(0, \tau) = 2\pi\delta(6\tau + 4)e^{j3\tau} + 2\pi\delta(6\tau - 4)e^{-j3\tau}$.

Solution 3.4. The Wigner distribution of the impulse response is

$$WD_h(t, \Omega) = 2\pi\delta(\Omega - \alpha t).$$

For the input signal we get

$$WD_x(t, \Omega) = 2\sqrt{\frac{\pi}{a}}e^{-at^2}e^{-\Omega^2/a}.$$

The Wigner distribution of the output signal is a convolution in time of the previous two,

$$WD_y(t, \Omega) = \int_{-\infty}^{\infty} WD_x(t - \tau, \Omega) WD_h(\tau, \Omega) d\tau = \frac{4\pi\sqrt{\pi/a}}{\alpha} e^{-a(\alpha t - \Omega)^2/\alpha^2} e^{-\Omega^2/a}.$$

Solution 3.5. The Fourier transform of $x(t)$ is (3.69)

$$X(\Omega) = \int_{-\infty}^{\infty} e^{-(1/(2\alpha^2) + ja)t^2} e^{-j(\Omega - b)t} dt = \sqrt{\frac{\pi}{\frac{1}{2\alpha^2} - ja}} \exp\left(\frac{-(\Omega - b)^2}{4(\frac{1}{2\alpha^2} - ja)}\right).$$

Its absolute value is

$$|X(\Omega)| = C \exp\left(\frac{-(\Omega - b)^2\alpha^2}{2(1 + 4\alpha^4a^2)}\right),$$

where C does not depend on frequency. The Fourier transform of $x_r(t)$ is

$$|X_r(\Omega)| \leq \frac{C}{2} \exp\left(\frac{-(\Omega - b)^2\alpha^2}{2(1 + 4\alpha^4a^2)}\right) + \frac{C}{2} \exp\left(\frac{-(\Omega + b)^2\alpha^2}{2(1 + 4\alpha^4a^2)}\right).$$

Obviously, $|X(\Omega)|$ and $2|X_r(\Omega)|$ differ for

$$|X_n(\Omega)| = C \exp\left(\frac{-(\Omega + b)^2\alpha^2}{2(1 + 4\alpha^4a^2)}\right).$$

The ratio of $C / |X_n(\Omega)|$ is greater than e^5 at $\Omega = 0$ for

$$b^2\alpha^2 > 10(1 + 4\alpha^4a^2).$$

The ratio increases as Ω increases. For time unlimited (pure) linear frequency-modulated signal, when $\alpha \rightarrow \infty$, we get $0 > 40a^2$, which cannot be satisfied for any a and b , except for a pure sinusoid, with $a = 0$, when $b^2\alpha^2 > 10$ should hold for a large α for almost any $b > 0$. For a modulated Gaussian signal, with $a = 0$, it is sufficient to have $b^2\alpha^2 > 10$.

Solution 3.6. The general relation for the Wigner distribution as a basis function is

$$AF_g(\theta, \tau) = c(\theta, \tau) \text{FT}_{t, \Omega}\{WD(t, \Omega)\} = c(\theta, \tau)AF(\theta, \tau).$$

We know that in this system the Rihaczek distribution has the kernel $c(\theta, \tau) = e^{-j\theta\tau/2}$, since

$$\begin{aligned} CD(t, \Omega) &= \frac{1}{2\pi} \int_{-\infty}^{\infty} \int_{-\infty}^{\infty} \int_{-\infty}^{\infty} e^{-j\theta\tau/2} x(u + \tau/2)x^*(u - \tau/2)e^{j\theta t - j\Omega\tau - j\theta u} du d\tau d\theta \\ &= \int_{-\infty}^{\infty} \int_{-\infty}^{\infty} \delta(t - \tau/2 - u)x(u + \tau/2)x^*(u - \tau/2)e^{-j\Omega\tau} du d\tau \\ &= \int_{-\infty}^{\infty} x(t)x^*(t - \tau)e^{-j\Omega\tau} d\tau. \end{aligned}$$

The Choi-Williams distribution has the kernel in the form $c(\theta, \tau) = e^{-\theta^2\tau^2/\sigma^2}$, by definition.

Obviously, if we take the Rihaczek distribution as the basic distribution,

$$CD(t, \Omega) = \frac{1}{2\pi} \int_{-\infty}^{\infty} \int_{-\infty}^{\infty} \int_{-\infty}^{\infty} c_1(\theta, \tau)x(u)x^*(u - \tau)e^{j\theta t - j\Omega\tau - j\theta u} du d\tau d\theta$$

then the Wigner distribution will have the kernel

$$c_{WD}(\theta, \tau) = e^{j\theta\tau/2}$$

while the Choi-Williams distribution will have the kernel

$$c_{CW}(\theta, \tau) = e^{j\theta\tau/2}e^{-\theta^2\tau^2/\sigma^2}.$$

If we assume the Choi-Williams distribution as the basic one, then the Wigner distribution should be obtained with the kernel $c(\theta, \tau) = e^{\theta^2 \tau^2 / \sigma^2}$. For the region where the Choi-Williams distribution reduced the terms, for $\theta^2 \tau^2 / \sigma^2 \gg 1$, it would mean that the Choi-Williams distribution form in the ambiguity domain should be multiplied with extremely large values $c(\theta, \tau) = e^{\theta^2 \tau^2 / \sigma^2}$ to get the Wigner distribution. This would significantly increase all kinds of errors and would not be acceptable. For the sinc distribution, when part of the ambiguity plane is multiplied by zero, recovery to the Wigner distribution would not be possible, even in theory.

Solution 3.7. In the considered case local, auto-correlation function is

$$R(t, \tau) = x(t + \tau)x^*(t)$$

and the corresponding distribution is

$$D(t, \Omega) = \int_{-\infty}^{\infty} x(t + \tau)x^*(t)e^{-j\Omega\tau} d\tau = x^*(t)X(\Omega)e^{j\Omega t} = RD^*(t, \Omega)$$

The obtained distribution is a complex-conjugated Rihaczek distribution.

The mean of the Rihaczek and this distribution is

$$\begin{aligned} & \frac{1}{2}[RD(t, \Omega) + D(t, \Omega)] = \frac{1}{2}[RD(t, \Omega) + RD^*(t, \Omega)] \\ &= \operatorname{Re}\left\{\int_{-\infty}^{\infty} x(t + \tau)x^*(t)e^{-j\Omega\tau} d\tau\right\} = \operatorname{Re}\{x^*(t)X(\Omega)e^{j\Omega t}\} = \operatorname{Re}\{x(t)X^*(\Omega)e^{-j\Omega t}\}. \end{aligned}$$

Its kernel (kernel of the Margenau-Hill distribution) is

$$c(\theta, \tau) = \frac{1}{2}[e^{j\theta\tau/2} + e^{-j\theta\tau/2}] = \cos(\theta\tau/2).$$

Obviously, it satisfies the marginal property conditions, $c(0, \tau) = c(\theta, 0) = 1$.

Solution 3.8. We have to check if

$$\frac{\partial^2 \ln [\rho(t_1, t_2)]}{\partial t_1 \partial t_2} = 0$$

where

$$\begin{aligned}\rho(t_1, t_2) &= \frac{1}{2\pi} \int_{-\infty}^{\infty} P\left(\frac{t_1+t_2}{2}, \Omega\right) e^{j\Omega(t_1-t_2)} d\Omega \\ &= \frac{1}{2\pi} \int_{-\infty}^{\infty} ae^{-(a(t_1+t_2))^2/4} be^{-(b\Omega)^2} e^{j\Omega(t_1-t_2)} d\Omega\end{aligned}$$

we get

$$\frac{\partial^2 \ln[\rho(t_1, t_2)]}{\partial t_1 \partial t_2} = \frac{1}{2} \left(\frac{1}{b^2} - a^2 \right)$$

and finally $P(t, \Omega)$ is the Wigner distribution if $a = 1/b$. The signal follows from

$$\rho(t_1, t_2) = x(t_1)x^*(t_2)$$

with $|x(0)| = x(0)$.

Solution 3.9. The coordinate transform matrix, for the signal $y(t) = [(x(t)e^{jt^2}) * (2e^{j2t^2})] e^{jt^2}$, is

$$\mathbf{L} = \begin{bmatrix} 1 & 0 \\ -2 & 1 \end{bmatrix} \begin{bmatrix} 1 & -1/4 \\ 0 & 1 \end{bmatrix} \begin{bmatrix} 1 & 0 \\ -2 & 1 \end{bmatrix} = \begin{bmatrix} 3/2 & -1/4 \\ -5 & 3/2 \end{bmatrix}$$

Now we can calculate the Wigner distribution of $y(t)$ as

$$WD_y(t, \Omega) = WD\left(\frac{3}{2}t - \frac{1}{4}\Omega, -5t + \frac{3}{2}\Omega\right) = e^{-\frac{13}{4}t^2 - \frac{1}{4}t\Omega - \frac{5}{16}\Omega^2}.$$

For further work, we suggest to the reader to find a linear transformation which produces a separable coordinate form of the Wigner distribution and to calculate products of effective duration measures in time and frequency, in all cases. When this product is minimal?

Solution 3.10. The Cohen class of distributions may be written as

$$CD(t, \Omega) = \int_{-\infty}^{\infty} R_{CD}(t, \tau) e^{-j\Omega\tau} d\tau = \text{FT}\{c_T(t, \tau) *_t R(t, \tau)\}$$

with

$$R_{CD}(t, \tau) = \frac{1}{2\pi} \int_{-\infty}^{\infty} CD(t, \Omega) e^{j\Omega\tau} d\Omega$$

$$\frac{\partial R_{CD}(t, \tau)}{\partial \tau} = \frac{1}{2\pi} \int_{-\infty}^{\infty} j\Omega CD(t, \Omega) e^{j\Omega\tau} d\Omega.$$

Therefore,

$$\Omega(t) = \frac{-j \frac{\partial R_{CD}(t, \tau)}{\partial \tau}|_{\tau=0}}{R_{CD}(t, 0)} = -j \frac{\frac{\partial c_T(t, \tau)}{\partial \tau}|_{\tau=0} *_t R(t, 0) + c_T(t, 0) *_t \frac{\partial R(t, \tau)}{\partial \tau}|_{\tau=0}}{R_{CD}(t, 0)}$$

with the kernel relation $c_T(t, \tau) = \frac{1}{2\pi} \int_{-\infty}^{\infty} c(\theta, \tau) e^{j\theta t} d\theta$, the condition $\frac{\partial c(\theta, \tau)}{\partial \tau}|_{\tau=0} = 0$ means $\frac{\partial c_T(t, \tau)}{\partial \tau}|_{\tau=0} = 0$, producing

$$\frac{\partial c_T(t, \tau)}{\partial \tau}|_{\tau=0} *_t R(t, 0) = 0,$$

while for $c(\theta, 0) = \int_{-\infty}^{\infty} c_T(t, 0) e^{j\theta t} dt = 1$, obviously $c_T(t, 0) = \delta(t)$, with

$$c_T(t, 0) *_t \frac{\partial R(t, \tau)}{\partial \tau}|_{\tau=0} = \frac{\partial R(t, \tau)}{\partial \tau}|_{\tau=0}.$$

So, we get

$$\Omega(t) = -j \frac{\frac{\partial R(t, \tau)}{\partial \tau}|_{\tau=0}}{|x(t)|^2}.$$

with $R_{CD}(t, 0) = c(\theta, 0) |x(t)|^2 = A^2(t)$. From the Wigner distribution properties we know that

$$\frac{\partial R(t, \tau)}{\partial \tau}|_{\tau=0} = j\phi'(t)A^2(t),$$

resulting in

$$\Omega(t) = \phi'(t).$$

Solution 3.11. The Cohen class of distributions of a signal $y(t) = x(t)e^{jat^2/2}$ is

$$\begin{aligned} CD_y(t, \Omega) &= \frac{1}{2\pi} \int_{-\infty}^{\infty} \int_{-\infty}^{\infty} \int_{-\infty}^{\infty} c(\theta, \tau) e^{jau\tau} x(u + \tau/2) x^*(u - \tau/2) e^{j\theta t - j\Omega\tau - j\theta u} du d\tau d\theta \\ &= \frac{1}{2\pi} \int_{-\infty}^{\infty} \int_{-\infty}^{\infty} \int_{-\infty}^{\infty} c(\theta, \tau) x(u + \tau/2) x^*(u - \tau/2) e^{j\theta t - j\Omega\tau - j(\theta - a\tau)u} du d\tau d\theta \end{aligned}$$

with a change of variables $\theta - a\tau = \vartheta$ follows

$$\begin{aligned} CD_y(t, \Omega) &= \frac{1}{2\pi} \int_{-\infty}^{\infty} \int_{-\infty}^{\infty} \int_{-\infty}^{\infty} c(\vartheta + a\tau, \tau) x\left(u + \frac{\tau}{2}\right) x^*\left(u - \frac{\tau}{2}\right) \\ &\quad \times e^{j\vartheta t - j(\Omega - at)\tau - j\vartheta u} du d\tau d\vartheta = CD_x(t, \Omega - at) \end{aligned}$$

if $c(\theta + a\tau, \tau) = c(\theta, \tau)$.

Solution 3.12. If $C(\Omega)$ is a given auto-term function, for the linear frequency modulated signal $x(t) = \exp(jat^2/2 + jbt)$, then the product kernel $c(\theta, \tau) = c(\theta\tau)$, which will produce this auto-term form, is defined by

$$\begin{aligned} CD(t, \Omega) &= \frac{1}{2\pi} \int_{-\infty}^{\infty} \int_{-\infty}^{\infty} \int_{-\infty}^{\infty} c(\theta\tau) e^{jau\tau + jb\tau} e^{j\theta t - j\Omega\tau - j\theta u} du d\tau d\theta \\ &= \int_{-\infty}^{\infty} \int_{-\infty}^{\infty} c(\theta\tau) \delta(a\tau - \theta) e^{jb\tau} e^{j\theta t - j\Omega\tau} d\tau d\theta = \int_{-\infty}^{\infty} c(a\tau^2) e^{j(b+at)\tau} e^{-j\Omega\tau} d\tau \\ &= C(\Omega - (b + at)) \end{aligned}$$

with

$$c(\theta\tau) = \frac{1}{2\pi} \int_{-\infty}^{\infty} C(\Omega) e^{j\Omega\tau} d\Omega \Big|_{a\tau^2 \rightarrow \theta\tau}$$

where a is the instantaneous frequency coefficient in $x(t)$. Assume $a = 1$, without loss of generality. For the triangular auto term function $C(\Omega) = k(1 - |\Omega|)$ for $|\Omega| < 1$ and $C(\Omega) = 0$ elsewhere (coefficient k will follow from the condition that $c(0, 0) = 1$), we get

$$c(\theta\tau) = \frac{\sin^2(\sqrt{|\theta\tau|/2})}{|\theta\tau|/2}. \quad (3.184)$$

This kernel decreases in (θ, τ) plane as $1/|\theta\tau|$.

Solution 3.13. Hint: Use the fact that the inner product kernel $G_T(v_1, v_2)$ in the S-method is factorized in the Hankel form

$$c_T \left(-\frac{v_1 + v_2}{2}, v_1 - v_2 \right) = G_T(v_1, v_2) = 2w(v_1)p(v_1 + v_2)w(v_2).$$

The Toeplitz factorization of the kernel

$$c_T \left(-\frac{v_1 + v_2}{2}, v_1 - v_2 \right) = G_T(v_1, v_2) = 2w(v_1)p(v_1 - v_2)w(v_2)$$

results in the smoothed spectrogram. These are the matrices whose eigenvalues decomposition is to be found. In addition, the window $p(v)$ is the inverse Fourier transform of the rectangular window with L samples.

Solution 3.14. The reassignment steps in the time and frequency domain are defined by

$$\begin{aligned} \hat{t}(t, \Omega) &= t + \operatorname{Re} \left\{ \frac{SM_{\tau w, w}(t, \Omega)}{SM_{w, w}(t, \Omega)} \right\} \\ \hat{\Omega}(t, \Omega) &= \Omega - \operatorname{Im} \left\{ \frac{SM_{D_w, w}(t, \Omega)}{SM_{w, w}(t, \Omega)} \right\} \end{aligned}$$

where

$$\tau w \rightarrow \tau w(\tau), D_w \rightarrow \partial w(\tau)/\partial \tau$$

and

$$STFT_w(t, \Omega) = \int_{-\infty}^{\infty} x(t + \tau)w(\tau)e^{-j\Omega\tau}d\tau.$$

The S-method kernel in the time-frequency domain is $2p(2t)WD_w(t, \Omega)$, where $WD_w(t, \Omega)$ is the Wigner distribution of the lag window and $p(t)$ is the inverse Fourier transform of the S-method window $P(\theta)$. Thus, from the general reassignment formula (3.176) follows that the S-method based reassignment in time is proportional to the S-method calculated with the window $2tp(2t)$ of $dP(\theta)/d\theta/2$ in the S-method definition. If the frequency-domain window $P(\theta)$ is rectangular, of the width $2\theta_p$, then, from

$$\int_{-\infty}^{\infty} G(\Omega, t, \theta) \frac{dP(\theta)}{d\theta} d\theta = G(\Omega, t, -\theta_p) - G(\Omega, t, \theta_p),$$

follows

$$\hat{t}(t, \Omega) = t + \text{Im} \left\{ \frac{\text{STFT}_w(t, \Omega + \theta_p) \text{STFT}_w^*(t, \Omega - \theta_p)}{\text{SM}_{w,w}(t, \Omega)} \right\}. \quad (3.185)$$

If for a time-frequency point (t, Ω) the window width wider than the auto-term width is used in $\text{STFT}_w(t, \Omega)$ then $\text{STFT}_w(t, \Omega + \theta_p) \text{STFT}_w^*(t, \Omega - \theta_p) = 0$ and $\hat{t}(t, \Omega) = t$, as expected. The S-method is then locally equal to the Wigner distribution, when no correction is to be done, within an auto-term. It proves once more that the S-method is locally equal to the Wigner distribution.

One of the simplest forms of a reassigned distribution would be to use time domain only reassigned S-method as

$$\text{SM}_{\text{reassign}}(t, \Omega) = \int_{-\infty}^{\infty} \text{SM}(u, v) \delta(t - \hat{t}(u, v)) du,$$

with $\hat{t}(t, \Omega)$ as in (3.185).

Using recursive realization of the STFT, it can be implemented online or in real time by an appropriate hardware structure.

Solution 3.15. The instantaneous frequency can be written as

$$\Omega_0(t) = \frac{\int_{-\infty}^{\infty} \Omega \text{WD}(t, \Omega) d\Omega}{\int_{-\infty}^{\infty} \text{WD}(t, \Omega) d\Omega}.$$

Consider now the Wigner distribution $\text{WD}_{X_\alpha}(t, \Omega)$ of a fractional Fourier transform of $x(t)$ denoted by $X_\alpha(t)$. It is related to the Wigner distribution of $x(t)$ through rotation. Its projection (marginal property) is

$$\frac{1}{2\pi} \int_{-\infty}^{\infty} \text{WD}_{X_\alpha}(t, \Omega) d\Omega = |X_\alpha(t)|^2.$$

The ambiguity function of $X_\alpha(t)$ is the two-dimensional Fourier transform of the Wigner distribution

$$AF_{X_\alpha}(\theta, \tau) = \frac{1}{2\pi} \int_{-\infty}^{\infty} \int_{-\infty}^{\infty} \text{WD}_{X_\alpha}(t, \Omega) e^{-j(\theta t - \Omega \tau)} dt d\Omega.$$

We can also write

$$\begin{aligned} \int_{-\infty}^{\infty} WD_{X_\alpha}(t, \Omega) e^{j\Omega\tau} d\Omega &= \int_{-\infty}^{\infty} AF_{X_\alpha}(\theta, \tau) e^{j\theta t} d\theta \\ \int_{-\infty}^{\infty} j\Omega WD_{X_\alpha}(t, \Omega) d\Omega &= \frac{\partial}{\partial \tau} \int_{-\infty}^{\infty} AF_{X_\alpha}(\theta, \tau) e^{j\theta t} d\theta|_{\tau=0} \\ AF_{X_\alpha}(\theta, \tau)|_{\tau=0} &= \frac{1}{2\pi} \int_{-\infty}^{\infty} \int_{-\infty}^{\infty} WD_{X_\alpha}(t, \Omega) d\Omega e^{-j\theta t} dt = \int_{-\infty}^{\infty} |X_\alpha(t)|^2 e^{-j\theta t} dt. \end{aligned} \quad (3.186)$$

Therefore,

$$\Omega_0(t) = \frac{\int_{-\infty}^{\infty} \Omega WD(t, \Omega) d\Omega}{2\pi |x(t)|^2} = \frac{1}{j2\pi |x(t)|^2} \int_{-\infty}^{\infty} \frac{\partial AF_{X_\alpha}(\theta, \tau)}{\partial \tau} e^{j\theta t} d\theta \Big|_{\tau=0}. \quad (3.187)$$

Consider values close to $\tau = 0$ and arbitrary θ . A small change in α corresponds to a small rotation of τ axis. Thus, for values close to $\tau = 0$ the change in τ , caused by a small rotation, is $d\tau = \theta d\alpha$. It means that

$$\frac{\partial AF_{X_\alpha}(\theta, \tau)}{\partial \tau} = \frac{\partial AF_{X_\alpha}(\theta, \tau)}{\partial \alpha} \frac{d\alpha}{d\tau} = \frac{\partial AF_{X_\alpha}(\theta, \tau)}{\theta \partial \alpha}$$

for τ and α close to $\tau = 0$ and $\alpha = 0$

or, according to (3.186),

$$\frac{\partial AF_{X_\alpha}(\theta, \tau)}{\partial \tau} \Big|_{\tau=0} = \frac{\partial}{\theta \partial \alpha} \int_{-\infty}^{\infty} |X_\alpha(t)|^2 e^{-j\theta t} dt \Big|_{\alpha=0}$$

resulting in, (3.187),

$$\Omega_0(t) = \frac{1}{j2\pi |x(t)|^2} \int_{-\infty}^{\infty} \int_{-\infty}^{\infty} \frac{1}{\theta} \frac{\partial |X_\alpha(u)|^2}{\partial \alpha} e^{-j\theta u} e^{j\theta t} du d\theta|_{\alpha=0}$$

Taking into account that $\Omega_0(t)$ assumes real values, with $|x(t)| = |X_0(t)|$, we get

$$\Omega_0(t) = \frac{1}{2\pi |X_0(t)|^2} \int_{-\infty}^{\infty} \int_{-\infty}^{\infty} \frac{\partial |X_\alpha(u)|^2}{\partial \alpha} \Bigg|_{\alpha=0} \frac{\sin(\theta(t-u))}{\theta} du d\theta.$$

Supposing that the derivative of the fractional power spectra is a continuous function of u , we change the order of integration. Then we obtain that

$$\begin{aligned}\Omega_0(t) &= \frac{1}{2|X_0(t)|^2} \int_{-\infty}^{\infty} \left. \frac{\partial |X_\alpha(u)|^2}{\partial \alpha} \right|_{\alpha=0} \operatorname{sgn}(t-u) du, \\ &= \frac{1}{2|X_0(t)|^2} \left[\left. \frac{\partial |X_\alpha(t)|^2}{\partial \alpha} \right|_{\alpha=0} *_t \operatorname{sgn}(t) \right]\end{aligned}$$

where $\operatorname{sgn}(t)$ is

$$\frac{1}{\pi} \int_{-\infty}^{\infty} \frac{\sin(\theta t)}{\theta} d\theta = \operatorname{sgn}(t) = \begin{cases} 1 & \text{for } t > 0, \\ 0 & \text{for } t = 0, \\ -1 & \text{for } t < 0. \end{cases} \quad (3.188)$$

since

$$\begin{aligned}\int_{-\infty}^{\infty} \operatorname{sgn}(t) e^{-j\Omega t} dt &= \lim_{\beta \rightarrow 0} \left(\int_{-\infty}^0 (-e^{\beta t}) e^{-j\Omega t} dt + \int_0^{\infty} e^{-\beta t} e^{-j\Omega t} dt \right) = \frac{2}{j\Omega} \\ \text{IFT}\left\{\frac{2}{j\Omega}\right\} &= \int_{-\infty}^{\infty} \frac{e^{j\Omega t}}{j\pi\Omega} d\Omega = \frac{1}{\pi} \int_{-\infty}^{\infty} \frac{\sin(\Omega t)}{\Omega} d\Omega = \operatorname{sgn}(t).\end{aligned}$$

Thus, we get for the signal $x(t) = |X_0(t)| \exp[j\varphi_0(t)]$, that its phase derivative $\varphi'_0(t) = d\varphi_0(t)/dt = \Omega_0(t)$ is determined by the fractional Fourier transform intensity $|X_0(t)|^2$ and the convolution of the signum function with the angular derivative of the fractional power spectrum $\partial |X_\alpha(u)|^2 / \partial \alpha$ at the angle $\alpha = 0$. This derivative can be approximated from two close values of $|X_\alpha(u)|^2$. Therefore, the signal phase can be reconstructed based on the two absolute values of the the fractional Fourier transform or two projections of the Wigner distribution, for two close angles.

The discrete reconstruction of the instantaneous frequency is

$$\Omega_0(n\Delta t) = \frac{\Delta t}{2|X_0(n\Delta t)|^2} \frac{\left[|X_\alpha(n\Delta t)|^2 - |X_{-\alpha}(n\Delta t)|^2 \right]}{2\alpha} *_n \operatorname{sgn}(n\Delta t),$$

resulting in the signal reconstruction

$$\hat{X}_0(n\Delta t) = |X_0(n\Delta t)| \exp \left[j \sum_{m=-M}^n \Omega_0(m\Delta t) \Delta t \right].$$

After we reconstruct the signal, up to the phase constant, the Wigner distribution, for all time and frequency points, can be calculated. The result can be easily generalized for any angle β

$$\Omega_\beta(t) = \frac{1}{2|X_\beta(t)|^2} \left[\frac{\partial |X_\alpha(t)|^2}{\partial \alpha} \Big|_{\alpha=\beta} *_t \text{sgn}(t) \right].$$

Solution 3.16. Time-frequency representations of the signal $x_0(t) = \exp(j\Phi(t))$ are given in Fig. 3.29. We leave to the reader to comment on how a signal with constant amplitude may behave as a multicomponent signal.

Solution 3.17. (a) The uncertainty principle for effective durations of windowed observations of pendulum angular motion in time and frequency is

$$\sigma_\Omega^2 \sigma_t^2 \geq \frac{1}{4},$$

For the inverse length $1/\sqrt{l}$ the uncertainty relation is obtained by using $\Omega = \sqrt{g/l}$ or $\sqrt{1/l} = \Omega/\sqrt{g}$ as

$$\sigma_{1/\sqrt{l}}^2 \sigma_t^2 = \frac{\sigma_\Omega^2 \sigma_t^2}{g} \geq \frac{1}{4g}. \quad (3.189)$$

If we observe the pendulum in a room with acceleration $a = L^2 g$, then the uncertainty relation for the inverse length $\sqrt{1/l}$ to time determination is

$$\sigma_{1/\sqrt{l}}^2 \sigma_t^2 \geq \frac{1}{4L^2 g}.$$

This uncertainty improvement, with respect to (3.189), can be explained by considering the angular movement $s_a(t + \tau)$ in the accelerating room. It is described as

$$\begin{aligned} s_a(t + \tau) w(\tau) &= \theta_0 \exp \left(j \left(\sqrt{\frac{a}{l}}(t + \tau) \right) + j\phi_0 \right) w(\tau) \\ &= \theta_0 \exp \left(j \sqrt{\frac{g}{l}} L \tau + j \sqrt{\frac{g}{l}} L t + j\phi_0 \right) w(\tau) \end{aligned}$$

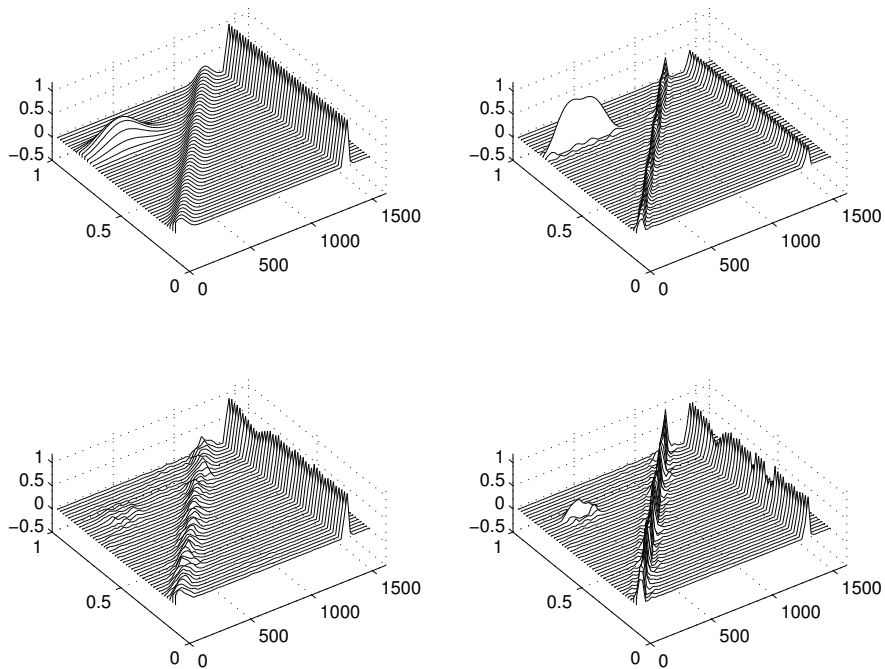


Figure 3.29 Time-frequency representation of the multicomponent signal by the spectrogram (left) and by the S-method (right). The original multicomponent signal $x(t) = |A(t)|\exp(j\Phi(t))$ is represented in the upper subplots, while the signal with a constant amplitude and phase from the original multicomponent signal $x_0(t) = \exp(j\Phi(t))$ is shown in the lower subplots.

$$\begin{aligned}
 STFT_a(t, \Omega) &= \int_{-\infty}^{\infty} \theta_0 \exp \left(j \sqrt{\frac{g}{l}} L \tau + j\phi(t) \right) w(\tau) e^{-jL\Omega\tau} d\tau \\
 &= \frac{1}{L} \int_{-\infty}^{\infty} \theta_0 \exp \left(jL \left[\sqrt{\frac{g}{l}} \frac{\tau}{L} + j\phi(t)/L \right] \right) w(\tau/L) e^{-j\Omega\tau} d\tau \\
 |STFT_a(t, \Omega)|^2 &= \frac{1}{L^2} \theta_0^2 W_{LT}^2 \left(\Omega - \sqrt{\frac{g}{l}} \right)
 \end{aligned}$$

where $W_{2LT}(\Omega)$ is the Fourier transform of $w(\tau/L)$, whose width in τ is $2LT$. A mathematical form of this transformation is the S-distribution form (in this case the S-short time Fourier transform)

$$\begin{aligned} STFT_L(t, \Omega) &= \int_{-\infty}^{\infty} w_L(\tau/L) x^{[L]}(t + \tau/L) e^{-j\Omega\tau} d\tau \\ &= \int_{-\infty}^{\infty} w\left(\frac{\tau}{L}\right) \theta_0 \exp(jL(\sqrt{\frac{g}{l}}\frac{\tau}{L} + j\phi(t)/L + j\phi_0/L)) e^{-j\Omega\tau} d\tau \\ |STFT_L(t, \Omega)|^2 &= \theta_0^2 W_{2LT}^2 \left(\Omega - \sqrt{\frac{g}{l}} \right). \end{aligned}$$

It reduces the uncertainty for L^2 . In theory, we transform a signal $x(t) = A \exp(j\varphi(t))$ to $x^{[L]}(t) = A \exp(jL\varphi(t/L))$. In this experimental observation of a pendulum, it means moving the pendulum to a observation room with acceleration a , such that $L = \sqrt{a/g}$.

Thus, we may conclude that keeping the same observation lag interval, that is, $w_L(\tau/L) = w(\tau/L)$, the frequency resolution of a constant frequency signal is improved, reducing the uncertainty relation. In the cases of a very small observation interval (lower than the oscillation of signal period), frequency is kept at the same position, while the observation interval is virtually increased (by oversampling in discrete realizations).

(b) Another point of view is when we can assume that the observation interval is large enough, however changes in the length $l(t)$ exists. For a linear length change $l(t) = l_0 + kt$, the angular motion is approximated by

$$\theta(t) \cong \theta_0(t) \cos \left(\frac{2\sqrt{g}}{k} \left(\sqrt{l_0} + \frac{k}{2\sqrt{l_0}} t - \frac{1}{4} \frac{k^2}{\sqrt{l_0^3}} t^2 / 2 + \dots \right) - 3\pi/4 \right).$$

Its complex form is

$$\theta \cong \theta_0(t) \exp \left(j \left(\sqrt{\frac{g}{l_0}} t - \frac{1}{2} \frac{k\sqrt{g}}{\sqrt{l_0^3}} t^2 / 2 + \dots \right) + j\phi_0 \right).$$

Then

$$\begin{aligned}
 s_a(t + \tau)w(\tau) &= \\
 &= \theta_0(t) \exp \left(j \left(\sqrt{\frac{a}{l_0}}(t + \tau) - \frac{1}{2} \frac{k\sqrt{a}}{\sqrt{l_0^3}}(t + \tau)^2/2 + \dots \right) + j\phi_0 \right) w(\tau) \\
 &= \theta_0(t) \exp \left(j \left(L \sqrt{\frac{g}{l_0}}(t + \tau) - \frac{1}{2} \frac{kL\sqrt{g}}{l_0\sqrt{l_0}}(t + \tau)^2/2 + \dots \right) + j\phi_0 \right) w(\tau),
 \end{aligned}$$

since we may assume that $\theta_0(t + \tau) \cong \theta_0(t)$. The Fourier transform of this signal, at frequency $L\Omega$, is

$$\begin{aligned}
 STFT_a(t, \Omega) &= \int_{-\infty}^{\infty} \theta_0(t) \exp \left(j \left[L \sqrt{\frac{g}{l_0}} \left(1 - \frac{1}{2} \frac{k}{l_0} t \right) \tau - \frac{1}{2} \frac{kL\sqrt{g}}{l_0\sqrt{l_0}} \tau^2/2 + \dots \right] + j\phi(t) \right) \\
 &\quad \times w(\tau) e^{-jL\Omega\tau} d\tau \\
 &= \frac{1}{L} \int_{-\infty}^{\infty} \theta_0(t) \exp \left(j \left[\sqrt{\frac{g}{l_0}} \left(1 - \frac{1}{2} \frac{k}{l_0} \right) \tau - \frac{1}{2} \frac{k\sqrt{g}}{l_0\sqrt{l_0}} \frac{\tau^2}{2L} + \dots \right] + j\phi(t) \right) w\left(\frac{\tau}{L}\right) e^{-j\Omega\tau} d\tau.
 \end{aligned}$$

If we keep the same number of samples in the analysis, that is, the same width for both $w(\tau)$ and $w_a(\tau/2)$, then we achieve

$$\begin{aligned}
 |STFT_a(t, \Omega)|^2 &= \frac{1}{L^2} \theta_0^2(t) W^2 \left(\Omega - \sqrt{\frac{g}{l_0}} \left(1 - \frac{1}{2} \frac{k}{l_0} \right) \right) \\
 &\quad *_{\Omega} \text{FT} \left\{ \exp \left(-j \frac{1}{2} \frac{k\sqrt{g}}{l_0\sqrt{l_0}} \tau^2 / (2L) \dots \right) \right\}.
 \end{aligned}$$

The spread factor is reduced L times with respect to the original STFT analysis, where

$$\begin{aligned}
 |STFT(t, \Omega)|^2 &= \theta_0^2(t) W^2 \left(\Omega - \sqrt{\frac{g}{l_0}} \left(1 - \frac{1}{2} \frac{k}{l_0} \right) \right) \\
 &\quad *_{\Omega} \text{FT} \left\{ \exp \left(-j \frac{1}{2} \frac{k\sqrt{g}}{l_0\sqrt{l_0}} \tau^2 / 2 \dots \right) \right\}.
 \end{aligned}$$

Thus, we can conclude that keeping the same number of samples in the new oversampled signal, $w_L(\tau/L) = w(\tau)$, the representation of a sinusoidal signal

will not change. However, nonlinearities in the signal instantaneous frequency are reduced by factor of $\sqrt{a/g} = L$, since the phase is locally linearized. (This effect will be used in the L-Wigner distribution realization examples in Chapter 4.)

It is possible to combine these two effects described in (a) and (b). For example, by using $L = 4$ with a double number of samples, we would increase the resolution of a sinusoid two times and also reduce nonlinearity effects by a factor of 2.

In this way, by analyzing the signal with S-distribution (similar results are obtained with the L-distributions), we may control in which way to improve the result, by selecting to keep the invariant observation time interval, with oversampling, or to keep the same number of samples.

Hint: The same analysis holds for a rotating point of mass m , with radius R , having in mind that momentum is constant, $m\Omega R = \text{const}$. Changing m , in the same geometric setup, we change the frequency and observation of, for example, $R(t)$.

Solution 3.18. One possible solution is

```
function PWD=PWD_calc(x,w)
M=length(x);
N=length(w);
N2=(N-1)/2;
t=N2+1:M-N2;
PWD=zeros(N,length(t));
tau=(-N2:N2);
for k=1:length(t)
    PWD(:,k)=w.*w.*x(t(k)+tau).*conj(x(t(k)-tau));
end
PWD=fft(ifftshift(PWD,1));
```

The pseudo Wigner distribution for each t is calculated as the Fourier transform over τ of $w(\tau/2)w(\tau/2)x(t + \tau/2)x^*(t - \tau/2)$. A symmetric window $w(-\tau/2) = w(\tau/2)$ is assumed.

In the case of an even number of samples, one of possible changes in order to get a real-valued pseudo Wigner distribution for a window with the first value in the vector $w(1) = 0$ (with symmetric rest values with respect to their central sample) is

```
function PWD=PWD_calc_E(x,w)
M=length(x);
N=length(w);
N2=N/2;
```

```

t=N2+1:M-N2;
PWD=zeros(N,length(t));
tau=(-N2:N2-1);
for k=1:length(t)
    xL=x(t(k)+tau);
    xLn=[xL(1); xL(N:-1:2)];
    PWD(:,k)=w.*w.*xL.*conj(xLn);
end
PWD=fft(ifftshift(PWD,1));

```

We leave to the reader to unify these two codes, into one by checking first if the lag window length is an odd or even number and then executing appropriate commands for these window lengths.

Solution 3.19. The considered problem can be solved as

```

t=(-32:(255+32))';
x1=sin(9*pi/16*t-pi/10/128*(t-128).^2-pi/2)+...
    sin(pi/18*t)+...
    1.2*sin(15*pi/16*t-pi/8/128*(t-128).^2-pi/2).*...
        exp(-((t-180)/40).^2)+...
    1.2*sin(4*pi/16*t-pi/32/128*(t-128).^2-pi/2).*...
        exp(-((t-64)/40).^2);
x=hilbert(x1);
PWD=PWD_calc(x,hanning(129));
imagesc(real(PWD))

```

The imaginary part of the pseudo Wigner distribution should be equal to 0. However, due to a numerical error, negligible values of the imaginary part are present in the results. Note that the maximal value of the imaginary part of the pseudo Wigner distribution compared to the maximal value of the pseudo Wigner distribution real part is of the order of numerical precision (10^{-16} for double precision).

Four auto-terms can be identified, corresponding to the constant frequency component, linear frequency-modulated component, and two Gaussian chirps. Five cross-terms could be seen. Note that there is no significant cross-term between Gaussian chirps since the applied time domain window was able to reduce (eliminate) them.

For an even number of samples, for example, 128, we should call

```
PWD=PWD_calc_E(x,hanning(128));
```

Solution 3.20. Assuming that rows correspond to frequency and columns correspond to time, the required function could be implemented as

```
function SM=SM_calc(ST,L)
N=size(ST,1);
SM=abs(ST).^2;
for k=1:L
    SM(1+k:N-k,:) = SM(1+k:N-k,:)+...
        2*real(ST(1:N-2*k,:).*conj(ST(1+2*k:N,:)));
end
```

Solution 3.21. The code reads:

```
t=(-64:(255+64))';
x1=sin(9*pi/16*t-pi/10/128*(t-128).^2-pi/2)+...
    sin(pi/18*t)+...
    1.2*sin(15*pi/16*t-pi/8/128*(t-128).^2-pi/2).*...
    exp(-((t-180)/40).^2)+...
    1.2*sin(4*pi/16*t-pi/32/128*(t-128).^2-pi/2).*...
    exp(-((t-64)/40).^2);
ST=STFT_calc(x1,hanning(128),1);
SM=SM_calc(ST,2);
imagesc(SM)
```

Solution 3.22. The main code reads:

```
% Signal definition
t=(0:(254))';
N=256;
x1=sin(9*pi/16*t-pi/10/128*(t-128).^2-pi/2)+...
    sin(pi/18*t)+...
    1.2*sin(15*pi/16*t-pi/8/128*(t-128).^2-pi/2).*...
    exp(-((t-180)/40).^2)+...
    1.2*sin(4*pi/16*t-pi/32/128*(t-128).^2-pi/2).*...
    exp(-((t-64)/40).^2);
x1=[zeros(127,1);x1;zeros(127,1)];
x=hilbert(x1);

CD=CD_KD(x,N);
```

```
imagesc(CD)
title(['CWD by using kernel decomposition'])
```

Supporting functions are:

```
function CD=CD_KD(x,N)
% Signal x, Kernel size (N+1)x(N+1)
% Kernel form is in function kernel.m
theta=-pi:2*pi/N:pi;
m=0;
for tau=-N/2:N/2; m=m+1;n=0;
    for t=-N/2:N/2; n=n+1;
        c=kernel(t-tau,theta);
        FS(m,n)=sum(c.*exp(-j*((t+tau)*theta)));
    end
end
[Q,L]=eig(real((FS)));
[p,ind]=sort(-abs(diag(L)));
% Distribution calculation
CD=0;
for p=1:length(diag(L))
    k=ind(p);
    SP=abs(STFT_calc(x,Q(:,k),1)).^2;
    CD=CD+L(k,k)*SP;
    % Eigenvalues squared not less than 1% of the
    % maximal eigenvalue are used in calculation
    if abs(L(k,k))<sqrt(0.01)*max(abs(diag(L)))
        break
    end
end

function CD=kernel(tau,theta)
CD=exp(-(tau.*theta/3).^2);
% Normalized region for -N/2<tau<N/2
% and -pi<theta<pi is used.
% The distribution parameter shoud be set
% to take this into account.
```

Solution 3.23. The code reads:

```

% Signal definition
t=(0:(254))';
x1=sin(9*pi/16*t-pi/10/128*(t-128).^2-pi/2)+...
    sin(pi/18*t)+...
    1.2*sin(15*pi/16*t-pi/8/128*(t-128).^2-pi/2).*...
        exp(-((t-180)/40).^2)+...
    1.2*sin(4*pi/16*t-pi/32/128*(t-128).^2-pi/2).*...
        exp(-((t-64)/40).^2);
x1=[zeros(127,1);x1;zeros(127,1)];
x=hilbert(x1);

% WD calculation
% (as PWD with long enough rectangular window)
WD=real(PWD_calc(x,ones(255,1)));

% Kernel definition
theta=(-127:127)*pi/127;
tau=-127:127;
[theta2,tau2]=meshgrid(theta,tau);
c=exp(-(theta2.*tau2).^2/20);
PI=fftshift(fft2(ifftshift(c)));
PI=real(PI);

% 2D convolution
CD=conv2(WD,PI,'same');

% Displaying results
imagesc(CD)

```

Solution 3.24. The code reads:

```

Ls=12;
Nc=30;
N=256;

t=(-N/2:N/2)';
x= exp(-j*1*pi*t.^2/N/25).*exp(-(t/96).^2)+...
    sqrt(2.5)*exp(j*t*3*pi/4).*exp(-(t/16).^2)+...
    sqrt(2.4)*exp(j*t*pi/2).*exp(-((t+N/4)/16).^2)+...

```

```

sqrt(2.3)*exp(j*t*pi/4).*exp(-((t-N/4)/16).^2)+...
sqrt(2.2)*exp(-j*t*pi/4).*exp(-((t+N/4)/16).^2)+...
sqrt(2.1)*exp(-j*t*pi/2).*exp(-((t-N/4)/16).^2)+...
sqrt(2.0)*exp(-j*t*3*pi/4).*exp(-(t/16).^2);

% Oversampling by 2 and zero padding
X=fft(x);
X=[X(1:N/2+1);zeros(N,1);X(N/2+2:N+1)];
x=2*ifft(X);
x=[zeros(N,1);x;zeros(N,1)];

% Short-time Fourier transform
X=zeros(2*N+1);
for k=1:2*N+1
    X(:,k)=x(k+(0:2*N));
end
F=fft([X(N+1:2*N+1,:);zeros(2*N,2*N+1);X(1:N,:)]);
F=F([2*N+2:4*N+1,1:2*N+1],:);

% S-method
ind=2*N+1+(-N:N);%(N+1):(3*N+1);
S=abs(F(ind,:)).^2;
SL=F;SD=conj(F);
for l=1:Ls
    i1=ind+l;i1(i1>4*N+1)=i1(i1>4*N+1)-(4*N+1);
    i2=ind-l;i2(i2<1)=i2(i2<1)+(4*N+1);
    S=S+2*real(SL(i1,:).*SD(i2,:));
end

% Decomposition
WDSM=S/(4*N+1);
WDF=ifft(WDSM([N+2:2*N+1,1:N+1],:));
WDF=WDF([N+2:2*N+1,1:N+1],:);
RW=zeros(N+1);
for n=1:N+1;
    v=N+n;
    k=n;
    for m=1:N+1;

```

```

RW(n,m)=WDF(v,k);
v=v-1;k=k+1;
end
end
opt.disp=0;
[V,D]=eigs(RW,Nc,'lm',opt);
D=abs(diag(D));
Dsm=D;

figure(1)
stem(Dsm)
figure(2)
x3=sqrt(Dsm(3))*V(:,3);
plot(real(x3))

```

Solution 3.25. If we decompose the given function, as described in the Problem 3.24, the largest eigenvector will correspond to the signal whose Wigner distribution has minimal squared error as compared to the given function. The code reads:

```

N=256;
w=linspace(-pi,pi,2*N+1);
t2=-N/2:0.5:N/2;
[tt,ww]=meshgrid(t2,w);
WD=exp(-(tt/4-32*ww/pi).^4-(tt/32).^4);

WDF=ifft(WD([N+2:2*N+1,1:N+1],:));
WDF=WDF([N+2:2*N+1,1:N+1],:);
RW=zeros(N+1);
for n=1:N+1;
    v=N+n;
    k=n;
    for m=1:N+1;
        RW(n,m)=WDF(v,k);
        v=v-1;k=k+1;
    end
end
opt.disp=0;
[V,D]=eigs(RW,30,'lm',opt);

```

```
D=abs(diag(D));
Dsm=D;

figure(1)
stem(Dsm)

t=(-N/2:N/2)';
x1=sqrt(Dsm(1))*V(:,1);
figure(2)
plot(t,real(x1),'b',t,imag(x1),'r')
```

Note that in this way we may also check if the given two-dimensional function is the proper Wigner distribution. In that case, only one eigenvalue should be nonzero.

Chapter 4

Higher-Order Time-Frequency Representations

The higher-order spectral analysis has found its applications in many fields: radars, sonars, biomedicine, plasma physics, seismic data processing, image reconstruction, time-delay estimation, and adaptive filtering. The higher-order statistics, known as cumulants, and their Fourier transforms, known as higher-order spectra (poly-spectra), are the basic forms in this analysis. Some of the appealing properties of the higher-order statistics will be listed next. They can provide additional information in the case of non-Gaussian processes. The Gaussian noise of unknown mean and variance can be suppressed. Some of the higher-order spectra preserve the signal's phase information. In the case of nonlinear systems, including a special case of quadratic phase coupling system, more information about the system can be obtained by using the higher-order spectra than the linear or quadratic signal transforms.

Based on these forms, higher-order time-varying spectra are introduced and analyzed. The basic representation in the time-varying higher-order spectral analysis is the Wigner higher-order spectra. After presenting full forms of the higher-order time-varying spectra, two forms of distributions reduced to the two-dimensional time-frequency plane are analyzed: the L-Wigner distributions (sliced version of the higher-order spectra) and the polynomial Wigner-Ville distributions (a projection of the higher-order spectra). Due to slicing or projecting operation, these distributions will lose some of the basic properties of the higher-order spectra, but will be able to enhance some other desirable properties for nonstationary signal

analysis. A highly concentrated distribution based on complex-lag argument is presented as well. Higher-order ambiguity functions analysis, as a tool for higher-order polynomial phase signals, concludes this chapter.

4.1 THIRD-ORDER TIME-FREQUENCY REPRESENTATIONS

Since the higher-order spectra will be introduced based on the random signal analysis let us shortly review these forms here.

4.1.1 Second-Order Moment and Spectrum

The second-order moment of a random stationary signal $x(t)$ is its auto-correlation function. It is defined by

$$m_2^x(\tau) = R(t, \tau) = E\{x^*(t)x(t + \tau)\}. \quad (4.1)$$

The second-order cumulant is equal to

$$c_2^x(\tau) = m_2^x(\tau) - (m_1^x)^2$$

where $m_1^x = E\{x(t)\}$, represents the mean value of the signal (first-order moment). For a zero-mean signal $x(t)$, the second-order cumulant is equal to the second-order moment. The second-order cumulant at $\tau = 0$ is the variance.

In the case of stationary signals, $R(t, \tau) = R(\tau)$. The Fourier transform, of the auto-correlation function, of a stationary random signal is given by

$$\text{FT}\{R(\tau)\} = E\left\{x^*(t) \int_{-\infty}^{\infty} x(t + \tau)e^{-j\Omega\tau} d\tau\right\} = E\left\{x^*(t)X(\Omega)e^{j\Omega t}\right\}.$$

Assume that the stationary random signal $x(t)$ is ergodic in auto-correlation. It means that its expected value over all realizations is equal to the mean value over time,

$$R(\tau) = E\{x^*(t)x(t + \tau)\} = \lim_{T \rightarrow \infty} \frac{1}{2T} \int_{-T}^T x^*(t)x(t + \tau) dt. \quad (4.2)$$

Then

$$\text{FT}\{R(\tau)\} = \lim_{T \rightarrow \infty} \frac{1}{2T} \int_{-T}^T x^*(t)X(\Omega)e^{j\Omega t} dt = \langle X(\Omega)X^*(\Omega) \rangle = S(\Omega), \quad (4.3)$$

where $\langle \cdot \rangle$ denotes the above limit value. $S(\Omega)$ is the spectral power density. Thus, for a stationary random signal $x(t)$, the auto-correlation and the spectral power density function form the Fourier transform pair,

$$\begin{aligned} S(\Omega) &= \text{FT}\{R(\tau)\} = \int_{-\infty}^{\infty} R(\tau) e^{-j\Omega\tau} d\tau \\ R(\tau) &= \text{IFT}\{S(\Omega)\} = \frac{1}{2\pi} \int_{-\infty}^{\infty} S(\Omega) e^{j\Omega\tau} d\Omega \end{aligned}$$

with the signal power $E\{|x(t)|^2\}$ being equal to the integral of spectral power density function,

$$E\left\{|x(t)|^2\right\} = R(0) = \frac{1}{2\pi} \int_{-\infty}^{\infty} S(\Omega) d\Omega. \quad (4.4)$$

A discrete form that is used in numerical realizations is

$$R(n, m) = E\{x^*(n)x(n+m)\}.$$

For stationary random discrete signals, when $R(n, m)$ does not depend on n the spectral power density is

$$\begin{aligned} S(k) &= \text{DFT}\{R(m)\} = E\left\{x^*(n) \sum_{m=0}^{N-1} x(n+m) e^{-j2\pi mk/N}\right\} \\ &= E\left\{x^*(n)X(k)e^{j2\pi nk/N}\right\} = \frac{1}{N} X^*(k)X(k) = \frac{1}{N} |X(k)|^2. \end{aligned} \quad (4.5)$$

In the final step, the ergodicity in auto-correlation is assumed when the expectation can be replaced by averaging over time.

We assumed stationarity and ergodicity for random signals, meaning that the second-order statistics parameters are time-independent. Assumption of time invariance led to power signals, with power and spectral power representations (since the power of such signals is finite). For deterministic signals, it is more common to consider signals within energy framework. The energy of a signal is defined by

$$E_x = \int_{-\infty}^{\infty} |x(t)|^2 dt = \frac{1}{2\pi} \int_{-\infty}^{\infty} |X(\Omega)|^2 d\Omega.$$

Here $X(\Omega)X^*(\Omega) = |X(\Omega)|^2$ is a spectral density of energy. In the case of deterministic signals, the local auto-correlation function (second-order instantaneous moment)

$$R(t, \tau) = x^*(t)x(t + \tau),$$

is also used. Its relation to the spectral energy density (inspired by (4.2)-(4.3)) is

$$X(\Omega)X^*(\Omega) = \int_{-\infty}^{\infty} \left(\int_{-\infty}^{\infty} R(t, \tau) dt \right) e^{-j\Omega\tau} d\tau. \quad (4.6)$$

The Fourier transform of a local auto-correlation function is the Richazek distribution. The auto-correlation function (for random signals) and local auto-correlation function (for deterministic signals) may be defined with a symmetric lag arguments (symmetric second-order instantaneous moment), as

$$\begin{aligned} R(t, \tau) &= E\{x^*(t - \tau/2)x(t + \tau/2)\}, \text{ and} \\ R(t, \tau) &= x^*(t - \tau/2)x(t + \tau/2), \end{aligned}$$

respectively, when the mean of arguments in the signal is t , that is, $(t - \tau/2 + t + \tau/2)/2 = t$. In a deterministic signal case, this form of the local auto-correlation function produces the Wigner distribution as its Fourier transform.

4.1.2 Third-Order Moment and Bispectrum

The previous relations may be extended to the higher-order statistics. The third-order moment $m_3^x(\tau_1, \tau_2)$, for stationary signals, is defined by

$$m_3^x(\tau_1, \tau_2) = E\{x^*(t)x(t + \tau_1)x(t + \tau_2)\}. \quad (4.7)$$

The third-order cumulant, in terms of the first-, second-, and third-order moment, is defined as

$$c_3^x(\tau_1, \tau_2) = m_3^x(\tau_1, \tau_2) - m_1^x(m_2^x(\tau_1) + m_2^x(\tau_2) + m_2^x(\tau_1 - \tau_2)) + 2(m_1^x)^3.$$

Without loss of generality, assume that $m_1^x = 0$, when $c_3^x(\tau_1, \tau_2) = m_3^x(\tau_1, \tau_2)$.

The two-dimensional Fourier transform of $m_3^x(\tau_1, \tau_2)$ is called the bispectrum of a random signal,

$$B(\Omega_1, \Omega_2) = \int_{-\infty}^{\infty} \int_{-\infty}^{\infty} m_3^x(\tau_1, \tau_2) e^{-j(\Omega_1\tau_1 + \Omega_2\tau_2)} d\tau_1 d\tau_2. \quad (4.8)$$

The following relationship holds

$$\mathbb{E}\{x^*(t)x(t+\tau_1)x(t+\tau_2)\} = \lim_{T \rightarrow \infty} \frac{1}{2T} \int_{-T}^T x^*(t)x(t+\tau_1)x(t+\tau_2)dt,$$

for a stationary random signal, ergodic in the third-order moment. Then, the bispectrum is obtained in the same way as (4.3), in the form

$$B(\Omega_1, \Omega_2) = \lim_{T \rightarrow \infty} \frac{1}{2T} X^*(\Omega_1 + \Omega_2)X(\Omega_1)X(\Omega_2) = \langle X^*(\Omega_1 + \Omega_2)X(\Omega_1)X(\Omega_2) \rangle. \quad (4.9)$$

The integral of bispectrum is

$$\frac{1}{4\pi^2} \int_{-\infty}^{\infty} \int_{-\infty}^{\infty} B(\Omega_1, \Omega_2) d\Omega_1 d\Omega_2 = m_3^x(0,0) = \mathbb{E}\{x^*(t)x(t)x(t)\}.$$

Here we will just mention that $m_3^x(0,0)$ is related to an interesting parameter, which indicates the symmetry of the signal's probability density function, the skewness. The bispectrum of a Gaussian signal is equal to zero. Thus, one of important areas of its application is in detection of nonGaussian signals in a Gaussian environment. In addition, the bispectrum preserves signal phase information.

We can easily write the discrete form of bispectrum of a random (stationary and ergodic) signal as

$$\begin{aligned} B(k_1, k_2) &= \text{DFT}\{m_3^x(m_1, m_2)\} \\ &= \mathbb{E}\left\{x^*(n)X(k_1)e^{j2\pi nk_1/N}X(k_2)e^{j2\pi nk_2/N}\right\} = \frac{1}{N}X^*(k_1+k_2)X(k_1)X(k_2), \end{aligned} \quad (4.10)$$

where the expectation is calculated by averaging over time n .

In the second-order analysis of deterministic signals, the representations based on the signal energy $E_x = \int_{-\infty}^{\infty} x^*(t)x(t)dt$ are considered, instead of the signal power $P(t) = x^*(t)x(t)$ based forms. It means that, for deterministic signals, instead of $x^*(t)x(t)x(t)$ we will here consider its integral over time

$$S_3 = \int_{-\infty}^{\infty} x^*(t)x(t)x(t)dt \quad (4.11)$$

and instead of $m_3^x(\tau_1, \tau_2)$ its local form

$$R_2(t, \tau_1, \tau_2) = x^*(t)x(t + \tau_1)x(t + \tau_2). \quad (4.12)$$

Then, following the from in (4.6), we get the definition of bispectrum of a deterministic signal, as two-dimensional Fourier transform, over lags τ_1 and τ_2 of the the integral of the second-order local auto-correlation function,

$$\begin{aligned} B(\Omega_1, \Omega_2) &= \int_{-\infty}^{\infty} \int_{-\infty}^{\infty} \left(\int_{-\infty}^{\infty} R_2(t, \tau_1, \tau_2) dt \right) e^{-j(\Omega_1 \tau_1 + \Omega_2 \tau_2)} d\tau_1 d\tau_2 \\ &= \int_{-\infty}^{\infty} \int_{-\infty}^{\infty} \int_{-\infty}^{\infty} x^*(t)x(t + \tau_1)x(t + \tau_2)e^{-j(\Omega_1 \tau_1 + \Omega_2 \tau_2)} dt d\tau_1 d\tau_2 \\ &= X^*(\Omega_1 + \Omega_2)X(\Omega_1)X(\Omega_2). \end{aligned} \quad (4.13)$$

The inverse two-dimensional Fourier transform of the bispectrum of a deterministic signal is

$$\frac{1}{4\pi^2} \int_{-\infty}^{\infty} \int_{-\infty}^{\infty} B(\Omega_1, \Omega_2) e^{j(\Omega_1 \tau_1 + \Omega_2 \tau_2)} d\Omega_1 d\Omega_2 = \int_{-\infty}^{\infty} x^*(t)x(t)x(t)dt.$$

While in the second-order analysis there is a clear distinction in notation of the signal power-based (random) cases and signal energy-based (deterministic) cases, here we will continue to use the same notation $B(\Omega_1, \Omega_2)$ for:

(a) The bispectrum of random signals,

$$B(\Omega_1, \Omega_2) = \langle X^*(\Omega_1 + \Omega_2)X(\Omega_1)X(\Omega_2) \rangle, \quad (4.14)$$

defined based on the bispectral density of the signal skewness $E\{x^*(t)x(t)x(t)\}$, assuming third-order ergodicity and

(b) The bispectrum of deterministic signals

$$B(\Omega_1, \Omega_2) = X^*(\Omega_1 + \Omega_2)X(\Omega_1)X(\Omega_2), \quad (4.15)$$

defined as the bispectral density of $\int_{-\infty}^{\infty} x^*(t)x(t)x(t)dt$.

Example 4.1. Calculate the bispectrum of deterministic signals

$$x_1(t) = \exp(j\Omega_0 t + \varphi_1),$$

$$x_2(t) = \exp(j\Omega_0 t + \varphi_1) + \exp(j2\Omega_0 t + \varphi_2)$$

and

$$x_3(t) = \exp(j\Omega_{01}t + \varphi_1) + \exp(j\Omega_{02}t + \varphi_2) + \exp(j(\Omega_{01} + \Omega_{02})t + \varphi_{12}).$$

★ The bispectrum of $x_1(t) = \exp(j\Omega_0 t + \varphi_1)$ is zero for all frequencies,

$$B(\Omega_1, \Omega_2) \equiv 0$$

since $X_1(\Omega) = 2\pi\delta(\Omega - \Omega_0)e^{j\varphi_1}$ and

$$(2\pi)^3 \delta(\Omega_1 - \Omega_0) \delta(\Omega_2 - \Omega_0) \delta(\Omega_1 + \Omega_2 - 2\Omega_0) = 0$$

for all Ω_1 and Ω_2 and $\Omega_0 \neq 0$.

For the signal $x_2(t)$ there will be a nonzero value (a peak) in the bispectrum,

$$B(\Omega_1, \Omega_2) = (2\pi)^3 \delta(\Omega_1 - \Omega_0) \delta(\Omega_2 - \Omega_0) \delta(\Omega_1 + \Omega_2 - 2\Omega_0) e^{j(2\varphi_1 - \varphi_2)},$$

at $\Omega_1 = \Omega_0$ and $\Omega_2 = \Omega_0$. All other terms in $B(\Omega_1, \Omega_2)$ are zero. Thus, the bispectrum will produce a peak in the frequency-frequency domain in the case of phase coupled signals. These kind of signals result when a sum of sinusoids passes through a nonlinear system, like

$$y(t) = x_1(t) + x_1^2(t) = x_2(t). \quad (4.16)$$

They are often referred to as the quadratic phase coupled signals. The bispectrum can efficiently detect when phase coupling occurs. A similar situation will appear for $x_3(t)$ when

$$\begin{aligned} B(\Omega_1, \Omega_2) &= (2\pi)^3 [\delta(\Omega_1 - \Omega_{01}) \delta(\Omega_2 - \Omega_{02}) \delta(\Omega_1 + \Omega_2 - (\Omega_{01} + \Omega_{02})) \\ &\quad + \delta(\Omega_1 - \Omega_{02}) \delta(\Omega_2 - \Omega_{01}) \delta(\Omega_1 + \Omega_2 - (\Omega_{01} + \Omega_{02}))] e^{j(\varphi_1 + \varphi_2 - \varphi_{12})}. \end{aligned}$$

It indicates that a coupling of two sinusoidal signals, with frequencies Ω_{01} and Ω_{02} , has occurred in the third signal component, with frequency equal to the sum of these frequencies (Fig. 4.1). Bispectrum is symmetric,

$$B(\Omega_1, \Omega_2) = B(\Omega_2, \Omega_1). \quad (4.17)$$

An interesting application of the bispectrum is that it could be used as the indicator of a quality of musical instruments. There are claims that the design requirement for a "good" musical instrument is that it should have the third formant frequency region containing the sum of the first two formant frequencies. Thus, one of the quality criteria could be a maximization of the bispectrum for a given signal energy.

□

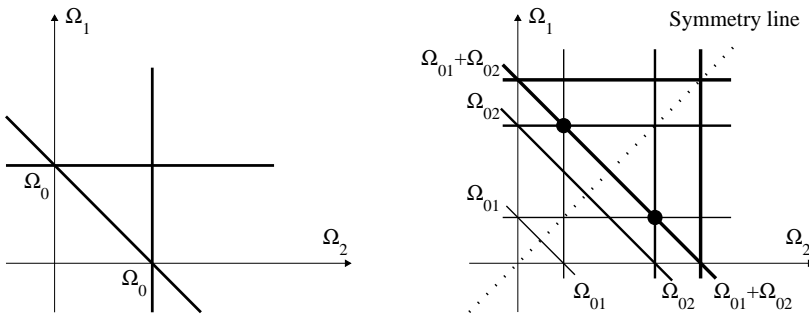


Figure 4.1 Bispectrum illustration of a one-component signal (left) and a three-component signal with phase coupling (right).

4.1.3 The Wigner Bispectrum

In general, the third-order moment can be written as

$$m_3^x(\tau_1, \tau_2) = E\{x^*(t + \alpha)x(t + \tau_1 + \alpha)x(t + \tau_2 + \alpha)\} \quad (4.18)$$

where α is an arbitrary constant. For deterministic signals, the third-order moment $m_3^x(\tau_1, \tau_2)$ is replaced by the third-order instantaneous moment (with two lag arguments)

$$R_2(t, \tau_1, \tau_2) = x^*(t + \alpha)x(t + \tau_1 + \alpha)x(t + \tau_2 + \alpha), \quad (4.19)$$

corresponding to a local two-lag auto-correlation function. The Wigner bispectrum (WB) is obtained from a two-dimensional Fourier transform of $R_2(t, \tau_1, \tau_2)$, over τ_1, τ_2 ,

$$WB(t, \Omega_1, \Omega_2) = \int_{-\infty}^{\infty} \int_{-\infty}^{\infty} x^*(t + \alpha)x(t + \tau_1 + \alpha)x(t + \tau_2 + \alpha)e^{-j(\Omega_1 \tau_1 + \Omega_2 \tau_2)} d\tau_1 d\tau_2. \quad (4.20)$$

This form was introduced by Gerr. The value of α is chosen in such a way that the mean value of the signal's arguments, in (4.20), is equal to t ,

$$\frac{(t + \alpha) + (t + \tau_1 + \alpha) + (t + \tau_2 + \alpha)}{3} = t,$$

$$\alpha = -\frac{\tau_1}{3} - \frac{\tau_2}{3}. \quad (4.21)$$

Then the Wigner bispectrum is defined as

$$WB(t, \Omega_1, \Omega_2) = \int_{-\infty}^{\infty} \int_{-\infty}^{\infty} x^* \left(t - \frac{\tau_1}{3} - \frac{\tau_2}{3} \right) x \left(t + \frac{2\tau_1}{3} - \frac{\tau_2}{3} \right) \\ \times x \left(t - \frac{\tau_1}{3} + \frac{2\tau_2}{3} \right) e^{-j(\Omega_1 \tau_1 + \Omega_2 \tau_2)} d\tau_1 d\tau_2, \quad (4.22)$$

or in terms of the signal's Fourier transform as

$$WB(t, \Omega_1, \Omega_2) = \frac{1}{2\pi} \int_{-\infty}^{\infty} X^* \left(\Omega_1 + \Omega_2 + \frac{\theta}{3} \right) X \left(\Omega_1 - \frac{\theta}{3} \right) X \left(\Omega_2 - \frac{\theta}{3} \right) e^{-j\theta t} d\theta. \quad (4.23)$$

This form is obtained by replacing the signal with its Fourier transform in (4.22), after some straightforward, but lengthy calculations.

The time marginal property of the Wigner bispectrum (4.22) is

$$\frac{1}{4\pi^2} \int_{-\infty}^{\infty} \int_{-\infty}^{\infty} WB(t, \Omega_1, \Omega_2) d\Omega_1 d\Omega_2 = x^*(t) x(t) x(t) = |x(t)|^2 x(t).$$

The marginal of the Wigner bispectrum over time is of the bispectrum form. It follows from (4.23)

$$\int_{-\infty}^{\infty} WB(t, \Omega_1, \Omega_2) dt = X^*(\Omega_1 + \Omega_2) X(\Omega_1) X(\Omega_2).$$

Example 4.2. Calculate the Wigner bispectrum of signals $x_1(t) = A \exp(j(\Omega_0 t + \varphi))$ and $x_2(t) = A \delta(t - t_0) e^{j\varphi}$.

★ The Wigner bispectrum behaves differently from the bispectrum. For the sinusoidal signal,

$$x(t) = A \exp(j(\Omega_0 t + \varphi)),$$

it will always produce a nonzero value, due to the varying θ . Here by using (4.22), we get

$$WB(t, \Omega_1, \Omega_2) = (2\pi)^2 A^3 \delta(\Omega_1 - \frac{2\Omega_0}{3}) \delta(\Omega_2 - \frac{2\Omega_0}{3}) e^{j\varphi} e^{j\Omega_0 t}.$$

From (4.23), we would get

$$WB(t, \Omega_1, \Omega_2) = 3(2\pi)^2 A^3 \delta(\Omega_1 + 2\Omega_2 - 2\Omega_0) \delta(\Omega_1 - \Omega_2) e^{j\varphi} e^{-j3(\Omega_2 - \Omega_0)t}.$$

It reduces to the previous one. The Wigner bispectrum peak value is at $(\Omega_1, \Omega_2) = (2\Omega_0/3, 2\Omega_0/3)$. Its phase is time varying. It is equal to the signal's phase $\Omega_0 t + \varphi$. Note that the Wigner bispectrum value is obtained with a shift in frequency lag in (4.23) for $\theta/3 = -\Omega_0/3$. The frequency lag shift is signal dependent. This conclusion is in agreement with the bispectrum value

$$B(\Omega_1, \Omega_2) = \int_{-\infty}^{\infty} WB(t, \Omega_1, \Omega_2) dt = 0$$

for $\Omega_0 \neq 0$.

For the signal $x_2(t) = A\delta(t - t_0)\exp(j\varphi)$, the Fourier transform is $X_2(\Omega) = A\exp(-jt_0\Omega)\exp(j\varphi)$, with

$$\begin{aligned} WB(t, \Omega_1, \Omega_2) &= \frac{1}{2\pi} A^3 \int_{-\infty}^{\infty} e^{j(\Omega_1 + \Omega_2 + \frac{\theta}{3})t_0} e^{-j(\Omega_1 - \frac{\theta}{3})t_0} e^{-j(\Omega_2 - \frac{\theta}{3})t_0} e^{j\varphi} e^{-j\theta t} d\theta \\ &= A^3 \delta(t - t_0) e^{j\varphi}. \end{aligned}$$

The bispectrum of this signal (scaled by the duration) would be $B(\Omega_1, \Omega_2) = A^3 \exp(j\varphi)$, preserving phase term, without time resolution.

In conclusion, the Wigner bispectrum has produced, in these two cases, ideal time and frequency representations, preserving the phase information.

□

Finally, let us mention that the third-order moment can be defined by using various combinations of the conjugated and the nonconjugated terms (signal must be at least once in the conjugated form and at least once in the nonconjugated form). Possible forms of the third-order moments, with corresponding bispectra of random

signals, are

$$\begin{aligned}
 E\{x^*(t)x(t+\tau_1)x(t+\tau_2)\} &\leftrightarrow \langle X^*(\Omega_1 + \Omega_2)X(\Omega_1)X(\Omega_2) \rangle \\
 E\{x(t)x^*(t+\tau_1)x(t+\tau_2)\} &\leftrightarrow \langle X(-\Omega_1 - \Omega_2)X^*(-\Omega_1)X(\Omega_2) \rangle \\
 E\{x(t)x(t+\tau_1)x^*(t+\tau_2)\} &\leftrightarrow \langle X(-\Omega_1 - \Omega_2)X(\Omega_1)X^*(-\Omega_2) \rangle \\
 E\{x^*(t)x^*(t+\tau_1)x(t+\tau_2)\} &\leftrightarrow \langle X^*(\Omega_1 + \Omega_2)X^*(-\Omega_1)X(\Omega_2) \rangle \\
 E\{x^*(t)x(t+\tau_1)x^*(t+\tau_2)\} &\leftrightarrow \langle X^*(\Omega_1 + \Omega_2)X(\Omega_1)X^*(-\Omega_2) \rangle \\
 E\{x(t)x^*(t+\tau_1)^*x(t+\tau_2)\} &\leftrightarrow \langle X(-\Omega_1 - \Omega_2)X^*(-\Omega_1)X^*(-\Omega_2) \rangle. \quad (4.24)
 \end{aligned}$$

All these forms produce similar results. For example, the last moment form is just a conjugated form of the first one. In the same way we may write corresponding bispectra of deterministic signals and Wigner bispectrum forms for all of these variations of conjugated and nonconjugated terms.

Before continuing with higher-order generalizations, an overview of the trispectrum will be presented. The trispectrum of deterministic signals is defined by

$$T(\Omega_1, \Omega_2, \Omega_3) = X^*(\Omega_1 + \Omega_2 + \Omega_3)X(\Omega_1)X(\Omega_2)X(\Omega_3). \quad (4.25)$$

The trispectrum of random signals is defined in an analog way to the bispectrum of random signals,

$$\begin{aligned}
 T(\Omega_1, \Omega_2, \Omega_3) &= \int_{-\infty}^{\infty} \int_{-\infty}^{\infty} \int_{-\infty}^{\infty} m_4^x(\tau_1, \tau_2, \tau_3) e^{-j(\Omega_1 \tau_1 + \Omega_2 \tau_2 + \Omega_3 \tau_3)} d\tau_1 d\tau_2 d\tau_3 \\
 &= \langle X^*(\Omega_1 + \Omega_2 + \Omega_3)X(\Omega_1)X(\Omega_2)X(\Omega_3) \rangle.
 \end{aligned}$$

The fourth-order moment with zero lags, $m_4^x(0, 0, 0) = E\{x^*(t)x(t)x(t)x(t)\}$, is used to define the kurtosis, $k_x = m_4^x(0, 0, 0) / [m_2^x(0)]^3 - 3$, as a measure of peakedness of random signal distribution. It was inspiration for some concentration measures in time-frequency analysis as well.

The trispectrum may be also written in variety of conjugate and nonconjugated terms. An interesting result is obtained with an equal number of conjugated and nonconjugated terms,

$$T(\Omega_1, \Omega_2, \Omega_3) = X^*(\Omega_1 + \Omega_2 + \Omega_3)X^*(-\Omega_1)X(\Omega_2)X(\Omega_3). \quad (4.26)$$

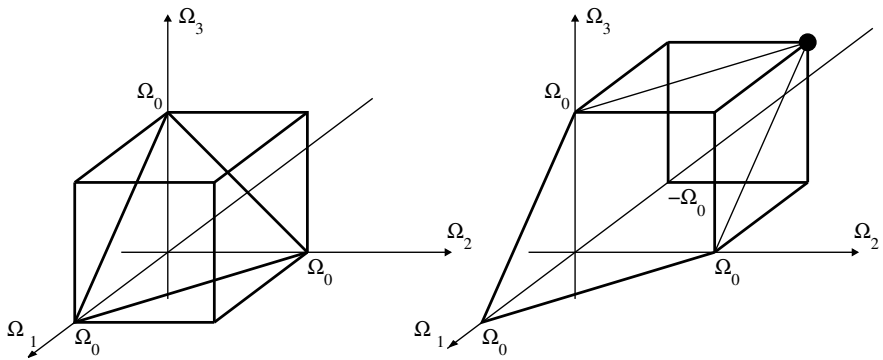


Figure 4.2 Illustration of trispectrum of a complex sinusoid with: one conjugated term in trispectrum, when there is no intersection of the four planes (left) and with two conjugated terms in trispectrum, when there is an intersection of the four planes (right).

Then the trispectrum is different from zero even for the case of one complex sinusoid $x(t) = A \exp(j\Omega_0 t)$, since

$$T(\Omega_1, \Omega_2, \Omega_3) = (2\pi)^4 \delta(\Omega_1 + \Omega_2 + \Omega_3 - \Omega_0) \delta(\Omega_1 + \Omega_0) \delta(\Omega_2 - \Omega_0) \delta(\Omega_3 - \Omega_0). \quad (4.27)$$

It is nonzero for $\Omega_1 = -\Omega_0$, $\Omega_2 = \Omega_0$ and $\Omega_3 = \Omega_0$. The trispectra defined by (4.25) and (4.26), are illustrated in Fig. 4.2. For the first one, there is no a common point (intersection) for all planes $\Omega_1 = \Omega_0$, $\Omega_2 = \Omega_0$, $\Omega_3 = \Omega_0$, and $\Omega_1 + \Omega_2 + \Omega_3 = \Omega_0$, while for the second one there is a common point (intersection) of all the planes $\Omega_1 = -\Omega_0$, $\Omega_2 = \Omega_0$, $\Omega_3 = \Omega_0$, and $\Omega_1 + \Omega_2 + \Omega_3 = \Omega_0$.

4.2 WIGNER HIGHER-ORDER SPECTRA

Following the idea of (4.20), the Wigner higher-order spectra of order k of a deterministic signal $x(t)$ are defined by Nikias and Fonollosa as the k -dimensional Fourier transform of the k -lag instantaneous moment function,

$$R_k(t, \tau_1, \dots, \tau_k) = x^*(t - \alpha) \prod_{i=1}^{L-1} x^*(t - \alpha + \tau_i) \prod_{i=L}^k x(t - \alpha + \tau_i) \quad (4.28)$$

$$W_k(t, \Omega_1, \dots, \Omega_k) = \int_{-\infty}^{\infty} \int_{-\infty}^{\infty} \dots \int_{-\infty}^{\infty} R_k(t, \tau_1, \dots, \tau_k) \prod_{i=1}^k \left(e^{-j\Omega_i \tau_i} d\tau_i \right) \quad (4.29)$$

with L conjugated terms ($1 \leq L \leq k$) and

$$\alpha = \frac{1}{k+1} \sum_{i=1}^k \tau_i. \quad (4.30)$$

The value of α is chosen in such a way that the instantaneous moment function $R_k(t, \tau_1, \tau_2, \dots, \tau_k)$ is centered at the time instant t , that is, the mean value of all signal arguments is

$$\frac{1}{k+1} [(t - \alpha) + \sum_{i=1}^k (\tau_i - \alpha)] = t.$$

For $k = 1$ (and $L = 0$) the Wigner distribution is obtained, while with $k = 2$ and $L = 1$ the Wigner bispectrum (4.22) follows. The distribution with $k = 3$ and $L = 1$ is the Wigner trispectrum. It is also used in analysis as an extension of trispectrum.

In terms of the signal's Fourier transform, the Wigner higher-order spectra of order k is

$$W_k(t, \Omega_1, \Omega_2, \dots, \Omega_k) = \frac{1}{2\pi} \int_{-\infty}^{\infty} X^* \left(\sum_{i=1}^k \Omega_i + \frac{\theta}{k+1} \right) \prod_{i=1}^{L-1} X^* \left(-\Omega_i + \frac{\theta}{k+1} \right) \prod_{i=L}^k X \left(\Omega_i - \frac{\theta}{k+1} \right) e^{-j\theta t} d\theta. \quad (4.31)$$

4.2.1 Instantaneous Frequency in the Wigner Higher-Order Spectra

One of the substantial properties of a time-frequency representation is that its central point over the multifrequency space is proportional to the instantaneous frequency. The mean frequency of the Wigner higher-order spectra is defined by

$$\Omega_m(t) = \frac{\int_{-\infty}^{\infty} \dots \int_{-\infty}^{\infty} \Omega_m W_k(t, \Omega_1, \dots, \Omega_k) \prod_{i=1}^k d\Omega_i}{\int_{-\infty}^{\infty} \dots \int_{-\infty}^{\infty} W_k(t, \Omega_1, \dots, \Omega_k) \prod_{i=1}^k d\Omega_i}, \quad (4.32)$$

for

$$m = 1, 2, \dots, k.$$

For a signal $x(t) = A \exp(j\varphi(t))$, having in mind the k -dimensional Fourier transform pair,

$$R_k(t, \tau_1, \dots, \tau_k) = \frac{1}{(2\pi)^k} \int_{-\infty}^{\infty} \int_{-\infty}^{\infty} \dots \int_{-\infty}^{\infty} W_k(t, \Omega_1, \dots, \Omega_k) \prod_{i=1}^k (e^{j\Omega_i \tau_i} d\Omega_i)$$

with

$$\frac{\partial}{\partial \tau_m} (R_k(t, \tau_1, \dots, \tau_k)) = \frac{1}{(2\pi)^k} \int_{-\infty}^{\infty} \int_{-\infty}^{\infty} \dots \int_{-\infty}^{\infty} j\Omega_m W_k(t, \Omega_1, \dots, \Omega_k) \prod_{i=1}^k (e^{j\Omega_i \tau_i} d\Omega_i)$$

it reduces to

$$j\Omega_m(t) = \frac{\frac{\partial}{\partial \tau_m} (R_k(t, \tau_1, \dots, \tau_k))_{\tau_1=\tau_2=\dots=\tau_k=0}}{R_k(t, \tau_1, \tau_2, \dots, \tau_k)_{\tau_1=\tau_2=\dots=\tau_k=0}}. \quad (4.33)$$

During the calculation of derivatives over τ_m , for $1 \leq m \leq k$, the dependence of α on τ_m , (4.30), should be taken into account. The signal is conjugated for $m \leq L-1$. The final result is

$$\Omega_m(t) = \varphi'(t) \left[\frac{L}{k+1} \pm 1 - \frac{1}{k+1}(k-L+1) \right],$$

where ± 1 is -1 for $m \leq L-1$ and $+1$ for $L \leq m \leq k$. In order to prove this relation, let us start from (4.33)

$$j\Omega_m(t) = \frac{\frac{\partial}{\partial \tau_m} \left[x^*(t-\alpha) \prod_{i=1}^{L-1} x^*(t-\alpha+\tau_i) \prod_{i=L}^k x(t-\alpha+\tau_i) \right]_{\tau_1=\tau_2=\dots=\tau_k=0}}{\left[x^*(t-\alpha) \prod_{i=1}^{L-1} x^*(t-\alpha+\tau_i) \prod_{i=L}^k x(t-\alpha+\tau_i) \right]_{\tau_1=\tau_2=\dots=\tau_k=0}}.$$

The derivative of the product function, at $\tau_1 = \tau_2 = \dots = \tau_k = 0$, with $\partial \alpha / \partial \tau_m = 1/(k+1)$, gives

$$\begin{aligned} j\Omega_m(t) &= \frac{\frac{-1}{k+1} x^{*\prime}(t) x^{*L-1}(t) x^{k-L+1}(t)}{x^{*L}(t) x^{k-L+1}(t)} \\ &+ \frac{\sum_{i=1}^{L-1} x^*(t) \left(\frac{-1}{k+1} + \delta(i-m) \right) x^{*\prime}(t) x^{*L-2}(t) x^{k-L+1}(t)}{x^{*L}(t) x^{k-L+1}(t)} \\ &+ \frac{\sum_{i=L}^k x^*(t) x^{*L-1}(t) \left(\frac{-1}{k+1} + \delta(i-m) \right) x'(t) x^{k-L}(t)}{x^{*L}(t) x^{k-L+1}(t)} \end{aligned}$$

since all conjugate and nonconjugate terms from the product function, contribute to the derivative with the same value. From the previous relation, we may write

$$\begin{aligned} j\Omega_m(t) &= \frac{-1}{k+1} \frac{x^{*l}(t)}{x^*(t)} + \sum_{i=1}^{L-1} \left(\frac{-1}{k+1} + \delta(i-m) \right) \frac{x^{*l}(t)}{x^*(t)} \\ &\quad + \sum_{i=L}^k \left(\frac{-1}{k+1} + \delta(i-m) \right) \frac{x'(t)}{x(t)}. \end{aligned}$$

Now, for $x(t) = A(t) \exp(j\phi(t))$, with

$$\frac{x'(t)}{x(t)} = \frac{A'(t)}{A(t)} + j\phi'(t) \quad (4.34)$$

and

$$\frac{x^{*l}(t)}{x^*(t)} = \frac{A'(t)}{A(t)} - j\phi'(t) \quad (4.35)$$

for the frequency along the m th axis, where $L \leq m \leq k$, we get

$$j\Omega_m(t) = L \frac{-1}{k+1} \frac{x^{*l}(t)}{x^*(t)} + (k-L+1) \frac{-1}{k+1} \frac{x'(t)}{x(t)} + \frac{x'(t)}{x(t)}$$

or

$$\begin{aligned} j\Omega_m(t) &= \frac{-L-k+L-1+k+1}{k+1} \frac{A'(t)}{A(t)} + j \frac{L-k+L-1+k+1}{k+1} \phi'(t) \\ &= j\phi'(t) \frac{2L}{k+1}. \end{aligned} \quad (4.36)$$

Thus,

$$\Omega_m(t) = \phi'(t) \frac{2L}{k+1}, \quad (4.37)$$

for $L \leq m \leq k$. In a similar way, for $m \leq L-1$, we get,

$$j\Omega_m(t) = L \frac{-1}{k+1} \frac{x^{*l}(t)}{x^*(t)} + \frac{x^{*l}(t)}{x^*(t)} + (k-L+1) \frac{-1}{k+1} \frac{x'(t)}{x(t)}$$

resulting in

$$\Omega_m(t) = \phi'(t) \left[\frac{2L}{k+1} - 2 \right]. \quad (4.38)$$

For a special case of $L = 1$, we get

$$\Omega_m(t) = \frac{2}{k+1} \phi'(t). \quad (4.39)$$

This is in agreement with our previous Wigner bispectrum ($k = 2$) analysis of a sinusoidal signal, when we have obtained that the Wigner bispectrum peak is located at $(\Omega_1, \Omega_2) = (2\Omega_0/3, 2\Omega_0/3)$. The locations of peaks, in general, are biased with respect to the true instantaneous frequency position, by an order-dependent constant $2/(k+1)$. An interesting case, which will be used later, is for $L = (k+1)/2$, when the instantaneous frequency positions are unbiased

$$\Omega_m(t) = \pm \phi'(t), \quad m = 1, 2, \dots, k, \quad (4.40)$$

up to a sign, since $\Omega_m(t) = \phi'(t)$ or $\Omega_m(t) = -\phi'(t)$ is obtained for different m . In this case the number of conjugated and nonconjugated terms is equal. Sign minus is for the index m corresponding to the axes associated with the conjugated terms, while $\Omega_m(t) = +\phi'(t)$ stands for the axes corresponding to the nonconjugated terms in $\prod_{i=1}^{L-1} x^*(t - \alpha + \tau_i) \prod_{i=L}^k x(t - \alpha + \tau_i)$.

Example 4.3. Derive the instantaneous frequency relation for $k = 3$ and $L = 2$.

★ The fourth-order Wigner spectra (Wigner trispectrum), with $k = 3$ and $L = 2$, produces

$$\begin{aligned} \Omega_1(t) &= -j \frac{\frac{\partial}{\partial \tau_1} [x^*(t - \alpha)x^*(t - \alpha + \tau_1)x(t - \alpha + \tau_2)x(t - \alpha + \tau_3)]|_{\tau_1=\tau_2=\tau_3=0}}{x^*(t)x^*(t)x(t)x(t)} \\ &= -j \frac{x^{*\prime}(t) \frac{-1}{k+1} x^*(t)x(t)x(t) + x^*(t)x^{*\prime}(t) (\frac{-1}{k+1} + 1)x(t)x(t)}{x^*(t)x^*(t)x(t)x(t)} \\ &\quad - j \frac{x^*(t)x^*(t)x'(t) \frac{-1}{k+1} x(t) + x^*(t)x^*(t)x(t)x'(t) \frac{-1}{k+1}}{x^*(t)x^*(t)x(t)x(t)}. \end{aligned}$$

For $x(t) = A(t)e^{j\phi(t)}$, with $x^{*\prime}(t)/x^*(t) = A'(t)/A(t) - j\phi'(t)$ and $x'(t)/x(t) = A'(t)/A(t) + j\phi'(t)$, follows

$$\begin{aligned} \Omega_1(t) &= \frac{1}{k+1} \phi'(t) + \left(\frac{1}{k+1} - 1 \right) \phi'(t) - \frac{1}{k+1} \phi'(t) - \frac{1}{k+1} \phi'(t) \\ &= -\phi'(t). \end{aligned}$$

In a similar way, $\Omega_2(t) = -\phi'(t)$, $\Omega_3(t) = \phi'(t)$, and $\Omega_4(t) = \phi'(t)$ is obtained. □

Example 4.4. Calculate the position of the Wigner higher-order spectra of $x(t) = \exp(j\Omega_0 t)$ along frequency axes in a multifrequency space. What is the position of this signal in the Wigner distribution?

★ The Wigner higher-order spectra of this signal is a pulse at

$$\Omega_m = \begin{cases} \Omega_0 \left[\frac{2L}{k+1} - 2 \right] & \text{for } m \leq L-1 \\ \Omega_0 \frac{2L}{k+1} & \text{for } L \leq m \leq k \end{cases}$$

For $L = (k+1)/2$ we get $\Omega_m = -\Omega_0$ for $m \leq L-1$ and $\Omega_m = \Omega_0$ for $L \leq m \leq k$.

For the Wigner distribution $k = 1$, $L = 1$ thus, $L = (k+1)/2$. Then in the product $\prod_{i=1}^{L-1} x^*(t - \alpha + \tau_i) \prod_{i=L}^k x(t - \alpha + \tau_i)$ there is only one term. It is a nonconjugated term $x(t - \alpha + \tau_1) = x(t + \tau_1/2)$. Thus, $\Omega_1 = \Omega_0$, as expected. □

4.2.2 Wigner Multitime Distribution

A distribution dual to the Wigner higher-order spectra (4.29) and (4.31) is introduced and defined as the multitime Wigner higher-order distribution (MTWD). The multitime Wigner higher-order distribution, in terms of a signal $x(t)$ in the time domain, reads as

$$W_k(\Omega, t_1, \dots, t_k) = \int_{-\infty}^{\infty} x^*\left(\sum_{i=1}^k t_i + \frac{\tau}{k+1}\right) \prod_{i=1}^{L-1} x^*\left(-t_i + \frac{\tau}{k+1}\right) \prod_{i=L}^k x\left(t_i - \frac{\tau}{k+1}\right) e^{j\tau\Omega} d\tau. \quad (4.41)$$

All the properties of the multitime Wigner higher-order distribution are dual to the properties for the Wigner higher-order spectra. For example, for $k = 2$ and $L = 1$, the frequency marginal property (integral of $W_k(\Omega, t_1, \dots, t_k)$ over frequency) of

$$W_2(\Omega, t_1, t_2) = \int_{-\infty}^{\infty} x^*(t_1 + t_2 + \frac{\tau}{3}) x(t_1 - \frac{\tau}{3}) x(t_2 - \frac{\tau}{3}) e^{j\tau\Omega} d\tau \quad (4.42)$$

is a form dual to bispectrum of deterministic signals,

$$\frac{1}{2\pi} \int_{-\infty}^{\infty} W_2(\Omega, t_1, t_2) d\Omega = x^*(t_1 + t_2) x(t_1) x(t_2).$$

It can be used for detection of coupled components in the time domain, for example, $Y(\Omega) = X(\Omega) + X^2(\Omega)$, corresponding to $y(t) = x(t) + x(t) * x(t)$. It also preserves

the signal phase information. The location of a pulse $x(t) = \delta(t - d)$ in the lag space is at $\tau/3 = -2d/3$. This location is signal-dependent.

In a similar way, we may define a distribution dual to the Wigner trispectrum. For example, with $L = 1$,

$$W_3(\Omega, t_1, t_2, t_3) = \int_{-\infty}^{\infty} x^*(t_1 + t_2 + t_3 + \frac{\tau}{4})x(t_1 - \frac{\tau}{4})x(t_2 - \frac{\tau}{4})x(t_3 - \frac{\tau}{4})e^{j\tau\Omega}d\tau.$$

Its marginal value over frequency is

$$\frac{1}{2\pi} \int_{-\infty}^{\infty} W_3(\Omega, t_1, t_2, t_3) d\Omega = x^*(t_1 + t_2 + t_3)x(t_1)x(t_2)x(t_3).$$

Example 4.5. A distribution dual to the Wigner trispectrum could be written in different forms, for various combinations of conjugated and nonconjugated terms. Show that the location of the delta pulse $x(t) = \delta(t - d)$, in the lag domain, for the form

$$W_3(\Omega, t_1, t_2, t_3) = \int_{-\infty}^{\infty} x^*(t_1 + t_2 + t_3 + \frac{\tau}{4})x^*(-t_1 + \frac{\tau}{4})x(t_2 - \frac{\tau}{4})x(t_3 - \frac{\tau}{4})e^{j\tau\Omega}d\tau,$$

does not depend on the signal's position in time d .

★The location of the delta pulse $x(t) = \delta(t - d)$, in the lag domain, follows as a solution of the system

$$\begin{aligned} t_1 + t_2 + t_3 + \frac{\tau}{4} &= d, \\ -t_1 + \frac{\tau}{4} &= d, \\ t_2 - \frac{\tau}{4} &= d, \\ t_3 - \frac{\tau}{4} &= d, \end{aligned} \tag{4.43}$$

as

$$\tau = 0.$$

Here the number of conjugated and nonconjugated terms in the dual Wigner trispectrum was equal. The location of this signal in the τ domain is signal-independent. The locations of the signal along t_1 , t_2 , and t_3 are at $-t_1 = t_2 = t_3 = d$.

For a further exercise, write some other forms of the dual Wigner trispectrum (with at least one conjugated and at least one nonconjugated signal form) and show that the locations depend on the signal's position if the number of conjugated and nonconjugated terms is not equal. □

4.2.2.1 Auto-Terms and Cross-Terms Location

Consider a multicomponent signal, formed as a sum of short duration signals

$$x(t) = \sum_{m=1}^M x_m(t - d_m), \quad (4.44)$$

where $x_m(t)$ ($m = 1, 2, \dots, M$) are such that $x_m(t) = 0$ for $|t| \geq \varepsilon$, with ε being small.

The integrand in (4.41) is different from zero only if the following inequalities are satisfied

$$\begin{aligned} & \left| \sum_{i=1}^k t_i + \frac{\tau}{k+1} - d_m \right| < \varepsilon, \\ & \left| -t_i + \frac{\tau}{k+1} - d_{m_i} \right| < \varepsilon, \quad i = 1, 2, \dots, L-1 \\ & \left| t_i - \frac{\tau}{k+1} - d_{m_i} \right| < \varepsilon, \quad i = L, L+1, \dots, k \end{aligned} \quad (4.45)$$

where $m, m_i = 1, 2, \dots, M$.

In order to analyze the auto-terms, consider first the case $M = 1$ with $d_1 = d$, when the cross-terms do not exist. Eliminating t_1, t_2, \dots, t_k from the first inequality in (4.45), and τ from the remaining ones, we get

$$\begin{aligned} & \left| \frac{\tau}{k+1} - \frac{(2L-k-1)d}{k+1} \right| < \varepsilon, \\ & \left| -t_i + \frac{(2L-k-1)d}{k+1} - d \right| < 2\varepsilon \frac{k}{k+1}, \quad i = 1, 2, \dots, L-1 \\ & \left| t_i - \frac{(2L-k-1)d}{k+1} - d \right| < 2\varepsilon \frac{k}{k+1}, \quad i = L, L+1, \dots, k. \end{aligned} \quad (4.46)$$

From this analysis, we can conclude that the location of auto-terms along τ depends on the signal's position d , for any L , except for $L = (k+1)/2$. This case was also preferred in the cumulant analysis. When $L = (k+1)/2$, the auto-terms are located at the τ axis origin and its vicinity. Also, we may conclude that for $L = (k+1)/2$ the auto-terms lie, in the k -dimensional t_1, t_2, \dots, t_k space, along the line s defined by

$$s : t_1 = -t, t_2 = -t, \dots, t_{L-1} = -t, \quad (4.47)$$

$$t_L = t, t_{L+1} = t, \dots, t_k = t$$

at the points $t = d_m$.

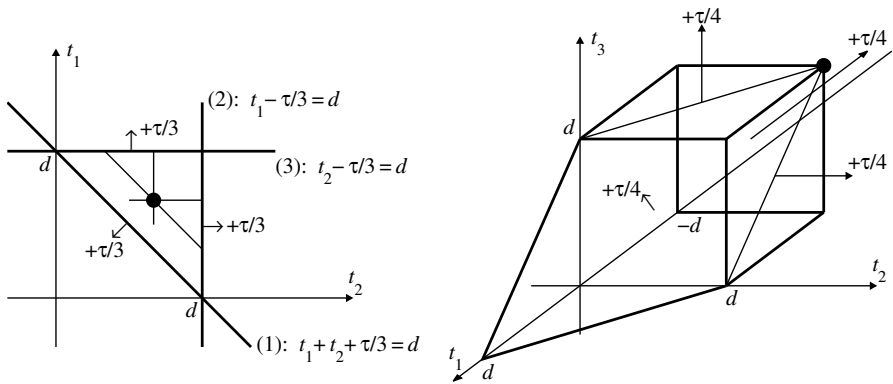


Figure 4.3 Illustration of the multitime Wigner higher-order distribution of the: second-order (left) and third-order (right).

The illustration of multitime Wigner higher-order distribution of the second-order with $k = 2$, dual to the Wigner bispectrum is given in Fig. 4.3. It cannot satisfy the condition $L = (k + 1)/2$. The multitime Wigner higher-order distribution of the third-order (with $k = 3$, dual to the Wigner trispectrum) is illustrated in Fig. 4.3. It is the lowest higher-order form that may satisfy the condition of equal number of conjugated and nonconjugated terms in the definition, $L = (k + 1)/2$ (if one does not count the well-known Wigner distribution). Similar conclusions can be made if we consider the group delay function along the m th axis $t_m(\Omega)$ dual to (4.33).

If $M > 1$, then for $L = (k + 1)/2$, considering only line s , the regions where the integrand in (4.41) is different from zero, may be obtained from (4.45) with $m_i = n$

$$\begin{aligned} \left| \frac{\tau}{k+1} - \frac{d_m - d_n}{k+1} \right| &< \varepsilon, \\ \left| -t_i + \frac{d_m - (k+2)d_n}{k+1} \right| &< 2\varepsilon \frac{k}{k+1}, \quad i = 1, 2, \dots, L-1 \\ \left| t_i - \frac{d_m + kd_n}{k+1} \right| &< 2\varepsilon \frac{k}{k+1}, \quad i = L, L+1, \dots, k. \end{aligned} \quad (4.48)$$

It follows from (4.48) that the components of the integrand in (4.41), corresponding to the cross-terms, $m \neq n$, are dislocated from the τ -axis origin. They are around $\tau = d_m - d_n$.

4.3 THE L-WIGNER DISTRIBUTION

The multitime Wigner higher-order distribution, with $L = (k + 1)/2$, along the line s , given by (4.47), is equal to the L-Wigner distribution. It is defined as

$$LWD_L(t, \Omega) = \int_{-\infty}^{\infty} x^{*L} \left(t - \frac{\tau}{2L} \right) x^L \left(t + \frac{\tau}{2L} \right) e^{-j\Omega\tau} d\tau. \quad (4.49)$$

For $L = 1$, the L-Wigner distribution reduces to the Wigner distribution. In the problems section, it will be shown that the L-Wigner distribution may be derived as a projection of the multitime Wigner higher-order spectra. The L-Wigner distribution was introduced before the time-varying higher spectra, as a distribution that improves time-frequency concentration along the instantaneous frequency.

Its pseudo form is defined by introducing a lag localization window $w_L(\tau)$,

$$LWD_L(t, \Omega) = \int_{-\infty}^{\infty} w_L(\tau) x^{*L} \left(t - \frac{\tau}{2L} \right) x^L \left(t + \frac{\tau}{2L} \right) e^{-j\Omega\tau} d\tau. \quad (4.50)$$

Since we will use only this form in the analysis and realizations, we will not introduce a new notation for the pseudo L-Wigner distribution. For a signal $x(t) = A \exp(j\phi(t))$, expanding $\phi(t \pm \tau/2L)$ into a Taylor series around t , up to the third-order term, we get

$$LWD_L(t, \Omega) = 2\pi A^{2L} \delta(\omega - \phi'(t)) *_{\Omega} W_L(\Omega) *_{\Omega} \text{FT} \left\{ e^{j \frac{\phi'''(t)}{24L^2} \tau^3 + \dots} \right\} \quad (4.51)$$

where $*_{\Omega}$ denotes the frequency domain convolution and $W_L(\Omega) = \text{FT}\{w_L(\tau)\}$. From (4.51) one may conclude that the generalized power A^{2L} is concentrated at the instantaneous frequency $\phi'(t)$. The distortions caused by the shape of the phase function are due to the existence of its third- and higher-order derivatives. If the instantaneous frequency is a linear function of time, then the Wigner distribution ($L = 1$) produces the ideal concentration. However, if that is not the case, then $L > 1$ reduces the distortion. In other words, the pseudo L-Wigner distribution locally linearize the instantaneous frequency function, by reducing the spreading term $\text{FT} \left\{ \exp(j \frac{\phi'''(t)}{24L^2} \tau^3 + \dots) \right\}$ influence by L^2 .

The pseudo L-Wigner distribution of an order L can be calculated based on the L-Wigner distribution of order $L/2$ as

$$LWD_L(t, \Omega) = LWD_{L/2}(t, 2\Omega) *_{\Omega} LWD_{L/2}(t, 2\Omega). \quad (4.52)$$

To prove this relation, let us start with,

$$\begin{aligned} & w_L(\tau) x^{*L} \left(t - \frac{\tau}{2L} \right) x^L \left(t + \frac{\tau}{2L} \right) \\ &= \left[w_{L/2}(\tau/2) x^{*L/2} \left(t - \frac{\tau/2}{2L/2} \right) x^{L/2} \left(t + \frac{\tau/2}{2L/2} \right) \right]^2, \end{aligned}$$

producing

$$\begin{aligned} LWD_L(t, \Omega) &= 2 \int_{-\infty}^{\infty} \left[w_{L/2}(\tau) x^{*L/2} \left(t - \frac{\tau}{2L/2} \right) x^{L/2} \left(t + \frac{\tau}{2L/2} \right) \right]^2 e^{-j2\Omega\tau} d\tau \\ &= \frac{1}{\pi} \int_{-\infty}^{\infty} \int_{-\infty}^{\infty} w_{L/2}(\tau) x^{*L/2} \left(t - \frac{\tau}{2L/2} \right) x^{L/2} \left(t + \frac{\tau}{2L/2} \right) \\ &\quad \times LWD_{L/2}(t, \theta) e^{-j(2\Omega-\theta)\tau} d\theta d\tau \\ &= \frac{1}{\pi} \int_{-\infty}^{\infty} LWD_{L/2}(t, 2\Omega - \theta) LWD_{L/2}(t, \theta) d\theta. \end{aligned}$$

Finally, with a change of variables $\theta \rightarrow \Omega + \theta$, follows

$$LWD_L(t, \Omega) = \frac{1}{\pi} \int_{-\infty}^{\infty} LWD_{L/2}(t, \Omega - \theta) LWD_{L/2}(t, \Omega + \theta) d\theta. \quad (4.53)$$

In order recursive realizations the lag window changes with order,

$$w_L(\tau) = w_{L/2}(\tau/2) w_{L/2}(\tau/2). \quad (4.54)$$

This can be concluded from the above derivation. The order independent window is the window of the form $w_L(\tau) = \exp(-|\tau|/\alpha)$. Since it is not well localized, it will be used only in analytical derivations, to show the improvements in the pseudo L-Wigner distribution (that will not be influenced by a changing window form, see Problem 3.17 for additional comments on the lag window role in the pseudo L-Wigner distribution)

Example 4.6. Calculate the pseudo L-Wigner distribution of a cubic phase signal (quadratic frequency modulated)

$$x(t) = \exp(j8\pi t^3)$$

by using: (a) the order independent lag window $w(\tau) = \exp(-|\tau|)$ and (b) the Hann(ing) window $w(\tau) = \cos^2(\tau\pi/2)$ for $|\tau| \leq 1$.

★ (a) The pseudo L-Wigner distribution value is

$$LWD_L(t, \Omega) = \int_{-\infty}^{\infty} \exp(-|\tau|) \exp(j8\pi\tau^3/(4L^2)) \exp(-j(\Omega - 24\pi t^2)\tau) d\tau$$

since $\exp(-|\tau|) = \exp(-|\tau/2|)\exp(-|\tau/2|)$. If L is large enough (for example $L = 8$), so that $8\pi\tau^3/(4L^2)$ is small within the lag window, approximately for $|\tau| < 1$, we get $|8\pi\tau^3/(4L^2)| < \pi/32$, then we should not use the stationary phase method, but write

$$\begin{aligned} LWD_8(t, \Omega) &\cong \int_{-\infty}^{\infty} \exp(-|\tau|) \exp(-j(\Omega - 24\pi t^2)\tau) d\tau \\ &= \frac{1}{1 + (\Omega - 24\pi t^2)^2}. \end{aligned}$$

(b) For the Hann(ing) window, we will get

$$\begin{aligned} LWD_8(t, \Omega) &\cong \int_{-1}^1 \cos^2(\tau\pi/2) \exp(-j(\Omega - 24\pi t^2)\tau) d\tau \\ &= \frac{\pi^2 \sin(\Omega - 24\pi t^2)}{(\Omega - 24\pi t^2)(\pi^2 - (\Omega - 24\pi t^2)^2)}. \end{aligned}$$

In this way, a high concentration along the instantaneous frequency $\Omega(t) = 24\pi t^2$ is achieved without inner interferences. □

Example 4.7. The pseudo Wigner distribution, along with the pseudo L-Wigner distributions, with $L = 2$, $L = 4$ and $L = 8$, are shown in Fig. 4.4 for a sinusoidally frequency modulated signal

$$x(t) = \exp(-j32\cos(\pi t/64)).$$

The signal is sampled with $\Delta t = 1$. A Hann(ing) window (257 samples) is used as a lag window in all cases. This simple example shows how the pseudo L-Wigner distribution reduces the inner interferences in a sinusoidally modulated signal. The same resulting lag window is used in all four time-frequency representations. Thus, the auto-term concentration is not compromised. □

Example 4.8. For a sinusoidally frequency modulated signal $x(t) = \exp(-j32\cos(\pi t/64))$, from the previous example, calculate an approximate value of the pseudo L-Wigner distribution, with $L = 8$ and a window $w_8(\tau)$ of the width $T = 32$.

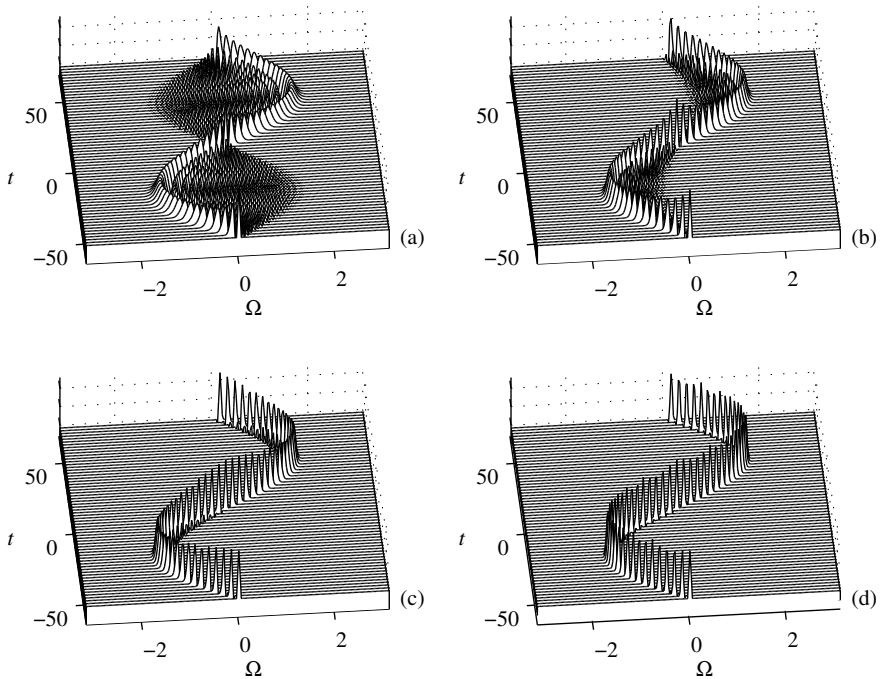


Figure 4.4 Time-frequency representation of a sinusoidally (nonlinear) frequency modulated signal: (a) pseudo Wigner distribution, (b) pseudo L-Wigner distribution with $L = 2$, (c) pseudo L-Wigner distribution with $L = 4$, and (d) pseudo L-Wigner distribution with $L = 8$.

★ The pseudo L-Wigner distribution of this signal, with $L = 8$, is

$$LWD_8(\Omega, t) = \int_{-32}^{32} e^{j256\cos(\pi(t-\tau/16)/64)} e^{-j256\cos(\pi(t+\tau/16)/64)} w_8(\tau) e^{-j\Omega\tau} d\tau.$$

By using the Taylor expansion

$$\begin{aligned} \cos\left(\pi t/64 \pm \frac{\pi\tau}{16 \cdot 64}\right) &= \cos(\pi t/64) \mp \frac{\pi}{16 \cdot 64} \sin(\pi t/64)\tau \\ &- \left(\frac{\pi}{16 \cdot 64}\right)^2 \cos(\pi t/64) \frac{\tau^2}{2} + \left(\frac{\pi}{16 \cdot 64}\right)^3 \sin(\pi t/64) \frac{\tau^3}{6}, \end{aligned}$$

with $|\tau_{1,2}| \leq 32$ in the Taylor series reminder, we get

$$LWD_8(\Omega, t) = \int_{-32}^{32} e^{j\pi/2 \sin(\pi t/64)\tau} e^{j256 \frac{\pi^3}{16^3 \cdot 64^3} \sin(\pi t/64) \frac{\tau_1^3 + \tau_2^3}{6}} w_8(\tau) e^{-j\Omega\tau} d\tau.$$

Obviously, $\left| 256 \frac{\pi^3}{16^3 \cdot 64^3} \sin(\pi t/64) \frac{\tau_1^3 + \tau_2^3}{6} \right| \leq 0.081$, since $|\tau_{1,2}| \leq 32$. Thus, we may write

$$LWD_8(\Omega, t) \cong W_8(\Omega - \pi/2 \sin(\pi t/64)),$$

where $W_8(\Omega)$ is the Fourier transform of window $w_8(\tau)$. For a Hann(ing) window this approximation holds for wider windows as well, since its values toward the ending points are small, meaning that the effective window width is lower than the window width itself. \square

4.4 THE POLYNOMIAL WIGNER-VILLE DISTRIBUTION

The polynomial Wigner-Ville distributions (PWVD) were proposed by Boashash et al. to improve the concentration of time-frequency representation for signals whose instantaneous frequencies are polynomial functions of time. It also has been shown that the polynomial Wigner-Ville distribution is a unique projection of the Wigner higher-order spectra. The projection axis is defined by the coefficients of the polynomial Wigner-Ville distribution. The projection step is necessary to achieve a highly concentrated time-frequency representation of nonlinear frequency-modulated signals. However, this step causes problems in dealing with multicomponent signals. It is possible, to develop such projection schemes that can both achieve the high concentration and be free from the constant amplitude cross-terms, as will be shown later in this chapter.

Here the polynomial Wigner-Ville distributions are derived based on the condition that the distribution of a frequency modulated signal $x(t) = \exp(j\phi(t))$, having a polynomial phase function

$$\phi(t) = \sum_{i=0}^p a_i t^i,$$

is equal to the ideally concentrated one, that is,

$$PD(t, \Omega) = 2\pi\delta(\Omega - \phi'(t)). \quad (4.55)$$

Such a distribution may be obtained as a Fourier transform of the polynomial kernel

$$K_x(t, \tau) = \prod_{k=-q/2}^{q/2} x^{b_k}(t + c_k \tau),$$

with respect to τ ,

$$PD(t, \Omega) = \int_{-\infty}^{\infty} \prod_{k=-q/2}^{q/2} x^{b_k}(t + c_k \tau) e^{-j\Omega\tau} d\tau, \quad (4.56)$$

where $q \geq p$ is an even number. Coefficients b_k and c_k should be determined, for a given p and q , so that the ideal distribution is achieved. A derivation of coefficients will be presented in the next section, for commonly used higher-order distributions, including the polynomial Wigner-Ville distributions. Here we will outline the most commonly used fourth-order polynomial Wigner-Ville distribution, with $q = 4$. It is defined as

$$PD(t, \Omega) = \int_{-\infty}^{\infty} x^2(t + 0.675\tau) x^{*2}(t - 0.675\tau) x^*(t + 0.85\tau) x(t - 0.85\tau) e^{-j\Omega\tau} d\tau. \quad (4.57)$$

Example 4.9. Calculate the fourth-order polynomial Wigner-Ville distribution of a polynomial phase signal

$$x(t) = e^{j(45\pi t + 120t^3)}.$$

Its value is close to

$$PD(t, \Omega) = 2\pi\delta(\Omega - 45\pi - 360t^2).$$

It is presented, for $-1 \leq t \leq 1$, in Fig. 4.5. \square

4.5 PHASE DERIVATIVE ESTIMATION

Let us consider a signal of the form

$$x(t) = A e^{j\varphi(t)} \quad (4.58)$$

with the instantaneous frequency

$$\Omega(t) = \frac{d\varphi(t)}{dt}. \quad (4.59)$$

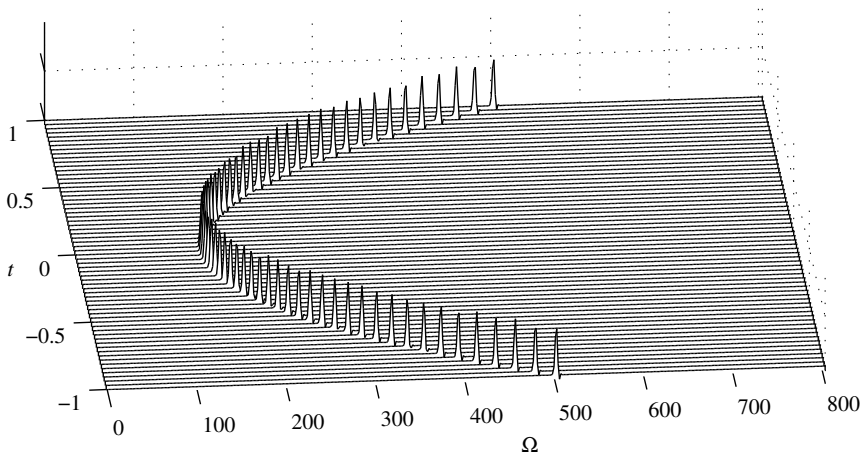


Figure 4.5 Polynomial Wigner-Ville distribution of a signal with the fourth-order polynomial phase.

In order to estimate the instantaneous frequency from the phase function, we can use various relations for the first derivative approximation.

4.5.1 Quadratic Distributions

First-order backward estimation is defined by

$$\Omega(t) \approx \frac{\varphi(t) - \varphi(t - \tau)}{\tau} = \frac{d\varphi(t)}{dt} + O(\varphi''(\tau)) \quad (4.60)$$

with error $O(\varphi''(\tau))$ of the second-order in τ . The time-frequency distribution corresponding to this estimation is the Richazek distribution

$$RD(t, \Omega) = \int_{-\infty}^{\infty} x(t)x^*(t - \tau)e^{-j\Omega\tau} d\tau.$$

The Richazek distribution is the Fourier transform of $A^2 \exp(j[\varphi(t) - \varphi(t - \tau)])$, thus being concentrated at the $\Omega(t) = d\varphi(t)/dt$ with the spread factor depending on $\varphi''(\tau)$.

Symmetric derivative estimation,

$$\Omega(t) \approx \frac{\varphi(t + \tau/2) - \varphi(t - \tau/2)}{\tau} = \frac{d\varphi(t)}{dt} + O(\varphi'''(\tau)), \quad (4.61)$$

obviously corresponds to the Wigner distribution

$$WD(t, \Omega) = \int_{-\infty}^{\infty} x\left(t + \frac{\tau}{2}\right)x^*\left(t - \frac{\tau}{2}\right)e^{-j\Omega\tau}d\tau,$$

with the spread factor depending on $\varphi'''(\tau)$. For a linear frequency modulated (quadratic phase) signal, there is no estimation error in derivative. Therefore, in this case, the Wigner distribution is ideally concentrated, as it is well known.

The generalized Wigner distribution,

$$GWD(t, \Omega) = \int_{-\infty}^{\infty} x(t + \alpha\tau)x^*(t + (\alpha - 1)\tau)e^{-j\Omega\tau}d\tau,$$

where α is a constant, follows from the first derivative estimator

$$\Omega(t) \approx \frac{\varphi(t + \alpha\tau) - \varphi(t + (\alpha - 1)\tau)}{\tau} = \frac{d\varphi(t)}{dt} + O(\varphi''(\tau)).$$

Any $\alpha \neq 1/2$ will increase the error value from $O(\varphi'''(\tau))$ in the Wigner distribution to $O(\varphi''(\tau))$.

4.5.2 Higher-Order Distributions

We can further improve the derivative estimation accuracy, at the cost of the estimator complexity. For example, the well-known first derivative estimator

$$\begin{aligned} \Omega(t) &\approx \frac{-\varphi(t - \tau/6) + 8\varphi(t - \tau/12) - 8\varphi(t + \tau/12) + \varphi(t + \tau/6)}{\tau} \\ &= \frac{d\varphi(t)}{dt} + O(\varphi^{(5)}(\tau)) \end{aligned} \quad (4.62)$$

corresponds to a distribution

$$PD(t, \Omega) = \int_{-\infty}^{\infty} x^*(t - \tau/6)x^8(t - \tau/12)x^{*8}(t + \tau/12)x(t + \tau/6)e^{-j\Omega\tau}d\tau.$$

This distribution is fully concentrated along the instantaneous frequency up to the fourth-order polynomial phase of the signal. However, it is of quite a high order with all drawbacks from a highly increased distribution order.

The polynomial Wigner-Ville distribution defined by (4.57) is obtained from the estimator

$$\begin{aligned}\Omega(t) &\approx \frac{2\varphi(t+0.675\tau)-2\varphi(t-0.675\tau)-\varphi(t+0.85\tau)+\varphi(t-0.85\tau)}{\tau} \\ &= \frac{d\varphi(t)}{dt} + O(\varphi^{(5)}(\tau))\end{aligned}$$

that is of lower order than the previous one, with the same estimation error order $O(\varphi^{(5)}(\tau))$.

In general, an instantaneous frequency estimator may be written as

$$\Omega(t) \approx \frac{\sum_i b_i \varphi(t+c_i\tau)}{\tau} = \frac{d\varphi(t)}{dt} + O(\varphi^{(p)}(\tau)). \quad (4.63)$$

A general distribution corresponding to (4.63) reads as

$$W_G(t, \Omega) = \int_{-\infty}^{\infty} \prod_i x^{b_i}(t+c_i\tau) e^{-j\Omega\tau} d\tau. \quad (4.64)$$

The coefficients b_i and c_i follow from the system of equations, obtained by expanding $b_i \varphi(t+c_i\tau)$ into a Taylor series around t ,

$$\begin{aligned}b_i \varphi(t+c_i\tau) &= \\ b_i \varphi(t) + b_i \varphi'(t)c_i\tau + b_i \varphi''(t) \frac{(c_i\tau)^2}{2!} + b_i \varphi'''(t) \frac{(c_i\tau)^3}{3!} + b_i \varphi^{(4)}(t) \frac{(c_i\tau)^4}{4!} + \dots\end{aligned}$$

with the conditions that:

- (a) The sum of coefficients with $\varphi(t)$ is equal to 0.
- (b) The sum of coefficients with $\varphi'(t)$ is equal to 1.
- (c) The sum of coefficients with $\varphi^{(n)}(t)$ is equal to 0 up to the desired order.

Condition (a) could be omitted, since the absolute value of the distribution could be used in estimation, with $|\exp(j\sum_i b_i \varphi(t))| = 1$.

For a fourth-order polynomial Wigner-Ville distribution, we get:

$$\begin{aligned} b_1 + b_2 + b_3 + b_4 &= 0 \\ b_1 c_1 + b_2 c_2 + b_3 c_3 + b_4 c_4 &= 1 \\ b_1 c_1^2 + b_2 c_2^2 + b_3 c_3^2 + b_4 c_4^2 &= 0 \\ b_1 c_1^3 + b_2 c_2^3 + b_3 c_3^3 + b_4 c_4^3 &= 0 \\ b_1 c_1^4 + b_2 c_2^4 + b_3 c_3^4 + b_4 c_4^4 &= 0. \end{aligned} \quad (4.65)$$

If we add the requirement that a distribution is real-valued, then

$$b_1 = -b_2, c_1 = -c_2$$

$$b_3 = -b_4, c_3 = -c_4,$$

resulting in a reduced system of equations

$$b_1 c_1 + b_3 c_3 = 1/2 \quad (4.66)$$

$$b_1 c_1^3 + b_3 c_3^3 = 0. \quad (4.67)$$

Example 4.10. Assuming the lowest possible integer values (signal powers) $b_1 = 2$ and $b_3 = -1$, we get the polynomial Wigner-Ville distribution (4.57) with coefficients $c_1 \simeq 0.675$ and $c_3 \simeq 0.85$. Negative b corresponds to a conjugation of signal, for example, for $b = -2$ we use with $x^{*2}(t)$. Another approach that was used in literature to define the polynomial Wigner-Ville distribution, was to assume values for c_1 and c_2 , appropriate for discrete realization without interpolation. It results in rational values of b_1 and b_3 , that is, rational signal powers. \square

Example 4.11. A complex-time distribution that preserves energy and time marginal condition for frequency modulated signals may be derived from a similar analysis, allowing complex arguments. For example, the fourth-order form of (4.64) follows from (4.66) for $b_1 = 1$ and $b_3 = j$, when we get $c_1 = 1/4$ and $c_3 = -j/4$ with frequency (first derivative) estimator

$$\Omega(t) \approx \frac{\phi(t + \frac{\tau}{4}) - \phi(t - \frac{\tau}{4}) + j\phi(t - j\frac{\tau}{4}) - j\phi(t + j\frac{\tau}{4})}{\tau}. \quad (4.68)$$

The corresponding distribution

$$CTD(t, \Omega) = \int_{-\infty}^{\infty} x(t + \tau/4)x^*(t - \tau/4)x^j(t - j\tau/4)x^{-j}(t + j\tau/4)e^{-j\Omega\tau}d\tau \quad (4.69)$$

will be presented in Section 4.6. \square

The general distribution (4.64) can be considered as a convolution of the Fourier transforms of individual signals,

$$W_G(t, \Omega) = \text{FT}\{x^{b_1}(t + c_1\tau)\} *_{\Omega} \text{FT}\{x^{b_2}(t + c_2\tau)\} *_{\Omega} \dots *_{\Omega} \text{FT}\{x^{b_k}(t + c_k\tau)\},$$

where $*_{\Omega}$ denotes a convolution in frequency.

4.5.3 Real-Time Causal Distributions

An interesting approximation

$$\Omega(t) \approx \frac{\varphi(t - \tau) - 4\varphi(t - \tau/2) + 3\varphi(t)}{\tau} = \frac{d\varphi(t)}{dt} + O(\varphi'''(\tau)) \quad (4.70)$$

leads to a distribution that is fully concentrated for linear frequency modulated signals, as the Wigner distribution. However, in contrast to the Wigner distribution that uses past and future time values (arguments $t + \tau/2$ and $t - \tau/2$ are used), this distribution uses past signal values only,

$$RTD(t, \Omega) = \int_0^{\infty} x(t - \tau) x^{*4} \left(t - \frac{\tau}{2} \right) x^3(t) e^{-j\Omega\tau} d\tau,$$

for the estimation of the instantaneous frequency at the current instant t . Its pseudo form is

$$RTD(t, \Omega) = \int_0^T w(\tau) x(t - \tau) x^{*4} \left(t - \frac{\tau}{2} \right) x^3(t) e^{-j\Omega\tau} d\tau.$$

This distribution can be efficiently used in many applications when it is important to produce a result in real time and to estimate the instantaneous frequency at the current, last point of the considered time interval. Note that using the common forms of time-frequency representations, the instantaneous frequency is estimated in the middle point of the analyzed interval (as the pseudo Wigner distribution does for the middle point of the lag window). An example of such importance is in radar signals, when the estimation of the target parameters at the middle of the considered interval (coherent integration time may be of the order of seconds) could be quite late and inappropriate for a decision.

4.5.4 Instantaneous Rate Estimation

In some cases, a parameter of interest is the signal rate, defined as the second derivative of the phase function,

$$a(t) = \frac{d^2\varphi(t)}{dt^2}, \quad (4.71)$$

for the signal $x(t) = Ae^{j\varphi(t)}$. Its estimation could be done according to

$$a(t) \approx \frac{\varphi(t + \tau/2) - 2\varphi(t) + \varphi(t - \tau/2)}{\tau^2} = \frac{1}{2} \frac{d^2\varphi(t)}{dt^2} + O(\varphi^{(4)}(\tau)).$$

A corresponding time-rate signal representation is

$$R(t, \Theta) = \int_{-\infty}^{\infty} x\left(t + \frac{\tau}{2}\right) x^{*2}(t) x\left(t - \frac{\tau}{2}\right) e^{-j\Theta\tau^2} d\tau.$$

Since, in most cases, the estimation is performed based on $|R(t, \Theta)|$, the signal $x^{*2}(t)$ could be omitted, since it does not influence the representation form. Then the representation

$$R(t, \Theta) = \int_{-\infty}^{\infty} x\left(t + \frac{\tau}{2}\right) x\left(t - \frac{\tau}{2}\right) e^{-j\Theta\tau^2} d\tau \quad (4.72)$$

follows. It was introduced by O'Shea.

In a similar way, like in the instantaneous frequency estimation case, other forms of the instantaneous rate estimator can be defined. In addition, any order phase derivative phase estimator may be defined as well.

4.6 COMPLEX-LAG DISTRIBUTIONS

Complex argument distributions are introduced by Stanković and Stanković in order to improve the time-frequency representation concentration. They are interesting from a theoretical point of view, since they use complex frequency argument (in the Laplace domain) and the corresponding complex-lag argument in the time domain.

These forms are able to produce almost completely concentrated representations along the group delay or the instantaneous frequency.

When the higher-order derivatives in signal's phase exist, then the signal representation can be improved by introducing signal with a complex argument. One such distribution was mentioned in Example 4.11. In the frequency domain, the notion of complex frequency is well established and studied in the signals and systems within the Laplace transform framework. Thus, this analysis will start with the distribution in the frequency domain, dual to (4.69). The complex argument distribution in the frequency domain is defined as

$$\begin{aligned} CTD(t, \Omega) = & \frac{1}{2\pi} \int_{-\infty}^{\infty} X\left(j\Omega + j\frac{\theta}{4}\right) X^*\left(j\Omega - j\frac{\theta}{4}\right) \\ & \times X^j\left(j\Omega + \frac{\theta}{4}\right) X^{-j}\left(j\Omega - \frac{\theta}{4}\right) e^{j\theta t} d\theta, \end{aligned} \quad (4.73)$$

where $X(j\Omega \pm \theta/4)$ is the Laplace transform $X(s)$ of signal $x(t)$, at $s = \pm\theta/4 + j\Omega$. The coefficients for this distribution will be justified next (they are already introduced in Example 4.11). The notation used here is

$$\begin{aligned} X\left(j\Omega \pm \frac{\theta}{4}\right) &= \int_{-\infty}^{\infty} x(t) e^{\mp\theta t/4} e^{-j\Omega t} dt, \\ X\left(j\Omega \pm j\frac{\theta}{4}\right) &= \int_{-\infty}^{\infty} x(t) e^{-j(\Omega \pm \theta/4)t} dt. \end{aligned} \quad (4.74)$$

It is important to note that only here will we use the notation $X(j\Omega)$ instead of $X(\Omega)$ for the Fourier transform. Namely, in the literature, there are two ways to denote a Fourier transform of the signal $x(t)$. One is $X(\Omega)$ and the other is $X(j\Omega)$. The first one is shorter and more appropriate for a book in which the Fourier transform will not be used along with the Laplace transform. That is the case here. However, if the Laplace transform is going to be used, then, common notation for the Laplace transform is $X(s)$, with s being a complex number, $s = \sigma + j\Omega$. The Fourier transform is obtained as the Laplace transform along $\sigma = 0$. So, in the Laplace domain notation, the Fourier transform is $X(j\Omega)$. The Laplace domain notation will be used just here and we hope that this change in the Fourier transform notation will not cause confusion that it was worth using the longer notation $X(j\Omega)$ for the Fourier transform throughout the rest of book.

The Laplace transform converges for $\int_{-\infty}^{\infty} |x(t) \exp(\mp \theta t/4)| dt < \infty$. The problem may appear in numerical calculation since (4.74), although being finite, can assume large values for some θ .

The complex argument distribution of a signal $X(j\Omega) = A e^{j\varphi(\Omega)}$ is concentrated along the group delay

$$t_g(\Omega) = -\varphi'(\Omega)$$

with the lowest spreading term being of the fifth order, that is,

$$CTD(t, \Omega) = A^2 \delta(t + \varphi'(\Omega)) *_t \text{IFT}_\theta \{ e^{j(\varphi^{(5)}(\Omega)\theta^5/(4^4 5!) + \varphi^{(9)}(\Omega)\theta^9/(4^8 9!))} \}. \quad (4.75)$$

To prove this claim, consider an expansion of the complex argument function $\varphi(\Omega \pm j\theta/4)$ into a complex valued Taylor series,

$$\varphi(\Omega \pm j\theta/4) = \varphi(\Omega) + \varphi'(\Omega)(\pm j\theta/4) + \varphi''(\Omega)(\pm j\theta/4)^2/2! + \dots \quad (4.76)$$

It results in

$$\begin{aligned} X^j \left(j\Omega + \frac{\theta}{4} \right) X^{-j} \left(j\Omega - \frac{\theta}{4} \right) &= e^{\varphi(\Omega + j\frac{\theta}{4}) - \varphi(\Omega - j\frac{\theta}{4})} \\ &= e^{j(\varphi'(\Omega)\frac{\theta}{2} - 2\varphi^{(3)}(\Omega)\frac{\theta^3}{4^3 3!} + 2\varphi^{(5)}(\Omega)\frac{\theta^5}{4^5 5!} + \dots)}. \end{aligned} \quad (4.77)$$

Recall that

$$\begin{aligned} X \left(j\Omega + j\frac{\theta}{4} \right) X^* \left(j\Omega - j\frac{\theta}{4} \right) &= A^2 e^{j\varphi(\Omega + \frac{\theta}{4}) - j\varphi(\Omega - \frac{\theta}{4})} \\ &= A^2 e^{j(\varphi'(\Omega)\frac{\theta}{2} + 2\varphi^{(3)}(\Omega)\frac{\theta^3}{4^3 3!} + 2\varphi^{(5)}(\Omega)\frac{\theta^5}{4^5 5!} + \dots)}. \end{aligned} \quad (4.78)$$

So, we get

$$\begin{aligned} X^j \left(j\Omega + \frac{\theta}{4} \right) X^{-j} \left(j\Omega - \frac{\theta}{4} \right) X \left(j\Omega + j\frac{\theta}{4} \right) X^* \left(j\Omega - j\frac{\theta}{4} \right) \\ = A^2 e^{j(\varphi'(\Omega)\theta + \varphi^{(5)}(\Omega)\frac{\theta^5}{4^4 5!} + \dots)}. \end{aligned}$$

Its inverse Fourier transform produces (4.75). The notation $\text{IFT}_\theta \{ \cdot \}$ is used for the inverse Fourier transform on θ . It is interesting to note that form (4.76)

$$\varphi(\Omega + j\theta/4) = \varphi(\Omega) + j\theta/4 \varphi'(\Omega) + \varphi''(\Omega)(j\theta/4)^2/2! + \dots$$

was reintroduced in mathematical journals as a derivative estimator, a few years after it was used in signal processing to this aim, as

$$\varphi'(\Omega) \approx \text{Im}\{\varphi(\Omega + j\theta)/\theta\}. \quad (4.79)$$

Relation (4.75) means that $CTD(t, \Omega)$ is a distribution with amplitude A^2 concentrated along the group delay, with the lowest disturbing term depending on the fifth derivative of the phase function, divided by a factor of $4^4 5! = 30545 \sim 10^4$. So we will get a completely concentrated distribution for the phase of up to the fourth-order polynomial function of time.

In practice, the instantaneous frequency is more common signal parameter than the group delay. A time-frequency representation producing improved concentration along the instantaneous frequency can be introduced by replacing frequency with time, since any definition in the frequency domain can be reintroduced in its dual form. In order to define a representation with complex-valued argument, we have to introduce the quantity that will be related to the time axis in the same way as the complex frequency is related to the frequency axis. This mathematical quantity will be referred to as the complex-time or complex-lag argument.

According to the previous analysis in the Fourier domain, we can conclude that a significant improvement in concentration, along the instantaneous frequency, can be achieved by defining a distribution with the complex-lag argument, dual to (4.73). The complex-lag distribution is defined by

$$CTD(t, \Omega) = \int_{-\infty}^{\infty} x\left(t + \frac{\tau}{4}\right) x^*\left(t - \frac{\tau}{4}\right) x^{-j}\left(t + j\frac{\tau}{4}\right) x^j\left(t - j\frac{\tau}{4}\right) e^{-j\Omega\tau} d\tau. \quad (4.80)$$

The spread factor $Q(t, \tau)$ for this distribution, according to (4.75), is

$$Q(t, \tau) = \varphi^{(5)}(t) \frac{\tau^5}{4^4 5!} + \varphi^{(9)}(t) \frac{\tau^9}{4^8 9!} + \dots \quad (4.81)$$

since

$$x^{-j}(t + j\tau/4)x^j(t - j\tau/4) = \exp(\varphi(t + j\tau/4) - \varphi(t - j\tau/4)).$$

The dominant term in $Q(t, \tau)$ is of the fifth order. All existing terms causing inner interferences are significantly reduced as compared to the respective ones in the Wigner distribution. Its form is

$$CTD(t, \Omega) = 2\pi A^2 \delta(\Omega - \varphi'(t)) *_{\Omega} \text{FT}\{e^{j\varphi^{(5)}(t)\tau^5/(4^4 5!) + \dots}\}.$$

Example 4.12. For a sinusoidally frequency modulated signal $x(t) = e^{-j32\cos(\pi t/64)}$ calculate an approximate value of the complex-lag distribution, with a window $w(\tau)$ of the width $T = 32$.

★ For this signal

$$\begin{aligned}\varphi'(t) &= \pi/2 \sin(\pi t/64) \\ \varphi^{(5)}(t) &= 32(\pi/64)^5 \sin(\pi t/64).\end{aligned}$$

The complex-lag distribution of this signal is

$$CTD(\Omega, t) = \int_{-32}^{32} e^{j\pi/2 \sin(\pi t/64)\tau} e^{j32(\pi/64)^5 \sin(\pi t/64)(\tau^5/(4^4 5!) + \dots)} w(\tau) e^{-j\Omega\tau} d\tau$$

where $|\tau| \leq 32$. Obviously $|32(\pi/64)^5 \sin(\pi t/64)\tau^5/(4^4 5!)| \leq \pi^5/(4^4 5!) = 0.01$. Thus, we may write

$$CTD(\Omega, t) \cong W(\Omega - \pi/2 \sin(\pi t/64)),$$

where $W(\Omega)$ is the Fourier transform of window $w(\tau)$. □

The continuous form of the complex-lag signal is dual to the Laplace transform of $x(t)$. Complex time is denoted by $\zeta = t + j\tau$.

$$x(\zeta) = x(t + j\tau) = \frac{1}{2\pi} \int_{-\infty}^{\infty} X(j\Omega) e^{-\Omega\tau} e^{j\Omega t} d\Omega.$$

The signal with a complex-lag argument could be calculated in the same way as the Laplace transform is calculated from the Fourier transform. According to the analysis for the complex-frequency, it is easy to conclude that $x(\zeta)$ converges within the entire complex plane ζ if $x(t)$ is a band-limited signal.

In theory, numerical realization of the complex argument distributions will be simple if we know the analytic expression for the signal. However, in practical realizations, the values of $x(n)$ are available as a set of data along the real axis only. The values of signal with complex argument are not known. They must be determined from the values on the real time axis. Note that this problem is mathematically well studied, known as an analytical extension (continuation) of the real argument function. An analytic extension of the signal $x(n)$ is defined as a sum of the analytic extensions of complex exponential functions. It is of the form

$$x(\eta) = x(n + jm) = \frac{1}{N} \sum_{k=-N/2}^{N/2-1} X(k) e^{-\frac{2\pi}{N} mk} e^{j\frac{2\pi}{N} nk}. \quad (4.82)$$

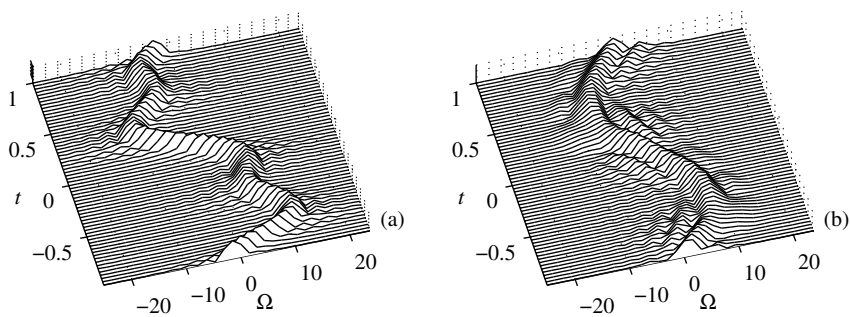


Figure 4.6 Time-frequency representation of a signal with fast-varying instantaneous frequency: (a) the complex-time distribution and (b) the pseudo Wigner distribution.

If we multiply

$$X(k) = \text{DFT}\{x(n)\}$$

by $\exp(-2\pi mk/N)$, for a given m , then $x(n + jm)$ is obtained as

$$x(n + jm) = \text{IDFT}\left\{X(k)e^{-2\pi mk/N}\right\}. \quad (4.83)$$

The presented form of $x(n + jm)$ could directly be used for the realization of a complex-lag distribution. Real exponential functions $\exp(-2\pi mk/N)$, for large $-mk$, may be out of the computer precision range, significantly worsening the results. Thus, one should carefully use the above relations in the direct numerical realization. The procedure for reduced cross-terms calculation can be defined based on the approach presented in the next section. An illustration of the complex-time distribution of signal

$$x(t) = e^{j[3\cos(\pi t) + \cos(3\pi t - \pi/3)/3]}$$

with $\Delta t = 2/N$, $N = 64$ and $-1 \leq t \leq 1$, by using $w(\tau) = \exp(-(4\tau)^{10})$ is presented in Fig. 4.6.

4.7 S-METHOD-BASED REALIZATION

Here we will extend the S-method-based approach to the realization of the higher-order time-frequency forms, obtained by reducing the full higher-order forms to the

two-dimensional time-frequency plane. This approach will provide two substantial advantages over the direct calculation: (1) it produces the higher-order distributions, without need for signal oversampling, and (2) in the case of multicomponent signals the cross-terms are reduced (eliminated). A detailed analysis of the S-method is presented in Chapter 3. The analysis presented there may directly be applied here. Therefore, we will just outline the basic steps in the higher-order distributions realizations by using this method.

4.7.1 The L-Wigner Distribution Realization

The relationship between the L-Wigner distribution of an order $2L$ and L-Wigner distribution of an order L is of the form

$$LWD_{2L}(t, \Omega) = \frac{1}{\pi} \int_{-\infty}^{\infty} LWD_L(t, \Omega + \theta) LWD_L(t, \Omega - \theta) d\theta. \quad (4.84)$$

The realization of cross-terms and alias-free version of the L-Wigner distribution may be efficiently done in the discrete domain, by using the S-method realization form as

$$LWD_{2L}(n, k) = LWD_L^2(n, k) + 2 \sum_{i=1}^{L_P} LWD_L(n, k+i) LWD_L(n, k-i), \quad (4.85)$$

with $LWD_1(n, k) = SM(n, k)$, calculated according to the described procedure in Chapter 3,

$$LWD_1(n, k) = |STFT(n, k)|^2 + 2 \sum_{i=1}^{L_P} \operatorname{Re}\{STFT(n, k+i) STFT^*(n, k-i)\}. \quad (4.86)$$

Form (4.85) is very convenient for software and hardware realizations since the same blocks, connected in cascade, can provide a simple and efficient system for higher-order time-frequency analysis, based on the STFT in the initial step, and the signal sampled according to the sampling theorem.

Example 4.13. Let us present the pseudo L-Wigner distribution realization for the signal from Fig. 4.4. The spectrogram is shown in Fig. 4.7(a). The pseudo Wigner distribution realized according to (4.86), without oversampling, is shown in Fig. 4.7(b). The pseudo L-Wigner distributions, calculated using (4.85), without any oversampling, are presented in Fig. 4.7(c) and (d), for $L = 2$ and $L = 8$, respectively. The only

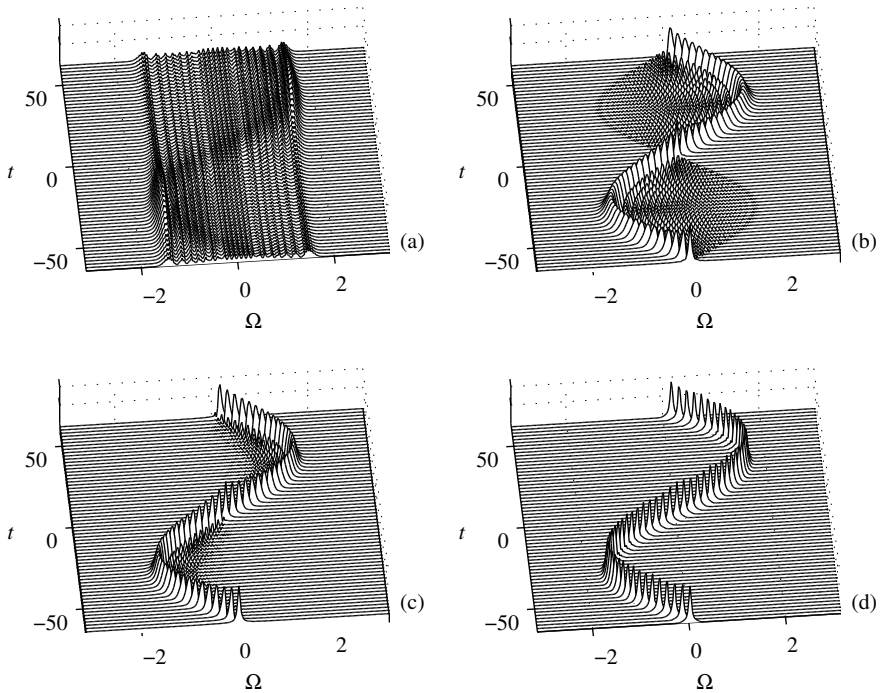


Figure 4.7 Time-frequency representation of a sinusoidally frequency modulated signal by: (a) spectrogram, (b) the pseudo Wigner distribution, (c) the L-Wigner distribution with $L = 2$, and (d) the L-Wigner distribution with $L = 8$ realized in a recursive manner.

difference from Fig. 4.4 is that here we used a lag window $w(\tau) = \exp(-|\tau/\sigma|)$ that is order invariant, $w(\tau) = w(\tau/2)w(-\tau/2) = w^2(\tau/2)w^2(-\tau/2) = \dots$, so that we can make fair comparisons of different order distributions. \square

Example 4.14. Similar calculations were repeated for a two-component signal. In this case, in order to provide a good graphical presentation at the point of intersection (where the distribution values increases with a power of $2L$) the distribution values are normalized, for each time instant n , with a maximal value for that instant over all k , that is, in Fig. 4.8 the value $LWD_{2L}(n,k)/\max_k(LWD_{2L}(n,k))$ for each n , is plotted. \square

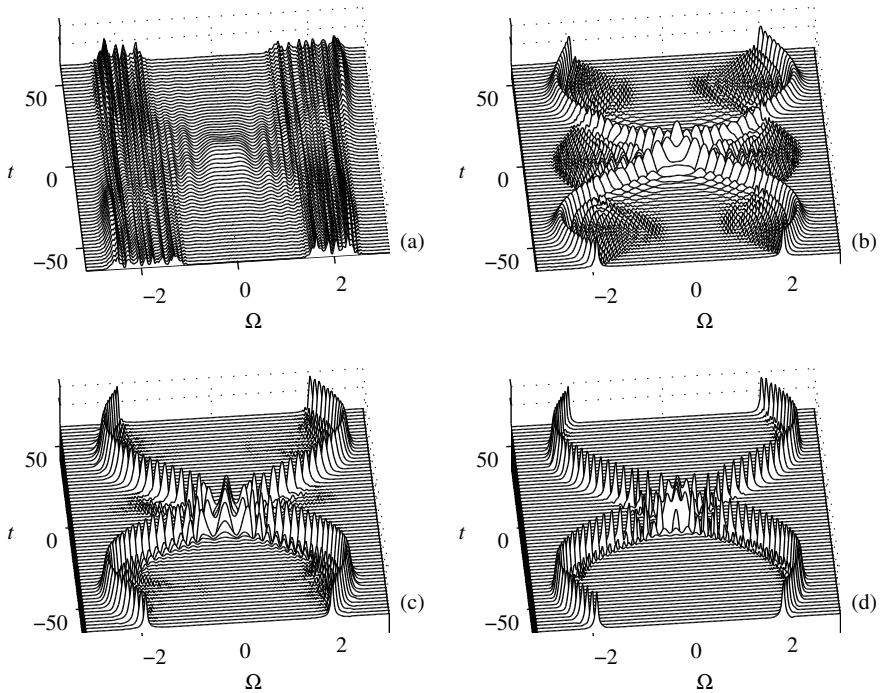


Figure 4.8 Time-frequency representation of a multicomponent signal by: (a) apertrogram, (b) cross-terms free pseudo Wigner distribution, realized by the S-method, (c) the pseudo L-Wigner distribution with $L = 2$, and (d) the pseudo L-Wigner distribution with $L = 8$ realized in a recursive manner.

4.7.2 Real-Time Causal Distribution Realization

The pseudo form of real-time distribution will be used for the presentation of a quite general approach to the efficient higher-order distributions realization.

The pseudo form of the real-time distribution can be written as

$$\begin{aligned} RTD(t, \Omega) &= \int_0^T x(t - \tau) x^*{}^4(t - \tau/2) x^3(\tau) e^{-j\Omega\tau} d\tau \\ &= x^3(t) STFT_x(t, \Omega) *_{\Omega} STFT_{x^4}(t, \Omega) \end{aligned} \quad (4.87)$$

where the rectangular window $w(\tau)$ for $0 \leq \tau \leq T$ is assumed, with $\chi(t) = x^*(t - \tau/2)$ and $STFT_{\chi^4}(t, \Omega) = \text{FT}\{w(\tau)x^{*4}(t - \tau/2)\}$ is given by

$$STFT_{\chi^4}(t, \Omega) = STFT_{\chi}(t, \Omega) *_{\Omega} STFT_{\chi}(t, \Omega) *_{\Omega} STFT_{\chi}(t, \Omega) *_{\Omega} STFT_{\chi}(t, \Omega).$$

Let us now assume that components in $STFT_{\chi}(t, \Omega)$ are localized, so that a value of $STFT_{\chi}(t, \Omega)$ at any frequency Ω_0 is related to the other values in $STFT_{\chi}(t, \Omega)$, over a finite local region $[\Omega_0 - \Omega_L/2, \Omega_0 + \Omega_L/2]$. Localization here means that the values of $STFT_{\chi}(t, \Omega)$ far from Ω_0 are not related to the value of $STFT_{\chi}(t, \Omega)$ at Ω_0 . For example, a multicomponent signal, whose components are dominantly within the regions whose width is narrower than Ω_L , is just a signal of this kind. Values from within one signal component are not related to the values within the other components. In general, the localization assumption is not equivalent to the assumption that $STFT_{\chi}(t, \Omega)$ is nonzero only within one local region $[\Omega_0 - \Omega_L/2, \Omega_0 + \Omega_L/2]$. Note that there is no assumption about the location of the central frequencies (that are, in general, time-varying) nor about the number of components (that also can change in time). Then

$$\begin{aligned} STFT_{\chi^2}(t, \Omega) &= STFT_{\chi}(t, \Omega) *_{\Omega} STFT_{\chi}(t, \Omega) \\ &= \frac{1}{2\pi} \int_{-\infty}^{\infty} STFT_{\chi}(t, \Omega - \xi) STFT_{\chi}(t, \xi) d\xi \\ &= \frac{1}{4\pi} \int_{-\infty}^{\infty} STFT_{\chi}\left(t, \frac{\Omega}{2} + \frac{\xi}{2}\right) STFT_{\chi}\left(t, \frac{\Omega}{2} - \frac{\xi}{2}\right) d\xi \\ &= \frac{1}{4\pi} \int_{-\Omega_L}^{\Omega_L} STFT_{\chi}\left(t, \frac{\Omega}{2} + \frac{\xi}{2}\right) STFT_{\chi}\left(t, \frac{\Omega}{2} - \frac{\xi}{2}\right) d\xi. \end{aligned} \quad (4.88)$$

This may be considered a windowed convolution, corresponding to the S-method. It will also reduce possible cross-terms between the distribution values more than $2\Omega_L$ apart. The region of interest $[\Omega_0 - \Omega_L/2, \Omega_0 + \Omega_L/2]$ in $STFT_{\chi}(t, \Omega)$ becomes $[2\Omega_0 - \Omega_L, 2\Omega_0 + \Omega_L]$ in $STFT_{\chi^2}(t, \Omega)$.

The value of $STFT_{\chi^4}(t, \Omega)$ is obtained by repeating this procedure

$$\begin{aligned} STFT_{\chi^4}(t, \Omega) &= STFT_{\chi^2}(t, \Omega) *_{\Omega} STFT_{\chi^2}(t, \Omega) \\ &= \frac{1}{4\pi} \int_{-2\Omega_L}^{2\Omega_L} STFT_{\chi^2}\left(t, \frac{\Omega}{2} + \frac{\xi}{2}\right) STFT_{\chi^2}\left(t, \frac{\Omega}{2} - \frac{\xi}{2}\right) d\xi \end{aligned} \quad (4.89)$$

with the region of interest corresponding to $[4\Omega_0 - 2\Omega_L, 4\Omega_0 + 2\Omega_L]$.

The final step is to make local convolution of $STFT_{\chi^4}(t, \Omega)$ with $STFT_x(t, \Omega)$ in Ω . It is important to relate the corresponding regions in these two transforms. For an arbitrary Ω_0 local region $[\Omega_0 - \Omega_L, \Omega_0 + \Omega_L]$ in $STFT_\chi(t, \Omega)$ is transformed to the region $[4\Omega_0 - 2\Omega_L, 4\Omega_0 + 2\Omega_L]$ in (4.89), as explained. The same region in $STFT_\chi(t, \Omega)$ corresponds to the region $[-2\Omega_0 - \Omega_L, -2\Omega_0 + \Omega_L]$ in the reversed transform $STFT_x(t, -\Omega)$, since this is the transform of $x(t - \tau)$, while $STFT_\chi(t, \Omega)$ is the transform of $x^*(t - \tau/2)$.

For both functions the same local frequency range should be used. The realization formula, then becomes

$$RTD(t, \Omega) = \frac{1}{4\pi} \int_{-2\Omega_L}^{2\Omega_L} STFT_x \left(t, -\frac{\Omega}{2} - \frac{\xi}{2} \right) STFT_{\chi^4}(t, \Omega - \xi) d\xi, \quad (4.90)$$

for all Ω . This approach can be applied to any distribution of form (4.56). In order to present discrete time form of this approach, let us consider a single time instant t and discrete time samples $x_t(n)$ of a continuous signal $x(t - \tau)$ sampled along τ . We will assume that a rectangular window function $w(n)$ of length N is used.

Step 1: Calculate a discrete time signal $\chi_t(n)$ as samples of $x^*(t - \tau/2)$. Its Fourier transform is $STFT_1(t, k) = FT\{\chi_t(n)\}$ for $-N/2 \leq k \leq N/2 - 1$.

Step 2: Calculate $STFT_2(t, k) = FT\{\chi_t^2(n)\}$ by convolution

$$STFT_2(t, k) = \sum_p STFT_1(t, p) STFT_1(t, k - p). \quad (4.91)$$

Let us assume that components in $STFT_1(t, k)$ are localized in discrete frequency, that is, that a component at any k_0 is related to the local components from the region $[k_0 - L, k_0 + L]$. It means that only frequency range $[k - L, k + L]$ will be used for calculation of $STFT_2(t, k)$ for all k since k_0 is unknown. The limits on p in (4.91) are $k_0 - L \leq p \leq k_0 + L$ and $k_0 - L \leq k - p \leq k_0 + L$. Eliminating unknown k_0 , we get

$$k/2 - L \leq p \leq k/2 + L.$$

The component in $STFT_1(t, k)$, corresponding to k_0 , is located in $STFT_2(t, k)$ within the range $[2k_0 - 2L, 2k_0 + 2L]$.

Step 3: The second convolution is performed in the same manner as in Step 2, to obtain

$$STFT_4(t, k) = FT\{\chi_t^4(n)\} = \sum_p STFT_2(t, p) STFT_2(t, k - p).$$

A similar analysis, as in Step 2, leads to the summation limits $\frac{k}{2} - 2L \leq p \leq \frac{k}{2} + 2L$. Note that component corresponding to k_0 in $STFT_1(t, k)$ is located in $STFT_4(t, k)$ within the range $[4k_0 - 4L, 4k_0 + 4L]$. Convolution $STFT_4(t, k)$ contains $4N - 3$ frequency samples in total.

Step 4: We will now calculate $STFT_x(t, k) = DFT\{x_t(n)\}$. For a component corresponding to k_0 in $STFT_1(t, k)$, the corresponding component in $STFT_x(t, k)$ is located within $[-2k_0 - 4L, -2k_0 + 4L]$. It is obvious, since $STFT_1(t, \Omega) = FT\{x^*(t - \tau/2)\}$ and $STFT_x(t, \Omega) = FT\{x(t + \tau)\}$.

The final distribution, with local calculation, is

$$RTD(t, k) = x^3(t) \sum_p STFT_x(t, k) STFT_4(t, k - p) \quad (4.92)$$

where limits for p are $-k - 4L \leq p \leq -k + 4L$. In the presentation of $|RTD(t, k)|$ the signal $x^3(t)$ could be omitted.

A signal dependent realization can be performed as follows. Check each next term, for $p = k/2 \pm 1, p = k/2 \pm 2, \dots$ against a reference level, before it is included in the summation. If the new correction term, for example, in two subsequent values of p , is lower than the reference level, then stop further summation. In this way, it is possible to avoid cross-terms between close components and improve representation, in a computationally very efficient way.

A realization of the STFT, the S-method (cross-terms free Wigner distribution) and the real-time causal distribution (calculated by using the presented calculation procedure) on a two-component signal

$$\begin{aligned} x(n) = & \exp(j230\pi(n/N) + j24\pi(n/N)^2 - j9(n/N)^3) \\ & + \exp(-j240\pi(n/N) - j20\pi(n/N)^2 + j2(n/N)^3), \end{aligned}$$

with $N = 256$ and $L = 7$ is presented in Fig. 4.9. Note that the instantaneous frequency representation in the real time causal distribution corresponds to the current instant (last available instant in calculation), while the instantaneous frequency in the Wigner distribution is significantly delayed with respect to this instant (Fig. 4.9). In the spectrogram we can see that the instantaneous frequency, corresponding to the current instant, is at the position of one of the ending frequencies in the wide auto-term (depending on fact whether the instantaneous frequency increases or decreases). In the Wigner distribution the instantaneous frequency is in the middle of the STFT's auto-term.

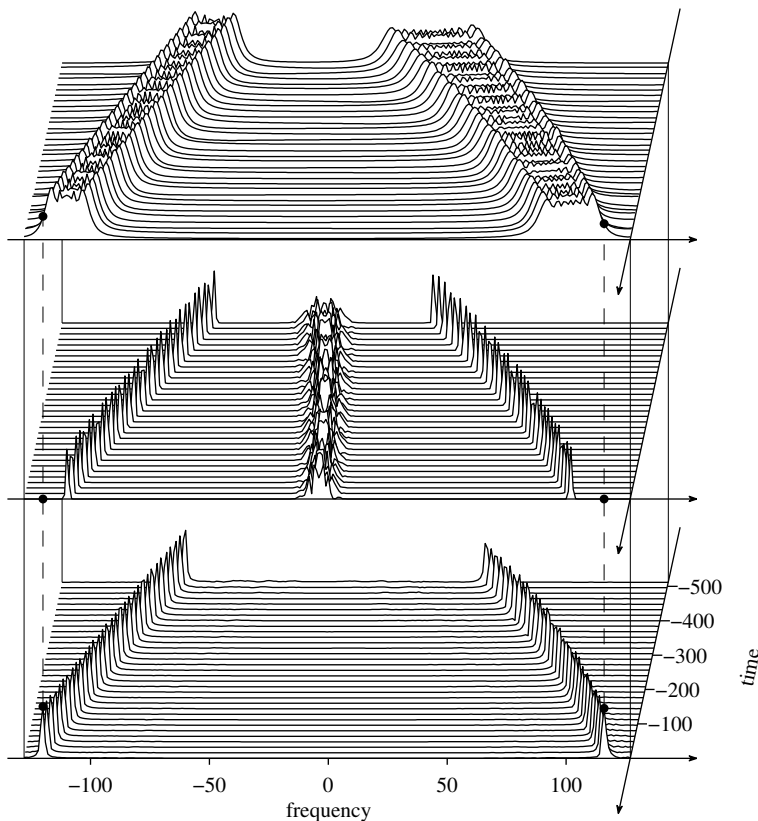


Figure 4.9 Time-frequency representation of a two-component signal: spectrogram (top), the cross-terms free form of the Wigner distribution, calculated by using the S-method (middle), and the real-time causal distribution with cross-terms free (reduced) realization (bottom). Vertical dashed lines indicate true instantaneous frequencies, at the initial time instant, for each component.

4.7.3 Polynomial Wigner-Ville Distribution Realization

The modification of the presented method for the realization of the polynomial Wigner-Ville distribution is straightforward. The fourth-order polynomial Wigner-Ville distribution

$$PD(t, \Omega) = \int_{-\infty}^{\infty} x^2(t + 0.675\tau) x^{*2}(t - 0.675\tau) x^*(t + 0.85\tau) x(t - 0.85\tau) e^{-j\Omega\tau} d\tau \quad (4.93)$$

can be written, by using the change of variables $0.675\tau \rightarrow \tau/4$ (or $\tau \rightarrow \tau/2.7$) as

$$PD(t, \Omega) = \int_{-\infty}^{\infty} x^2\left(t + \frac{\tau}{4}\right) x^{*2}\left(t + \frac{\tau}{4}\right) x^*\left(t + \frac{1.7}{2.7} \frac{\tau}{2}\right) x\left(t + \frac{1.7}{2.7} \frac{\tau}{2}\right) e^{-j\tau\Omega/2.7} d\tau.$$

In a frequency scaled form

$$PD(t, \Omega) = \frac{1}{2.7} \int_{-\infty}^{\infty} x^2\left(t + \frac{\tau}{4}\right) x^{*2}\left(t - \frac{\tau}{4}\right) x^*\left(t + A \frac{\tau}{2}\right) x\left(t - A \frac{\tau}{2}\right) e^{-j\tau\Omega_s} d\tau, \quad (4.94)$$

where $A = 0.85/1.35$ and $\Omega_s = \Omega/2.7$. Note that

$$PD(t, \Omega_s) = \frac{1}{2.7} LWD_2(t, \Omega_s) *_{\Omega_s} WD^A(t, \Omega_s), \quad (4.95)$$

where

$$W^A(t, \Omega_s) = \text{FT} \left\{ x^*\left(t + A \frac{\tau}{2}\right) x\left(t - A \frac{\tau}{2}\right) \right\}$$

is a scaled and frequency reversed version (due to order of conjugate terms) of the pseudo Wigner distribution and

$$LWD_2(t, \Omega_s) = \text{FT} \left\{ x^2\left(t + \frac{\tau}{4}\right) x^{*2}\left(t - \frac{\tau}{4}\right) \right\}$$

is the L-Wigner distribution with $L = 2$. The cross-terms free realization of the pseudo Wigner distribution and the pseudo L-Wigner distribution is already presented. In the discrete implementation of the above relation, the only remaining problem is the evaluation of $WD^A(t, \Omega_s)$ on the discrete set of points on the frequency axis, $\Omega_s = -k\Delta\Omega_s$. Since $WD^A(t, \Omega_s)$ is, by definition, a scaled and frequency reversed version of $WD(t, \Omega)$. Therefore, the values of $WD^A(t, \Omega_s)$ at $\Omega_s = -k\Delta\Omega_s$ are the values of $WD(t, \Omega)$ at $\Omega_s = k\Delta\Omega_s/A$. However, these points do not correspond to any sample location along the frequency axis grid. Thus, the interpolation of the pseudo Wigner distribution has to be done (one way of doing it is in an appropriate zero padding of the signal).

A discrete form of convolution (4.94), including rectangular window $P(\theta)$ and the above considerations, is

$$PD(n, k) = \sum_{i=-L_P}^{L_P} LW_2(n, k+i) \hat{WD}(n, k+i/A) \quad (4.96)$$

where $2L_P + 1$ is the width of $P(\theta)$ in the discrete domain, while $\hat{WD}(n, k+i/A)$ is the pseudo Wigner distribution approximation. We can simply use $\hat{WD}(n, k+i/A) = SM_x(n, k+[i/A])$ where $[i/A]$ is the nearest integer to i/A , or use the linear interpolation of the pseudo Wigner distribution (S-method) values at two nearest integers. The terms in (4.96), when $k+i$, or $k+[i/A]$ is outside the basic period, are considered as zero in order to avoid aliasing.

Example 4.15. Consider a real-valued multicomponent signal

$$x(t) = \cos(15 \sin(\pi t) + 35\pi t) + \sin(15 \cos(\pi t) + 100\pi t),$$

within $-1 \leq t < 1$, with $\Delta t = 1/128$. In the realization, a Hann(ing) window of the width $T = 2$ is used. Based on the STFT (using its positive frequencies), the cross-terms free pseudo Wigner distribution is obtained from (4.86) with $L_P = 15$, and denoted by the S-method (Fig. 4.10(a)). Then the pseudo L-Wigner distribution, with $L = 2$, is calculated according to (4.85). It is combined with the linearly interpolated S-method value into the polynomial Wigner-Ville distribution (4.96), shown in Fig. 4.10(b). For the precise implementation of $[i/A]$, the lag window has been zero-padded by a factor of 2. \square

4.8 LOCAL POLYNOMIAL WIGNER DISTRIBUTION

A full concentration of a polynomial phase signals may be achieved by the local polynomial Fourier transform (LPFT), presented in Chapter 2. However, in the local polynomial Fourier transform case of a signal with third-order polynomial phase one should use three coefficients to match the phase parameters. Optimization over a set of three coefficients may be computationally complex. A distribution, being an extension of the local polynomial Fourier transform, is the polynomial Wigner distribution

$$WDP(t, \Omega; \beta) = \int_{-\infty}^{\infty} x\left(t + \frac{\tau}{2}\right) x^*\left(t - \frac{\tau}{2}\right) e^{-j\beta\tau^3} e^{-j\Omega\tau} d\tau. \quad (4.97)$$

With respect to the signal, this is a quadratic distribution, with one optimization parameter β . Introducing a lag window, it becomes a local polynomial Wigner

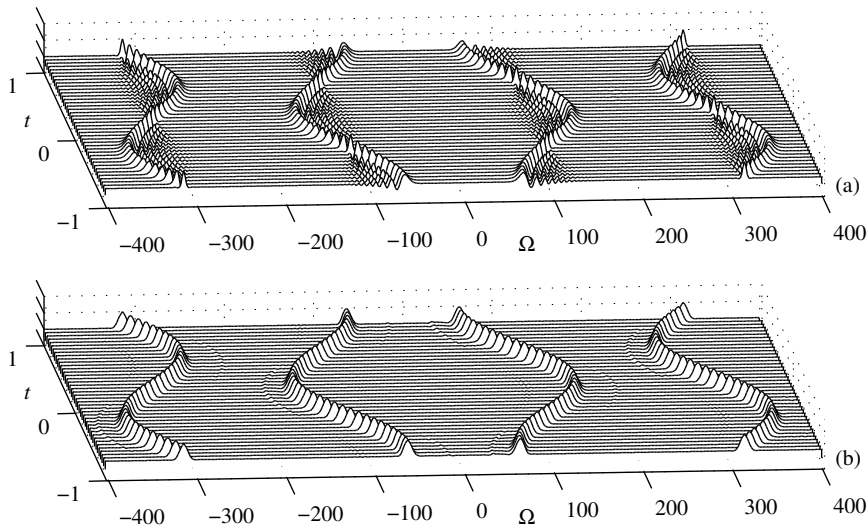


Figure 4.10 Time-frequency representation of a real-valued multicomponent signal: (a) the S-method (cross-terms and alias-free version of the pseudo Wigner distribution) and (b) polynomial Wigner-Ville distribution realized based on the STFT by using the S-method and its order recursive form.

distribution. It can achieve full concentration of the signal with phase up to the fourth-order

$$x(t) = A \exp(j(a_0 + a_1 t + a_2 t^2 + a_3 t^3 + a_4 t^4)),$$

when we get

$$WDP(t, \Omega; \beta) = 2\pi A^2 \delta(\Omega - a_1 - 2a_2 t - 3a_3 t^2 - 4a_4 t^3),$$

for $\beta = a_3/4 + ta_4$. This concentration is equivalent to the one achieved by the fourth-order polynomial Wigner-Ville distribution that is not using any parameter (nonparametric estimator). For a signal of the form $x(t) = A \exp(j(a_0 + a_1 t + a_2 t^2 + a_3 t^3))$ the parameter $\beta = a_3/4$ is time invariant. The distribution $WDP(t, \Omega; \beta = a_3/4)$ is the same as the one presented in Fig. 4.5 for the signal $x(t) = \exp(j(45\pi t + 120t^3))$. The simplest way to estimate parameter β is to vary its values within the set of possible values and to choose the one producing maximal distribution concentration for each time instant. The number of parameters in the

local polynomial Wigner distribution may be increased by adding odd power terms in τ . The next one would be $\exp(-j\gamma\tau^5)$ for signals up to the sixth-order polynomial phase. The polynomial Wigner distribution satisfies the time marginal (and energy) property.

4.9 HIGHER-ORDER AMBIGUITY FUNCTIONS

A specific class of nonlinear frequency modulated signals is the polynomial phase signals. This case is of importance not only when the phase is of polynomial form, but also in quite general case, when signals within a smaller time intervals can be approximated by finite order polynomial functions, using the Taylor series. By using the multilag higher-order instantaneous moments, the polynomial order of the phase function is reduced, in several steps, to the linear one. The Fourier transform of the multilag instantaneous moments, known as the multilag higher-order ambiguity function, is used to estimate the highest phase coefficient. After the original signal is demodulated, the procedure is repeated until all parameters of the phase are estimated. The product higher-order ambiguity function (PHAF) is introduced to estimate the polynomial phase signal coefficients in the case of multicomponent signals.

4.9.1 Monocomponent Polynomial Phase Signals

Consider a deterministic polynomial phase signal

$$x(t) = A \exp(j\varphi(t)) = A \exp\left(j \sum_{p=0}^P \alpha_p t^p\right) \quad (4.98)$$

and see what will be the result of an operation corresponding the studied symmetric phase derivative estimation

$$\hat{\Omega}(t) = \frac{\varphi(t + \tau_1) - \varphi(t - \tau_1)}{2\tau_1}.$$

In terms of signal, it means

$$\begin{aligned} x(t + \tau_1)x^*(t - \tau_1) &= A^2 \exp(j(\varphi(t + \tau_1) - \varphi(t - \tau_1))) \\ &= A^2 \exp\left(j \sum_{p=0}^P \alpha_p (t + \tau_1)^p - j \sum_{p=0}^P \alpha_p (t - \tau_1)^p\right). \end{aligned} \quad (4.99)$$

The highest-order phase term is transformed into

$$\alpha_P(t + \tau_1)^P - \alpha_P(t - \tau_1)^P = 2\alpha_P\tau_1[(t + \tau_1)^{P-1} + (t + \tau_1)^{P-2}(t - \tau_1) + \dots + (t - \tau_1)^{P-1}].$$

Thus, the phase order in t is reduced in $x(t + \tau_1)x^*(t - \tau_1)$ to $P - 1$,

$$R(t, \tau_1) = x(t + \tau_1)x^*(t - \tau_1) = A^2 \exp \left(\sum_{p=0}^{P-1} \beta_p(\tau_1)t^p \right). \quad (4.100)$$

The first-order instantaneous moment $R_1(t, \tau_1)$, corresponding to the local auto-correlation function, will be used without index, that is, $R(t, \tau_1) = R_1(t, \tau_1)$.

The highest-order coefficient, with t^{P-1} , in $R(t, \tau_1)$ is

$$\beta_{P-1}(\tau_1) = 2\alpha_P\tau_1 P. \quad (4.101)$$

It is possible to continue in this way by forming

$$R_2(t, \tau_1, \tau_2) = R(t + \tau_2, \tau_1)R^*(t - \tau_2, \tau_1) = A^4 \exp \left(\sum_{p=0}^{P-2} \gamma_p(\tau_1, \tau_2)t^p \right).$$

The highest-order coefficient in $R_2(t, \tau_1, \tau_2)$, according to (4.101), is

$$\gamma_{P-2}(\tau_1, \tau_2) = 2\beta_{P-1}(\tau_1)\tau_2(P-1) = 4\alpha_P\tau_1\tau_2 P(P-1).$$

After $P - 1$ steps, a pure complex sinusoidal signal in $R_{P-1}(t, \tau_1, \tau_2, \dots, \tau_{P-1})$ is obtained. The functions $R_{P-1}(t, \tau_1, \tau_2, \dots, \tau_{P-1})$ are called the multilag higher-order instantaneous moments. The coefficient with t in the final sinusoid is obtained as

$$\Omega_0 = 2^{P-1}\alpha_P\tau_1\tau_2\dots\tau_{P-1}P!. \quad (4.102)$$

It can be calculated using the multilag higher-order ambiguity function, defined as the Fourier transform of the multilag higher-order instantaneous moment,

$$X_{P-1}(\Omega, \tau_1, \tau_2, \dots, \tau_{P-1}) = \int_{-\infty}^{\infty} R_{P-1}(t, \tau_1, \tau_2, \dots, \tau_{P-1})e^{-j\Omega t} dt, \quad (4.103)$$

as

$$\begin{aligned}\Omega_0 &= \arg \left\{ \max_{\Omega} X_{P-1}(\Omega, \tau_1, \tau_2, \dots, \tau_{P-1}) \right\}, \\ \hat{\alpha}_P &= \frac{\Omega_0}{2^{P-1} \tau_1 \tau_2 \dots \tau_{P-1} P!}.\end{aligned}\quad (4.104)$$

Now the original signal is demodulated by

$$x_1(t) = x(t) \exp(-j\hat{\alpha}_P t^P),$$

producing, in an ideal case, a signal with a lower ($P - 1$) order of the phase,

$$x_1(t) = A \exp \left(j \sum_{p=0}^{P-1} \alpha_p t^p \right).$$

All previous steps are repeated on $x_1(t)$ to produce the next highest coefficient $\hat{\alpha}_{P-1}$. Here $P - 2$ steps are performed. In this way lower and lower order of coefficients is estimated. Note that if an error in the estimation of a coefficient $\hat{\alpha}_P$ occurs, it will propagate and cause inaccurate lower-order coefficients estimation.

Example 4.16. Consider a third-order ($P = 3$) polynomial phase signal

$$x(t) = A e^{j(a_0 + a_1 t + a_2 t^2 + a_3 t^3)}.$$

Estimate its phase coefficients.

★The multilag higher-order instantaneous moments of the signal $x(t)$ are:

$$R_0(t) = x(t) = A e^{j(a_0 + a_1 t + a_2 t^2 + a_3 t^3)},$$

$$R(t, \tau_1) = x(t + \tau_1)x^*(t - \tau_1) = |A|^2 e^{j2a_1 \tau_1 + 2ja_3 \tau_1^3} e^{j4a_2 \tau_1 t} e^{ja_3 6t^2 \tau_1},$$

$$R_2(t, \tau_1, \tau_2) = R(t + \tau_2, \tau_1)R^*(t - \tau_2, \tau_1) = |A|^4 e^{j8a_2 \tau_1 \tau_2} e^{ja_3 24 \tau_1 \tau_2 t}.$$

The multilag higher-order ambiguity function is the Fourier transform (over t) of $R_2(t, \tau_1, \tau_2)$, that is,

$$X_2(\Omega, \tau_1, \tau_2) = \text{FT}_t \{R_2(t, \tau_1, \tau_2)\} = 2\pi |A|^4 e^{j8a_2 \tau_1 \tau_2} \delta(\Omega - 24a_3 \tau_1 \tau_2).$$

Obviously, from the position of the Fourier transform maximum, at

$$\Omega_0 = 24a_3 \tau_1 \tau_2, \quad (4.105)$$

follows

$$\hat{a}_3 = \frac{\Omega_0}{24\tau_1\tau_2} = a_3.$$

The estimated coefficient can be used to unwrap the original signal to

$$\begin{aligned} x_1(t) &= x(t)e^{-j\hat{a}_3 t^3} = Ae^{j(a_0+a_1t+a_2t^2+a_3t^3)}e^{-ja_3t^3} \\ &= Ae^{j(a_0+a_1t+a_2t^2)}. \end{aligned}$$

Now the multilag higher-order instantaneous moments of the signal $x_1(t)$ are calculated

$$\begin{aligned} x_1(t) &= Ae^{j(a_0+a_1t+a_2t^2)} \\ R(t, \tau_1) &= x_1(t + \tau_1)x_1^*(t - \tau_1) = |A|^2 e^{j2a_1\tau_1} e^{ja_2 4t\tau_1}. \end{aligned}$$

The Fourier transform is

$$X(\Omega, \tau_1) = \text{FT}_t\{R(t, \tau_1)\} = 2\pi|A|^2 e^{j2a_1\tau_1} \delta(\Omega - 4a_2\tau_1)$$

with $\Omega_0 = 4a_2\tau_1$ and $\hat{a}_2 = \Omega_0/(4\tau_1) = a_2$.

The estimated coefficient is used to dechirp $x_1(t)$, as

$$\begin{aligned} x_2(t) &= x_1(t)e^{-j\hat{a}_2 t^2} = Ae^{j(a_0+a_1t+a_2t^2)}e^{-ja_2t^2} \\ &= Ae^{j(a_0+a_1t)}. \end{aligned}$$

Now the Fourier transform of $x_2(t)$, $X_1(\Omega) = 2\pi A e^{ja_0} \delta(\Omega - a_1)$, produces a_1 and a_0 . □

4.9.2 Multicomponent Polynomial Phase Signals

When $x(t)$ is a multicomponent polynomial phase signal, that is,

$$x(t) = \sum_{k=1}^K A_k \exp\left(j \sum_{p=0}^P a_p^k t^p\right), \quad (4.106)$$

where a_p^k are the coefficients of the k th component, the P th-order multilag higher instantaneous moments will contain K sinusoids that correspond to the auto-terms. Each auto-term has the frequency proportional to the corresponding highest-order phase coefficient. In addition to the auto-terms, the multilag higher-order instantaneous moments will contain a large number of cross-terms which are, in general,

P th-order polynomial phase signals. When the highest-order phase coefficients of some components coincide, the corresponding cross-terms are complex sinusoids, implying that some of the peaks in the multilag higher-order ambiguity function correspond to the cross-terms. The maxima based estimation of phase coefficients is ambiguous, since a peak corresponding to a cross-term can be detected as a maximum, leading to a false estimation.

The effect of cross-terms can be considerably attenuated by using the product higher-order ambiguity function (PHAF). The PHAF is based on the fact that, unlike the cross-terms, the auto-terms are at frequencies proportional to the product of time lags used for the calculation of the multilag higher-order ambiguity function. Therefore, in the PHAF, L sets of the time lags are used

$$\mathbf{T}_{P-1}^L = \begin{bmatrix} \tau_1^{(1)}, \tau_2^{(1)}, \dots, \tau_{P-1}^{(1)} \\ \tau_1^{(2)}, \tau_2^{(2)}, \dots, \tau_{P-1}^{(2)} \\ \dots \\ \tau_1^{(L)}, \tau_2^{(L)}, \dots, \tau_{P-1}^{(L)} \end{bmatrix}. \quad (4.107)$$

The PHAF is defined as a product of the scaled transforms (4.103)

$$X_{P-1}^L(\Omega, \mathbf{T}_{P-1}^L) = \prod_{l=1}^L X_{P-1}(\beta^{(l)}\Omega, \tau_1^{(l)}, \tau_2^{(l)}, \dots, \tau_{P-1}^{(l)}) \quad (4.108)$$

with the scaling coefficient

$$\beta^{(l)} = \frac{\prod_{k=1}^{P-1} \tau_k^{(l)}}{\prod_{k=1}^{P-1} \tau_k^{(1)}}.$$

In the resulting PHAF, obtained as a product of the frequency scaled higher-order ambiguity functions, calculated for different sets of lags (4.108), the auto-terms are enhanced more significantly than the cross-terms. They are at the same positions in the scaled frequency for each multilag higher-order ambiguity function, which is not the case for the cross-terms.

Example 4.17. In order to illustrate the procedure of the PHAF calculation, we will consider a two-component second-order ($P = 2$) polynomial phase signal

$$x(t) = A_1 e^{j(a_0^1 + a_1^1 t + a_2^1 t^2)} + A_2 e^{j(a_0^2 + a_1^2 t + a_2^2 t^2)}.$$

The multilag higher-order instantaneous moment of the signal $x(t)$ is

$$\begin{aligned} R(t, \tau_1) = & |A_1|^2 e^{j2a_1^1 \tau_1} e^{j4a_2^1 \tau_1 t} + |A_2|^2 e^{j2a_2^2 \tau_1} e^{j4a_2^2 \tau_1 t} + \\ & + A_1 A_2^* e^{j((a_0^1 - a_0^2) + (a_1^2 - a_1^1)t + (a_1^1 + a_1^2)\tau_1 + (a_2^2 - a_2^1)(t^2 + \tau_1^2) + (a_1^1 + a_2^2)2t\tau_1)} \\ & + A_2 A_1^* e^{j((a_0^2 - a_0^1) + (a_1^2 - a_1^1)t + (a_1^2 + a_1^1)\tau_1 + (a_2^2 - a_2^1)(t^2 + \tau_1^2) + (a_2^2 + a_1^1)2t\tau_1)}. \end{aligned} \quad (4.109)$$

The first two terms in the second-order instantaneous moment, proportional to the a_2^1 and a_2^2 , respectively, are the auto-terms. The frequency of the auto-terms is as well, proportional to the value of the used time-lag τ_1 . The third and fourth terms are obtained as a result of interferences of two signal components and are the cross-terms. The frequencies of the cross-terms are not proportional to the value of the used time-lag τ_1 . This is the reason for introducing different sets of time lags and for multiplication of the corresponding multilag higher-order ambiguity functions in the PHAF.

Let us consider two sets of the time lags, $L = 2$ in (4.107)

$$\mathbf{T}_1^2 = \begin{bmatrix} \tau_1^{(1)} \\ \tau_1^{(2)} \end{bmatrix}.$$

The PHAF calculated with these time lags is (4.108)

$$X_1^2(\Omega, \mathbf{T}_1^2) = X_1\left(\Omega, \tau_1^{(1)}\right) X_1\left(\frac{\tau_1^{(2)}}{\tau_1^{(1)}}\Omega, \tau_1^{(2)}\right). \quad (4.110)$$

Let us consider further the component of the PHAF that corresponds to the first auto-term in (4.109), that is, to $x'(t) = A'_1 e^{j4a_2^1 \tau_1^{(1)} t}$. The PHAF is obtained as the product of two higher-order ambiguity functions (4.110). The first higher-order ambiguity function is the Fourier transform of the signal $x'(t) = A'_1 e^{j4a_2^1 \tau_1^{(1)} t}$, that is, a peak at the frequency $4a_2^1 \tau_1^{(1)}$. When lag $\tau_1^{(2)}$ is used, the resulting Fourier transform is a peak at the frequency $4a_2^1 \tau_1^{(2)}$. After scaling over frequency, the position of the maximum is changed to $4a_2^1 \tau_1^{(2)} / \beta^{(2)} = 4a_2^1 \tau_1^{(2)} / \tau_1^{(2)} \tau_1^{(1)} = 4a_2^1 \tau_1^{(1)}$. It becomes the same as the position of the maximum in the first higher-order ambiguity function calculated for $\tau_1^{(1)}$. The same alignment will occur for the second auto-term in (4.109). Therefore, by multiplying the frequency-scaled multilag higher-order ambiguity functions calculated for the different values of the time-lag sets, the auto-terms are enhanced in the resulting PHAF. The cross-terms in (4.109) are not proportional to the used time lags. Therefore, after frequency scaled higher-order ambiguity functions (calculated for different time lags) are multiplied (4.110), the cross-terms are almost completely eliminated (attenuated comparing to the auto-terms) in the resulting PHAF. \square

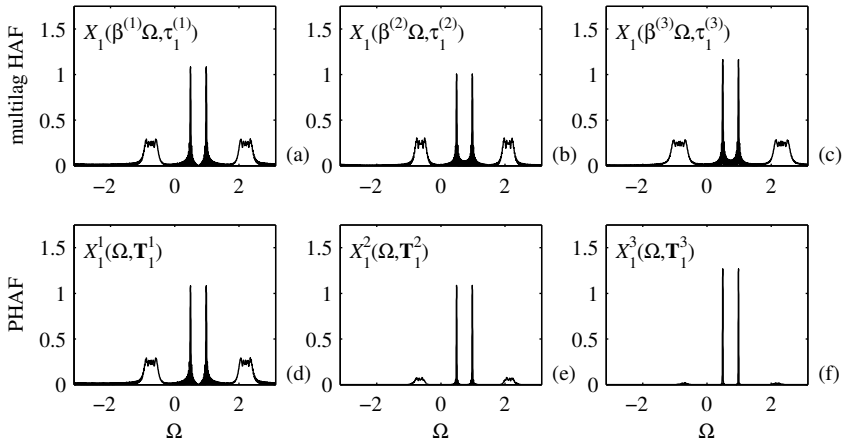


Figure 4.11 Frequency-scaled multilag higher-order ambiguity functions (HAF) calculated for three different values of time lag (a - c) and the product higher-order ambiguity functions (PPAF) obtained by multiplying scaled multilag higher-order ambiguity functions for one, two, and three sets of lags (d - f).

Example 4.18. In this example, a two-component signal

$$x(t) = e^{j(-56\pi t + 20\pi t^2)} + e^{j(64\pi t + 40\pi t^2)}$$

is analyzed with three sets of time lags are used for the PPHAF calculation. The PPHAF is obtained as

$$X_1^3(\Omega, \mathbf{T}_1^3) = \prod_{l=1}^3 X_1 \left(\beta^{(l)} \Omega, \tau_1^{(l)} \right). \quad (4.111)$$

In Fig. 4.11 all steps in the calculation of the PPHAF are shown: the multilag higher-order ambiguity function obtained for the first value of time lag $\tau_1^{(1)}$ (Fig. 4.11(a)) which is equal to the PPHAF, calculated for one set of time lags, depicted in Fig. 4.11(d); the frequency-scaled multilag higher-order ambiguity functions, calculated for the second value of time lag $\tau_1^{(2)}$ (second term in product (Fig. 4.11(b)); the resulting PPHAF for two sets of time lags (Fig. 4.11(e)); the third term in the product (4.111) (Fig. 4.11(c)), and the PPHAF for the three sets of time lags (Fig. 4.11(f)). It is obvious that the auto-terms are enhanced by using this procedure, while the influence of cross-terms is decreased.

In the considered case, true values of phase coefficients of the first component are: $a_1^1 = -56\pi$ and $a_2^1 = 20\pi$. Estimated values are: $\hat{a}_1^1 = -55.9906\pi$ and $\hat{a}_2^1 = 20.011\pi$. The true values of the phase coefficients of the second component are:

$a_1^2 = 64\pi$ and $a_2^2 = 40\pi$. Estimated values are $\hat{a}_1^2 = 63.975\pi$ and $\hat{a}_2^2 = 39.9968\pi$. The lag values $\tau_1^{(1)} = 128$, $\tau_1^{(2)} = 138$, and $\tau_1^{(3)} = 118$ are used here, since $N = 512$ signal samples are available, $P = 2$, and recommendation given by Barbarossa et al., is to use lag values close to $N/(2P)$. \square

The advantages of the PHAF, as an estimator of phase coefficients, are: (a) it is quite efficient from the point of numerical implementation; (b) it is robust to the deviation of signal model, including slowly varying amplitude or nonpolynomial (but continual) phase; and (c) it provides accuracy of the obtained estimation similar to the accuracy that would be obtained by considering monocomponent case. However, it can be concluded from the presented example that a difference between the estimated and the true value, although very small, exists. In addition, an error on the PHAF estimates of the highest order phase coefficients propagates to the other, lower-order, coefficients.

4.10 PROBLEMS

Problem 4.1. Calculate the bispectrum of a signal

$$x(t) = 1.2e^{j2\pi t} + e^{j3\pi t} + 0.9e^{j4\pi t - j\pi/4} + 0.5e^{j5\pi t + j\pi/3}.$$

Problem 4.2. Show that the Wigner higher-order spectra in terms of the signal in the time domain (4.22) is equal to its version (4.23) with signal in frequency domain.

Problem 4.3. Let the higher-order instantaneous moment functions, of different order, be defined by

$$R(t, \lambda_1) = x(t + \frac{\lambda_1}{2})x^*(t - \frac{\lambda_1}{2})$$

$$\begin{aligned} R_2(t, \lambda_1, \lambda_2) &= R(t, \frac{\lambda_1}{4} + \frac{\lambda_2}{4})R(t, \frac{\lambda_1}{4} - \frac{\lambda_2}{4}) \\ &= [x(t + \frac{\lambda_1}{4} + \frac{\lambda_2}{4})x^*(t - \frac{\lambda_1}{4} + \frac{\lambda_2}{4})][x(t + \frac{\lambda_1}{4} - \frac{\lambda_2}{4})x^*(t - \frac{\lambda_1}{4} - \frac{\lambda_2}{4})] \end{aligned}$$

$$\begin{aligned}
R_3(t, \lambda_1, \lambda_2, \lambda_3) = & [x(t + \frac{\lambda_1}{8} + \frac{\lambda_2}{8} + \frac{\lambda_3}{8})x^*(t - \frac{\lambda_1}{8} + \frac{\lambda_2}{8} + \frac{\lambda_3}{8})] \\
& \times [x(t + \frac{\lambda_1}{8} - \frac{\lambda_2}{8} + \frac{\lambda_3}{8})x^*(t - \frac{\lambda_1}{8} - \frac{\lambda_2}{8} + \frac{\lambda_3}{8})] \\
& \times [x(t + \frac{\lambda_1}{8} + \frac{\lambda_2}{8} - \frac{\lambda_3}{8})x^*(t - \frac{\lambda_1}{8} + \frac{\lambda_2}{8} - \frac{\lambda_3}{8})] \\
& \times [x(t + \frac{\lambda_1}{8} - \frac{\lambda_2}{8} - \frac{\lambda_3}{8})x^*(t - \frac{\lambda_1}{8} - \frac{\lambda_2}{8} - \frac{\lambda_3}{8})] \\
& \dots
\end{aligned}$$

with corresponding higher-order spectra defined by

$$\begin{aligned}
WH_2(t, \Omega_1, \Omega_2) &= \int_{-\infty}^{\infty} \int_{-\infty}^{\infty} R_2(t, \lambda_1, \lambda_2) e^{-j\lambda_1 \Omega_1 - j\lambda_2 \Omega_2} d\lambda_1 d\lambda_2. \\
WH_3(t, \Omega_1, \Omega_2, \Omega_3) &= \int_{-\infty}^{\infty} \int_{-\infty}^{\infty} \int_{-\infty}^{\infty} R_3(t, \lambda_1, \lambda_2, \lambda_3) e^{-j\lambda_1 \Omega_1 - j\lambda_2 \Omega_2 - j\lambda_3 \Omega_3} d\lambda_1 d\lambda_2 d\lambda_3 \\
& \dots
\end{aligned}$$

Show that the L-Wigner distributions may be understood as a projection of this higher-order spectra onto the time t and the frequency Ω_1 plane,

$$\begin{aligned}
LWD_2(t, \Omega_1) &= \frac{1}{4\pi^2} \int_{-\infty}^{\infty} WH_2(t, \Omega_1, \Omega_2) d\Omega_2 \\
LWD_4(t, \Omega_1) &= \frac{1}{8\pi^3} \int_{-\infty}^{\infty} \int_{-\infty}^{\infty} WH_3(t, \Omega_1, \Omega_2, \Omega_3) d\Omega_2 d\Omega_3 \\
& \dots
\end{aligned}$$

Problem 4.4. Calculate on the pseudo L-Wigner distribution of a signal $x(t) = \exp(j \sin(\pi t^2) - j8\pi t^2)$ by using the window $w(\tau) = \exp(-\tau^2)$. Comment the value as L increases.

Problem 4.5. Find the coefficients in the following fourth-order polynomial Wigner distribution

$$PD(t, \Omega) = \int_{-\infty}^{\infty} x^{b_1}(t + \tau/2)x^{b_3}(t + \tau)x^{-b_1}(t - \tau/2)x^{-b_3}(t - \tau)e^{-j\Omega\tau} d\tau.$$

Hint: This distribution should produce $\delta(\Omega - a_1 - 2a_2t - 3a_3t^2 - 4a_4t^3)$ for $x(t) = \exp(j(a_0 + a_1t + a_2t^2 + a_3t^3 + a_4t^4))$.

Problem 4.6. Assuming that the coefficients b_1, c_1, b_3 , and c_3 in the following fourth-order polynomial Wigner distribution

$$PD(t, \Omega) = \int_{-\infty}^{\infty} x^{b_1}(t + \tau/c_1)x^{b_3}(t + \tau/c_3)x^{-b_1}(t - \tau/c_1)x^{-b_3}(t - \tau/c_3)e^{-j\Omega\tau}d\tau$$

are integers, find the smallest values of the parameters in the set of integers b_1, c_1 , and c_3 if $b_3 = -1$ and $c_1 \neq 0, c_3 \neq 0$.

Problem 4.7. Write a system of equations for the sixth-order polynomial Wigner-Ville distribution. Then find one possible form of this distribution.

Problem 4.8. Derive the fourth-order time-rate representation for the estimation of the instantaneous signal rate.

Problem 4.9. Calculate, by definition, the complex-lag distribution of the signal

$$x(t) = A \exp(j(a_0 + a_1t + a_2t^2 + a_3t^3 + a_4t^4)).$$

Problem 4.10. Consider a polynomial phase signal

$$x(t) = \exp(j \sum_{i=0}^P a_i t^i)$$

. What is the order of polynomial distribution calculated as

$$CP(t, \Omega) = \int_{-\infty}^{\infty} e^{-j\text{Re}\{\ln(x(t+j\tau))\}} e^{-j\Omega\tau} d\tau.$$

Show that

$$CR(t, \Theta) = \int_{-\infty}^{\infty} e^{-j\text{Im}\{\ln(x(t+j\tau))\}} e^{-j\Theta\tau^2} d\tau$$

could be used as the instantaneous rate estimator for the signal whose phase is up to the third polynomial order.

Problem 4.11. The phase function of a signal $\varphi(t)$, like any other function, can be written in the Cauchy integral form

$$\varphi(t) = \frac{1}{2\pi j} \oint_C \frac{\varphi(z)}{z-t} dz,$$

where C is a boundary circle of the function domain and the function $\varphi(z)$ is complex differentiable. Describe the time-frequency representations, as the instantaneous frequency estimators, within this framework.

Problem 4.12. Calculate the discrete time version of the real-time distribution

$$RTD(t, \Omega) = \int_0^1 x(t-\tau)x^*(t-\tau/2)x^3(t)e^{-j\Omega\tau} d\tau$$

for the signal $x(t) = \exp(j(12\pi t + 32\pi t^2))$ at the instant $t = 1$. The signal is sampled at $\Delta t = 1/256$. Only the past values $x(1-m\Delta t)$ for $m = 0, 1, 2, \dots, 256$ are available for calculation (including $t = 1$). What is the estimate of the instantaneous frequency by using the real-time distribution and the Wigner distribution over the same set of data $x(m\Delta t)$, $0 \leq m\Delta t \leq 1$?

Problem 4.13. Estimate the polynomial coefficients in the polynomial phase signal

$$x(t) = e^{j(a_0 + a_1 t + a_2 t^2 + a_3 t^3 + a_4 t^4)}$$

by using the first-order instantaneous moment $R(t, \tau_1) = x(t + \tau_1)x^*(t - \tau_1)$ and its local polynomial Wigner distribution,

$$WDP(t, \Omega; \beta) = \int_{-\infty}^{\infty} R\left(t + \frac{\tau}{2}, \tau_1\right) R^*\left(t - \frac{\tau}{2}, \tau_1\right) e^{-j\beta\tau^3} e^{-j\Omega\tau} d\tau,$$

instead of the Fourier transform. Here τ_1 is a parameter (like in the HAF and the PHAF approaches). Generalize.

Problem 4.14. Calculate the product higher-order ambiguity function of a three-component second-order ($P = 2$) polynomial phase signals (PPS)

$$x(t) = e^{j(100+25t+2t^2)} + 2e^{j(200+50t+t^2)} + 3e^{j(150+75t+2.5t^2)}.$$

Use the set of time lags

$$\mathbf{T}_1^2 = \begin{bmatrix} 0.5 \\ 0.48 \end{bmatrix}, \quad (4.112)$$

where the optimal lag value is $\tau = T/2P$ and $T = 2$ is the signal duration.

Problem 4.15. Write code for recursive fourth-order L-Wigner distribution realization for real-valued signal defined as

$$\begin{aligned} x(t) = & \cos(120t^3 + 45\pi t) + e^{-t^2} \cos(25\pi t) \\ & + e^{-25t^2} \cos(40\pi t^2 + 150\pi t) \end{aligned}$$

sampled with $\Delta t = 1/256$. The time axis of the obtained distribution should cover continuous time interval $-1 \leq t \leq 1$. Use the 256-point Hann(ing) window for STFT calculation and $L_p = 3$ for L-Wigner distribution.

Problem 4.16. Write a program for the fourth-order polynomial Wigner distribution calculation, if an analytical expression for the signal is given. Calculate the distribution for the signal $x(t) = e^{j96\pi t^3 - j48\pi t}$, with lag discretization $\tau = -1 : 1/64 : 1$ for the time instants $t = -0.5 : 1/64 : 0.5$.

4.11 SOLUTIONS

Solution 4.1. The bispectrum of signal

$$x(t) = 1.2e^{j2\pi t} + e^{j3\pi t} + 0.9e^{j4\pi t - j\pi/4} + 0.5e^{j5\pi t + j\pi/3}$$

could be easily obtained from the Fourier transform of signal

$$\begin{aligned} X(\Omega) = & 2.4\pi\delta(\Omega - 2\pi) + 2\pi\delta(\Omega - 3\pi) \\ & + 1.8\pi\delta(\Omega - 4\pi)e^{-j\pi/4} + \pi\delta(\Omega - 5\pi)e^{j\pi/3}. \end{aligned}$$

The bispectrum of deterministic signal is

$$\begin{aligned}
 B(\Omega_1, \Omega_2) &= X^*(\Omega_1 + \Omega_2)X(\Omega_1)X(\Omega_2) \\
 &= [2.4\pi\delta(\Omega_1 + \Omega_2 - 2\pi) + 2\pi\delta(\Omega_1 + \Omega_2 - 3\pi) \\
 &\quad + 1.8\pi\delta(\Omega_1 + \Omega_2 - 4\pi)e^{j\pi/4} + \pi\delta(\Omega_1 + \Omega_2 - 5\pi)e^{-j\pi/3}] \\
 &\quad \times [2.4\pi\delta(\Omega_1 - 2\pi) + 2\pi\delta(\Omega_1 - 3\pi) \\
 &\quad + 1.8\pi\delta(\Omega_1 - 4\pi)e^{-j\pi/4} + \pi\delta(\Omega_1 - 5\pi)e^{j\pi/3}] \\
 &\quad \times [2.4\pi\delta(\Omega_2 - 2\pi) + 2\pi\delta(\Omega_2 - 3\pi) \\
 &\quad + 1.8\pi\delta(\Omega_2 - 4\pi)e^{-j\pi/4} + \pi\delta(\Omega_2 - 5\pi)e^{j\pi/3}] \\
 &= 1.8\pi\delta(\Omega_1 + \Omega_2 - 4\pi)e^{j\pi/4}2.4\pi\delta(\Omega_1 - 2\pi)2.4\pi\delta(\Omega_2 - 2\pi) \\
 &\quad + \pi\delta(\Omega_1 + \Omega_2 - 5\pi)e^{-j\pi/3}2.4\pi\delta(\Omega_1 - 2\pi)2\pi\delta(\Omega_2 - 3\pi) \\
 &\quad + \pi\delta(\Omega_1 + \Omega_2 - 5\pi)e^{-j\pi/3}2\pi\delta(\Omega_1 - 3\pi)2.4\pi\delta(\Omega_2 - 2\pi).
 \end{aligned}$$

There are three nonzero values in $B(\Omega_1, \Omega_2)$ at: $(\Omega_1, \Omega_2) = (2\pi, 2\pi)$, $(\Omega_1, \Omega_2) = (2\pi, 3\pi)$, and $(\Omega_1, \Omega_2) = (3\pi, 2\pi)$.

Solution 4.2. From the Wigner bispectrum definition

$$\begin{aligned}
 WB(t, \Omega_1, \Omega_2) &= \int_{-\infty}^{\infty} \int_{-\infty}^{\infty} x^* \left(t - \frac{\tau_1}{3} - \frac{\tau_2}{3} \right) x \left(t + \frac{2\tau_1}{3} - \frac{\tau_2}{3} \right) \\
 &\quad \times x \left(t - \frac{\tau_1}{3} + \frac{2\tau_2}{3} \right) e^{-j(\Omega_1\tau_1 + \Omega_2\tau_2)} d\tau_1 d\tau_2,
 \end{aligned}$$

follows

$$\begin{aligned}
 WB(t, \Omega_1, \Omega_2) &= \frac{1}{8\pi^3} \int_{-\infty}^{\infty} \int_{-\infty}^{\infty} \int_{-\infty}^{\infty} \int_{-\infty}^{\infty} X^*(\theta_1) e^{-j(t - \frac{\tau_1}{3} - \frac{\tau_2}{3})\theta_1} X(\theta_2) e^{j(t + \frac{2\tau_1}{3} - \frac{\tau_2}{3})\theta_2} \\
 &\quad \times X(\theta_3) e^{j(t - \frac{\tau_1}{3} + \frac{2\tau_2}{3})\theta_3} e^{-j(\Omega_1\tau_1 + \Omega_2\tau_2)} d\theta_1 d\theta_2 d\theta_3 d\tau_1 d\tau_2, \\
 &= \frac{1}{2\pi} \int_{-\infty}^{\infty} \int_{-\infty}^{\infty} \int_{-\infty}^{\infty} \int_{-\infty}^{\infty} X^*(\theta_1) X(\theta_2) X(\theta_3) \delta \left(\Omega_1 - \frac{\theta_1}{3} - \frac{2\theta_2}{3} + \frac{\theta_3}{3} \right) \\
 &\quad \times \delta \left(\Omega_2 - \frac{\theta_1}{3} + \frac{\theta_2}{3} - \frac{2\theta_3}{3} \right) e^{-j(\theta_1 - \theta_2 - \theta_3)t} d\theta_1 d\theta_2 d\theta_3.
 \end{aligned}$$

With $\theta_1 = \theta + \theta_2 + \theta_3$

$$\begin{aligned} WB(t, \Omega_1, \Omega_2) &= \frac{1}{2\pi} \int_{-\infty}^{\infty} \int_{-\infty}^{\infty} \int_{-\infty}^{\infty} \int_{-\infty}^{\infty} X^*(\theta + \theta_2 + \theta_3) X(\theta_2) X(\theta_3) \delta\left(\Omega_1 - \frac{\theta}{3} - \theta_2\right) \\ &\quad \times \delta\left(\Omega_2 - \frac{\theta}{3} - \theta_3\right) e^{-j\theta t} d\theta_2 d\theta_3 d\theta, \end{aligned}$$

the Wigner bispectrum in terms of the signal's Fourier transform is obtained, after integration over θ_2 and θ_3 , as

$$WB(t, \Omega_1, \Omega_2) = \frac{1}{2\pi} \int_{-\infty}^{\infty} X^*\left(\Omega_1 + \Omega_2 + \frac{\theta}{3}\right) X\left(\Omega_1 - \frac{\theta}{3}\right) X\left(\Omega_2 - \frac{\theta}{3}\right) e^{-j\theta t} d\theta.$$

Solution 4.3. The L-Wigner distribution, with $L = 2$, easily follows as the Fourier transform of $R_2(t, \lambda_1, 0)$, since the integration $\int_{-\infty}^{\infty} WH_2(t, \Omega_1, \Omega_2) d\Omega_2$ produces $\delta(\lambda_2)$. For $L = 4$ case the L-Wigner distribution is a Fourier transform of $R_3(t, \lambda_1, 0, 0)$.

Solution 4.4. The pseudo L-Wigner distribution of signal $x(t) = \exp(j \sin(\pi t^2) - j8\pi t^2)$ is

$$\begin{aligned} LWD_L(t, \Omega) &= \int_{-\infty}^{\infty} \exp(-\tau^2) \exp(jL \sin(\pi(t + \frac{\tau}{2L})^2) - jL8\pi(t + \frac{\tau}{2L})^2) \\ &\quad \times \exp(-jL \sin(\pi(t - \frac{\tau}{2L})^2) + jL8\pi(t - \frac{\tau}{2L})^2) \exp(-j\Omega t) d\tau. \end{aligned}$$

Since

$$\begin{aligned} &L \sin(\pi(t + \frac{\tau}{2L})^2) - L \sin(\pi(t - \frac{\tau}{2L})^2) \\ &\cong 2t\pi \cos(\pi t^2)\tau - \frac{3\pi^2 t \sin(\pi t^2) + 2\pi^3 t^3 \cos(\pi t^2)}{6L^2} \tau^3. \end{aligned}$$

This term can be also obtained as

$$2L \sin\left(\frac{\pi t \tau}{L}\right) \cos\left(\pi t^2 + \frac{\pi \tau^2}{4L^2}\right) \cong 2\pi t \tau \cos(\pi t^2).$$

Finally we get

$$LWD_L(t, \Omega) \cong \sqrt{\pi} e^{-\left(\Omega - 2t\pi \cos(\pi t^2) - 16\pi t\right)^2/4}$$

for

$$\left| \frac{3\pi^2 t \sin(\pi t^2) + 2\pi^3 t^3 \cos(\pi t^2)}{6L^2} \tau^3 \right| \ll 1$$

or

$$\left| \frac{\pi t \tau}{L} \right| \ll 1.$$

If we assume that the considered interval is $|t| < 1$, then we can use $L \geq 8$.

Solution 4.5. For the distribution

$$PD(t, \Omega) = \int_{-\infty}^{\infty} x^{b_1}(t + \tau/2)x^{b_3}(t + \tau)x^{-b_1}(t - \tau/2)x^{-b_3}(t - \tau)e^{-j\Omega\tau}d\tau$$

we have $c_1 = 1/2$ and $c_3 = 1$. Then from

$$\begin{aligned} b_1/2 + b_3 &= 1/2 \\ b_1/8 + b_3 &= 0 \end{aligned}$$

follow $b_1 = 4/3$ and $b_3 = -1/6$, producing the fourth-order polynomial Wigner distribution in the form

$$PD(t, \Omega) = \int_{-\infty}^{\infty} x^{4/3}(t + \tau/2)x^{*1/6}(t + \tau)x^{*4/3}(t - \tau/2)x^{1/6}(t - \tau)e^{-j\Omega\tau}d\tau.$$

Solution 4.6. From the set of equations

$$\begin{aligned} b_1/c_1 + b_3/c_3 &= 1/2 \\ b_1/c_1^3 + b_3/c_3^3 &= 0 \end{aligned}$$

with $b_3 = -1$ we get

$$\begin{aligned} b_1 c_3 - c_1 &= c_1 c_3 / 2 \\ b_1 c_3^3 - c_1^3 &= 0 \end{aligned}$$

resulting in

$$c_1 = \pm c_3 \sqrt{c_3/2 + 1}$$

where the values of c_1 and c_3 are nonzero integers. By direct inspection it is easy to conclude that the lowest c_3 , when $c_3\sqrt{c_3/2 + 1}$ is a nonzero integer, is $c_3 = 6$. Then $c_1 = \pm 12$ with $b_1 = \pm 8$. Thus, the lowest integers satisfying these equations are $c_1 = 12$, $c_3 = 6$, $b_1 = 8$ and $b_3 = -1$ or $c_1 = -12$, $c_3 = 6$, $b_1 = -8$ and $b_3 = -1$. It is easy to write the corresponding polynomial Wigner-Ville distributions.

Solution 4.7. For a sixth-order polynomial Wigner-Ville distribution we get

$$\begin{aligned} b_1 + b_2 + b_3 + b_4 + b_5 + b_6 &= 0 \\ b_1 c_1 + b_2 c_2 + b_3 c_3 + b_4 c_4 + b_5 c_5 + b_6 c_6 &= 1 \\ b_1 c_1^2 + b_2 c_2^2 + b_3 c_3^2 + b_4 c_4^2 + b_5 c_5^2 + b_6 c_6^2 &= 0 \\ b_1 c_1^3 + b_2 c_2^3 + b_3 c_3^3 + b_4 c_4^3 + b_5 c_5^3 + b_6 c_6^3 &= 0 \\ b_1 c_1^4 + b_2 c_2^4 + b_3 c_3^4 + b_4 c_4^4 + b_5 c_5^4 + b_6 c_6^4 &= 0 \\ b_1 c_1^5 + b_2 c_2^5 + b_3 c_3^5 + b_4 c_4^5 + b_5 c_5^5 + b_6 c_6^5 &= 0 \\ b_1 c_1^6 + b_2 c_2^6 + b_3 c_3^6 + b_4 c_4^6 + b_5 c_5^6 + b_6 c_6^6 &= 0. \end{aligned}$$

If we add the requirement that a distribution is real valued, that is, that the estimator is symmetric, then

$$\begin{aligned} b_1 &= -b_2, c_1 = -c_2 \\ b_3 &= -b_4, c_3 = -c_4 \\ b_5 &= -b_6, c_5 = -c_6 \end{aligned}$$

resulting in the system of equations

$$\begin{aligned} b_1 c_1 + b_3 c_3 + b_5 c_5 &= 1/2 \\ b_1 c_1^3 + b_3 c_3^3 + b_5 c_5^3 &= 0 \\ b_1 c_1^5 + b_3 c_3^5 + b_5 c_5^5 &= 0, \end{aligned}$$

or in a matrix form

$$\begin{bmatrix} c_1 & c_3 & c_5 \\ c_1^3 & c_3^3 & c_5^3 \\ c_1^5 & c_3^5 & c_5^5 \end{bmatrix} \begin{bmatrix} b_1 \\ b_3 \\ b_5 \end{bmatrix} = \begin{bmatrix} 1/2 \\ 0 \\ 0 \end{bmatrix}.$$

This system has an infinite number of solutions.

For $b_1 = 1$, $b_3 = 1$, and $b_5 = -1$ we get $c_1 = 0.625$, $c_3 = 0.75$, and $c_5 = 0.875$, that approximately satisfy the previous system.

The sixth-order polynomial Wigner-Ville distribution, corresponding to these coefficient values, is

$$W_6(t, \Omega) = \int_{-\infty}^{\infty} x(t + 0.625\tau)x^*(t - 0.625\tau) \\ \times x(t + 0.75\tau)x^*(t - 0.75\tau)x^*(t + 0.875\tau)x(t - 0.875)e^{-j\Omega\tau}d\tau.$$

Solution 4.8. The generalized time-rate representation is

$$R_G(t, \Theta) = \int_{-\infty}^{\infty} \prod_i x^{b_i}(t + c_i\tau)e^{-j\Theta\tau^2}d\tau.$$

Coefficients b_i and c_i for the instantaneous signal rate estimation follow from the system of equations, obtained by expanding $b_i\varphi(t + c_i\tau)$ into a Taylor series around t ,

$$b_i\varphi(t + c_i\tau) = \\ b_i\varphi(t) + b_i\varphi'(t)c_i\tau + b_i\varphi''(t)\frac{(c_i\tau)^2}{2!} + b_i\varphi'''(t)\frac{(c_i\tau)^3}{3!} + b_i\varphi^{(4)}(t)\frac{(c_i\tau)^4}{4!} + \dots$$

The conditions are that:

1. The sum of coefficients with $\varphi'(t)$ is equal to 0.
2. The sum of coefficients with $\varphi''(t)$ is equal to 1.
3. The sum of coefficients with $\varphi^{(n)}(t)$ is equal to 0 up to the fourth-order:

$$\begin{aligned} b_1c_1 + b_2c_2 + b_3c_3 + b_4c_4 &= 0, \\ b_1c_1^2 + b_2c_2^2 + b_3c_3^2 + b_4c_4^2 &= 1, \\ b_1c_1^3 + b_2c_2^3 + b_3c_3^3 + b_4c_4^3 &= 0, \\ b_1c_1^4 + b_2c_2^4 + b_3c_3^4 + b_4c_4^4 &= 0. \end{aligned}$$

If we add the requirement that the estimator is symmetric, then

$$\begin{aligned} b_1 &= b_2, & c_1 &= -c_2 \\ b_3 &= b_4, & c_3 &= -c_4, \end{aligned}$$

resulting in the system of equations

$$\begin{aligned} b_1 c_1^2 + b_3 c_3^2 &= 1/2 \\ b_1 c_1^4 + b_3 c_3^4 &= 0. \end{aligned}$$

Taking, for example, $b_1 = -1$ and $b_3 = 4$, we get

$$\begin{aligned} -c_1^2 + 4c_3^2 &= 1/2 \\ -c_1^4 + 4c_3^4 &= 0 \end{aligned}$$

The solutions are $c_1 = \pm\sqrt{2}c_3$ and $c_1 = \pm j\sqrt{2}c_3$ with $4c_3^2 = 1/2 + c_1^2 = 1/2 \pm 2c_3^2$. Thus, $2c_3^2 = 1/2$ or $6c_3^2 = 1/2$. The solution $c_3 = 1/2$ and $c_1 = 1/\sqrt{2}$ is one of possible solutions. The fourth-order time-rate representations, corresponding to this solution, is

$$R(t, \Theta) = \int_{-\infty}^{\infty} x^*(t + \frac{\tau}{\sqrt{2}})x^*(t - \frac{\tau}{\sqrt{2}})x^4(t + \frac{\tau}{2})x^4(t - \frac{\tau}{2})e^{-j\Theta\tau^2}d\tau.$$

Solution 4.9. For the signal $x(t) = A \exp(j(a_0 + a_1 t + a_2 t^2 + a_3 t^3 + a_4 t^4))$, we have

$$\begin{aligned} &x(t + \frac{\tau}{4})x^*(t - \frac{\tau}{4})x^{-j}(t + j\frac{\tau}{4})x^j(t - j\frac{\tau}{4}) \\ &= A^2 e^{j(a_0 + a_1(t + \tau/4) + a_2(t + \tau/4)^2 + a_3(t + \tau/4)^3 + a_4(t + \tau/4)^4)} \\ &\quad \times e^{-j(a_0 + a_1(t - \tau/4) + a_2(t - \tau/4)^2 + a_3(t - \tau/4)^3 + a_4(t - \tau/4)^4)} \\ &\quad \times e^{(a_0 + a_1(t + j\tau/4) + a_2(t + j\tau/4)^2 + a_3(t + j\tau/4)^3 + a_4(t + j\tau/4)^4)} \\ &\quad \times e^{-(a_0 + a_1(t - j\tau/4) + a_2(t - j\tau/4)^2 + a_3(t - j\tau/4)^3 + a_4(t - j\tau/4)^4)} \\ &= A^2 e^{j(a_1\tau/2 + a_2\tau + 3a_3t^2\tau/2 + 2a_3(\tau/4)^2 + 4a_4t^3\tau/2 + 12a_4t(\tau/4)^3)} \\ &\quad \times e^{(ja_1t\tau/2 + ja_2t\tau + 3ja_3t^2\tau/2 - 2ja_3(\tau/4)^2 + 4ja_4t^3\tau/2 - 12ja_4t(\tau/4)^3)} \\ &= A^2 e^{j(a_1\tau + 2a_2t\tau + 3a_3t^2\tau + 4a_4t^3\tau)} \end{aligned}$$

producing

$$\begin{aligned} CTD(t, \Omega) &= \int_{-\infty}^{\infty} A^2 e^{j(a_1\tau + 2a_2t\tau + 3a_3t^2\tau + 4a_4t^3\tau)} e^{-j\Omega\tau} d\tau \\ &= 2\pi A^2 \delta(\Omega - (a_1 + 2a_2t + 3a_3t^2 + 4a_4t^3)). \end{aligned}$$

Solution 4.10. For a polynomial phase signal $x(t) = \exp(j \sum_{i=0}^P a_i t^i)$, we can write

$$\begin{aligned} -\operatorname{Re}\{\ln(x(t + j\tau))\} &= -\operatorname{Re}\left\{j \sum_{i=0}^P a_i (t + j\tau)^i\right\} \\ &= a_1\tau + 2a_2t\tau + 3a_3t^2\tau - a_3\tau^3 + \dots \end{aligned}$$

Obviously, for the linear-frequency modulated signal ($P = 2$)

$$CP(t, \Omega) = \int_{-\infty}^{\infty} e^{-j\operatorname{Re}\{\ln(x(t + j\tau))\}} e^{-j\Omega t} dt = 2\pi \delta(\Omega - a_1 - 2a_2 t),$$

like in the Wigner distribution case.

For the signal whose phase is up to the third-order, we get a disturbing term

$$CP(t, \Omega) = 2\pi \delta(\Omega - a_1 - 2a_2 t - 3a_3 t^2) * \operatorname{FT}\{e^{-ja_3\tau^3}\},$$

that is of the same order as in the Wigner distribution (but with a larger coefficient).

For the representation

$$CR(t, \Theta) = \int_{-\infty}^{\infty} e^{-j\operatorname{Im}\{\ln(x(t + j\tau))\}} e^{-j\Theta t^2} d\tau,$$

we use

$$\begin{aligned} \operatorname{Im}\{\ln(x(t + j\tau))\} &= \operatorname{Im}\left\{j \sum_{i=0}^P a_i (t + j\tau)^i\right\} \\ &= a_0 + a_1 t + a_2 t^2 - a_2 \tau^2 + a_3 t^3 - 3a_3 t \tau^2 + \dots \end{aligned}$$

If the signal phase is up to the third-order, then the representation

$$|CR(t, \Theta)| = \left| \int_{-\infty}^{\infty} e^{j(a_2 + 3a_3 t - \Theta)\tau^2} d\tau \right|$$

produces maximum at the instantaneous signal rate

$$\Theta = a_2 + 3a_3 t = \frac{1}{2} \frac{d^2 \varphi(t)}{dt^2}.$$

Solution 4.11. The instantaneous frequency, within the Cauchy integral definition, is

$$\Omega(t) = \varphi'(t) = \frac{1}{2\pi j} \oint_C \frac{\varphi(z)}{(z-t)^2} dz.$$

For $z = t + \tau e^{j\alpha}$ we can write

$$\varphi'(t) = \frac{1}{2\pi j} \int_0^{2\pi} \frac{\varphi(t + \tau e^{j\alpha})}{(\tau e^{j\alpha})^2} d(\tau e^{j\alpha}).$$

Thus,

$$\varphi'(t)\tau = \frac{1}{2\pi} \int_0^{2\pi} \varphi(t + \tau e^{j\alpha}) e^{-j\alpha} d\alpha.$$

The ideal time-frequency representation, for a signal $x(t) = \exp(j\varphi(t))$, would be

$$ITF(t, \Omega) = \int_{-\infty}^{\infty} e^{j\varphi'(t)\tau} e^{-j\Omega\tau} d\tau = \int_{-\infty}^{\infty} \exp \left[\frac{j}{2\pi} \int_0^{2\pi} \varphi(t + \tau e^{j\alpha}) e^{-j\alpha} d\alpha \right] e^{-j\Omega\tau} d\tau.$$

The form of commonly used time-frequency representations is obtained from

$$\begin{aligned} \varphi'(t)\tau &= \frac{1}{2\pi} \int_0^{2\pi} \varphi(t + \tau e^{j\alpha}) e^{-j\alpha} d\alpha \\ &\cong \frac{1}{2\pi} \sum_{p=0}^{N-1} \varphi(t + \tau e^{j2\pi p/N}) e^{-j2\pi p/N} \frac{2\pi}{N}. \end{aligned}$$

For a very rough estimation, using $N = 1$, we get the STFT (or the Rihaczek distribution) estimator

$$\varphi'(t)\tau \cong \varphi(t + \tau).$$

The case with $N = 2$ produces

$$\begin{aligned} 2\varphi'(t)\tau &\cong [\varphi(t + \tau) - \varphi(t - \tau)] \\ \varphi'(t)\tau &\cong \left[\varphi(t + \frac{\tau}{2}) - \varphi(t - \frac{\tau}{2}) \right] \end{aligned}$$

corresponding to the Wigner distribution. For $N = 4$

$$\begin{aligned} 4\varphi'(t)\tau &\cong [\varphi(t + \tau) - j\varphi(t + j\tau) - \varphi(t - \tau) + j\varphi(t - j\tau)] \\ \varphi'(t)\tau &\cong \left[\varphi(t + \frac{\tau}{4}) - j\varphi(t + j\frac{\tau}{4}) - \varphi(t - \frac{\tau}{4}) + j\varphi(t - j\frac{\tau}{4}) \right]. \end{aligned}$$

This is the estimator for the complex-lag distribution.

Solution 4.12. The distribution can be written as

$$RTD(t, \Omega) = \int_0^1 x(t - \tau)x^{*4}(t - \tau/2)x^3(\tau)\exp(-j\Omega\tau)d\tau.$$

The instantaneous frequency of signal $x(t) = \exp(j(12\pi t + 32\pi t^2))$ at the instant $t = 1$ is $\Omega_i = 76\pi$.

The discrete version of $RTD(t, \Omega)$, at $t = 1$, is

$$\begin{aligned} RTD(1, \Omega) &= x^3(1) \sum_{m=0}^N x(1 - m\Delta t)x^{*4}(1 - m\Delta t/2)\exp(-jkm\Delta\Omega\Delta t)\Delta t \\ &= x^3(1) \sum_{m=0}^N \exp(j[12\pi(1 - m\Delta t) + 32\pi(1 - m\Delta t)^2]) \\ &\quad \times \exp(-j4[12\pi(1 - m\Delta t/2) + 32\pi(1 - m\Delta t/2)^2])\exp(-jkm\Delta\Omega\Delta t)\Delta t \\ &= \sum_{m=0}^N \exp(j[-12\pi m\Delta t - 64\pi m\Delta t]) \\ &\quad \times \exp(+j4[12\pi m\Delta t/2 + 32\pi m\Delta t])\exp(-jkm\Delta\Omega\Delta t)\Delta t \\ &= \sum_{m=0}^N \exp(j[12\pi m\Delta t + 64\pi m\Delta t])\exp(-jkm\Delta\Omega\Delta t)\Delta t \\ &= N\Delta t\delta(76\pi\Delta t - k\Delta\Omega\Delta t). \end{aligned}$$

Maximal value is reached at $k\Delta\Omega = 76\pi$, what is the frequency at the ending instant of the considered time interval.

In the case of the Wigner distribution, using the same time interval $0 \leq t \leq 1$, we would obtain

$$\begin{aligned} WD(1/2, \Omega) &= \sum_{m=-N/2}^{N/2} x(1/2 + m\Delta t/2)x^*(1/2 - m\Delta t/2)\exp(-jkm\Delta\Omega\Delta t)\Delta t \\ &= \sum_{m=-N/2}^{N/2} \exp(j[12\pi(1/2 + m\Delta t/2) + 32\pi(1/2 + m\Delta t/2)^2]) \\ &\quad \times \exp(-j[12\pi(1/2 - m\Delta t/2) + 32\pi(1/2 - m\Delta t/2)^2])\exp(-jkm\Delta\Omega\Delta t)\Delta t \\ &= \sum_{m=-N/2}^{N/2} \exp(j[12\pi m\Delta t + 32\pi m\Delta t])\exp(-jkm\Delta\Omega\Delta t)\Delta t \\ &= N\Delta t \delta(44\pi\Delta t - k\Delta\Omega\Delta t). \end{aligned}$$

Maximal Wigner distribution value is reached at $k\Delta\Omega = 44\pi$, which is the frequency at the middle instant of the considered time interval. Delay in the instantaneous frequency estimation is $t = 1/2$.

Solution 4.13. For the signal $x(t) = e^{j(a_0 + a_1t + a_2t^2 + a_3t^3 + a_4t^4)} = e^{j\varphi(t)}$ the first-order instantaneous moment is

$$\begin{aligned} R(t, \tau_1) &= x(t + \tau_1)x^*(t - \tau_1) = e^{j\varphi(t + \tau_1) - j\varphi(t - \tau_1)} \\ &= e^{j2(a_1 + 2a_2t + 3a_3t^2 + 4a_4t^3)\tau_1 + j(6a_3 + 24a_4t)\tau_1^3/3} \\ &= e^{j(2a_1\tau_1 + 2a_3\tau_1^3)}e^{jt(4a_2\tau_1 + 8a_4\tau_1^3)}e^{jt^2(6a_3\tau_1)}e^{jt^3(8a_4\tau_1)}. \end{aligned}$$

Three the highest-order coefficients may be estimated from this moment, by using the local polynomial Wigner distribution form

$$WDP(t, \Omega; \beta) = \int_{-\infty}^{\infty} R\left(t + \frac{\tau}{2}, \tau_1\right) R^*\left(t - \frac{\tau}{2}, \tau_1\right) e^{-j\beta\tau^3} e^{-j\Omega\tau} d\tau.$$

By changing the value of parameter β , the maximal value of $WDP(t, \Omega; \beta)$ is achieved for

$$\begin{aligned}\beta &= (8a_4\tau_1)/4, \\ \hat{a}_4 &= \frac{\beta}{2\tau_1}.\end{aligned}$$

The local polynomial Wigner distribution, at $\beta = 2a_4\tau_1$, is

$$WDP(t, \Omega; \beta = 2a_4\tau_1) = 2\pi\delta(\Omega - 4a_2\tau_1 - 8a_4\tau_1^3 - 12ta_3\tau_1 - 24t^2a_4\tau_1).$$

By using any two maxima of $WDP(t, \Omega; \beta = 2a_4\tau_1)$, for example, at (t_1, Ω_1) and (t_2, Ω_2) , we get

$$\begin{aligned}\Omega_1 &= 4a_2\tau_1 + 8a_4\tau_1^3 + 12t_1a_3\tau_1 + 24t_1^2a_4\tau_1 \\ \Omega_2 &= 4a_2\tau_1 + 8a_4\tau_1^3 + 12t_2a_3\tau_1 + 24t_2^2a_4\tau_1,\end{aligned}$$

resulting in

$$\hat{a}_3 = \frac{\Omega_1 - \Omega_2}{12(t_1 - t_2)\tau_1} - 2\hat{a}_4(t_1 + t_2)$$

and

$$\hat{a}_2 = \frac{\Omega_1 - 8\hat{a}_4\tau_1^3 - 12t_1\hat{a}_3\tau_1 - 24t_1^2\hat{a}_4\tau_1}{4\tau_1}.$$

After three the highest-order coefficients are estimated, two the lowest-order coefficients follow from

$$\text{FT}_t\{x(t)e^{-j(\hat{a}_4t^4 + \hat{a}_3t^3 + \hat{a}_2t^2)}\} = \text{FT}_t\left\{e^{j(a_0 + a_1t)}\right\} = 2\pi\delta(\Omega - a_1)e^{ja_0}.$$

Hint: Generalize the approach for a signal $x(t) = \exp(\sum_{p=0}^P a_p t^p)$.

Solution 4.14. The multilag higher-order instantaneous moments are

$$x(t) = e^{j(100+25t+2t^2)} + 2e^{j(200+50t+t^2)} + 3e^{j(150+75t+2.5t^2)}$$

$$\begin{aligned}
R(t, \tau_1) &= x(t + \tau_1)x^*(t - \tau_1) = & (4.113) \\
&= e^{j(50\tau_1 + 8t\tau_1)} + 4e^{j(100\tau_1 + 4t\tau_1)} + 9e^{j(150\tau_1 + 10t\tau_1)} + \\
&2e^{j(-100 + 75\tau_1 + \tau_1^2)}e^{j((-25 + 6\tau_1)t + t^2)} + 3e^{j(-50 + \tau_1 - 0.5\tau_1^2)}e^{j((-50 + 9\tau_1)t - 0.5t^2)} + \\
&2e^{j(100 + 75\tau_1 - \tau_1^2)}e^{j((25 + 6\tau_1)t - t^2)} + 6e^{j(50 + 125\tau_1 - 1.5\tau_1^2)}e^{j((-25 + 7\tau_1)t - 1.5t^2)} + \\
&3e^{j(50 + 100\tau_1 + 0.5\tau_1^2)}e^{j((50 + 9\tau_1)t + 0.5t^2)} + 6e^{j(-50 + 125\tau_1 + 1.5\tau_1^2)}e^{j((25 + 7\tau_1)t + 1.5t^2)}.
\end{aligned}$$

The PHAF is obtained as

$$X_1^2(\Omega, \mathbf{T}_1^2) = \prod_{l=1}^2 X_1(\beta^{(l)}\Omega, \tau_1^{(l)}).$$

We will first calculate the HAFs. The first three terms in (4.113) are the auto-terms. The HAF of the auto-terms calculated with $\tau_1^{(1)} = 0.5$ is

$$\left| X_1(\Omega, \tau_1^{(1)}) \right| = 2\pi\delta(\Omega - 8\tau_1^{(1)}) + 8\pi\delta(\Omega - 4\tau_1^{(1)}) + 18\pi\delta(\Omega - 10\tau_1^{(1)}).$$

They will appear in the Fourier transform over t as sharp peaks at the frequencies $4a_2^i\tau_1^{(1)}$, $i = 1, 2, 3$, respectively (a_2^i is the coefficient with t^2 in the i th component of the signal).

Similarly, the auto-terms in the frequency-scaled HAF $X_1(\beta^{(2)}\Omega, \tau_1^{(2)})$ will be

$$\begin{aligned}
\left| X_1(\beta^{(2)}\Omega, \tau_1^{(2)}) \right| &= 2\pi/\beta^{(2)}\delta(\Omega - 8\tau_1^{(2)}/\beta^{(2)}) + 8\pi/\beta^{(2)}\delta(\Omega - 4\tau_1^{(2)}/\beta^{(2)}) \\
&\quad + 18\pi/\beta^{(2)}\delta(\Omega - 10\tau_1^{(2)}/\beta^{(2)}), & (4.114)
\end{aligned}$$

that is, the peaks at the frequencies $4a_2^i\tau_1^{(2)}/\tau_1^{(2)}\tau_1^{(1)} = 4a_2^i\tau_1^{(1)}$, for $i = 1, 2, 3$, respectively. The second lag is $\tau_1^{(2)} = 0.48$. Consequently, the auto-terms will be at the same position in each HAF. They will be preserved in

$$X_1^2(\Omega, \mathbf{T}_1^2) = X_1(\Omega, \tau_1^{(1)})X_1(\beta^{(2)}\Omega, \tau_1^{(2)}).$$

However, the last six terms in (4.113) are the cross-terms. They are in a form of linear-frequency modulated signals. The HAFs of these signals can be approximated, for a large a , by using the method of stationary phase

$$\int_{-\infty}^{\infty} A(t)e^{j\phi(t)}e^{-j\Omega t}dt \simeq A(t_0)e^{j\phi(t_0)}e^{-j\Omega t_0}\sqrt{\frac{2\pi j}{\phi''(t_0)}},$$

where t_0 is solution of

$$\phi'(t_0) = \Omega.$$

By using this method the HAF of the first cross-term can be approximated as

$$X_1(\Omega, \tau_1^{(1)}) \cong 2e^{j(-100+75\tau_1^{(1)}+(\tau_1^{(1)})^2)} e^{j((-25+6\tau_1^{(1)})t_0+t_0^2)} e^{-j\Omega t_0} w(t_0) \sqrt{\frac{2\pi j}{2}},$$

where, $w(t)$ is the rectangular window defined by the signal's duration and $t_0 = (\Omega + 25 - 6\tau_1^{(1)})/2$. The absolute value of the HAF is

$$|X_1(\Omega, \tau_1^{(1)})| \cong 2w\left(\frac{\Omega + 25 - 6\tau_1^{(1)}}{2}\right) \sqrt{\frac{2\pi}{2}}. \quad (4.115)$$

The HAF of the cross-term is, approximately, in the form of the used window (this approximation will produce closer results for smooth windows). It is centered at $\Omega = (-25 + 6\tau_1^{(1)}) = -22$, while its width is approximately $W = 2T$, where T is the signal duration in the time domain, $W = 4$.

The absolute value of the frequency-scaled HAF of this cross-term, can be written as

$$|X_1(\beta^{(2)}\Omega, \tau_1^{(2)})| \cong 2/\beta^{(2)} w\left(\frac{\Omega + (25 - 6\tau_1^{(2)})/\beta^{(2)}}{2/(\beta^{(2)})^2}\right) \sqrt{\frac{2\pi}{2}}.$$

The frequency-scaled HAF of the cross-term is still in a form of the used window. However, it is centered at $\Omega = (-25 + 6\tau_1^{(2)})/\tau_1^{(2)}\tau_1^{(1)} = (-25/\tau_1^{(2)}\tau_1^{(1)} + 6\tau_1^{(1)}) = -23.0417$, while its width is $W = 4$. Therefore, the PHAF of the cross-term is

$$\begin{aligned} X_1^2(\Omega, \mathbf{T}_1^2) &= X_1(\Omega, \tau_1^{(1)}) X_1(\beta^{(2)}\Omega, \tau_1^{(2)}) \\ &= \begin{cases} 4\pi/\beta^{(2)} & \text{for } -24 < \Omega < -21.0417 \\ 0 & \text{for other } \Omega. \end{cases} \end{aligned}$$

By using only two time lags, the window width of the PHAF is decreased to the width of approximately $W_1 = 2.9583$. Moreover, in the HAFs the ratio of the lowest auto-term and this cross-term is $2\pi/(2\sqrt{\pi}) = \sqrt{\pi}$, while in the PHAF calculated with the set of two time lags, this ratio is $4\pi^2/(4\pi) = \pi$.

If we use one more time lag, for example, $\tau_1^{(3)} = 0.52$, the HAF will be

$$\left| X_1(\beta^{(3)}\Omega, \tau_1^{(3)}) \right| = 2/\beta^{(3)}w \left(\frac{\Omega + (25 - 6\tau_1^{(2)})/\beta^{(3)}}{2/(\beta^{(3)})^2} \right) \sqrt{\frac{2\pi}{2}}.$$

It is centered at the frequency $\Omega = -21.0385$. The PHAF calculated with three time lags will be

$$\begin{aligned} X_1^2(\Omega, T_1^2) &= X_1(\Omega, \tau_1^{(1)})X_1(\beta^{(2)}\Omega, \tau_1^{(2)})X_1(\beta^{(3)}\Omega, \tau_1^{(3)}) \\ &= \begin{cases} 8\pi\sqrt{\pi}/\beta^{(2)}/\beta^{(3)} & \text{for } -23.0385 < \Omega < -21.0417 \\ 0 & \text{for other } \Omega. \end{cases} \end{aligned}$$

The window width of the PHAF is decreased to $W_1 = 1.9968$, while the ratio of the lowest auto-term and this cross-term is $8\pi^3/(8\pi\sqrt{\pi}) = \pi\sqrt{\pi}$. In general, for the signal composed of three components we should use a higher number of time lags. The ratio among the auto-terms and cross terms will be additionally increased by each additional time lag making auto-terms easier to detect.

Solution 4.15. The code reads as

```
% Signal definition
t=(-1.5:1/256:1.5)';
x=cos(120*t.^3+45*pi*t)+...
    exp(-t.^2).*cos(25*pi*t)+...
    1*exp(-25*t.^2).*cos(40*pi*t.^2+150*pi*t);

N=256;
Lp=3;

ST=STFT_calc(x,hanning(N),1);
% First-order LWD
LWD_1=abs(ST).^2;
for k=1:Lp
    LWD_1(1+k:N-k,:)=LWD_1(1+k:N-k,:)... 
        +2*real(ST(1:N-2*k,:).*conj(ST(1+2*k:N,:)));
end
% Second-order LWD
LWD_2=abs(LWD_1).^2;
```

```

for k=1:Lp
    LWD_2(1+k:N-k,:) = LWD_2(1+k:N-k,:)... 
        + 2*LWD_1(1:N-2*k,:).*LWD_1(1+2*k:N,:);
end
% Fourth-order LWD
LWD_4=abs(LWD_2).^2;
for k=1:Lp
    LWD_4(1+k:N-k,:) = LWD_4(1+k:N-k,... 
        + 2*LWD_2(1:N-2*k,:).*LWD_2(1+2*k:N,:);
end
imagesc(LWD_4)

```

Solution 4.16. Code for the fourth-order polynomial Wigner distribution reads as

```

function PWD4
N=64;
tau=-1:1/N:1; %lag value

k=0;
for t=-.5:1/N:.5
    k=k+1;
    r=sig(t+.675*tau).^2.*conj(sig(t-.675*tau).^2).*...
        conj(sig(t+.85*tau)).*sig(t-.85*tau);

    %PWD4(k,:)=fftshift(fft(r));
    PWD4(k,:)=fftshift(fft(r.*hanning(2*N+1)'));
    plot(abs(PWD4(k,:))), pause(.001)
end
waterfall(abs(PWD4)), view([10 80])

function x=sig(t)
    %Signal definition
x=exp(j*96*pi*t.^3-j*48*pi*t);

```

Chapter 5

Analysis of Noisy Signals

Disturbances that can be modeled by noise are inherent in all signal processing applications. If there were no noise, then many problems would have been solved in an easy and direct way. The presence of noise means that many obvious and mathematically well-established solutions cannot be used in practice, because they fail to produce any result in real-life cases, even with small to moderate noises. Thus, any engineering-oriented analysis would not be complete without taking into account noise presence. In this chapter, an analysis of noise influence to the commonly used time-frequency representations is presented. The Wigner distribution, as the basic time-frequency representation, is studied in details. The influence of noise on the Wigner distribution-based instantaneous frequency estimation is studied. This analysis, presented on the Wigner distribution, may be used for any time-frequency representation. An algorithm for the estimation of the optimal window width is presented. The analysis of noise is extended to other quadratic distributions as well. Generalizations to different types of additive and multiplicative noise, including stationary white noise, nonstationary white noise, and colored stationary noise, are made. The exact expressions for the mean value and variance of quadratic distributions for each point in the time-frequency plane are given. The noise analysis is extended to various noise types, including heavy-tailed noise. This analysis leads to robust definitions and calculation methods of time-frequency representations for various noise classes. A special attention has been paid to the impulse noise, when some signal samples are so highly corrupted that their complete omission is done. At this point, when highly corrupted signal values are omitted due to the high impulse noise (equivalent to the case when they are not available at all), this analysis meets the area of sparse signal processing. Thus, robust signal processing tools, dealing with heavily corrupted signals at some instants, approach the compressive sensed

signal processing, dealing with the signal measurements not available at the same instants.

5.1 SHORT-TIME FOURIER TRANSFORM OF NOISY SIGNALS

The STFT is the windowed Fourier transform. The noise influence on the STFT can be considered in the same way as in the case of the Fourier transform. Here a short review of some results from Chapter 1, will be presented.

Consider a discrete noisy signal

$$x(n) = s(n) + \varepsilon(n), \quad (5.1)$$

where $s(n)$ is a deterministic signal and $\varepsilon(n)$ is an additive noise. The STFT of this signal is

$$\begin{aligned} STFT_x(n, k) &= \sum_{m=0}^{N-1} w(m) (s(n+m) + \varepsilon(n+m)) e^{-j2\pi km/N} \\ &= STFT_s(n, k) + STFT_\varepsilon(n, k). \end{aligned} \quad (5.2)$$

Its mean value is

$$E\{STFT_x(n, k)\} = STFT_s(n, k) + STFT_{\mu_\varepsilon}(n, k),$$

where $\mu_\varepsilon(n) = E\{\varepsilon(n)\}$. In the case of zero-mean noise $\mu_\varepsilon(n) = 0$. Then the STFT mean value is equal to the STFT of the signal $s(n)$

$$E\{STFT_x(n, k)\} = STFT_s(n, k). \quad (5.3)$$

The variance of $STFT(n, k)$, for zero-mean noise, is

$$\begin{aligned} \sigma_{STFT}^2(n, k) &= E\{STFT_x(n, k)STFT_x^*(n, k)\} - STFT_s(n, k)STFT_s^*(n, k) \\ &= \sum_{m_1=0}^{N-1} \sum_{m_2=0}^{N-1} w(m_1)w(m_2) E\{\varepsilon(n+m_1)\varepsilon^*(n+m_2)\} e^{-j2\pi k(m_1-m_2)/N}. \end{aligned} \quad (5.4)$$

In the case of white noise, whose auto-correlation is given by

$$R_{\varepsilon\varepsilon}(n+m_1, n+m_2) = E\{\varepsilon(n+m_1)\varepsilon^*(n+m_2)\} = \sigma_\varepsilon^2 \delta(m_1 - m_2),$$

where σ_ϵ^2 is the noise variance, the STFT variance is

$$\sigma_{STFT}^2(n, k) = \sigma_\epsilon^2 \sum_{m=0}^{N-1} w^2(m) = \sigma_\epsilon^2 E_w. \quad (5.5)$$

Example 5.1. Signal $x(n)$ is composed of a deterministic complex sinusoid $s(n) = A \exp(j2\pi k_0 n/N)$, with a frequency index k_0 (an integer) and a Gaussian complex white noise, with independent real and imaginary parts of variance $\sigma_\epsilon^2/2$. Find the mean value and variance of the STFT for the Hann(ing) window. Compare the maximal STFT value of the deterministic part of signal with the STFT variance.

★ The STFT mean value and variance are

$$\begin{aligned} E\{STFT_x(n, k)\} &= STFT_s(n, k) \\ &= A \frac{N}{4} (\delta(k - k_0 + 1) + 2\delta(k - k_0) + \delta(k - k_0 - 1)), \\ \sigma_{STFT}^2(n, k) &= \sigma_\epsilon^2 \sum_{m=0}^{N-1} w^2(m) = \frac{3N}{8} \sigma_\epsilon^2. \end{aligned} \quad (5.6)$$

The peak signal-to-noise ratio that is relevant for signal detection in high noise environment is

$$SNR_{out} = \frac{\max_k |STFT_s(n, k)|^2}{\sigma_{STFT}^2} = \frac{2N}{3} \frac{A^2}{\sigma_\epsilon^2}.$$

For the rectangular window, it would be $SNR_{out} = NA^2/\sigma_\epsilon^2$. The signal-to-noise ratio in the STFT increases with N . \square

The usage of any other than the rectangular lag window in the STFT calculation may be considered as the STFT smoothing in frequency, (5.6). This smoothing reduces the maximal STFT value amplitude. In the Hann(ing) window case, the amplitude is reduced to 1/2 of the original value, while the variance is reduced by a factor of $1/16 + 1/4 + 1/16 = 3/8$. Thus, we have overall reduction in the SNR_{out} coefficient from N to $2N/3$. However, the analysis in the previous example has been performed with the assumption that the frequency of the analyzed signal is on the frequency grid. In reality, that is never the case. Then significant side lobes in the STFT, as well as changes in the STFT amplitude, worsen the rectangular window performance to the level that this window is just one of the windows used in the analysis.

In the case of frequency-modulated signals $s(n) = A \exp(j\phi(n))$, assuming that the phase variations within the window of width N are high, an approximation

of the STFT value of the signal $s(n)$ can be obtained by using the stationary-phase method of the corresponding continuous time signal. The maximal STFT value will be proportional to the signal amplitude and inversely proportional to the instantaneous frequency derivative (as explained in Chapter 2). It will not depend on the window width. Therefore, the signal-to-noise ratio SNR_{out} will not increase with the window width N , as in the constant frequency case. In addition, the signal's STFT is spread over a wide frequency region, increasing the probability that some of its noisy samples, not corresponding (or not even being near) to the instantaneous frequency position, exceed the STFT value at the true instantaneous frequency. It may result in a wrong conclusion about the frequency position. An approach to the performance analysis of time-frequency representations, as instantaneous frequency estimators, will be presented later in this chapter.

In processing noisy signals, influence of random disturbance to the signal can be reduced by smoothing the resulting function (here the STFT or the spectrogram). Smoothing would further decrease signal concentration in the time-frequency domain. Another approach is to compose the STFTs in a counter direction, increasing the time-varying signal concentration toward the Wigner distribution via the S-method. In the case of the linear frequency-modulated signal, full concentration is achieved by the Wigner distribution, since it behaves the same for all signals with linear and constant frequency. The spectrogram, as the squared modulus of the STFT, is a member of quadratic time-frequency distributions as well. So we will focus on quadratic distributions of noisy signals, starting with the Wigner distribution as their main representative.

5.2 WIGNER DISTRIBUTION OF NOISY SIGNALS

Consider the pseudo Wigner distribution of a discrete-time noisy signal $x(n) = s(n) + \varepsilon(n)$,

$$PWD_x(n, \omega) = \sum_{m=-\infty}^{\infty} w(m)w(-m)x(n+m)x^*(n-m)e^{-j2\omega m}, \quad (5.7)$$

where $w(m)$ is a real-valued lag window, such that $w(0) = 1$. The frequency variable will be kept in continuous form since we will use its derivatives in the explanations that follow. A signal $s(n)$ is a deterministic signal and noise $\varepsilon(n) = \varepsilon_r(n) + j\varepsilon_i(n)$ is a complex-valued white Gaussian noise with independent and identically distributed real and imaginary parts (i.i.d. $\mathcal{N}(0, \sigma_\varepsilon^2/2)$). The auto-correlation function of this

noise is

$$R_{\epsilon\epsilon}(m) = \text{E}\{\epsilon(n)\epsilon^*(n-m)\} = \sigma_\epsilon^2 \delta(m). \quad (5.8)$$

The Wigner distribution mean, for the noisy signal $x(n) = s(n) + \epsilon(n)$, is

$$\begin{aligned} \text{E}\{PWD_x(n, \omega)\} &= \text{E}\left\{\sum_{m=-\infty}^{\infty} w(m)w(-m)[s(n+m)s^*(n-m)\right. \\ &\quad + s(n+m)\epsilon^*(n-m) + \epsilon(n+m)s^*(n-m) \\ &\quad \left.+ \epsilon(n+m)\epsilon^*(n-m)]e^{-j2\omega m}\right\}. \end{aligned}$$

Having in mind that

$$\begin{aligned} \text{E}\{\epsilon(n \pm m)\} &= 0 \\ \text{E}\{\epsilon(n+m)\epsilon^*(n-m)\} &= R_{\epsilon\epsilon}(2m), \end{aligned}$$

it follows

$$\begin{aligned} \text{E}\{PWD_x(n, \omega)\} &= \sum_{m=-\infty}^{\infty} w(m)w(-m)s(n+m)s^*(n-m)e^{-j2\omega m} \\ &\quad + \sum_{m=-\infty}^{\infty} w(m)w(-m)R_{\epsilon\epsilon}(2m)e^{-j2\omega m}. \end{aligned} \quad (5.9)$$

The first term is the Fourier transform of the product of $w(m)w(-m)s(n+m)s^*(n-m)$ at 2ω . It can be written as the convolution of the Fourier transform $W(e^{j\omega})$ of $w(m)w(-m)$

$$W(e^{j\omega}) = \sum_{m=-\infty}^{\infty} w(m)w(-m)e^{-j\omega m}$$

and the original Wigner distribution $WD_s(n, \omega)$ of $s(n)$ without a lag window

$$WD_s(n, \omega) = \sum_{m=-\infty}^{\infty} s(n+m)s^*(n-m)e^{-j2\omega m}.$$

The second term is equal to σ_ϵ^2 , since $R_{\epsilon\epsilon}(m) = \sigma_\epsilon^2 \delta(m)$. Thus,

$$\text{E}\{PWD_x(n, \omega)\} = \frac{1}{\pi} \int_{-\pi/2}^{\pi/2} WD_s(n, \omega - \alpha)W(e^{j2\alpha})d\alpha + \sigma_\epsilon^2, \quad (5.10)$$

where the convolution integration is performed over the discrete time Wigner distribution period, $-\pi/2 < \omega \leq \pi/2$.

5.2.1 Pseudo Wigner Distribution Bias

The pseudo Wigner distribution is biased. In addition to the random noise-caused bias factor σ_e^2 , the lag window $w(m)$ causes a deterministic bias in the pseudo Wigner distribution, since it differs from the original Wigner distribution without a lag window. By expanding $WD_s(n, \omega - \alpha)$ into a Taylor series, around ω ,

$$WD_s(n, \omega - \alpha) = WD_s(n, \omega) + \frac{\partial WD_s(n, \omega)}{\partial \omega} \alpha + \frac{1}{2} \frac{\partial^2 WD_s(n, \omega)}{\partial \omega^2} \alpha^2 + \dots,$$

we get

$$\frac{1}{\pi} \int_{-\pi/2}^{\pi/2} WD_s(n, \omega - \alpha) W(e^{j2\alpha}) d\alpha = WD_s(n, \omega) + \frac{1}{8} \frac{\partial^2 WD_s(n, \omega)}{\partial \omega^2} m_2 + \dots, \quad (5.11)$$

where

$$\begin{aligned} \frac{1}{2\pi} \int_{-\pi}^{\pi} W(e^{j\omega}) d\omega &= w^2(0) = 1, \\ m_1 &= \frac{1}{2\pi} \int_{-\pi}^{\pi} \omega W(e^{j\omega}) d\omega = 0, \\ m_2 &= \frac{1}{2\pi} \int_{-\pi}^{\pi} \omega^2 W(e^{j\omega}) d\omega. \end{aligned} \quad (5.12)$$

The first moment m_1 (and all other odd moments) of $W(e^{j\omega})$ is equal to zero, since $W(e^{j\omega})$ is an even function (as the Fourier transform of an even, real-valued window function $w(m)w(-m)$).

From (5.11) follows that the first term is the original Wigner distribution, while the remaining terms introduce the pseudo Wigner distribution deterministic distortion. They can be approximated by

$$\begin{aligned} \frac{1}{\pi} \int_{-\pi/2}^{\pi/2} WD_s(n, \omega - \alpha) W(e^{j2\alpha}) d\alpha - WD_s(n, \omega) &= \frac{1}{8} \frac{\partial^2 WD_s(n, \omega)}{\partial \omega^2} m_2 + \dots \\ &\cong \frac{1}{8} \frac{\partial^2 WD_s(n, \omega)}{\partial \omega^2} m_2 = \frac{1}{8} b(n, \omega) m_2. \end{aligned}$$

The pseudo Wigner distribution bias is

$$\text{bias}_{PWD}(n, \omega) = \text{bias}_\varepsilon + \text{bias}(n, \omega) = \sigma_\varepsilon^2 + \frac{1}{8}b(n, \omega)m_2. \quad (5.13)$$

The second part of the Wigner distribution bias is highly time-frequency dependent. For the regions where the Wigner distribution variations in the frequency direction are small, as described by the second- and higher-order derivatives, this bias is small and vice versa. Since the first part of the bias in (5.13) is just a constant for all (n, ω) , it will be disregarded in most of the following analysis.

5.2.2 Pseudo Wigner Distribution Variance

The pseudo Wigner distribution variance, at the considered point (n, ω) , is defined by

$$\sigma_{PWD}^2(n, \omega) = E\{PWD_x(n, \omega)PWD_x^*(n, \omega)\} - E\{PWD_x(n, \omega)\}E\{PWD_x^*(n, \omega)\}. \quad (5.14)$$

For a noisy signal (5.1), it results in

$$\begin{aligned} \sigma_{PWD}^2(n, \omega) &= \sum_{m_1=-\infty}^{\infty} \sum_{m_2=-\infty}^{\infty} w(m_1)w(-m_1)w(m_2)w(-m_2)e^{-j2\omega(m_1-m_2)} \\ &\quad \times [s(n+m_1)s^*(n+m_2)R_{\varepsilon\varepsilon}(n-m_2, n-m_1) \\ &\quad + s^*(n-m_1)s(n-m_2)R_{\varepsilon\varepsilon}(n+m_1, n+m_2) \\ &\quad + s(n+m_1)s(n-m_2)R_{\varepsilon\varepsilon^*}^*(n-m_1, n+m_2) \\ &\quad + s^*(n-m_1)s^*(n+m_2)R_{\varepsilon\varepsilon^*}(n+m_1, n-m_2) \\ &\quad + R_{\varepsilon\varepsilon}(n+m_1, n+m_2)R_{\varepsilon\varepsilon}(n-m_2, n-m_1) \\ &\quad + R_{\varepsilon\varepsilon^*}(n+m_1, n-m_2)R_{\varepsilon\varepsilon^*}^*(n-m_1, n+m_2)], \end{aligned} \quad (5.15)$$

where

$$R_{\varepsilon\varepsilon}(n, m) = E\{\varepsilon(n)\varepsilon^*(m)\}.$$

The fourth-order moment of the noise

$$m_4^\varepsilon = E\{\varepsilon(n+m_1)\varepsilon^*(n-m_1)\varepsilon^*(n+m_2)\varepsilon(n-m_2)\}$$

is reduced to the auto-correlation function by using the relation

$$E\{z_1z_2z_3z_4\} = E\{z_1z_2\}E\{z_3z_4\} + E\{z_1z_3\}E\{z_2z_4\} + E\{z_1z_4\}E\{z_2z_3\}, \quad (5.16)$$

which holds for Gaussian zero-mean random variables z_i , $i = 1, 2, 3, 4$.

For the considered complex noise

$$R_{\varepsilon\varepsilon}(n, m) = \sigma_\varepsilon^2 \delta(n - m)$$

and

$$\begin{aligned} R_{\varepsilon\varepsilon^*}(n, m) &= E\{[\varepsilon_r(n) + j\varepsilon_i(n)][\varepsilon_r(m) + j\varepsilon_i(m)]\} \\ &= E\{\varepsilon_r(n)\varepsilon_r(m)\} - E\{\varepsilon_i(n)\varepsilon_i(m)\} = 0. \end{aligned}$$

The variance of the pseudo Wigner distribution estimator reduces to

$$\sigma_{PWD}^2(n, \omega) = \sigma_\varepsilon^2 \sum_{m=-\infty}^{\infty} w^2(m)w^2(-m) [2|s(n+m)|^2 + \sigma_\varepsilon^2]. \quad (5.17)$$

It is frequency independent. For constant amplitude signals, $s(n) = A \exp(j\phi(n))$, the pseudo Wigner distribution variance is constant (both time and frequency independent),

$$\sigma_{PWD}^2(n, \omega) = \sigma_\varepsilon^2 E_w (2A^2 + \sigma_\varepsilon^2), \quad (5.18)$$

where

$$E_w = \sum_{m=-\infty}^{\infty} [w(m)w(-m)]^2,$$

is the energy of window $w(m)w(-m)$. A finite energy lag window is sufficient to make the variance of $PWD_x(n, \omega)$ finite for Gaussian, zero-mean, white noise.

Other types of noise will be introduced later in general analysis of quadratic time-frequency distributions.

5.2.3 On the Optimal Window Width

The optimal lag window width can be obtained by minimizing the mean squared error (MSE)

$$e^2 = \text{bias}^2(n, \omega) + \sigma_{PWD}^2(n, \omega). \quad (5.19)$$

Example 5.2. Consider a constant amplitude signal, $x(n) = A \exp(j\phi(n))$ and the Hann(ing) window $w(m)w(-m)$ of the width N . Calculate the optimal window width as a function of the Wigner distribution derivatives.

★For the Hann(ing) window, $E_w = 3N/8$ and $m_2 = 2\pi^2/N^2$, so we get

$$e^2 \cong \frac{\pi^4}{16N^4} \left(\frac{\partial^2 WD_s(n, \omega)}{\partial \omega^2} \right)^2 + \frac{3N}{8} \sigma_\varepsilon^2 (2A^2 + \sigma_\varepsilon^2). \quad (5.20)$$

It has been assumed that the fourth and other higher-order Wigner distribution derivatives can be neglected. From $\partial e^2/\partial N = 0$, the approximation of optimal window width, for the pseudo Wigner distribution of noisy signals, follows

$$N_{opt}(n, \omega) \cong \sqrt[5]{\frac{2b^2(n, \omega)\pi^4}{3\sigma_\varepsilon^2(2A^2 + \sigma_\varepsilon^2)}} \quad (5.21)$$

with $b(n, \omega) = \partial^2 WD_s(n, \omega)/\partial \omega^2$. Roughly speaking, this relation means that small values of the window width (intensive smoothing in frequency direction) should be used at the points where there are no Wigner distribution variations in frequency, that is, for small $b^2(n, \omega)$. When $b^2(n, \omega)$ is large, then window should be wide, meaning less intensive smoothing, that is, keeping the original Wigner distribution form, for the points when its variations are high. As far as the noise is concerned, low noise cases (small σ_ε^2) do not require any smoothing of the original Wigner distribution in frequency direction. Thus, wide lag windows should be used. For a high noise, the Wigner distribution smoothing will improve results.

In general, the fourth and other higher-order derivatives and window moments should be included as well. \square

Of course, we do not know anything about the signal or its form in the Wigner distribution in advance. An algorithm for estimation of $N_{opt}(n, \omega)$, without using the value of $b^2(n, \omega)$, will be presented later in this chapter.

Calculation of higher-order moments and cross-correlation function for the Wigner distribution of noisy signals could be found in literature (for the correlation calculation, see the problems).

5.3 WIGNER DISTRIBUTION BASED INSTANTANEOUS FREQUENCY ESTIMATION

The instantaneous frequency estimators based on maxima of time-frequency representations are often used. They are based on the property of time-frequency distributions to concentrate the energy of a signal, in the time-frequency plane, at and around the instantaneous frequency. As it has been shown in Chapter 3, the Wigner distribution produces the best concentration along the linear instantaneous frequency out of the Cohen class of distributions, with a signal-independent kernel. Thus, here we present the Wigner distribution-based estimation. The same approach and analysis may be easily extended to any other distribution or representation presented in the previous chapters. These extensions are quite straightforward and may be found in literature.

Consider the problem of the instantaneous frequency estimation from the discrete-time observations,

$$x(n\Delta t) = s(n\Delta t) + \varepsilon(n\Delta t), \quad (5.22)$$

where

$$s(t) = A \exp(j\phi(t)),$$

Δt is a sampling interval and $\varepsilon(n\Delta t)$ is a complex-valued white Gaussian noise with independent and identically distributed real and imaginary parts, $\mathcal{N}(0, \sigma_\varepsilon^2/2)$. The total variance of the noise is equal to σ_ε^2 . The instantaneous frequency, by definition, is the first derivative of the phase $\Omega(t) = \phi'(t)$. It is assumed that $\Omega(t)$ is an arbitrary smooth differentiable function of time with bounded derivatives. Here we will use continuous time signal notation with samples

$$x(n\Delta t) = x(t)|_{t=n\Delta t},$$

since we are going to use derivatives over time.

The pseudo Wigner distribution notation to be used here is

$$PWD(t, \Omega) = \sum_{m=-\infty}^{\infty} w_T(m\Delta t) x(t + m\Delta t) x^*(t - m\Delta t) e^{-j2\Omega m\Delta t}, \quad (5.23)$$

where the equivalent window of a width T

$$w_T(m\Delta t) = w_0(m\Delta t/T)\Delta t/T,$$

is used, with $w_0(t)$ being a real-valued symmetric window,

$$w_0(t) = w(t)w(-t).$$

We also assume that $w_0(t)$ has the unity width (i.e., $w_0(t) = 0$, for $|t| > 1/2$). Here the window width T will be a varying (and later optimization) parameter, so it has been added as an index into the window notation and corresponding estimates.

According to the instantaneous frequency analysis, we have concluded that we may expect maximal distribution value at the instantaneous frequency. Therefore, the instantaneous frequency estimate, obtained by using the window of the width T in the pseudo Wigner distribution calculation, is a solution of

$$\hat{\Omega}_T(t) = \arg[\max_{\Omega} PWD(\Omega, t)]. \quad (5.24)$$

Next we will analyze the performance of this estimator. The presented analysis, although it uses the pseudo Wigner distribution as a study case, may be applied to any time-frequency representation.

5.3.1 Estimation Error

The estimation error, at a time instant t , is equal to the difference between the true instantaneous frequency $\Omega(t)$ and the position of maximum in the pseudo Wigner distribution $\hat{\Omega}_T(t)$. These two may differ due to various reasons that will be studied here. The error is defined by

$$\Delta\hat{\Omega}_T(t) = \Omega(t) - \hat{\Omega}_T(t). \quad (5.25)$$

The instantaneous frequency estimation error is partly deterministic, caused by the form of the signal and the form of the Wigner distribution, as an estimation tool. Also, there is a part of the error caused by noise. The deterministic part of the error contributes to the estimation bias. Since the analysis is quite complex, the deterministic part of error will be studied first, introducing disturbing factors one by one.

5.3.1.1 Deterministic Error

The stationary point of $PWD(t, \Omega)$ is determined by the zero value of its derivative

$$\frac{\partial PWD(t, \Omega)}{\partial \Omega} = \sum_{m=-\infty}^{\infty} w_T(m\Delta t) x(t + m\Delta t) x^*(t - m\Delta t) (-j2m\Delta t) e^{-j2m\Delta t \Omega}. \quad (5.26)$$

The deterministic part of $x(t + m\Delta t)x^*(t - m\Delta t)$ can be written in the form

$$s(t + m\Delta t)s^*(t - m\Delta t) = |A|^2 \exp(j[2\phi'(t)m\Delta t + \Delta\phi(t, m\Delta t)])$$

since

$$\phi(t + m\Delta t) - \phi(t - m\Delta t) = 2\phi'(t)m\Delta t + \Delta\phi(t, m\Delta t).$$

The Taylor series expansion of $\phi(t + m\Delta t)$ and $\phi(t - m\Delta t)$, around t , can be used to get the residue value $\Delta\phi(t, m\Delta t)$,

$$\phi(t \pm m\Delta t) = \phi(t) \pm \phi'(t)m\Delta t + \frac{1}{2!}\phi''(t)(m\Delta t)^2 \pm \frac{1}{3!}\phi'''(t)(m\Delta t)^3 + \dots$$

$$\Delta\phi(t, m\Delta t) = \phi(t + m\Delta t) - \phi(t - m\Delta t) - 2\phi'(t)m\Delta t = 2\frac{(m\Delta t)^3}{3!}\Omega^{(2)}(t) + \dots$$

where $\Omega^{(2)}(t) \equiv \phi'''(t)$.

The analysis will be done, introducing factors that influence the instantaneous frequency estimation, step by step. Consider first the simplest case, when the higher-order phase derivatives can be neglected,

$$s(t + m\Delta t)s^*(t - m\Delta t) = |A|^2 \exp(j2\phi'(t)m\Delta t).$$

The pseudo Wigner distribution derivative $\partial PWD(t, \Omega)/\partial \Omega$ is of the form

$$\frac{\partial PWD(t, \Omega)}{\partial \Omega} = |A|^2 \sum_{m=-\infty}^{\infty} w_T(m\Delta t)(-j2m\Delta t)e^{-j2m\Delta t(\Omega - \phi'(t))}.$$

For a symmetric window

$$\sum_{m=-\infty}^{\infty} (m\Delta t)w_T(m\Delta t) = 0,$$

$$\frac{\partial PWD(t, \Omega)}{\partial \Omega} = 0 \text{ at } \Omega = \phi'(t). \quad (5.27)$$

The point $\Omega = \phi'(t)$ is the stationary point of $PWD(t, \Omega)$. We will use notation with index $|_0$, to indicate this $\Omega = \phi'(t)$ point,

$$\left. \frac{\partial PWD(t, \Omega)}{\partial \Omega} \right|_0 = |A|^2 \sum_{m=-\infty}^{\infty} w_T(m\Delta t)(-j2m\Delta t) = 0. \quad (5.28)$$

It states that the pseudo Wigner distribution of a linear frequency-modulated signal reaches its maximal value for $\Omega = \phi'(t)$. This is the fact that we already knew. In this case, there is no any estimation error. The instantaneous frequency estimation $\hat{\Omega}_T(t)$, based on the maximum of $PWD(\Omega, t)$ over Ω , for a given t , would be exact, in this simple case.

In the next step, assume that there are small higher-order terms in the phase function,

$$s(t + m\Delta t)s^*(t - m\Delta t) = |A|^2 \exp(j(\phi'(t) \cdot 2m\Delta t) \exp(j\Delta\phi(t, m\Delta t))),$$

with a small $\Delta\phi(t, m\Delta t)$ value within the lag window. Then the approximation

$$\exp(j\Delta\phi(t, m\Delta t)) \simeq 1 + j\Delta\phi(t, m\Delta t), \quad (5.29)$$

can be used. It results in

$$\frac{\partial PWD(t, \Omega)}{\partial \Omega} = |A|^2 \sum_{m=-\infty}^{\infty} w_T(m\Delta t) (-j2m\Delta t) [1 + j\Delta\phi(t, m\Delta t)] e^{-j2m\Delta t(\Omega - \phi'(t))}. \quad (5.30)$$

The higher-order term in the phase function will result in a shift of stationary point, from $\Omega = \phi'(t)$ to $\Omega = \phi'(t) + \Delta\Omega$, causing an error $\Delta\Omega$ in the instantaneous frequency estimation. Our aim is to find and analyze this error. The stationary point of the pseudo Wigner distribution is now

$$\left. \frac{\partial PWD(t, \Omega)}{\partial \Omega} \right|_{\Omega=\phi'(t)+\Delta\Omega} = 0. \quad (5.31)$$

By using the first-order (linear) Taylor expansion of $\partial PWD(t, \Omega)/\partial \Omega$, around the true instantaneous frequency value $\Omega = \phi'(t)$, we can write

$$\left. \frac{\partial PWD(t, \Omega)}{\partial \Omega} \right|_{\Omega=\phi'(t)+\Delta\Omega} = \left. \frac{\partial PWD(t, \Omega)}{\partial \Omega} \right|_{\Omega=\phi'(t)} + \left. \frac{\partial^2 PWD(t, \Omega)}{\partial \Omega^2} \right|_{\Omega=\phi'(t)} \Delta\Omega, \quad (5.32)$$

just as we would write $F(\Omega_0 + \Delta\Omega) \cong F(\Omega_0) + \Delta\Omega dF(\Omega)/d\Omega|_{\Omega=\Omega_0}$ for any differentiable function $F(\Omega)$ and sufficiently small $\Delta\Omega$, when we can replace the approximation sign with the (almost) equality sign. The second derivative of PWD in the stationary point is

$$\begin{aligned} \left. \frac{\partial^2 PWD(t, \Omega)}{\partial \Omega^2} \right|_{\Omega=\phi'(t)} &= |A|^2 \sum_{m=-\infty}^{\infty} w_T(m\Delta t) (-j2m\Delta t)^2 e^{-j2m\Delta t(\Omega - \phi'(t))} \Big|_{\Omega=\phi'(t)} \\ &= |A|^2 \sum_{m=-\infty}^{\infty} w_T(m\Delta t) (-j2m\Delta t)^2. \end{aligned} \quad (5.33)$$

By replacing the value of (5.30), (5.31), and (5.33) into (5.32), it follows

$$\begin{aligned} 0 &= |A|^2 \sum_{m=-\infty}^{\infty} w_T(m\Delta t) (-j2m\Delta t) + |A|^2 \sum_{m=-\infty}^{\infty} w_T(m\Delta t) (-j2m\Delta t) j\Delta\phi(t, m\Delta t) \\ &\quad + |A|^2 \sum_{m=-\infty}^{\infty} w_T(m\Delta t) (-j2m\Delta t)^2 \Delta\Omega. \end{aligned} \quad (5.34)$$

Let us introduce a symbolic notation of the terms in the above equation:

- The first term in summation is equal to (5.28). It represents the first derivative value of the pseudo Wigner distribution, as an estimator, if there were no higher-order phase terms. For this term, the notation introduced in (5.28) will be used.
- The second term is a contribution of the higher-order phase terms $\Delta\phi(t, m\Delta t)$ to $\partial PWD(t, \Omega)/\partial\Omega$. It is a cause of deviation in the estimation. Thus, for this term we will use a symbolic notation

$$\left. \frac{\partial PWD(t, \Omega)}{\partial\Omega} \right|_0 \delta_{\Delta\phi} = |A|^2 \sum_{m=-\infty}^{\infty} w_T(m\Delta t) (-j2m\Delta t) j\Delta\phi(t, m\Delta t)$$

indicating the deviation of $\partial PWD(t, \Omega)/\partial\Omega$ value at $\Omega = \phi'(t)$, caused by a nonzero value of $\Delta\phi(t, m\Delta t)$.

- The third term is the linear change of $\partial PWD(t, \Omega)/\partial\Omega$ when the frequency is shifted for small $\Delta\Omega$. This change is calculated with respect to the stationary point $\Omega = \phi'(t)$, without the higher-order disturbing term $\Delta\phi(t, m\Delta t)$. Its symbolic notation is

$$\left. \frac{\partial^2 PWD(t, \Omega)}{\partial\Omega^2} \right|_0 = -|A|^2 \sum_{m=-\infty}^{\infty} w_T(m\Delta t) (2m\Delta t)^2. \quad (5.35)$$

With the introduced symbolic notations, (5.34) may be rewritten as

$$0 = \left. \frac{\partial PWD(t, \Omega)}{\partial\Omega} \right|_0 + \left. \frac{\partial PWD(t, \Omega)}{\partial\Omega} \right|_0 \delta_{\Delta\phi} + \left. \frac{\partial^2 PWD(t, \Omega)}{\partial\Omega^2} \right|_0 \Delta\Omega. \quad (5.36)$$

This is a linear model of the instantaneous frequency estimation analysis. A full linearization model follows when the noise is added. This model can be widely used (and it has been used) as a model for the instantaneous frequency estimation analysis of various time-frequency representations as instantaneous frequency estimators, including the STFT, the Cohen class of distributions and higher-order time-frequency representations.

From (5.36), the deterministic error in the instantaneous frequency estimation can be found. If we denote the stationary point of (5.31) as $\Omega = \hat{\Omega}(t)$, the estimation error is $\Delta\hat{\Omega}_T(t) = \Delta\Omega$. Its value is

$$\Delta\hat{\Omega}_T(t) = -\frac{\left. \frac{\partial PWD(t, \Omega)}{\partial\Omega} \right|_0 \delta_{\Delta\phi}}{\left. \frac{\partial^2 PWD(t, \Omega)}{\partial\Omega^2} \right|_0}. \quad (5.37)$$

A full evaluation of the window-dependent expressions in (5.37) is simple. It will be done later in this chapter.

5.3.1.2 Random Error

In the final phase of the instantaneous frequency estimator analysis, let us add the noise. For a noisy signal (5.22),

$$\begin{aligned} x(t + m\Delta t)x^*(t - m\Delta t) &= s(t + m\Delta t)s^*(t - m\Delta t) + \\ &s(t + m\Delta t)\varepsilon^*(t - m\Delta t) + \varepsilon(t + m\Delta t)s^*(t - m\Delta t) + \varepsilon(t + m\Delta t)\varepsilon^*(t - m\Delta t). \end{aligned}$$

The pseudo Wigner distribution derivative of signal $x(n\Delta t)$ is

$$\begin{aligned} \frac{\partial PWD(t, \Omega)}{\partial \Omega} &= \sum_{m=-\infty}^{\infty} w_T(m\Delta t)(-j2m\Delta t)s(t + m\Delta t)s^*(t - m\Delta t)e^{-j2m\Delta t\Omega} \\ &+ \sum_{m=-\infty}^{\infty} w_T(m\Delta t)(-j2m\Delta t)s(t + m\Delta t)\varepsilon^*(t - m\Delta t)e^{-j2m\Delta t\Omega} \\ &+ \sum_{m=-\infty}^{\infty} w_T(m\Delta t)(-j2m\Delta t)\varepsilon(t + m\Delta t)s^*(t - m\Delta t)e^{-j2m\Delta t\Omega} \\ &+ \sum_{m=-\infty}^{\infty} w_T(m\Delta t)(-j2m\Delta t)\varepsilon(t + m\Delta t)\varepsilon^*(t - m\Delta t)e^{-j2m\Delta t\Omega}. \end{aligned}$$

The first term is deterministic and its form has already been studied in details. The last three terms are the contribution of noise to the estimation model. They will be denoted by

$$\begin{aligned} \frac{\partial PWD(t, \Omega)}{\partial \Omega}|_0 \delta_\varepsilon &= \sum_{m=-\infty}^{\infty} w_T(m\Delta t)(-j2m\Delta t)s(t + m\Delta t)\varepsilon^*(t - m\Delta t)e^{-j2m\Delta t\Omega} \\ &+ \sum_{m=-\infty}^{\infty} w_T(m\Delta t)(-j2m\Delta t)\varepsilon(t + m\Delta t)s^*(t - m\Delta t)e^{-j2m\Delta t\Omega} \\ &+ \sum_{m=-\infty}^{\infty} w_T(m\Delta t)(-j2m\Delta t)\varepsilon(t + m\Delta t)\varepsilon^*(t - m\Delta t)e^{-j2m\Delta t\Omega}. \end{aligned} \tag{5.38}$$

The linear model that includes the noise is the extended form of (5.36),

$$\begin{aligned} &\left. \frac{\partial PWD(t, \Omega)}{\partial \Omega} \right|_0 + \left. \frac{\partial^2 PWD(t, \Omega)}{\partial \Omega^2} \right|_0 \Delta \Omega \\ &+ \left. \frac{\partial PWD(t, \Omega)}{\partial \Omega} \right|_0 \delta_{\Delta \phi} + \left. \frac{\partial PWD(t, \Omega)}{\partial \Omega} \right|_0 \delta_\varepsilon = 0 \end{aligned} \tag{5.39}$$

where $|_0$ means that the corresponding derivatives are calculated at the original stationary point, without other disturbances. The term $\partial \text{PWD}(t, \Omega) / \partial \Omega |_0 \delta_{\Delta\phi}$ is a deviation in estimation caused by the higher-order phase derivative. It is calculated at $\Omega = \phi'(t)$, without noise influence, $\varepsilon(m\Delta t) = 0$. The term $\partial \text{PWD}(t, \Omega) / \partial \Omega |_0 \delta_\varepsilon$ is a deviation in estimation caused by the small noise. It is analyzed at $\Omega = \phi'(t)$, neglecting $\Delta\phi$. Thus, the simultaneous influence of small values $\Delta\phi$ and ε , is neglected in the analysis. It is lower for an order than the individual influence of any of these disturbances.

Equation (5.39) gives the approximation error

$$\Delta\hat{\Omega}_T(t) = \Delta\Omega = \frac{\left. \frac{\partial \text{PWD}(t, \Omega)}{\partial \Omega} \right|_0 \delta_{\Delta\phi}}{-\left. \frac{\partial^2 \text{PWD}(t, \Omega)}{\partial \Omega^2} \right|_0} + \frac{\left. \frac{\partial \text{PWD}(t, \Omega)}{\partial \Omega} \right|_0 \delta_\varepsilon}{-\left. \frac{\partial^2 \text{PWD}(t, \Omega)}{\partial \Omega^2} \right|_0}. \quad (5.40)$$

The first part of error $\Delta\hat{\Omega}_T(t)$ is deterministic, while the second part is random. The error can be written in a compact form

$$\Delta\hat{\Omega}_T(t) = \frac{L_T(t)}{2F_T} + \frac{\Xi_T}{2F_T |A|^2}, \quad (5.41)$$

introducing the notation that will be explained next. The value of F_T is

$$\begin{aligned} F_T &= \sum_{m=-\infty}^{\infty} w_T(m\Delta t)(m\Delta t)^2 \\ &= \sum_{m=-\infty}^{\infty} w_0(m\Delta t/T)(m\Delta t)^2 \Delta t/T. \end{aligned} \quad (5.42)$$

The previous sum, for small Δt , can be approximated by integral

$$F_T \rightarrow \int_{-T/2}^{T/2} w_0(t/T)t^2 dt/T = T^2 \int_{-1/2}^{1/2} w_0(t)t^2 dt = T^2 F,$$

where T is the window width and F is a constant, for a given window form. For example, for the rectangular window $F = 1/12$.

The value of $L_T(t)$ is

$$L_T(t) = \sum_{m=-\infty}^{\infty} w_T(m\Delta t) \Delta\phi(t, m\Delta t) m\Delta t \simeq \frac{\phi^{(3)}(t)}{3} \sum_{m=-\infty}^{\infty} w_T(m\Delta t) (m\Delta t)^4$$

$$L_T(t) \rightarrow \frac{\phi^{(3)}(t)}{3} T^4 \int_{-1/2}^{1/2} w_0(t) t^4 dt = \frac{\Omega^{(2)}(t)}{3} T^4 \int_{-1/2}^{1/2} w_0(t) t^4 dt = \frac{\Omega^{(2)}(t)}{3} T^4 L,$$

while

$$\Xi_T = \frac{1}{2} \left. \frac{\partial WD(t, \Omega)}{\partial \Omega} \right|_0 \delta_\varepsilon. \quad (5.43)$$

5.3.2 Instantaneous Frequency Estimation Bias

The instantaneous frequency estimation bias is obtained, according to (5.41), as

$$E\{\Delta\hat{\Omega}_T(t)\} = \frac{L_T(t)}{2F_T} + \frac{1}{2F_T |A|^2} E\{\Xi_T\}. \quad (5.44)$$

The expected value of Ξ_T follows from (5.38). The expected value of the first two sums in (5.38) is obviously zero, for a zero-mean noise. The expectation of the third sum in (5.38) is

$$\begin{aligned} & \sum_{m=-\infty}^{\infty} w_T(m\Delta t) (-j2m\Delta t) E\{\varepsilon(t+m\Delta t) \varepsilon^*(t-m\Delta t)\} e^{-j2m\Delta t \Omega} \\ &= \sum_{m=-\infty}^{\infty} w_T(m\Delta t) (-j2m\Delta t) \sigma_\varepsilon^2 \delta(m) e^{-j2m\Delta t \Omega} = 0. \end{aligned}$$

The expected value of the random estimation error is

$$E\{\Xi_T\} = 0. \quad (5.45)$$

In this way, it has been shown that the bias in the estimation error is equal to the deterministic error. The bias of the estimate can be written in the form

$$E\{\Delta\hat{\Omega}_T(t)\} = \frac{L_T(t)}{2F_T} \rightarrow T^2 \frac{\Omega^{(2)}(t)}{6} \frac{\int_{-1/2}^{1/2} w_0(t) t^4 dt}{\int_{-1/2}^{1/2} w_0(t) t^2 dt} = T^2 G \Omega^{(2)}(t), \quad (5.46)$$

with a constant

$$G = \frac{L}{6F}.$$

For the rectangular window $G = 1/40$.

5.3.3 Instantaneous Frequency Estimation Variance

The instantaneous frequency estimation variance, following from (5.41), is

$$\text{var}\{\Delta\hat{\Omega}_T(t)\} = \frac{1}{4F_T^2 |A|^4} \text{E}\{\Xi_T^2\}.$$

After some simple calculations, as in (5.15), the variance is obtained in the form

$$\begin{aligned} \text{var}\{\Delta\hat{\Omega}_T(t)\} &= \frac{\sigma_\epsilon^2}{2|A|^2} \left(1 + \frac{\sigma_\epsilon^2}{2|A|^2} \right) \frac{E_T}{F_T^2}, \\ E_T &= \sum_{m=-\infty}^{\infty} w_T^2(m\Delta t)(m\Delta t)^2 \rightarrow T\Delta t \int_{-1/2}^{1/2} w_0^2(t)t^2 dt = T\Delta t E \end{aligned} \quad (5.47)$$

or

$$\text{var}\{\Delta\hat{\Omega}_T(t)\} = \frac{\sigma_\epsilon^2}{2|A|^2} \left(1 + \frac{\sigma_\epsilon^2}{2|A|^2} \right) \frac{\Delta t}{T^3} \frac{E}{F^2} \quad (5.48)$$

where the constants F and E depend on the window type only. All constants, used in these formulae, are summarized in Table 5.1.

The mean square error is

$$\begin{aligned} \text{E}\{\Delta\hat{\Omega}_T(t)\}^2 &= \text{var}\{\Delta\hat{\Omega}_T(t)\} + |\text{E}\{\Delta\hat{\Omega}_T(t)\}|^2 \\ &= \frac{\sigma_\epsilon^2}{2|A|^2} \left(1 + \frac{\sigma_\epsilon^2}{2|A|^2} \right) \frac{\Delta t}{T^3} \frac{E}{F^2} + \left(T^2 G \Omega^{(2)}(t) \right)^2. \end{aligned} \quad (5.49)$$

For small noise $1 + \sigma_\epsilon^2/(2|A|^2) \cong 1$ and we can write

$$\text{E}\{\Delta\hat{\Omega}_T(t)\}^2 \cong \frac{\sigma_\epsilon^2}{2|A|^2} \frac{\Delta t}{T^3} \frac{E}{F^2} + \left(T^2 G \Omega^{(2)}(t) \right)^2. \quad (5.50)$$

Table 5.1

Window-Dependent Constants in the Instantaneous Frequency Estimation Relations

$$\begin{aligned} F &= \int_{-1/2}^{1/2} w_0(t)t^2 dt & L &= \int_{-1/2}^{1/2} w_0(t)t^4 dt \\ G &= \frac{1}{6F} \int_{-1/2}^{1/2} w_0(t)t^4 dt & E &= \int_{-1/2}^{1/2} w_0^2(t)t^2 dt \end{aligned}$$

Example 5.3. If the window is rectangular, then $E = F = 1/12$ and $G = 1/40$. The MSE can be written in the form

$$E\{\Delta\hat{\Omega}_T(t)\}^2 = \text{var}\{\Delta\hat{\Omega}_T(t)\} + |E\{\Delta\hat{\Omega}_T(t)\}|^2 \quad (5.51)$$

$$E\{\Delta\hat{\Omega}_T(t)\}^2 = \frac{6\sigma_\varepsilon^2}{|A|^2} \frac{\Delta t}{T^3} + \left(\frac{1}{40} T^2 \Omega^{(2)}(t) \right)^2. \quad (5.52)$$

From (5.52) it is clear that by increasing the window width T , the bias increases, while the variance decreases. The optimization of T in (5.52), minimizing the MSE, results in

$$T_o(t) = \left[\frac{7200\sigma_\varepsilon^2 \Delta t}{|A|^2 (\Omega^{(2)}(t))^2} \right]^{1/7}. \quad (5.53)$$

□

The optimal window width $T_0(t)$ gives the optimal bias-variance trade-off, usual for nonparametric estimation, depending on the signal-to-noise ratio $|A|^2/\sigma_\varepsilon^2$, the sampling interval Δt and the second instantaneous frequency derivative $\Omega^{(2)}(t)$. Thus, the optimal choice of the width T depends on the instantaneous frequency derivative $\Omega^{(2)}(t)$. This derivative is unknown because the instantaneous frequency itself is to be estimated. Note that if the second derivative $\Omega^{(2)}(t)$ is significantly different for different t , then the optimization of the estimation accuracy requires a time-varying window width $T(t)$.

5.4 ADAPTIVE ALGORITHM

A general form of an optimization algorithm will be presented next. To accomplish this aim, we will generalize the notation. A generalized form of the MSE, for an estimate $\hat{f}_h(t)$ of a function $f(t)$, by using an estimator varying parameter h , is

$$MSE = \frac{V}{h^m} + B(t)h^n, \quad (5.54)$$

where the variance and the bias of estimate $\hat{f}_h(t)$, for a given parameter h , are

$$\sigma^2(h) = V/h^m, \quad \text{bias}(t, h) = \sqrt{B(t)h^n}. \quad (5.55)$$

The expected value of $B(t)$ depends on $f(t)$ variations in time. With $m = 3$ and $n = 4$ in (5.54), the MSE for the instantaneous frequency estimation (5.52) follows, with $h = T$. Values of m and n are different for various estimations, but the algorithm remains the same, in principle. Thus, its generalized form, valid not only for the instantaneous frequency estimation and the Wigner distribution, is presented.

The MSE in (5.54) has a minimum with respect to h . This minimum occurs for the optimal value of h given by

$$h_{opt}(t) = [mV/(nB(t))]^{1/(m+n)}. \quad (5.56)$$

Note that this relation is not useful in practice, because its right side contains $B(t)$, which depends on derivatives of the unknown value to be estimated. Therefore, a method that can be useful in practice should produce an estimate of $h_{opt}(t)$ without having to know the value of $B(t)$. The optimal value of parameter h , according to (5.54), is obtained from

$$\frac{\partial MSE}{\partial h} = -m \frac{V}{h^{m+1}} + nB(t)h^{n-1} = 0|_{h=h_{opt}}. \quad (5.57)$$

Multiplying (5.57) by h , a relationship between the bias and the standard deviation, (5.55), for $h = h_{opt}$, is obtained

$$\text{bias}(t, h_{opt}) = \sqrt{\frac{m}{n}} \sigma(h_{opt}). \quad (5.58)$$

It will be assumed, without loss of generality, that the bias is positive.

The estimate $\hat{f}_h(t)$ (obtained by using the parameter h) is a random variable distributed around the true value $f(t)$ with the bias $\text{bias}(t, h)$ and the standard deviation $\sigma(h)$. Thus, one may write,

$$|f(t) - (\hat{f}_h(t) - \text{bias}(t, h))| \leq \kappa\sigma(h), \quad (5.59)$$

where the inequality holds with probability $P(\kappa)$ depending on parameter κ . If we assume, for example, that the random variable $\hat{f}_h(t)$ is Gaussian, with the central value

$$M = f(t) + \text{bias}(t, h)$$

and the standard deviation $\sigma(h)$, then the probability that $\hat{f}_h(t)$ takes a value within the interval

$$[M - \kappa\sigma(h), M + \kappa\sigma(h)]$$

is $P(\kappa) = 0.95$ for $\kappa = 2$, and $P(\kappa) = 0.997$ for $\kappa = 3$. Assume that κ is such that $P(\kappa) \rightarrow 1$.

Introduce now a set H of discrete dyadic values of parameter h ,

$$H = \{h_s \mid h_s = 2h_{s-1}, s = 1, 2, \dots, J\}. \quad (5.60)$$

Define the confidence intervals

$$D_s = [L_s, U_s]$$

of the estimates, with the following upper and lower bounds

$$\begin{aligned} L_s &= \hat{f}_{h_s}(t) - (\kappa + \Delta\kappa)\sigma(h_s), \\ U_s &= \hat{f}_{h_s}(t) + (\kappa + \Delta\kappa)\sigma(h_s), \end{aligned} \quad (5.61)$$

where $\hat{f}_{h_s}(t)$ is an estimate of $f(t)$, with the parameter $h = h_s$, and $\sigma(h_s)$ is its standard deviation. Assume that a parameter value denoted by $h_{s^+} \in H$ is close to h_{opt} , $h_{s^+} \sim h_{opt}$. Since, in general, h_{opt} does not correspond to any h_s from the set H , for the analysis that follows we can write $h_{s^+} = 2^p h_{opt}$, where p is a constant close to 0. According to (5.60), all other parameter values can be written as a function of h_{s^+} as

$$\begin{aligned} h_s &= h_{s^+} 2^{(s-s^+)} = h_{opt} 2^{s-s^++p}, \\ (s-s^+) &= \dots, -2, -1, 0, 1, 2, \dots. \end{aligned} \quad (5.62)$$

With this notation, having in mind (5.58), the standard deviation and bias from (5.55) can be expressed by

$$\sigma(h_s) = \sqrt{V/h_s^m} = \sigma(h_{opt}) 2^{-(s-s^++p)m/2},$$

$$\text{bias}(t, h_s) = \sqrt{B(t)/h_s^n} = \sqrt{m/n} \sigma(h_{opt}) 2^{(s-s^++p)n/2}. \quad (5.63)$$

For small values of h_s , when $s \ll s^+$, the bias of $\hat{f}_{h_s}(t)$ is negligible, thus

$$f(t) \in D_s$$

(with probability $P(\kappa + \Delta\kappa) \rightarrow 1$). Then obviously,

$$D_{s-1} \cap D_s \neq \emptyset,$$

since at least the true value $f(t)$ belongs to both confidence intervals.

For large values of h_s , when $s \gg s^+$, the variance is small, but the bias is large. It is clear that for $\text{bias}(t, h_s) \neq 0$ there exists such a large s that

$$D_s \cap D_{s+1} = \emptyset$$

for a finite $\kappa + \Delta\kappa$.

The idea behind the algorithm is that $\Delta\kappa$ in D_s can be found in such a way that the largest s , for which the sequence of the pairs of the confidence intervals D_{s-1} and D_s has at least a point in common, is $s = s^+$. Such a value of $\Delta\kappa$ exists because the bias and the variance are monotonically increasing and decreasing functions of h , respectively, (5.63). As soon as this value of $\Delta\kappa$ is found the intersection of the confidence intervals D_{s-1} and D_s could be expressed as

$$|\hat{f}_{h_{s-1}}(t) - \hat{f}_{h_s}(t)| \leq (\kappa + \Delta\kappa)[\sigma(h_{s-1}) + \sigma(h_s)], \quad (5.64)$$

works as an indicator of the event $s = s^+$, that is, the event

$$h_s = h_{s^+} \sim h_{opt}.$$

The value of h_{s^+} is the last h_s when (5.64) is still satisfied.

Table 5.2

Parameters in the Adaptive Algorithm for Various m, n, κ : $m = 3, n = 4$ for the Spectrogram, Wigner and L-Wigner Distribution-Based Instantaneous Frequency Estimators; $m = 3, n = 8$ for the Fourth-Order Polynomial Wigner-Ville Distribution, and Local Polynomial Distribution-Based Instantaneous Frequency Estimators; $m = 1, n = 4$ for the Wigner Distribution as a Spectrum Estimator.

m	1	1	3	3	3	3	3	3
n	4	4	4	4	4	8	8	8
κ	2	3	2	3	5	2	3	5
$\Delta\kappa$	0.86	1.29	0.39	0.58	0.97	0.09	0.14	0.23
p	0.99	1.22	0.34	0.51	0.72	-0.13	-0.03	0.11
p_1	1.18	1.41	0.59	0.76	0.97	0.19	0.30	0.43

5.4.1 Parameters in the Adaptive Algorithm

There are three possible approaches to choosing algorithm parameters κ , $\Delta\kappa$, and p . Their performances do not differ significantly.

The first approach is when our knowledge about the variance and bias behavior, given by (5.54), is not quite reliable, an approximate approach for κ , $\Delta\kappa$, and p determination can be used. Then we can assume a value of $\kappa \cong 2.5$, such that $P(\kappa) \cong 0.99$ for Gaussian distribution of estimation error. The value of $\Delta\kappa$ should take into account the bias for the expected optimal window width (5.58). It is common to assume that, for the optimal value of h , the bias and variance are of the same order, resulting in $\Delta\kappa \cong 1$. Then we can expect that the obtained value h_{s^+} is close to h_{opt} , thus $p \cong 0$, and all parameters for the key algorithm equation (5.64) are defined. This simple heuristic form has been successfully used in applications, and it is highly recommended for most of practical applications. Estimation of the standard deviation $\sigma(h_s)$ will be discussed within the numerical examples that follow. In the case when correlation between random deviations of consecutive estimates cannot be excluded, lower values of $(\kappa + \Delta\kappa)$ should be used. In some image processing applications values, as low as, $\kappa + \Delta\kappa$ of order 1 or lower have been efficiently used.

The second approach when the knowledge about the variance and bias behavior is reliable, that is, when (5.54) accurately describes the estimation error, then we can calculate all the algorithm parameters. According to the algorithm basic idea, only three confidence intervals, D_{s^+-1}, D_{s^+} , and D_{s^++1} , should be considered. The

confidence intervals D_{s^+-1} and D_{s^+} should have, while D_{s^+} and D_{s^++1} should not have, at least one point in common. Assuming that relation (5.59) holds, and that the bias is positive, this condition means that the minimal possible value of the upper D_{s^+-1} bound, (5.61), denoted by $\min\{U_{s^+-1}\}$, is always greater than or equal to the maximal possible value of the lower D_{s^+} bound, denoted by $\max\{L_{s^+}\}$, that is,

$$\min\{U_{s^+-1}\} \geq \max\{L_{s^+}\}.$$

The condition that D_{s^+} and D_{s^++1} do not intersect is given by

$$\max\{U_{s^+}\} < \min\{L_{s^++1}\}.$$

According to (5.59) and (5.61), the above analysis results in

$$\text{bias}(h_{s^+-1}) + \Delta\kappa\sigma(h_{s^+-1}) \geq \text{bias}(h_{s^+}) - \Delta\kappa\sigma(h_{s^+}),$$

$$\text{bias}(h_{s^+}) + (2\kappa + \Delta\kappa)\sigma(h_{s^+}) < \text{bias}(h_{s^++1}) - (2\kappa + \Delta\kappa)\sigma(h_{s^++1}). \quad (5.65)$$

Since the inequalities are written for the worst case, we can calculate the algorithm parameters by using the corresponding equalities. With (5.63) we get

$$\Delta\kappa = \frac{2\kappa}{2^{(m+n)/2} - 1},$$

$$2^p = \left[\frac{\Delta\kappa \sqrt{n/m} (2^{m/2} + 1)}{1 - 2^{-n/2}} \right]^{2/(m+n)}. \quad (5.66)$$

Values of the parameters $\Delta\kappa$ and p for various distributions, that is, for various values of m and n , are given in Table 5.2.

For further and very fine tuning of the algorithm parameters, one may want that the adaptive parameter value is unbiased in logarithmic, instead of linear scale (due to definition (5.60)). The estimation bias and variance are exponential functions with respect to m and n , (5.63). Thus, the confidence interval limits vary as $2^{(s-s^+)(m+n)/2}$. The mean value for this exponential function, for two successive confidence intervals, for example, $(s-s^+) = 0$ and $(s-s^+) = 1$, is $(1 + 2^{(m+n)/2})/2$. It is shifted with respect to the geometrical mean $\sqrt{2^{(m+n)/2}}$ of these two intervals, by approximately

$$\Delta p \cong \left[\log_2 \left((1 + 2^{(m+n)/2})/2 \right) \right] \frac{2}{m+n} - \frac{1}{2},$$

resulting in the total logarithmic shift

$$p_1 = p + \Delta p,$$

presented in Table 5.2. Therefore, the adaptive parameter value (as an estimate of the optimal parameter value) should be

$$\hat{h}_{opt} = h_{s^+}/2^{p_1}.$$

Note that the set H of parameter values h is a priori assumed. Therefore, as long as we can calculate p_1 , we can use it in the following ways: (a) to calculate distribution with the new parameter value,

$$h_a = h_{s^+}/2^{p_1}$$

as the best estimate of h_{opt} , and (b) to remain within the assumed set of $h_s \in H$, and to decide only whether to correct the obtained h_{s^+} or not. For example, if $|p_1| \leq 1/2$ the correction is smaller than the parameter discretization step. Thus, we can use $h_a = h_{s^+}$. For $1/2 < p_1 \leq 3/2$, it is better to use

$$h_a = h_{s^+}/2 = h_{s^+-1},$$

as the adaptive parameter value. Fortunately, the loss of accuracy for the adaptive parameters h_a , as far as they are of h_{opt} order, is not significant since the MSE varies slowly around its stationary point. Thus, in numerical implementations we can use only the parameter values from the given set H .

The third approach for the parameter $(\kappa + \Delta\kappa)$ estimation is based on the statistical nature of confidence intervals, and a posteriori check of the fitting quality.

Example 5.4. Optimal Width Estimation: In this illustrative example we have simulated the estimates of a function $f_i(t)$ as a random variable

$$\hat{f}_h(t) = \mathbf{a}\sqrt{V/h^m} + \sqrt{B(t)h^n} + f_i(t), \quad (5.67)$$

having the MSE given by (5.54), where $\mathbf{a} = \mathcal{N}(0, 1)$ is a Gaussian (zero-mean, unity-variance) random variable, $m = 3$, $n = 4$, and $V = 1$. For the true value $f_i(t)$, at a given t , any constant can be assumed. The bias parameter $B(t)$ in $\hat{f}_h(t)$ logarithmically varies within

$$\frac{1}{7} \log_2 \left(\frac{mV}{nB(t)} \right) \in [-4, 3],$$

with step 0.05.

For each value of parameter $B(t)$, we have calculated the optimal window width according to (5.56), and plotted $\log_2(h_{opt})$ as a thick line in Fig. 5.1. The problem considered here is to find the adaptive parameter h , by using the presented algorithm, for various values of bias parameter $B(t)$, and to compare it with the optimal one, h_{opt} .

The value of $\hat{f}_h(t)$ was simulated (generated) using (5.67) for each $B(t)$ and $h_s \in H$.

The assumed set of possible window widths was

$$H = \{1/16, 1/8, 1/4, 1/2, 1, 2, 4, 8, 16, 32\},$$

and $\kappa = 2$. The key algorithm relation (5.64) was tested each time, with the known standard deviation

$$\sigma(h_s) = \sqrt{V/h_s^m}.$$

The largest value of h_s when the key relation (5.64) was still satisfied was denoted by h_{s+} . Value $\Delta\kappa = 0.39$, corresponding to $m = 3$, $n = 4$, $\kappa = 2$, is used (Table 5.2). The adaptive values $h_a = h_{s+}/2^{p_1}$, $p_1 = 0.59$ (Table 5.2), produced in this way, are connected with the optimal window line, by thin vertical lines in Fig. 5.1. The simulation is repeated for $\kappa = 3$ and $\kappa = 5$.

We can conclude that the presented algorithm almost always chooses the width h_s from set H , which is the nearest to the optimal one. However, for relatively small $\kappa = 2$, there are few complete misses of the optimal window width, since (5.59) is satisfied only with probability $P(2) = 0.95$. For $\kappa = 2$, two successive confidence intervals do not intersect when the bias is small, producing false result, with probability of $2(0.05)^2 \sim 10^{-2}$ order. The same experiment is repeated with the uniform noise, when $P(\kappa) = 1$ may be achieved without approximation, as well as with the Laplace impulsive noise, when a large κ is needed to achieve $P(\kappa) \rightarrow 1$. The results are presented in Fig. 5.1. \square

Example 5.5. Adaptive Smoothing of a Nonstationary Signal: Application of the adaptive algorithm on the smoothing of a nonstationary signal $f(t)$, corrupted by a zero mean stationary Gaussian additive noise $\varepsilon(t)$ of variance σ_ε^2 , will be presented here. Let us illustrate the presented algorithm on one specific, very simple example. Consider the estimation of $f(t)$ from

$$x(t) = f(t) + \varepsilon(t)$$

based on a simple smoothing

$$\hat{f}(t) = \frac{1}{h} \int_{-h/2}^{h/2} x(t+\tau) d\tau.$$

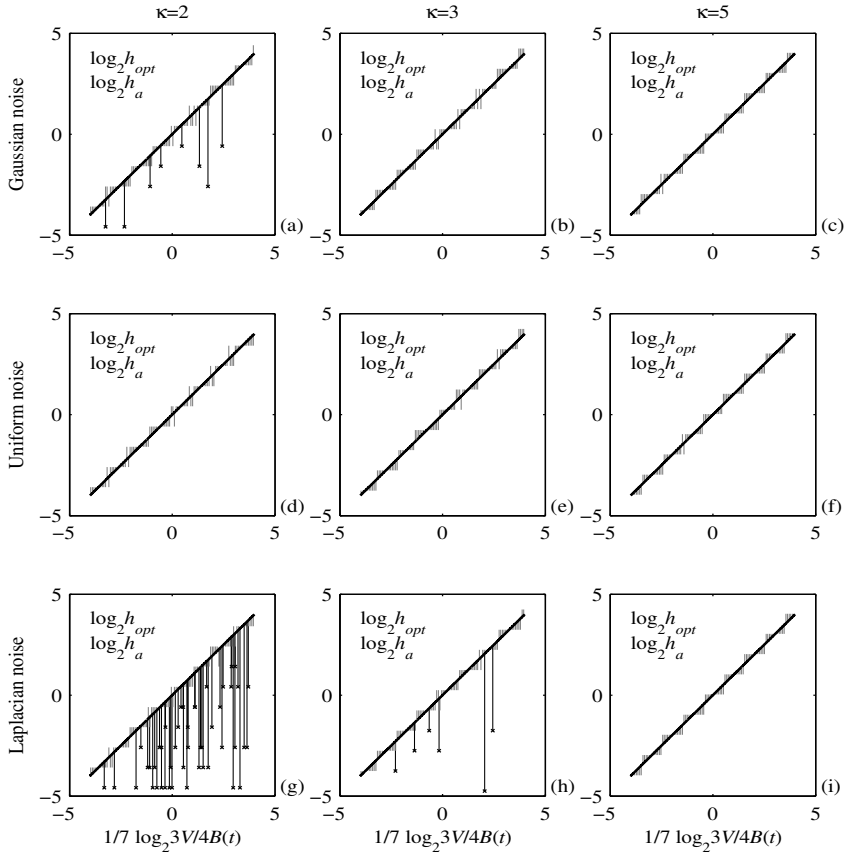


Figure 5.1 (a - i) Optimal window width (straight thick line), and adaptive window widths (end of vertical lines, starting from the optimal window width line) for $m = 3$, $n = 4$, $V = 1$. The variance-to-bias ratio $V/B(t)$ is logarithmically varied. The adaptive width $h_a = h_{s^+}/2^{p_1}$ is obtained from h_{s^+} , according to (5.64), after correction for the corresponding values of p_1 , given in Table 5.2. The Gaussian, uniform, and Laplacian noise are considered with $\kappa = 2, 3$, and 5.

Bias of this estimator is

$$\begin{aligned}\text{bias}(t, h) &= E\{\hat{f}(t)\} - f(t) \\ &= \frac{1}{h} \int_{-h/2}^{h/2} f(t + \tau) d\tau - f(t) \cong f''(t) \frac{h^2}{24},\end{aligned}$$

where the Taylor expansion

$$f(t + \tau) = f(t) + f'(t)\tau + f''(t)\tau^2/2 + \dots$$

is used.

The bias, given by the last equation, is only an approximation up to the second-order term. The bias increases as parameter h increases. However, the bias cannot increase infinitely as $h \rightarrow \infty$. In this example, it is obvious that there is a limit for the bias. The maximal possible bias is equal to the maximal possible difference in the signal, that is,

$$|\text{bias}(t, h)| \leq \max_{t_1, t_2} |x(t_1) - x(t_2)|.$$

We should be aware of this fact, especially in order to avoid using extremely large values for κ .

The variance of the estimator is

$$\sigma^2(h) = \frac{\sigma_\varepsilon^2}{h}.$$

Therefore, this case approximately corresponds to the described model, with $m = 1$ and $n = 4$.

For illustration, we will consider

$$f(t) = \frac{1}{1 + (t/7.5)^{40}} \quad (5.68)$$

within the interval $|t| < 25$, with the step $\Delta t = 1/25$. The nonnoisy signal is shown in Fig. 5.2(a), while the signal with additive Gaussian white noise, with standard deviation $\sigma_\varepsilon = 0.1$, is shown in Fig. 5.2(b). The noise standard deviation value σ_ε , needed for the algorithm, is estimated by using

$$\hat{\sigma}_\varepsilon = \frac{\text{median } |x(n) - x(n-1)|}{0.6745\sqrt{2}}. \quad (5.69)$$

In our case it resulted in $\hat{\sigma}_\varepsilon = 0.101$, what is very close to the original σ_ε value. Values of $a = 2$ and $\kappa = 2$ are used, while $\Delta\kappa = 0.86$ is taken from Table 5.2. Mean absolute errors (MAE) are: $MAE = 0.041$ for constant h with 129 smoothing points (Fig. 5.2(d)) $MAE = 0.047$ for constant h with three smoothing points, Fig. 5.2(f), and $MAE = 0.009$ for the adaptive parameter h (Fig. 5.2(e)). Note that in Fig. 5.2 the

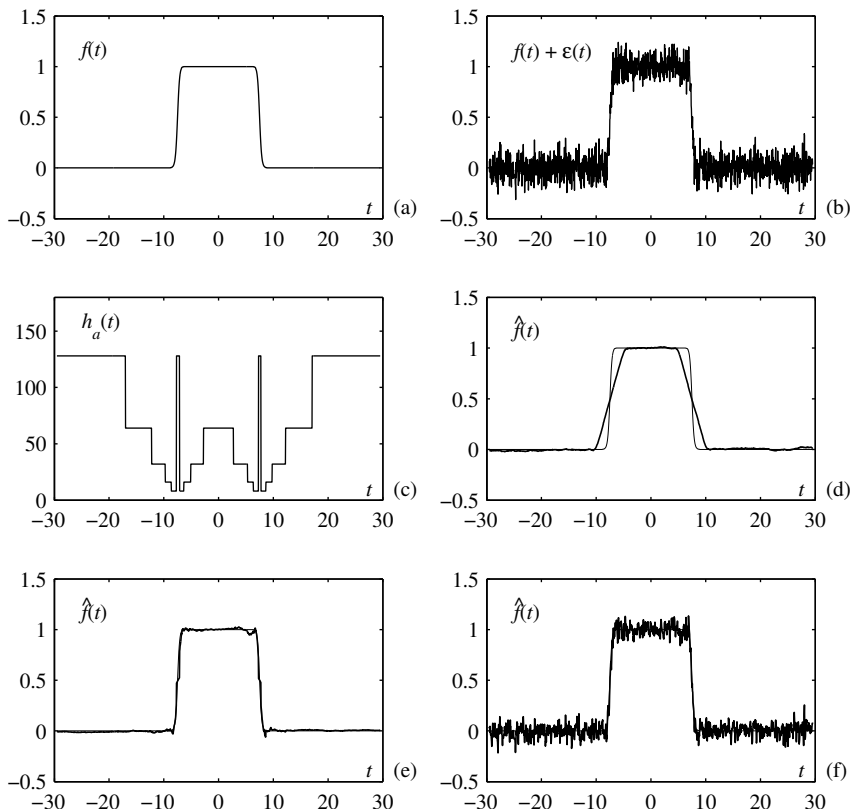


Figure 5.2 Illustration of noisy signal smoothing by using the considered algorithm: (a) original signal, (b) noisy signal, (c) adaptive parameter $h_a(t)$, (d) signal smoothed in a wide range with constant $2h(t) + 1 = 129$, (e) adaptive smoothed signal by using the widths $h_a(t)$ from (c), and (f) signal smoothed in a narrow range with constant $2h(t) + 1 = 3$.

total number of smoothing points is $2h(t) + 1$. In the adaptive algorithm the set of $h \in \{1, 2, 4, 8, 32, 64, 128, 256\}$ is used. For each instant t the smoothed value $\hat{f}(t)$ is calculated. Two subsequent estimates are compared according to (5.64), to find the best smoothing value h . \square

Example 5.6. Pseudo Wigner distribution-Based Instantaneous Frequency Estimation: In this example, a frequency-modulated signal, with the given instantaneous

frequency,

$$\Omega_i(n\Delta t) = 256 \arctan(250(n\Delta t - 0.5)) + 256\pi,$$

and the phase

$$\phi(n\Delta t) = \Delta t \sum_{m=0}^n \Omega_i(m\Delta t),$$

is considered. The signal amplitude was $A = 1$, and

$$20 \log(A/\sigma_\varepsilon) = 10 \text{ [dB]}$$

($A/\sigma_\varepsilon = 3.16$). Considered time interval was $0 \leq n\Delta t \leq 1$, with $\Delta t = 1/1024$. The instantaneous frequency is estimated by using the discrete Wigner distribution, with a rectangular lag-window, calculated with the standard DFT routines.

The algorithm is implemented as follows:

1. A set H of window widths h_s , corresponding to the following number of signal samples

$$N = \{4, 8, 16, 32, 64, 128, 256, 512\},$$

is assumed. In order to have the same number of frequency samples, as well as to reduce the quantization error, all windows are zero-padded up to the maximal window width.

2. For a given time instant $t = n\Delta t$, the pseudo Wigner distributions are calculated starting from the smallest toward the wider window widths h_s .
3. The instantaneous frequency is estimated using (5.24) and the pseudo Wigner distribution.
4. The confidence intervals intersection, (5.64), is checked for the estimated instantaneous frequency, $\hat{\Omega}_{h_s}(t)$, and

$$\sigma(h_s) = \sqrt{6\sigma_\varepsilon^2 \Delta t / (A^2 h_s^3)}$$

with, for example, $\kappa + \Delta\kappa = 6$, when $p_1 \cong 1$, and $P(\kappa) \rightarrow 1$ (see Table 5.2 and the comment that follows).

5. The adaptive window width $h_a = h_{s^+}/2$ is obtained from the last $h_s = h_{s^+}$ when (5.64) is still satisfied. Return to 2.

The estimation of the signal and noise parameters A and σ_ε^2 can be done by using

$$|\hat{A}|^2 + \hat{\sigma}_\varepsilon^2 = \frac{1}{N} \sum_{n=1}^N |x(n\Delta t)|^2.$$

The variance is estimated by

$$\hat{\sigma}_\varepsilon^2 = \hat{\sigma}_{\varepsilon r}^2 + \hat{\sigma}_{\varepsilon i}^2,$$

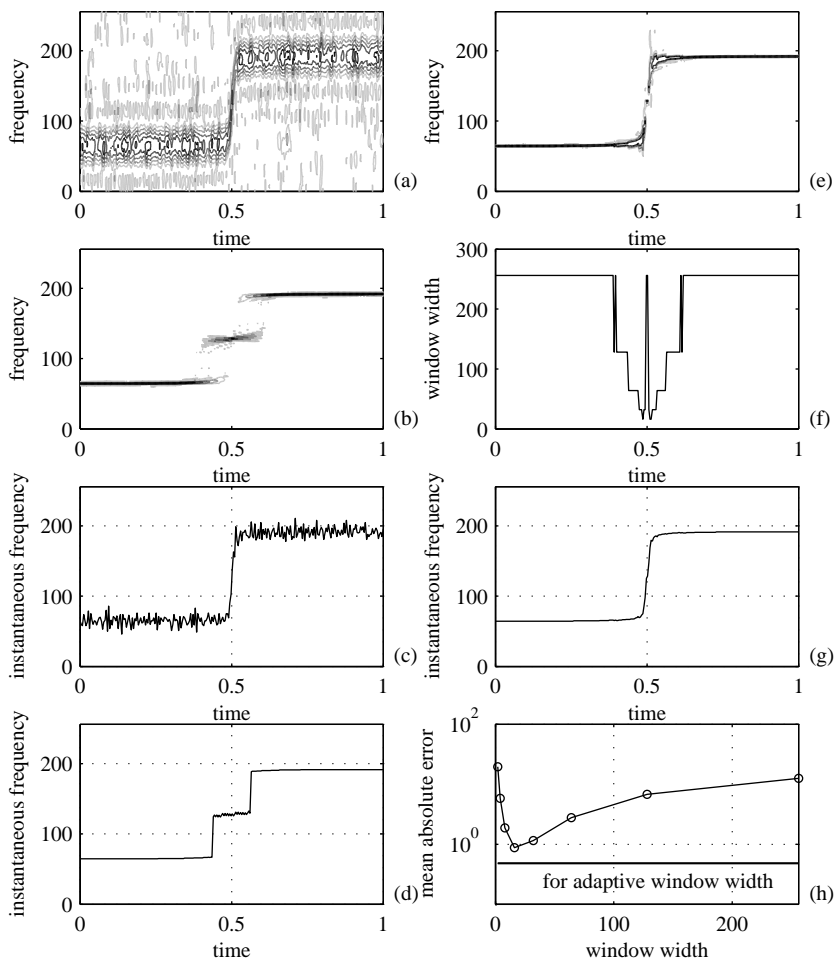


Figure 5.3 Time-frequency analysis of a noisy signal: (a) pseudo Wigner distribution with $N = 16$, (b) pseudo Wigner distribution with $N = 256$, (c) estimated instantaneous frequency using the pseudo Wigner distribution with $N = 16$, (d) estimated instantaneous frequency using the pseudo Wigner distribution with $N = 256$, (e) pseudo Wigner distribution with adaptive window width, (f) adaptive window width as a function of time, (g) estimated instantaneous frequency using the pseudo Wigner distribution with the adaptive window width, and (h) absolute mean error as a function of the window width. The horizontal line represents the mean absolute error value for the adaptive window width. The frequency $f = \Omega/2\pi$ is presented.

where

$$\hat{\sigma}_{\varepsilon r,i} = \frac{\operatorname{median}_{n=2,\dots,N}(|x_{r,i}(n\Delta t) - x_{r,i}((n-1)\Delta t)|)}{0.6745\sqrt{2}}, \quad (5.70)$$

with $x_r(n\Delta t)$ and $x_i(n\Delta t)$ being the real and imaginary parts of $x(n\Delta t)$. It is assumed that N is large, and Δt is small. For this estimation we oversampled the signal by a factor of four.

The pseudo Wigner distributions with constant window widths $N = 16$ and $N = 256$ are presented in Fig. 5.3(a), and Fig. 5.3(b), respectively. The instantaneous frequency estimates using the pseudo Wigner distributions with constant window widths $N = 16$, and $N = 256$ are given in Fig. 5.3(c) and Fig. 5.3(d). Fig. 5.3(e) shows the pseudo Wigner distribution with adaptive window width. Values of the adaptive window width, determined by the algorithm, are presented in Fig. 5.3(f). We can see that when the instantaneous frequency variations are small, the algorithm uses the widest window in order to reduce the variance. Around the point $n\Delta t = 0.5$, where the instantaneous frequency variations are fast, the windows with smaller widths are used. The instantaneous frequency estimate with adaptive window width is presented in Fig. 5.3(g). Mean absolute error, normalized to the discretization step, is shown in Fig. 5.3(h) for each considered window width. The horizontal line represents value of the mean absolute error for the adaptive window. \square

5.5 INFLUENCE OF HIGH NOISE ON THE INSTANTANEOUS FREQUENCY

We have seen that the instantaneous frequency estimation by using Wigner distribution (and other time-frequency representations) is based on the detection of the distribution maxima positions. The sources of estimation error that have been studied are: the bias and random deviation of the maxima within the auto-term, caused by the small noise (this noise can make some of the auto-term points surpass the value of true maximum at the instantaneous frequency), being represented by the estimation variance. In addition to these two kinds of errors, there are large random errors that could appear due to false maxima detection, far outside of the auto-term. It happens when the noise is so high that some of the distribution values outside the auto-term surpass the values inside the auto-term. This error can significantly degrade the estimation. Here we will focus on this type of error.

5.5.1 Estimation Error

Consider the discrete Wigner distribution

$$WD_x(n, k) = \sum_{m=-N/2}^{N/2-1} x(n+m)x^*(n-m)e^{-j4\pi mk/N} \quad (5.71)$$

of a frequency-modulated signal

$$x(n) = s(n) + \varepsilon(n) = Ae^{j\phi(n)} + \varepsilon(n),$$

corrupted by a Gaussian white complex noise $\varepsilon(n)$ with variance $\sigma_\varepsilon^2 = 2\sigma^2$. For a given instant n the instantaneous frequency ($\omega(n)$ or $\Omega(n\Delta t) = \omega(n)/\Delta t$) is estimated according to the Wigner distribution maximum position

$$\hat{k} = \arg\left\{\max_k WD_x(n, k)\right\}.$$

For the analysis of high noise influence, note that the Wigner distribution mean value is $WD_s(n, m) + 2\sigma^2$, while the variance, according to (5.18), is

$$\sigma_{WD}^2 = N\sigma_\varepsilon^2(2A^2 + \sigma_\varepsilon^2) = 4N\sigma^2(A^2 + \sigma^2).$$

The constant factor $2\sigma^2$ in the mean value will be omitted. Since there is a large number of terms in sum (5.71), we will assume that the central limit theorem may be applied to the Wigner distribution values. Thus, the Wigner distribution values are Gaussian in nature, with zero mean and standard deviation σ_{WD} , that is, $\mathcal{N}(0, \sigma_{WD})$, outside the auto-term, and with A_{WD} mean, $\mathcal{N}(A_{WD}, \sigma_{WD})$, within the auto-term. Here A_{WD} is the auto-term maximal value of a signal $s(n)$, for given n ,

$$A_{WD} = \max_k \{WD_s(n, k)\}.$$

The above assumption is statistically checked later in the example.

The probability density function (pdf) for the Wigner distribution values at the auto-term is then

$$p(\xi) = \frac{1}{\sqrt{2\pi}\sigma_{WD}} e^{-(\xi - A_{WD})^2/(2\sigma_{WD}^2)}, \quad (5.72)$$

while probability density function for the Wigner distribution values outside the auto-term is

$$q(\xi) = \frac{1}{\sqrt{2\pi}\sigma_{WD}} e^{-\xi^2/(2\sigma_{WD}^2)}.$$

The Wigner distribution outside the auto-term takes a value greater than Ξ , with probability

$$Q(\Xi) = \frac{1}{\sqrt{2\pi}\sigma_{WD}} \int_{\Xi}^{\infty} e^{-\xi^2/(2\sigma_{WD}^2)} d\xi = 0.5 \operatorname{erfc} \left(\frac{\Xi}{\sqrt{2}\sigma_{WD}} \right). \quad (5.73)$$

The probability that a Wigner distribution value outside the auto-term is lower than Ξ is $[1 - Q(\Xi)]$. The probability that M independent Wigner distribution values outside the auto-term are lower than Ξ is $[1 - Q(\Xi)]^M$. Probability that at least one of M Wigner distribution values outside the auto-terms is greater than Ξ , is

$$G(\Xi) = 1 - [1 - Q(\Xi)]^M. \quad (5.74)$$

When a Wigner distribution value outside the auto-term surpasses the value within auto-term, then a large instantaneous frequency estimation error occurs. To calculate this probability, consider the auto-term value at and around ξ . The auto-term value is within ξ and $\xi + d\xi$ with probability $p(\xi)d\xi$, where $p(\xi)$ is defined by (5.72). The probability that at least one of M Wigner distribution values outside auto-terms is above ξ is $G(\xi) = 1 - [1 - Q(\xi)]^M$. Thus, the probability that the auto-term value is within ξ and $\xi + d\xi$ and that, at the same time, at least one of the Wigner distribution values outside the auto-term exceeds the auto-term value is

$$G(\xi)p(\xi)d\xi.$$

Considering all possible values of ξ , from (5.72) and (5.74), follows that the probability of high estimation error

$$P_E = \int_{-\infty}^{\infty} G(\xi)p(\xi)d\xi. \quad (5.75)$$

When this error occurs, then the estimated instantaneous frequency can be any value from the whole frequency interval. This error is then of an impulsive nature, and its values are uniformly distributed over the entire frequency interval.

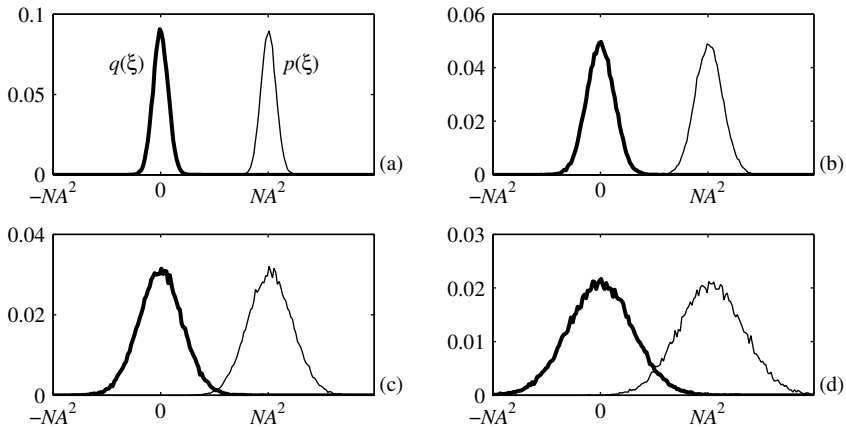


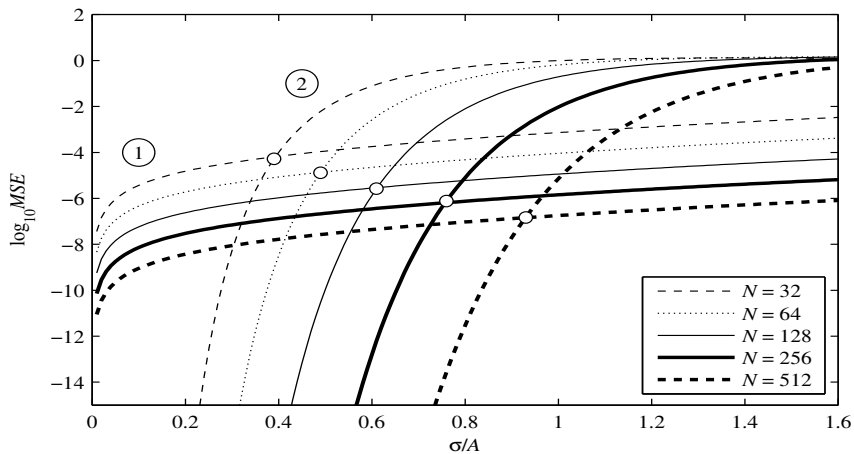
Figure 5.4 Histograms of the Wigner distribution values for: (a) $\sigma/A = 0.5$, (b) $\sigma/A = 0.8$, (c) $\sigma/A = 1.1$, and (d) $\sigma/A = 1.4$. Thin lines: histograms of the Wigner distribution values along the instantaneous frequency; thick lines: histograms of the Wigner distribution values outside the auto-term.

Relation (5.75) is illustrated with linear frequency-modulated signal $s(n) = A \exp(jan^2/2)$. In order to avoid the discretization error, the value of a is chosen so that the exact instantaneous frequency lies along the frequency grid. This a and large N in (5.71) produce highly concentrated auto-term and eliminate, for this signal, the errors within the auto-term. Then $A_{WD} = NA^2$, and $M = N - 1$. In this way the only remaining error is due to false auto-term position detection. The histograms of the Wigner distribution values along the instantaneous frequency, $p(\xi)$, and outside the auto-term, $q(\xi)$, are presented in Fig. 5.4, for various σ/A . These histograms are compared with the corresponding Gaussian probability density functions. The agreement is extremely high. For small noise, the histograms are well separated, meaning that there will be no false detection of maxima. The instantaneous frequency estimation will be reliable. However, for higher noise values, the histograms intersect, meaning that there is a significant probability of false maxima position detection. The expected and obtained numbers of false detections (in total number of 5120 random realizations, according to (5.75)), for various σ/A and $N = 256$, are given in Table 5.3.

Table 5.3

Expected and Obtained Numbers of False Detections in 5120 Realizations.

σ/A	P_E	<i>Expected</i>	<i>Obtained</i>
0.2	7.4793e-224	0	0
0.4	2.8395e-038	0	0
0.6	7.9544e-014	0	0
0.8	3.9741e-006	0	0
1.0	4.7100e-003	24	21
1.2	9.0217e-002	469	451
1.4	3.2033e-001	1640	1674
1.6	5.6288e-001	2882	2907

**Figure 5.5** MSE of instantaneous frequency estimation for various N : 1-MSE caused by the small variations of maxima within the auto-term, and 2-MSE caused by false maxima detection.

Approximation of P_E : For well-separated histograms (i.e., for small σ/A) according to (5.74), we can write

$$G(\xi)p(\xi) \approx MQ(\xi)p(\xi).$$

Then it is easy to derive that

$$P_E \approx \frac{M}{2\pi\sigma_{WD}^2} \int_{-\infty}^{\infty} \int_x^{\infty} e^{-y^2/2\sigma_{WD}^2} e^{-(x-A_{WD})^2/2\sigma_{WD}^2} dx dy = \frac{M}{2} \operatorname{erfc}\left(\frac{A_{WD}}{2\sigma_{WD}}\right). \quad (5.76)$$

Thus, the relevant parameter for this error is the maximal auto-term to distribution standard deviation ratio.

5.5.2 Mean Square Error

For the Wigner distribution with N samples along the frequency axis, the true instantaneous frequency value $\hat{\omega}(n) = \omega(n)$ is obtained with probability $1 - P_E$, while other (false) values are detected with probability $P_E/(N-1)$. Considering the frequencies $\omega_k = k\pi/N$, $-N/2 \leq k < N/2$, the mean estimation error for a large number of samples N is

$$\mathbb{E}\{\Delta\hat{\omega}(n)\} \approx P_E \omega(n). \quad (5.77)$$

The error depends on $\omega(n)$. It is smallest for the instantaneous frequency at the middle point $\omega(n) = 0$. Then the error is uniformly distributed from the minimal ($\omega_{\min} = -\pi/2$ in the Wigner distribution) to the maximal frequency value ($\omega_{\max} = \pi/2$). The variance of uniformly distributed random variable from $-\pi/2$ to $\pi/2$ is $\pi^2/12$. Therefore,

$$\mathbb{E}\{\Delta\hat{\omega}^2(n)\} \approx P_E \pi^2/12.$$

The largest MSE,

$$\mathbb{E}\{\Delta\hat{\omega}^2(n)\} \approx P_E \pi^2/3, \quad (5.78)$$

is obtained for $\omega(n) = \pm\pi/2$ when the error is uniformly distributed from 0 to π , or from $-\pi$ to 0. The mean value of the MSE is of order $e_m \approx 2P_E$.

To compare this kind of error with the error due to the small instantaneous frequency deviations within the auto-term, recall that its MSE is ((5.52) for rectangular window)

$$e_s = \frac{12\sigma^2}{A^2 N^3} \left(1 + \frac{\sigma^2}{A^2}\right).$$

This kind of error is always present when the auto-term is not completely concentrated at a single point along the frequency axis. The values of e_m and e_s for various N are presented in Fig. 5.5. The errors are of different orders of magnitude, before and after their intersection point. Thus, in each region, only one of them could be considered as dominant.

The increase in the estimation variance is well known for all quadratic and higher-order representations, as compared to the linear ones. This effect is especially exhibited in high noise cases. In lower noise cases, the analysis is more focused on correct unbiased representations, when quadratic (or higher-order) representations are superior. In order to illustrate this effect and to indicate a way for its reduction, we will present an example.

Example 5.7. Consider a simplified case of a sinusoidal signal $s(n) = A \exp(j2\pi k_0 n/N)$ and a disturbance of the same form at frequency k_1 with amplitude E_1 . What is the condition for correct frequency estimate, based on

$$\hat{k}_0 = \arg \left\{ \max_k |X(k)| \right\},$$

where $X(k)$ is the DFT of noisy signal $s(n) + \varepsilon(n)$? What is the condition if the DFT of squared signal value is used in the estimation?

★The DFT of this signal is

$$X(k) = AN\delta(k - k_0) + E_1 N\delta(k - k_1),$$

where $E_1 N\delta(k - k_1)$ is the disturbing term. The correct estimate of frequency $\hat{k}_0 = \arg \left\{ \max_k |X(k)| \right\}$ is when the disturbing term is lower than the desired signal, that is, when

$$A > E_1.$$

Now consider a case corresponding to a quadratic distribution, requiring the squared value of $x(n)$. Let us simplify again and consider the DFT of $x^2(n)$. Then its DFT is

$$X(k) *_k X(k) = A^2 N^2 \delta(k - 2k_0) + E_1^2 N^2 \delta(k - 2k_1) + 2AE_1 N^2 \delta(k - k_0 - k_1).$$

It is clear that if $A > E_1$ then $A^2 > E_1^2$, that is, the first two terms in $X(k) *_k X(k)$, representing the auto-terms of signal and disturbing term in convolution, will not influence the estimation precision, at all. However, the cross-term $2AE_1 N^2 \delta(k - k_0 - k_1)$ is introduced as well. For the correct estimation, here we must have

$$A > 2E_1. \quad (5.79)$$

Thus, the estimation condition is worsened two times. It corresponds to the well-known 6 dB worsening with each higher-order degree, in the case of constant frequency signals. In the case of signals with varying frequency, this effect is partly compensated by increase in signal concentration, using higher-order representations. Anyway, the results will be improved if we can remove or reduce cross-terms, as much as possible (in an ideal case to get *modified* $\{X(k) *_k X(k)\} = A^2 \delta(k - 2k_0) + E_1^2 \delta(k - 2k_1)$) and to obtain the estimation quality as high as if we did not use quadratic distributions, at the same time keeping the property of significant improvement with respect to the bias.

□

If the quadratic distributions, including the idea presented in the previous example, cannot produce satisfactory results in a high noise case then, it is recommended to return to a linear signal transform. The optimal case would be if the signal form were known. Then we could project the noisy signal onto a set of basis functions containing the signal proportional to the one of the basis functions. In many cases, we can assume that the signal phase is polynomial, at least within local intervals. Then the estimate based on the LPFT,

$$\omega(n) = \arg \left\{ \max_{\omega, a_2, \dots, a_K} \left| \sum_{m=-\infty}^{\infty} w(m)x(n+m)e^{-j(\omega m + a_2 m^2/2 + \dots + a_K m^K / K!)} \right| \right\}$$

should produce results without increasing the signal and noise order. Here a multidimensional minimization over additional parameters a_2, a_3, \dots, a_K is required. These parameters may be time-dependent as well. A combination of the nonparametric STFT-based initial estimation (with a possibly time-varying window, corresponding to time variations of the parameters) and the parametric LPFT estimation (on a signal demodulated by the initial estimate) is an efficient way to proceed in this case.

5.6 NOISE IN QUADRATIC TIME-FREQUENCY DISTRIBUTIONS

Now we will extend the analysis of noise influence to the general form of shift covariant time-frequency distributions, including more general forms of the noise. A discrete-time form of the Cohen class of distributions in the time-lag domain is used as the starting point for this analysis. First, consider a distribution in the time-frequency plane of noise $\varepsilon(n)$ only

$$CD_\varepsilon(n, \omega) = \sum_{l=-\infty}^{\infty} \sum_{m=-\infty}^{\infty} c_T(m, l) \varepsilon(n+m+l) \varepsilon^*(n+m-l) e^{-j2\omega l}, \quad (5.80)$$

where $c_T(m, l)$ is the kernel in the discrete time-lag domain.

The mean value of a distribution from the Cohen class, for a general nonstationary noise, is

$$E\{CD_\varepsilon(n, \omega)\} = \sum_{l=-\infty}^{\infty} \sum_{m=-\infty}^{\infty} c_T(m, l) R_{\varepsilon\varepsilon}(n+m+l, n+m-l) e^{-j2\omega l},$$

where $R_{\varepsilon\varepsilon}(m, n)$ is the noise auto-correlation function. For special cases of noise, the values of $E\{CD_\varepsilon(n, \omega)\}$ follow:

1.) Stationary white noise, $R_{\varepsilon\varepsilon}(m, n) = \sigma_\varepsilon^2 \delta(m - n)$,

$$\mathbb{E}\{CD_\varepsilon(n, \omega)\} = \sigma_\varepsilon^2 \sum_{m=-\infty}^{\infty} c_T(m, 0) = \sigma_\varepsilon^2 c(0, 0). \quad (5.81)$$

2.) Nonstationary white noise, $R_{\varepsilon\varepsilon}(m, n) = I(n) \delta(m - n)$, $I(n) \geq 0$,

$$\mathbb{E}\{CD_\varepsilon(n, \omega)\} = \sum_{m=-\infty}^{\infty} c_T(m, 0) I(n + m). \quad (5.82)$$

3.) Stationary colored noise, $R_{\varepsilon\varepsilon}(m, n) = R_{\varepsilon\varepsilon}(m - n)$,

$$\mathbb{E}\{CD_\varepsilon(n, \omega)\} = \int_{-\pi}^{\pi} C_\Omega(0, 2(\omega - \alpha)) S_{\varepsilon\varepsilon}(\alpha) d\alpha, \quad (5.83)$$

where

$$S_{\varepsilon\varepsilon}(\omega) = \text{FT}\{R_{\varepsilon\varepsilon}(m)\}$$

is the noise power spectrum density, and the kernel forms in the time-lag $c_T(m, l)$, Doppler-lag $c(v, l)$, and Doppler-frequency $C_\Omega(v, \omega)$ domains are related as

$$\sum_{m=-\infty}^{\infty} c_T(m, l) e^{-j2\theta m} = c(\theta, l) = \frac{1}{2\pi} \int_{-\pi}^{\pi} C_\Omega(\theta, \omega) e^{j\omega l} d\omega.$$

The variance of $CD_\varepsilon(n, \omega)$ is defined by

$$\sigma_{\varepsilon\varepsilon}^2(n, \omega) = \mathbb{E}\{CD_\varepsilon(n, \omega) CD_\varepsilon^*(n, \omega)\} - \mathbb{E}\{CD_\varepsilon(n, \omega)\} \mathbb{E}\{CD_\varepsilon^*(n, \omega)\}.$$

For Gaussian noise, as in (5.14) and (5.15), we get

$$\begin{aligned} \sigma_{\varepsilon\varepsilon}^2(n, \omega) &= \sum_{l_1=-\infty}^{\infty} \sum_{l_2=-\infty}^{\infty} \sum_{m_1=-\infty}^{\infty} \sum_{m_2=-\infty}^{\infty} c_T(m_1, l_1) c_T^*(m_2, l_2) \\ &\times [R_{\varepsilon\varepsilon}(n + m_1 + l_1, n + m_2 + l_2) R_{\varepsilon\varepsilon}^*(n + m_1 - l_1, n + m_2 - l_2) \\ &+ R_{\varepsilon\varepsilon}^*(n + m_1 + l_1, n + m_2 - l_2) R_{\varepsilon\varepsilon}(n + m_1 - l_1, n + m_2 + l_2)] e^{-j2\omega(l_1 - l_2)}. \end{aligned} \quad (5.84)$$

The form of $\sigma_{\varepsilon\varepsilon}^2(n, \omega)$ for specific noises will be presented next.

5.6.1 Complex Stationary and Nonstationary White Noise

For nonstationary complex white noise, with independent real and imaginary parts of equal variance, the auto-correlation is of the form

$$\begin{aligned} R_{\epsilon\epsilon}(m, n) &= I(n)\delta(m - n), \\ R_{\epsilon\epsilon^*}(n, m) &= 0, \end{aligned}$$

producing

$$\begin{aligned} \sigma_{\epsilon\epsilon}^2(n, \omega) &= \sum_{l=-\infty}^{\infty} \sum_{m=-\infty}^{\infty} |c_T(m, l)|^2 I(n+m+l) I^*(n+m-l) \\ &= CD_I(n, 0; |c_T|^2) \end{aligned} \quad (5.85)$$

where $CD_I(n, \omega; |c_T|^2)$ stands for the Cohen-class distribution of $I(n)$ calculated with the time-lag kernel $|c_T(m, l)|^2$.

For stationary white noise, $I(n) = \sigma_{\epsilon}^2$, the variance is proportional to the kernel energy,

$$\sigma_{\epsilon\epsilon}^2(n, \omega) = \sigma_{\epsilon}^4 \sum_{l=-\infty}^{\infty} \sum_{m=-\infty}^{\infty} |c_T(m, l)|^2. \quad (5.86)$$

It is constant over time and frequency.

5.6.2 Colored Stationary Noise

For complex colored stationary noise, with spectral density $S_{\epsilon\epsilon}(\omega) = \text{FT}\{R_{\epsilon\epsilon}(m)\}$, the variance (5.84) can be rewritten as

$$\begin{aligned} \sigma_{\epsilon\epsilon}^2(n, \omega) &= \sum_{l_1=-\infty}^{\infty} \sum_{m_1=-\infty}^{\infty} c_T(m_1, l_1) \sum_{l_2=-\infty}^{\infty} \sum_{m_2=-\infty}^{\infty} c_T^*(m_2, l_2) \\ &\times [R_{\epsilon\epsilon}(m_1 - m_2 + l_1 - l_2) R_{\epsilon\epsilon}^*(m_1 - m_2 - (l_1 - l_2))] e^{-j2\omega(l_1 - l_2)}, \end{aligned}$$

or

$$\sigma_{\epsilon\epsilon}^2(n, \omega) = \sum_{l=-\infty}^{\infty} \sum_{m=-\infty}^{\infty} c_T(m, l) \left\{ c_T(m, l) *_{(l, m)} [R_{\epsilon\epsilon}^*(m+l) R_{\epsilon\epsilon}(m-l) e^{j2\omega l}] \right\}^*,$$

where “ $*_{(l,m)}$ ” denotes a two-dimensional convolution in l, m . Consider the product of $c_T(m, l)$ and the function

$$Y^*(m, l) = \left\{ c_T(m, l) *_{(l,m)} [R_{\varepsilon\varepsilon}^*(m+l) R_{\varepsilon\varepsilon}(m-l) e^{j2\omega l}] \right\}^*.$$

Two-dimensional Fourier transforms of these two terms are

$$C_\Omega(\theta, \xi) = \text{FT}\{c_T(m, l)\}$$

and

$$\begin{aligned} y(\theta, \xi) &= \text{FT} \left\{ c_T(m, l) *_{(l,m)} [R_{\varepsilon\varepsilon}^*(m+l) R_{\varepsilon\varepsilon}(m-l) e^{j2\omega l}] \right\} \\ &= \text{FT}\{c_T(m, l)\} \times \text{FT}\left\{ R_{\varepsilon\varepsilon}^*(m+l) R_{\varepsilon\varepsilon}(m-l) e^{j2\omega l} \right\} \\ &= \frac{1}{2} C_\Omega(\theta, \xi) S_{\varepsilon\varepsilon} \left(\omega - \frac{\xi - \theta}{2} \right) S_{\varepsilon\varepsilon}^* \left(\omega - \frac{\xi + \theta}{2} \right). \end{aligned}$$

According to Parseval's theorem, we get

$$\begin{aligned} \sigma_{\varepsilon\varepsilon}^2(n, \omega) &= \frac{1}{8\pi^2} \int_{-\pi}^{\pi} \int_{-\pi}^{\pi} |C_\Omega(\theta, \xi)|^2 S_{\varepsilon\varepsilon}^* \left(\omega - \frac{\xi - \theta}{2} \right) S_{\varepsilon\varepsilon} \left(\omega - \frac{\xi + \theta}{2} \right) d\theta d\xi \\ &= CD_{S_{\varepsilon\varepsilon}}(0, \omega; |C_\Omega|^2), \end{aligned} \quad (5.87)$$

where $CD_{S_{\varepsilon\varepsilon}}(0, \omega; |C_\Omega|^2)$ denotes the Cohen class distribution of $S_{\varepsilon\varepsilon}(\omega)$ calculated at $n = 0$ with the squared absolute frequency-Doppler kernel $C_\Omega(\omega, \theta)$.

Note that the Fourier transform of a colored stationary noise is a white nonstationary noise, with auto-correlation in the frequency domain

$$\begin{aligned} R_{\Xi\Xi}(\omega_1, \omega_2) &= \sum_{m=-\infty}^{\infty} \sum_{n=-\infty}^{\infty} \text{E}\{\varepsilon(m) \varepsilon^*(n)\} e^{-j\omega_1 m + j\omega_2 n} \\ &= S_{\varepsilon\varepsilon}(\omega_2) \delta_p(\omega_1 - \omega_2), \end{aligned}$$

where $\delta_p(\omega)$ is a periodic delta function with period 2π . Thus, (5.87) is just a form dual to (5.85).

5.6.3 Analytic Noise

In the numerical implementation of quadratic distributions, an analytic part of the signal is commonly used, rather than the signal itself. The analytic part of noise can be written as

$$\varepsilon_a(n) = \varepsilon(n) + j\varepsilon_h(n),$$

where $\varepsilon_h(n)$ is the Hilbert transform of $\varepsilon(n)$. The spectral power density of $\varepsilon_a(n)$, within the basic period $|\omega| < \pi$, for the white noise $\varepsilon(n)$, is

$$S_{\varepsilon_a \varepsilon_a}(\omega) = 2\sigma_\varepsilon^2 u(\omega),$$

where $u(\omega)$ is the unit step function (in discrete-time case signal spectrum is periodic with 2π). The variance follows from (5.87) in the form

$$\sigma_{\varepsilon \varepsilon}^2(n, \omega) = 2\sigma_\varepsilon^4 \frac{1}{4\pi^2} \int_{-\pi}^{\pi} \int_{-d(\omega, \xi)}^{d(\omega, \xi)} |C_\Omega(\theta, \xi)|^2 d\xi d\theta \quad (5.88)$$

for $|\omega| \leq \pi$, where the integration limits are periodic and defined by

$$d(\omega, \xi) = 2 |\arcsin(\sin((\omega - \xi)))|.$$

The kernel $C_\Omega(\theta, \xi)$ is mainly concentrated at and around the (θ, ξ) origin and the $\xi = 0$ axis. Having this in mind, as well as the fact that $|C_\Omega(\theta, \xi)|^2$ is always positive, we may easily conclude that the minimal value of $\sigma_{\varepsilon \varepsilon}^2(n, \omega)$ is for $\omega = 0$. The maximal value will be obtained for $|\omega| = \pi/2$. It is very close to

$$\begin{aligned} \max\{\sigma_{\varepsilon \varepsilon}^2(n, \omega)\} &\cong \sigma_\varepsilon^4 \frac{1}{2\pi^2} \int_{-\pi}^{\pi} \int_{-\pi}^{\pi} |C_\Omega(\theta, \xi)|^2 d\xi d\theta \\ &= 2\sigma_\varepsilon^4 \sum_{l=-\infty}^{\infty} \sum_{m=-\infty}^{\infty} |c_T(m, l)|^2. \end{aligned} \quad (5.89)$$

5.6.4 Real-Valued Noise

Now consider a real-valued stationary white Gaussian noise $\varepsilon(n)$ with variance σ_ε^2 . In this case, variance (5.84) contains all terms. It can be written as

$$\sigma_{\varepsilon \varepsilon}^2(n, \omega) = \sigma_\varepsilon^4 \sum_{l=-\infty}^{\infty} \sum_{m=-\infty}^{\infty} [|c_T(m, l)|^2 + c_T(m, l)c_T^*(m, -l)e^{-j4\omega l}]. \quad (5.90)$$

For distributions whose kernel is symmetric with respect to lag l , relation

$$c_T(m, l) = c_T(m, -l)$$

holds. The Fourier transform is therefore applied to the positive and even function $|c_T(m, l)|^2$. The transform's maximal value is reached at $\omega = 0$, and $|\omega| = \pi/2$. Accordingly,

$$\max \{ \sigma_{\epsilon\epsilon}^2(n, \omega) \} = 2\sigma_\epsilon^4 \sum_{l=-\infty}^{\infty} \sum_{m=-\infty}^{\infty} |c_T(m, l)|^2. \quad (5.91)$$

The crucial parameter in all previous cases is the kernel energy

$$E_C = \sum_{l=-\infty}^{\infty} \sum_{m=-\infty}^{\infty} |c_T(m, l)|^2. \quad (5.92)$$

Its minimization is studied in literature by Amin et al. It was concluded that, out of all the quadratic distributions satisfying the marginal and time-support conditions, the Born-Jordan distribution is optimal with respect to this parameter.

5.6.5 Noisy Signals

Analysis of deterministic signals $s(n)$ corrupted by noise,

$$x(n) = s(n) + \epsilon(n),$$

is highly signal dependent. It can be easily shown that the distribution variance $\sigma_{CD}^2(n, \omega)$ consists of two components

$$\sigma_{CD}^2(n, \omega) = \sigma_{\epsilon\epsilon}^2(n, \omega) + \sigma_{s\epsilon}^2(n, \omega). \quad (5.93)$$

The first variance component and the distribution mean value have already been studied in detail. For the analysis of the second signal-dependent component $\sigma_{s\epsilon}^2(n, \omega)$, we will use the inner product form of the Cohen class of distributions

$$CD_x(n, \omega; \tilde{c}_T) = \sum_{l=-\infty}^{\infty} \sum_{m=-\infty}^{\infty} \tilde{c}_T(m, l) [x(n+m)e^{-j\omega m}] \left[x(n+l)e^{-j\omega l} \right]^*, \quad (5.94)$$

where

$$\tilde{c}_T(m, l) = c_T((m+l)/2, (m-l)/2).$$

In the Cohen class notation, the kernel function \tilde{c}_T , in this domain, has been added. For a real and symmetric $c_T(m, l)$, and complex noise, we get

$$\begin{aligned}\sigma_{s\epsilon}^2(n, \omega) &= 2 \sum_{l_1=-\infty}^{\infty} \sum_{m_1=-\infty}^{\infty} \sum_{l_2=-\infty}^{\infty} \sum_{m_2=-\infty}^{\infty} \tilde{c}_T(m_1, l_1) \tilde{c}_T^*(m_2, l_2) s(n+m_1) \\ &\quad \times s^*(n+m_2) R_{\epsilon\epsilon}(n+l_2, n+l_1) e^{-j\omega(m_1-l_1-m_2+l_2)},\end{aligned}$$

which can be written as

$$\begin{aligned}\sigma_{s\epsilon}^2(n, \omega) &= 2 \sum_{m_1=-\infty}^{\infty} \sum_{m_2=-\infty}^{\infty} \tilde{\Phi}(m_1, m_2) \\ &\quad \times [s(n+m_1) e^{-j\omega m_1}] [s(n+m_2) e^{-j\omega m_2}]^*,\end{aligned}\tag{5.95}$$

where the new kernel $\tilde{\Phi}(m_1, m_2)$ is given by

$$\begin{aligned}\tilde{\Phi}(m_1, m_2) &= \sum_{l_1=-\infty}^{\infty} \sum_{l_2=-\infty}^{\infty} \tilde{c}_T(m_1, l_1) \tilde{c}_T^*(m_2, l_2) \\ &\quad \times e^{-j\omega(l_2-l_1)} R_{\epsilon\epsilon}(n+l_2, n+l_1).\end{aligned}\tag{5.96}$$

In general, this kernel is also time-frequency-dependent.

The signal-dependent part of the variance $\sigma_{s\epsilon}^2(n, \omega)$ is a quadratic distribution of the signal, with the new kernel $\tilde{\Phi}(m_1, m_2)$ in the inner product form, that is,

$$\sigma_{s\epsilon}^2(n, \omega) = 2CD_s(n, \omega; \tilde{\Phi}).$$

Now several special cases of noise will be presented in the sense of (5.96).

5.6.5.1 White Stationary Complex Noise

For this kind of noise, with independent, identically distributed real and imaginary parts, the auto-correlation function is

$$R_{\epsilon\epsilon}(n+l_2, n+l_1) = \sigma_{\epsilon}^2 \delta(l_2 - l_1).$$

It produces

$$\tilde{\Phi}(m_1, m_2) = \sigma_{\epsilon}^2 \sum_{l=-\infty}^{\infty} \tilde{c}_T(m_1, l) \tilde{c}_T^*(m_2, l).\tag{5.97}$$

We assume realness and symmetry of the kernel, that is, $\tilde{c}_T^*(m_2, l) = \tilde{c}_T(l, m_2)$. Thus, for finite limits, relation (5.97) takes a matrix multiplication form,

$$\tilde{\Phi} = \sigma_\varepsilon^2 \tilde{\mathbf{c}}_T \cdot \tilde{\mathbf{c}}_T^* = \sigma_\varepsilon^2 \tilde{\mathbf{c}}_T^2.$$

Boldface letters, without arguments, are used to denote a matrices. For example, $\tilde{\mathbf{c}}_T$ is a matrix with elements $\tilde{c}_T(m, l)$. Thus,

$$\sigma_{se}^2(n, \omega) = 2CD_s(n, \omega; \sigma_\varepsilon^2 \tilde{\mathbf{c}}_T^2). \quad (5.98)$$

Example 5.8. Show that any two distributions with kernels $\tilde{c}_{T1}(m, l) = \tilde{c}_{T2}(m, -l)$ have the same variance.

★ It follows from

$$\begin{aligned} \sum_{l=-\infty}^{\infty} \tilde{c}_{T1}(m_1, l) \tilde{c}_{T1}^*(m_2, l) &= \sum_{l=-\infty}^{\infty} \tilde{c}_{T2}(m_1, -l) \tilde{c}_{T2}^*(m_2, -l) \\ &= \sum_{l=-\infty}^{\infty} \tilde{c}_{T1}(m_1, l) \tilde{c}_{T1}^*(m_2, l). \end{aligned}$$

□

Example 5.9. Show that a distribution with real and symmetric product kernel $c(\theta\tau)$ and the distribution with its dual kernel,

$$c_d(\theta\tau) = \text{FT}_{\alpha,\beta}^{2D} \{c(\alpha\beta)\}$$

have the same variance.

★ Consider all coordinates in the analog domain. The time-lag domain forms of $c(\theta\tau)$,

$$c_T(t, \tau) = \text{FT}_V \{c(\theta\tau)\},$$

and

$$c_{Td}(t, \tau) = \text{FT}_\theta \{c_d(\theta\tau)\}$$

are related by

$$c_T(t, \tau) = c_{Td}(\tau, t).$$

In the rotated domain this relation produces

$$\tilde{c}_T(t_1, t_2) = \tilde{c}_{Td}(t_1, -t_2),$$

which ends the proof, according to the previous example. □

Example 5.10. The Wigner distribution has the kernel

$$\begin{aligned} c(\theta\tau) &= 1, \\ \tilde{c}_T(m, l) &= \delta(m + l). \end{aligned}$$

According to the previous example, the Wigner distribution has the same variance as its dual kernel counterpart, with

$$\begin{aligned} c(\theta\tau) &= \delta(\theta)\delta(\tau), \\ \tilde{c}_T(m, l) &= \delta(m - l). \end{aligned} \tag{5.99}$$

This dual kernel corresponds to the signal energy

$$E_x = \sum_{m=-\infty}^{\infty} |x(n+m)|^2$$

(see (5.94)). Thus, the Wigner distribution and the signal energy have the same variance. \square

Example 5.11. The smoothed spectrogram and the S-method, whose kernels are

$$\tilde{c}_T(m, l) = w(m)p(m+l)w(l),$$

and

$$\tilde{c}_T(m, l) = w(m)p(m-l)w(l),$$

respectively, have the same variance, for symmetric lag windows. This conclusion follows directly from the fact that any two distributions with kernels

$$\tilde{c}_{T1}(m, l) = \tilde{c}_{T2}(m, -l)$$

have the same variance. \square

Eigenvalue decomposition: Assume that both the summation limits and values of $\tilde{c}_T(m, l)$ are finite. It is true when the kernel $c_T(m, l)$ is calculated from the well defined kernel in a finite Doppler-lag domain,

$$c_T(m, l) = \text{FT}_\theta \{c(\theta, l)\},$$

using a finite number of samples. The signal-dependent part of the variance $\sigma_{se}^2(n, \omega)$ can be calculated, like other distributions from the Cohen class, by using the eigenvalue decomposition of matrix $\tilde{\mathbf{c}}_T$, described in Chapter 3. The distribution

of a nonnoisy signal (5.94) is

$$CD_s(n, \omega) = \sum_{i=1}^N \lambda_i |STFT_s(n, \omega; q_i)|^2 = CD_s(n, \omega; [\lambda, q]), \quad (5.100)$$

where λ_i and $q_i(m)$ are eigenvalues and eigenvectors of the matrix $\tilde{\mathbf{c}}_T$, respectively, and

$$STFT_s(n, \omega; q_i) = \sum_{m=-N/2}^{N/2-1} s(n+m) q_i(m) e^{-j\omega m}$$

is the STFT of signal $s(n)$ calculated by using $q_i(m)$ as a lag window. Since

$$\tilde{\Phi} = \sigma_\varepsilon^2 \tilde{\mathbf{c}}_T^2,$$

its eigenvalues and eigenvectors are $\sigma_\varepsilon^2 |\lambda_i|^2$ and $q_i(m)$, respectively. Thus, according to (5.98),

$$\begin{aligned} \sigma_{se}^2(n, \omega) &= 2\sigma_\varepsilon^2 \sum_{i=1}^N |\lambda_i|^2 |STFT_s(n, \omega; q_i)|^2 \\ &= 2\sigma_\varepsilon^2 CD_s(n, \omega; [\lambda^2, q]) \end{aligned} \quad (5.101)$$

Relation between the original kernel and variance $\sigma_{se}^2(n, \omega)$ kernel: According to (5.100), we can conclude that the original kernel in the Doppler-lag domain can be decomposed into

$$c(\theta, l) = \sum_{i=1}^N \lambda_i a_i(\theta, l),$$

where $a_i(\theta, l)$ are ambiguity functions of eigenvectors $q_i(m)$. The kernel of

$$CD_s(n, \omega; [\lambda^2, q]),$$

in (5.101) is

$$c_\sigma(\theta, l) = \sum_{i=1}^N |\lambda_i|^2 a_i(\theta, l).$$

A detailed analysis of distributions, with respect to their eigenvalue properties, has already been presented. In the sense of that analysis, the signal-dependent variance is just an energetic map of the time-frequency distribution of the original signal.

The mean value of variance (5.95) is

$$\overline{\sigma_{se}^2(n, \omega)} = \frac{1}{2\pi} \int_{-\pi}^{\pi} \sigma_{se}^2(n, \omega) d\omega = 2\sigma_e^2 \sum_{m=-\infty}^{\infty} \tilde{\Phi}(m, m) |s(n+m)|^2. \quad (5.102)$$

For frequency-modulated signals $s(n) = A \exp(j\phi(n))$, it is a constant proportional to the kernel energy.

Example 5.12. Consider the signal

$$\begin{aligned} x(t) = & \exp(j1150(t+0.1)^2) \\ & + e^{-25(t-0.25)^2} \exp(j1600(t+0.2)^2 + j600(t-0.75)^3) \\ & + e^{-25(t-0.67)^2} \exp(j1000(t-0.4)^2) + \exp(j960\pi t) + \varepsilon(t), \end{aligned}$$

within the interval $[0, 1]$, sampled at $\Delta t = 1/1024$. A Hann(ing) lag window of the width $T_w = 1/4$ is used. A stationary white complex noise with variance $\sigma_e^2 = 2$ is assumed. The spectrogram, smoothed spectrogram, S-method, Choi-Williams distribution, and the pseudo Wigner distribution of a signal without noise are presented in the first column of Fig. 5.6, respectively. For the Choi-Williams distribution, the kernel $c(\theta, \tau) = \exp(-(\theta\tau)^2)$ is used, with normalized coordinates $-\sqrt{\pi N/2} \leq \theta < \sqrt{\pi N/2}$, $-\sqrt{\pi N/2} \leq \tau < \sqrt{\pi N/2}$, and 128 samples within the intervals. Elements of the matrix $\tilde{\mathbf{c}}_T$ were calculated as

$$\tilde{c}_T(m, l) = \sum_{p=-N/2}^{N/2} c(p\Delta\theta, (m-l)\Delta\tau) \exp(-j(m+l)p/(2N)) \Delta\theta.$$

The normalized eigenvalues of the matrix $\tilde{\Phi}$ were

$$\lambda_i = \{1, -0.87, 0.69, -0.58, 0.41, -0.30, \dots\}$$

and

$$\mu_i = |\lambda_i|^2 = \{1, 0.76, 0.47, 0.33, 0.17, 0.09, \dots\}.$$

In the spectrogram and smoothed spectrogram, the whole signal dependent part of variance is located just on the signal components, while in the pseudo Wigner distribution it is spread over the entire time-frequency plane. Variance behavior in other two distributions is between these two extreme cases. As was shown, the variances in the smoothed spectrogram and the S-method are the same (Fig. 5.6). \square

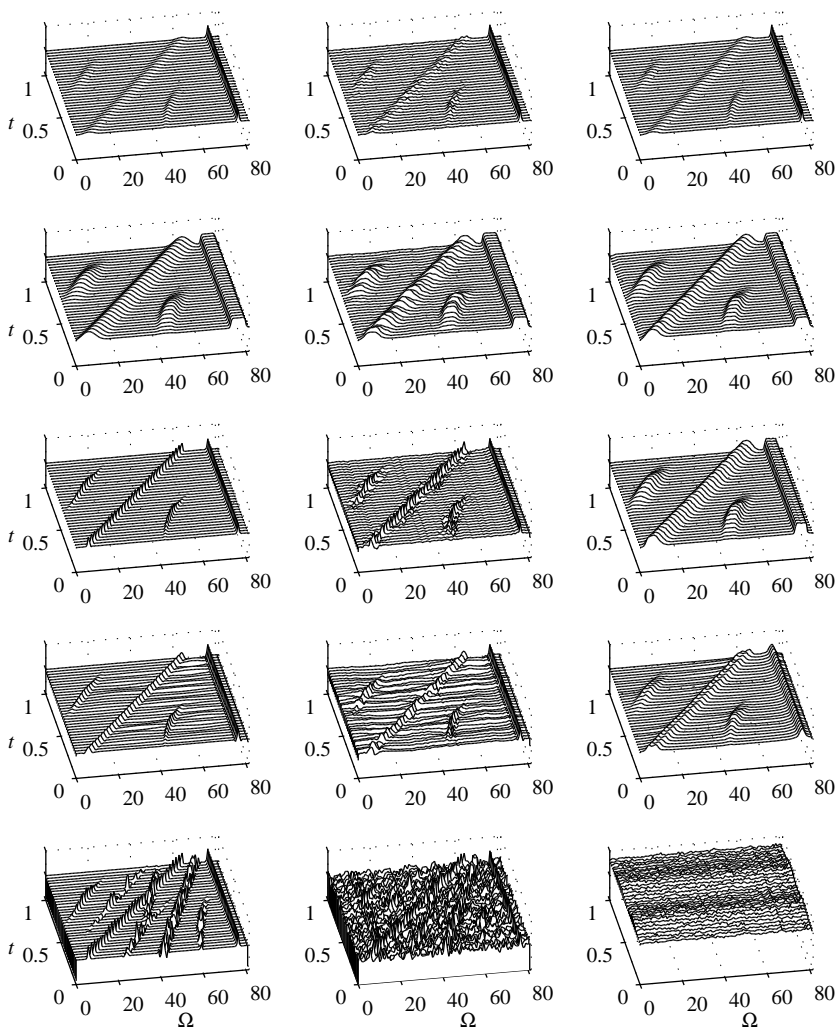


Figure 5.6 Time-frequency representations of a noise-free signal (first column); one realization of time-frequency representations of the signal corrupted by a white stationary complex noise (second column); variances of the distributions, obtained numerically by averaging over 1000 realizations (third column), and rows: the spectrogram, the smoothed spectrogram, the S-method, the Choi-Williams distribution, and the pseudo Wigner distribution.

5.6.5.2 Some Other Forms of Noise

For nonstationary white complex noise, (5.96) results in

$$\tilde{\Phi}(m_1, m_2) = \sum_{l=-N/2}^{N/2-1} I(n+l) \tilde{c}_T(m_1, l) \tilde{c}_T^*(m_2, l), \quad (5.103)$$

or

$$\tilde{\Phi} = \tilde{\mathbf{c}}_T \mathbf{I}_n \tilde{\mathbf{c}}_T^*, \quad (5.104)$$

where \mathbf{I}_n is a diagonal matrix, with the elements $I(n+l)$. For the quasi-stationary case,

$$I(n+l_1) \delta(l_1 - l_2) \cong I(n) \delta(l_1 - l_2),$$

we have that the eigenvalues of $\tilde{\Phi}$ are $I(n) |\lambda_i|^2$, with all other parameters as in (5.101).

In the case of colored stationary complex noise, relations dual to those in special case 2 hold (like (5.85) and (5.87)).

Let

$$x(n) = s(n)(1 + \mu(n)),$$

where $\mu(n)$ is a multiplicative noise. We can write

$$x(n) = s(n) + s(n)\mu(n) = s(n) + \varepsilon(n), \quad (5.105)$$

where $\varepsilon(n) = s(n)\mu(n)$ is an additive noise. Thus, the case of this kind of multiplicative noise can be analyzed in the same way as the additive noise. For example, if the noise $\mu(n)$ is a nonstationary white complex one with

$$R_{\mu\mu}(m, n) = I_\mu(n) \delta(n - m),$$

then

$$R_{\varepsilon\varepsilon}(m, n) = I_\varepsilon(n) \delta(n - m),$$

where

$$I_\varepsilon(n) = |s(n)|^2 I_\mu(n). \quad (5.106)$$

The variance values of some time-frequency distributions in the case of white nonstationary complex noise with

$$R_{\varepsilon\varepsilon}(m, n) = I(n) \delta(m - n), I(n) \geq 0,$$

are summarized next:

- Pseudo Wigner distribution $PWD_s(n, \omega; w)$, with $\tilde{c}_T(m, l) = w(m)\delta(m + l)w(l)$

$$\sigma_{WD}^2(n, \omega) = \sigma_{\epsilon\epsilon}^2(n, \omega) + \sigma_{s\epsilon}^2(n, \omega) = PWD_I(n, 0; w^2) + 2PWD_{I,|s|^2}(n, 0; w^2),$$

where $PWD_{I,|s|^2}$ denotes the cross pseudo Wigner distribution for $I(n)$ and $|s(n)|^2$.

- Spectrogram $S_s(n, \omega; w)$, with $\tilde{c}_T(m, l) = w(m)w(l)$

$$\sigma_{SPEC}^2(n, \omega) = S_I(n, 0; w^2) + 2STFT_I(n, 0; w^2)S_s(n, \omega; w). \quad (5.107)$$

The STFT of $I(n)$, calculated using the window $w^2(m)$, is denoted by $STFT_I(n, \omega; w^2)$.

- A general quadratic distribution, with kernel

$$\tilde{c}_T(m, l) = c_T((m+l)/2, (m-l)/2),$$

in (5.80) or (5.94), and $\tilde{\mathbf{c}}_T$ being a matrix with elements $\tilde{c}_T(m, l)$

$$\sigma_{CD}^2(n, \omega) = CD_I(n, 0; |c_T|^2) + 2CD_s(n, \omega; \tilde{\mathbf{c}}_T \mathbf{I}_n \tilde{\mathbf{c}}_T). \quad (5.108)$$

Expressions for stationary white noise follow with $I(n) = \sigma_\epsilon^2$. Dual expressions hold for a colored stationary noise.

5.7 ROBUST TIME-FREQUENCY ANALYSIS

Huber's estimation theory gives fundamental principles for solving a wide class of problems when the signal is corrupted by impulsive disturbances. The standard Fourier transform and other Fourier transform based time-frequency representations presented up to now can be obtained by solving a proper minimization problem with the squared absolute error as a loss function. Within the estimation theory framework, they are the maximum likelihood (ML) estimates of the nonnoisy signal transform for the Gaussian noise environment. However, for the impulse kind of noise, the standard Fourier transform and the Fourier transform-based representations may produce poor results.

Applying results from the Huber's estimation theory, the robust M -Fourier transform is defined. This method has been extended to the robust time-frequency

analysis of nonstationary signals embedded in impulse noise. The robust M -Fourier transform definition is based on the absolute error as a loss function. Since this type of loss function does not produce a closed-form solution, the iterative procedures are used in calculation of the robust M -Fourier transform. Procedures producing the robust Fourier transform, without iterative procedures, by using the L-statistics approach and median are defined by Katkovnik, Djurović, Stanković, et al. as well.

5.7.1 Robust Short-Time Fourier Transform

In order to explain this approach, let us first introduce the well-known standard Fourier transform and the short-time Fourier transform (STFT) within this framework.

The standard discrete Fourier transform coefficient $X(k)$ of a signal $x(n)$ for a given frequency k could be seen as a projection of the signal onto the complex sinusoid $e^{j2\pi kn/N}$. It means that the value of $X(k)$ is the amplitude of complex sinusoid, at a frequency k , that is the closest (the most similar) to our signal. If we use the mean square error as a similarity measure of the signal $x(n)$ and complex sinusoid, then we have to minimize the error

$$e(k, n) = x(n) - X(k)e^{j2\pi kn/N} \quad (5.109)$$

in the mean squared sense, over all available time instants n .

The value of $X(k)$ is equal to the value of parameter m that minimizes

$$\begin{aligned} \sum_{n=-N/2}^{N/2-1} |e(k, n)|^2 &= \sum_{n=-N/2}^{N/2-1} |x(n) - me^{j2\pi kn/N}|^2 \\ &= \sum_{n=-N/2}^{N/2-1} |x(n)e^{-j2\pi kn/N} - m|^2. \end{aligned}$$

Therefore, we can say that the Fourier transform coefficient $X(k)$ is a solution of the minimization problem

$$X(k) = \arg \left\{ \min_m I(k, m) \right\} \quad (5.110)$$

where

$$I(k, m) = \sum_{n=-N/2}^{N/2-1} |x(n)e^{-j2\pi kn/N} - m|^2. \quad (5.111)$$

The minimization is performed by taking the first derivative over the minimization parameter m ,

$$\frac{I(k, m)}{\partial m^*} = 2 \sum_{n=-N/2}^{N/2-1} \left(x(n) e^{-j2\pi kn/N} - m \right) = 0,$$

resulting in

$$m = \frac{1}{N} \sum_{n=-N/2}^{N/2-1} x(n) e^{-j2\pi kn/N}$$

that minimizes $I(k, m)$. Thus, the normalized DFT follows

$$X(k) = \arg \left\{ \min_m I(k, m) \right\} = \frac{1}{N} \sum_{n=-N/2}^{N/2} x(n) e^{-j2\pi kn/N}.$$

The standard STFT of signal $x(n\Delta t)$, calculated at a given point (t, Ω) , can be defined as a solution to the following optimization problem

$$STFT(t, \Omega) = \arg \left\{ \min_m I(t, \Omega, m) \right\}, \quad (5.112)$$

$$I(t, \Omega, m) = \sum_{n=-N/2}^{N/2-1} w(n\Delta t) \mathbf{F}(e(t, \Omega, n)), \quad (5.113)$$

where the loss function is assumed as

$$\mathbf{F}(e) = |e|^2, \quad (5.114)$$

$w(n\Delta t)$ is a window function and Δt is a sampling interval. The error function has the form

$$e(t, \Omega, n) = x(t + n\Delta t) e^{-j\Omega n\Delta t} - m, \quad (5.115)$$

where m is a complex-valued optimization parameter in (5.112). The error function can be considered as a residuum expressing the “similarity” between the signal and a given harmonic $\exp(j\Omega n\Delta t)$.

The solution of (5.112) easily follows from

$$\frac{\partial I(t, \Omega, m)}{\partial m^*} = 0, \quad (5.116)$$

that is, with (5.115), from

$$\frac{\partial}{\partial m^*} \left[\sum_{n=-N/2}^{N/2-1} w(n\Delta t) |x(t+n\Delta t)e^{-j\Omega n\Delta t} - m|^2 \right] = 0$$

$$2 \sum_{n=-N/2}^{N/2-1} w(n\Delta t) (x(t+n\Delta t)e^{-j\Omega n\Delta t} - m) = 0,$$

in the form of the well-known standard STFT definition (used in this book) as

$$STFT(t, \Omega) = m = \frac{1}{a_w} \sum_{n=-N/2}^{N/2-1} w(n\Delta t) x(t+n\Delta t) e^{-j\Omega n\Delta t}, \quad (5.117)$$

normalized with a constant

$$a_w = \sum_{n=-N/2}^{N/2-1} w(n\Delta t). \quad (5.118)$$

5.7.1.1 Loss Function

The maximum likelihood (ML) approach can be used for selection of appropriate loss function $\mathbf{F}(e)$ if the pdf $p(e)$ of the noise is known. The ML approach suggests the loss function

$$\mathbf{F}(e) \sim -\log p(e). \quad (5.119)$$

For example, the loss function

$$\mathbf{F}(e) = |e|^2$$

gives the standard STFT, as the ML estimate of spectra for signals corrupted with the Gaussian noise, whose pdf is

$$p(e) \sim \exp(-|e|^2). \quad (5.120)$$

The standard STFT produces poor results for signals corrupted by impulse noise. Additionally, in many cases the ML estimates are quite sensitive to deviations from the parametric model and the hypothetical distribution. Even a slight deviation from the hypothesis can result in a strong degradation of the ML estimate. The minimax robust approach has been developed in statistics, as an alternative to the

conventional ML in order to decrease the ML estimates sensitivity, and to improve the efficiency in an environment with the heavy-tailed pdfs. The loss function

$$\mathbf{F}(e) = |e| = \sqrt{\operatorname{Re}^2\{e\} + \operatorname{Im}^2\{e\}} \quad (5.121)$$

is recommended by the robust estimation theory for a wide class of heavy-tailed pdfs. It is worth noting that the loss function

$$\mathbf{F}(e) = |\operatorname{Re}\{e\}| + |\operatorname{Im}\{e\}| \quad (5.122)$$

is the ML selection for the Laplacian distribution of independent real and imaginary parts of the complex valued noise.

Nonquadratic loss functions in (5.113) can improve filtering properties for impulse noises. In particular, the robust M -STFT has been derived by using the absolute error loss function

$$\mathbf{F}(e) = |e|,$$

when

$$\begin{aligned} \frac{\partial}{\partial m^*} \left[\sum_{n=-N/2}^{N/2-1} w(n\Delta t) \sqrt{|x(t+n\Delta t)e^{-j\Omega n\Delta t} - m|^2} \right] &= 0 \\ \sum_{n=-N/2}^{N/2-1} \left(\frac{w(n\Delta t)x(t+n\Delta t)e^{-j\Omega n\Delta t}}{|x(t+n\Delta t)e^{-j\Omega n\Delta t} - m|} - \frac{w(n\Delta t)m}{|x(t+n\Delta t)e^{-j\Omega n\Delta t} - m|} \right) &= 0. \end{aligned}$$

The robust M -STFT follows as a solution of the nonlinear equation

$$m = \frac{1}{\sum_{n=-N/2}^{N/2-1} \frac{w(n\Delta t)}{|x(t+n\Delta t)e^{-j\Omega n\Delta t} - m|}} \sum_{n=-N/2}^{N/2-1} \frac{w(n\Delta t)x(t+n\Delta t)e^{-j\Omega n\Delta t}}{|x(t+n\Delta t)e^{-j\Omega n\Delta t} - m|}$$

with $STFT(t, \Omega) = m$, being the solution of the previous equation

$$STFT(t, \Omega) = \frac{1}{a_w(t, \Omega)} \sum_{n=-N/2}^{N/2-1} d(t, \Omega, n) x(t+n\Delta t) e^{-j\Omega n\Delta t}, \quad (5.123)$$

where

$$d(t, \Omega, n) = \frac{w(n\Delta t)}{|x(t+n\Delta t)e^{-j\Omega n\Delta t} - STFT(t, \Omega)|}, \quad (5.124)$$

and

$$a_w(t, \Omega) = \sum_{n=-N/2}^{N/2-1} d(t, \Omega, n). \quad (5.125)$$

5.7.1.2 Iterative Procedure for the Realization of the Robust STFT

The expression (5.123) includes $STFT(t, \Omega)$ on the right side. Therefore, to get the robust STFT, we have to solve a nonlinear equation of the form $y = f(y)$. Here we will use the fixed point iterative algorithm $y_i = f(y_{i-1})$, with the stopping rule $|y_i - y_{i-1}|/|y_i| < \eta$, where η defines the solution precision. This procedure, applied to (5.123), can be summarized as follows.

Step 0: Calculate the standard STFT (5.117)

$$STFT^{(0)}(t, \Omega) = STFT(t, \Omega),$$

and set $i = 0$.

Step 1: Set $i = i + 1$. Calculate

$$d^{(i)}(t, \Omega, n) = \frac{w(n\Delta t)}{|x(t + n\Delta t)e^{-j\Omega n\Delta t} - STFT^{(i-1)}(t, \Omega)|}$$

for $STFT^{(i-1)}(t, \Omega)$ determined by (5.124). Calculate $STFT^{(i)}(t, \Omega)$ as

$$STFT^{(i)}(t, \Omega) = \frac{1}{\sum_{n=-N/2}^{N/2-1} d^{(i)}(t, \Omega, n)} \sum_{n=-N/2}^{N/2-1} d^{(i)}(t, \Omega, n) x(t + n\Delta t) e^{-j\Omega n\Delta t}. \quad (5.126)$$

Step 2: If the maximal relative absolute difference between two iterations is smaller than η

$$\max_{(t, \Omega)} \left\{ \frac{|STFT^{(i)}(t, \Omega) - STFT^{(i-1)}(t, \Omega)|}{|STFT^{(i)}(t, \Omega)|} \right\} \leq \eta, \quad (5.127)$$

then the robust STFT is obtained as $STFT(t, \Omega) = STFT^{(i)}(t, \Omega)$. Otherwise return to 1.

Example 5.13. Consider the signal

$$s(n) = e^{j12\pi n/N} + e^{j18\pi n/N}, \text{ with } N = 64,$$

with a strong additive impulse Laplacian noise $\varepsilon(n)$ in 75% of the arbitrary positioned instants n (Fig. 5.7(a, b)). Its standard STFT transform and the robust STFT, calculated in nine iterations at $n = 32$, are shown in Fig. 5.7(c, d). If the amplitudes of the signal components were different, this procedure would favor the strongest component. One way to proceed in that case would be to eliminate the strongest component, after it had been found, and to repeat the procedure on the rest of the signal. \square

5.7.1.3 Vector Filter Approach

Note that the standard STFT (5.117) can be treated as an estimate of the mean, calculated over a set of complex-valued observations

$$\mathbf{E}^{(t,\Omega)} = \{x(t + n\Delta t)e^{-j\Omega n\Delta t} : n \in [-N/2, N/2]\}, \quad (5.128)$$

that is,

$$STFT(t, \Omega) = \underset{n \in [-\frac{N}{2}, \frac{N}{2}]}{\text{mean}} \{x(t + n\Delta t)e^{-j\Omega n\Delta t}\}.$$

If we restrict possible values of m in (5.112) to the set $\mathbf{E}^{(t,\Omega)}$, the vector filter concept can be applied to get a simple approximation of the robust estimate of the STFT. Here the coordinates of vector-valued variable are real and imaginary parts of $x(t + n\Delta t)e^{-j\Omega n\Delta t}$. The vector estimate of the STFT is defined as $STFT(t, \Omega) = m$, where $m \in \mathbf{E}^{(t,\Omega)}$, and for all $k \in [-N/2, N/2]$ the following inequality holds

$$\begin{aligned} & \sum_{n=-N/2}^{N/2-1} \mathbf{F} \left(\left| m - x(t + n\Delta t)e^{-j\Omega n\Delta t} \right| \right) \leq \\ & \sum_{n=-N/2}^{N/2-1} \mathbf{F}(|x(t + k\Delta t)e^{-j\Omega k\Delta t} - x(t + n\Delta t)e^{-j\Omega n\Delta t}|). \end{aligned} \quad (5.129)$$

For $\mathbf{F}(e) = |e|$ this estimate is called the vector median.

The marginal median can be used for independent estimation of real and imaginary parts of m . It results in

$$\begin{aligned} \text{Re}\{STFT(t, \Omega)\} &= \underset{n \in [-\frac{N}{2}, \frac{N}{2}]}{\text{median}} \{\text{Re}\{x(t + n\Delta t)e^{-j\Omega n\Delta t}\}\}, \\ \text{Im}\{STFT(t, \Omega)\} &= \underset{n \in [-\frac{N}{2}, \frac{N}{2}]}{\text{median}} \{\text{Im}\{x(t + n\Delta t)e^{-j\Omega n\Delta t}\}\}. \end{aligned} \quad (5.130)$$

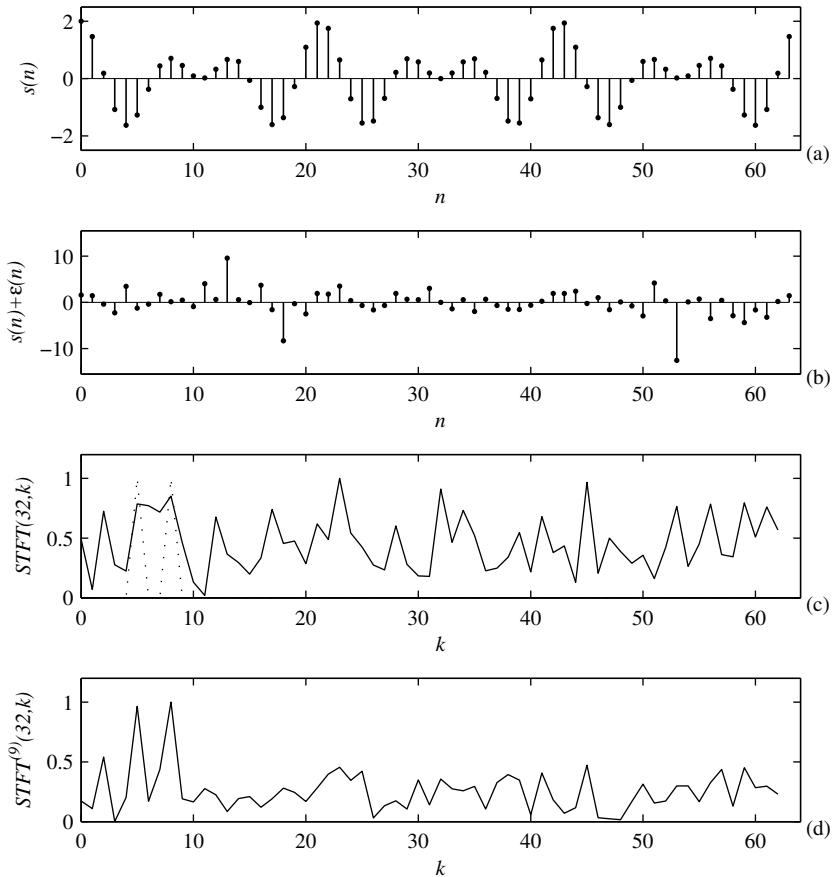


Figure 5.7 Illustration of the robust STFT: (a) noise-free signal, (b) signal with a strong impulse noise in 75% of the randomly positioned instants, (c) standard STFT of noisy signal, and (d) robust STFT of noisy signal. Real parts of signals are presented in (a) and (b), while the absolute normalized values of the transforms are presented in (c) and (d).

The separate estimation of the real and imaginary parts of $STFT(t, \Omega)$ assumes independence of the real and imaginary parts of $x(t + n\Delta t)e^{-j\Omega n\Delta t}$, which in general, does not hold here. However, in numerous experiments, the accuracy of the median estimates (5.129) and (5.130) is of the same order. A simplicity of calculation is the advantage of these median estimates over the iterative procedures.

5.7.2 Robust Wigner Distribution

For rectangular window, the standard Wigner distribution (normalized with the number of samples, to follow the robust framework notation) can be treated as an estimate of the mean, calculated over a set of complex-valued observations

$$\mathbf{G} = \{x(t + n\Delta t)x^*(t - n\Delta t)e^{-j2\Omega n\Delta t} : n \in [-N/2, N/2]\}, \quad (5.131)$$

that is,

$$\begin{aligned} WD(t, \Omega) &= \frac{1}{N+1} \sum_{n=-N/2}^{N/2} x(t + n\Delta t)x^*(t - n\Delta t)e^{-j2\Omega n\Delta t} \\ &= \underset{n \in [-\frac{N}{2}, \frac{N}{2}]}{\text{mean}} \{x(t + n\Delta t)x^*(t - n\Delta t)e^{-j2\Omega n\Delta t}\}. \end{aligned} \quad (5.132)$$

Since the Wigner distribution is real-valued, minimization similar to (5.113) can be done with respect to the real part of $x(t + n\Delta t)x^*(t - n\Delta t)e^{-j2\Omega n\Delta t}$ only. A form of the robust Wigner distribution, the median Wigner distribution, can be introduced as

$$WD(t, \Omega) = \underset{n \in [-\frac{N}{2}, \frac{N}{2}]}{\text{median}} \{\text{Re}\{x(t + n\Delta t)x^*(t - n\Delta t)e^{-j2\Omega n\Delta t}\}\}. \quad (5.133)$$

Generally, it can be shown that any robust time-frequency distribution, obtained by using the Hermitian local auto-correlation function, $R_x(t, n\Delta t) = R_x^*(t, -n\Delta t)$ in the minimization, is real-valued. In the Wigner distribution case, this condition is satisfied, since

$$R_x(t, n\Delta t) = x(t + n\Delta t)x^*(t - n\Delta t).$$

For a general quadratic distribution from the Cohen class with a Hermitian generalized local auto-correlation function, the robust version reads as

$$CD(t, \Omega) = \underset{n \in [-\frac{N}{2}, \frac{N}{2}]}{\text{median}} \{\text{Re}\{R_{CD}(t, n\Delta t)e^{-j2\Omega n\Delta t}\}\}, \quad (5.134)$$

where $R_{CD}(t, n\Delta t)$ includes the kernel in time-lag domain.

Note that for an input Gaussian noise the resulting noise in the Wigner distribution, has both Gaussian and impulse component, due to the Wigner distribution quadratic nature. Thus, robust Wigner distribution forms can improve performance of the standard Wigner distribution, even in a high Gaussian noise environment.

Example 5.14. Consider a signal

$$x(t) = e^{j128 \cos(\pi t + \pi/3)} + \alpha(\varepsilon_1^3(t) + j\varepsilon_2^3(t)) \quad (5.135)$$

sampled with $T = 1/1024$ and $N = 128$. The standard and the robust Wigner distributions of $x(t)$ for $\alpha = 0.4$ and $\alpha = 0.9$ are shown in Fig. 5.8. For the graphical presentation, the standard Wigner distributions are limited to the value of the Wigner distribution maximum for nonnoisy signal. It can be concluded that the robust Wigner distribution filters the heavy-tailed noise significantly better than the standard Wigner distribution. \square

5.7.3 L-Estimation

Signals are often corrupted not by a pure Gaussian or impulse noise but by their combination. In time-frequency representations, due to their quadratic nature, the resulting noise is a mixture of the Gaussian and impulse noise for the input noise being purely Gaussian. Theoretically, when we have a sum of Gaussian and impulse noise (of a known type), we can derive the pdf function and its corresponding loss function for the ML estimation. However, this loss function will be of the form that is not practically applicable in the minimization. Huber's estimation theory provides solutions for this kind of problems. They are based on the L - and R -estimation approaches. The L -estimation will be demonstrated on the Wigner distribution case. The basic idea in the L -estimation is not to use a simple mean of all values (being the ML estimate for a Gaussian noise) nor the simple median (being the ML estimate for Laplacian noise), but to eliminate the extreme values and to use a (weighted) sum of the remaining values.

The L -estimate of the Wigner distribution can be introduced as

$$WD_L(n, k) = \sum_{i=0}^N a_i \mathbf{x}_{(i)}(n, k), \quad (5.136)$$

with

$$\sum_{i=0}^{N-1} a_i = 1.$$

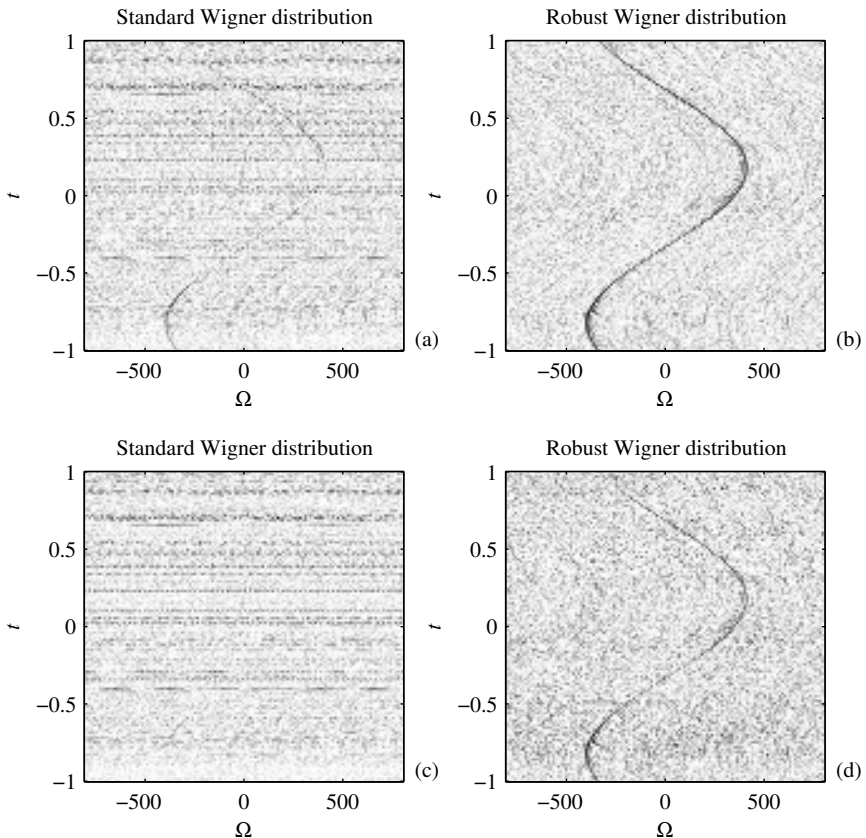


Figure 5.8 Standard Wigner distribution and robust Wigner distribution of sinusoidally modulated signal with $\alpha = 0.4$ (a) and (b) and $\alpha = 0.9$ (c) and (d).

The values $\mathbf{x}_{(i)}(n, k)$ are the order statistics of

$$\mathbf{E}_{n,k} = \left\{ \operatorname{Re}\{x(n+m)x^*(n-m)\exp(-j4\pi km/(N+1))\} : m \in [-\frac{N}{2}, \frac{N}{2}] \right\}.$$

ordered into a nonincreasing sequence

$$\mathbf{x}_{(0)}(n, k) \geq \dots \geq \mathbf{x}_{(i)}(n, k) \geq \mathbf{x}_{(i+1)}(n, k) \geq \dots \geq \mathbf{x}_N(n, k). \quad (5.137)$$

The basic idea here is to avoid $\mathbf{x}_{(i)}(n, k)$ with extremely high absolute values, that is, values at the beginning and at the end of (5.137), and to use the remaining ones in the Wigner distribution calculation.

Note that the standard Wigner distribution, that is, the mean-based Wigner distribution (5.132), and the Wigner distribution form based on the median (5.130) can be obtained as special cases of (5.136):

1.) The standard Wigner distribution follows with

$$a_i = 1/(N+1), \quad i = 0, \dots, N,$$

since the ordering of terms, in this case, does not affect the sum in (5.136).

2.) The robust median-based Wigner distribution result, for

$$a_i = \begin{cases} 1 & i = N/2 \\ 0 & i \neq N/2 \end{cases} \quad \text{for even } N, \quad (5.138)$$

when only the middle term of the sorted sequence is used.

A special attention will be paid to the form of coefficients in (5.136), which can be written in analogy to the α -trimmed mean in the nonlinear digital filter theory. The coefficients a_i , for even N , are given by

$$a_i = \begin{cases} \frac{1}{(N+1)(1-2\alpha)+2\alpha} & \text{for } N\alpha \leq i \leq N - \alpha N \\ 0 & \text{elsewhere.} \end{cases} \quad (5.139)$$

Obviously, the lowest $N\alpha$ values of $\mathbf{x}_{(i)}(n, k)$ are eliminated (not used in (5.136) calculation). These are the terms with the biggest negative values. The same is done with the highest positive values. Then the Wigner distribution is calculated with the remaining terms, based on (5.136). Here the L-estimation forms of the time-frequency representations meet the time-frequency representation of the compressive sensed signals. In the L-estimation some randomly positioned signal samples are eliminated, as unreliable, while in the compressive sensing some signal samples are inherently unavailable.

From (5.139), the standard form follows for $\alpha = 0$, whereas $\alpha = 0.5$ produces the median-based form. For $0 < \alpha < 0.5$ performance between these two limit cases is obtained.

For a mixture of Gaussian and impulse noise, the L-estimation with a properly chosen value of α can produce more accurate results than either the standard and the median-based forms. This is especially important for quadratic and higher-order time-frequency representations, like the Wigner distribution, where the resulting noise inherently has a form of this mixture.

5.7.4 Resulting Noise Distribution in the Local Auto-Correlation Function

Next we will show that the L -estimation-based Wigner distribution can outperform the standard Wigner distribution, even in the case of Gaussian input noise.

Let the signal $s(n)$ be corrupted by an additive noise $\varepsilon(n)$. The local auto-correlation function is given by

$$\begin{aligned} x(n+m)x^*(n-m) &= s(n+m)s^*(n-m) + s(n+m)\varepsilon^*(n-m) + \\ \varepsilon(n+m)s^*(n-m) + \varepsilon(n+m)\varepsilon^*(n-m) &= r_s(n,m) + \Psi(n,m), \end{aligned} \quad (5.140)$$

where

$$r_s(n,m) = s(n+m)s^*(n-m)$$

is the signal component, while the noise influenced term is

$$\Psi(n,m) = s(n+m)\varepsilon^*(n-m) + \varepsilon(n+m)s^*(n-m) + \varepsilon(n+m)\varepsilon^*(n-m).$$

Assume that the input noise is of the form $\varepsilon(n) = \varepsilon_1(n) + j\varepsilon_2(n)$, where $\varepsilon_i(n)$, $i = 1, 2$, are mutually independent white Gaussian noises, with variance $\mathcal{N}(0, \sigma^2)$. The component $s(n+m)\varepsilon^*(n-m) + \varepsilon(n+m)s^*(n-m)$ is a Gaussian white non-stationary noise with variance depending on the signal $s(n)$. The noise local auto-correlation function $r_\varepsilon(n,m) = \varepsilon(n+m)\varepsilon^*(n-m)$ can be written as

$$\begin{aligned} \varepsilon(n+m)\varepsilon^*(n-m) &= \\ \varepsilon_1(n+m)\varepsilon_1(n-m) + \varepsilon_2(n+m)\varepsilon_2(n-m) - \\ j\varepsilon_1(n+m)\varepsilon_2(n-m) + j\varepsilon_2(n+m)\varepsilon_1(n-m). \end{aligned} \quad (5.141)$$

For $m = 0$, it is equal to

$$r_\varepsilon(n,0) = \text{Re}\{\varepsilon(n)\varepsilon^*(n)\} = \varepsilon_1^2(n) + \varepsilon_2^2(n).$$

The pdf of this noise is

$$p(\xi) = \exp(-\xi/(2\sigma^2))/(2\sigma^2)$$

for $\xi > 0$ and $p(\xi) = 0$ for $\xi < 0$. For $m \neq 0$ the real and imaginary parts of noise

$$r_\varepsilon(n,m) = r_1(n,m) + jr_2(n,m)$$

in (5.141) can be written as

$$r_i(n, m) = \varepsilon_a \varepsilon_b + \varepsilon_c \varepsilon_d, \quad (5.142)$$

where ε_a , ε_b , ε_c , and ε_d are mutually independent Gaussian noises. Then components $r_i(n, m) = \varepsilon_a \varepsilon_b + \varepsilon_c \varepsilon_d$ have the Laplacian pdf

$$p(\xi) = \exp(-|\xi|/\sigma^2)/(2\sigma^2). \quad (5.143)$$

They are dominant with respect to $r_\varepsilon(n, 0)$, since they exist for each $m \neq 0$.

Thus, we can conclude that for a Gaussian input noise, the resulting noise in the Wigner distribution $\Psi(n, m)$ is a mixture of the Gaussian and Laplacian impulse noise.

5.8 SPARSE SIGNAL ANALYSIS IN TIME-FREQUENCY

In signal processing representations a signal is transformed from one domain into another. In many cases it happens that a signal that covers whole considered interval in one domain (dense in that domain) is located within much smaller regions in the other domain (sparse in this domain). For example, a discrete time complex sinusoidal signal with N samples in the discrete-time domain is just one sample in the DFT domain (if the frequency is on a grid position). Similarly, M complex sinusoids covering N points in the discrete-time domain, are represented by M values in the frequency domain. This simple illustration leads to the conclusion that, for a complex signal containing M complex sinusoids, we do not need N samples in the time domain to reconstruct M samples in the frequency domain. Of course, the Fourier domain is just one of possible domains to transform a signal (many of them, with linear signal transformation, are discussed in Chapter 2). A signal may not be sparse in the time domain or in the Fourier domain, but could be, for example, sparse in polynomial Fourier domain or in the fractional Fourier domain (a linear frequency-modulated signal transforms into a one value in frequency and rate domain) or in the STFT domain (Example 2.13). Then we will also be able to reconstruct the original signal if some samples are missing.

The samples could be missed due to their physical or measurements unavailability. In applications it could happen that some arbitrarily positioned samples of the signal are so heavily corrupted by disturbances that it is better to omit them in the analysis. This is especially true for the impulse noise. In quadratic and higher-order signal representations, impulse noise appears even in the case of the Gaussian input

noise (as shown earlier in this chapter). The robust analysis is defined to minimize the influence of extreme signal values. In some cases these samples are omitted (for example, after the L-statistics method is applied). Then these signals could be also considered within the framework of missing values. A similar situation appears in the cases when some signal samples (also randomly positioned) are not available (compressive sensing). Under some conditions, the processing could be performed with the remaining samples, almost as in the case if missing samples were available. Of course, some a priori information about the nature of the analyzed signal, its sparsity in a known domain, should be used. Compressive sensing is a field dealing with this problem and provides a solution that differs from the classical signal theory approach. Sparsity is one of the main requirements that should be satisfied in order to efficiently apply the compressive sensing methods for signal reconstruction.

Here we will start with quite simple examples in order to introduce basic concepts of processing sparse signals. Consider the simplest case first. Since the Fourier analysis is based on the sinusoidal decomposition of any signal, let us consider the case when a sampled signal is a pure real-valued sinusoid. Then we know that its form, $y(t) = A \cos(\Omega_0 t + \varphi)$, requires three equations to determine three unknown parameters A , Ω_0 , and φ . If a signal $y(t)$ is a real-valued sinusoid, then only three of its independent values should be sufficient to reconstruct it (see Problem 1.14).

Example 5.15. Four samples of a simple complex-valued signal in the discrete-time domain are considered, $x(0) = 0.6929 + j0.2870$, $x(1)$ is missing, $x(2) = -0.6929 - j0.2870$, and $x(3) = 0.2870 - j0.6929$. The second sample is missing (heavily corrupted or not available). We know that the signal is sparse in Fourier domain, as well as that its amplitude is somewhere between 0 and 2. Find the value of the second sample that will produce the best concentrated Fourier transform of this signal.

★For the signal $x(n)$, with the missing sample being replaced by $\alpha e^{j\beta}$, the DFT is of the form

$$\begin{aligned} X(k) &= \sum_{n=0}^3 x(n) e^{-j n k \pi / 2} \\ &= x(0) + \alpha e^{j \beta} e^{-j k \pi / 2} + x(2) e^{-j k \pi} + x(3) e^{-j 3 k \pi / 2} \\ X(0) &= 0.2870 - j0.6929 + \alpha e^{j \beta} \\ X(1) &= 2.0787 + j0.8610 - j \alpha e^{j \beta} \\ X(2) &= -0.2870 + j0.6929 - \alpha e^{j \beta} \\ X(3) &= 0.6929 + j0.2870 + j \alpha e^{j \beta}. \end{aligned}$$

Using the measure of concentration (explained in Chapter 2) of the resulting DFT in the form

$$M(\alpha, \beta) = \sum_{k=0}^3 |X(k)| \quad (5.144)$$

and varying parameters α from 0 to 2, with step 0.25, and β from $-\pi$ to π , with step $\pi/8$, we get the global minimum of $M(\alpha, \beta)$ at

$$M(0.75, 1.9635) = 3.$$

It means that the missing sample, producing the best concentrated DFT, is

$$x(1) = 0.75 \exp(j1.9635) = -0.2870 + j0.6929.$$

Then $X(0) = 0$, $X(1) = 2.7716 + j1.1481$, $X(2) = 0$ and $X(3) = 0$.

Now reformulate this problem into matrix form. Denote the full DFT transformation matrix with

$$\mathbf{W} = \begin{bmatrix} 1 & 1 & 1 & 1 \\ 1 & e^{-j2\pi/N} & e^{-j4\pi/N} & e^{-j6\pi/N} \\ 1 & e^{-j4\pi/N} & e^{-j8\pi/N} & e^{-j12\pi/N} \\ 1 & e^{-j6\pi/N} & e^{-j12\pi/N} & e^{-j18\pi/N} \end{bmatrix}$$

$$\mathbf{X} = \mathbf{W}\mathbf{x}$$

$$\mathbf{x} = \mathbf{W}^{-1}\mathbf{X}$$

where \mathbf{x} is a vector column with the signal values and \mathbf{X} is a vector column with the DFT values. In the case of the missing second signal sample, for the DFT coefficients calculation, we get three equations

$$\text{instant 0 : } x(0) = \frac{1}{4} (X(0) + X(1) + X(2) + X(3))$$

instant 1 : Missing value and equation

$$\text{instant 2 : } x(2) = \frac{1}{4} (X(0) + X(1)e^{j4\pi/N} + X(2)e^{j8\pi/N} + X(3)e^{j12\pi/N})$$

$$\text{instant 3 : } x(3) = \frac{1}{4} (X(0) + X(1)e^{j6\pi/N} + X(2)e^{j12\pi/N} + X(3)e^{j18\pi/N})$$

The transformation matrix

$$\mathbf{W}^{-1} = \frac{1}{N} \begin{bmatrix} 1 & 1 & 1 & 1 \\ 1 & e^{j2\pi/N} & e^{j4\pi/N} & e^{j6\pi/N} \\ 1 & e^{j4\pi/N} & e^{j8\pi/N} & e^{j12\pi/N} \\ 1 & e^{j6\pi/N} & e^{j12\pi/N} & e^{j18\pi/N} \end{bmatrix}$$

is now reduced, by omitting the second row, to

$$\mathbf{A} = \frac{1}{N} \begin{bmatrix} 1 & 1 & 1 & 1 \\ 1 & e^{j4\pi/N} & e^{j8\pi/N} & e^{j12\pi/N} \\ 1 & e^{j6\pi/N} & e^{j12\pi/N} & e^{j18\pi/N} \end{bmatrix}$$

with

$$\mathbf{y} = \mathbf{AX}. \quad (5.145)$$

Thus, we have three equations with three signal samples $x(n)$ in the vector

$$\mathbf{y} = [x(0), x(2), x(3)]^T$$

and four unknown DFT values $X(k)$ in vector

$$\mathbf{X} = [X(0), X(1), X(2), X(3)]^T.$$

Thus, by varying the value for $x(1)$, we have solved undetermined problem, as a minimization problem,

$$\min \|\mathbf{X}\| \text{ subject to } \mathbf{y} = \mathbf{AX}, \quad (5.146)$$

where for $\|\mathbf{X}\|$, the absolute value concentration measure is used, presented, and discussed in Chapter 2,

$$\|\mathbf{X}\| = \sum_{k=0}^{N-1} |X(k)|. \quad (5.147)$$

This measure is known as the l_1 norm, in notation $\|\mathbf{X}\|_{l_1}$. Of course, other concentration measures are possible as well.

It is important to note that the minimization solution with the l_2 norm would be trivial in this case. For this norm, we would attempt to minimize

$$\|\mathbf{X}\|_{l_2} = \sum_{k=0}^{N-1} |X(k)|^2.$$

According to Parseval's theorem

$$\|\mathbf{X}\|_{l_2} = N \sum_{n=0}^{N-1} |x(n)|^2. \quad (5.148)$$

Since any value than $x(n) = 0$ for the nonavailable (missing) signal samples, would increase $\|\mathbf{X}\|_2$, then the solution for the nonavailable samples, with respect to the l_2 norm, is trivial. This was the reason why this norm was not used as a concentration measure.

□

Based on the previous example we may easily write a general sparse signal processing formulation.

Let the original signal be $x(n)$ with $n = 0, 1, \dots, N - 1$. Suppose that an arbitrary number of $N - K$ signal values are missing. Then the available K signal values are denoted by vector \mathbf{y} . If we denote by \mathbf{A} the inverse transformation matrix \mathbf{W}^{-1} with omitted rows, corresponding to missing signal values, then for the DFT coefficients we have to solve K equations

$$\mathbf{y} = \mathbf{AX}$$

with N unknowns. Thus, we have to find the best concentrated \mathbf{X} , solving the minimization problem

$$\min \|\mathbf{X}\| \text{ subject to } \mathbf{y} = \mathbf{AX} \quad (5.149)$$

$$\text{where } \|\mathbf{X}\| = \sum_{k=0}^{N-1} |X(k)|.$$

The condition that we will obtain a satisfactory result is that the considered signal is sparse in the DFT domain.

Example 5.16. A signal with $N = 8$ samples is considered. However, tree samples, $x(0)$, $x(3)$, and $x(4)$, are removed by using the L -statistics (or are not available for calculation). It is known that the signal is sparse in the DFT domain. Formulate the problem in a sparse signal processing sense.

★The available signal values are

$$\mathbf{y} = [x(1), x(2), x(5), x(6), x(7)]^T.$$

Thus, the transformation matrix is obtained by removing the first, fourth, and fifth row in the inversion matrix, corresponding to $x(0)$, $x(3)$, and $x(4)$,

$$\mathbf{A} = \frac{1}{N} \begin{bmatrix} 1 & e^{j\frac{2\pi}{N}} & e^{j\frac{4\pi}{N}} & e^{j\frac{6\pi}{N}} & e^{j\frac{8\pi}{N}} & e^{j\frac{10\pi}{N}} & e^{j\frac{12\pi}{N}} & e^{j\frac{14\pi}{N}} \\ 1 & e^{j\frac{4\pi}{N}} & e^{j\frac{8\pi}{N}} & e^{j\frac{12\pi}{N}} & e^{j\frac{16\pi}{N}} & e^{j\frac{20\pi}{N}} & e^{j\frac{24\pi}{N}} & e^{j\frac{28\pi}{N}} \\ 1 & e^{j\frac{10\pi}{N}} & e^{j\frac{20\pi}{N}} & e^{j\frac{30\pi}{N}} & e^{j\frac{40\pi}{N}} & e^{j\frac{50\pi}{N}} & e^{j\frac{60\pi}{N}} & e^{j\frac{70\pi}{N}} \\ 1 & e^{j\frac{12\pi}{N}} & e^{j\frac{24\pi}{N}} & e^{j\frac{36\pi}{N}} & e^{j\frac{48\pi}{N}} & e^{j\frac{60\pi}{N}} & e^{j\frac{72\pi}{N}} & e^{j\frac{84\pi}{N}} \\ 1 & e^{j\frac{14\pi}{N}} & e^{j\frac{28\pi}{N}} & e^{j\frac{42\pi}{N}} & e^{j\frac{56\pi}{N}} & e^{j\frac{70\pi}{N}} & e^{j\frac{84\pi}{N}} & e^{j\frac{98\pi}{N}} \end{bmatrix}.$$

Thus, the minimization formulation is (5.149). Of course, here it would still be possible to minimize the problem by a direct search over three complex values. □

However, if we would have a large number of signal samples with a significant percent of the being unavailable, that would mean a problem with a lot of unknowns. Then the direct search would not be possible. Here linear programming algorithms for minimization should be used. Their description is out of the scope of this book. For a simplified method to consider this kind of problems see Problem 5.16.

Consider now a signal of the form

$$x(n) = e^{j0.1n^2} e^{j\pi n/4}, \quad \text{for } n = 0, 1, 2, 3, 4, 5, 6, 7$$

whose values are

$$\mathbf{x} = [1, -0.1 + j0.99, -0.92 - j0.39, 0.78 - j0.62, \\ -0.03 + j, -0.6 - j0.8, 0.9 + j0.44, -0.98 - j0.19]^T.$$

Its DFT is not sparse since,

$$\mathbf{X} = [0.05 + j0.44, 0.26 + j0.79, 2 + j1.45, 3.72 - j6, \\ 1.84 + j1.67, 0.13 + j0.84, -0.01 + j0.45, 0.00 + j0.36]^T.$$

Thus, processing within the DFT domain formulation would not produce a satisfactory result. However, the polynomial Fourier transform

$$X(k, \alpha) = \text{DFT}\{x(n)e^{-j\alpha n^2}\}$$

contains a domain where the signal is sparse. Namely, for $\alpha = 0.1$ the signal is sparse in the polynomial DFT domain. A similar situation is in the fractional Fourier domain.

The sparse processing formulation is as follows. Consider the case when some randomly positioned samples are omitted or are not available. The vector with remaining available signal values is \mathbf{y} . Its form with signal values multiplied by $e^{-j\alpha n^2}$ is \mathbf{y}_α . Then the matrix \mathbf{A} is formed by omitting the row in transformation matrix corresponding to unavailable samples. It follows from

$$\mathbf{X}_\alpha = \begin{bmatrix} 1 & 1 & \cdots & 1 \\ 1 & e^{-j2\pi/N} & \cdots & e^{-j2\pi(N-1)/N} \\ \vdots & \vdots & \ddots & \vdots \\ 1 & e^{-j2\pi(N-1)/N} & \cdots & e^{-j2\pi(N-1)(N-1)/N} \end{bmatrix} \begin{bmatrix} x(0) \\ x(1)e^{-j\alpha} \\ \vdots \\ x(N-1)e^{-j\alpha(N-1)^2} \end{bmatrix}.$$

It is the same as in the DFT case. The minimization problem is now

$$\begin{aligned} \min \| \mathbf{X}_\alpha \| & \text{ subject to } \mathbf{y}_\alpha = \mathbf{A} \mathbf{X}_\alpha \\ \text{where } \| \mathbf{X}_\alpha \| &= \sum_{k=0}^{N-1} |X_\alpha(k)|. \end{aligned} \quad (5.150)$$

Minimization is performed with α as parameter (repeating procedure for various possible values of α), and the final solution is the best concentrated \mathbf{X}_α out of the values obtained for all possible α values.

If the number of unavailable values is small, a direct search could be performed over the missing values and the parameter α space. In the case of large number of missing values, sophisticated sparse processing (linear programming) algorithms should be applied (for a simple solution, see also Problem 5.16).

In this way, it is possible to process a signal of the form

$$x(n) = \sum_{i=1}^K e^{j\alpha_0 n^2} e^{j\omega_i n}$$

with different frequencies ω_i and the same chirp rate α_0 . If the chirp rates are different, then formulation is not straightforward.

Consider a signal with unavailable samples, knowing that it is well concentrated and sparse in the Wigner distribution domain. If a small number of samples is missing (eliminated), then we can still calculate the Wigner distribution with missing samples as parameters and find the parameter values (missing samples) that produce the best concentration. For example, they would follow as the ones producing a minimum of

$$\mu[WD(n,k)] = \sum_{k=1}^N \sum_{n=1}^N |WD(n,k)|^{1/2},$$

since the Wigner distribution is energy distribution (the same form we used for an energetic version of the Fourier transform $\| \mathbf{X} \| = \sum_{k=0}^{N-1} |X(k)|$). More often, the measure with power 1 is used rather than $1/2$, corresponding to the l_1 norm. If the exponent is 0, it will be the l_0 norm.

Another approach to the Wigner distribution sparse processing is in the Fourier domain formulation of the Wigner distribution proposed by Flandrin and Borgnat. It is a two-dimensional Fourier transform of the ambiguity function

$$AF(p,l) = \frac{1}{N} \sum_{k=1}^N \sum_{n=1}^N WD(n,k) e^{-j2\pi(np-kl)/N}. \quad (5.151)$$

This relation was used for efficient definition of the reduced interference distribution. The ambiguity function was multiplied by a lowpass kernel function (as explained in detail in Chapter 3). Here we will use a different approach. A large part of the ambiguity domain values will be not multiplied by zero kernel function, but they will just be omitted and considered as unavailable. Only a small region around the ambiguity origin, where we know that the auto-terms are located, is used. Then we try to reconstruct other values (now missing, since we removed them from analysis). Then the linear programming formulation is based on

$$\min \left\| \sum_{k=1}^N \sum_{n=1}^N |WD(n,k)| \right\| \text{ subject to} \quad (5.152)$$

$$\frac{1}{N} \sum_{k=1}^N \sum_{n=1}^N WD(n,k) e^{-j2\pi(np-kl)/N} = AF(p,l), \text{ for } K \text{ selected points in } (p,l).$$

In a matrix form, relation (5.151) can be rewritten as

$$\mathbf{AF}_1 = \mathbf{W}_{2D} \cdot \mathbf{WD}_1$$

where \mathbf{AF}_1 is the matrix column, of the ambiguity function values formed by concatenating all columns into one,

$$AF_1(p + (l-1)N) = AF(p,l).$$

In a similar way, a vector column of the Wigner distribution \mathbf{WD}_1 is formed as

$$WD_1(n + (k-1)N) = WD(n,k),$$

while the matrix of coefficients is an $N^2 \times N^2$ matrix, formed as

$$W_{2D}(p + (l-1)N, n + (k-1)N) = \frac{1}{N} e^{-j2\pi(np-kl)/N}.$$

After the ambiguity function values $AF(p,l)$, for some (p,l) , are removed, then the corresponding rows in \mathbf{W}_{2D} , at $(p + (l-1)N)$, are also removed. The matrix \mathbf{A} is formed, as the matrix with remaining rows of the coefficients matrix \mathbf{W}_{2D} . If we keep 10×10 central values of the ambiguity function, it means that 100 rows of \mathbf{W}_{2D} are used in the matrix \mathbf{A} .

Now, we have a complete formulation of the problem within the sparse signal processing framework. We have reduced the formulation of this problem to

the linear programming problem with norm one. It can be then solved by using appropriate minimization algorithms.

Possible variation of this approach is when using highly concentrated distributions with reduced cross-terms, for example, the S-method. Then the ambiguity function of this distribution $AF_{SM}(p, l)$ is used in the appropriate minimization problem over $SM(n, k)$. In this case, we make two different efforts to the same direction, to obtain a highly concentrated representation without cross-terms. The marginal properties will be satisfied if within the K selected points in (p, l) all the values of $AF(p, l)$ along $p = 0$ or $l = 0$ are included.

Example 5.17. A signal

$$x(n) = \exp(j20\pi t^3 - j29\pi t) + \exp(-t^2) \exp(-j49\pi t) + 1.5 \exp(-(6t)^2) \exp(j21\pi t)$$

is considered within $-1 + 4\Delta t < t < 1 - 6\Delta t$ with step $\Delta t = 1/64$ in lag and $2\Delta t$ in time, with a Hann(ing) window of the width $N = 64$. In the S-method calculation the reference level with $Q = 10$ is used. The pseudo Wigner distribution and the S-method are calculated and matrices of dimension 60×60 (3600 points) are obtained, Fig. 5.9 (upper row). Their nonnegative parts are presented in an image format in Fig. 5.9 (middle row). The two-dimensional Fourier transforms of both the Wigner distribution and the S-method are calculated, transforming them into ambiguity domain. It is then assumed that the ambiguity domain functions are sparse and a mask of size 7×7 (1.4% of the total number of ambiguity points) around the ambiguity domain origin is applied. The sparse Wigner distribution and the S-method are then reconstructed according to (5.152), with linear programming method for the l_1 norm. They are presented in Fig. 5.9(bottom row). It can be concluded that the reconstructed distributions correspond to the original ones with reduced cross-terms. \square

5.9 COMPRESSIVE SENSING AND ROBUST TIME-FREQUENCY ANALYSIS

The compressive sensing (CS) processing of sparse signals was recently used in time-frequency analysis in combination with the L-statistics by Stanković, Orović, Stanković and Amin. Two forms were considered. One form is used to reconstruct the missing measurements in time and/or lag domain, after they are removed by the L-statistics approach, described in Section 5.7.3 (for example, by (5.136)). The other form of compressive sensing application in the time-frequency analysis is to separate a set of time-varying signals from an unknown sparse signal in the Fourier domain, being represented by a sum of sinusoids. Next these two CS based time-frequency forms will be presented.

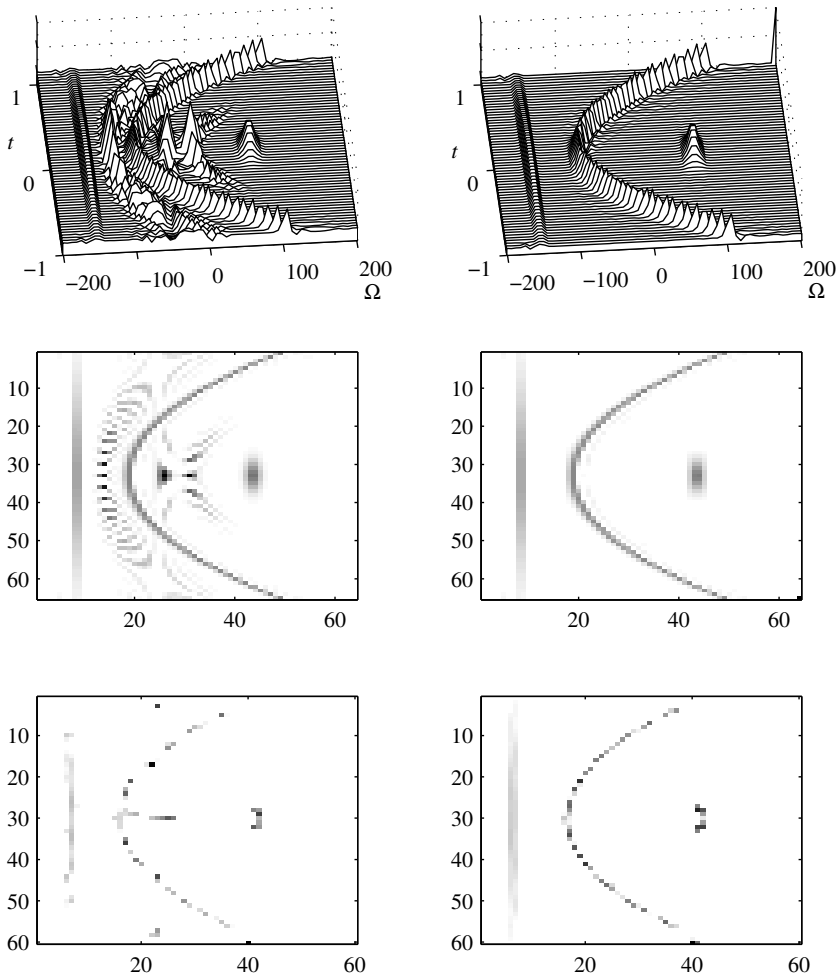


Figure 5.9 The pseudo Wigner distribution and the S-method (upper row). Their nonnegative parts in an image format (middle row). The sparse Wigner distribution and the sparse S-method (bottom row).

5.9.1 Compressive Sensing-Based Processing of the L-estimated Time-Frequency Representations

In the L-estimation form of the time-frequency representations, the highest values of the product of the signal (or local auto-correlation function) and the basis functions are discarded and the mean of the remaining set is calculated. The highest values are assumed to be corrupted by impulse random noise. They are randomly positioned in the time-lag domain. Thus, after the highest values are discarded, the L-estimation may be described as the time-frequency analysis with the remaining (an incomplete set of) signal or local auto-correlation samples. The removal effect is described by using zero signal values at these time-lag instants. It causes an effect similar to noise, smaller than the initial impulse noise, but still significant.

Example 5.18. Consider the STFT of complex sinusoidal signal $s(n) = A \exp(j2\pi k_0 n/N)$ with frequency k_0 . Assume that it contains high impulse noise $\varepsilon(n)$, appearing in $Q\%$ ($Q = 70\%$) of the signal values within a set of N samples, that is, appearing in N_Q signals values. Then the STFT of noisy signal $x(n) = s(n) + \varepsilon(n)$ is

$$STFT(n, k) = \sum_{m=0}^{N-1} (A \exp(j2\pi k_0 (n+m)/N) + \varepsilon(n+m)) e^{-j2\pi m k/N}. \quad (5.153)$$

The result will be unacceptable if the STFT is calculated with impulse noise values (as illustrated in Problem 5.14). Thus, first we have to remove the signal values with a high noise. It is done by discarding the highest $M > N_Q$ values of $|x(n+m)| = |x(n+m)e^{-j2\pi m k/N}|$, as described by (5.137). Let us analyze the result if we just continue with the L-estimation, being the same as using zeros for the discarded $x(n+m)$ values.

Now M of the total number of signal samples are removed and the rest of the samples contain nonnoisy signal $s(n)$. Consider the following cases:

- 1.) Case for $k = k_0$, corresponding to the signal's frequency position. At this frequency, all terms in sum (5.153) are the same and equal to $A \exp(j2\pi k_0 n/N)$. Thus, the L-estimation value of $STFT(n, k_0)$, in notation $STFT_L(n, k)$, after M values are removed, is

$$STFT_L(n, k_0) = (N - M)A \exp(j2\pi k_0 n/N) = (N - M)s(n).$$

- 2.) Case for $k = k_0 + l$, with $l \neq 0$, that is, STFT samples where STFT frequency index does not correspond to the signal frequency. The discarded values in (5.153) are of the form

$$x_l(n, m) = x(n)e^{-j2\pi ml/N}.$$

With respect to the original signal $s(n)$, the disturbance caused by discarding the values is

$$x_l(n, m) = s(n)e^{-j2\pi ml/N}.$$

For a given time instant n , $e^{-j2\pi ml/N}$ randomly assumes a value from the set

$$\Phi = \{e^{-j2\pi ml/N}, m = 0, 1, 2, \dots, M - 1\}. \quad (5.154)$$

The mean value of $x_l(n, m)$ is

$$E\{x_l(n, m)\} = 0$$

resulting in

$$E\{STFT_L(n, k)\} = (N - M)s(n)\delta(k - k_0).$$

In this process, M statistically independent signal samples are removed from the STFT summation. With respect to the nonnoisy signal $s(n)$, this is the same as setting its value to zero. It corresponds to a new disturbance (noise)

$$\varepsilon_L(n) = \begin{cases} 0 & \text{for remaining signal samples} \\ -s(n) = -Ae^{j2\pi k_0 n/N} & \text{for removed signal samples.} \end{cases}$$

Since samples are removed randomly, the variance of the STFT with removed samples is

$$\sigma_L^2 = MA^2, \text{ for } k \neq k_0.$$

Therefore, by using the L-estimation (necessary to remove high impulse noise), the detection is still compromised in two ways: (1) reduced value of $|STFT(n, k_0)|$ to $|STFT_L(n, k_0)| = A(N - M)$, for $k = k_0$, and (2) random variations of $STFT_L(n, k)$, with variance $\sigma_L^2 = MA^2$, for $k \neq k_0$, are introduced, corresponding to noise. \square

Example 5.19. Consider the signal

$$s(n) = e^{j12\pi n/N} + e^{j18\pi n/N}, N = 64,$$

with 75% of its arbitrary positioned values, being unavailable (Fig. 5.10(b)). The unavailable values in this CS signal may be due to the avoiding the signal values contaminated by a high impulse noise or due to the CS measurements of the signal itself. The standard STFT transform of this CS signal, calculated at $n = 0$, is shown in Fig. 5.10(c). Next, the robust STFT of the CS signal is calculated in five iterations, according to (5.126), from the previous section. It is presented in Fig. 5.10(d). Since, this procedure is sensitive to different amplitudes in the signal components, it could be considered just as one simplified way to process a CS signal. A solution could also be obtained by using the method presented in Problem 5.16. \square

Example 5.20. If the result of a minimization process is a sparse function, then the cost function that would count a number of nonzero error values is,

$$\mathbf{F}(e) = |e|^{1/p}, \quad (5.155)$$

with $p \rightarrow \infty$,

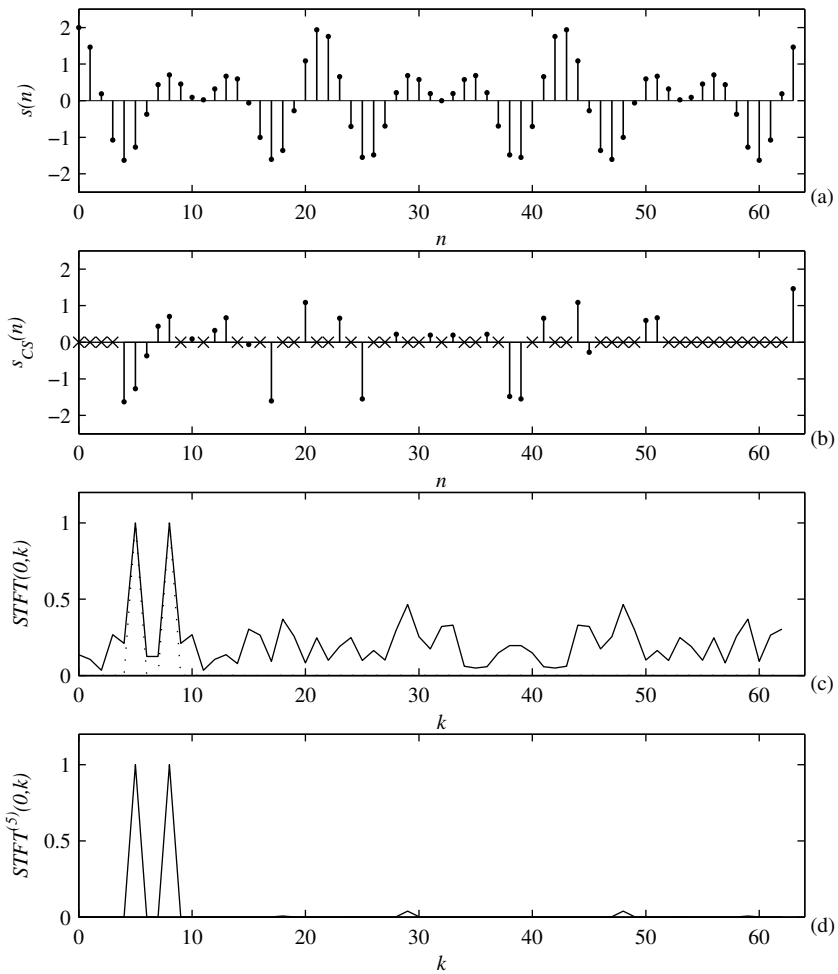


Figure 5.10 (a) Original signal, (b) CS signal with 75% unavailable randomly positioned values, denoted by "x" (or omitted values due to a high impulse noise contamination), (c) the standard STFT of the CS signal, and (d) the robust STFT of the CS, after five iterations. Real parts of signals are presented in (a) and (b), while the absolute normalized values of the transforms are presented in (c) and (d).

This function, as a concentration measure, would minimize the number of nonzero values in the result. It has been discussed as a concentration measure in Chapter 2. This loss function corresponds to the l_0 norm. In implementations, an approximation of the l_0 norm based loss function in the form $\mathbf{F}(e) = 1 - \exp(-p|e|)$ with large p is used as well. However, the minimization with the loss function of the form (5.155) corresponding to the l_0 norm is quite complex. Thus, the l_1 norm is considered as a good trade-off between a good matching of the loss function form to the error distribution and the calculation complexity. \square

The original time-frequency representation (here the STFT) could be restored if we assume that it is sparse in the frequency domain, for a considered time instant n . Then the remaining values, after the L-statistics-based elimination, denoted by $\mathbf{x}_{CS}(n)$, are processed by using the CS methods as

$$\begin{aligned} \min \| \mathbf{STFT}(n) \| &= \min \sum_{k=0}^{N-1} |STFT(n, k)| \\ \text{subject to } \mathbf{x}_{CS}(n) &= \mathbf{A}_{CS} \mathbf{STFT}(n), \end{aligned} \quad (5.156)$$

where \mathbf{A}_{CS} is the inverse Fourier transform matrix with removed rows corresponding to the removed signal values in $\mathbf{x}_{CS}(n)$.

In the case of the Wigner distribution, the CS formulation for reconstructing the distribution, after the L-estimation (when high noise samples in the local auto-correlation function are removed) is

$$\begin{aligned} \min \| \mathbf{WD}(n) \| &= \min \sum_{k=0}^{N-1} |WD(n, k)| \text{ subject to} \\ \mathbf{r}_{CS}(n) &= \mathbf{A}_{CS} \mathbf{WD}(n), \end{aligned} \quad (5.157)$$

where $\mathbf{r}_{CS}(n)$ are the remaining values of the local auto-correlation function vector

$$\mathbf{r}(n) = [..., x(n-1)x^*(n+1), x(n)x^*(n), x(n+1)x^*(n-1), ...]$$

after the L-statistics is applied and heavily corrupted values in $\mathbf{r}(n)$ are removed. The matrix \mathbf{A}_{CS} is the inverse Fourier transform (corresponding to the Wigner distribution calculation, based on the local auto-correlation function), with removed rows for discarded values in $\mathbf{r}(n)$.

If the conditions assumed here are satisfied then, by using the L-estimation, we remove the samples with high impulse noise, and then based on the rest of the signal (local auto-correlation) values, we achieve almost perfect reconstruction of nonnoisy time-frequency representations, for example, $STFT_s(n, k)$ or $WD_s(n, k)$.

5.9.2 CS-Based Separation of Signals in Time-Frequency Domain

A time-frequency domain CS approach has been used to separate a set of time-varying signals from an unknown sparse signal in the Fourier domain, being represented by a sum of sinusoids (stationary signals). It is assumed that these two sets of components overlap in a significant part of the time-frequency plane. Different components of a stationary sparse signal intersect nonstationary components at different time-varying points. By removing a large number of overlapping points or intervals, a signal with large number of missing measurements in the time-frequency plane is formed, corresponding to a CS signal with a frequency-varying CS matrix. The CS observations are taken in the time-frequency domain, rather than in the time domain. It is difficult to imagine such a situation if we look at the signal in the time or frequency domain separately. However, this situation can be easily found in time-frequency problem formulations. This case can be encountered in radar signal processing, where in many applications there are micro-Doppler effects that can obscure rigid body points, rendering the radar image ineffective. A similar situation may, for example, appear in communications, when narrowband signals are disturbed by a frequency-hopping jammer that is of shorter duration than the considered time interval. Any other nonstationary jammer, with high values and a large number of crossing points, leads to the same time-frequency varying CS formulation. Since we assumed that components overlap in a significant part of the time-frequency plane here we will use linear signal transforms in order to avoid dealing with emphatic cross-terms, spread over the entire time-frequency or ambiguity plane. Since the final aim is the signal reconstruction, by using linear time-frequency representations the components phases will be preserved.

The theory presented here may be considered as the CS approach in the time-frequency domain being applied to a time-frequency varying form of the STFT. The standard CS approach in the time domain can be viewed as a special case. In the standard CS definition, some points in the time domain are not available. In the time-frequency domain it would mean that these values are not available for some time intervals and all frequencies, corresponding to these intervals. Thus, the standard CS approach in the time domain is just a special case of the case with missing arbitrary positioned measurements in the time-frequency domain.

Consider a signal $x(n)$ of length N and its Fourier transform $X(k)$. The STFT, with a rectangular window of the width M , is

$$STFT(n, k) = \sum_{m=0}^{M-1} x(n+m)e^{-j2\pi mk/M}.$$

In matrix form, it can be written as

$$\text{STFT}_M(n) = \mathbf{W}_M \mathbf{x}(n)$$

where $\text{STFT}_M(n)$ and $\mathbf{x}(n)$ are vectors defined as

$$\begin{aligned}\text{STFT}_M(n) &= [STFT(n,0), STFT(n,1), \dots, STFT(n,M-1)]^T \\ \mathbf{x}(n) &= [x(n), x(n+1), \dots, x(n+M-1)]^T\end{aligned}\quad (5.158)$$

and \mathbf{W}_M is the $M \times M$ Fourier transform matrix with coefficients $W(m,k) = \exp(-j2\pi km/M)$.

After calculating the value of $\text{STFT}_M(n)$, assume first that the STFT do not overlap in the time domain. Then the next STFT will be calculated at the instant $n+M$ as follows

$$\text{STFT}_M(n+M) = \mathbf{W}_M \mathbf{x}(n+M).$$

All the STFT vectors, calculated at $n = 0, M, 2M, \dots, N-M$ (with N/M being an integer) may be written in one resulting vector as

$$\begin{bmatrix} \text{STFT}_M(0) \\ \text{STFT}_M(M) \\ \vdots \\ \text{STFT}_M(N-M) \end{bmatrix} = \begin{bmatrix} \mathbf{W}_M & \mathbf{0}_M & \dots & \mathbf{0}_M \\ \mathbf{0}_M & \mathbf{W}_M & \dots & \mathbf{0}_M \\ \vdots & \vdots & \ddots & \vdots \\ \mathbf{0}_M & \mathbf{0}_M & \dots & \mathbf{W}_M \end{bmatrix} \begin{bmatrix} \mathbf{x}(0) \\ \mathbf{x}(M) \\ \vdots \\ \mathbf{x}(N-M) \end{bmatrix} \quad (5.159)$$

where $\mathbf{0}_M$ is an $M \times M$ zero matrix.

The vector $[\mathbf{x}(0), \mathbf{x}(M), \dots, \mathbf{x}(N-M)]^T$ is the signal vector,

$$[x(0), x(1), \dots, x(N-1)]^T = [\mathbf{x}(0), \mathbf{x}(M), \dots, \mathbf{x}(N-M)]^T = \mathbf{x}.$$

Since we are going to minimize the sum of the signal's DFT absolute values, we will rewrite the previous matrix relation in terms of the DFT of the signal

$$\begin{bmatrix} \text{STFT}_M(0) \\ \text{STFT}_M(M) \\ \vdots \\ \text{STFT}_M(N-M) \end{bmatrix} = \begin{bmatrix} \mathbf{W}_M & \mathbf{0}_M & \dots & \mathbf{0}_M \\ \mathbf{0}_M & \mathbf{W}_M & \dots & \mathbf{0}_M \\ \vdots & \vdots & \ddots & \vdots \\ \mathbf{0}_M & \mathbf{0}_M & \dots & \mathbf{W}_M \end{bmatrix} \mathbf{W}_N^{-1} \begin{bmatrix} X(0) \\ X(1) \\ \vdots \\ X(N-1) \end{bmatrix} \quad (5.160)$$

where \mathbf{W}_N^{-1} denotes $N \times N$ the inverse DFT matrix, since

$$\mathbf{x} = \mathbf{W}_N^{-1} \mathbf{X},$$

where \mathbf{X} is the DFT vector. Finally, we may write the STFT values in terms of the DFT as

$$\mathbf{STFT} = \mathbf{A} \mathbf{X}.$$

As previously explained, we will not use all the STFT points, since a large number of them will be considered as corrupted and thus will be omitted. Consequently, they will be considered as unavailable. This corresponds to the CS approach in the time-frequency domain, where only some of the STFT values (measurements) are available.

The separation of time-frequency points, that can be declared as the CS points (intervals), belonging to the sparse stationary signal, will be done using the L-statistics. For each frequency k , a vector of STFT in time is formed

$$\mathbf{S}_k(n) = [STFT(n, k), n = 0, M, \dots, N - M].$$

After sorting the elements of $\mathbf{S}_k(n)$, for a given frequency k , we obtain a new ordered set of elements

$$\Psi_k(n) \in \mathbf{S}_k(n)$$

such that

$$|\Psi_k(0)| \leq |\Psi_k(M)| \leq \dots \leq |\Psi_k(N - M)|.$$

In the L-statistics form, we omit N_Q of the highest values of $\Psi_k(n)$ for each k . Note that, in some cases, the overlapping components of the same order of amplitude may decrease the intersection value. This happens when a disturbing component of the same value crosses the desired signal with the opposite phase. These cases may also efficiently be treated within the L-statistics framework, by omitting some of the lowest L-statistics values, in addition to N_Q highest values. The omitted values of the STFT are heavily corrupted. Thus, they are declared as useless or unavailable in the CS framework. The rest of the STFT values is considered as CS in the time-frequency plane.

Denote now the vector of available STFT values by \mathbf{STFT}_{CS} . The corresponding CS matrix \mathbf{A}_{CS} is formed by omitting the rows corresponding to the omitted STFT values. We want to reconstruct the original sparse stationary signal, since it produces the best concentrated Fourier transform $X(k)$. Therefore, the corresponding minimization problem can be defined as follows

$$\min \|\mathbf{X}\| = \min \sum_{k=0}^{N-1} |X(k)| \quad (5.161)$$

subject to $\mathbf{STFT}_{CS} = \mathbf{A}_{CS} \mathbf{X}$.

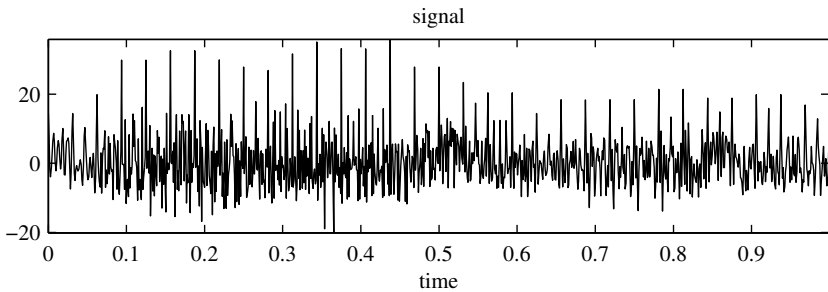


Figure 5.11 Signal composed of a stationary part (sparse in frequency domain) and nonstationary part.

Thus, based on the STFT_{CS} values, we are going to reconstruct the missing values such to provide minimal $\sum_{k=0}^{N-1} |X(k)|$. This is a well-known CS formulation of the problem that can be solved by using linear programming tools.

Example 5.21. In this example, we consider a signal that consists four complex sinusoids

$$x(n) = e^{j256\pi n/N} + 1.5e^{-j256\pi n/N+j\pi/8} + 0.7e^{j512\pi n/N+j\pi/4} + e^{-j512\pi n/N-j\pi/3},$$

with nonstationary disturbance in form of several short duration sinusoidal signals (some of them are at the same frequencies as the stationary sinusoids) and four sinusoidally modulated signals. The signal in the time domain is shown in Fig. 5.11.

Its STFT is calculated for $N = 1024$ and $M = 32$. The STFT of the signal is presented in Fig. 5.12 (left). After the L-statistics is performed and 50% of the largest values are removed, along with 10% of the smallest values, the CS form of the STFT, with only 40% of the original values, is obtained (Fig. 5.12 (middle)). The STFT values that remained after the L-statistics based removal are shown in Fig. 5.12 (right). The reconstruction is performed, based on the STFT values from Fig. 5.12 (right). The reconstructed signal's Fourier transform is equal to the original Fourier transform, preserving amplitude and phase. Its amplitude is shown in Fig. 5.13 (bottom), along with the original Fourier transform of the signal Fig. 5.13 (top). \square

5.9.3 Compressive Sensing and Signal Inversion in Overlapping STFT

Consider now an overlapping case, with, for example, a Hann(ing) window of the width M with time step $M/2$ in the STFT calculation. Here we may get a simple, CS convenient, matrix formulation. The STFT with a Hann(ing) (or any other window)

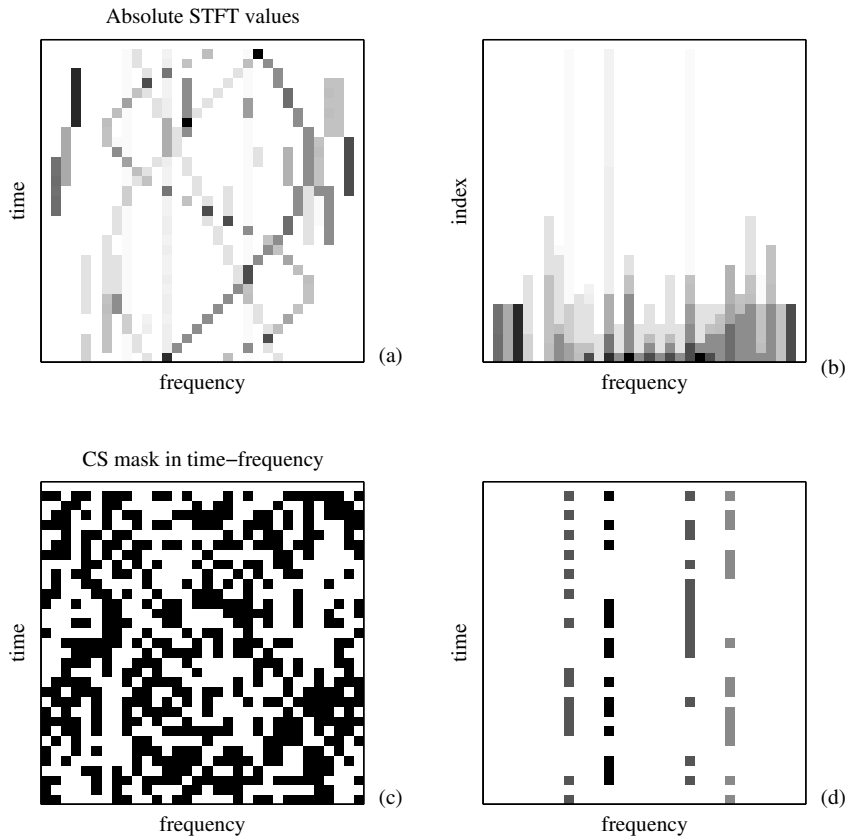


Figure 5.12 (a) The STFT of the composite signal. (b) Its sorted values. (c) The compressive sensing mask corresponding to the L-statistics-based STFT values. (d) The STFT values that remain after applying the compressive sensing mask on the absolute values of the STFT.

may be written in matrix form as

$$\begin{aligned}
 STFT(n, k) &= \sum_{m=0}^{M-1} w(m) x(n+m) e^{-j2\pi mk/M} \\
 &= \mathbf{W}_M \mathbf{H}_M \mathbf{x}(n),
 \end{aligned} \tag{5.162}$$

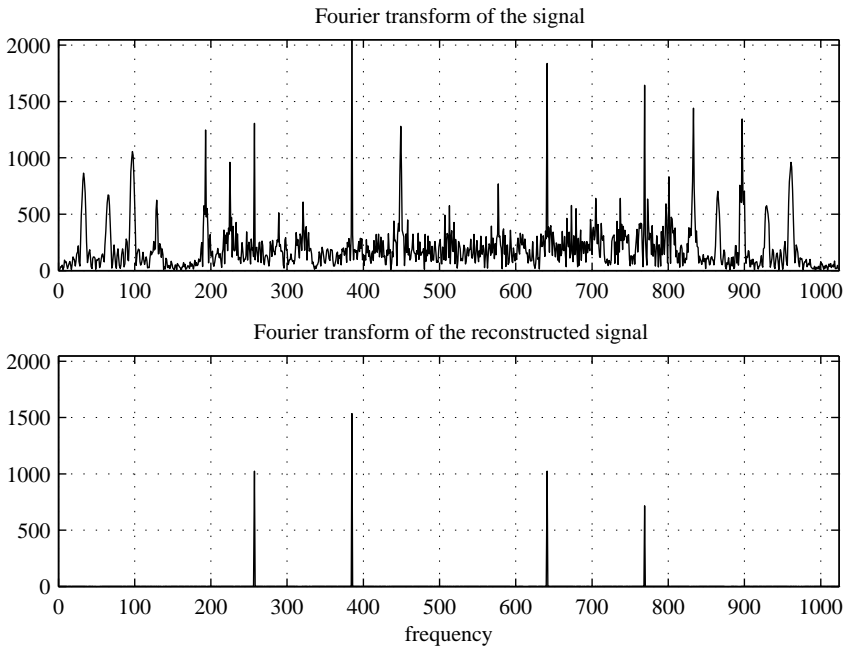


Figure 5.13 Reconstructed Fourier transform by using the compressive sensing values of the STFT presented in Fig. 5.12(d) corresponding to stationary part of the composite signal (bottom) and the Fourier transform of the composite signal (top).

where \mathbf{H}_M is a diagonal $M \times M$ matrix with the window values on the diagonal, $H(i, i) = w(i)$, $i = 0, 1, \dots, M - 1$. In addition, introduce the first STFT with a half of the window width, as

$$STFT_{1/2}(0, k) = \sum_{m=0}^{M/2-1} w(M/2 + m)x(m)e^{-j2\pi mk/(M/2)} = \mathbf{W}_{M/2}\mathbf{H}_{M/2}^+\mathbf{x}_{M/2}(0)$$

Here $\mathbf{H}_{M/2}^+$ denotes a diagonal $M/2 \times M/2$ matrix,

$$H_{M/2}^+(i, i) = w(i + M/2), \quad i = 0, 1, \dots, M/2 - 1$$

and

$$\mathbf{x}_{M/2}(0) = [x(0), x(1), \dots, x(M/2 - 1)]^T.$$

In the same way, the last STFT, with a half of the window, is defined as

$$\begin{aligned} STFT_{1/2}(N - M/2, k) &= \sum_{m=0}^{M/2-1} w(m)x(N - M/2 + m)e^{-j2\pi mk/(M/2)} \\ &= \mathbf{W}_{M/2}\mathbf{H}_{M/2}^-\mathbf{x}_{M/2}(N - M/2), \end{aligned}$$

where $\mathbf{H}_{M/2}^-$ denotes a diagonal $M/2 \times M/2$ matrix

$$H_{M/2}^-(i, i) = w(i), i = 0, 1, \dots, M/2 - 1,$$

and

$$\mathbf{x}_{M/2}(N - M/2) = [x(N - M/2), \dots, x(N - 2), x(N - 1)]^T.$$

Now it is possible to split the calculation into two nonoverlapping sets

$$\begin{aligned} \begin{bmatrix} STFT_M(0) \\ STFT_M(M) \\ \dots \\ STFT_M(N - M) \end{bmatrix} &= \begin{bmatrix} \mathbf{W}_M & \mathbf{0}_M & \dots & \mathbf{0}_M \\ \mathbf{0}_M & \mathbf{W}_M & \dots & \mathbf{0}_M \\ \dots & \dots & \dots & \dots \\ \mathbf{0}_M & \mathbf{0}_M & \dots & \mathbf{W}_M \end{bmatrix} \\ &\times \begin{bmatrix} \mathbf{H}_M & \mathbf{0}_M & \dots & \mathbf{0}_M \\ \mathbf{0}_M & \mathbf{H}_M & \dots & \mathbf{0}_M \\ \dots & \dots & \dots & \dots \\ \mathbf{0}_M & \mathbf{0}_M & \dots & \mathbf{H}_M \end{bmatrix} \begin{bmatrix} \mathbf{x}(0) \\ \mathbf{x}(M) \\ \dots \\ \mathbf{x}(N - M) \end{bmatrix}, \end{aligned} \quad (5.163)$$

or in a full matrix notation

$$\mathbf{STFT} = \mathbf{W}_{M,N}\mathbf{H}_{M,N}\mathbf{x},$$

where $\mathbf{W}_{M,N}$ and $\mathbf{H}_{M,N}$ denotes the transformation and the window matrices of $M \times M$, extended in blocks into $N \times N$ matrix, according to the previous detailed

matrix relation. The other nonoverlapping set is

$$\begin{bmatrix} \text{STFT}_{M/2}(0) \\ \text{STFT}_M(M/2) \\ \vdots \\ \text{STFT}_M(N-3M/2) \\ \text{STFT}_{M/2}(N-M/2) \end{bmatrix} = \begin{bmatrix} \mathbf{W}_{M/2} & \mathbf{0} & \dots & \mathbf{0} & \mathbf{0} \\ \mathbf{0} & \mathbf{W}_M & \dots & \mathbf{0} & \mathbf{0} \\ \vdots & \vdots & \ddots & \vdots & \vdots \\ \mathbf{0} & \mathbf{0} & \dots & \mathbf{W}_M & \mathbf{0} \\ \mathbf{0} & \mathbf{0} & \dots & \mathbf{0} & \mathbf{W}_{M/2} \end{bmatrix} \times \begin{bmatrix} \mathbf{H}_{M/2}^+ & \mathbf{0} & \dots & \mathbf{0} & \mathbf{0} \\ \mathbf{0} & \mathbf{H}_M & \dots & \mathbf{0} & \mathbf{0} \\ \vdots & \vdots & \ddots & \vdots & \vdots \\ \mathbf{0} & \mathbf{0} & \dots & \mathbf{H}_M & \mathbf{0} \\ \mathbf{0} & \mathbf{0} & \dots & \mathbf{0} & \mathbf{H}_{M/2}^- \end{bmatrix} \begin{bmatrix} \mathbf{x}_{M/2}(0) \\ \mathbf{x}(M/2) \\ \vdots \\ \mathbf{x}(N-3M/2) \\ \mathbf{x}_{M/2}(N-M/2) \end{bmatrix},$$

or

$$\text{STFT}^{1/2} = \mathbf{W}_{M,N}^{1/2} \mathbf{H}_{M,N}^{1/2} \mathbf{x},$$

where $\mathbf{W}_{M,N}^{1/2}$ and $\mathbf{H}_{M,N}^{1/2}$ are notations of the transformation and the window matrices of $M \times M$, extended in blocks into $N \times N$ matrix. However, here the first and the last block are made by using a half size matrices, $M/2 \times M/2$, as in the previous detailed matrix relation, and $\text{STFT}^{1/2}$ denotes corresponding STFT matrix.

Let us just note that the inversion (important to get a result free of the block effects) follows from

$$\mathbf{H}_{M,N} \mathbf{x} + \mathbf{H}_{M,N}^{1/2} \mathbf{x} = (\mathbf{H}_{M,N} + \mathbf{H}_{M,N}^{1/2}) \mathbf{x} = \mathbf{I}_N \mathbf{x} = \mathbf{x}.$$

The same inversion relation holds for the Hamming and triangular windows. It can be extended, in straightforward way, to other overlappings and time steps of $M/4, M/8, M/16, \dots, 1$ (Chapter 2).

The CS formulation for the overlapping case is

$$\begin{bmatrix} \text{STFT} \\ \text{STFT}^{1/2} \end{bmatrix} = \begin{bmatrix} \mathbf{W}_{M,N} \mathbf{H}_{M,N} \\ \mathbf{W}_{M,N}^{1/2} \mathbf{H}_{M,N}^{1/2} \end{bmatrix} \mathbf{x},$$

resulting in

$$\begin{bmatrix} \text{STFT} \\ \text{STFT}^{1/2} \end{bmatrix} = \begin{bmatrix} \mathbf{W}_{M,N} \mathbf{H}_{M,N} \\ \mathbf{W}_{M,N}^{1/2} \mathbf{H}_{M,N}^{1/2} \end{bmatrix} \mathbf{W}_N^{-1} \mathbf{x}. \quad (5.164)$$

In general, the values in **STFT** and **STFT**^{1/2} are related in neighboring time instants. In general, disturbance can be high in one STFT, at one frequency, while in a neighboring STFT it could be significantly reduced at that frequency. In this way, by using overlapped STFTs, we may improve time resolution of the separation.

The approach has been extended to the time- and frequency-varying windows, including linear frequency-modulated signals, sparse in the local polynomial Fourier domain. The time-varying windows are easily included by using varying window widths in (5.160). As an example of frequency varying windows let us consider a form that corresponds to the wavelet lattice in time-frequency plane.

5.9.4 Compressive Sensing Formulation with Frequency-Varying Windows (Wavelets)

The STFT can be calculated using the signal's Fourier transform instead of the signal itself. There is a direct relation between the time domain and the frequency domain STFT via coefficients of the form $\exp(j2\pi nk/M)$.

A dual form of the STFT is

$$\begin{aligned} \text{STFT}(n, k) &= \frac{1}{M} \sum_{m=0}^{M-1} X(k+m) e^{j2\pi mn/M}, \\ \text{STFT}_M(k) &= \mathbf{W}_M^{-1} \mathbf{X}(k), \end{aligned} \quad (5.165)$$

where a rectangular frequency-domain window of the width M is assumed. Now we can repeat the analysis from the time domain. A form corresponding to frequency-varying windows is

$$\begin{bmatrix} \text{STFT}_{M_0}(0) \\ \text{STFT}_{M_1}(M_0) \\ \vdots \\ \text{STFT}_{M_L}(N-M_L) \end{bmatrix} = \begin{bmatrix} \mathbf{W}_{M_0}^{-1} & \mathbf{0} & \dots & \mathbf{0} \\ \mathbf{0} & \mathbf{W}_{M_1}^{-1} & \dots & \mathbf{0} \\ \dots & \dots & \dots & \dots \\ \mathbf{0} & \mathbf{0} & \dots & \mathbf{W}_{M_L}^{-1} \end{bmatrix} \begin{bmatrix} X(0) \\ X(1) \\ \vdots \\ X(N-1) \end{bmatrix}. \quad (5.166)$$

Its CS form is obtained by omitting the unavailable STFT values and corresponding rows in the transformation matrix.

For example, a special form of the frequency-varying windows is a form corresponding to a wavelet transform, when

$$\begin{bmatrix} \text{STFT}_1(0) \\ \text{STFT}_1(1) \\ \text{STFT}_2(2) \\ \text{STFT}_4(4) \\ \dots \\ \text{STFT}_{N/2}(N/2) \end{bmatrix} = \begin{bmatrix} 1 & 0 & 0 & \dots & \dots & 0 \\ 0 & 1 & 0 & \dots & \dots & 0 \\ 0 & 0 & \mathbf{W}_2^{-1} & 0 & \dots & 0 \\ \dots & \dots & \dots & \mathbf{W}_4^{-1} & \dots & 0 \\ \dots & \dots & \dots & \dots & \dots & 0 \\ 0 & 0 & 0 & 0 & \dots & \mathbf{W}_{N/2}^{-1} \end{bmatrix} \begin{bmatrix} X(0) \\ X(1) \\ X(2) \\ \dots \\ X(N-1) \end{bmatrix}$$

Here for low frequencies, $k = 0$ and $k = 1$, the best frequency resolution is achieved (without time resolution) by using the Fourier transform itself, $\text{STFT}_1(0) = X(0)$. Note that $X(0)$ is here just a scalar. Then in each step, the time resolution is improved by a factor of 2, decreasing the frequency resolution for the same factor.

The CS formulation, when some of the STFT (wavelet) coefficients are missing, for this kind of problem is

$$\begin{aligned} \min \|\mathbf{X}\| &= \min \sum_{k=0}^{N-1} |X(k)| \\ \text{subject to } \text{STFT}_{CS} &= \mathbf{A}_{CS} \mathbf{X} \end{aligned} \quad (5.167)$$

where STFT_{CS} is the CS matrix of the STFT (wavelet) coefficients and \mathbf{A}_{CS} is the corresponding transformation matrix, with omitted rows for unavailable values. \square

5.10 WIGNER SPECTRUM AND TIME-VARYING FILTERING

In the case of random signals, the expected value of the Wigner distribution, the Wigner spectrum, is used instead of the Wigner distribution,. It is defined as

$$E\{WD(t, \Omega)\} = \int_{-\infty}^{\infty} E\left\{x\left(t + \frac{\tau}{2}\right)x^*\left(t - \frac{\tau}{2}\right)\right\} e^{-j\Omega\tau} d\tau. \quad (5.168)$$

Properties of this spectrum may be derived in analogy with the case of the Wigner distribution.

In the case of the random multicomponent signals

$$x(t) = \sum_{i=1}^M x_i(t),$$

when the components are not correlated,

$$\mathbb{E}\{x_i(t_1)x_j^*(t_2)\} = 0 \text{ for } i \neq j,$$

the Wigner spectrum is equal to the sum of the expected values of individual components

$$\begin{aligned} \mathbb{E}\{WD(t, \Omega)\} &= \sum_{i=1}^M \int_{-\infty}^{\infty} \mathbb{E}\left\{x_i\left(t + \frac{\tau}{2}\right)x_i^*\left(t - \frac{\tau}{2}\right)\right\} e^{-j\Omega\tau} d\tau \\ &= \sum_{i=1}^M \mathbb{E}\{WD_{x_i}(t, \Omega)\}. \end{aligned} \quad (5.169)$$

Thus, the problem of cross-terms does not exist in the Wigner spectrum, if we are able to use a large number of random signals belonging to the same random process.

Analysis and processing of stationary signals are usually performed either in the time domain or in the frequency domain. However, when signals exhibit nonstationary characteristics more efficient processing of such signals may be done by using joint time-frequency domain tools, which are based on time-frequency representations.

Time-varying filtering is one of challenging areas where one may benefit from the joint time-frequency representations. It is defined as

$$y(t) = H\{x(t)\} = \int_{-\infty}^{\infty} h(t, \tau)x(\tau)d\tau, \quad (5.170)$$

where $h(t, \tau)$ is the impulse response of the time-varying system H . If the signal $x(t)$ is a sum of a desired signal $s(t)$ and noise $v(t)$, then the optimal system H may be determined by minimizing the mean square error

$$H_{\text{opt}} = \arg \min_H \mathbb{E} \left\{ |s(t) - H\{x(t)\}|^2 \right\}. \quad (5.171)$$

The ideal case would be a system that produces

$$\begin{aligned} H\{x(t)\} &= s(t) \\ H\{v(t)\} &= 0. \end{aligned} \quad (5.172)$$

Time-varying filtering may produce better results, in the nonstationary signal cases, than processing of signals in either the time or the frequency domain separately.

However, in the definition of time-varying filtering, there is a certain amount of freedom that has resulted in several solutions for this approach.

Example 5.22. Here we will present a solution based on the following formulation of the time-varying filtering

$$y(t) = H\{x(t)\} = \int_{-\infty}^{\infty} h\left(t + \frac{\tau}{2}, t - \frac{\tau}{2}\right) x(t + \tau) d\tau. \quad (5.173)$$

The optimal value of H will be derived by analogy with the Wiener filter in the stationary signal cases. For the nonstationary stochastic process $x(t) = s(t) + v(t)$, we know that when the mean square error $e^2 = E\{|s(t) - y(t)|^2\}$ reaches its minimum, the error $s(t) - y(t)$ is orthogonal to the data $x^*(t + \alpha)$. From this fact we get

$$E\left\{ \left(s(t) - \int_{-\infty}^{\infty} h\left(t + \frac{\tau}{2}, t - \frac{\tau}{2}\right) x(t + \tau) d\tau \right) x^*(t + \alpha) \right\} = 0. \quad (5.174)$$

The expected value of the ambiguity function is defined by

$$E\{AF_{xx}(\theta, \tau)\} = \int_{-\infty}^{\infty} E\left\{ x\left(t + \frac{\tau}{2}\right) x^*\left(t - \frac{\tau}{2}\right) \right\} e^{-j\theta t} dt.$$

Taking the Fourier transform of (5.174) over t , by using appropriate substitutions

$$\int_{-\infty}^{\infty} E\{s(t)x^*(t + \alpha)\} e^{-j\theta t} dt = E\{AF_{sx}(\theta, -\alpha)\} e^{j\alpha\theta/2}$$

and

$$\int_{-\infty}^{\infty} E\{x(t + \tau)x^*(t + \alpha)\} e^{-j\theta t} dt = E\{AF_{xx}(\theta, \tau - \alpha)\} e^{j(\alpha+\tau)\theta/2}$$

we get

$$E\{AF_{sx}(\theta, \alpha)\} e^{-j\alpha\theta/2} = \int_{-\infty}^{\infty} \int_{-\infty}^{\infty} A_H(u, -\tau) E\{AF_{xx}(\theta - u, \alpha - \tau)\} e^{-j\frac{(\alpha+\tau)(\theta-u)}{2}} d\tau du \quad (5.175)$$

where

$$A_H(\theta, \tau) = \int_{-\infty}^{\infty} h\left(t + \frac{\tau}{2}, t - \frac{\tau}{2}\right) e^{-j\theta t} dt. \quad (5.176)$$

In the cases when we can assume that

$$|\theta\tau - u\alpha - u\tau|/2 \ll \pi,$$

when $e^{j(\theta\tau - u\alpha - u\tau)/2} \cong 1$, (5.175) can be simplified as

$$\mathbb{E}\{AF_{sx}(\theta, \alpha)\} = \int_{-\infty}^{\infty} \int_{-\infty}^{\infty} A_H(u, -\tau) \mathbb{E}\{AF_{xx}(\theta - u, \alpha - \tau)\} d\tau du. \quad (5.177)$$

Taking the two-dimensional Fourier transform of (5.177), we get

$$\mathbb{E}\{WD_{sx}(t, \Omega)\} = L_H(t, \Omega) \mathbb{E}\{WD_{xx}(t, \Omega)\}$$

where

$$\begin{aligned} \mathbb{E}\{WD_{xx}(t, \Omega)\} &= \text{FT}_{\theta, \alpha}^{\text{2D}} \{ \mathbb{E}\{AF_{xx}(\theta, \alpha)\} \} \\ &= \int_{-\infty}^{\infty} \mathbb{E}\left\{ x\left(t + \frac{\tau}{2}\right) x^*\left(t - \frac{\tau}{2}\right) \right\} e^{-j\Omega\tau} d\tau \end{aligned}$$

is the Wigner spectrum. The Weyl symbol of the filter impulse response is denoted by

$$L_H(t, \Omega) = \int_{-\infty}^{\infty} h\left(t + \frac{\tau}{2}, t - \frac{\tau}{2}\right) e^{-j\Omega\tau} d\tau. \quad (5.178)$$

Therefore, the optimal filter in time-frequency domain is defined by

$$L_H(t, \Omega) = \frac{\mathbb{E}\{WD_{sx}(t, \Omega)\}}{\mathbb{E}\{WD_{xx}(t, \Omega)\}} \quad (5.179)$$

which corresponds to the well-known Wiener filter in the stationary cases $H(\Omega) = S_{sx}(\Omega)/S_{xx}(\Omega)$; here $S_{sx}(\Omega) = \text{FT}\{r_{sx}(\tau)\}$, since $r_{sx}(\alpha) = \mathbb{E}\{s(t)x^*(t + \alpha)\}$ and $r_{xx}(\tau - \alpha) = \mathbb{E}\{x(t + \tau)x^*(t + \alpha)\}$.

For a signal not correlated with noise follows

$$L_H(t, \Omega) = \frac{\mathbb{E}\{WD_{ss}(t, \Omega)\}}{\mathbb{E}\{WD_{ss}(t, \Omega)\} + \mathbb{E}\{WD_{vv}(t, \Omega)\}}. \quad (5.180)$$

This expression may be used in the filter optimization for nonstationary processes.

□

5.11 PROBLEMS

Problem 5.1. Find the auto-correlation

$$R_{STFT}(n_1, k_1, n_2, k_2) = E\{STFT(n_1, k_1)STFT^*(n_2, k_2)\}$$

of the STFT values

$$STFT(n, k) = \sum_{m=0}^{N-1} x(n+m)e^{-j2\pi km/N},$$

if the signal $x(n) = \varepsilon(n)$ is complex Gaussian, zero mean white noise, with independent real and imaginary parts of equal variances, $R_{\varepsilon\varepsilon}(n) = \sigma_\varepsilon^2 \delta(n)$. The STFT values are calculated for instants $n, n+N, \dots, N+kN, \dots$, that is, without overlapping. What is the value of auto-correlation if the Hann(ing) window is used with overlapping in time for a half of the window length?

Problem 5.2. Find the auto-correlation

$$R_{WD}(n_1, k_1, n_2, k_2) = E\{WD(n_1, k_1)WD(n_2, k_2)\}$$

of the Wigner distribution values

$$WD(n, k) = \sum_{m=0}^{N-1} x(n+m)x^*(n-m)e^{-j4\pi km/N},$$

if the signal $x(n) = \varepsilon(n)$ is the complex Gaussian, zero mean white noise, with independent real and imaginary parts of equal variances, $R_{\varepsilon\varepsilon}(n) = \sigma_\varepsilon^2 \delta(n)$. What is the value of auto-covariance of the Wigner distribution?

Problem 5.3. Show that the expected value of the Wigner distribution of random signal

$$x(t) = \sum_{i=1}^M A_i(t)e^{j(\phi_i(t)+\varphi_i)},$$

where the phases φ_i are random, statistically independent, uniformly distributed values over $[0, 2\pi)$, is cross-terms free.

Problem 5.4. Consider the STFT of a sampled signal $x(n) = Ae^{j2\pi k_0 n} + \varepsilon(n)$. Noise samples $\varepsilon(n)$ are the complex Gaussian, zero mean white noise, with independent real and imaginary parts of equal variances, $R_{\varepsilon\varepsilon}(n) = \sigma_\varepsilon^2 \delta(n)$. We want to estimate the STFT of nonnoisy signal with a rectangular window. What is the MSE and what is the MSE ratio when the rectangular and the Hann(ing) windows are used?

Problem 5.5. Consider N samples of a noisy signal $x(n) = e^{j(2\pi nk_0/N + an^2)} + \varepsilon(n)$, where $\varepsilon(n)$ is the complex Gaussian, zero mean white noise, with independent real and imaginary parts of equal variances, $R_{\varepsilon\varepsilon}(n) = \sigma_\varepsilon^2 \delta(n)$. We want to estimate the Wigner distribution with a rectangular window, but we use in the calculation: (a) Hann(ing) window, (b) the squared value of the Hann(ing) window, and (c) the Blackman window of the width N in

$$WD(n, k) = \sum_{m=0}^{N-1} w(m)x(n+m)x^*(n-m)e^{-j4\pi km/N}.$$

In all three cases calculate the mean square error, being measure of the calculated distribution expected deviation from the nonnoisy Wigner distribution with a rectangular window.

Problem 5.6. Consider a noisy signal $x(n) = f(n) + \varepsilon_a(n)$, when the noise $\varepsilon_a(n)$ is an analytic part of a stationary noise with $S_{\varepsilon_a}(\omega) = \text{FT}\{R_{\varepsilon_a\varepsilon_a}(n-m)\} = 2\sigma_\varepsilon^2$ for $\omega > 0$ and $S_{\varepsilon_a\varepsilon_a}(\omega) = 0$ for $\omega < 0$. The periodicity in ω is assumed for any discrete-time signal. Find the mean value and the variance of the Wigner distribution.

Problem 5.7. The Wigner distribution is calculated by using special hardware where the normalized signal values are stored in registers b bits long. A lag window with N samples is used in calculation. The signal values and the results of arithmetic operations are rounded as well. Fixed point arithmetic is used. The quantized values of a complex-valued signal could be written as $x(n) = f(n) + \varepsilon(n)$, where $\varepsilon(n) = \varepsilon_r(n) + j\varepsilon_i(n)$ is a random uniformly distributed quantization noise, $-2^{-b}/2 \leq \varepsilon_r(n) < 2^{-b}/2$ and $-2^{-b}/2 \leq \varepsilon_i(n) < 2^{-b}/2$. (a) Write a model for the Wigner distribution calculation by using these registers. (b) Find the mean and the variance of the Wigner distribution, and (c) write the noise-to-signal ratio in the case when the input signal $f(n)$ is a complex-valued Gaussian random signal with independent real and imaginary parts of equal variances. The total signal variance is σ_f^2 .

Problem 5.8. Consider a function

$$f(\theta) = \sum_{n=-\infty}^{\infty} jnF_n e^{j\theta n}.$$

Assume that it has zero value at $\theta = \theta_0$. Write the linearization model for the zero value position of a disturbed function

$$f_d(\theta) = \sum_{n=-\infty}^{\infty} jn(F_n + v_n) e^{j\Delta\phi(n)} e^{j\theta n}$$

with small disturbances v_n and $\Delta\varphi(n)$.

Problem 5.9. Consider an arbitrary continuous and differentiable function $f(\theta)$, having zero value at $\theta = \theta_0$. Assume that there are a small additive and a small shift disturbance factor $v(\theta)$ and $\mu(\theta)$, respectively. Then instead of $f(\theta)$, use a function $f_d(\theta)$ described by

$$f_d(\theta) = f(\theta + \mu(\theta)) + v(\theta).$$

Find the shift of the zero value position for $f_d(\theta)$ with respect to $f(\theta)$.

Problem 5.10. Consider samples of a signal $x(t) = e^{j(a_0+a_1t+a_2t^2+a_3t^3)}$ taken at Δt , with a small instantaneous frequency deviations from the linear one, that is, a_3 is small. The instantaneous frequency is estimated by using the pseudo Wigner distribution

$$PWD(t, \Omega) = \sum_{m=-\infty}^{\infty} w_h(m\Delta t) x(t - m\Delta t) x^*(t + m\Delta t) e^{-j2\Omega m\Delta t},$$

where the window $w_h(m\Delta t) = w_0(m\Delta t/h)\Delta t/h$ is used, with $w_0(t)$ being rectangular window of the width $|t| \leq 1/2$. Write the linearization model for the instantaneous frequency estimation for this signal and find the expression for the estimation error. If the frequency is estimated without a frequency-domain interpolation (or any other technique for reducing frequency domain discretization error), find the mean square estimation error and the optimal window width.

Problem 5.11. For the signal $x(t) = e^{j(a_0+a_1t+a_2t^2+a_3t^3/6)} + \varepsilon(t)$, with small a_3 and $\varepsilon(t)$, the Wigner distribution is used for the instantaneous frequency estimation, by using the following set of windows

$$\{w_0(m\Delta t), w_1(m\Delta t), w_2(m\Delta t), \dots\}$$

where $w_h(m\Delta t) = w_0^h(m\Delta t)\Delta t$ with $w_0(t)$ being Hann(ing) window of the width $|t| \leq 1/2$. Find the optimal window form as a function of a_3 and σ_ε^2 .

Problem 5.12. We have measured and estimated a random variable $\mathbf{x}(t)$, for example the instantaneous frequency, at an instant t , by using parameters $h = \{1, 2, 4, 8, 16, 32, 64, 128\}$ and obtained the values

$$\{0.0037, -0.1438, 0.1294, 0.0337, 0.1470, 0.1999, 0.5114, 2.0413\}.$$

(a) Our knowledge about the bias behavior is not reliable, except that a distribution of random variable could be considered as Gaussian with variance, as function of parameter h , being $\text{var}\{\mathbf{x}(t)\} = 0.1/h$. Assume that, for the optimal value of h , the bias and variance are of the same order. What is the best estimate of $\mathbf{x}(t)$?

(b) We know the bias behavior of this random variable is $\text{bias}\{\mathbf{x}(t)\} = B(t)h^2$, with a signal-dependent unknown value $B(t)$, while the variance as function of parameter h is $\text{var}\{\mathbf{x}(t)\} = \sigma^2(h) = 0.1/h$. What is the best estimate of the value of $\mathbf{x}(t)$?

Problem 5.13. Consider the sinc distribution with kernel

$$c(\theta\tau) = \begin{cases} 1 & \text{for } |\theta\tau| < 1/2 \\ 0, & \text{elsewhere.} \end{cases}$$

In the time-frequency analysis its finite ambiguity domain region is used $|\theta| < 5$, $|\tau| < 5$. The analyzed signal is a linear frequency-modulated one, $x(t) = s(t) + \varepsilon(t)$, with $s(t) = A \exp(jat^2/2)$ for $0 \leq a \leq 1$. Noise is a Gaussian complex zero mean with independent real and imaginary parts of variance $\sigma_\varepsilon^2/2$. Samples of signal and noise, sampled at Δt , are available. Find the maximal distribution value in the case of nonnoisy signal, as a function of a . Find the variance of this distribution for the noise only. Find the ratio of the maximal distribution value and deviation $\sigma_{\varepsilon\varepsilon}$. Using the symmetry, write the value of this ratio, for example, for $a = -2$ (find the corresponding value of a within $0 \leq a \leq 1$).

Problem 5.14. Calculate:

(a) The STFT of eight samples signals $x(n) = s(n) + \varepsilon(n) = \exp(j6\pi n/8) + \varepsilon(n)$ at $n = 0$ with impulse noise

$$\varepsilon(m) = [0.01, -0.13, 0.17, 0.02, 15.5, -0.035, 11.2, 0.05],$$

by definition.

(b) By using the L-statistics-based definition, when two the largest samples of the local-correlation function multiplied by basis functions $(s(m)e^{-j2\pi mk/8})$ are removed.

(c) After two samples are removed (the same case as if they were not available in advance), find estimates of two values of $s(m)$ for the removed m by a direct search over all values ranging from the minimal amplitude m_0 to the maximal amplitude M_0 in the rest of the signal values. Take the amplitude and the phase increment as $s(m) = (m_0 + 0.1p)\exp(-jq)$ where p ranges from 0 up to

$m_0 + 0.1p = M_0$ and q ranges from 0 to 2π with step $\pi/10$. Out of the STFT values plot the best concentrated one with minimal measure

$$\mu[STFT(n, k)] = \frac{(\sum_n \sum_k |STFT(n, k)|^{2/p})^p}{\sum_n \sum_k |STFT(n, k)|^2}$$

with $p = 2$.

Problem 5.15. Calculate the Wigner distribution at $n = 0$ of nine samples signals $x(n) = s(n) + \varepsilon(n) = \exp(j\pi(n+1)^2/9) + \varepsilon(n)$ with impulse noise $\varepsilon(n) = [0.1, -0.3, 0.7, 0.2, 15.5, -0.35, 11.2, 0.5, .1]$, for $n = -4, -3, \dots, 3, 4$ in a direct way, by definition

$$WD(0, k/2) = \sum_{m=-4}^4 x(0+m)x^*(0-m)e^{-j2\pi km/9}.$$

Compare the result with the L-statistics-based one when the three largest samples of the local-correlation function multiplied by basis functions $(s(m)s^*(-m)e^{-j2\pi mk/9})$ are removed. What is the result if $\varepsilon(0) = 755.5$ and $\varepsilon(2) = 531.4$?

Problem 5.16. Consider a discrete signal

$$x(n) = 1.2e^{j2\pi n/16+j\pi/4} + 1.5e^{j14\pi n/16-j\pi/3} + 1.7e^{j12\pi n/16},$$

for $0 \leq n \leq 15$, sparse in the DFT domain since only three DFT values are different than zero. Assume now that its samples $x(2), x(4), x(11)$, and $x(14)$ are not available (CS signal). Show that, in this case, the exact DFT reconstruction may be achieved by: (1) calculating the initial DFT estimate by setting unavailable sample values to zero, (2) detecting the positions of maximal three DFT values, k_{01}, k_{02} , and k_{03} , and (3) Calculating the reconstructed DFT values at k_{01}, k_{02} , and k_{03} from system

$$\sum_{i=1}^3 X(k_{0i})e^{j2\pi k_{0i}n_{cs}/16} = x(n_{cs}),$$

where n_{cs} are the instants where the signal is available. Since there are more equations than unknowns, the system $\mathbf{AX} = \mathbf{B}$, could be solved, in the least square sense, by using MATLAB operation $\mathbf{X} = \mathbf{A} \setminus \mathbf{B}$.

Problem 5.17. Write a MATLAB function for the pseudo Wigner distribution-based instantaneous frequency estimation. Inputs are signal samples and a window

for pseudo Wigner distribution calculation while output should be estimated discrete frequency. Assume that signal is complex with instantaneous frequency within the interval $[-\frac{\pi}{2}, \frac{\pi}{2}]$. Additionally, write code for the instantaneous frequency estimation in the case of the signal

$$x(t) = \exp(j16\sin(\pi t/64) + j6\sin(\pi t/48))$$

sampled with $\Delta t = 1$, corrupted with complex Gaussian noise with total variance $\sigma^2 = 0.25$. The instantaneous frequency estimation should be performed over time interval $0 \leq t \leq 511$. Use a 129-point Hann(ing) window for the pseudo Wigner distribution calculation.

Problem 5.18. Write a code for smoothing the signal $x(t) = f(t) + \varepsilon(t)$, $f(t) = 1/(1+(t/7.5)^{40})$, within the interval $|t| < 25$, with the step $\Delta t = 1/25$. Additive Gaussian white noise, with standard deviation $\sigma_\varepsilon = 0.1$, is assumed. Smoothing should be done by adaptive window width. Values $\kappa = 2$ and $\Delta\kappa = 1$ are used. Compare the results with the ones obtained with one narrow window and one wide window. The set of smoothing window widths is $h \in \{0, 1, 2, 4, 8, 16, 128, 256, 512\}$.

Problem 5.19. Write a code for the robust STFT calculation by using the median of the real and imaginary parts of the transform, as well as by using the iterative procedure. Signal is of the form $s(n) = \exp(j12\pi n/N) + \exp(j20\pi n/N)$, while the noise is Cauchy impulse noise of the form $\chi(n) = \varepsilon_1^3(n) + j\varepsilon_2^3(n)$, where $\varepsilon_1(n)$ and $\varepsilon_2(n)$ are the Gaussian noises with unity variance. Total number of points in calculation is $N = 64$, while the stopping criterion in the iterative procedure is when the transform absolute values changes for less than 1% of the maximal transform value in two subsequent iterations. Maximal number of iterations is 15.

5.12 SOLUTIONS

Solution 5.1. The auto-correlation of the STFT values in the case of nonoverlapping calculation with rectangular window is

$$\begin{aligned} R_{STFT}(n_1, k_1, n_2, k_2) &= E\{STFT(n_1, k_1)STFT^*(n_2, k_2)\} \\ &= \sum_{m_1=0}^{N-1} \sum_{m_2=0}^{N-1} E\{\varepsilon(n_1+m_1)\varepsilon^*(n_2+m_2)\} e^{-j2\pi(m_1k_1-m_2k_2)/N}. \end{aligned}$$

Since the STFT values do not overlap, relation between n_1 and n_2 is $n_1 = kN + n_2$. Thus, it is not possible that noise in $\varepsilon(n_1+m_1)$ and $\varepsilon^*(n_2+m_2)$ assume the same

value of argument for $k \neq 0$. Therefore,

$$\mathbb{E}\{\varepsilon(n_1 + m_1)\varepsilon^*(n_2 + m_2)\} = 0,$$

except for $n_1 = n_2$ when

$$\mathbb{E}\{\varepsilon(n_1 + m_1)\varepsilon^*(n_1 + m_2)\} = \sigma_\varepsilon^2 \delta(m_1 - m_2),$$

producing

$$\begin{aligned} R_{STFT}(n_1, k_1, n_2, k_2) &= \delta(n_1 - n_2) \sigma_\varepsilon^2 \sum_{m=0}^{N-1} e^{-j2\pi m(k_1 - k_2)/N} \\ &= N \sigma_\varepsilon^2 \delta(n_1 - n_2) \delta(k_1 - k_2). \end{aligned}$$

Solution 5.2. The auto-correlation of the Wigner distribution values

$$\begin{aligned} R_{WD}(n_1, k_1, n_2, k_2) &= \mathbb{E}\{WD(n_1, k_1)WD^*(n_2, k_2)\} \\ &= \sum_{m_1=0}^{N-1} \sum_{m_2=0}^{N-1} \mathbb{E}\{\varepsilon(n_1 + m_1)\varepsilon^*(n_1 - m_1)\varepsilon^*(n_2 + m_2)\varepsilon(n_2 - m_2)\} e^{-j4\pi(m_1 k_1 - m_2 k_2)/N} \\ &= \sum_{m_1=0}^{N-1} \sum_{m_2=0}^{N-1} \sigma_\varepsilon^4 [\delta(2m_1)\delta(2m_2) + \delta(n_1 + m_1 - n_2 - m_2)\delta(n_2 - m_2 - n_1 + m_1)] \\ &\quad \times e^{-j4\pi(m_1 k_1 - m_2 k_2)/N} \\ &= \sigma_\varepsilon^4 + \sigma_\varepsilon^4 \delta(n_1 - n_2) \sum_{m=0}^{N-1} e^{-j4\pi m(k_1 - k_2)/N} = \sigma_\varepsilon^4 [1 + N\delta(n_1 - n_2)\delta(k_1 - k_2)], \end{aligned}$$

since $\delta(2(k_1 - k_2)) = \delta(k_1 - k_2)$ within the basic frequency period. The auto-covariance is

$$\begin{aligned} c_{WD}(n_1, k_1, n_2, k_2) &= \mathbb{E}\{[WD(n_1, k_1) - \mathbb{E}\{WD(n_1, k_1)\}][WD^*(n_1, k_1) - \mathbb{E}\{WD^*(n_1, k_1)\}]\} \\ &= R_{WD}(n_1, k_1, n_2, k_2) - \mathbb{E}^2\{WD(n_1, k_1)\} \\ &= \sigma_\varepsilon^4 N \delta(n_1 - n_2) \delta(k_1 - k_2). \end{aligned}$$

Therefore, the Wigner distribution values of a Gaussian complex white noise, with independent real and imaginary parts, behave as a two-dimensional white noise.

Solution 5.3. The expected value of the Wigner distribution of signal

$$x(t) = \sum_{i=1}^M A_i(t) e^{j(\phi_i(t) + \varphi_i)}$$

is

$$\mathbb{E}\{WD(t, \Omega)\} = \sum_{i=1}^M \sum_{k=1}^M \int_{-\infty}^{\infty} A_i(t + \frac{\tau}{2}) A_k(t - \frac{\tau}{2}) e^{j(\phi_i(t + \frac{\tau}{2}) - \phi_k(t - \frac{\tau}{2}))} \mathbb{E}\{e^{j\varphi_i - j\varphi_k}\} e^{-j\Omega\tau} d\tau.$$

Since $\mathbb{E}\{e^{j\varphi_i - j\varphi_k}\} = \delta(i - k)$, all cross-terms are averaged out, so we get the auto-terms only,

$$\mathbb{E}\{WD(t, \Omega)\} = \sum_{i=1}^M \int_{-\infty}^{\infty} A_i(t + \frac{\tau}{2}) A_i(t - \frac{\tau}{2}) e^{j(\phi_i(t + \frac{\tau}{2}) - \phi_i(t - \frac{\tau}{2}))} e^{-j\Omega\tau} d\tau.$$

Solution 5.4. The STFT of this signal is

$$STFT(n, k) = \sum_{m=-N/2}^{N/2-1} w(m) x(n+m) e^{-j2\pi mk/N}.$$

In the case of a rectangular window, we have

$$STFT(n, k) = NA\delta(k - k_0) + \sum_{m=-N/2}^{N/2-1} \varepsilon(n+m) e^{-j2\pi mk/N},$$

with mean

$$\mathbb{E}\{STFT(n, k)\} = NA\delta(k - k_0)$$

and variance

$$\text{var}\{STFT(n, k)\} = N\sigma_{\varepsilon}^2.$$

Means square error, in this case, is

$$MSE_R = N\sigma_{\varepsilon}^2.$$

In the case of the Hann(ing) window, we get

$$\mathbb{E}\{STFT(n, k)\} = \frac{N}{2}A\delta(k - k_0) + \frac{N}{4}A\delta(k - k_0 + 1) + \frac{N}{4}A\delta(k - k_0 - 1)$$

and

$$\text{var}\{STFT(n, k)\} = \sigma_\varepsilon^2 \sum_{m=-N/2}^{N/2-1} w^2(m) = \frac{3}{8} \sigma_\varepsilon^2 N.$$

Thus, the transform is spread (degraded) and the variance is reduced. The mean square error, if the rectangular window form (a delta pulse for a sinusoidal signal) is considered as the ideal one, is

$$\begin{aligned} MSE_H &= \sum_{k=0}^{N-1} A^2 \left[N\delta(k-k_0) - \frac{N}{2}\delta(k-k_0) - \frac{N}{4}\delta(k-k_0+1) - \frac{N}{4}\delta(k-k_0-1) \right]^2 \\ &\quad + \frac{3}{8}\sigma_\varepsilon^2 N = \frac{3}{8}N^2A^2 + \frac{3}{8}\sigma_\varepsilon^2 N. \end{aligned}$$

The ratio of the MSEs in these two cases is

$$\frac{MSE_H}{MSE_R} = \frac{\frac{3}{8}N^2A^2 + \frac{3}{8}\sigma_\varepsilon^2 N}{\sigma_\varepsilon^2 N} = \frac{3}{8}N\frac{A^2}{\sigma_\varepsilon^2} + \frac{3}{8}.$$

Solution 5.5. For the signal $x(n) = \exp(j(2\pi nk_0/N + an^2)) + \varepsilon(n)$, the Wigner distribution is of the form

$$\begin{aligned} WD(n, k) &= \sum_{m=0}^{N-1} w(m) [e^{j(4\pi mk_0/N + 4ann)} + e^{j(2\pi(n+m)k_0/N + a(n+m)^2)} \varepsilon^*(n-m) \\ &\quad + \varepsilon(n+m)e^{-j(2\pi(n-m)k_0/N + a(n-m)^2)} + \varepsilon(n+m)\varepsilon^*(n-m)] e^{-j4\pi km/N}. \end{aligned}$$

Its expected value for the rectangular, Hann(ing), squared Hann(ing), and Blackman windows is:

$$\begin{aligned} E\{WD_R(n, k)\} &= N\delta(k_0 + an\frac{N}{\pi}), \\ E\{WD_H(n, k)\} &= \frac{N}{2}\delta(k_0 + an\frac{N}{\pi}) + \frac{N}{4}\delta(k_0 + an\frac{N}{\pi} + 1) + \frac{N}{4}\delta(k_0 + an\frac{N}{\pi} - 1), \\ E\{WD_{H^2}(n, k)\} &= \frac{3N}{8}\delta(k_0 + an\frac{N}{\pi}) + \frac{N}{4}\delta(k_0 + an\frac{N}{\pi} + 1) + \frac{N}{16}\delta(k_0 + an\frac{N}{\pi} + 2) \\ &\quad + \frac{N}{4}\delta(k_0 + an\frac{N}{\pi} - 1) + \frac{N}{16}\delta(k_0 + an\frac{N}{\pi} - 2), \\ E\{WD_B(n, k)\} &= 0.42N\delta(k_0 + an\frac{N}{\pi}) + 0.25N\delta(k_0 + an\frac{N}{\pi} + 1) \\ &\quad + 0.04N\delta(k_0 + an\frac{N}{\pi} + 2) + 0.25N\delta(k_0 + an\frac{N}{\pi} - 1) + 0.04N\delta(k_0 + an\frac{N}{\pi} - 2). \end{aligned}$$

It is assumed that anN/π is an integer, for the considered instant n . The variance in all of these cases are obtained from

$$\text{var}\{WD(n,k)\} = \sigma_\varepsilon^2 \sum_{m=0}^{N-1} w^2(m)(2 + \sigma_\varepsilon^2).$$

By using Parseval's theorem and knowing the Fourier transforms of each of the previous windows, easily follows,

$$\text{var}\{WD_R(n,k)\} = (2 + \sigma_\varepsilon^2)\sigma_\varepsilon^2 N,$$

$$\text{var}\{WD_H(n,k)\} = (2 + \sigma_\varepsilon^2)\sigma_\varepsilon^2 \left(\frac{N}{4} + \frac{N}{16} + \frac{N}{16}\right) = 3(2 + \sigma_\varepsilon^2)\sigma_\varepsilon^2 N/8,$$

$$\begin{aligned} \text{var}\{WD_{H^2}(n,k)\} &= (2 + \sigma_\varepsilon^2)\sigma_\varepsilon^2 \left(\frac{9N}{64} + \frac{N}{16} + \frac{N}{256} + \frac{N}{16} + \frac{N}{256}\right) \\ &= (2 + \sigma_\varepsilon^2) \frac{35\sigma_\varepsilon^2}{128} N, \end{aligned}$$

$$\begin{aligned} \text{var}\{WD_B(n,k)\} &= (2 + \sigma_\varepsilon^2)\sigma_\varepsilon^2 N(0.1764 + 0.0625 + 0.0016 + 0.0625 + 0.0016) \\ &= 0.3046(2 + \sigma_\varepsilon^2)\sigma_\varepsilon^2 N. \end{aligned}$$

The MSE is calculated, for example, for the Hann(ing) window, as

$$MSE_H = (\text{E}\{WD_H(n,k) - WD_R(n,k)\})^2 + \text{var}\{WD_H(n,k)\}.$$

Solution 5.6. The analytic part of a noise $\varepsilon(n)$ is defined by

$$\varepsilon_a(n) = \varepsilon(n) + j\varepsilon_h(n)$$

where $\varepsilon_h(n)$ is the Hilbert transform of $\varepsilon(n)$. The analytic signal is commonly used in the calculation of the Wigner distribution. In that case the noise has real and imaginary parts that are related via the Hilbert transform, thus being correlated. If the spectral power density of the input noise is $\sigma_\varepsilon^2/2$, the spectral power density of analytic noise is

$$S_{\varepsilon_a \varepsilon_a}(\omega) = 2\sigma_\varepsilon^2 u(\omega)$$

for $|\omega| < \pi$, where $u(\omega)$ is the step function.

For the analytic signal, the variance component, depending on the noise only, is given by

$$\begin{aligned} \text{var}\{WD_{\varepsilon_a}(n, \omega)\} &= E\left\{\sum_{m_1=-\infty}^{\infty} \sum_{m_2=-\infty}^{\infty} \varepsilon_a(n+m_1) \varepsilon_a^*(n-m_1) e^{-j2\omega m_1} \right. \\ &\quad \times \left. \varepsilon_a^*(n+m_2) \varepsilon_a(n-m_2) e^{j2\omega m_2}\right\} - \\ &- \sum_{m_1=-\infty}^{\infty} \sum_{m_2=-\infty}^{\infty} E\{\varepsilon_a(n+m_1) \varepsilon_a^*(n-m_1)\} e^{-j2\omega m_1} \\ &\quad \times E\{\varepsilon_a^*(n+m_2) \varepsilon_a(n-m_2)\} e^{j2\omega m_2}. \end{aligned}$$

Using $E\{z_1 z_2 z_3 z_4\} = E\{z_1 z_2\}E\{z_3 z_4\} + E\{z_1 z_3\}E\{z_2 z_4\} + E\{z_1 z_4\}E\{z_2 z_3\}$ and

$$\begin{aligned} R_{\varepsilon_a \varepsilon_a}(m_1 - m_2) &= E\{\varepsilon_a(n+m_1) \varepsilon_a^*(n+m_2)\} \\ R_{\varepsilon_a \varepsilon_a^*}(m_1 + m_2) &= E\{\varepsilon_a(n+m_1) \varepsilon_a(n-m_2)\} = 0 \end{aligned}$$

follows

$$\text{var}\{WD_{\varepsilon_a}(n, \omega)\} = \sum_{m_1=-\infty}^{\infty} \sum_{m_2=-\infty}^{\infty} R_{\varepsilon_a \varepsilon_a}(m_1 - m_2) e^{-j2\omega(m_1 - m_2)}.$$

for $|2\omega| < \pi$. It may be interpreted as a sum of the Fourier transform of the product $R_{\varepsilon_a \varepsilon_a}(m)R_{\varepsilon_a \varepsilon_a}(m)$ where $m = m_1 - m_2$, that is,

$$\text{var}\{WD_{\varepsilon_a}(n, \omega)\} = \sum_{m_1=-\infty}^{\infty} S_{\varepsilon_a \varepsilon_a}(2\omega) *_{\omega} S_{\varepsilon_a \varepsilon_a}(2\omega),$$

since $S_{\varepsilon_a \varepsilon_a}(\omega) = \text{FT}\{R_{\varepsilon_a \varepsilon_a}(m)\}$. For $S_{\varepsilon_a \varepsilon_a}(\omega) = 2\sigma_{\varepsilon}^2 u(\omega)$ the convolution is

$$S_{\varepsilon_a \varepsilon_a}(2\omega) *_{\omega} S_{\varepsilon_a \varepsilon_a}(2\omega) = 4\sigma_{\varepsilon}^4 |\omega/\pi|$$

within the basic period of ω . Therefore

$$\text{var}\{WD_{\varepsilon_a}(n, \omega)\} = \lim_{L \rightarrow \infty} \left\{ 4\sigma_{\varepsilon}^4 \sum_{m_1=-L}^L |\omega/\pi| \right\} = 4\sigma_{\varepsilon}^4 |\omega/\pi| \lim_{L \rightarrow \infty} (2L+1).$$

The signal-dependent part of variance is

$$\sigma_{f\varepsilon}^2 = \sum_{m_1=-\infty}^{\infty} \sum_{m_2=-\infty}^{\infty} [f(n+m_1) f^*(n+m_2) R_{\varepsilon_a \varepsilon_a}(m_1 - m_2)]$$

$$+f^*(n-m_1)f(n-m_2)R_{\varepsilon_a\varepsilon_a}(m_1-m_2)]e^{-j2\omega(m_1-m_2)}.$$

The previous expression can be understood as

$$\sigma_{f\varepsilon}^2 = \sum_{m_1=-\infty}^{\infty} \{f(n+m_1)[f^*(n+m_1)*_{m_1} R_{\varepsilon_a\varepsilon_a}(m_1)e^{-j2\omega m_1}]$$

$$+f^*(n-m_1)[f(n-m_1)*_{m_1} R_{\varepsilon_a\varepsilon_a}(m_1)e^{-j2\omega m_1}]\}$$

where $*_{m_1}$ denotes convolution in m_1 .

Using Parseval's theorem

$$\begin{aligned} & \sum_{m_1=-\infty}^{\infty} f(n+m_1) \times [f^*(n+m_1)*_{m_1} R_{\varepsilon_a\varepsilon_a}(m_1)e^{-j2\omega m_1}] \\ &= \frac{1}{2\pi} \int_{-\pi}^{\pi} \text{FT}\{f(n+m_1)\} \times \text{FT}^*\{[f(n+m_1)*_{m_1} R_{\varepsilon_a\varepsilon_a}^*(m_1)e^{j2\omega m_1}]\} d\theta \end{aligned}$$

we get

$$\begin{aligned} \sigma_{f\varepsilon}^2 &= \frac{2}{2\pi} \int_{-\pi}^{\pi} |F(e^{j\theta})|^2 S_{\varepsilon_a\varepsilon_a}(2\omega - \theta) d\theta \\ &= \frac{4}{2\pi} \sigma_{\varepsilon}^2 \left\{ \begin{array}{ll} \int_0^{2\omega} |F(e^{j\theta})|^2 d\theta & 0 \leq \omega < \pi/2 \\ \int_{\pi+2\omega}^{\pi} |F(e^{j\theta})|^2 d\theta & -\pi/2 \leq \omega < 0 \end{array} \right. \\ &\leq 4E_f \sigma_{\varepsilon}^2. \end{aligned} \quad (5.181)$$

We can see that both components are strongly dependent on ω and equal to zero for $\omega = 0$. Besides, $\sigma_{f\varepsilon}^2$ is a nondecreasing function, where ω ranges from 0 to $\pi/2$. The variance reaches maximum for $|\omega| = \pi/2$, the maximum values being $\sigma_{xx}^2 = 4E_f \sigma_{\varepsilon}^2 + 2N\sigma_{\varepsilon}^4$, where E_f is the energy of the analytic signal $f(n)$.

Solution 5.7. (a) The effects of quantization of the signal $f(n)$ are modeled by the additive noise $\varepsilon(n)$. Thus, the Wigner distribution is calculated for a noisy signal signal $x(n) = f(n) + \varepsilon(n)$, where the noise $\varepsilon(n) = \varepsilon_r(n) + j\varepsilon_i(n)$ is a random uniformly distributed noise $-2^{-b}/2 \leq \varepsilon_r(n), \varepsilon_i(n) < 2^{-b}/2$. Its variance is $\sigma_{\varepsilon}^2 =$

$2\sigma_b^2 = 2 \cdot 2^{-2b} / 12$. The Wigner distribution model for analysis is

$$\begin{aligned} WD(n, m) &= \sum_{k=-L}^L \{[x(n+k)x^*(n-k) + e(n, k)]e^{-j\frac{4\pi}{N}km} + \mu(n, k, m)\} \\ &= WD_x(n, m) + \sum_{k=-L}^L [e(n, k)e^{-j\frac{4\pi}{N}km} + \mu(n, k, m)] \end{aligned}$$

where $e(n, k)$ and $\mu(n, k, m)$ are also quantization noises due to the quantization of the product $x(n+k)x^*(n-k)$ and its product with the basis functions $e^{-j4\pi km/N}$ (with $N = 2L+1$). They are also uniform noises with variances $\sigma_e^2 = \sigma_\mu^2 = 4\sigma_b^2 = 2^{-2b}/3$. In the last expression we have taken into account all the quantization errors except the one of the basis functions.

(b) The mean and variance of the Wigner distribution are

$$\begin{aligned} E\{WD(n, m)\} &= E\{WD_x(n, m)\} = WD_f(n, m) + \sigma_\epsilon^2, \\ \sigma_{WD}^2 &= \sigma_x^2 + N\sigma_e^2 + N\sigma_\mu^2 = \sigma_x^2 + \frac{N}{3}2^{-2b} \end{aligned}$$

where σ_x^2 is the variance of $WD_x(n, m)$.

(c) For a random Gaussian input signal $\sigma_x^2 = \text{var}\{WD_x(n, m)\} \cong N(\sigma_f^2 + \sigma_\epsilon^2)^2$. The noise-to-signal ratio (NSR) will be defined as

$$NSR = \frac{\sigma_{WD}^2 - \sigma_{WD| \text{without quantization noise}}^2}{\sigma_{WD| \text{without quantization noise}}^2}. \quad (5.182)$$

where $\sigma_{WD| \text{without quantization noise}}^2 = N\sigma_f^4$ for the white complex random signal with the variance σ_f^2 . Thus, we have

$$NSR = (2\sigma_\epsilon^2\sigma_f^2 + \sigma_\epsilon^4 + \sigma_e^2 + \sigma_\mu^2)/\sigma_f^4. \quad (5.183)$$

The direct calculation of DFT, by its definition, is rarely used in practice. However, for the fixed-point arithmetic the same results are valid for the FFT algorithms.

Solution 5.8. For a function

$$f(\theta) = \sum_{n=-\infty}^{\infty} jnF_n e^{j\theta n}$$

with a zero value at $\theta = \theta_0$, the model of disturbed function

$$f_d(\theta) = \sum_{n=-\infty}^{\infty} jn(F_n + v_n)e^{j\theta n}e^{j\Delta\varphi(n)}$$

with small disturbances v_n and $\Delta\varphi(n)$, produces the position of zero of $f_d(\theta)$ that will be shifted due to the disturbances. Assume that this shift $\Delta\theta = \theta - \theta_0$, caused by small v_n and $\Delta\varphi(n)$, is also small. Thus, the zero value of $f_d(\theta)$ is

$$\begin{aligned} f_d(\theta_0 + \Delta\theta) = 0 &= \sum_{n=-\infty}^{\infty} jn(F_n + v_n)e^{j(\theta_0 + \Delta\theta)n}e^{j\Delta\varphi(n)} \cong f_d(\theta_0) + \frac{df_d(\theta)}{d\theta}|_{\theta=\theta_0} \Delta\theta \\ &= \sum_{n=-\infty}^{\infty} jn(F_n + v_n)e^{j\theta_0 n}e^{j\Delta\varphi(n)} - \Delta\theta \sum_{n=-\infty}^{\infty} n^2(F_n + v_n)e^{j\theta_0 n}e^{j\Delta\varphi(n)}. \end{aligned}$$

Having in mind that $\Delta\theta$, v_n and $\Delta\varphi(n)$ (with $e^{j\Delta\varphi(n)} \cong 1 + j\Delta\varphi(n)$) are so small that all their products can be neglected, we get

$$0 = \sum_{n=-\infty}^{\infty} jnF_n e^{j\theta_0 n} + \sum_{n=-\infty}^{\infty} j\Delta\varphi(n) jnF_n e^{j\theta_0 n} + \sum_{n=-\infty}^{\infty} jnv_n e^{j\theta_0 n} - \Delta\theta \left[\sum_{n=-\infty}^{\infty} n^2 F_n e^{j\theta_0 n} \right]$$

resulting in

$$0 = f(\theta)|_0 + f(\theta)|_0 \delta_{\Delta\varphi(n)} + f(\theta)|_0 \delta_v + \frac{df(\theta)}{d\theta}|_0 \Delta\theta$$

where:

1.)

$$f(\theta)|_0 \delta_v = \sum_{n=-\infty}^{\infty} jnv_n e^{j\theta_0 n} = \sum_{n=-\infty}^{\infty} jn(F_n + v_n)e^{j\theta_0 n}e^{j\Delta\varphi(n)}$$

at $\theta = \theta_0$, $\Delta\varphi(n) = 0$, and $F_n = 0$. It is a contribution of v_n to $f_d(\theta)$ at the zero value point of $f(\theta)$, that is, at $\theta = \theta_0$, with all other disturbances being neglected.

2.)

$$\begin{aligned} f(\theta)|_0 \delta_{\Delta\varphi(n)} &= \sum_{n=-\infty}^{\infty} j\Delta\varphi(n) jnF_n e^{j\theta_0 n} \\ &\cong \sum_{n=-\infty}^{\infty} jn(F_n + v_n)e^{j\theta_0 n}e^{j\Delta\varphi(n)} \end{aligned}$$

at $\theta = 0$, $v_n = 0$, and $F_n = 0$, with $e^{j\Delta\varphi(n)} \cong 1 + j\Delta\varphi(n)$. It is a contribution of $\Delta\varphi(n)$ to $f_d(\theta)$ at the zero value point of $f(\theta)$, that is, at $\theta = \theta_0$, with all other disturbances being neglected.

3.)

$$\frac{df(\theta)}{d\theta} \Big|_{\theta=0} = - \sum_{n=-\infty}^{\infty} n^2 F_n e^{j\theta_0 n}$$

is a derivative of $f(\theta)$ at $\theta = \theta_0$ when all disturbances v_n and $\Delta\varphi(n)$ are neglected.

Solution 5.9. Consider the function $f_d(\theta)$ described by

$$f_d(\theta) = f(\theta + \mu(\theta)) + v(\theta).$$

In this case $f_d(\theta) = 0$ at $\theta = \theta_1 \neq \theta_0$. With enough small disturbances, θ_1 is close to θ_0 . In general, for a point θ close to θ_0 , we can write

$$\begin{aligned} f_d(\theta) &= f_d(\theta_0) + \frac{df_d(\theta)}{d\theta} \Big|_{\theta=\theta_0} (\theta - \theta_0) + \dots \\ &\cong f_d(\theta_0) + \frac{df_d(\theta)}{d\theta} \Big|_{\theta=\theta_0} (\theta - \theta_0) \\ &= [f(\theta_0 + \mu(\theta_0)) + v(\theta_0)] + \frac{d}{d\theta} (f(\theta + \mu(\theta)) + v(\theta)) \Big|_{\theta=\theta_0} \Delta\theta. \end{aligned}$$

Assume that $v(\theta_0)$ and $\mu(\theta_0)$ are small, as well as that $\Delta\theta = \theta - \theta_0$ is small. Then with

$$[f(\theta_0 + \mu(\theta_0)) + v(\theta_0)] = f(\theta_0) + \frac{df_d(\theta)}{d\theta} \Big|_{\theta=\theta_0} \mu(\theta_0) + v(\theta_0) \quad (5.184)$$

$$\begin{aligned} \frac{d}{d\theta} (f(\theta + \mu(\theta)) + v(\theta)) \Big|_{\theta=\theta_0} \Delta\theta &= \frac{df(\theta)}{d\theta} \Big|_{\theta=\theta_0} \Delta\theta \\ &\quad + \frac{d^2 f(\theta)}{d\theta^2} \Big|_{\theta=\theta_0} \mu(\theta_0) \Delta\theta + \frac{dv(\theta)}{d\theta} \Big|_{\theta=\theta_0} \Delta\theta, \end{aligned}$$

neglecting any product of two or more small values (for example, products $\mu(\theta_0)\Delta\theta$, $v(\theta_0)\Delta\theta$, ...), a linearized model of the previous relation follows

$$f_d(\theta) \cong f(\theta_0) + \frac{df(\theta)}{d\theta} \Big|_{\theta=\theta_0} \mu(\theta_0) + v(\theta_0) + \frac{df(\theta)}{d\theta} \Big|_{\theta=\theta_0} \Delta\theta.$$

By denoting the point $\theta = \theta_0$ by index 0, the previous relation can be rewritten, at the zero value of the disturbed function $f_d(\theta_1) = 0$, as

$$f_d(\theta_1) = 0 = f(\theta)|_0 + f(\theta)|_0 \delta_\mu + f(\theta)|_0 \delta_v + \frac{df(\theta)}{d\theta}|_0 \Delta\theta \quad (5.185)$$

where $f(\theta)|_0 = 0$, by assumption; $f(\theta)|_0 \delta_\mu = \frac{df(\theta)}{d\theta}|_0 \mu(\theta_0)$ denotes a small contribution of $\mu(\theta)$ to $f_d(\theta)$ at $\theta = \theta_0$, when all other disturbances are neglected; and $f(\theta)|_0 \delta_v = v(\theta_0)$ denotes a small contribution of $v(\theta)$ to $f_d(\theta)$ at $\theta = \theta_0$, when all other disturbances are neglected; $\frac{df(\theta)}{d\theta}|_0 \Delta\theta$ denotes increase of $f(\theta)$ from $\theta = \theta_0$ to $\theta = \theta_1$, when all other disturbances are neglected.

To illustrate this relation, consider $f(\theta) = \sin(\theta)$, around $t = 0$, with disturbances $\mu(\theta) = 0.01(\sin(\theta) + 1)$ and $v(\theta) = -0.03 \exp(\theta)$. From (5.185), we get

$$\begin{aligned} 0 &= f(0) + \left. \frac{df(\theta)}{d\theta} \right|_{\theta=0} \mu(0) + v(0) + \left. \frac{df(\theta)}{d\theta} \right|_{\theta=0} \Delta\theta \\ 0 &= 0 + 1 \cdot 0.01 + (-0.03) + 1 \cdot \Delta\theta \\ \Delta\theta &= 0.02 \end{aligned} \quad (5.186)$$

Meaning that the zero of $f(\theta)$, being at $\theta_0 = 0$, is shifted in

$$f_d(\theta) = \sin(\theta + 0.01(\sin(\theta) + 1)) - 0.03 \exp(\theta)$$

for about $\Delta\theta = 0.02$, that is, we have $f_d(0.02) \cong 0$. Indeed, the true zero of $f_d(\theta)$ is at $\theta = 0.02042$. The value of neglected terms, for example, $\Delta\theta d v(\theta)/d\theta|_{\theta=\theta_0}$, in (5.184) is $-0.03\Delta\theta$. It is much lower than the other terms in linear model (5.186). It would change the result to $\Delta\theta = 0.0206$.

Solution 5.10. For the signal $x(t) = e^{j(a_0+a_1t+a_2t^2+a_3t^3)}$ with a small a_3 , we write

$$\begin{aligned} x(t+m\Delta t)x^*(t-m\Delta t) &= e^{j(2a_1m\Delta t+4a_2tm\Delta t+6a_3t^2m\Delta t)} e^{j2a_3(m\Delta t)^3} \\ &= e^{j\Omega_i(t)2m\Delta t} e^{j\Delta\phi(t,m\Delta t)} \cong e^{j2m\Delta t\Omega_i(t)} (1 + j2a_3(m\Delta t)^3), \end{aligned}$$

$$\frac{\partial PWD(t, \Omega)}{\partial \Omega} = \sum_{m=-\infty}^{\infty} -j2m\Delta t w_h(m\Delta t) x(t-m\Delta t) x^*(t+m\Delta t) e^{-j2\Omega m\Delta t}.$$

Let us now write the value $\partial PWD(t, \Omega)/\partial \Omega$ close to the stationary point, at a point $\Omega + \Delta\Omega$ of undisturbed signal $x_{ud}(t) = e^{j(a_0+a_1t+a_2t^2)}$ when $a_3 = 0$. This point is

indicated with index 0

$$\begin{aligned}\frac{\partial PWD(t, \Omega)}{\partial \Omega} &= \sum_{m=-\infty}^{\infty} -(2m\Delta t)^2 w_h(m\Delta t) x(t-m\Delta t) x^*(t+m\Delta t) e^{-j2\Omega m\Delta t} \\ &= \frac{\partial PWD(t, \Omega)}{\partial \Omega}|_0 + \frac{\partial^2 PWD(t, \Omega)}{\partial \Omega^2}|_0 \Delta \Omega + \frac{\partial PWD(t, \Omega)}{\partial \Omega}|_0 \delta_{\Delta \phi}\end{aligned}$$

with the elements as follows

$$\begin{aligned}\frac{\partial^2 PWD(t, \Omega)}{\partial \Omega^2}|_0 &= \sum_{n=-\infty}^{\infty} -(2m\Delta t)^2 w_h(m\Delta t) x(t-m\Delta t) x^*(t+m\Delta t) e^{-j2\Omega m\Delta t}|_{a_3=0, \Omega=\Omega_i(t)} \\ &= -|A|^2 \sum_{n=-\infty}^{\infty} w_h(m\Delta t) (2m\Delta t)^2\end{aligned}$$

$$\begin{aligned}\frac{\partial PWD(t, \Omega)}{\partial \Omega}|_0 \delta_{\Delta \phi} &= \sum_{m=-\infty}^{\infty} -j2m\Delta t w_h(m\Delta t) x(t-m\Delta t) x^*(t+m\Delta t) e^{-j2\Omega m\Delta t}|_{a_3=small, \Omega=\Omega_i(t)} \\ &= |A|^2 \sum_{n=-\infty}^{\infty} w_h(m\Delta t) 2a_3(m\Delta t)^3 (2m\Delta t).\end{aligned}$$

Since $\partial PWD(t, \Omega)/\partial \Omega = 0$, at the stationary point, the approximation error

$$\begin{aligned}\Delta \Omega_h(t) &= \frac{\frac{\partial PWD(t, \Omega)}{\partial \Omega}|_0 \delta_{\Delta \phi}}{-\frac{\partial^2 PWD(t, \Omega)}{\partial \Omega^2}|_0} = \frac{\sum_{n=-\infty}^{\infty} w_h(m\Delta t) 2a_3(m\Delta t)^3 (2m\Delta t)}{\sum_{n=-\infty}^{\infty} w_h(m\Delta t) (2m\Delta t)^2} \\ &\cong a_3 h^{2-1/2} \frac{\int_{-1/2}^{1/2} w_0(t) t^4 dt}{\int_{-1/2}^{1/2} w_0(t) t^2 dt} = \frac{3}{20} a_3 h^2.\end{aligned}$$

Assume now that the instantaneous frequency is estimated without any interpolation or displacement technique for the frequency estimation. Then the frequency step (by

using the DFT in the Wigner distribution calculation) is

$$\Delta\Omega = \frac{2\Omega_m}{N} = \frac{2\pi/\Delta t}{N} = \frac{2\pi}{h}$$

where h is the window duration. Then the frequency quantization squared error is

$$e_Q = \frac{\Delta\Omega^2}{12} = \frac{\pi^2}{3h^2}.$$

The total squared error is

$$MSE = \frac{9}{400}a_3^2h^4 + \frac{\pi^2}{3h^2}.$$

The optimal window is obtained from

$$\frac{9}{100}a_3^2h^3 - \frac{2\pi^2}{3h^3} = 0 \quad \text{as} \quad h = \sqrt[6]{\frac{200\pi^2}{27a_3^2}}.$$

Solution 5.11. For the set of windows

$$\{w_0(m\Delta t), w_1(m\Delta t), w_2(m\Delta t), \dots\}$$

where $w_k(m\Delta t) = w_0^k(m\Delta t)\Delta t$ with $w_0(t)$ being Hann(ing) window of width 1 holds

$$\frac{\int_{-1/2}^{1/2} (w_0^k(t))^2 t^2 dt}{\left(\int_{-1/2}^{1/2} w_0^k(t)t^2 dt\right)^2} \cong 12.36k^{3/2}, \quad \left(\frac{\int_{-1/2}^{1/2} w_0^k(t)t^4 dt}{\int_{-1/2}^{1/2} w_0^k(t)t^2 dt} \right)^2 \cong 36 \left(\frac{0.152}{k} \right)^2$$

The values of the previous approximations of the normalized moment ratios are obtained numerically and shown in Fig. 5.14.

Therefore, we have

$$E(\Delta\hat{\Omega}_h(t))^2 = 12.36 \frac{\sigma_\varepsilon^2}{2|A|^2} \Delta t k^{3/2} + 36a_3^2 \left(\frac{0.152}{k} \right)^2.$$

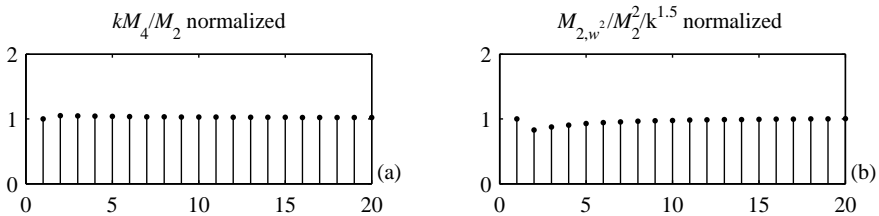


Figure 5.14 Normalized moments ratios for the mean square error calculation.

The optimal order k follows from $\partial E(\Delta\hat{\Omega}_h(t))^2 / \partial k = 0$, that is,

$$12.36 \frac{3\sigma_\epsilon^2}{4|A|^2} \Delta t k^{1/2} = 72a_3^2 \frac{0.152^2}{k^3} \quad k = \left(\frac{0.18a_3^2 |A|^2}{\Delta t \sigma_\epsilon^2} \right)^{2/7}.$$

Solution 5.12. (a) For the Gaussian distribution we can assume $\kappa = 2$, meaning that our confidence interval intersection approach will work with a probability of 0.95. Since the bias and variance are of the same order for an optimal parameter h , we can use $\Delta\kappa = 1$. Now we check the relation

$$|x_{h_{s-1}}(t) - x_{h_s}(t)| \leq (\kappa + \Delta\kappa)[\sigma(h_{s-1}) + \sigma(h_s)]$$

for the signal

$$x \in \{0.0037, -0.1438, 0.1294, 0.0337, 0.1470, 0.1999, 0.5114, 2.0413\}.$$

The relations are

$$\begin{aligned} |0.0037 + 0.1438| &= 0.1475 \leq (2+1)(\sqrt{\frac{0.1}{1}} + \sqrt{\frac{0.1}{2}}) = 1.6195, \top \\ |-0.1438 - 0.1294| &= 0.2732 \leq 1.1452, \top \\ |0.1294 - 0.0337| &= 0.0957 \leq 0.8098, \top \\ |0.0337 - 0.1470| &= 0.1133 \leq 0.5726, \top \\ |0.1470 - 0.1999| &= 0.0529 \leq 0.4049, \top \\ |0.1999 - 0.5114| &= 0.3115 \leq 0.2863, \perp \\ |0.5114 - 2.0413| &= 1.5299 \leq 0.2024, \perp. \end{aligned}$$

Thus, the estimate of the optimal parameter is the last value of h for which the inequality still holds. It is $h_{opt} = 32$ with $\sigma(h_{opt}) = \sqrt{0.1}/\sqrt{32} = 0.056$, producing $\mathbf{x}(t) = 0.1999$ as the best estimate, at this instant.

(b) By using a more reliable analysis with probability 0.999 and $\kappa = 3$ for the case $m = 1$ and $n = 4$ we get the values $\Delta\kappa = 1.29$, $p = 1.22$, and $p_1 = 1.41$ (from Table 5.2). Therefore, the the best estimate of h_{opt} is

$$h_a = h_{s^+}/2^{p_1} \cong h_{s^+}/2 = h_{s^+-1},$$

since $1/2 < p_1 \leq 3/2$. In this case, we use $h_{opt} = 32/2 = 16$ with $\mathbf{x}(t) = 0.1470$ as the best estimate.

Solution 5.13. The ambiguity function of the signal $s(t) = A \exp(jat^2/2)$ is

$$A(\theta, \tau) = \int_{-\infty}^{\infty} A^2 \exp(jat\tau) e^{-j\theta t} dt = 2\pi A^2 \delta(\theta - a\tau).$$

Thus, the distribution is a two-dimensional Fourier transform of the product $A(\theta, \tau)c(\theta\tau)$,

$$\begin{aligned} SD_s(t, \Omega) &= \frac{1}{2\pi} \int_{-\infty}^{\infty} \int_{-\infty}^{\infty} A(\theta, \tau) c(\theta\tau) e^{j\theta t - j\Omega\tau} d\theta d\tau \\ &= \iint_{\substack{|\theta\tau| < 1/2 \\ |\theta| < 5, |\tau| < 5}} A^2 \delta(\theta - a\tau) e^{j\theta t - j\Omega\tau} d\theta d\tau. \end{aligned}$$

For $0 \leq a \leq 1/50$

$$\begin{aligned} SD_s(t, \Omega) &= \iint_{\substack{|\theta| < 5, |\tau| < 5}} A^2 \delta(\theta - a\tau) e^{j\theta t - j\Omega\tau} d\theta d\tau \\ &= \int_{-5}^5 A^2 e^{jat\tau - j\Omega\tau} d\tau = 2A^2 \frac{\sin[5(at - \Omega)]}{(at - \Omega)} \\ \max\{SD_s(t, \Omega)\} &= 10A^2. \end{aligned}$$

For most of the range for a , that is, for $1/50 < a \leq 1$,

$$SD_s(t, \Omega) = \int_{-1/\sqrt{2a}}^{1/\sqrt{2a}} A^2 e^{jat\tau - j\Omega\tau} d\tau = 2A^2 \frac{\sin[\frac{(at-\Omega)}{\sqrt{2a}}]}{(at-\Omega)}$$

$$\max\{SD_s(t, \Omega)\} = \sqrt{2} \frac{A^2}{\sqrt{a}}.$$

It is a dependent. The case of $a = -2$, behaves the same as $a = 1/2$, due to symmetry in the ambiguity domain kernel.

The distribution variance in the noise-only case is proportional to the kernel energy

$$\sigma_{\epsilon\epsilon}^2 = \frac{\sigma_\epsilon^4}{2\pi} \int_{-5}^5 \int_{-5}^5 |c(\theta, \tau)|^2 d\theta d\tau = \frac{\sigma_\epsilon^4}{2\pi} 4[5 \cdot \frac{1}{10} + \int_{1/10}^5 \frac{1}{2\tau} d\tau] = \frac{\sigma_\epsilon^4}{\pi} [1 + \ln 5 + \ln 10].$$

The ratio of the squared maximal value and distribution variance, $1/50 < a \leq 1$, is

$$\frac{\max^2\{SD_s(t, \Omega)\}}{\sigma_{\epsilon\epsilon}^2} = \frac{2}{a} \frac{A^4}{1.56\sigma_\epsilon^4} = \frac{1.28}{a} \frac{A^4}{\sigma_\epsilon^4}.$$

The result can be generalized for the kernel $|\theta\tau| < 1/(2B)$ and $|\theta| < 5, |\tau| < 5$. Then

$$\sigma_{\epsilon\epsilon}^2 = \frac{\sigma_\epsilon^4}{2\pi} 4[5 \cdot \frac{1}{10B} + \int_{1/10B}^5 \frac{1}{2B\tau} d\tau] = \frac{\sigma_\epsilon^4}{\pi B} [1 + \ln 5 + \ln 10 + \ln B].$$

For most of the range for a , that is, for $1/(50B) < a \leq 1$,

$$SD_s(t, \Omega) = \int_{-1/\sqrt{2Ba}}^{1/\sqrt{2Ba}} A^2 e^{jat\tau - j\Omega\tau} d\tau$$

$$= 2A^2 \frac{\sin[\frac{(at-\Omega)}{\sqrt{2aB}}]}{(at-\Omega)}$$

$$\max\{SD_s(t, \Omega)\} = \sqrt{2} \frac{A^2}{\sqrt{aB}}, \text{ for } \Omega = at.$$

The ratio of the squared maximal value and the distribution variance, for $1/(50B) < a \leq 1$, is

$$\frac{\max^2\{SD_s(t, \Omega)\}}{\sigma_{\varepsilon\varepsilon}^2} = \frac{2\pi}{a} \frac{A^4}{\sigma_\varepsilon^4} \frac{1}{1 + 2\ln 5 + \ln 2 + \ln B}.$$

As the kernel becomes narrower, B increases, and then this signal-to-noise ratio decreases, meaning that reduction of noise is slower than the signal degradation. Thus, we have to be careful in the reduced interference distribution application for noisy signals. They may degrade the signal auto-terms more than they reduce the noise.

Solution 5.14. (a) The STFT of eight samples signals $x(n) = s(n) + \varepsilon(n) = \exp(j6\pi n/8) + \varepsilon(n)$ at $n = 0$ with

$$\varepsilon(m) = [0.01, -0.13, 0.17, 0.02, 15.5, -0.035, 11.2, 0.05],$$

calculated in a direct way is

$$\begin{aligned} STFT(0, k) &= \sum_{m=0}^7 s(m) e^{-j2\pi mk/8} \\ &= [0, 0, 0, 8, 0, 0, 0, 0]. \end{aligned}$$

For noisy signal we get

$$\begin{aligned} STFT(0, k) &= \sum_{m=0}^7 x(m) e^{-j2\pi mk/8} = [27.8, -15.5 + j11.1, 4.1 + j0.2, \\ &- 7.4 - j10.9, 27, -15.4 + j10.9, 4.1 - j0.2, -15.5 - j11.1]. \end{aligned}$$

(b) By using the L-statistics-based one, when two largest samples of the signal multiplied by basis functions ($s(m)e^{-j2\pi mk/8}$) are removed, we get

$$\begin{aligned} &STFT_{L_stat}(0, k) \\ &= [1.08 - j, -0.036 - j0.081, 0.84 + j1.23, 6.1 + j0.26, \\ &1.27 - j1, 0.056 - j0.26, 0.84 + j0.76, -2.036 + j0.081]. \end{aligned}$$

(c) After two samples are removed (the same case as if they were not available in advance at all), two new values are added by a direct search over the values ranging from the minimal amplitude m_0 to the maximal amplitude M_0 in the rest of the

values. The amplitude increment was $(m_0 + 0.1p)\exp(-jq)$ where p ranges from 0 up to $m_0 + 0.1p = M_0$ and q ranges from 0 to 2π with step $\pi/10$, that is.

$$x(5), x(7) \in \{A \exp(j\phi) \mid A \in [0.8 : 0.1 : 1.2], \phi \in [0 : \pi/10 : 2\pi]\}.$$

Out of all the STFTs, the best concentrated one is obtained for values $x(5) = 1.1 \exp(j\pi)$ and $x(7) = 1 \exp(j\pi/2)$. These two values produced the best concentration measure

$$\mu[\text{SPEC}(n, k)] = \frac{(\sum_n \sum_k |\text{STFT}(n, k)|)^2}{\sum_n \sum_k |\text{STFT}(n, k)|^2}.$$

The STFT with these reconstructed values is

$$\begin{aligned} & \text{STFT}_{L,\text{stat},\text{REC}}(0, k) \\ &= [-0.01, 0.064 - j0.081, -0.26 + j0.23, 8.16 + j0.26, \\ & \quad 0.17, 0.156 - j0.26, -0.26 - j0.23, 0.064 + j0.081]. \end{aligned}$$

The results are shown in Fig. 5.15.

Solution 5.15. Values of the nonnoisy signal $s(n) = \exp(j\pi(n+1)^2/9)$ Wigner distribution are

$$\begin{aligned} WD(0, k/2) &= \sum_{m=-4}^4 s(m)s^*(-m)e^{-j2\pi mk/9} = \sum_{m=-4}^4 e^{j4m\pi/9}e^{-j2\pi mk/9} \\ &= [0, 0, 0, 0, 0, 0, 9, 0, 0] \\ &\text{for } k = -4, -3, -2, -1, 0, 1, 2, 3, 4. \end{aligned}$$

The Wigner distribution of the noisy signal

$$x(n) = \exp(j\pi(n+1)^2/9) + [0.1, -0.3, 0.7, 0.2, 15.5, -0.35, 11.2, 0.5, 0.1]$$

is

$$\begin{aligned} WD(0, k) &= \sum_{m=-4}^4 x(m)x^*(-m)e^{-j2\pi mk/9} \\ &= [293, 245, 238, 283, 303, 268, 243, 259, 302]. \end{aligned}$$

If we remove the three biggest values of $x(m)x^*(-m)e^{-j2\pi mk/9}$ for $m = -4, -3, \dots, 3, 4$ and sum the rest of six of the lowest terms, we get the L-statistics-based Wigner

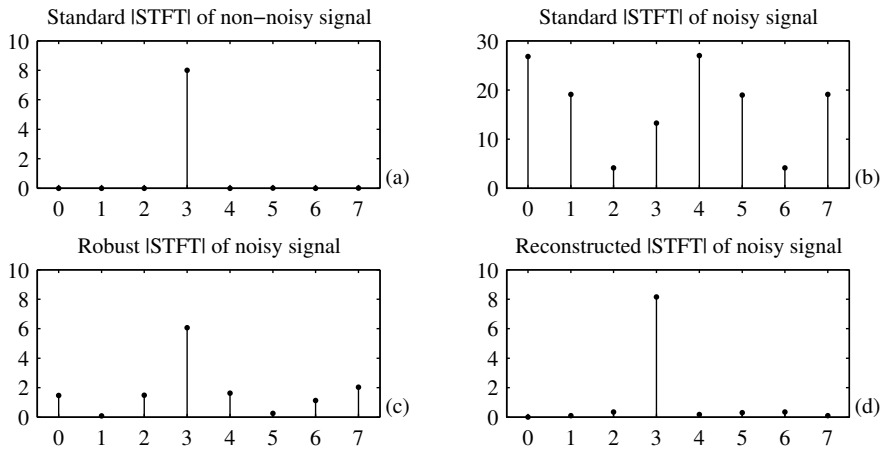


Figure 5.15 (a) The absolute value of the STFT of nonnoisy signal. (b) The standard STFT of a signal with high impulse noise. (c) The L-statistics-based robust STFT of a signal with high impulse noise. (d) The L-statistics-based robust STFT after the removed values are reconstructed by a direct search, producing the best concentrated STFT.

distribution value

$$WD_{Lstat}(0, k) = [1.47, -3.02, -3.45, 0.24, -0.81, -1.55, 6.73, -0.93, 1.33].$$

In this case, there is quite clear peak value $WD_{Lstat}(0, k) = 6.73$ for $k = 1$. Results are presented in Fig. 5.16.

For noise

$$\varepsilon(m) = [0.1, -0.3, 0.7, 0.2, 755.5, -0.35, 531.4, 0.5, 0.1]$$

the L-statistics-based distribution would be the same, since the three the highest terms are removed and they do not influence the value of $WD_{Lstat}(0, k)$. Further improvement of the results can be achieved by reconstructing the removed values, as in the previous or in the next problem.

Solution 5.16. For the discrete signal

$$x(n) = 1.2 e^{j2\pi n/16 + j\pi/4} + 1.5 e^{j14\pi n/16 - j\pi/3} + 1.7 e^{j12\pi n/16},$$

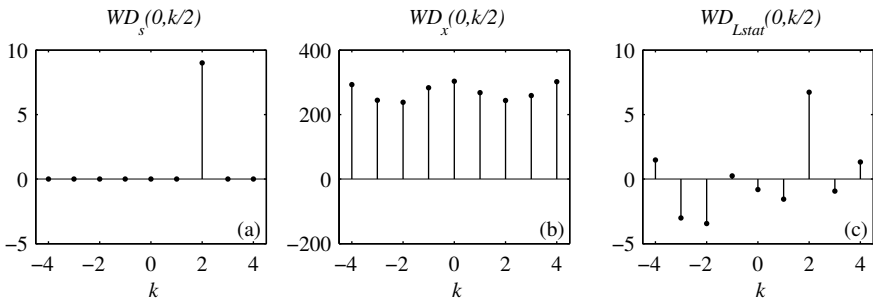


Figure 5.16 (a) The Wigner distribution of noise-free signal. (b) The standard Wigner distribution of a signal with high impulse noise. (c) The L-statistics-based robust Wigner distribution of a signal with high impulse noise.

with $0 \leq n \leq 15$, time domain is shown in Fig. 5.17. The signal is sparse in the DFT domain since only three DFT values are different than zero (Fig. 5.17(second row)). The CS signal, with missing samples $x(2)$, $x(4)$, $x(11)$, and $x(14)$, being set to 0 for the initial DFT estimation, is shown in Fig. 5.17 (third row). The DFT of the signal, with missing values being set to 0, is calculated and presented in Fig. 5.17 (fourth row). There are three DFT values, at $k_{01} = 1$, $k_{02} = 6$, and $k_{03} = 7$ above the assumed threshold, for example at level of 11. The rest of the the DFT values is set to 0. This is justified by using the assumption that the signal is sparse. Now, we form a set of equations, for these frequencies $k_{01} = 1$, $k_{02} = 6$, and $k_{03} = 7$ as

$$\sum_{i=1}^3 X(k_{0i}) e^{j2\pi k_{0i} n_{CS}/16} = x(n_{CS}),$$

where $n_{CS} = 0, 2, 3, 5, 6, 7, 8, 9, 10, 12, 13, 15$ are the instants where the signal is available. Since there are more equations than unknowns, the system $\mathbf{AX} = \mathbf{B}$, is solved in the least square sense, by using MATLAB operation $\mathbf{X} = \mathbf{A} \setminus \mathbf{B}$. The obtained reconstructed values are exact, for all frequencies k , as in Fig. 5.17(second row). They are shown in Fig. 5.17 (fifth row).

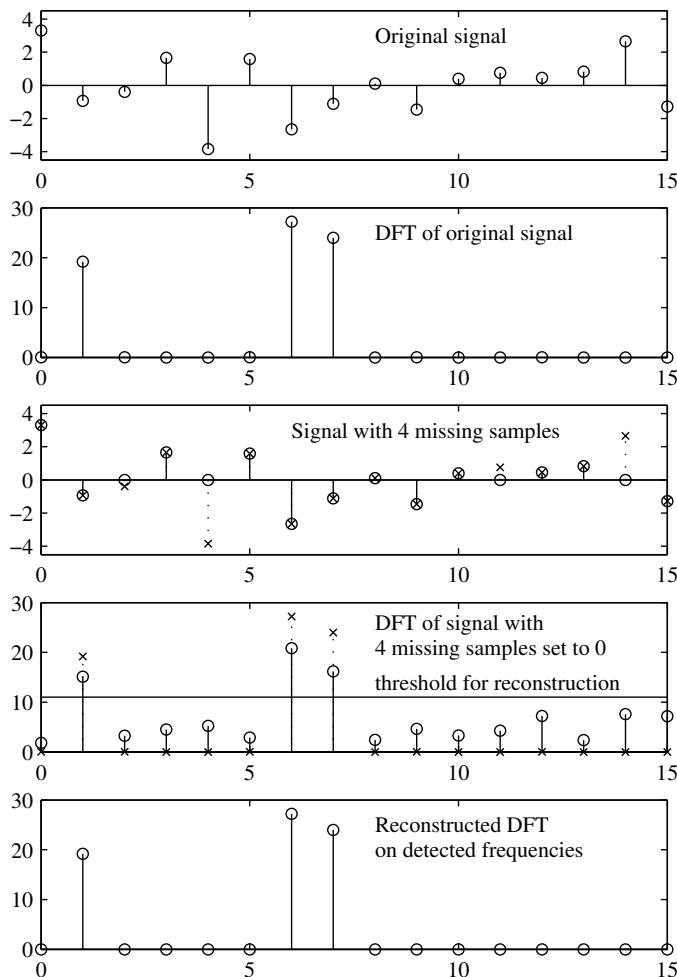


Figure 5.17 Original signal in the time domain (first row); the DFT of the original signal (second row); the CS signal with four missing samples at $n = 2, 4, 11$, and 14 (third row); and the DFT of signal with missing values being set to 0 (fourth row). The reconstructed signal assuming that the DFT contains components only at frequencies where the initial DFT is above threshold (fifth row). Absolute values of the DFT are shown.

Solution 5.17. The function for instantaneous frequency estimation can be implemented as:

```
function Freq=IFestWD(x,w);
% WD based instantaneous frequency estimation
% complex input signal and odd window length assumed
PWD=PWD_calc(x,w);
PWD=fftshift(real(PWD),1);
[d,k]=max(PWD);
N=length(w);
Freq=pi*(k-(N+1)/2)/N;
```

The instantaneous frequency can be estimated with

```
s=sqrt(0.25);
t=(-64:511+64)';
t1=0:511;
x0=exp(j*16*sin(pi*t/64) + j*6*sin(pi*t/48));
TrueIF=(pi/4)*cos(pi*t1/64) + (pi/8)*cos(pi*t1/48);
noise=s/sqrt(2)*(randn(size(x0))+j*randn(size(x0)));
x=x0+noise;
wf=hanning(129);
% If the number of samples were even
% the appropriate PWD should be used
Freq=IFestWD(x, wf);
plot(t1, Freq, t1, TrueIF)
```

Solution 5.18. The code is:

```
%Set of possible parameter h values
h=[0 1 2 4 8 16 32 64 128 256 512];
m=1; n=4; %Estimator description
k=2; dk=1; %Assumed values,
%Signal and noise
t=-50:1/25:50;
f=1.0./(1+(t/7.5).^40);
noise=0.1*randn(1,length(t));
```

```
x=f+noise;
%Estimation of the noise variance
V=median(abs(diff(x)))/sqrt(2)/0.6745;
%Algorithm
for i=1+max(h):length(t)-max(h)
    sgm0=sqrt(V^2/((2*h(1)+1)^m));
    j=2;
    f0=x(i);
    while (abs(f0-mean(x(i-h(j):i+h(j))))...
        <=(sgm0+sqrt(V^2/((2*h(j)+1)^m)))*(k+dk))...
        &j<length(h);
        f0=mean(x(i-h(j):i+h(j)));
        sgm0=sqrt(V^2/(2*h(j)+1)^m);
        j=j+1;
    end
%Smoothing with adaptive and constant widths of h
ha(i)=h(j-2);
f_fil(i)=mean(x(i-h(j-2):i+h(j-2)));
f_fill(i)=mean(x(i-1:i+1));
f_fil64(i)=mean(x(i-64:i+64));
end
%Graphic presentation
tsk=[1+max(h):length(t)-max(h)];
figure(1), subplot(3,2,1)
plot(t(tsk),f(tsk),'k'), axis([-30 30 -.5 1.5])
subplot(3,2,2)
plot(t(tsk),x(tsk),'k'), axis([-30 30 -.5 1.5])
subplot(3,2,3)
plot(t(tsk),ha(tsk),'k'), axis([-30 30 0 180])
subplot(3,2,5),
plot(t(tsk),f_fil(tsk),t(tsk),f(tsk),'k-');
axis([-30 30 -.5 1.5])
subplot(3,2,4),
plot(t(tsk),f_fil64(tsk),t(tsk),f(tsk),'k-');
axis([-30 30 -.5 1.5])
subplot(3,2,6),
plot(t(tsk),f_fill(tsk),'b',t(tsk),f(tsk),'k-');
axis([-30 30 -.5 1.5])
```

Solution 5.19. Program for the robust STFT calculation by using the median and the iterative procedure

```

N=64; n=0:N-1;
s=exp(j*12*pi/N*n)+exp(j*20*pi/N*n); %Signal
x=s+randn(1,N).^3+j*rand(1,N).^3; %Cauchy impulse noise
subplot(311),plot(n,s,n,x)
for k=1:N
    STFTx(k)=mean(x.*exp(-j*2*pi/N*(k-1)*n));
    STFTs(k)=mean(s.*exp(-j*2*pi/N*(k-1)*n));
    STFTsM(k)=median(real(x.*exp(-j*2*pi/N*(k-1)*n)))...
        +j*median(imag(x.*exp(-j*2*pi/N*(k-1)*n)));
end
subplot(312)
plot(n-1,abs(STFTsM)/max(abs(STFTsM)), 'r',...
    n-1,abs(STFTx)/max(abs(STFTx)), '--g',...
    n-1,abs(STFTs)/max(abs(STFTs)), ':')
STFTr=STFTx;
for i=1:15 %Iteration: Maximal number of iterations 15
    %Iterative robust STFT
    for k=1:N
        d=1.0./abs(x.*exp(-j*2*pi/N*(k-1)*n)-STFTr(k));
        STFTrN(k)=sum(d.*x.*exp(-j*2*pi/N*(k-1)*n))/sum(d);
    end
    % Stopping criterion:
    % changes smaller than 1% of the maximal value
    if max(abs(STFTrN-STFTr))<0.01*max(abs(STFTr)),
        disp('number of iteration'), i, break,
    else, STFTr=STFTrN; end
    subplot(313),plot(n-1,abs(STFTr)),pause(1)
end

```

Chapter 6

Applications of Time-Frequency Analysis

Just a few of many possible applications of time-frequency analysis will be presented here. The basic principles of these application areas, with their formulation within the time-frequency framework, will be explained. The benefits of the time-frequency representations over the classical tools will be emphasized. Since many of the presented time-frequency methods may be then applied, on such a formulated problem, we will just present one of the possible results. It is left to the reader to try to apply some other time-frequency methods, with their possible advantages and drawbacks. Previously discussed implementation details will not be repeated here. Some applications, such as radar signal processing, will be presented in detail, while some others will be only briefly covered or just listed.

6.1 RADAR SIGNAL PROCESSING

When radar transmits an electromagnetic signal to a target, the signal reflects from it and returns to radar. The reflected signal, as compared to the transmitted signal, is delayed, changed in amplitude, and possibly shifted in frequency. These parameters of the received signal contain information about the target's characteristics. For example, delay is related to the target's distance from the radar (range), while the target's velocity is related to the shift in frequency (Doppler shift). The basic property in spectral analysis is that a higher concentration of the Fourier transform is achieved by using longer signal sequences. However, within longer time intervals, the target point velocity may change. These changes cause corresponding frequency changes that spread the Fourier transform and decrease radar efficiency. In addition, target motion can also be three-dimensional, changing the velocity projection along

the target-radar line in a very complex way. Classical techniques for these kind of problems are based on movement compensation.

Inverse synthetic aperture radar (ISAR) is a method for obtaining a high-resolution image of a target based on the change in viewing angle of the target with respect to the fixed radar. Rotation as a result of this angle change introduces additional velocity proportional to the rotation speed and the distance from the rotation center. A component of the velocity in direction of the radar-target line is proportional to the normal distance of the point from the center of rotation (cross-range). Thus, in the case of ISAR, the distance and the velocity locate the target point in the range/cross-range domain. Since the range and cross-range information are contained in two-dimensional sinusoids with corresponding frequencies, a common technique used for the ISAR signal analysis is the two-dimensional Fourier transform. Fourier transform application on the ISAR signal of a point target results in a highly concentrated function at a point whose position corresponds to the range and cross-range values. However, the target movement almost never can reduce to a pure uniform (constant) velocity thus, we have to deal with a signal with varying frequencies. The SAR imaging is a method for obtaining high resolution image of a target based on the change in viewing angle of the radar with respect to the fixed target. In theory, a similar effect may appear as in ISAR.

Another problem in radar imaging is in the micro-Doppler effect processing. Namely, very fast moving parts of a target can cause micro-Doppler effect, producing fast frequency changes (usually in the cross-range domain). These parts have increased speed, projecting themselves in a different scale than the scale of slow-moving parts. They can also cover slow moving (rigid) parts of a target and degrade the ISAR/SAR image. The separation of patterns caused by rigid parts of the target from the patterns caused by fast moving parts is an interesting area of time-frequency analysis application.

6.1.1 Analytic CW Radar Signal Model

For the analytic model derivation, consider a continuous wave (CW) radar that transmits signal in a form of coherent series of chirps

$$v_p(t) = \begin{cases} \exp(j\pi B f_r t^2), & \text{for } 0 \leq t \leq T_r \\ 0, & \text{otherwise} \end{cases} \quad (6.1)$$

where T_r is the repetition time and $f_r = 1/T_r$ is the repetition frequency.

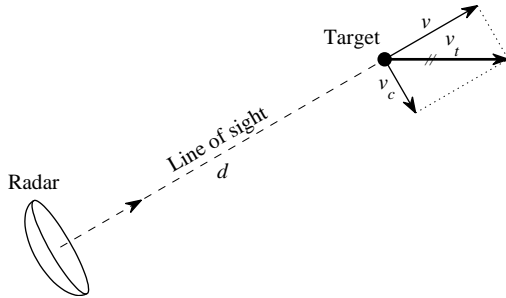


Figure 6.1 Illustration of the radar and target positions.

In one revisit, the transmitted signal consists of M such chirps

$$v(t) = \exp(-j\Omega_0 t) \sum_{m=0}^{M-1} v_p(t - mT_r) \quad (6.2)$$

where Ω_0 is the radar operating frequency. The total signal duration is $T_c = MT_r$. It is called coherent integration time (CIT).

The signal of form (6.2) is transmitted toward a target (Fig. 6.1). If the target distance from radar is d (referred to as range), then the received signal is delayed with respect to the transmitted signal for $t_d = 2d/c$, where c is the propagation rate, equal to the speed of light. The phase of the received signal is changed for

$$\phi = 2kd = \frac{4\pi d}{\lambda} = \frac{4\pi d f_0}{c} = \Omega_0 \frac{2d}{c},$$

where $f_0 = \Omega_0/(2\pi)$ if the radar operating frequency in [Hz], $\lambda = c/f_0$ is the wavelength, and $k = 2\pi/\lambda$ is the wavenumber of radar signal.

Thus, the form of the received signal is

$$u(t) = \sigma \exp\left(-j\Omega_0\left(t - \frac{2d}{c}\right)\right) \sum_{m=0}^{M-1} v_p\left(t - \frac{2d}{c} - mT_r\right)$$

where σ is the reflection coefficient. The received signal is mixed (multiplied) with the complex-conjugate of the transmitted signal, shifted for constant delay T_0 .

$$\begin{aligned} q(t) &= u(t)v^*(t - T_0) \\ &= \sigma \exp\left(j\Omega_0 \frac{2d}{c}\right) \sum_{m_1=0}^{M-1} \sum_{m_2=0}^{M-1} v_p\left(t - \frac{2d}{c} - m_1 T_r\right) v_p^*(t - T_0 - m_2 T_r) \end{aligned}$$

We will assume that a constant distance is properly compensated (i.e., $T_0 = 0$).

Example 6.1. Assume that the repetition time is $T_r = 0.5$ ms, $B = 300$ MHz and $f_0 = \Omega_0/(2\pi) = 1$ GHz, also assume that a target, reflecting the signal with $\sigma = 1$, exists at a distance $d = 1.5$ km. The returned signal comes back to the radar with a delay $t_d = 2d/c = 10^{-5} = 0.01$ ms, where $c = 3 \times 10^8$ m/s. Consider a product of the corresponding chirps $m_1 = m_2 = m$ in the product $q(t)$ of the received signal with the conjugated transmitted signal

$$\begin{aligned} q(m, t) &= \sigma \exp\left(j\Omega_0 \frac{2d}{c}\right) v_p^*(t - mT_r) v_p(t - mT_r - t_d) \\ &= \sigma \exp\left(j\Omega_0 \frac{2d}{c}\right) \exp(-j\pi B f_r (t - mT_r)^2) \exp(j\pi B f_r (t - mT_r - t_d)^2) \end{aligned}$$

within $t_d \leq t - mT_r \leq T_r$ or 0.01 ms $\leq t - mT_r \leq 0.5$ ms. This product results in a pure sinusoid

$$q(t) = \exp(-j2\pi B f_r t_d) \exp(j\phi) = \exp(-j2\pi 6t 10^6) \exp(j\phi)$$

with $\phi = \pi B f_r t_d^2 + 2\pi B f_r m T_r + 2\Omega_0 d / c$. It means that the target at distance $d = 1.5$ km produces a pure sinusoid at the frequency 6 MHz. A distance of 1 m corresponds to the frequency 4 kHz. Of course, if there are many targets we get many sinusoids at corresponding frequencies. Note that for $0 \leq t - mT_r \leq t_d$ two successive chirps are multiplied, since the delayed received chirp overlaps (within this small interval) with the previous chirp in the transmitted signal. \square

Example 6.2. Assume the same parameters as in the previous example, and see what will happen if we only multiply the received signal with the conjugated transmitted signal of the next chirp. Then we get

$$\begin{aligned} q(t) &= \sigma \exp\left(j\Omega_0 \frac{2d}{c}\right) v_p(t - t_d) v_p^*(t - T_r) \\ &= \sigma \exp\left(j\Omega_0 \frac{2d}{c}\right) \exp(-j\pi B f_r (t - T_r)^2) \exp(j\pi B f_r (t - t_d)^2) \end{aligned}$$

within $0 \leq t \leq t_d$. This product results in a sinusoid

$$q(t) = \exp(-j2\pi Bf_r(t_d + T_r)t) \exp(j\phi) = \exp(-j2\pi[6+300]t10^6)) \exp(j\phi)$$

with $\phi = \pi Bf_r(t_d^2 + T_r^2) + 2\Omega_0 d/c$. It means that a target at $d = 1.5$ km produces here an additional sinusoid at the frequency $(6+300)$ MHz. Obviously, it is at a much higher frequency 306 MHz, than the basic one at 6 MHz. Thus, it can be easily filtered out and neglected in further analysis. \square

According to the previous example, it is clear that we can consider mixed signal in the form

$$\begin{aligned} q(t) &= \sum_{m=0}^{M-1} q(m,t) \\ q(m,t) &= \sigma \exp\left(j\Omega_0 \frac{2d}{c}\right) v_p\left(t - \frac{2d}{c} - mT_r\right) v_p^*(t - mT_r) \end{aligned} \quad (6.3)$$

since the time shift due to delay is small and the product of the components (6.1) for different chirps is a sinusoid at a very high frequency, which can easily be filtered out.

By substituting values for signal components $v_p(t)$, we get

$$\begin{aligned} q(m,t) &= \sigma \exp\left(j\Omega_0 \frac{2d}{c}\right) \exp\left(j\pi Bf_r\left(t - \frac{2d}{c} - mT_r\right)^2\right) \exp(-j\pi Bf_r(t - mT_r)^2) \\ &= \sigma \exp\left(j\Omega_0 \frac{2d}{c}\right) \exp\left(-j2\pi Bf_r(t - mT_r) \frac{2d}{c}\right) \exp(j\phi_0). \end{aligned} \quad (6.4)$$

The constant phase shift $\exp(j\phi_0)$ is usually omitted.

The position of the maxima in the two-dimensional Fourier transform of $q(m,t)$ will contain information about the Doppler shift and the range of target. Namely, the second term $\exp(-j2\pi Bf_r(t - mT_r) \frac{2d}{c})$, where time t is sampled as

$$t - mT_r = nT_s,$$

with T_s being a sampling interval within a chirp,

$$T_s = \frac{T_r}{N},$$

reduces to

$$\exp(-j2\pi Bf_r(t - mT_r) \frac{2d}{c}) = \exp(-j\gamma n),$$

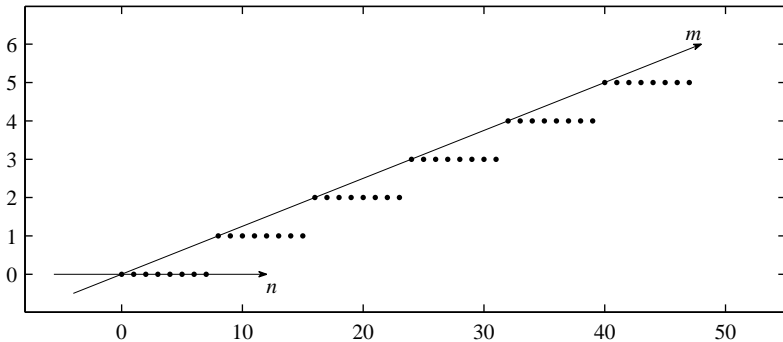


Figure 6.2 Illustration of one chirp series discretization in coordinates m (chirp index, slow time) and n (time within one chirp, fast time). The case of $M = 6$ chirps in one revisit and $N = 8$ samples within chirp is presented.

where

$$\gamma = 2\pi B f_r T_s \frac{2d}{c}.$$

Thus,

$$q(m, n) = \sigma \exp\left(j\Omega_0 \frac{2d}{c}\right) \exp(-j\gamma n) \exp(j\phi_0). \quad (6.5)$$

The illustration of the signal radar discretization in coordinates m (chirp index, slow time) and n (time within one chirp, fast time) is presented in Fig. 6.2. The Fourier transform of $\exp(-j\gamma n)$ results in a pulse at the discrete angular frequency

$$\omega = -\gamma = -\frac{4\pi B f_r T_s}{c} d,$$

being proportional to the range d .

Since the calculation is based on the DFT, it is known that taking DFT of $\exp(-j\gamma n)$ with N samples, we get the resolution $\Delta\omega = 2\pi/N$ in discrete frequency ($\omega = \Omega T_s$). Thus, the resolution in $\gamma = 2\pi B f_r T_s 2d/c$ will be

$$\Delta\gamma = 2\pi/N.$$

Then the resolution in d is

$$\Delta d = \frac{\Delta\gamma c}{4\pi B f_r T_s} = \frac{2\pi c/N}{4\pi B f_r T_s} = \frac{c}{2T_r f_r B} = \frac{c}{2B}.$$

Finally, the range resolution is defined by $R_{\text{range}} = \Delta d$,

$$R_{\text{range}} = \frac{c}{2B}. \quad (6.6)$$

All these derivations are done assuming that target is stationary, that is, that distance d does not change within one chirp, that is, within interval T_r . Note that T_r is significantly shorter than $T_c = MT_r$ so the assumption that d does not change significantly within T_r does not mean that d does not change significantly within T_c . Later we will see that T_c is related to the Doppler change in frequency. Changing distance d resulting in a time-varying frequency and relates this field to the time-frequency analysis instead of the classical Fourier transform.

6.1.2 Signal and Resolution in the Doppler Domain

In order to find the resolution in Doppler shift, consider the following part of (6.5) with time-varying distance $d = d(t)$,

$$s(t) = \sigma \exp\left(j\frac{\Omega_0}{c}2d(t)\right) \quad (6.7)$$

Assume that the target within T_c moves with a constant velocity v , that is, that $d(t) = d_0 + vt$. Then

$$s(t) = \sigma \exp(j\Omega_0 2(d_0 + vt)/c).$$

In general, $t = mT_r + nT_s$. For this part we will consider only chirp index m , with discrete slow-time notation of the signal $s(m)$. The chirp index m is called “slow time” since the sampling interval for this index is much higher compared with the “fast time” index n (considered and included in the range analysis part of the signal). It is equal to the chirp duration T_r . The signal $s(m)$ is a sinusoid along m

$$s(m) = \sigma \exp(j2\Omega_0 v m T_r / c) \exp(j\psi)$$

with discrete-frequency $\omega = 2\Omega_0 v T_r / c$. All phase terms that do not depend on m are denoted by ψ . The Fourier transform of the complex sinusoid $s(m)$ produces a peak at the position

$$\omega_d = \frac{2\Omega_0 T_r}{c} v \quad (6.8)$$

proportional to the target velocity. The DFT of $s(m)$, calculated by taking M samples, produces a resolution $2\pi/M$ in frequency $\omega = 2\Omega_0 v T_r / c$. The Doppler

shift in frequency is defined by

$$\Delta\Omega_d = 2\Omega_0 \frac{v}{c}.$$

Its resolution follows from $\Delta\Omega_d = \omega_d/T_r$ in the form

$$R_{\text{Dopp}} = \frac{2\pi}{MT_r} = \frac{2\pi}{T_c}. \quad (6.9)$$

It means that longer CIT, that is, longer series of pulses will improve the resolution in the Doppler shift detection. It is interesting to note that resolutions in both (range and cross-range) directions depend only on T_c , c , and B .

6.1.3 Nonuniform Target Motion

In some cases the target motion over all M chirps, in one revisit, cannot be considered as the constant velocity motion. Then a higher-order approximation

$$d(t) \cong d_0 + v_0 t + a \frac{t^2}{2} + \dots,$$

should be used with

$$v(t) = v_0 + at + \dots$$

If we assume, for the beginning, that $v(t) = v_0 + at$, then the Doppler shift is linear function of time. Its rate is a . Thus, instead of the delta pulse concentrated at one frequency corresponding to v_0 we will obtain a Fourier transform of an linear frequency-modulated signal (or higher-order frequency-modulated signal), whose instantaneous frequency changes are proportional to velocity $v(t)$ changes. Instead of having the Doppler frequency concentrated at a point in the Fourier domain corresponding to v_0 , we will obtain a spread Fourier transform.

In order to analyze nonstationarities in the Fourier transform of (6.7), consider

$$\begin{aligned} S(\Omega) &= \int_{-T_c/2}^{T_c/2} \sigma \exp\left(j \frac{2\Omega_0}{c} d(t)\right) \exp(-j\Omega t) dt \\ &= \int_{-\infty}^{\infty} w(t) \sigma \exp\left(j \frac{2\Omega_0}{c} d(t)\right) \exp(-j\Omega t) dt, \end{aligned} \quad (6.10)$$

where $w(t)$ is the window defined by the coherent integration time T_c .

For time-varying $d(t)$, we can write a Taylor series expansion of $d(t)$ around $t = 0$

$$d(t) = d_0 + d'(0)t + \frac{1}{2}d''(0)t^2 + \dots = \sum_{n=0}^{\infty} \frac{1}{n!} d^{(n)}(0)t^n, \quad (6.11)$$

where $d^{(n)}(0)$ is the n th derivative of the distance, at $t = 0$, and

$$\frac{2\Omega_0 d'(0)}{c} = \Delta\Omega_d$$

is the Doppler shift in frequency, caused by speed $v(0) = d'(0)$.

The Fourier transform (6.10), with (6.11), is of the form

$$S(\Omega) = \int_{-\infty}^{\infty} w(t) \exp \left(j \frac{2\Omega_0}{c} \left(d(0) + d'(0)t + \sum_{n=2}^{\infty} \frac{1}{n!} d^{(n)}(0)t^n \right) \right) \exp(-j\Omega t) dt \quad (6.12)$$

This is the Fourier transform of a product of the window $w(t)$ and a function with higher-order derivatives, calculated at the frequency $\Omega - 2\Omega_0 d'(0)/c = \Omega - \Delta\Omega_d$. Its absolute value is

$$|S(\Omega)| = \left| W(\Omega - \Delta\Omega_d) *_{\Omega} \text{FT} \left\{ \exp \left(j \frac{2\Omega_0}{c} \sum_{n=2}^{\infty} \frac{1}{n!} d^{(n)}(0)t^n \right) \right\} \right|,$$

where $*_{\Omega}$ denotes convolution in frequency and $W(\Omega)$ is the Fourier transform of $w(t)$. The window in classical radar signal processing is defined by the coherent integration time. Thus, the Fourier transform is located at and around the Doppler shift $\Omega = \Delta\Omega_d$. It is spread by the factor

$$S_{\text{spread}}(\Omega) = \text{FT} \left\{ \exp \left(j \frac{2\Omega_0}{c} \sum_{n=2}^{\infty} \frac{1}{n!} \Delta d^{(n)}(0)t^n \right) \right\}.$$

This factor depends on the derivatives of the distance, starting from the second order (first-order derivative of the Doppler shift), that is, the spread factor depends on

$$s_f(t) = \frac{1}{2}d''(0)t^2 + \frac{1}{6}d'''(0)t^3 + \dots$$

It can significantly degrade the concentration of the radar image, obtained as a squared absolute Fourier transform,

$$P(\Omega) = |S(\Omega)|^2.$$

Concentration of radar images, that are blurred due to the long CIT and/or nonuniform target movement, can easily be improved by using the S-method form of the resulting image calculation as

$$SM(\Omega) = \frac{1}{\pi} \int_{-\infty}^{\infty} S(\Omega + \theta) S^*(\Omega - \theta) d\theta. \quad (6.13)$$

Here in contrast to standard S-method introduced in Chapter 3, the Fourier transform $S(\Omega)$ is used instead of the STFT. This form can improve the image concentration. By replacing $S(\Omega)$ from (6.12) into (6.13), we get

$$SM(\Omega) = W_e(\Omega - \Delta\Omega_d) *_{\Omega} \text{FT} \left\{ \exp \left(j \frac{2\Omega_0}{c} \left(\frac{1}{3!} d'''(0)t^3 + \dots \right) \right) \right\}, \quad (6.14)$$

with $W_e(\Omega)$ being the Fourier transform of $w(t/2)w(-t/2)$.

The radar image, based on this form, is located at the same position as the Fourier transform image, $\Omega = \Delta\Omega_d$, but with the spreading term, due to the target motion,

$$S_{\text{spread}}(\Omega) = \text{FT} \left\{ \exp \left(j \frac{2\Omega_0}{c} \left(\frac{1}{3!} d'''(0)t^3 + \dots \right) \right) \right\},$$

starting from the third derivative $d'''(0)$,

$$s_f(t) = \frac{1}{6} d'''(0)t^3 + \frac{1}{120} d^{(5)}(0)t^5 + \dots \quad (6.15)$$

Remember that in the Fourier transform-based image the spreading terms, due to the target motion, started from the second derivative $d''(0)$. It means that in this form, the points with linear Doppler changes

$$\frac{2\Omega_0}{c} d'(t) = \Delta\Omega_d(t) = \Delta\Omega_d(0) + at$$

will be fully concentrated without any spread, since here $s_f(t) = 0$.

A discrete version of (6.13) reduces to the S-method, applied on the DFT of the Doppler part of the signal

$$SM_L(k) = \sum_{i=-L}^L S(k+i)S^*(k-i) = |S(k)|^2 + 2\operatorname{Re}\left\{\sum_{i=1}^L S(k+i)S^*(k-i)\right\}$$

In theory, L should be such to provide calculation over the whole frequency range, when the pseudo Wigner distribution is obtained.

The first term is $|S(k)|^2$, that is, the squared absolute Fourier transform (classic radar image), while the terms $2\operatorname{Re}\{S(k+i)S^*(k-i)\}$, for $i = 1, 2, \dots$, are used to improve its concentration, in the case of a time-varying Doppler shift. Only few terms are enough to achieve high resolution. The S-method can be realized in a recursive form,

$$SM_L(k) = SM_{L-1}(k) + 2\operatorname{Re}\{S(k+L)S^*(k-L)\}, \quad (6.16)$$

with $SM_0(k) = |S(k)|^2$ being the standard radar image. Therefore, the S-method improvement can be achieved starting with the already obtained Fourier transform-based radar image, with an additional simple calculation according to (6.16). Here we applied a window $w(m)$ as well and calculated the Fourier transforms of $w(m)q(m,n)$. In the examples, we used a window such that that $w^2(m)$ is a Hann(ing) window.

6.1.4 ISAR Basic Definitions and Model

Inverse synthetic aperture radar (ISAR) is a method for obtaining a high resolution of a target based on the change in viewing angle of the target with respect to the fixed radar. The illustration of a target and relevant quantities are shown in Fig. 6.3. Suppose that a target consists of P point scatterers whose locations are (x_i, y_i) , $i = 1, 2, \dots, P$, in the coordinate system whose center is the center of target rotation. The coordinate in the direction of the line radar-target (range coordinate) is denoted by x_i , while y_i is coordinate in the normal direction to this line (cross-range coordinate). The target total movement can be considered as a superposition of translation and rotation. During the considered time interval t , the point scatterer rotates for $\theta_R(t) = \Omega_R t$. New coordinates of the scatterer are

$$\begin{bmatrix} x'_i \\ y'_i \end{bmatrix} = \begin{bmatrix} \cos(\theta_R(t)) & \sin(\theta_R(t)) \\ -\sin(\theta_R(t)) & \cos(\theta_R(t)) \end{bmatrix} \begin{bmatrix} x_i \\ y_i \end{bmatrix} \quad (6.17)$$

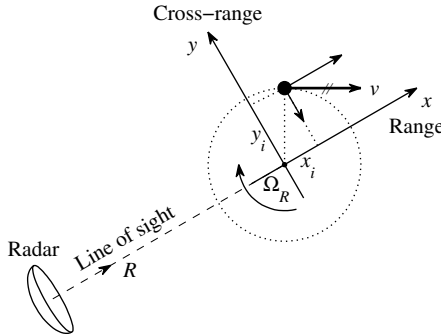


Figure 6.3 Geometry of the ISAR system.

The total range position is

$$\begin{aligned} d(t) &= \sqrt{(R + x'_i)^2 + y_i'^2} \\ &= \sqrt{[R + x_i \cos(\theta_R(t)) + y_i \sin(\theta_R(t))]^2 + [-x_i \sin(\theta_R(t)) + y_i \cos(\theta_R(t))]^2} \end{aligned} \quad (6.18)$$

In general, this definition for distance should be used in simulations and quantitative analysis. For a qualitative analysis, we will use approximations. Since $R \gg x_i$ and $R \gg y_i$, we can write

$$d(t) \cong R + x'_i = R + x_i \cos(\theta_R(t)) + y_i \sin(\theta_R(t))$$

Assuming that the rotation angle $\theta_R(t)$ is small, within the coherent integration time, then

$$\begin{aligned} \cos(\theta_R(t)) &\rightarrow 1, \\ \sin(\theta_R(t)) &\rightarrow \theta_R(t) \end{aligned}$$

and

$$d(t) \cong R + x_i + y_i \Omega_R t.$$

The distance $d(t)$ changes from $d(0) \cong R + x_i$ to $d(T_c) \cong R + x_i + y_i \Omega_R T_c$ within the coherent integration time that is relevant for the analysis of the Doppler part of signal. For the range analysis, the considered interval is $T_r = T_c/M \ll T_c$.

Thus, for the range calculation the distance changes from $d(0) \cong R + x_i$ to $d(T_c) \cong R + x_i + y_i\Omega_R T_c/M$. The distance changes, for the range calculation, are much lower (since it is considered within much shorter interval). That is why we usually consider only changes in the Doppler domain, while the range domain is considered as well concentrated. Another reason for this kind of analysis is in the existence of other methods for accurate estimation of the range position.

The Doppler shift is proportional to the velocity in direction of radar-target line (line of sight), (6.7),

$$\begin{aligned}\Delta\Omega_d &= \frac{2\Omega_0}{c} \frac{d}{dt}[d(t)] \cong \frac{2\Omega_0}{c} \frac{d}{dt}[R + x_i \cos(\theta_R(t)) + y_i \sin(\theta_R(t))] \\ &\cong \frac{2\Omega_0}{c} \frac{d}{dt}[R + x_i + y_i\Omega_R t]\end{aligned}$$

Another reason that we must not neglect the term $y_i\Omega_R t$ is in the fact that it is multiplied by a big constant $2\Omega_0/c$, in defining the phase of $\exp(2\Omega_0 d(t)/c)$. The Doppler shift is proportional to the cross-range y_i ,

$$\Delta\Omega_d = \frac{2\Omega_0}{c} y_i \Omega_R \sim y_i,$$

assuming, in addition to the above approximations, that the translation is compensated, $R(t) = R$.

Recall now that the two-dimensional Fourier transform of $q(m, n)$ is located, along the frequency corresponding to m , at the Doppler frequency $\Delta\Omega_d$, in the ISAR case proportional to y_i . The other coordinate contains the range information. Thus, the two-dimensional Fourier transform of mixed radar signal is the radar image, in an ideal case representing location of the reflecting point in the range/cross-range domain

$$Q(x, y) \sim \delta(x - x_i, y - y_i).$$

The ideal case here means that the distance does not change significantly, $d(t) \cong R + x_i$, during the pulse repetition time T_r , while the distance change may be considered as linear $d(t) = R + x_i + y_i\Omega_R t$ within the coherent integration time $T_c = M T_r$.

The two-dimensional Fourier transform of the received, dechirped lowpass filtered signal is

$$Q(k, l) = \sum_{m=0}^{M-1} \sum_{n=0}^{N-1} q(m, n) \exp(-j[2\pi m k / M + 2\pi n l / N]), \quad (6.19)$$

where time is discretized $t - mT_r = nT_s$. Again, index m corresponds to the chirp index (slow time), while index n is the index of signal sample within one chirp, fast-time. The illustration of the discrete $q(m, n)$ values is presented in Fig. 6.2. Note that due to the same sign minus in the range direction and the Fourier transform, (6.5), the inverse Fourier transform should be used along this direction or just the range coordinate should switch the sign in calculation. The coordinate axes should be scaled with the resolution parameters.

The absolute squared modulus of the Fourier transform (the periodogram)

$$P(k, l) = |Q(k, l)|^2$$

represents an ISAR image.

Cross-range resolution directly follows from the relation $\Delta\Omega_d = 2\Omega_0 y_i \Omega_R / c$, that is, form $y_i = \Delta\Omega_d / (2\Omega_0 \Omega_R / c)$. Since we already determined the resolution in Doppler shift by (6.9), the resolution in cross-range is obtained as $R_{\text{Dopp}} / (2\Omega_0 \Omega_R / c)$

$$R_{\text{cross-range}} = \frac{\pi c}{\Omega_0 T_c \Omega_R}. \quad (6.20)$$

A ratio of resolutions in the range and cross-range is

$$\frac{R_{\text{range}}}{R_{\text{cross-range}}} = \frac{\Omega_0 T_c \Omega_R}{2\pi B}.$$

Note that the cross-range resolution depends on the target parameter Ω_R .

In general, the conditions $\sin(\Omega_R t) = \Omega_R t$ and $\cos(\Omega_R t) = 1$ are not satisfied. A more realistic case is

$$\sin(\Omega_R t) = \Omega_R t - (\Omega_R t)^3 / 3! + \dots$$

and

$$\cos(\Omega_R t) = 1 - (\Omega_R t)^2 / 2! + \dots,$$

when the Doppler part of the signal is a linear (or higher-order) frequency-modulated signal with varying frequency. In that case time-frequency representations will improve a radar image.

Example 6.3. Assume that a target moves along a straight line parallel to the ground at a height h , that its ground distance from radar is z , meaning the range is $d = \sqrt{h^2 + z^2}$. From the radar position the target is seen at an angle α , $\sin(\alpha) = h/d$. In the next instant $t + \Delta t$ the target is moved to the new position corresponding to the ground

distance $z + \Delta z$, radar range is $\sqrt{h^2 + (z + \Delta z)^2}$, and it is seen from the radar at an angle $\alpha + \Delta\alpha$. Thus, this movement can be considered as a translation for Δd and rotation for $\Delta\alpha$.

If the target speed is v_t then $\Delta z = v_t \Delta t$. Since

$$\alpha = \arctan\left(\frac{h}{z}\right) \text{ and } \frac{\partial \alpha}{\partial z} = \frac{-h}{z^2 + h^2}$$

we get

$$\Delta\alpha \cong \frac{-h}{z^2 + h^2} \Delta z = -\frac{h}{d^2} \Delta z = -v_t \Delta t \frac{h}{d^2}$$

□

Example 6.4. The setup that we will consider for the ISAR illustration assumes: high-resolution radar operating at the frequency $f_0 = 10.1$ GHz, $\Omega_0 = 2\pi f_0$, bandwidth of linear frequency-modulated chirps $B = 300$ MHz, and pulse repetition frequency $f_r = 1/T_r = 2$ kHz with 2048 pulses in one revisit (image coherent integration time $T_c \cong 1$ s, cases with $T_c \cong 2$ s and $T_c \cong 4$ s are also considered). Pulse repetition time is $T_r = 0.5$ ms. The target is at 2 km distance from the radar, and rotates at $\Omega_R = 4 \frac{\pi}{180}$ 1/s = 4° /s. The nonlinear rotation with frequency $\Omega = \pi$ 1/s is superimposed, $\Omega_R(t) = \Omega_R + A \sin(\Omega t)$, and amplitude $A = 1.25 \frac{\pi}{180}$ 1/s corresponds to the total change in angular frequency Ω_R for $2.5 \frac{\pi}{180}$ 1/s. Note that here the range and the cross-range resolutions are $R_{\text{range}} = c/(2B) = 0.5$ m, and $R_{\text{cross-range}} = \pi c / (\Omega_0 T_c \Omega_R) = 0.106$ m (calculated for $T_c = 2$ s with $\Omega_R \cong 4 \frac{\pi}{180}$ 1/s, neglecting effects of nonlinear rotation). Assume that at $t = 0$ the line of points 1, 2, and 3 is parallel to the line of sight Fig. 6.4. Then at $t = 0$ we have $(x_1, y_1) = (-2.5, 1.44)$, $(x_2, y_2) = (0, 1.44)$, $(x_3, y_3) = (2.5, 1.44)$, $(x_4, y_4) = (1.25, -0.72)$, $(x_5, y_5) = (-1.25, -0.72)$, and $(x_6, y_6) = (0, -2.89)$. All coordinates are in meters. Note again that resolutions in both directions depend on T_c , c , and B , but not on T_r and N .

The signal model corresponding to one of six rotating parts is

$$d_i(t) = \sqrt{[R + x_i \cos(\theta_R(t)) + y_i \sin(\theta_R(t))]^2 + [-x_i \sin(\theta_R(t)) + y_i \cos(\theta_R(t))]^2}$$

$$\Delta\Omega_i = \frac{2\Omega_0}{c} \frac{d}{dt}[d_i(t)] \quad (6.21)$$

with

$$\theta'_R(t) = \Omega_R(t) = \Omega_R + A \sin(\Omega t),$$

$$\theta_R(t) = \Omega_R t - \frac{A}{\Omega} \cos(\Omega t) + \phi_0.$$

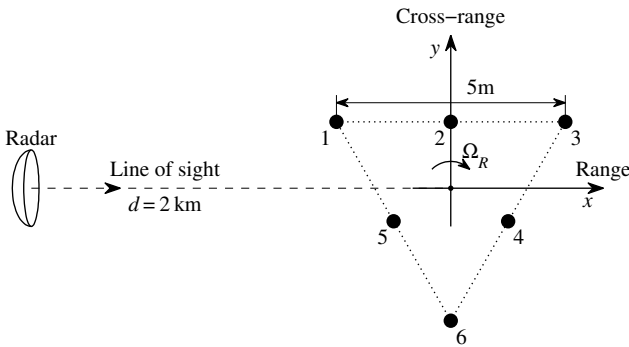


Figure 6.4 Illustration of the target simulation setup.

Thus, the signal model is of the form

$$q(m, t) = \sum_{p=1}^6 q_i(m, t) = \sum_{i=1}^6 \sigma_i \exp\left(j\Omega_0 \frac{2d_i(t)}{c}\right) \exp\left(-j2\pi B f_r(t - mT_r) \frac{2d_i(t)}{c}\right) \quad (6.22)$$

We assumed $T_0 = 0$ and neglected constant phase terms, with $t - mT_r = nT_s$. The model is completely defined for simulations.

The obtained results for several target positions are presented in Fig. 6.5. Radar images in the range/cross-range domain obtained by using the Fourier transform (periodogram), the S-method, and the Wigner distribution at time instants $t = 0, 4$, and 9 s are given. In order to keep the same scale for presentation, we presented nonnegative values of the Wigner distribution.

To illustrate the cause of the cross-range spread, in the analyzed ISAR images, consider the case at $t = 9$ s and the range bins at $x = -0.5$ m and $x = 1.5$ m. The distribution of the cross-range values over the considered coherent integration time is shown in Fig. 6.6. For $x = 1.5$ m from Fig. 6.6(b) we can see that the middle reflecting point is stationary in the Doppler shift, meaning that it will be highly concentrated in corresponding ISAR image Fig. 6.5(g). However, the remaining two reflecting points at this range move over the cross-range, resulting in the spread in ISAR image. \square

Example 6.5. The presented time-frequency-based method is applied to the models of Boeing 727 and Mig 25 that are often used as standard benchmarks for the ISAR imaging methods. In this example ISAR images are smeared due to nonuniform target motion during considered coherent integration time. The S-method is done according

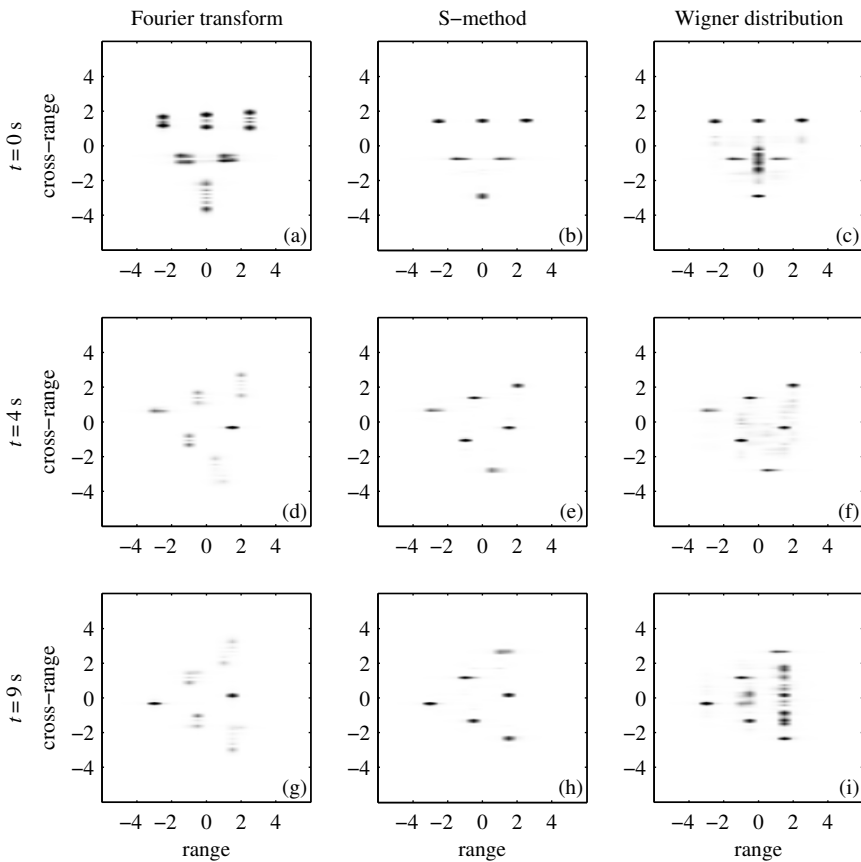


Figure 6.5 Radar image in the range/cross-range domain. The imaging method in (a, d, g) is a two-dimensional Fourier transform, in (b, e, h) it is the S-method, and in (c, f, i) it is the Wigner distribution. Three time instants are considered: (a - c) $t = 0$ s, (d - f) $t = 4$ s, and (g - i) $t = 9$ s.

to (6.16) for $L = 0$ (the standard Fourier transform), $L = 3$ and $L = 6$. The results are presented in Fig. 6.7. The readability improvement obtained by using the S-method is evident. \square

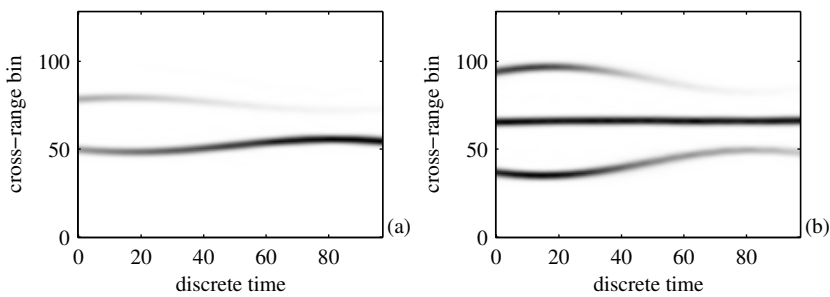


Figure 6.6 Time-frequency representation of the bin at range (a) $x = -0.5\text{ m}$ and (b) $x = 1.5\text{ m}$ at $t = 9\text{ s}$.

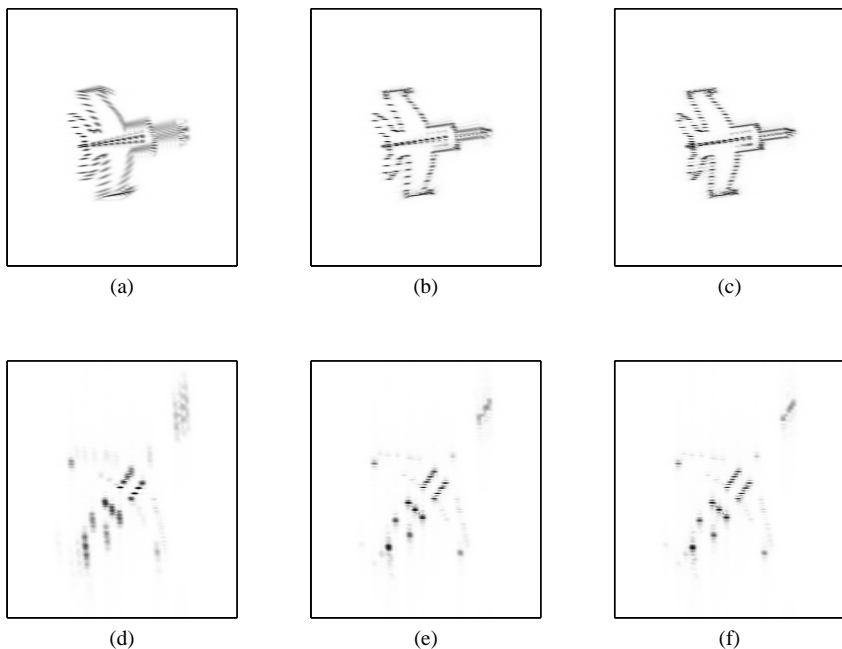


Figure 6.7 Radar images for (a - c) Mig 25 and (d - f) Boeing 727. (a, d) The standard two-dimensional Fourier transform images; (b, e) the S-method with $L = 3$; and (c, f) the S-method with $L = 6$.

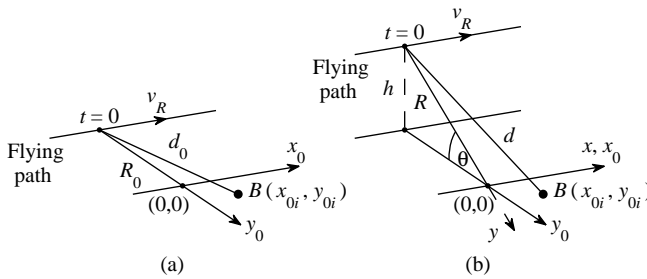


Figure 6.8 Geometry of the SAR systems: (a) $\theta = 0$ and (b) $\theta \neq 0$.

6.1.5 SAR Setup

In the SAR imaging the target is fixed while the radar moves and changes viewing angle (circular radar). Consider a SAR setup, as in Fig. 6.8. If the radar moves along the line, as it is plotted in Fig. 6.8, then, for a given instant t and small consideration interval, this movement can be approximated by an appropriate rotation, as discussed and illustrated within an ISAR example. Assume first that the radar movement (rotation or equivalent rotation) is parallel to the imaged terrain. This position of the radar will be described by the elevation angle $\theta = 0$. Denote the radar speed as \vec{v}_R and assume that it moves in a direction of the x_0 axis of the coordinate system, $\vec{v}_R = v_R \vec{i}_{x_0}$. Assume that the line of sight is in the direction of the y_0 axis, with unit vector \vec{i}_{y_0} . The distance of the radar to the center of the imaged terrain is denoted by $\vec{R}_0 = R_0 \vec{i}_{y_0}$. At one instant, the radar movement corresponds to the rotation of the terrain, with respect to the radar, with

$$\vec{v}_R = \vec{\Omega}_B \times (-\vec{R}_0). \quad (6.23)$$

Now assume that there is only one stationary reflecting point on the ground. Assume that it is located at (x_{0i}, y_{0i}, z_{0i}) from the center of image defined by \vec{R}_0 . Just to restate, x_{0i} is the point coordinate in the direction normal to the line of sight and normal to the rotation vector $\vec{\Omega}_B$, y_{0i} is the line of sight direction, and z_{0i} is normal to the line of sight and parallel to the rotation vector $\vec{\Omega}_B$. Taking into account that the image plane with reflecting point(s) rotate with $\vec{\Omega}_B$ around the center, point movement (trajectory) can be described by the simple rotation matrix, as in the

ISAR case, resulting in

$$\begin{aligned}x_{0i}(t) &= x_{0i} \cos(\Omega_B t) + y_{0i} \sin(\Omega_B t) \\y_{0i}(t) &= -x_{0i} \sin(\Omega_B t) + y_{0i} \cos(\Omega_B t) \\z_{0i}(t) &= z_{0i}.\end{aligned}$$

The signal $s_i(t)$ reflected from this point, as a function of the distance from the radar to that point $d_i(t)$, or distance traveled by the radar signal $2d_i(t)$, is of the form

$$s_i(t) = \sigma_i \exp\left(j \frac{\Omega_0}{c} 2d_i(t)\right) = \exp\left(j \frac{2\Omega_0}{c} \sqrt{x_{0i}^2(t) + (R_0 + y_{0i}(t))^2 + z_{0i}^2(t)}\right). \quad (6.24)$$

Since the distance R_0 is much greater than any point coordinate, for qualitative analysis, we may write

$$\begin{aligned}s_i(t) &\cong \sigma_i \exp\left(j \frac{2\Omega_0}{c} (R_0 + y_{0i}(t))\right), \\s_i(t) &= \sigma_i \exp\left(j \frac{2\Omega_0}{c} (-x_{0i} \sin(\Omega_B t) + y_{0i} \cos(\Omega_B t))\right),\end{aligned} \quad (6.25)$$

where the constant phase terms $\exp(j2\Omega_0 R_0/c)$ is omitted and we returned to the equality sign for simplicity of further notation. For small Ω_B we get

$$s_i(t) = \sigma_i \exp\left(-j \frac{2\Omega_0 \Omega_B}{c} x_{0i} t\right). \quad (6.26)$$

Thus, again the Fourier transform position is concentrated to the frequency proportional to the coordinate normal to the line of sight, here denoted by x .

In general, if radar is at $\theta \neq 0$, we have a new coordinate system, connected to the radar, in which the initial positions of the reflecting points are rotated for θ around x_0 axis (Fig. 6.8(b)) as

$$\begin{aligned}x_{0i}(\theta) &= x_{0i} \\y_{i0}(\theta) &= y_{0i} \cos(\theta) - z_{0i} \sin(\theta) \\z_{0i}(\theta) &= y_{0i} \sin(\theta) + z_{0i} \cos(\theta).\end{aligned} \quad (6.27)$$

The rotation in this coordinate system then remains the same as for $\theta = 0$, with the rotation vector

$$\vec{v}_R = \vec{\Omega}_B \times (-\vec{R})$$

$$v_R = \Omega_B R_0 / \cos(\theta) = \Omega_{B\theta} R_0.$$

The resulting rotation is

$$x_i(t) = x_{0i} \cos(\Omega_{B\theta} t) + y_{0i}(\theta) \sin(\Omega_{B\theta} t)$$

$$y_i(t) = -x_{0i} \sin(\Omega_{B\theta} t) + y_{0i}(\theta) \cos(\Omega_{B\theta} t)$$

$$z_i(t) = y_{0i} \sin(\theta) + z_{0i} \cos(\theta),$$

with $y_{0i}(\theta)$ defined by (6.27) and signal $s_i(t)$ is of the form

$$s_i(t) = \sigma_i \exp \left(j \frac{2\Omega_0}{c} (-x_{0i} \sin(\Omega_{B\theta} t) + [y_{0i} \cos(\theta) - z_{0i} \sin(\theta)] \cos(\Omega_{B\theta} t)) \right). \quad (6.28)$$

For small $\Omega_{B\theta}$, the signal form (6.26) follows.

Therefore, in a formal mathematical way the SAR and ISAR models could be treated in the same way.

6.1.6 Micro-Doppler Effects in ISAR/SAR Imaging

The micro-Doppler effect appears in the ISAR/SAR radar imaging when the target has one or more very fast moving parts. The analysis and processing of micro-Doppler effects are an excellent example of when the role of time-frequency analysis is not only to improve the presentation, but to be a crucial tool for considering and solving the practical problem. This effect can decrease readability of radar images. However, the micro-Doppler effect at the same time carries information about the features of moving parts (type, velocity, size). Thus, the primary goal is to remove this effect and to provide a radar image without this disturbance. However, in some applications the focus is just on the fast moving parts, whose parameters (size, way, and speed of movement) could help to describe and detect that parts. Here we should take into account that their presentation in cross-range is proportional not to the rigid body angular frequency, but to their much higher angular frequency, making them look much further in the cross-range domain.

Here we will illustrate this problem and one time-frequency-based solution by using the L-statistics forms (Chapter 5) of the time-frequency radar signal

representation, to separate the rigid body and micro-Doppler. The L-statistics will be performed on the spectrogram, while the rigid body signal synthesis will be done in the STFT domain. This time-frequency-based approach is very simple to use and produces good results.

6.1.6.1 Micro Doppler Description in ISAR

The common ISAR imaging models assume that all the point scatterers share the same angular motion (Fig. 6.3). Then the Doppler part of the received signal, within the m th radar sweep, corresponding to K rigid body points, can be written by

$$s(t) = \sum_{i=1}^K \sigma_{Bi} \exp \left(j \frac{2\Omega_0}{c} [R_B(t) + x_{Bi} \cos \theta_B(t) + y_{Bi} \sin \theta_B(t)] \right), \quad (6.29)$$

where the target's translation and angular motion are denoted as $R(t)$ and $\theta(t)$, with index B being added to indicate the rigid body points and parameters (as the basic ones in the radar image). For each point we have used the approximation $d_i(t) = \sqrt{(R+x_i)^2 + y_i^2} \cong R + x_i$ to obtain $d_{Bi}(t) \cong R_B(t) + x_{Bi} \cos(\theta_B(t)) + y_{Bi} \sin(\theta_B(t))$. The initial locations of points in the coordinate system for which the origin is in the center of the target rotation are (x_{Bi}, y_{Bi}) .

During the coherent integration time, $T_c = MT_r$, inequality $|\theta_B(t)| \ll 1$ holds for the rigid body, following in $\cos \theta_B(t) \approx 1$ and $\sin \theta_B(t) \approx \theta_B(t) = \Omega_B t$, where Ω_B is the effective body rotation rate after motion compensation.

Assume that there are P fast rotating points that rotate around (x_{R0i}, y_{R0i}) with a radius A_{Ri} . The index R is used to indicate fast moving points. The coordinates of this point are

$$\begin{aligned} x_i &= x_{R0i} + A_{Ri} \sin(\theta_R(t)) \\ y_i &= y_{R0i} + A_{Ri} \cos(\theta_R(t)) \end{aligned} \quad (6.30)$$

According to (6.17), we have

$$\begin{bmatrix} x'_i \\ y'_i \end{bmatrix} = \begin{bmatrix} \cos \theta_B(t) & \sin \theta_B(t) \\ -\sin \theta_B(t) & \cos \theta_B(t) \end{bmatrix} \begin{bmatrix} x_{R0i} + A_{Ri} \sin \theta_{Ri}(t) \\ y_{R0i} + A_{Ri} \cos \theta_{Ri}(t) \end{bmatrix}, \quad (6.31)$$

where $\theta_B(t)$ represents the angular velocity of rigid body. Assume now that the rotation speed of the i th fast rotating point is Ω_{Ri} as well as that the initial angle is zero then $\theta_{Ri}(t) = \Omega_{Ri}t$. After distance compensation range position of fast rotating

reflector is

$$\begin{aligned} d(t) &\cong x'_i = [x_{R0i} + A_{Ri} \sin(\theta_{R_i}(t))] \cos(\theta_B(t)) + [y_{R0i} + A_{Ri} \cos(\theta_{R_i}(t))] \sin(\theta_B(t)) \\ &= [x_{R0i} \cos(\theta_B(t)) + y_{R0i} \sin(\theta_B(t))] + A_{Ri} \sin(\theta_{R_i}(t) + \theta_B(t)). \end{aligned}$$

In the case of $|\theta_B(t)| \ll 1$, $\cos \theta_B(t) \approx 1$ and $\sin \theta_B(t) \approx \theta_B(t) = \Omega_B t$,

$$d(t) \cong x'_i = [x_{R0i} + y_{R0i} \Omega_B t] + A_{Ri} \sin((\Omega_{Ri} + \Omega_B)t),$$

or, after the distance x_{R0i} compensation, with $\Omega_{Ri} \gg \Omega_B$,

$$d(t) \cong y_{R0i} \Omega_B t + A_{Ri} \sin(\Omega_{Ri} t). \quad (6.32)$$

The received signal, including both rigid and fast rotating micro-Doppler points (indexed with R) can be written as

$$s(t) = \sum_{i=1}^K \sigma_{Bi} \exp \left(j \frac{2\Omega_0}{c} y_{Bi} \Omega_B t \right) + \sum_{i=1}^P \sigma_{Ri} \exp \left(j \frac{2\Omega_0}{c} [y_{R0i} \Omega_B t + A_{Ri} \sin(\Omega_{Ri} t)] \right). \quad (6.33)$$

The first term in (6.33) represents complex sinusoids concentrated at frequencies proportional to the position of the reflector y_{Bi} , $i \in [1, K]$ and rotating rate Ω_B .

Since the Doppler component in the received signal is considered, the analysis reduces to a one-dimensional signal and its Fourier transform in the continuous or discrete form

$$\begin{aligned} S(\Omega) &= \int_{-\infty}^{\infty} s(t) e^{-j\Omega t} dt, \\ S(k) &= \sum_{i=0}^{M-1} s(i) e^{-j2\pi ik/M}. \end{aligned} \quad (6.34)$$

If we calculate the Fourier transform of the signal corresponding to one point of the rigid body, we get a delta pulse at the position $\Omega = 2\Omega_0 \Omega_B y_{Bi}/c$ proportional to the cross-range coordinate y_{Bi} . Note that the delta pulse position depends not only on the radar parameters that are constant, but also on the rotation speed Ω_B .

However, the Doppler part of the radar signal that corresponds to a rotating reflector is a sinusoidally modulated signal, with the frequency

$$\Omega_{Ri}(t) = \frac{2\Omega_0}{c} [y_{R0i} \Omega_B + A_{Ri} \Omega_{Ri} \cos(\Omega_{Ri} t)]. \quad (6.35)$$

It can be concluded that the location of rotating scattering points in the cross-range coordinate is proportional to its true location multiplied by the rigid body rotation speed. In addition, its resulting rotating rate $\Omega_{Ri} = \theta'_{Ri}(t)$ is significantly higher than the rotating rate of the rigid body Ω_B . Therefore, the radar image of rotating reflectors is not concentrated. It is spread over the interval proportional to its rotating rate and the radius of rotation. It is also important to note a different scale for the radar image of rotating reflector comparing to the radar image of the rigid body.

The Fourier transform of a sinusoidally modulated signal is known in the literature. Its coefficients are in the form of Bessel functions. The time-frequency representation of this part of the radar signal, within the coherent integration time would be concentrated around the sinusoidal instantaneous frequency $\Omega_{Ri}(t)$ (6.35) in the time-frequency plane. A similar form of the received signal is obtained in the case of vibrating points. If a reflecting point vibrates along the line parallel to the line of sight with the central point (x_{R0i}, y_{R0i}) and frequency Ω_{Vi} , reaching the maximum amplitude A_{Ri} from the central point, then

$$s(t) = \sum_{i=1}^K \sigma_{Bi} \exp \left(j \frac{2\Omega_0}{c} y_{Bi} \Omega_B t \right) + \sum_{i=1}^P \sigma_{Vi} \exp \left(j \frac{2\Omega_0}{c} [y_{R0i} \Omega_B t + A_{Ri} \sin(\Omega_{Vi} t)] \right).$$

Thus, the vibrations can be analyzed in the same way as the rotations. Oscillations or any other similar periodic movements can be easily described within the previous framework as well. Any other arbitrary motion can be described by using

$$\begin{aligned} x_i &= x_{R0i} + x_{arb}(t) \\ y_i &= y_{R0i} + y_{arb}(t) \end{aligned} \quad (6.36)$$

in (6.30). The Doppler part of the radar signal that corresponds to an arbitrary moving point is a frequency-modulated signal with the instantaneous frequency

$$\Omega_{Ri}(t) = \frac{2\Omega_0}{c} [y_{R0i} \Omega_B + d(x_{arb}(t))/dt],$$

with approximations as in the derivation of (6.32). Note that relations (6.30) and (6.31), without any approximation, can be used in simulations, instead of the presented compact form (6.32) that is appropriate for the qualitative analysis.

6.1.7 Micro-Doppler Description in SAR

Consider the Doppler part in the SAR signal (6.28)

$$s_i(t) = \sigma_i \exp \left(j \frac{2\Omega_0}{c} (-x_{0i} \sin(\Omega_B \theta t) + [y_{0i} \cos(\theta) - z_{0i} \sin(\theta)] \cos(\Omega_B \theta t)) \right). \quad (6.37)$$

Assume now that in addition to the pure rotation, caused by radar movement, the i th point rotates around its central point (x_{0i}, y_{0i}, z_{0i}) in the plane $x_0 O y_0$ with Ω_{R_i} . Then

$$\begin{aligned} x_i(t) &= [x_{0i} + A_i \sin(\Omega_{R_i} t)] \cos(\Omega_B \theta t) + [y_{0i} + A_i \cos(\Omega_{R_i} t)] \cos(\theta) \sin(\Omega_B \theta t) \\ y_i(t) &= -[x_{0i} + A_i \sin(\Omega_{R_i} t)] \sin(\Omega_B \theta t) + [y_{0i} + A_i \cos(\Omega_{R_i} t)] \cos(\theta) \cos(\Omega_B \theta t) \\ z_i(t) &= y_{0i} \sin(\theta) + z_{0i} \cos(\theta), \end{aligned}$$

with

$$\begin{aligned} s_i(t) &= \sigma_i \exp \left(j \frac{2\Omega_0}{c} y_i(t) \right) \\ &= \sigma_i \exp \left(j \frac{2\Omega_0}{c} (-[x_{0i} + A_i \sin(\Omega_{R_i} t)] \sin(\Omega_B \theta t) \right. \\ &\quad \left. + [y_{0i} + A_i \cos(\Omega_{R_i} t)] \cos(\theta) \cos(\Omega_B \theta t)) \right). \end{aligned}$$

Here the approximations $\Omega_B \theta t \ll 1$ and $A_i \sin(\Omega_{R_i} t) \ll x_{0i}$ hold, and

$$s_i(t) \cong \sigma_i \exp \left(j \frac{2\Omega_0}{c} [-x_{0i} \Omega_B \theta t + A_i \cos(\Omega_{R_i} t) \cos(\theta)] \right).$$

The corresponding instantaneous frequency, in the spectrum of signal, is

$$\Omega_i(t) = \frac{2\Omega_0 \Omega_B \theta}{c} \left(-x_{0i} - A_i \frac{\Omega_{R_i}}{\Omega_B \theta} \sin(\Omega_{R_i} t) \cos(\theta) \right) \quad (6.38)$$

Regarding to the theoretical analysis, the ISAR and SAR setup can be considered in a unified way.

Assume now that in addition to the pure rotation, caused by radar movement, the point has a fast arbitrary movement around (x_{0i}, y_{0i}, z_{0i}) , described by

$$\begin{aligned} x_i(t) &= x_{0i} + x_{arb}(t), \\ y_i(t) &= y_{0i} + y_{arb}(t), \\ z_i(t) &= z_{0i} + z_{arb}(t), \end{aligned} \quad (6.39)$$

where index $_{arb}$ is used to denote such a movement. With approximation $\Omega_{B\theta}t \ll 1$, appropriate distance compensation and by neglecting constant phase terms, we get

$$s_i(t) \cong \sigma_i \exp(j2(-x_0 i \Omega_{B\theta} t + [y_{arb}(t) \cos(\theta) - z_{arb}(t) \sin(\theta)]) \Omega_0/c).$$

In simulations, the form without approximations, should be used.

6.1.8 Time-Frequency Analysis and L-Statistics

A simplest way to localize the signal behavior in shorter intervals, within the coherent integration time, is in applying a window function to the standard Fourier transform. The resulting short-time Fourier transform in discrete form is

$$STFT(m, k) = \sum_{i=0}^{M-1} s(i) w(i-m) e^{-j2\pi ik/M},$$

where $w(i)$ is a window function used to truncate the considered signal within the coherent integration time. In most of the provided examples, we will use the Hann(ing) window. The window width is M_w , $w(i) \neq 0$ for $-M_w/2 \leq i \leq M_w/2 - 1$. In these applications, the window is zero-padded up to M , the same number of samples as in (6.34), so that we have the same frequency grid in the STFT as in the DFT. Then we can later easily reconstruct the Fourier transform, without interpolation, with the concentration close or equal to the concentration of the original DFT. We know that, by using a lag window $w(i)$ in the STFT, the concentration in frequency is reduced, as compared to the original DFT (6.34). For example, if the lag window width is M_w , then the concentration of a sinusoidal signal is reduced M/M_w times, that is, the STFT-based ISAR/SAR image of a rigid body point (the main lobe of the DFT of a sinusoid) would be approximately M/M_w times wider than the original DFT-based image of the same reflecting point. We will also refer to this effect as the concentration being lower M/M_w times in the STFT than in the original DFT.

6.1.8.1 Restoring the High DFT Concentration from the STFT

The concentration could be restored to the original one by summing all the low concentrated STFT (complex) values over m . Since we calculated $STFT(m, k)$ with the window of the width M_w , there are two possibilities for its summation: (1) For all time instants $0 \leq m \leq M - 1$, when the signal $s(i)$ has to be zero-padded for $-M_w \leq i < 0$ and $M \leq i < M + M_w - 1$; and (2) for instants $M_w/2 \leq m \leq M - M_w/2$,

when zero-padding of $s(i)$ is not used. The reconstruction formula (reconstruction of the DFT from the STFT), for the case when the signal is not zero-padded, is

$$\begin{aligned} \sum_{m=M_w/2}^{M-M_w/2} STFT(m, k) &= \sum_{i=0}^{M-1} s(i) \left[\sum_{m=M_w/2}^{M-M_w/2} w(i-m) \right] e^{-j2\pi ik/M} \\ &= \sum_{i=0}^{M-1} s(i) w_1(i) e^{-j2\pi ik/M} = S_{w_1}(k). \end{aligned} \quad (6.40)$$

In the case when the STFT is calculated for each time instant (time step one in the STFT calculation), the resulting window $w_1(i)$ is constant, $w_1(i) = \text{const}$, for $M_w - 1 \leq i \leq M - M_w$, for any window. It means that during the most of the coherent integration time interval we have the normalized resulting window $w_1(i)$ being close to the rectangular one, with a small transition at the ending M_w points. The DFT of the window obtained during the process of reconstruction produces a concentration very close to the full range rectangular window case (i.e., no window). It means that we will be able to reconstruct the DFT with a concentration close to the one in the original DFT, by using low concentrated STFTs, calculated with narrow windows. In this way, we will restore the high concentrated radar image, although we used low concentrated STFT in the analysis.

The transition at the ending points of $w_1(i)$ can be easily overcame by zero-padding the analyzed signal $s(i)$ with M_w samples on both sides as explained before. Then the pure rectangular window $w_1(i)$ would be obtained for any window $w(i)$. The analysis is not restricted to step 1 in the STFT calculation. The same resulting window would be obtained for a step equal to half of the window width ($M_w/2$) and a Hann(ing), Hamming, triangular, or rectangular window. The same is valid for steps equal to $M_w/4, M_w/8, \dots$

In order to explain how this mechanism of restoring the original concentration, by summing low-concentrated images, works, consider a signal $s(m) = \exp(j2\pi k_0 m/N)$. Its DFT is $S(k) = N\delta(k - k_0)$. The STFT of this signal produces

$$STFT(n, k) = W(k - k_0) \exp(j2\pi(k - k_0)n/M).$$

The discrete form of (6.40), for the considered signal, is

$$S(k) = \sum_{m=0}^{M-1} W(k - k_0) e^{j2\pi m(k - k_0)/M} \quad (6.41)$$

Let us now analyze the result of summing the STFT values over n :

- For $k = k_0$, constant values of $W(0)$ will be summed over time interval, with the same phase $\exp(j2\pi(k - k_0)m/M) = \exp(j0)$.
- For any other k not equal to k_0 , that is, when $k = k_0 + l$, $l \neq 0$, we will have the summation with $\exp(j2\pi lm/M)$. Therefore, all values for $k \neq k_0$ are, in theory, averaged out to zero by summing the low concentrated STFTs over time.

Values of $S(k)$, when the signal is not zero-padded, are close to (6.41).

6.1.8.2 The Basic Idea for the Separation of the Rigid Body and the Fast-Rotating Part

The presented mechanism of restoring the original concentration of the DFT, in the conjunction with the knowledge of the time-frequency patterns behavior of fast-moving and rigid scattering points, can be used to obtain a micro-Doppler free, highly concentrated, radar image. The rigid body and the fast-moving points behave differently in the time-frequency representation of the returned radar signal within the coherent integration time. The rigid body signal is almost constant in time (stationary), while the fast-varying micro-Doppler part of the signal is highly nonstationary. This part of signal keeps changing its position in the frequency direction.

For the illustration, let us assume that the signal is returned from a one-point rigid body scatterer and a one-point fast-rotating (micro-Doppler) scatterer. Two cases with different strengths of the micro-Doppler reflection are analyzed. In the first case, the reflection coefficient of the rigid body is $\sigma_B = 1$, while the reflection coefficient of the fast-moving scatterer is $\sigma_R = 0.8$. The STFT representation of the resulting signal is shown in Fig. 6.9(a). The second case is with a strong micro-Doppler, $\sigma_R = 15$, and the same σ_B as in the previous case. The STFT representation of this signal is shown in Fig. 6.9(c). In both cases, the rigid body part is at a constant frequency for all t within the coherent integration time, while the fast rotating part changes frequency. If we perform sorting over the time axis, as in Fig. 6.9(b, d), we will not change the result of the summation in (6.40) since it is a commutative operation. By summing the STFT values over time, from either of these two plots, presented in Fig. 6.9(a) or Fig. 6.9(b), we will get the original DFT of the corresponding signal (Fig. 6.9(e)). Note that any value of σ_R from (and including) the case without micro-Doppler $\sigma_R = 0$ up to $\sigma_R \gg \sigma_B$ will not significantly change the pattern.

The basic idea for separating the rigid body and the fast-rotating part is in the sorting of STFT values of the returned radar signal along the time axis, within the coherent integration time. Since the rigid body return is stationary, the sorting

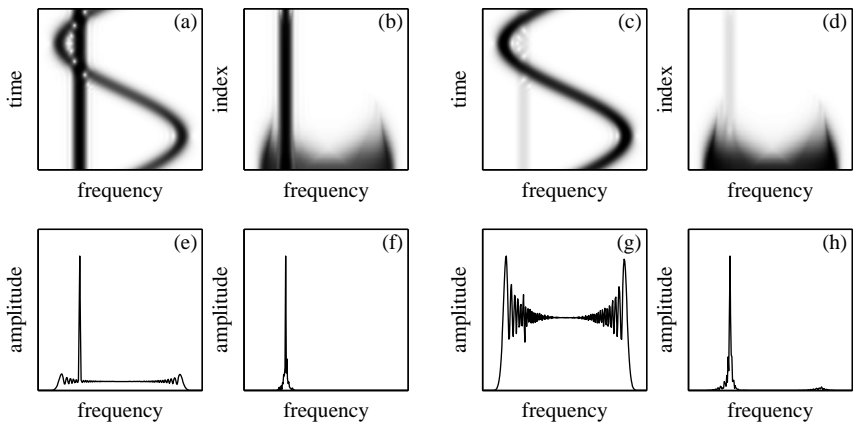


Figure 6.9 Simulated radar signals that correspond to a rigid body reflector with $\sigma_B = 1$ and a rotating reflector with reflection coefficient $\sigma_R = 0.8$ (a, b, e, f) and $\sigma_R = 15$ (c, d, g, h). (a, c) Absolute value of the STFT, (b, d) sorted STFT values, (e, g) the original Fourier transforms, and (f, h) the reconstructed Fourier transforms from 40% of the lowest values.

procedure will not significantly change the distribution of its values. However, the fast-varying micro-Doppler part of the signal is highly nonstationary, occupying different frequency bins for different time instants (in the case of flashes it exists for some time instants only). Its existence is short in time, for each frequency, over a wide range of frequencies. Thus, after sorting the STFT along the time axis, the micro-Doppler part of the signal has strong values for a wide frequency range but for a few instants only. By removing several strongest values of the sorted STFT, for each frequency, we eliminate most or all of the micro-Doppler part of the signal. Summing the rest of the STFT values over time, we will get the rigid body radar image.

Let us consider a set of M (or $M - M_w$ if the signal is not zero-padded) elements of the STFT, for a given frequency k ,

$$\mathbf{S}_k(m) = \{STFT(m, k), m = 0, 1, \dots, M - 1\}.$$

After sorting $S_k(m)$ along the time, for a given frequency k , we obtain a new ordered set of elements $\Psi_k(m) \in S_k(m)$ such that $|\Psi_k(0)| \leq |\Psi_k(1)| \leq \dots \leq |\Psi_k(M - 1)|$.

Of course, if we use the whole set, we get

$$\sum_{m=0}^{M-1} STFT(m, k) = \sum_{m=0}^{M-1} \Psi_k(m) = S(k). \quad (6.42)$$

In the L-statistics form of this summation, we will omit $M - M_Q$ of the highest values of $\Psi_k(m)$ for each k and produce the L-estimate of $S(k)$, denoted by $S_L(k)$, as

$$S_L(k) = \sum_{m=0}^{M_Q-1} \Psi_k(m) \quad (6.43)$$

where $M_Q = \text{int}[M(1 - Q/100)]$ and Q is the percent of omitted values.

To illustrate this procedure, we eliminated 60% of the strongest values of the sorted STFT from Fig. 6.9(b, d). In this way, we completely eliminated the micro-Doppler component from the time-frequency representation. We are left with the 40% lowest STFT values that contain only the rigid body. The DFT reconstruction is performed based on these values only. The reconstructed Fourier transforms for the cases of a weak and a strong micro-Doppler are shown in Fig. 6.9(f, h), respectively. The DFT of the rigid body is in both cases successfully reconstructed. Note that the result is not significantly influenced by the value of σ_R , since the points corresponding to the micro-Doppler signature are removed, meaning that their values are almost not important.

In the data analysis, this approach, based on elimination of a part of data, before analyzing the rest of the data, is known as L-statistics.

6.1.8.3 Analysis of the Missing Values

Since we have eliminated some of the time-frequency representation values, we will analyze the influence of incomplete sum in (6.40). This is the same theory as the L-statistics theory applied to the noisy or nonnoisy data.

Assume that only points in $m \in D_k$ are used in summation

$$S_L(k) = \sum_{m \in D_k} STFT(m, k), \quad (6.44)$$

where, for each k , D_k is a subset of $\{0, 1, 2, \dots, M - 1\}$ with M_Q elements.

Within the framework of the previous analysis, it means that there will be a highly concentrated component $S(k)$ surrounded by several low-concentrated values $\sum_{m \notin D_k} STFT(m, k)$. Note that the amplitude of $STFT(m, k)$ is M times lower than

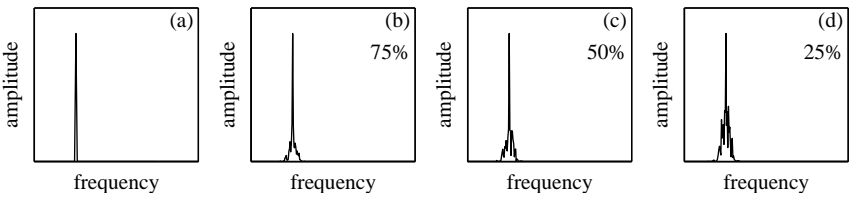


Figure 6.10 The Fourier transform of a sinusoidal signal: (a) original, (b) reconstructed by summing 75% of the smallest STFT values, for each k , (c) reconstructed by summing 50% of the smallest STFT values, and (d) reconstructed by summing 25% of the smallest STFT values.

the amplitude $S(k)$, since $S(k)$ is obtained as a sum of M values of the STFT. In general, by removing, for example, $(M - M_Q)$ values in m , we will get one very highly concentrated pulse, as in $S(k)$, and $(M - M_Q)$ values of low-concentrated components of the type $STFT(m,k)$, being spread around the peak of $S(k)$ and summed up by different random phases. Only the peak value is summed in phase. Consider:

- 1.) The case for $k = k_0$ corresponding to the position of the rigid body point: At this frequency, all terms in the sum are the same and equal to $W(0)$. Thus, the value of $S_L(k)$ does not depend on the positions of the removed samples. Its value is $S_L(k_0) = M_Q W(0)$.
- 2.) The case for $k = l + k_0$, where $l \neq 0$: Removed terms in (6.41) are of the form $\mathbf{x}_l(m) = W(l)e^{j2\pi ml/M}$. They assume values from the set $\Phi_l = \{W(l)e^{j2\pi ml/M}, m = 0, 1, 2, \dots, M-1\}$, with equal probability, for a given l . The statistical mean of these values is $E\{\mathbf{x}_l(m)\} = 0$ for $l \neq 0$, resulting in $E\{S_L(l+k_0)\} = 0$.

The resulting statistical mean for any k is

$$E\{S_L(k)\} = M_Q W(0) \delta(k - k_0). \quad (6.45)$$

The higher-order statistical analysis of this process could be easily performed as well. Here the influence of the number of missing points to the concentration of the reconstructed DFT will be illustrated by an example, shown in Fig. 6.10. Here we consider a constant frequency signal without micro-Doppler. Its DFT is calculated and presented in Fig. 6.10(a). Then the DFT is reconstructed based on the 75%, 50%, and 25% of the lowest STFT values for each k . We can see that even by taking a small number of STFT points, we still keep a strong peak, since it is summed in phase (Fig. 6.10(b - d)).

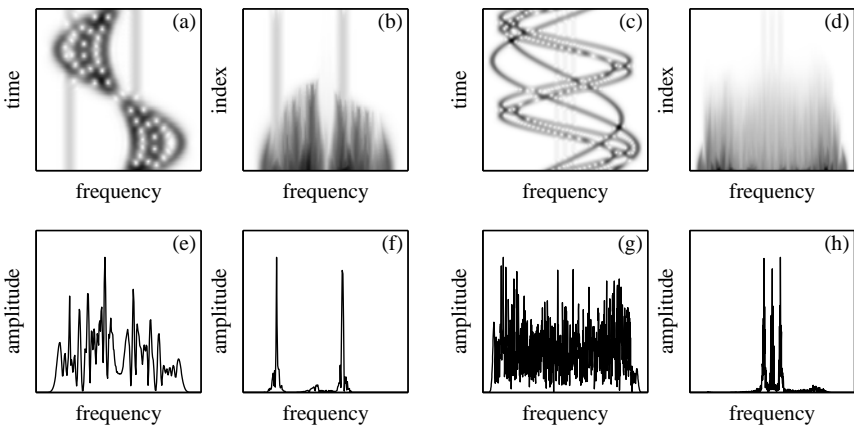


Figure 6.11 (a, b, e, f) A radar signal representing two rigid body points and four sinusoidally modulated components. (c, d, g, h) The signal consisted of three rigid body points and five sinusoidally modulated components. (a, c) The STFT of signals. (b, d) The sorted STFT values form (a, c). (e, g) The original Fourier transform of the signal. (f, h) The Fourier transform of rigid body, reconstructed by summing the lowest STFT values.

Example 6.6. A signal with two rigid body points and four sinusoidally modulated components (used to model rotating reflectors),

$$s(m) = \sigma_B \sum_{i=1}^K \exp(jy_{Bi}m) + \sigma_R \sum_{i=1}^P \exp(j[y_{R0i}m + A_{Ri} \cos(\Omega_{Ri}m + \varphi_i)]), \quad (6.46)$$

with $K = 2$, $P = 4$, $\sigma_B = 0.8$, $\sigma_R = 3$, $y_{B1} = 0.4\pi$, $y_{B2} = 1.2\pi$, $A_{Ri} = [96, 48, 64, 24]$, $\Omega_{Ri} = \pi/128$, $y_{R0i} = \pi$ and $\varphi_i = 0$, for $i = 1, 2, 3, 4$ is analyzed. The STFT of this signal is presented in Fig. 6.11(a). The micro-Doppler, although moderate, significantly covers the rigid body, that is, the part of the constant frequency component is almost invisible in the sinusoidal patterns. The sorted STFT is shown in Fig. 6.11(b). The highest STFT values are removed for each frequency in the reconstruction phase. The DFT reconstructed from the 40% lowest STFT samples is shown in Fig. 6.11(f). The rigid body is successfully reconstructed in the presence of the micro-Doppler. The original DFT of the analyzed signal is given in Fig. 6.11(e). \square

Example 6.7. Here we analyze a signal with eight components: $K = 3$ components with constant frequency (used to model rigid body reflectors) and $P = 5$ sinusoidally modulated components (used to model rotating reflectors), (6.46) with: $\sigma_B = 1$,

$\sigma_R = 12$, $y_{Bi} = [1.9\pi, 2\pi, 2.1\pi]$, $A_{Ri} = [150, 350, 200, 450, 200]$, $\Omega_{Ri} = [\pi/256, \pi/512, \pi/256, \pi/512, \pi/256]$, $y_{R0i} = 0$, and $\varphi_i = [0, \pi/6, \pi/6, -\pi/6, 0]$, for $i = 1, 2, 3, 4, 5$, $M = 1024$, and $M_w = 64$. The STFT of this signal is shown in Fig. 6.11(c). The constant components that correspond to the rigid body are not well separated in the time-frequency plane. Moreover, they are covered by the sinusoidally modulated patterns that represent the micro-Doppler effects of the rotating reflectors. If we sort the STFT values along time axis, then the representation of the rigid body parts does not change, since it is constant during the whole coherent integration time, Fig. 6.11(d). However, the fast-rotating parts occupy only small time intervals over a wide region of frequencies. They lie in high-value regions of the sorted transform. Thus, they will be eliminated by removing the highest STFT values for each frequency. The reconstructed Fourier transform, obtained by summing the 30% lowest STFT values (6.44) along the time, is shown in Fig. 6.11(h). We can clearly see three peaks that correspond to the three rigid body reflectors. The original DFT is shown in Fig. 6.11(g). It cannot be used even to determine the number of components in the analyzed signal. \square

Example 6.8. Helicopter Data Analysis: In this example, we first present a simulation approach to the data of a German Air Force Bell UH-1D Helicopter known also as Iroquois. Here the simulation is performed according to the variable flashing reflection coefficients. Several effects are emphasized in the time-frequency representation (Fig. 6.12(a)). The stationary patterns along the time axis correspond to the rigid body reflection. The motion of two main blades is modeled by two rotating reflectors, producing sinusoidal frequency-modulated signals with a large magnitude in the frequency direction, (6.47). The main rotor flashes are simulated by signals producing lines that connects extreme points of the sinusoidal frequency-modulated signal along the time axis. The smaller pulses that can be seen on the right side of Fig. 6.12(a) correspond to the tail rotor flashes, and they are simulated here by taking into account the physical meaning of its appearance. Namely, these flashes correspond to the periodic alignment of the main and tail rotors to maximally reflect the radar signal when they are normal to the line of sight. Therefore, we use here an angle-dependent reflection coefficient

$$\sigma(t) = \exp(-30|\sin(2\pi t/T_{Rot})|),$$

where the reflection takes value 1 when $t = kT_{Rot}/2$ and $|\sin(2\pi t/T_{Rot})| = 0$, while for other t , $30|\sin(2\pi t/T_{Rot})|$ assumes high values and the reflection coefficient is small. Note that other effects that can be observed in a radar image, including multipath, are not considered here. The simplified model of the reflected UH-1D signal can now be written as

$$s(t) = x_{RIG}(t) + x_{ROT}(t) + x_{FL_M}(t) + x_{FL_T}(t), \quad (6.47)$$

where $x_{RIG}(t)$, $x_{ROT}(t)$, $x_{FL_M}(t)$, and $x_{FL_T}(t)$ represent signals caused by the rigid body, rotation of the main rotor, and the main and tail rotor flashes, respectively.

The signal is considered within the interval of 400 ms, sampled with a rate of $\Delta t = 1/48$ ms. Four sinusoidal components, caused by the rigid body, are at the frequencies -10.3 kHz, -2.5 kHz, 2.3 kHz and 2.7 kHz. Two components at -0.4 kHz and 0.4 kHz correspond to the modulated time tones commonly added to the data tape. The sinusoidal frequency-modulated signals, corresponding to the rotation of the main rotor blades, are modeled as

$$x_{ROT}(t) = \sigma_{ROT} [e^{j2\pi A_{ROT} \sin(2\pi t/T_{ROT})} + e^{-j2\pi A_{ROT} \sin(2\pi t/T_{ROT})}],$$

where $\sigma_{ROT} = 10$, $T_{ROT} = 175$ ms, and $A_{ROT} = 529.19$. The main and tail rotor flashes are modeled as

$$x_{FL,M}(t) = 2.5 \sum_{k=1}^{128} \frac{k+64}{128} e^{-30|\sin(2\pi t/175)|} \cos\left(25.98k \sin\left(\frac{2\pi t}{175}\right)\right),$$

and

$$x_{FL,T}(t) = 2.5 \sum_{k=64}^{128} e^{-30|\sin(2\pi t/35.8)|} e^{(j(2.66k \sin(4\pi t/35.8)))}.$$

The signal is corrupted by a moderate Gaussian noise. The presented algorithm for the rigid body separation is applied to the simulated helicopter signal. The sorted STFT is shown in Fig. 6.12(b). We can see that the STFT values corresponding to the rotating parts are in the high-value region. The reconstructed DFT is shown in Fig. 6.12(e). All five reflectors that correspond to the rigid body are successfully recovered. The original DFT is presented in Fig. 6.12(c). The reconstructed DFT obtained by summing the absolute values of the remaining STFT samples is presented in Fig. 6.12(d). We can see that omitting phase information in summation significantly degrades the reconstructed DFT. \square

Example 6.9. Noncompensated Rigid Body Acceleration: In this case an accelerating rigid body target is considered and examined. The received radar signal that corresponds to an accelerating target in the ISAR systems is a linear frequency-modulated. Similarly, in the SAR systems the target motion may induce linear frequency modulation in the received radar signal. Therefore, we simulated three rigid body reflectors as three linear frequency-modulated components with the chirp rate a . In order to show that this algorithm will not remove only the micro-Doppler induced by vibrating and rotating targets, here we have also used a more complex form of the micro-Doppler. The STFT of the analyzed signal is presented in Fig. 6.13(a). We can clearly see that, as a result of the acceleration, the time-frequency representation of the rigid body part of the signal is not stationary during the time. Consequently, it is difficult to separate it from the micro-Doppler in the sorted STFT (Fig. 6.13(b)). Namely, if we perform the micro-Doppler separation by removing 50% of the highest STFT samples, as we did in the examples where there was no need for the motion

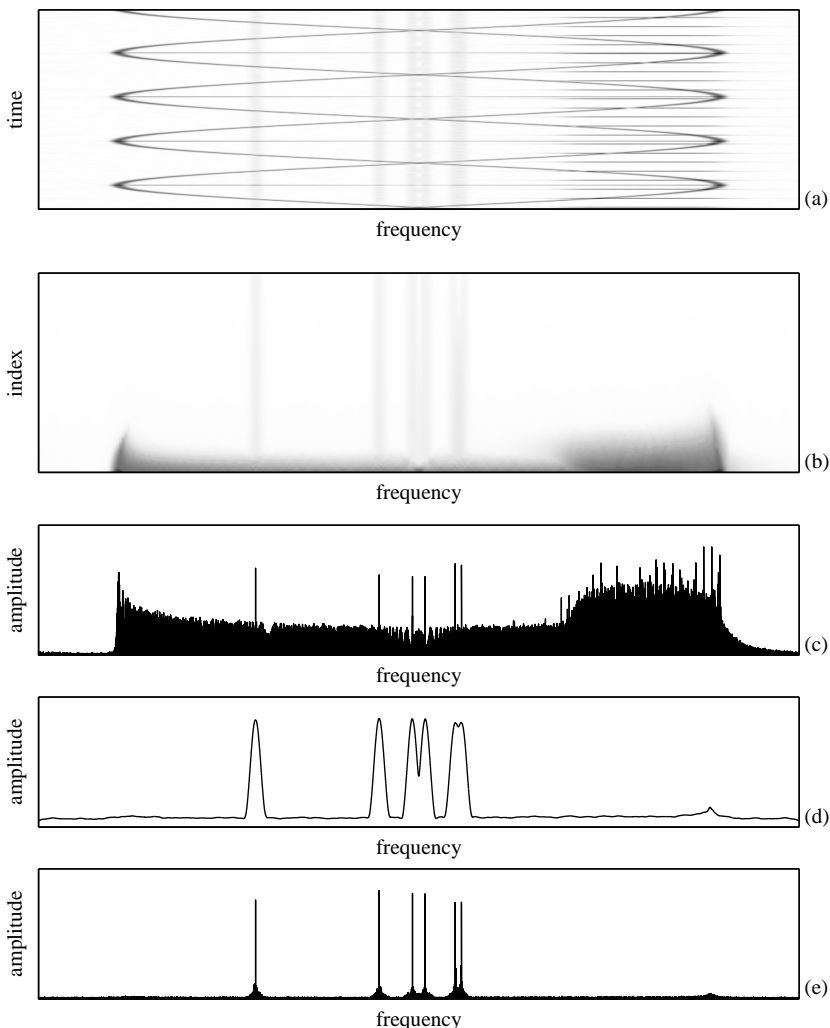


Figure 6.12 (a) The STFT of a simulated signal of a German Air Force Bell UH-1D Helicopter. (b) The sorted STFT of this signal. (c) The original Fourier transform of the signal. (d) The Fourier transform of the rigid body, reconstructed by summing the lowest absolute STFT values. (e) The Fourier transform of the rigid body, reconstructed after L-statistics is applied.

compensation, we would reconstruct the DFT of the rigid body as presented in Fig. 6.13(f). Here we would remove a significant part of the rigid body points as well. In the analysis of the rigid body with uncompensated acceleration, we should first compensate the remaining acceleration. This is not possible in the original signal, since the micro-Doppler signatures prevent us from properly compensating the remaining acceleration. However, the application of the L-statistics-based method for the micro-Doppler removal can solve this problem as well. We will use the local polynomial Fourier transform (LPFT)

$$LPFT(t, \Omega) = \int_{-\infty}^{\infty} s(\tau)w(\tau-t)e^{-j(\Omega\tau+\alpha\tau^2)}d\tau, \quad (6.48)$$

instead of the STFT, where the term $\exp(-j\alpha\tau^2)$ is used to compensate the linear frequency modulation of the rigid body part of the signal, $LPFT(t, \Omega) = \text{FT}\{s(\tau)e^{-j\alpha\tau^2}w(\tau-t)\}$. The parameter α is not known in advance, but we know that it can take values from a set $\Lambda = [-\alpha_{\max}, \alpha_{\max}]$, where α_{\max} is the chirp rate corresponding to the maximal expected acceleration (positive or negative). In this example we used $\Lambda = [-2 : 0.25 : 2]$. Now $\hat{\alpha}$ can be estimated as the value from the set Λ for which we obtain the highest concentration of the reconstructed rigid body (compensated Fourier transform) based on the LPFT and L-statistics with, for example, $Q = 50\%$. The reconstructed Fourier transform, by using 50% of the lower LPFT values, will be denoted by $S_{L,\alpha}(k)$. Its concentration is calculated based on normalized norm one (Chapter 2)

$$H(\alpha) = \frac{\sum_{k=0}^{M-1} |S_{L,\alpha}(k)|}{\sqrt{\sum_{k=0}^{M-1} |S_{L,\alpha}(k)|^2}}. \quad (6.49)$$

The LPFT, calculated with the estimated optimal value of $\hat{\alpha} = 1.25$, which results from $H(\alpha)$, is shown in Fig. 6.13(c). The linear frequency modulation is compensated by $\hat{\alpha}$ in (6.48). Thus, with optimal $\hat{\alpha}$ we have components with almost constant frequency in the time-frequency representation representation of the rigid body reflectors. In this way, we have successfully reconstructed the rigid body and removed the micro-Doppler part, as presented in Fig. 6.13(h). The procedure is not too sensitive to $\hat{\alpha}$. Very good results are obtained with neighboring values $\hat{\alpha} = 1.0$ and $\hat{\alpha} = 1.5$. Note that it would be impossible to estimate the chirp-rate $\hat{\alpha}$ from the original signal, without employing the algorithm for the micro-Doppler removal. \square

Example 6.10. The L-statistics-based method is applied on real data in this example. The examined data were collected using an X-band radar operating at 9.2GHz. The first real data represent three corner reflectors rotating at approximately 60rpm (all facing radar) and the rigid body observed by the radar with $T_r = 1$ kHz. The STFT of the

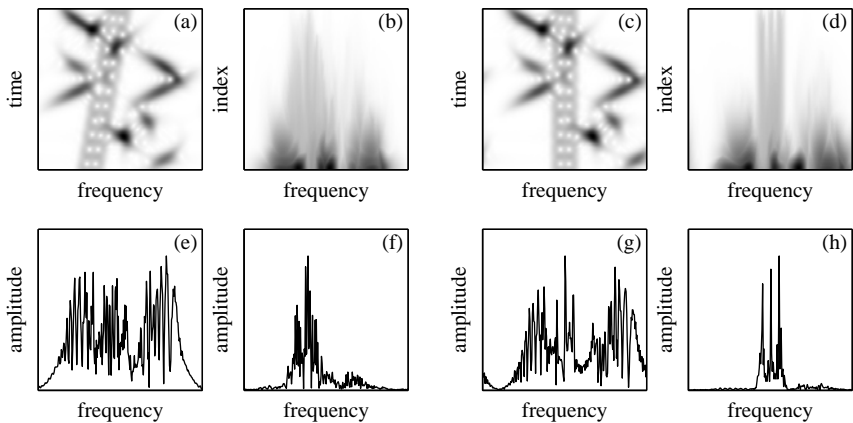


Figure 6.13 Accelerating rigid body with a complex form of the micro-Doppler. (a) Time-frequency representation of the signal without motion compensation. (b) Sorted time-frequency representation values of the original signal. (c) Time-frequency representation of the signal after motion compensation. (d) Sorted time-frequency representation values of acceleration compensated signal. (e) The original Fourier transform of the analyzed signal. (f) The reconstructed Fourier transform of the accelerating rigid body without motion compensation. (g) The Fourier transform of the original signal with motion compensation. (h) The reconstructed Fourier transform of the accelerating rigid body with motion compensation.

returned signal, for the given range bin, is shown in Fig. 6.14(a). After sorting the STFT over time Fig. 6.14(b), the constant frequency component corresponding to the rigid body becomes more visible, since the time-varying frequency content is spread over many frequencies, for each frequency bin. The rigid body is separated from the micro-Doppler and its DFT is successfully reconstructed by using 50% of the lowest STFT values, as shown in Fig. 6.14(e). If we compare it to the DFT of the original signal (Fig. 6.14(f)), we can see the improvement in the rigid body presentation. □

Example 6.11. In the second example, the real radar data corresponding to two outside corner reflectors, rotating at approximately 40 rpm (all facing radar) with rigid body, are analyzed. The same radar as in the previous example is used, while the reflectivity of rigid body is much higher than those of the rotating reflectors. The STFT representation of the observed signal is shown in Fig. 6.14(c). The sorted STFT is shown in Fig. 6.14(d). The original DFT is shown in Fig. 6.14(g). The reconstructed Fourier transform, obtained by summing 50% of the lowest STFT values is presented in Fig. 6.14(h). We have successfully removed most of the micro-Doppler. Moreover,

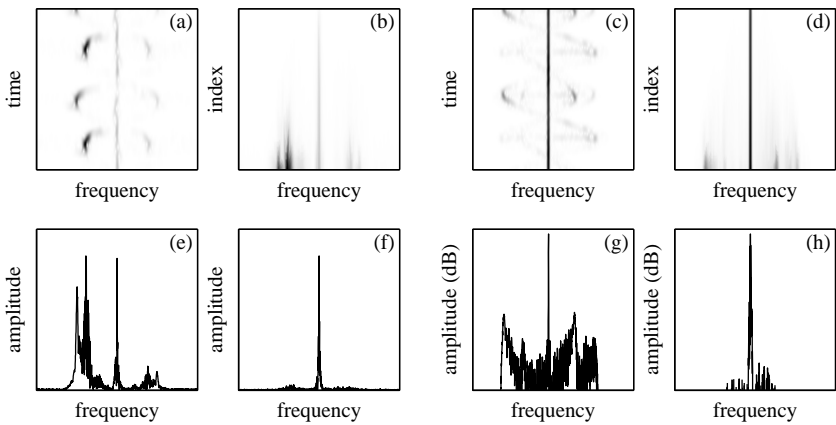


Figure 6.14 Real radar data corresponding to a rigid body and three corner reflectors rotating at ~ 60 RPM (a, b, e, f) and real radar data corresponding to a stronger rigid body and two corner reflectors rotating at ~ 40 RPM (c, d, g, h). (a, c) The STFT. (b, d) The sorted STFT. (e, g) The original Fourier transform. (f, h) The Fourier transform reconstructed by summing over 50% of the lowest STFT samples. A logarithmic amplitude scale is used in subplots (g) and (h).

we may use the removed STFT samples in order to estimate features of rotating reflectors. Here we used a logarithmic scale to present the reconstructed values, since the micro-Doppler values were very low. \square

6.1.8.4 Noise Influence

It is well-known that L-statistics is a tool for robust time-frequency analysis. The robustness comes from the fact that L-statistics-based calculation avoids the highest values, which are the most influenced by a noise. Therefore, we may expect that by using L-statistics we will not degrade the radar imaging performance in the case of noise. By using L-statistics we will eliminate a part of the signal that is summed in phase in the DFT, but we will also eliminate the signal values that are mostly corrupted by noise. Thus, with the elimination of the micro-Doppler, we will improve the overall performance in the noisy signal cases as well. In the case of impulse noise, we may expect significant improvement, even in the case without micro-Doppler, with pure rigid body. The effect of noise is statistically analyzed within the simulation study.

Example 6.12. One stationary reflector and one micro-Doppler reflector are considered. Complex-valued, white Gaussian noise $\varepsilon(t)$, with variance σ_ε^2 , is added

$$s(m) = e^{-j0.75\pi m} + \sigma_R e^{j58\cos(2\pi m/256)} + \varepsilon(t),$$

where σ_R is the reflection coefficient of the micro-Doppler reflector. The noise variance is varied within a wide range $0 \leq \sigma_\varepsilon^2 \leq 72$ (from the case without noise up to the case when noise dominates) with step 1. For each variance value from this range, 1000 Monte Carlo simulations are performed. In each realization, we have found the position of the maximum in the L-statistics-based estimate of the Fourier transform, $S_L(k)$. Then the error is calculated as a difference of this position and the true signal frequency. The mean absolute error is calculated for each variance for 1000 realizations and the mean absolute error is plotted for various noise variance values. For the rigid body DFT reconstruction we used for each frequency 50% of the smallest STFT values in the L-statistics summation. We start with the case of pure stationary point $\sigma_R = 0$, to see how the L-statistics approach, with 50% of values, influences the results. It is well known that the DFT transform is theoretically the best (ML) estimator for a pure sinusoid in Gaussian noise. The corresponding mean absolute error is depicted in Fig. 6.16(a). The solid line corresponds to the L-statistics-based method where 50% of the smallest STFT values are summed, while the dashed line corresponds to the full Fourier transform. The DFT is well reconstructed with the L-statistics-based method and the estimation results are not degraded with respect to the full Fourier transform, in this simple case, when the DFT is the ML estimator.

We have analyzed noise influences in the case of $\sigma_R = 5$ as well. For the noiseless case, the STFT is shown in Fig. 6.15(a), while the sorted STFT is shown in Fig. 6.15(b). The original DFT is presented in Fig. 6.15(e). The DFT reconstructed by summing, for each frequency, 50% of the lowest STFT samples is shown in Fig. 6.15(f). The plots for the case of $\sigma_\varepsilon^2 = 4.5$, $SNR = -6.53$ dB are shown in Fig. 6.15(c, d, g, h). The signal-to-noise ratio (SNR) is calculated as the rigid body part of the signal-to-noise ratio. We can see that the L-statistics-based method successfully reconstructs the DFT of the rigid body in the presence of micro-Doppler and noise. The mean absolute error of the presented method and the original DFT is shown in Fig. 6.16(b). This method successfully reconstructs the Fourier transform, eliminates the micro-Doppler effect, and outperforms the original Fourier transform, whose estimation performance is degraded by the micro-Doppler effect. \square

Example 6.13. We analyzed one more case of one stationary reflector and one micro-Doppler reflector in the presence of noise. Here the micro-Doppler reflector is stronger and closer to the stationary one. The corresponding signal is of the same form as in the previous example, but with $\sigma_R = 10$, while the rigid body reflector signal component is at the frequency $f_B = 0.125$ Hz. The same statistical analysis

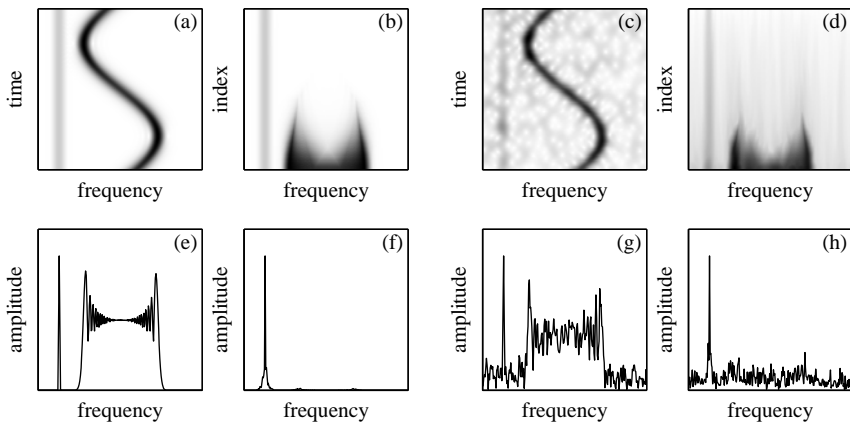


Figure 6.15 One rigid body reflector and one micro-Doppler reflector. Noise-free case (a, b, e, f) and noisy case (c, d, g, h) with $\sigma_e^2 = 4.5$. (a, c) The STFT absolute value. (b, d) Sorted STFT values. (c, g) The original Fourier transform. (d, h) The reconstructed Fourier transform.

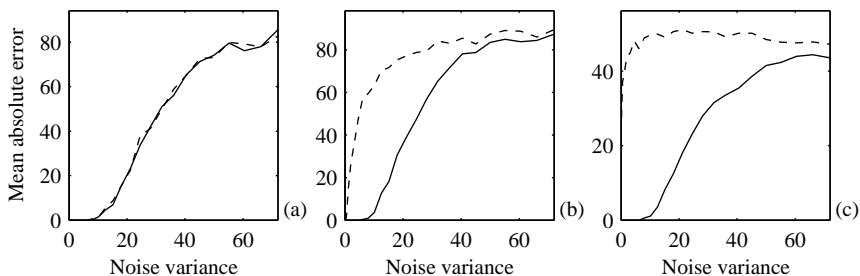


Figure 6.16 Mean absolute error as a function of the noise variance for the Fourier transform (dashed line) and the L-statistic-based rigid body detection (solid line). (a) The rigid body without micro-Doppler, (b) setup from Example 6.12, and (c) setup from Example 6.13.

and the reconstruction procedure as in the previous example are performed. For the noiseless case, the STFT is shown in Fig. 6.17(a), while the sorted STFT is shown in Fig. 6.17(b). The original DFT is presented in Fig. 6.17(e). The DFT reconstructed by summing, for each frequency, 50% of the lowest STFT samples is shown in Fig. 6.17(f). The plots for the case of $\sigma_e^2 = 4.5$, $SNR = -6.53$ dB are shown in Fig.

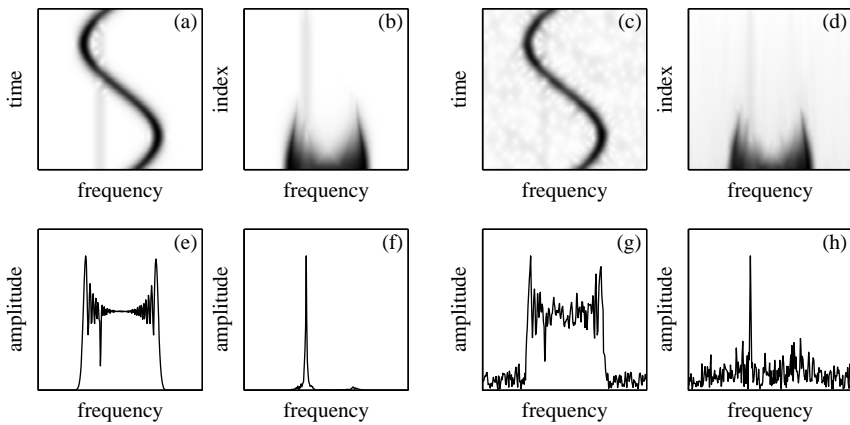


Figure 6.17 One rigid body reflector and one close micro-Doppler reflector. Noise-free case (a,b,c,e,f) and noisy case (c,d,g,h) with $\sigma_e^2 = 4.5$. (a,c) The STFT absolute value. (b,d) The sorted STFT. (e,g) The original Fourier transform. (f,h) The reconstructed Fourier transform.

6.17(c, d, g, h). We can see from Fig. 6.17 that the performance of the L-statistics-based method does not degrade even in the case of strong micro-Doppler reflector positioned close to the rigid body reflector; in this case, the stationary and micro-Doppler components are crossing in the STFT. This method continues to successfully reconstruct the DFT of the rigid body in the presence of noise, Fig. 6.17(h), while the DFT is not even able to indicate that there is a rigid body reflector, at all, Fig. 6.17(g). The mean absolute error of the L-statistics-based method and the original DFT are shown in Fig. 6.16(c). From the presented statistics, it is possible to conclude that, even in the presence of noise and close reflectors with strong micro-Doppler effects, this method successfully reconstructs the DFT of the rigid body, while the original DFT completely fails to indicate the rigid body existence. \square

6.1.8.5 High-Resolution Property

Consider the L-statistics application on two very close rigid body points

$$s(t) = e^{-j2(y_{Bi} - \Delta y_{Bi})\Omega_B t \Omega_0/c} + e^{-j2(y_{Bi} + \Delta y_{Bi})\Omega_B t \Omega_0/c}$$

with a very small Δy_{Bi} so that in the DFT of the signal $S(\Omega)$, calculated over the entire coherent integration time, we can not distinguish these components. Since the resolution in the Doppler direction is $R_{\text{Dopp}} = 2\pi/T_c$, it means $2\Delta y_{Bi} \sim 2\pi/T_c$.

It is surprising, but if we use low concentrated STFT and L-statistics, we will be able to separate these components. The STFT of these components is

$$\begin{aligned} STFT(t, \Omega) = & W(\Omega + (y_{Bi} - \Delta y_{Bi})) e^{-j\Omega t} e^{-j(y_{Bi} - \Delta y_{Bi})t} \\ & + W(\Omega + (y_{Bi} + \Delta y_{Bi})) e^{-j\Omega t} e^{-j(y_{Bi} + \Delta y_{Bi})t} \end{aligned}$$

with a normalized frequency Ω for $2\Omega_0\Omega_B/c = 1$.

Note that the STFTs of the components are phase shifted for $\Delta\varphi(t) = 2\Delta y_{Bi}t$. Even for small $2\Delta y_{Bi} \sim 2\pi/T_c$, the phase shift changes are of the order $\Delta\varphi(t) \sim 2\pi/T_c \times T_c$. It means that it could easily change during the coherent integration time within 0 to π or even more. Then there will be time instants in $|STFT(t, \Omega)|$ when the individual STFTs are summed in phase, that is, when $|STFT(t, \Omega)| \cong |W(\Omega + (y_{Bi} - \Delta y_{Bi})) + W(\Omega + (y_{Bi} + \Delta y_{Bi}))|$. Then the signal components cannot be separated. However, there will be also the instants in the STFT when the components are with opposite phase, $|STFT(t, \Omega)| \cong |W(\Omega + (y_{Bi} - \Delta y_{Bi})) - W(\Omega + (y_{Bi} + \Delta y_{Bi}))|$, so that the signal components are clearly separated, although on biased positions. We can see that in the first case the values of $|STFT(t, \Omega)|$ will be higher than in the other case. By using the L-statistics approach, the higher values will be eliminated, while the lower values, which are well separated, will remain. Thus, we may achieve high signal resolution by using the low concentrated STFT and L-statistics, even in the case when the separation is not possible in the original DFT over the whole coherent integration time. Positions of maxima are biased in this case and they do not correspond to the signal frequencies.

Example 6.14. Two very close rigid body reflectors in the presence of micro-Doppler effects are simulated in this example

$$s(m) = e^{-j171\pi m/M} + e^{-j175\pi m/M} + 10e^{j48\cos(2\pi m/M)+j60\pi/M},$$

where $M = 256$ samples are used. The window with $M_w = 32$ zero-padded to M is used for the STFT calculation. The STFT of the analyzed signal is presented on Fig. 6.18(a), while the sorted STFT is presented on Fig. 6.18(b). It can be seen in Fig. 6.18(a), that there are time instants when the STFTs of the close components are summed with opposite phase and they appear as separated. However, when the close components are summed in phase, they are not separated. Moreover, as it can be seen from the sorted STFT, presented in Fig. 6.18(b), when the STFTs are summed in

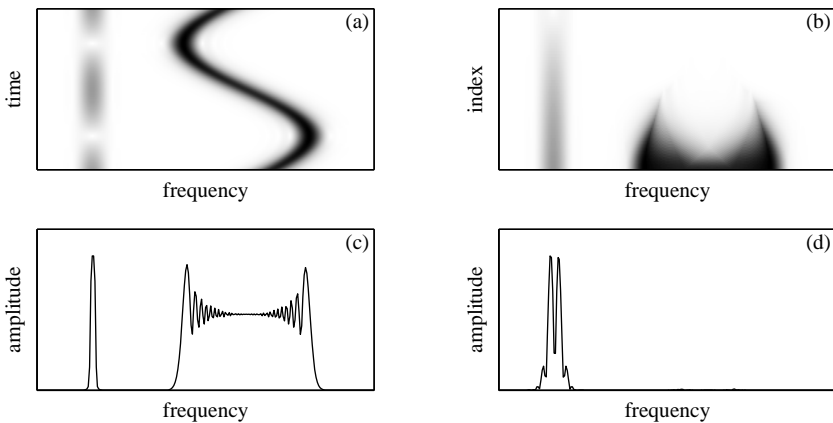


Figure 6.18 (a) The STFT of a signal consisted of two very close components with constant frequency and one sinusoidally modulated component. (b) The sorted STFT of the same signal. (c) The original Fourier transform of the signal. (d) The Fourier transform of rigid body, reconstructed by summing the lowest STFT values.

phase, the resulting STFT is higher. Consequently, by removing the highest values of the STFT, the remaining lower values are well separated; thus, the close components are separated. The DFT reconstructed by summing over time 40% of the lowest samples of the STFT is shown in Fig. 6.18(d), while the original DFT is shown in Fig. 6.18(c). We can see that the separation of the close components is achieved, although it is not possible in the Fourier transform. \square

6.2 INTERFERENCE REJECTION IN SPREAD SPECTRUM COMMUNICATION SYSTEMS

Spread spectrum is a transmission coding technique used in digital telecommunication systems, where pseudo-noise (PN), or pseudo-random code, independent of the information data, is employed as a modulation waveform. The pseudo-random code significantly expands the bandwidth of original signal. The spread signal has a lower power density, but the same total power. At the receiver side signal is “de-spread” using the synchronized replica of the pseudo-noise code. Spread spectrum technology has been recognized as a good alternative to both frequency division

multiple access (FDMA) and time division multiple access (TDMA) for the cellular systems. The most common spread spectrum systems are of the direct sequence (DS) or frequency hopping (FH) type.

Direct sequence spread spectrum systems employ a high-speed code sequence to introduce rapid phase transitions into the carrier containing the data. The result of modulating the carrier is a signal centered at the carrier frequency, but with main lobe bandwidth significantly wider than the original bandwidth. The FH spread spectrum achieves the band spreading by using the PN sequence to pseudo-randomly hop the carrier frequency.

While the influence of low power interfering signals is significantly reduced by despreading process at the receiver, in the case of very high power interferences, preprocessing is required. This is a common case, when the interference stations are much closer to the receiver than the signal transmitting station.

Different methods have been proposed by Amin and Wang, Barbarossa and Scaglione, Suleesathira and Chaparro, et al. for rejection or mitigation of interferences of this kind in order to improve robustness of spread spectrum systems and more reliable receiving and decoding of the useful signal. As an illustration of the time-frequency-based linear signal filtering application in the jammer excision, the local polynomial Fourier transform (LPFT) will be used here.

6.2.1 Direct Sequence Spread Spectrum Model

Let us assume a digital signal that is going to be transmitted in the waveform

$$x(t) = \sum_n x_n h_T(t - nT) \quad (6.50)$$

where $x = \{x_n : x_n \in \{+1, -1\}\}$ is the data sequence, T represents the data symbol duration, and $h_T(t)$ is a rectangular pulse of duration T .

In the DS spread spectrum systems, the PN sequence may be expressed in the following manner

$$a(t) = \sum_k a_k h_c(t - kT_c) \quad (6.51)$$

where $a = \{a_k : a_k \in \{+1, -1\}\}$ is a spreading sequence, and T_c is the PN symbol or chip period. Pseudo-random sequence is actually a periodic sequence with period N .

It is necessary that T is an integer multiple of T_c . The ratio $G = T/T_c$, defined as a number of PN chips per data symbol, is called the processing gain. There are two types of spreading codes, short codes and long codes. The short code is one

with $G = N$, that is, when the PN code length is equal to a data symbol. The long code has $G \ll N$, that is, the PN code length is much longer than the data symbol, so that a different chip pattern is associated with each symbol. The total transmitted signal may be expressed in the form

$$s(t) = \sum_n x_n a(t - nT) = \sum_n x_n \sum_k a_k h_c(t - kT_c - nT). \quad (6.52)$$

The received signal is of the following form

$$r(t) = s(t) + J(t) + \varepsilon(t), \quad (6.53)$$

where $s(t)$ is the desired signal, $J(t)$ is an interference, and $\varepsilon(t)$ is the uncorrelated white noise process with the auto-correlation function: $R_{\varepsilon\varepsilon}(t) = \sigma_\varepsilon^2 \delta(t)$. The amount of noise in the received signal is described by the signal-to-noise ratio (SNR), defined as $SNR = 20\log_{10}(A/\sigma_\varepsilon)$, where A is the signal amplitude. The interference (jammer) has the form

$$J(t) = a_J \cos(\varphi(t)), \quad (6.54)$$

where $\varphi(t)$ is the phase and a_J is the magnitude of the jammer.

Amount of the jammer in the received signal can be described by the jammer-to-signal ratio (JSR), defined as $JSR = 20\log_{10}(a_J/A)$. The block diagram of the DS spread spectrum (DSSS) system is given in Fig. 6.19.

6.2.2 Filtering and Reconstruction

First, let us use the STFT as the analysis tool for both filtering of the jammer and reconstruction of the desired signal. The STFT is defined by

$$STFT(t, \Omega) = \int_{-\infty}^{+\infty} x(t + \tau) w(\tau) e^{-j\Omega\tau} d\tau, \quad (6.55)$$

where $w(t)$ denotes a real-valued lag window function. The original signal can be fully recovered from its STFT (as shown in Chapter 2). The product of the signal and the window may be obtained by using the inverse Fourier transform, that is,

$$x(t + \tau) w(\tau) = \frac{1}{2\pi} \int_{-\infty}^{+\infty} STFT(t, \Omega) e^{j\Omega\tau} d\Omega. \quad (6.56)$$

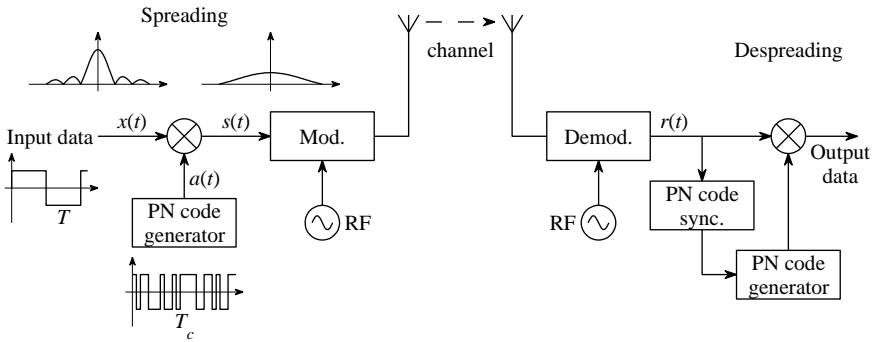


Figure 6.19 Block diagram of the DS spread spectrum system.

Based on this relation and the property of the window function that $w(0) = 1$, it follows

$$x(t) = \frac{1}{2\pi} \int_{-\infty}^{+\infty} STFT(t, \Omega) d\Omega. \quad (6.57)$$

The signal $x(t)$, at any instant, may be obtained by integrating its STFT, at the same instant, over the frequency. Of course, here we may reconstruct not only the signal at t but also within the region around t , where the window function has significant values. However, here we will assume a real-time implementation, when $STFT(t, \Omega)$ is calculated for each t and $STFT(t, \Omega)$ will be used to reconstruct $x(t)$ only.

The STFT is linear transform and therefore for the received signal it is composed of three components: the STFT of the desired signal, the STFT of the noise, and the STFT of the jammer. Because of spreading at the transmitter side, the bandwidth of the desired signal is wider than the bandwidth of jammer. We may assume that the desired signal and noise exist over all frequencies, while the jammer exists only in a certain frequency interval of the STFT. This assumption leads to the idea of filtering the jammer in the time-frequency plane. The desired signal is then reconstructed by inverting the filtered STFT. The filtering and signal reconstruction

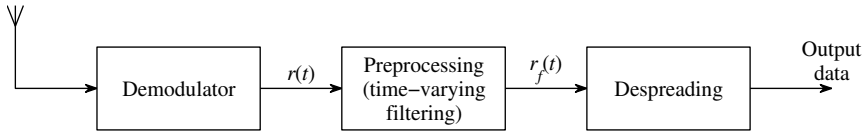


Figure 6.20 Block diagram of the direct sequence spread spectrum receiver in the case of a high power jammer.

may be modeled by the following expression

$$x_f(t) = \frac{1}{2\pi} \int_{-\infty}^{+\infty} L_f(t, \Omega) STFT(t, \Omega) d\Omega. \quad (6.58)$$

where $x_f(t)$ is the filtered signal, and $L_f(t, \Omega)$ is a rectangular support function used for filtering. Analytical expression of this window is given by

$$L_f(t, \Omega) = \begin{cases} 0, & \Omega \in B_j(t) \\ 1, & \text{elsewhere} \end{cases} \quad (6.59)$$

where $B_j(t)$ is the frequency band around the jammer's instantaneous frequency $\varphi'(t)$, that is, the region in which we assume that the jammer exists. Because of its narrow frequency band, it is easy to detect the jammer, even when its total power is lower or equal to the power of signal.

A block diagram of the direct sequence spread spectrum receiver in case of a high power jammer is shown in Fig. 6.20.

Now we will illustrate these simple and straightforward filtering forms on examples.

Example 6.15. Consider a signal defined by (6.52) and (6.53) with 128 chips per bit.

The same parameters are going to be used in all further examples. The standard deviation of the added white Gaussian noise was assumed to be $\sigma_e = 2A$, where A is the amplitude of the received signal. The jammer is assumed in the form of a linear frequency-modulated signal. The JSR was varied from 0 to 145 dB (relative to the signal's energy) in increments of 5 dB. Bit error rate (BER) values are calculated from the corresponding chip error rate (CER) values. The Hann(ing) and the Kaiser window in the STFT, both with length of 128 time samples, are considered. For the Kaiser window $\beta = 15$ is used. After time-varying filtering based on (6.58) and (6.59), the signal is reconstructed and the CER values are obtained. The BER values

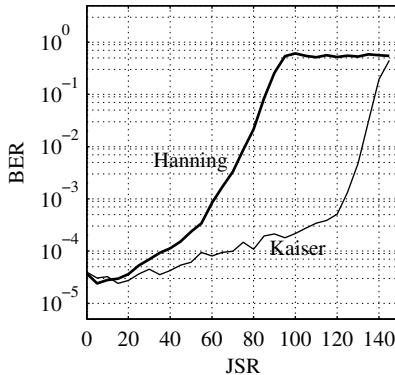


Figure 6.21 Bit error rate (BER) curves: thick line for the Hann(ing) window; thin line for the Kaiser window. Window width was 128 samples; beta value for the Kaiser window was 15.

are shown in Fig. 6.21. The Hann(ing) window has a narrower main lobe, producing slightly better results for low JSR, while the Kaiser window has much lower side lobes, resulting in a more robust system for high JSR. For high jammer values the jammer side lobes of the Hann(ing) window are stronger than the signal (JSR about 100 dB), so it failed to produce satisfactory results. \square

Example 6.16. Interference is taken as a linear frequency-modulated signal. The interference power was set to 30 dB (relative to the signal's energy). Here the modulation index (slope) of the interference in the STFT is varied from 0 (the case that corresponds to a pure sinusoidal interference) to the value at which interference sweeps the entire considered frequency area (the area where components of the desired signal exist). Filtering of the interference component in the received signal was done in the same way as in the previous example. The results are illustrated in Fig. 6.22(a). \square

Example 6.17. In this example two bits of the signal are considered. The Kaiser window of width 128 and beta value 15 was used. Interference is taken as a sinusoidal-frequency-modulated signal. JSR was set to 30 dB. Here we varied the interference frequency from 0 to the value at which interference (jammer) covers entire frequency range where the signal exist. Interference filtering was done in the same way as before. Results in BER as a function of the interference signal rate (amplitude of frequency change) are illustrated in Fig. 6.22(b). As expected, when the interference rate increases it occupies wider frequency range in the STFT, covering wider area of the desired signal, and thus increasing the BER. \square

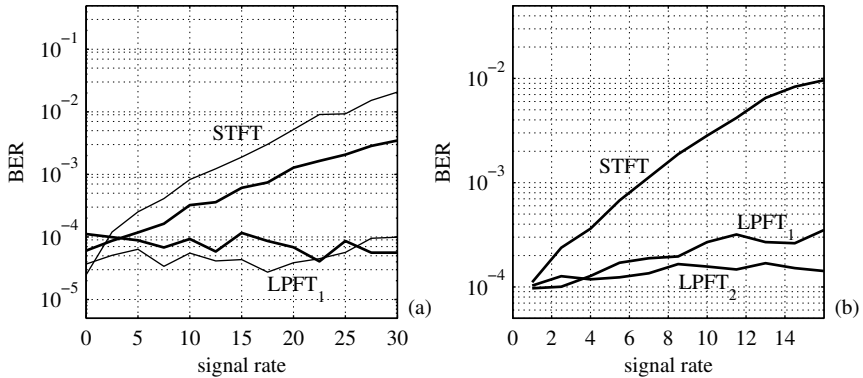


Figure 6.22 Bit error rate (BER) for (a) linear frequency-modulated signal and (b) sinusoidal frequency-modulated signal as a function of the interference signal rate. Thick lines for the Hann(ing) window; thin lines for the Kaiser window; JSR=30 dB. Window width was 128 samples. Algorithm with the STFT and LPFT up to the first and the second order (LPFT₁ and LPFT₂)-based filtering.

In order to define a more robust system to the jammer (interference) variation here we will consider the local polynomial Fourier transform (LPFT)

$$LPFT(t, \Omega; \Omega_1, \Omega_2, \dots, \Omega_N) = \int_{-\infty}^{+\infty} x(t + \tau) w(\tau) e^{-j(\Omega\tau + \Omega_1 \frac{\tau^2}{2!} + \dots + \Omega_N \frac{\tau^N}{N!})} d\tau, \quad (6.60)$$

where $\Omega = \{\Omega_1, \Omega_2, \dots, \Omega_N\}$ represents an N -dimensional parameter space. The LPFT preserves the linearity property of the STFT, with respect to the signal.

The original signal can be reconstructed from its LPFT by using

$$x(t) = \int_{-\infty}^{+\infty} LPFT(t, \Omega; \Omega_1, \Omega_2, \dots, \Omega_N) d\Omega. \quad (6.61)$$

It is interesting to note that the integral (6.61) does not depend on the parameters of the N -dimensional parameter space, $\Omega_1, \Omega_2, \dots, \Omega_N$.

The optimal LPFT is the transform that satisfies

$$LPFT_{opt}(t, \Omega) = \max_{\Omega_1, \Omega_2, \dots, \Omega_N} \{|LPFT(t, \Omega; \Omega_1, \Omega_2, \dots, \Omega_N)|\} \quad (6.62)$$

Basically, optimization can be done over the N -dimensional parameter space. Since the significance of the parameters decreases as their index increases, we can first optimize the LPFT with respect to Ω_1 , and then vary Ω_2 for the obtained fixed Ω_1 , and so on. In this way, the realization procedure is computationally efficient. However, in general, the optimization over all parameters $\Omega_1, \Omega_2, \dots, \Omega_N$, at the same time, should be done since optimal value over Ω_1 only usually does not mean that it is optimal when Ω_2 is used.

Filtering was done in the same way as in the STFT case, that is,

$$x_f(t) = \frac{1}{2\pi} \int_{-\infty}^{+\infty} L_f(t, \Omega) LPFT_{opt}(t, \Omega) d\Omega. \quad (6.63)$$

where $x_f(t)$ is the filtered received signal, $L_f(t, \Omega)$ is a rectangular excision function used for filtering. Analytical expression of this window is given by

$$L_f(t, \Omega) = \begin{cases} 0 & \text{for } \Omega \in B_j(t) \\ 1 & \text{elsewhere,} \end{cases} \quad (6.64)$$

where $B_j(t)$ is the frequency band where the concentrated jammer exists.

As a special case of the LPFT, let us first consider the simplest, first-order $LPFT_1$, $LPFT(t, \Omega; \Omega_1)$. The optimization of this transform can be done directly by varying the parameter Ω_1 . After the optimal (maximally concentrated) LPFT is found, the filtering relation (6.63) is performed. The optimization procedure may be done in a much more efficient way by exploiting the relations derived for the second-order LPFT moments (Chapter 2) or the fractional Fourier transform second-order moments (Chapter 3).

Now we are going to describe algorithm of adaptive interference rejection. The presented algorithm is order adaptive, which will provide additional savings in computation. It is based on the following property of the LPFT. Consider definition (6.60). It is easy to conclude that when we achieve that the jammer form and the LPFT order are matched within the window $w(t)$, then

$$LPFT(t, \Omega; \Omega_1, \Omega_2, \dots, \Omega_N) = a_J W(\Omega - \varphi'(t)). \quad (6.65)$$

Thus, the LPFT order is matched to the jammer form when the filtering region $L_f(t, \Omega)$, for a given t , is approximately equal to the width of the window's main lobe.

Step 1. Calculate $STFT(t, \Omega)$ for a given instant t and determine the filtering region $L_f(t, \Omega)$ (frequency range) covered by the jammer for that instant.

If the width of $L_f(t, \Omega)$ is approximately equal to the width of the main lobe of applied window, it means that the jammer frequency is constant within the considered time interval (width of the lag window in the frequency domain). Filtering is done according to relation (6.58). Go to step 4. Otherwise, go to the next step.

Step 2. Calculate the first-order LPFT and perform its optimization (maximizing of concentration) by varying the parameter Ω_1 . Optimization of the first-order LPFT can be done in an efficient manner by maximizing its second-order moment (see Chapter 2). If the width of such a determined $L_f(t, \Omega)$, in the optimal Ω_1 domain (for $\Omega_1 = \Omega_{1opt}$), is approximately equal to the width of the main lobe of the applied window, the filtering is realized based on relation (6.63). Go to step 4. Otherwise go to the next step.

Step 3. Calculate the second-order LPFT and perform its optimization by varying the parameter Ω_2 with $\Omega_1 = \Omega_{1opt}$ from step 2 (or in general by varying both Ω_1 and Ω_2). Apply filtering, like in the previous steps, and go to step 4. We may proceed with this algorithm, for the third, fourth..., order LPFT, but we will restrict ourselves to the second-order LPFT. The reason for that is in fact that the results obtained for up to the second-order LPFT are almost independent of the jammer rate. Note that in general, by increasing the order, the numerical complexity increases, since, in general, we may not assume that the best first-order coefficient is the best in the second-order distribution. Then all possible values for both parameters should be considered. In general, for K possible values for one coefficient and P coefficients, there are K^P possible coefficients combinations to check.

Step 4. Take a next time instant t , and go to step 1.

In the next two examples we will demonstrate contribution in the jammer excision provided by the described algorithm. As can be seen from Fig. 6.23, this contribution is reflected in “narrowing” the area corrupted by the jammer.

Example 6.18. Consider the received signal composed of the same components as in Example 6.16. Now, in addition to the standard STFT, we will use the presented algorithm. The jammer parameters are the same as in Example 6.16. Since the jammer is a linear frequency-modulated signal, the algorithm uses the first-order LPFT. After calculating the filtering range and interference filtration based on (6.63) and (6.64), we got results for BER illustrated in Fig. 6.22(a) (marked as LPFT₁). □

Example 6.19. Now consider the received signal composed of the same components as in Example 6.17 and apply the order-adaptive LPFT. Two forms of the algorithm are used. In the first case we limited the algorithm up to the first-order LPFT. In

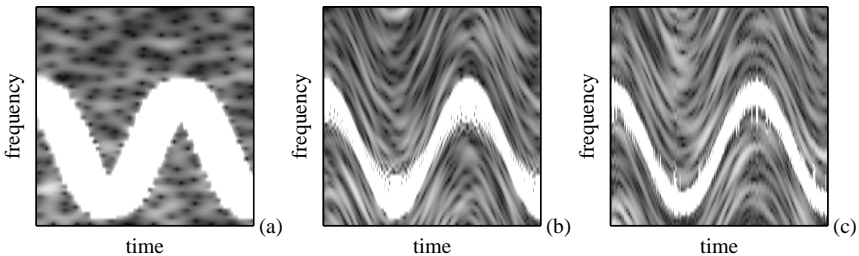


Figure 6.23 Absolute values of the transforms: (a) the STFT, (b) the transform obtained with the algorithm up to the first-order LPFT (LPFT_1), and (c) the transform obtained with the algorithm up to the second-order LPFT (LPFT_2) with corresponding filtered out areas for one realization of the received signal and sinusoidally frequency-modulated jammer.

the second case a full form of the presented algorithm was used (up to the second-order LPFT). In this way we obtained the filtered signal and BER curves denoted by LPFT_1 and LPFT_2 in Fig. 6.22(b). The algorithm, up to the first-order LPFT, improved significantly BER with respect to the one obtained by using the STFT. Further improvement is achieved by using the algorithm up to the second-order LPFT. As we can see, the algorithm here produces results almost independent of the signal rate (amplitude of the jammer frequency variations). It means that there is no need for increasing the LPFT order in the algorithm in this case.

Illustration of the filtering region for one realization and all three used filtering forms (STFT, LPFT_1 and LPFT_2) is given in Fig. 6.23. The filtered out area in the time-frequency plane is shown in white. Transforms are calculated for 2 bits of the signal with 128 chips in each bit. A sinusoidal jammer with $JSR = 30$ dB is considered. From this figure we see improvement in localization when the algorithm uses higher-order LPFTs. It results in the performance improvement. \square

6.3 CAR ENGINE SIGNAL ANALYSIS

Structure-borne sound signals and more seldom pressure signals are used for efficient combustion control of spark-ignition engines. This control can increase efficiency, reduce pollution and noise, and protect against knock. Knock is an abnormal combustion that causes rapid rise of the temperature and pressure. Its detection is an important problem since frequent knock occurrence can destroy the engine or significantly degrade its performances. By measuring the pressure

at a suitable point inside the cylinder, we can observe the combustions. However, pressure sensors are expensive, difficult to mount, and not robust enough. These are the reasons why their application is mainly limited to test beds. Sound signals can be considered as time-varying filtered versions of the pressure and can be used for the observation of diagnostic parameters as resonance frequencies that are function of temperature and resonance energies that indicate knock. The application of acceleration sensors on the surface of the engine is easy and economical, but sound signals are superimposed with mechanical noise that can significantly influence the analysis.

Such sound and pressure signals are highly nonstationary therefore, classical signal analysis tools in the time domain or in the frequency domain are not efficient here. Even the short-time Fourier transform and its energetic version spectrogram, as extensions of the Fourier analysis to the nonstationary problems, cannot be used due to high nonstationary effects in the car engine signals. These signals require joint time-frequency analysis. It has been shown by Böhme et al. that pressure signals and sound signals can be considered as frequency-modulated multicomponent signals with random amplitudes and phases of the components when low-frequency parts are neglected. Due to cyclostationarity and the property that the components of these signals are mutually not correlated, it has been found that the Wigner spectrum can be used as an efficient time-frequency tool for their analysis. The problem of cross-terms in the Wigner distribution was resolved by averaging over pressure or sound signals of different combustion cycles of the engine under similar working conditions. Since the components are not correlated, the cross-terms disappear and theoretically, using an infinite number of combustions, the mean of Wigner distributions converges to the Wigner-Ville spectrum containing the auto-terms only. The main disadvantage of this approach is that the elimination of cross-terms requires a large number of combustions, meaning a long observation time that can mask the effects in a single combustion or a decision based on the analysis can be too late for an action.

6.3.1 Car Engine Signal Models and Analysis

A pressure signal or an undisturbed sound signal can be described by a multicomponent frequency and amplitude modulated signal if low-frequency parts of the signals are filtered out. Consider first a very simple form of a real monocomponent signal,

$$\bar{y}(t) = 2A(t) \cos(\varphi(t)) \quad (6.66)$$

with

$$\varphi(t) = \Omega_0 \int_{-\infty}^t m(\tau) d\tau + \Phi \quad (6.67)$$

where $\Omega_0 m(t)$ is the instantaneous frequency and Φ is a random phase. If we suppose that the amplitude and phase are such functions that the Fourier transform of $A(t) \exp(j\varphi(t))$ is zero-valued for negative frequencies, then the analytic signal of $\bar{y}(t)$ can be written as

$$y(t) = A(t) e^{j\varphi(t)} \quad (6.68)$$

The Wigner distribution provides a time-frequency representation of the signal $y(t)$. Two properties of the Wigner distribution, which will be used here, are that the amplitude and the instantaneous frequency can be estimated using

$$\begin{aligned} \frac{1}{2\pi} \int_{-\infty}^{\infty} WD_y(t, \Omega) d\Omega &= A^2(t) \\ \varphi'(t) &= \arg \left\{ \max_{\Omega} WD_y(t, \Omega) \right\}. \end{aligned} \quad (6.69)$$

If the instantaneous frequency is not a linear function of time, we have either to use the general unbiased moment relation for the instantaneous frequency or we use the simple form (6.69), being aware that a biased value may be obtained. Therefore, if we know the pseudo Wigner distribution of a monocomponent frequency-modulated signal, then we can exactly reconstruct its amplitude and instantaneous frequency.

In reality sound and pressure car engine signals should be modeled as multi-component signals. The analysis slightly complicates in this case. Consider a signal

$$\bar{y}(t) = 2 \sum_{p=1}^P A_p(t) \cos(\varphi_p(t))$$

with

$$\varphi_p(t) = \Omega_p \int_{-\infty}^t m_p(\tau) d\tau + \Phi_p, \quad p = 1, 2, \dots, P,$$

where $\Omega_p m_p(t)$ are the instantaneous frequencies and Φ_p are the random independent phases of the components $p = 1, 2, \dots, P$. The analytic signal is approximately

equal to

$$y(t) \cong \sum_{p=1}^P y_p(t) = \sum_{p=1}^P A_p(t) e^{j\varphi_p(t)}.$$

In this case our goal is to get $A_p(t)$ and $\varphi'_p(t) = \Omega_p m_p(t)$, $p = 1, 2, \dots, P$. These values cannot be obtained from the Wigner distribution, because of the cross-term effects. This problem could be resolved by using a distribution

$$D(t, \Omega) = \sum_{p=1}^P WD_{y_p}(t, \Omega) \quad (6.70)$$

where $WD_{y_p}(t, \Omega)$ is the pseudo Wigner distribution of the component $y_p(t)$, correspondingly.

Note that if a large number of realizations of a stochastic process $y(t) \cong \sum_{p=1}^P y_p(t)$ were known and if the components were uncorrelated, $E\{y_p(n)y_q^*(m)\} = 0$, $p \neq q$, then averaging the Wigner distribution, or the product $y(t + \tau/2)y(t - \tau/2)$, using realizations from different combustions, would produce (6.70). However, if we want signal processing based on a single realization of $y(t)$, then this approach is not applicable.

Based on the S-method $SM_y(t, \Omega)$, the amplitudes of each signal component of a multicomponent signal can be estimated as

$$A_p^2(t) = \frac{1}{2\pi} \int_{\Omega \in D_{p|t}} SM_y(t, \Omega) d\Omega \quad (6.71)$$

and

$$\varphi'_p(t) = \arg \left\{ \max_{\Omega \in D_{p|t}} SM_y(t, \Omega) \right\}$$

where

$$D_{p|t} = (\Omega_{0p}(t) - B_p(t), \Omega_{0p}(t) + B_p(t))$$

denotes the frequency interval for which the STFT is greater than an assumed reference level, for a given t . The region D_p within the p th component determination will be based on an assumed reference level R^2 . The reference level can be defined as a few percents of the spectrogram or the S-method maximal value at a considered instant n ,

$$R_n^2 = \max_k \{SPEC(n, k)\} / Q^2.$$

Values within the interval $Q^2 \in [10, 200]$ are quite appropriate for this application. Note that if $Q \rightarrow \infty$, the Wigner distribution with full cross-terms will be obtained, while $Q = 1$ results in the pure spectrogram.

For a simpler graphical presentation of the results, the amplitude value $A_p^2(n)$ is assigned to the point $(n, k_p(n))$ in the time-frequency plane (n, k) . A new matrix

$$A_M(n, k) = \begin{cases} A_p^2(n) & \text{for } (n, k) = (n, k_p(n)) \\ 0 & \text{elsewhere} \end{cases} \quad (6.72)$$

is formed to that aim. It has zero values everywhere except for the points $(n, k_p(n))$. The matrix $A_M(n, k)$ contains full information about the instantaneous frequencies and squared amplitudes (instantaneous powers) and allow an easy presentation and energy calculation. The p th resonance energy is estimated by

$$E_p \cong \sum_n A_p^2(n) \Delta t, \quad (6.73)$$

where (6.69) is used. The summation over n is done within a signal component. The practical realization of this summation is performed using the matrix $A_M(n, k)$. At each following time instant n , the nonzero value of $A_M(n, k)$ placed according to (6.72) at $(n, k_p(n))$ is summed with the nonzero value from the previous time instant $(n - 1)$ if they belong to the same signal component. The indicator of the points $(n, k_p(n))$ and $(n - 1, k_p(n - 1))$ belonging to the same component is the intersection of the corresponding regions of support $D_{p|n}$ and $D_{p|n-1}$. If these regions overlap along the frequency axis, we say that they belong to the same component.

The decision if two points $(n, k_p(n))$ and $(n - 1, k_p(n - 1))$ belong to the same component can be also based on a simple analysis as follows. If the points in the time-frequency plane are dense enough and we assume that the instantaneous frequencies are smooth functions, then we may say that the points $(n, k_p(n))$ and $(n - 1, k_p(n - 1))$ belong to the same signal component if they are within a defined range along the frequency axis, for example, if $|k_p(n) - k_p(n - 1)| \leq b$, that is, if the instantaneous frequencies do not absolutely change for more than b frequency axis steps during one time-axis step. Note that too small b would cause that if the condition $|k_p(n) - k_p(n - 1)| \leq b$ is not satisfied for a given component p and instant n , then the algorithm stops summation (6.73) at instant n and considers the remaining part of the p th component as a new component with respect to energy calculation. Too large b can cause that the instantaneous frequencies of more than one component satisfy $|k_p(n) - k_p(n - 1)| \leq b$. For analyzed car engine signals, $b = 2$ is appropriate.

Table 6.1
Signal Parameters

p	1	2	3	4	5
A_p	6	14	15	15	35
d_p	5	3	6	4	8
c_{p2}	-12π	-12π	-12π	-12π	-12π
c_{p1}	36π	76π	116π	156π	196π

Example 6.20. The presented procedure is tested on a synthetic (simulated) five-component signal with linear frequency-modulated components

$$y(t) = 2 \sum_{p=1}^5 A_p(t) \cos(\varphi_p(t)) + \varepsilon(t) \quad (6.74)$$

where

$$\begin{aligned} \varphi_p(t) &= c_{p2}t^2 + c_{p1}t + \Phi_p, \\ A_p(t) &= \begin{cases} A_p t e^{-d_p t} & \text{for } t \geq 0 \\ 0 & \text{elsewhere} \end{cases} \\ p &= 1, 2, \dots, P. \end{aligned} \quad (6.75)$$

White Gaussian noise with standard deviation σ_n is denoted by $\varepsilon(t)$, while the random phases Φ_p are uniformly distributed within $[0, 2\pi]$. We assumed that the signal (6.74) begins at $t = 0$ and its main part is located within normalized unity time period $0 \leq t \leq 1$. The observation period was then widened to $-0.1 \leq t \leq 1.5$. The sampling interval was $\Delta t = 1/256$. The Hann(ing) window $w(\tau)$ was used. Its width was $T = N\Delta t = 1$ with $N = 256$ samples. Signal parameters A_p, d_p, c_{p2}, c_{p1} are given in Table 6.1.

Example 6.21. The signal defined by (6.74) and (6.75) with parameters given in Table 6.1 is presented in Fig. 6.24(a). Using this signal, we calculated the S-method with $L_P = 4$ (Fig. 6.24(e)). The time-frequency representation produced by the S-method is compared with two other basic time-frequency distributions: the Wigner distribution and the spectrogram. As it is known, the Wigner distribution suffers from the cross-terms. In the case of a five-component signal there are 10 cross-terms, many of them overlapping each other and overlapping signal components (Fig. 6.24(c)). The spectrogram is shown in Fig. 6.24(b). Its resolution is quite low and for these kind of signals it cannot be significantly improved by changing the window $w(\tau)$ form.

The S-method (Fig. 6.24(e)) produces the distribution that is equal to the sum of the Wigner distributions calculated for each signal component separately (Fig. 6.24(d)). The calculation of distribution presented in Fig. 6.24(d) is possible since in the simulation, and only in the simulation, we know the signal components separately. After the S-method is obtained, then the instantaneous frequencies, instantaneous powers, and energies as cumulative instantaneous powers of each signal component are calculated according to relations (6.69) - (6.73) (Fig. 6.24(f - h)). The reference level in was $Q^2 = 200$. The method's accuracy is checked by comparing the obtained values with the exact instantaneous frequencies, powers and energies, presented in Fig. 6.24(f - h) by lines. The agreement is very high. Note that a small deviation of the estimated instantaneous frequency from the exact one exists at the very beginning of each signal component, $t = 0$. This can be explained by the fact that here the amplitude variations are very fast and the assumption that the signal is linear frequency-modulated does not hold here. \square

Example 6.22. Experimental Data: The procedure is applied to sound and pressure signals of a six-cylinder engine measured in parallel at speed 1000rpm. The signals are shown in Fig. 6.25. Their time-frequency representations, obtained by using the S-method, instantaneous frequencies, powers, and cumulative powers corresponding to the selected pressure and sound signals are shown in Fig. 6.26. Both pressure and sound signals are highly nonstationary signals with the significant oscillations starting just after a 10° crank angle. The crank angle is measured in degrees from top dead center (TDC). In the sound signal (Fig. 6.26(h)) the algorithm recognized four separate components also just after 10° crank angle. The instantaneous power calculated prior that angle is assigned to one component only and is located between two components with higher instantaneous frequencies (Fig. 6.26(g)). The energies of oscillations in both pressure signal and sound signal are mainly located along three resonance time-varying frequencies. While in the pressure signal the energy is mostly concentrated in the middle component, in the sound signal the energy is mainly concentrated in the two other dominant components. In the pressure signal the dominant part of energy is located up to the crank angle just higher than 20° , while the oscillations in the sound signal last longer, up to a crank angle of about 35° . The linear frequency modulation, corresponding to temperature variations, is especially notable on the longer-lasting sound signal (Fig. 6.26(f)). It is easy to estimate that the instantaneous frequency law, for example, for the middle frequency component is

$$\varphi'(t) = -0.09\theta + 13.125 \text{ kHz} \quad (6.76)$$

where θ denotes the crank angle in degrees from TDC. We can also observe that the middle resonance frequency in the sound signal, corresponding to the strongest oscillation in the pressure signal, has significant power variations. A small resonance between two higher strong resonance components appeared in the sound signal as

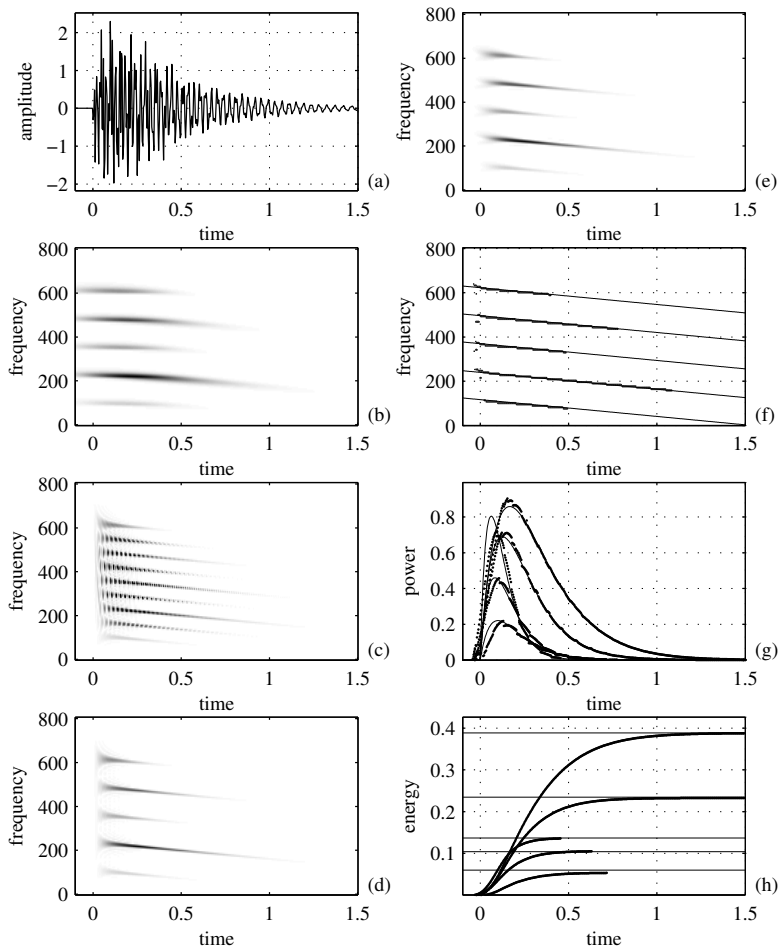


Figure 6.24 Time-frequency analysis of the simulated pressure or sound signal: (a) signal in the time domain, (b) spectrogram, (c) Wigner distribution, (d) time-frequency representation using the S-method with $L_P = 4$, (e) sum of the Wigner distributions calculated for each signal component separately. In (c) the same gray scale is used as in (d) and (e). (f) Instantaneous frequencies: exact (line) and calculated using the time-frequency representation (e) (thick line), (g) components instantaneous powers (squared amplitudes): exact (line) and calculated using the time-frequency representation (dotted), and (h) exact components energy (line) and cumulative component powers calculated using the time-frequency representation (thick line). Reference level is determined by $Q^2 = 200$.

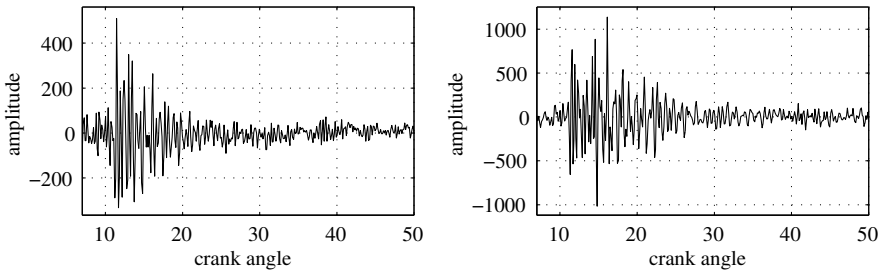


Figure 6.25 Pressure (left) and sound (right) signals of a six-cylinder engine measured in parallel at speed 1000rpm.

well. Most of these effects can be considered as a consequence of the existing evidences that the sound signal $y(t)$ can be seen as a time-variant filtered noisy version of the pressure signal $x(t)$

$$y(t) = \int_{-\infty}^t h(t, t - \tau)x(\tau)d\tau + n(t).$$

In the case of experimental data we are not able to check directly the presented algorithm and the calculation procedure, as in the case of simulated signals. But few rough check points can be indicated in the real data cases as well. If we have obtained correct results, we can expect, for example, that the following relation for the signal and calculated powers $|A_p(t)|^2$ holds

$$|y(t)| \leq 2 \sum_{p=1}^P |A_p(t)|$$

with equality for the points where all components in (6.74) are in phase $\varphi_p(t) = k\pi$. Considering, for example, the sound signal in Fig. 6.25(e - h) we can see a strong negative peak at a 15° crank angle. A high possibility is that the existing four components summed at this point in phase producing a sum of amplitudes. Calculating the amplitudes as square roots of the powers from Fig. 6.26(g) at $\theta = 15^\circ$ we roughly get $2 \sum_{p=1}^P A_p(t) = 2(\sqrt{45000} + \sqrt{16000} + \sqrt{16000} + \sqrt{2000}) = 1020$, which is in good agreement with the amplitude in Fig. 6.25(e - h). Once more we want to emphasize that this is a quite rough check. It can be influenced by the existing noise as well as by the fact that the components of a multicomponent signal very rarely take the same multiple of 2π phase. The procedure for the energy calculation can be

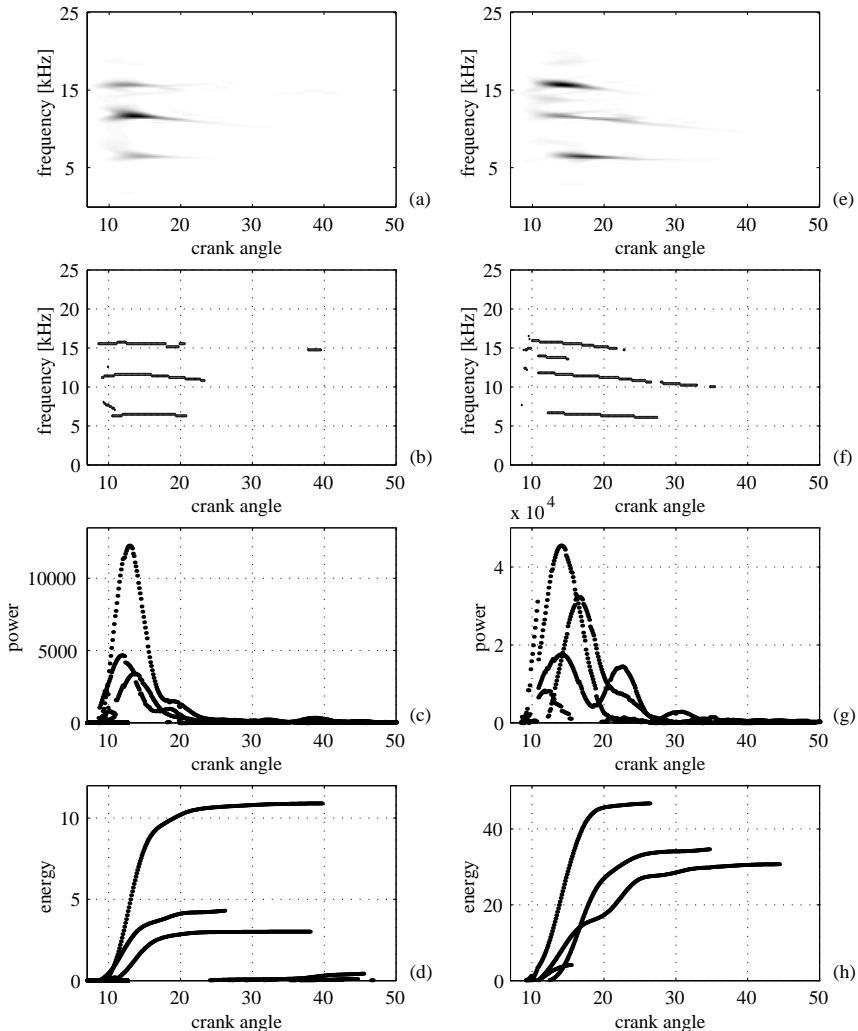


Figure 6.26 Time-frequency analysis of the pressure signal (a - d) and sound signal (e - h) with speed 1000 rpm: (a, e) time-frequency representation using the S-method with $L_P = 2$, (b, f) instantaneous frequencies, (c, g) components' instantaneous powers (squared amplitudes), and (d, h) components' cumulative power. Reference level is determined by $Q^2 = 100$. Time is measured in crank angle degrees from the TDC.

easily checked by comparing the area under a power curve and the corresponding energy. \square

6.4 ESTIMATION OF TIME-VARYING VELOCITIES IN VIDEO

In video signal processing, especially those related to the surveillance video systems, detection of moving objects and estimation of its speed are the main tasks. One of the approaches that are used to solve this problem is based on frame projections and the SLIDE (subspace-based line detection) algorithm. A key step of the SLIDE algorithm is to map a line into a complex sinusoid. By using frame projections onto the coordinate axes, the velocity of an object is mapped into an image containing lines. In order to transform the line parameters to the complex sinusoid parameters, the SLIDE algorithm with constant μ -propagation is applied. Very accurate results are obtained when objects have constant velocities, transforming to constant frequency sinusoidal signals. However, for time-varying velocities the SLIDE algorithm produces a frequency-modulated signal. This is the reason why the instantaneous frequency estimators based on the time-frequency distributions are introduced in this area.

Assume that a video-sequence $i(x,y,t)$ may be considered as a superposition of M relatively small moving objects $s^m(x,y)$, $m = 1, \dots, M$, and a stationary background $f(x,y)$, where (x,y) are spatial coordinates and t is a time instant. Let the moving objects be centered around positions given by the coordinate pairs $(\varphi_x^m(t), \varphi_y^m(t))$, $m = 1, \dots, M$, at an instant t . Then the video sequence can be modeled as

$$i(x,y,t) = f(x,y) + \sum_{m=1}^M s^m(x - \varphi_x^m(t), y - \varphi_y^m(t)). \quad (6.77)$$

The initial positions of objects are $(x_0^m, y_0^m) = (\varphi_x^m(0), \varphi_y^m(0))$, $m = 1, \dots, M$, while the projections of the velocities onto spatial coordinate axes are

$$(v_x^m(t), v_y^m(t)) = \left(\frac{d\varphi_x^m(t)}{dt}, \frac{d\varphi_y^m(t)}{dt} \right), m = 1, 2, \dots, M. \quad (6.78)$$

Velocity is represented in pixels per frame.

The main idea of this approach is in mapping the three-dimensional video-sequence (6.77) into two one-dimensional frequency-modulated signals in order to reduce the problem dimension and to employ highly accurate spectral analysis techniques for motion parameter estimation. These signals will contain information

about objects' motion parameters. The first step in this procedure is in determination of two synthetic images by using projections of the video sequence onto coordinate axes. Consider the projections of frames onto x and y axes

$$\begin{aligned} P_x(x, t) &= \int_{-\infty}^{\infty} i(x, y, t) dy \\ P_y(y, t) &= \int_{-\infty}^{\infty} i(x, y, t) dx. \end{aligned} \quad (6.79)$$

By inserting (6.77) in (6.79), the projection $P_x(x, t)$ can be written as

$$\begin{aligned} P_x(x, t) &= \int_{-\infty}^{\infty} i(x, y, t) dy \\ &= \int_{-\infty}^{\infty} f(x, y) dy + \int_{-\infty}^{\infty} \left[\sum_{m=1}^M s_x^m(x - \varphi_x^m(t), y - \varphi_y^m(t)) \right] dy \\ &= F_x(x) + \sum_{m=1}^M s_x^m(x - \varphi_x^m(t)), \end{aligned} \quad (6.80)$$

where

$$F_x(x) = \int_{-\infty}^{\infty} f(x, y) dy,$$

and

$$\begin{aligned} s_x^m(x, y) &= \int_{-\infty}^{\infty} s^m(x - \varphi_x^m(t), y - \varphi_y^m(t)) dy, \\ m &= 1, \dots, M, \end{aligned}$$

are projections of the background and the moving objects, respectively. A similar expression holds for the y -axis projection

$$P_y(y, t) = F_y(y) + \sum_{m=1}^M s_y^m(y - \varphi_y^m(t)). \quad (6.81)$$

In order to eliminate influence of the background, differentiation of $P_x(x, t)$ with respect to t is done

$$\frac{\partial P_x(x, t)}{\partial t} = \frac{\partial}{\partial t} \left[\sum_{m=1}^M s_x^m(x - \varphi_x^m(t)) \right] = \sum_{m=1}^M \frac{\partial s_x^m(x - \varphi_x^m(t))}{\partial \varphi_x^m(t)} \frac{\partial \varphi_x^m(t)}{\partial t}$$

The synthetic image $\partial P_x(x, t)/\partial t$ with x and t coordinates keeps information about objects' coordinate $\varphi_x^m(t)$, $m = 1, \dots, M$. A direct estimation of the motion parameters from $\partial P_x(x, t)/\partial t$ can be inaccurate due to the noise and other disturbances influence.

The transformation of the synthetic image $\partial P_x(x, t)/\partial t$ to an frequency-modulated signal is performed, in order to produce a signal whose parameters can be analyzed by the spectral analysis techniques. The constant μ -propagation can be used for this purpose. This technique stems from the detection of direction of arrival of a signal to a sensor array. Its application to the estimation of line parameters is proposed in literature. Mapping of the two-dimensional function $\partial P_x(x, t)/\partial t$ to the frequency domain, by using the constant μ -propagation, can be performed as

$$z_x(t) = \int_{-\infty}^{\infty} [\partial P(x, t)/\partial t] e^{j\mu x} dx. \quad (6.82)$$

Consider the special case of one object with constant velocity $v_x(t) = d\varphi_x(t)/dt = v_x$ with $\varphi_x(t) = v_x t + x_0$. Then

$$\frac{\partial P_x(x, t)}{\partial t} = \frac{\partial s_x(x - v_x t - x_0)}{\partial t} = v_x \Pi(x - v_x t - x_0),$$

with

$$\Pi(x) = -\frac{\partial s_x(x)}{\partial x}.$$

The signal $z_x(t)$ is

$$\begin{aligned} z_x(t) &= \int_{-\infty}^{\infty} v_x \Pi(x - v_x t - x_0) e^{j\mu x} dx \\ &= v_x \Phi(\mu) e^{j\mu(v_x t + x_0)} = v_x \Phi(\mu)^{j\mu\varphi_x(t)}, \end{aligned}$$

where $\Phi_x(\mu)$ is the Fourier transform of signal $\Pi_x(x)$

$$\Phi_x(\mu) = \int_{-\infty}^{\infty} \Pi_x(x) \exp(j\mu x) dx. \quad (6.83)$$

The Fourier transform of $z_x(t)$ is

$$Z_x(\Omega) = v_x \Phi(\mu) \exp(j\mu x_0) \delta(\Omega - \mu v_x). \quad (6.84)$$

Thus, the position of the Fourier transform maximum determines the object velocity

$$\begin{aligned} \Omega &= \arg \left\{ \max_{\Omega} |Z_x(\Omega)| \right\} = \mu v_x \\ v_x &= \Omega / \mu. \end{aligned} \quad (6.85)$$

This is the form of classical SLIDE algorithm for the case of constant velocities.

Consider now a linear velocity variation, with the position functions of M small moving objects,

$$\varphi_x^m(t) = x_0^m + v_{x0}^m t + a_x^m t^2 / 2, \quad m = 1, \dots, M, \quad (6.86)$$

where x_0^m is the initial position, v_{x0}^m is the initial velocity, and a_x^m is the acceleration. The objects' velocities are

$$v_x^m(t) = \frac{d\varphi_x^m(t)}{dt} = v_{x0}^m + a_x^m t. \quad (6.87)$$

The x -projection derivative is

$$\begin{aligned} \frac{\partial P_x(x, t)}{\partial t} &= \sum_{m=1}^M \frac{\partial s_x^m(x - a_x^m t^2 / 2 - v_{x0}^m t - x_0^m)}{\partial t} \\ &= - \sum_{m=1}^M (v_{x0}^m + a_x^m t) \frac{\partial s_x^m(x - a_x^m t^2 / 2 - v_{x0}^m t - x_0^m)}{\partial x}. \end{aligned}$$

The signal $z_x(t)$ can be represented as

$$\begin{aligned} z_x(t) &= \sum_{m=1}^M (v_{x0}^m + a_x^m t) \Phi_x^m(\mu) \exp(j\mu \varphi_x^m(t)) = \\ &= \sum_{m=1}^M v_x^m(t) \Phi_x^m(\mu) \exp(j\mu(x_0^m + v_{x0}^m t + a_x^m t^2 / 2)). \end{aligned} \quad (6.88)$$

The variable phase function associated with the m th object is given by

$$\phi_x^m(t) = \mu(x_0^m + v_{x0}^m t + a_x^m t^2/2) \quad (6.89)$$

while the corresponding instantaneous frequency is

$$\Omega_x^m(t) = \frac{d\phi_x^m(t)}{dt} = \mu(v_{x0}^m + a_x^m t) = \mu v_x^m(t). \quad (6.90)$$

It is time-varying. Therefore, the instantaneous frequency estimation based on the time-frequency representations should be used for analysis of object's velocity.

In general, for a phase function with all derivatives,

$$\begin{aligned} z_x(t) &= \int_{-\infty}^{\infty} [\partial P(x, t)/\partial t] e^{j\mu x} dx \\ &= \sum_{m=1}^M \left(\sum_{k=1}^{\infty} \frac{1}{k!} \frac{d^k \varphi_x^m(t)}{dt^k} \right) \int_{-\infty}^{\infty} \Pi_x^m(x - \varphi_x^m(t)) e^{j\mu x} dx \\ &= \sum_{m=1}^M \left(\sum_{k=1}^{\infty} \frac{1}{k!} \frac{d^k \varphi_x^m(t)}{dt^k} \right) \Phi_x^m(\mu) \exp(j\mu \varphi_x^m(t)) \end{aligned}$$

The motion parameters $\varphi_x^m(t)$ of moving objects can be extracted from the signal $z_x(t)$, by using some of the spectral analysis tools.

As a result of the object motion, the value of $\partial P_x(x, t)/\partial t$ will have two components: positive and negative. Since these two components produce the same spectral content, a modified function $\tilde{P}_x(x, t)$ with positive-only values is used. Therefore, the analysis of the object motion parameters is reduced to the analysis of motion of one of the object edges. We will assume that the function $\Pi_x^m(x)$ can approximately be written as

$$\Pi_x^m(x) \approx A_m \delta(x - \Delta x^m) \quad (6.91)$$

where Δx^m contains information about the object dimension. From (6.83) and (6.91) follows

$$\Phi_x^m(\mu) \approx A_m \exp(j\mu \Delta x^m). \quad (6.92)$$

This relationship holds for relatively small variations of object position between the consecutive frames.

For numerical analysis, it will also be assumed that the step in t is small enough, to use the derivative by finite difference approximation,

$$\frac{\partial P_x(x, t)}{\partial t} \cong P_x(x, t+1) - P_x(x, t) = \sum_{m=1}^M [s_x^m(x - \varphi_x^m(t+1)) - s_x^m(x - \varphi_x^m(t))].$$

Example 6.23. In a landscape image from Montenegro (size 1536×2048 pixels) as a background, two moving objects have been embedded. The motion of the first object is described by

$$\varphi_x^1(t) = 400 + 1.5t^2/500 + 0.1t - 2.5t^3/10^6$$

with

$$v_x^1(t) = 3t/500 + 0.1 - 7.5t^2/10^6.$$

The other coordinate of the first moving object changes according to

$$\varphi_y^1(t) = 60 + 2.5t,$$

for $0 \leq t \leq 500$ with step 1. The size of the first object in video sequence (due to motion) changes from 20 to 30 pixels in radius during the whole range of t . The second object's motion parameters are

$$\varphi_x^2(t) = 100 + 3t - t^2/1800 - 0.75t^3/10^6$$

with velocity

$$v_x^2(t) = 3 - t/900 - 2.25t^2/10^6$$

and y -coordinate changes as

$$\varphi_y^2(t) = 100 + 1.5t.$$

Object size changes from 15 to 25 pixels in radius during whole range of t . The image with object positions in each twentieth frame is shown in Fig. 6.27(a). The spectrogram with a Hann(ing) window of the width 256, along with the S-method, calculated based on this STFT, with $L = 8$ correcting terms, is shown in Fig. 6.27(b, c). The x -component of the velocity is analyzed by using the described approach. Since the signal analysis is performed with the STFT using a window of the width 256, then a movement in the video sequence with a speed v_x [pixels/frame] corresponds to the frequency number $k = 256v_x/(2\pi)$. Thus, the velocities in the frequency indices are

$$\begin{aligned} k_x^1 &= [3t/500 + 0.1 - 7.5t^2/10^6]128/\pi, \\ k_x^2 &= [3 - t/900 - 2.25t^2/10^6]128/\pi. \end{aligned}$$

These values, corresponding to the true velocities, are plotted by circles, along with the time-frequency representation.

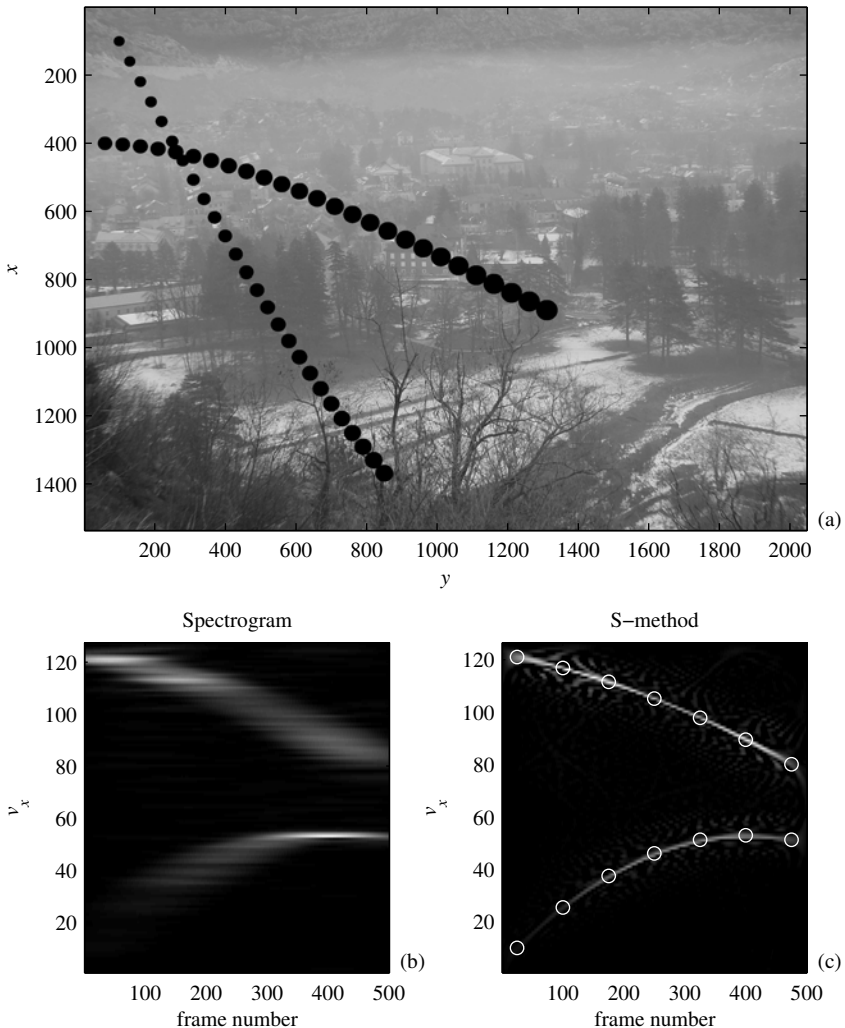


Figure 6.27 Video sequence with a landscape in background, and two moving objects. (a) Positions in every twentieth frame of the moving objects. (b) Time-frequency analysis of the processed x-axis projection based on the spectrogram, and (c) based on the S-method. Circles indicate the true objects velocities in selected frames. The time axis is here the number of the video frame, while the frequency axis is proportional to the velocity.

Example 6.24. A real video sequence is considered in this example. It lasts 29[s] and it contains 734 video-frames (25 frames/s) of the size 320×240 with 256 gray levels. The sequence is recorded by an iPhone in a MP4 format and converted into an avi format. The scene contains two moving objects (walkers) and the background. The objects positions in frames 100, 200, 400, and 600 are depicted in Fig. 6.28(a – d). Since the main objects movement is along the x -coordinate, we made only a velocity estimation of the x -component. The constant μ -propagation with $\mu = 1/\pi$ is applied. The spectrogram of the signal $z_x(t)$ is shown in Fig. 6.28(c), while the S-method is shown in Fig. 6.28(d). It is important to note that, in this case, an accurate velocity estimation would be very difficult by employing any specific parametric motion model.

□

6.5 TIME-FREQUENCY-BASED DETECTION OF DETERMINISTIC SIGNALS

The detection of an unknown deterministic signal in a high noise environment is of crucial interest in many real-world applications. In this case the problem is in testing the hypothesis

$$\begin{aligned} H_0 &: \text{Signal is not present in the observed noisy signal} \\ H_1 &: \text{Signal is present in the observed noisy signal} \end{aligned} \quad (6.93)$$

The deterministic signal may be deterministic with unknown parameters, for example, a sinusoidal signal with unknown amplitude, frequency, and phase, or may be of unknown form. In the case of a constant frequency sinusoidal signal, the Fourier transform concentrates all the signal's energy at one frequency point, while the noise is distributed over a wide frequency range. We have already shown that the Fourier transform-based representation provides the best signal concentration, with the minimization of the stationary white Gaussian noise influence. Thus, in the case of sinusoidal signal and a Gaussian white noise, the Fourier transform-based detectors are optimal. However, for time-varying signals, when the frequency content of a signal changes over time, the spectral content is time-varying. Then the Fourier transform-based detector will not provide the optimal result. The basic idea is to use time-frequency representation that produces highly-concentrated energy of the desired signal around the instantaneous frequency and then to apply integration along the instantaneous frequency line. In the case of high noise, an algorithm for finding possible instantaneous frequency paths should be defined. In this way, the

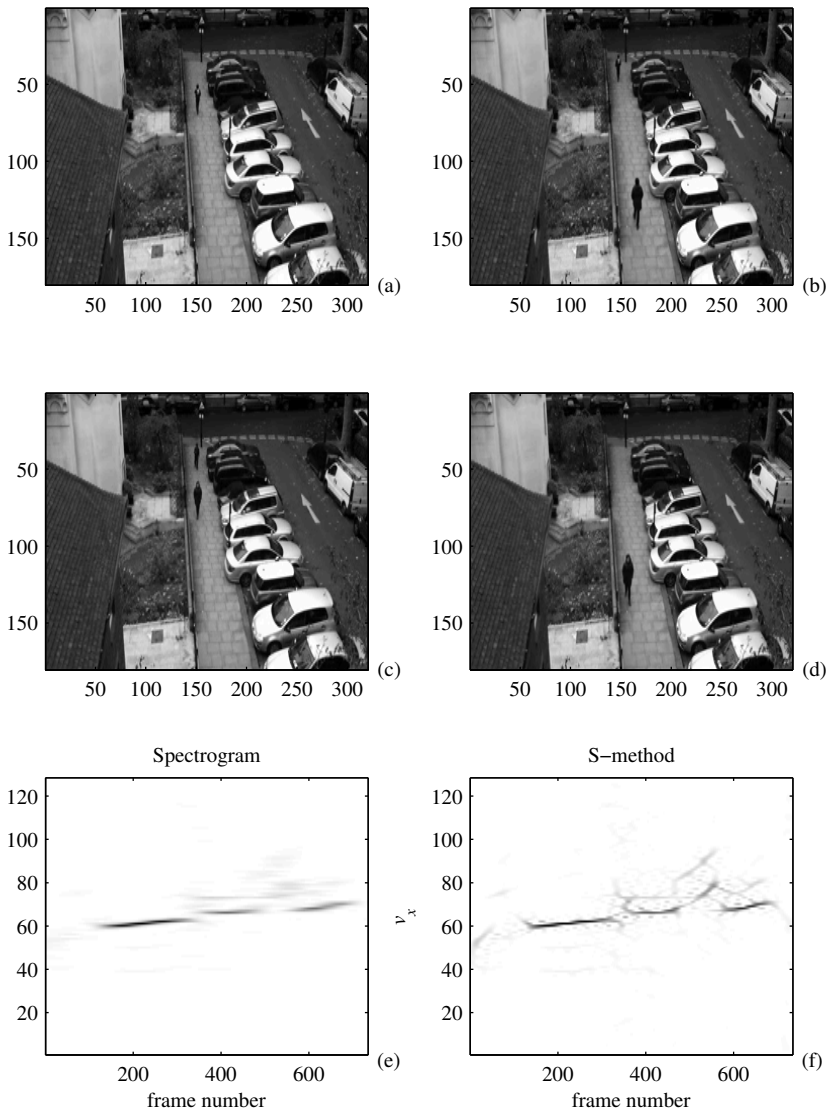


Figure 6.28 Velocity estimation in a real video sequence: (a- d) video frames at 100, 200, 400, and 600; (e) the spectrogram of the signal $z_x(t)$; and (f) the S-method concentrated along the object velocities.

performance of such a detector is close to the performance achieved for constant frequency signals by using the Fourier transform.

Thus, we will first review the Fourier-based detector, since it will be the basis for time-frequency generalization.

6.5.1 Signal Detection by Using the Fourier Transform

Let us consider a single component deterministic signal with unknown discrete frequency ω_0

$$x(n) = Ae^{j\omega_0 n},$$

and observation

$$s(n) = \xi \cdot x(n) + \varepsilon(n),$$

where $\varepsilon(n)$ is a complex zero mean Gaussian white noise with independent real and imaginary parts, with variance σ_ε^2 . Variable ξ can take values $\xi = 0$ (hypothesis H_0 : absence of the signal $x(n)$) and $\xi = 1$ (hypothesis H_1 : presence of the signal $x(n)$). Suppose that there are N samples of the discrete signal $s(n)$. The discrete Fourier transform of the signal $s(n)$ is

$$S(k) = \xi NA\delta(k - k_0) + \varepsilon_F(k), \quad (6.94)$$

where $\varepsilon_F(k)$ is also complex zero mean Gaussian white noise, with variance $\sigma_F^2 = N\sigma_\varepsilon^2$ and $k_0 = \omega_0 N / (2\pi)$ is an integer. It is optimal for this signal and noise. The expected value of the signal spectrum is

$$\begin{aligned} E\{|S(k)|^2\} &= N^2 |A|^2 \delta(k - k_0) + N\sigma_\varepsilon^2 && \text{for } H_1 : \xi = 1 \\ E\{|S(k)|^2\} &= N\sigma_\varepsilon^2 && \text{for } H_0 : \xi = 0 \end{aligned}$$

Now we can make a decision about the presence of the deterministic signal $x(n)$ in noisy samples $s(n)$ as

$$\hat{\xi} = \begin{cases} 1 & \text{for } \max[|S(k)|^2] > R_{S^2}, \\ 0 & \text{for } \max[|S(k)|^2] \leq R_{S^2}, \end{cases}$$

where R_{S^2} is the threshold level. False alarm probability P_{FA} can be determined by analyzing the statistical properties of the noise, while magnitude of the signal $x(n)$ must be known in order to determine the probability of signal detection P_D . A common method for determining the threshold level R_{S^2} is a constant false alarm rate method (CFAR), where the probability P_{FA} is kept constant. In the analyzed

case we have

$$\begin{aligned} P_{FA} &= P[|\varepsilon_F(k)|^2 > R_{S^2} \text{ for at least one } k] \\ &= 1 - P[|\varepsilon_F(k)|^2 \leq R_{S^2} \text{ for every } k] \\ &= 1 - \prod_{k=0}^{N-1} P[|\varepsilon_F(k)|^2 \leq R_{S^2}]. \end{aligned}$$

where $P[\cdot]$ denotes probability of event $[\cdot]$.

The square absolute value of a complex random variable with Gaussian probability distribution is a random variable with chi-square probability distribution with two degrees of freedom, so we have

$$P_{FA} = 1 - \left(1 - \exp \left(-\frac{R_{S^2}}{N\sigma_\varepsilon^2} \right) \right)^N, \quad (6.95)$$

Now we can determine the threshold level R_{S^2} , which depends on the probability P_{FA} ,

$$R_{S^2} = -N\sigma_\varepsilon^2 \ln(1 - \sqrt[N]{1 - P_{FA}}).$$

To determine the threshold level, the noise variance must be known. This variance can be estimated by using data samples of the signal $s(n)$ as

$$\sigma_\varepsilon^2 \cong 1.1 \left(\underset{1 \leq i < N}{\text{median}}(|\text{Re}[s(i) - s(i-1)]|)^2 + \underset{1 \leq i < N}{\text{median}}(|\text{Im}[s(i) - s(i-1)]|)^2 \right). \quad (6.96)$$

In many cases, the discrete frequency of the deterministic signal does not satisfy the relation $\omega_0 = 2\pi k_0/N$, where k_0 is an integer. In these cases, when $\omega_0 \neq 2\pi k_0/N$, the detection result can be improved (probability P_D increased), for example, by zero-padding before the Fourier transform calculation.

If the deterministic signal $x(n)$ is nonstationary, it can be written as

$$x(n) = A(n)e^{j\varphi(n)},$$

where $\varphi(n)$ is a nonlinear function. In this scenario, the Fourier-based detector is not the optimal one. When signals are nonstationary, the detection capability of the Fourier-based detector is limited. In these cases, the detection problem can be solved in a better way by using time-frequency analysis of the signal $s(n)$. Before we start time-frequency formulation, in order to better illustrate its efficiency, we will introduce an intermediate step, the parametric processing of nonstationary signals.

6.5.2 Parametric Extension of the Fourier Transform

A nonstationary signal of the form $x(n) = A(n)e^{j\varphi(n)}$ can be processed by using a parametric form of the Fourier transform

$$X(k) = \sum_{n=0}^{N-1} A(n)e^{j\varphi(n)}e^{-j\psi(n;a_0,a_1,\dots,a_P)}e^{-j2\pi kn/n},$$

where N is the signal's duration and $\psi(n;a_0,a_1,\dots,a_P)$ is a function with P parameters. If we are able to match the form of $\varphi(n)$ with $\psi(n;a_0,a_1,\dots,a_P)$ and find the parameters a_0, a_1, \dots, a_P such that $\varphi(n) - \psi(n;a_0,a_1,\dots,a_P)$ is a linear function of n , then $e^{j\varphi(n)}e^{-j\psi(n;a_0,a_1,\dots,a_P)}$ would be a pure sinusoid. Then all the conclusions valid for the Fourier transform-based detector could be applied. In order to match the form of $\varphi(n)$, we can apply instantaneous frequency estimation techniques, the fractional Fourier transform, or polynomial Fourier transform, if the signal phase is polynomial.

In order to illustrate these methods, which will lead to a nonparametric time-frequency-based signal detection, consider the discrete short time Fourier transform

$$STFT(n,k) = \sum_{m=-M/2}^{M/2-1} w(m)x(n+m)e^{-j2\pi km/M}$$

with Hann(ing) window $w(m)$. The spectrogram, a squared module of the STFT, will be used here as the time-frequency representation. We will consider two signals: a signal with linear frequency modulation, and a signal with sinusoidal frequency modulation. Signal-to-noise ratio in both cases is 0dB.

Fig. 6.29 and Fig. 6.30 illustrate the basic principle of the time-frequency-based detection. Subplots in Fig. 6.29(a - c) present time-frequency representation of the analyzed linearly frequency-modulated signal, illustrating the paths in the time-frequency plane and the summation of time-frequency values along the paths. In this case, the paths are parallel to the time axis and the summation along these paths is proportional to the Fourier transform of the analyzed signal. Fig. 6.29(d - f) presents the summation along the paths adjusted to the signal's instantaneous frequency by determining the parameters of the linear frequency-modulated signal. The maximum value of the summation along the paths is higher in the second case. This distinctly demonstrates that the detection of these types of signals is simple and straightforward using this approach.

Fig. 6.30 illustrates the detection of a sinusoidal frequency-modulated deterministic signal. Fig. 6.30(a - c) presents the summation along the paths equivalent

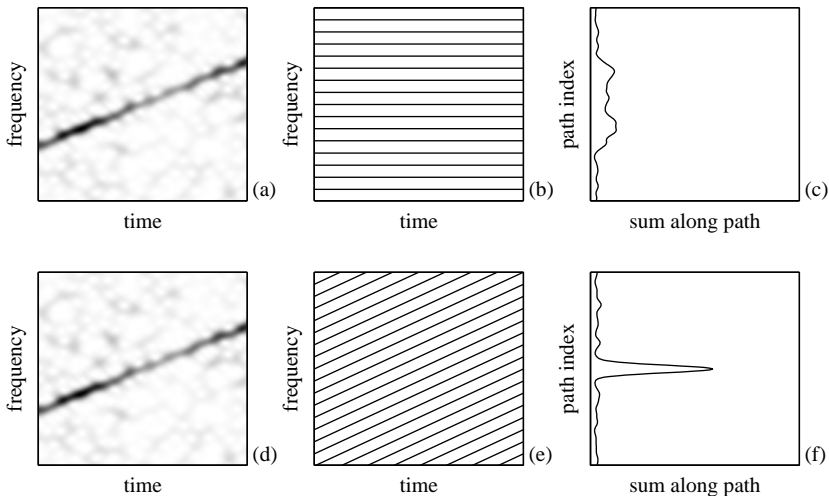


Figure 6.29 Detection example of a linear frequency-modulated signal. (a - c) Paths parallel to the time axis, equivalent to Fourier transform-based detector. (d - f) Paths parallel to the instantaneous frequency, equivalent to the time-frequency detector. (a, d) Time-frequency representation; (b, e) paths; and (c, f) sum of the time-frequency representation values along the paths.

to the Fourier transform. Fig. 6.30(d - f) presents the summation along the paths adjusted to the linear frequency-modulated signal from the previous figure, and Fig. 6.30(g - i) presents the summation along the paths adjusted to the instantaneous frequency and parameters of the analyzed signal. The maximum value is obtained when the path coincides with signal's instantaneous frequency. The detection method analyzed here is based on searching the best path (with the maximum summation of the time-frequency values along the path).

The above example shows that the detection of nonstationary signal can only be considered if we know the signal form and we are able to adjust the paths to the instantaneous frequency. However, in practice the signal form is not a priori known and the parametric approach to these types of applications is quite limited. We will next show that similar principles can be used in nonparametric formulation of the detection, without using a priori knowledge about the signal form.

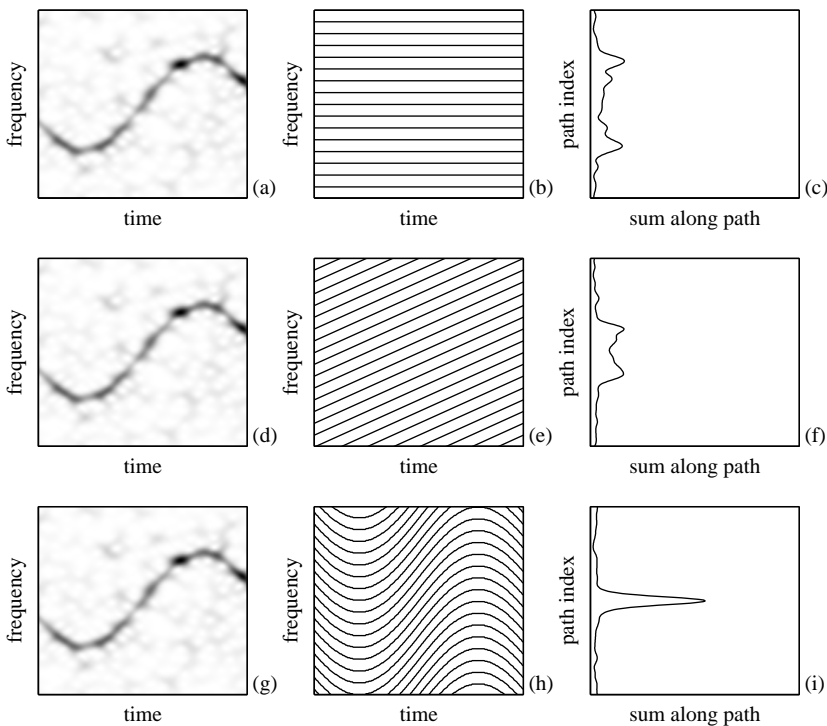


Figure 6.30 Detection example of a sinusoidal frequency-modulated signal. (a - c) Paths parallel to the time axis, equivalent to Fourier transform-based detector. (d - f) Paths used in the linear frequency-modulated signal. (g - i) Paths parallel to the instantaneous frequency, equivalent to the time-frequency detector. (a, d, g) Time-frequency representation; (b, e, h) paths; and (c, f, i) sum of the time-frequency representation values along the paths.

6.5.3 Detection in the Time-Frequency Domain

For signals whose spectral content varies over time, time-frequency distributions represent energy distribution over time and frequency. The basic quadratic time-frequency distribution is the Wigner distribution. The Wigner distribution has the best concentration among quadratic distributions. However, it cannot be used in practice due to the very exhibited cross-terms. In the case of multicomponent signals we have to use a distribution with reduced interference property. Appropriately

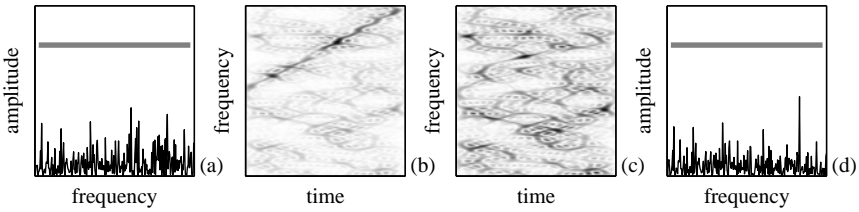


Figure 6.31 (a - d) The Fourier transform (with threshold level presented with thick gray line) and S-method of the signal $s(n)$ in the cases of the deterministic signal $x(n)$: (a, b) existence and (c, d) nonexistence.

chosen reduced interference distribution means a reduction of noise at the same time (note that, in general, the signal-to-noise ratio is not improved in the reduced interference distributions due to the auto-terms degradation). A simple distribution that can be used for this nonparametric approach is the S-method.

Let us consider a single component linearly frequency-modulated signal of the form

$$x(n) = A e^{jan^2}.$$

Let $S(n, k)$ denote the time-frequency representation of the signal $s(n)$. Fig. 6.31 shows the Fourier transform of the signal $s(n)$ for the cases $\xi = 1$ (Fig. 6.31(a)) and $\xi = 0$ (Fig. 6.31(d)). The time-frequency representation of the signal $s(n)$, for both cases, is also shown in Fig. 6.31(b, c). The S-method with rectangular window and $L = 12$ is used as the time-frequency representation of the signal. The number of samples is $N = 256$, the noise variance is $\sigma_e^2 = 4$, and the signal amplitude $A = 1$, so that the signal-to-noise ratio is approximately -6 dB. The reference level of the Fourier transform-based detector is calculated with the false alarm probability $P_{FA} = 0.0027$, and is shown in the first and last plots. The same realization of the noise is used for all four plots. Fig. 6.31 clearly shows the limited ability of the Fourier transform-based detector. However, it is easy to see if a deterministic component $x(n)$ exists in the time-frequency representation of the signal $s(n)$.

This example shows that the time-frequency analysis can be used for non-stationary signal detection in the presence of a strong noise. The basic problem is to automate the decision procedure. An algorithm for the signal detection in the arbitrary time-frequency representation is described below.

Let us consider time-frequency representation $S(n, k)$ of the signal $s(n)$, where $k = 0, 1, \dots, M - 1$ and $n = 0, 1, \dots, N - 1$. Assume that the instantaneous frequency of a deterministic signal $x(n)$ is a continuous function. We define a path in the time-frequency plane as an array of N frequency indices $\pi(n)$, with $0 \leq \pi(n) < M$ for every t . We then observe the ensemble Π_D of such paths having the property $|\pi(n) - \pi(n - 1)| \leq D$ for some specified value D and for all n . The value of D is the maximal allowed frequency index change for two consecutive time instants or the allowed frequency step. We then observe one path $\pi_m(n) \in \Pi_D$ and sum the time-frequency representation values along this path. That is,

$$J_m = \sum_{n=0}^{N-1} S(n, \pi_m(n)). \quad (6.97)$$

Denote the maximum of the observed sum over the ensemble Π_D as J_{\max} ,

$$J_{\max} = \max_{\pi_m \in \Pi_D} J_m = \sum_{n=0}^{N-1} S(n, \pi_{\max}(n)), \quad (6.98)$$

where π_{\max} is the best path. The quantity defined in this way represents a reliable criteria for determining the deterministic component existence in the time-frequency representation $S(n, k)$. Namely, if $J_{\max} > R_J$ holds, where R_J denotes the threshold level, it can be concluded that the deterministic component exists in the signal $s(n)$; in other words, $\hat{\xi} = 1$.

The basic problem in detector realization is in the threshold level R_J determination. In the case of the second-order time-frequency representation, we can assume that the level R_J is proportional to σ_{ϵ}^2 . For a specific time-frequency representation, known noise distribution, and a chosen probability P_{FA} , it is sufficient to determine the threshold level R_0 when the false alarm probability is equal to P_{FA} for the noise variance $\sigma_{\epsilon}^2 = 1$. The threshold level for nonunity noise variance can be calculated as $R_J = R_0 \sigma_{\epsilon}^2$. The determination of R_0 in this way demands the processing of many noise only data if P_{FA} is significantly small. However, this procedure should be used only once for a given time-frequency representation and for a given P_{FA} . The algorithm for the threshold level R_0 determination is described below.

1. Choose the time-frequency representation, probability of false alarm P_{FA} , and the maximum allowed frequency step D .
2. For $i = 1, 2, \dots, M_i$ where M_i is the number of iterations

- (a) Take a realization of noise-only signal $s(n)$ with unity noise variance $\sigma_\varepsilon^2 = 1$.
- (b) Calculate $S(n, k) = TFR[s(n)]$.
- (c) Find the best possible path $\pi_{\max}(t)$ and calculate

$$J_{\max}(i) = \sum_{t=0}^{N-1} S(t, \pi_{\max}(t)).$$

3. Calculate the threshold level R_0 such that in $M_i P_{FA}$ iterations we obtain $J_{\max}(i) > R_0$ (and $J_{\max}(i) \leq R_0$ in the remaining $M_i(1 - P_{FA})$ iterations).

The second problem is in specifying the number of path ensembles Π_D and in the determination of the best path. In order to decrease the total number of paths (of the order N^M), we can apply the following approach:

1. For each time index n , find the maximum $S_{\max}(n)$ and the position of maximum $k_{\max}(n)$

$$\begin{aligned} S_{\max}(n) &= \max_k S(n, k), \\ k_{\max}(n) &= \arg \max_k S(n, k). \end{aligned}$$

Assume that the best path $\pi_{\max}(n)$ passes through at least one of the selected maxima.

2. For each time index $n \in \{1, 2, \dots, N\}$, form the path $\pi_n(i)$ starting at the point $(n, k_{\max}(n))$ in the time-frequency plane.

- (a) Put point $(n, k_{\max}(n))$ into path: $\pi_n(n) = k_{\max}(n)$.
- (b) For $i = n + 1, n + 2, \dots, N$, the path point is

$$\pi_n(i) = \arg \max_{k \in K} S(i, k),$$

where set K includes frequency points $K = \{k | \pi_n(i-1) - D \leq k \leq \pi_n(i-1) + D\}$. Note that this procedure limits the frequency step between two consecutive time instants to D .

- (c) For $t = i-1, i-2, \dots, 1$, the path point is

$$\pi_n(i) = \arg \max_{k \in K} S(i, k), \quad (6.99)$$

where $K = \{k | \pi_n(i+1) - D \leq k \leq \pi_n(i+1) + D\}$.

3. Calculate the sum $J_n = \sum_{i=0}^{N-1} S(i, \pi_n(i))$.

4. The best path is the path with maximum J_n .

Note that the number of analyzed paths in this procedure is equal to N . The number of paths can be further decreased if, in step 2 of the previous procedure, we perform the path forming only if the starting point $(n, k_{\max}(n))$ is not included in any of the previous analyzed paths $\pi_{n-1}(i), \pi_{n-2}(i), \dots, \pi_1(i)$. This can be done because if the point $(n, k_{\max}(n))$ belongs to the path $\pi_p(i)$ for some p , then the path $\pi_n(i)$ coincides with the path $\pi_p(i)$. Also, note that in step 2 of the previous procedure we can process time instants n in an arbitrary order. We suggest that the value of $S_{\max}(n)$ determines the order of processing the time instants. That is, we process the time instant with the highest $S_{\max}(n)$ first and the time instant with the smallest $S_{\max}(n)$ should be the last one processed. This reordering cannot change the best path, but can change the total number of analyzed paths.

Fig. 6.32(a) presents the threshold estimation for the spectrogram with a 32-point Hann(ing) window. It should be noted that J_{\max} in Fig. 6.32(a) is plotted in a descending order. The signal length is 256 samples and the STFT is calculated over 256 frequency bins. The probability of false alarm is $P_{FA} = 0.01$. The threshold is estimated by analyzing the best paths in the noise only case with $\sigma_e^2 = 1$. The number of realizations is $M_i = 1000$. The threshold is determined according to the number of expected false alarms $M_i \cdot P_{FA} = 10$. In this way, we can implement the desired probability of false alarms.

Fig. 6.32(b) presents a histogram of the number of analyzed paths in the procedure for searching the best path in the noise only case. The mean number of the analyzed paths per realization is 12.

The performance of time-frequency-based signal detectors, with their comparison to the Fourier-based detector, are shown in Fig. 6.33. The case of a linearly frequency-modulated signal is considered

$$x(n) = e^{j\frac{\pi}{128}(n-128)^2},$$

for $0 \leq n \leq 256$ in the presence of additive Gaussian white noise. For each SNR, 200 realizations are observed and the detection is performed by using the Fourier transform and the S-method with $L = 4$, $L = 16$, and $L = 32$. The dependency of the probability P_D on the signal-to-noise ratio is shown in Fig. 6.33. As we expected, the S-method with large enough L is a good signal detector, even if the signal-to-noise ratio is small. The false alarm probability for all analyzed detectors is $P_{FA} = 0.01$. It

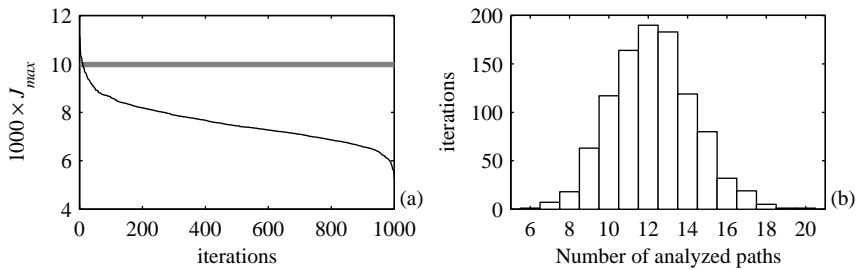


Figure 6.32 (a) Threshold estimation. The best achieved values of the path sum for 1000 realizations of random signal without deterministic component. The gray horizontal line represents the threshold $R_0 = 9973$ obtained with $P_{FA} = 0.01$. (b) Histogram of the number of analyzed paths for $M_i = 1000$ realizations. The average number of analyzed paths is 12.

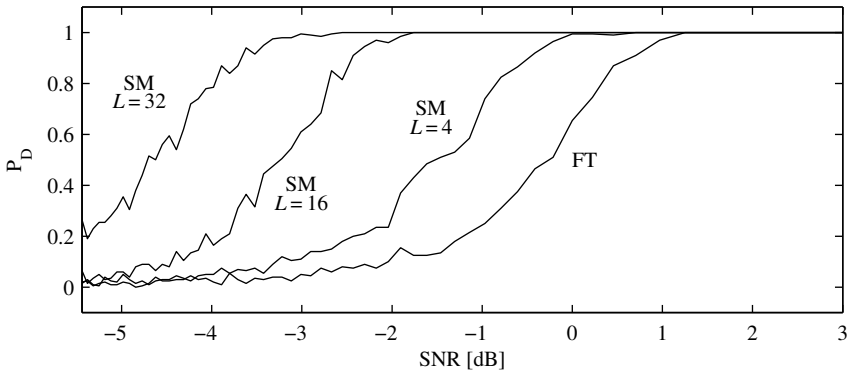


Figure 6.33 Probability of the signal detection for the case of Fourier transform-based detector and the S-method-based detector for $L = 4, 16$, and 32.

should be noted that the threshold estimation for the Fourier-based detector is very simple compared to a time-consuming threshold estimation for time-frequency-based detector.

6.5.4 Real Radar Data Analysis

Let us now consider detection of target signals in an experimental high-frequency surface-wave radar system. Suppose that the target velocity is high enough so that the sea clutter can be removed by highpass filtering.

Stationary Targets: The Fourier transform is the optimal detector in this case. Let us now consider a single range cell with the signal representing that range cell denoted by $x(n)$. The detection algorithm in the case of a constant false alarm rate is:

1. Choose the probability of false alarms P_{FA} .
2. Estimate the noise variance for the considered signal σ_e^2 . A good estimation can be obtained by using (6.96).
3. Calculate the reference level $R_{FT} = -\ln(P_{FA}/N)N\sigma_e^2$, where N is the signal length.
4. Calculate the discrete Fourier transform of the signal $X(k) = \text{DFT}_N\{x(n)\}$.
5. If there exists k such that $|X(k)|^2 > R_{FT}$, then we make a decision that a target signal exists.

Nonstationary Targets: The algorithm mentioned above is optimal in the case of stationary signals. When the target velocity changes in the considered time interval, the target's signal becomes nonstationary, and the Fourier transform is no longer an optimal detector. In these cases, we can use the time-frequency-based detector. Now the detection algorithm is:

1. Choose the probability of the false alarm P_{FA} .
2. Choose the time-frequency representation.
3. Consider the noise-only case with unit variance. Estimate the reference level R_0 so that the criterion $J_{\max} > R_0$ gives the false alarm rate as chosen in the step 1.
4. Estimate the noise variance σ_e^2 .
5. Calculate the time-frequency representation of the analyzed signal.
6. Find J_{\max} and compare it with the reference level $R_J = R_0\sigma_e^2$. If $J_{\max} > R_J$, we can make a decision that the target signal exists in the considered range cell.

Note that steps 1. - 3. should be performed only once, so the time-consuming step 3 does not slow down the detection process.

Example 6.25. Signals in the following analysis are experimental aircraft data collected by a high-frequency surface-wave radar (HFSWR), which use a 10-element linear receiving antenna array. The data was collected with a target present. The radar carrier frequency is 5.672 MHz and the pulse repetition frequency is 9.17762 Hz. There are six trials. Each trial corresponds to a block of 256 pulses. We consider five nonstationary cases (signals 1 - 5) and one stationary case (signal 6). The signals are highpass filtered in order to remove strong sea clutter. Fig. 6.34 presents the Fourier transform of the filtered analyzed signals with SNR = -2dB . The target signature is not clearly visible except in the stationary case Fig. 6.34(f). Time-frequency representations of the analyzed signals are presented in Fig. 6.35. Here we can see clear target signature in all analyzed signals. The S-method is chosen as the time-frequency representation with large L ($L = 64$). The reference level $R_0 = 1320$ is determined according to the previously described procedure. The false alarm probability is $P_{FA} = 0.0027$.

In order to estimate threshold values of the detector, we add noise to the analyzed signal so that a noisy signal is obtained. Note that in this example, deterministic signal $x(n)$ is experimental data and noise $\varepsilon(n)$ is artificial. Detection algorithms of stationary and nonstationary cases are then applied to the noisy signal. Table 6.2 shows the number of detected target signals for 100 noise realizations with varying signal-to-noise ratios (SNR). It is obvious that the time-frequency-based approach outperforms the Fourier-based detection approach when the target signal is nonstationary. In the case of a stationary signal (signal 6), the presented method is slightly worse than the Fourier-based approach. The Fourier-based detection is optimal in this case. The estimated probability of target detection with varying SNR is given in Fig. 6.36 for nonstationary cases using both the Fourier and the time-frequency-based detectors. Fig. 6.37 and Fig. 6.38 represent two typical realizations for nonstationary and stationary signals and its detection procedure, respectively. Both Table 6.2 and Fig. 6.36 also show that the time-frequency-based detector is able to detect the nonstationary target signals correctly when the SNR is higher than -8 dB . \square

These results confirm that the Fourier detector is optimal when the signals are stationary, whereas the time-frequency-based detector is a better choice for nonstationary signals.

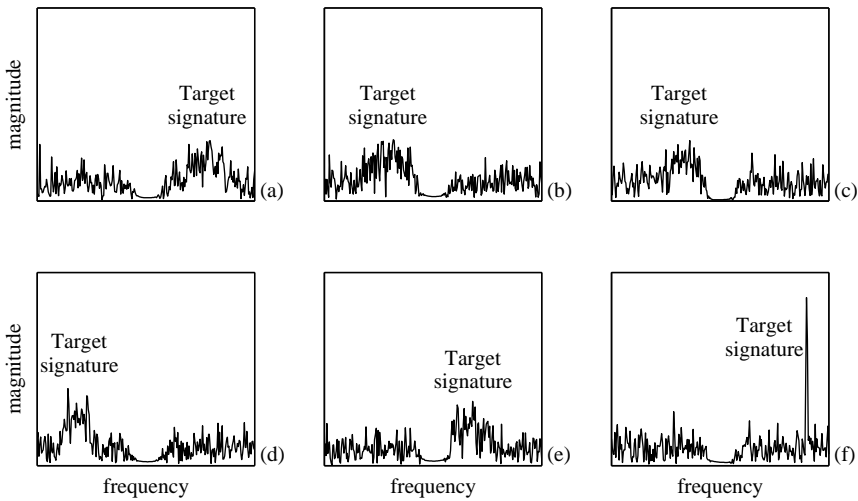


Figure 6.34 Fourier transform of the analyzed signals with SNR = -2 dB. (a – f) The analyzed signals 1–6. Stationary target movement case is (f), while the cases (a – e) present nonstationary target movement.

Table 6.2

Number of Detected Target Signals in 100 Trials for Various SNR with a Fourier-Based Detector (FT) and a Time-Frequency-Based Detector (T-F).

SNR [dB]	Signal 1		Signal 2		Signal 3		Signal 4		Signal 5		Signal 6	
	FT	T-F										
-2	79	100	67	100	87	100	94	100	80	100	100	100
-4	43	100	22	100	25	100	55	100	27	100	100	100
-6	12	100	8	100	8	100	19	100	9	100	100	100
-8	5	99	4	93	5	99	3	98	5	99	98	94
-10	2	85	1	62	1	73	2	81	4	69	80	77
-12	2	49	1	14	0	21	0	43	1	27	35	31
-14	0	13	0	4	1	8	1	11	0	6	14	13

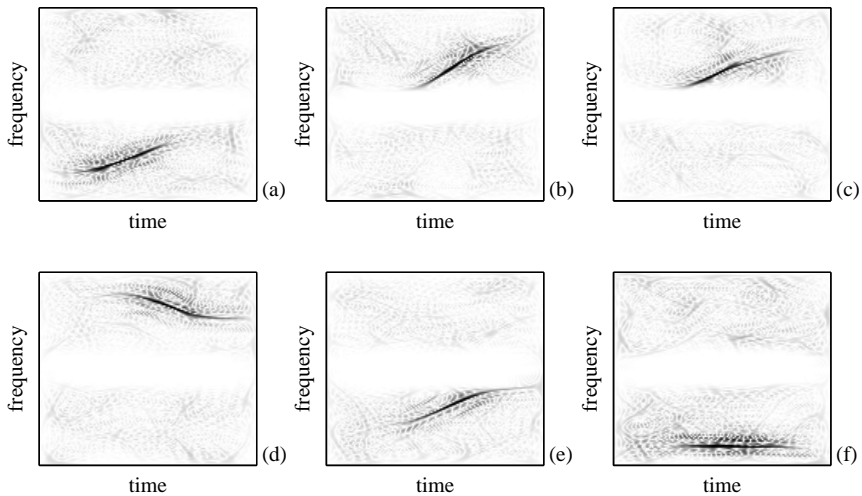


Figure 6.35 Time-frequency representation of the analyzed signals with SNR= -2 dB. (a - f) The analyzed signals 1 - 6. Stationary target movement case is (f), while cases (a - e) presents nonstationary target movement.

6.6 MULTIDIMENSIONAL SPACE-SPATIAL FREQUENCY ANALYSIS

Multidimensional space-spatial frequency analysis has attracted attention in many areas of signal processing, like compression, filtering, and digital watermarking in images and video sequences.

After the Wigner distribution was introduced in quantum mechanics in 1932, one of the earliest areas of its wide application was in optics, where it was introduced in 1960s to relate partial coherence to radiometry and then in the area of Fourier optics. While the position and momentum of a particle are the considered quantities in mechanics, time and frequency in signal analysis, the parameters related via the Wigner distribution in optics are the position and the direction (frequency) of a ray. The Wigner distribution representation of an optical field in terms of a ray picture is invariant to the cases when the light is partially coherent or completely coherent. Application of the Wigner distribution representation is useful when the optical signals and systems can be described by quadratic-phase functions. It means that they are within the first-order optics, including cases of

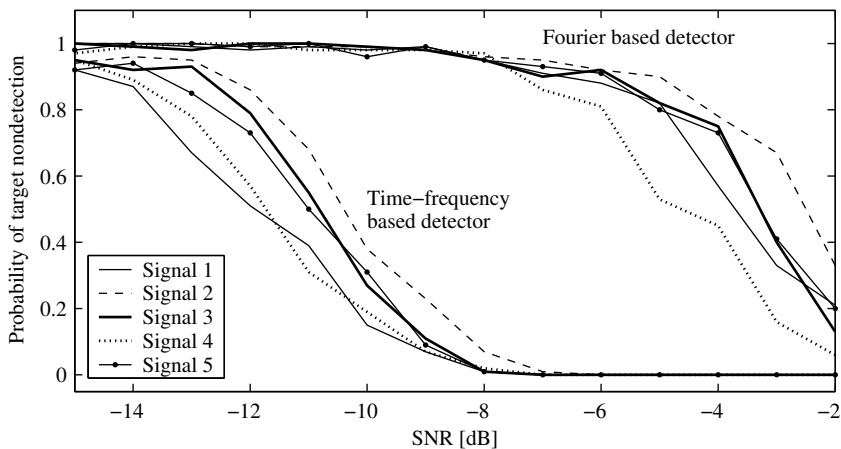


Figure 6.36 Estimated probability of target detection versus SNR for nonstationary cases using both Fourier transform and time-frequency-based detectors.

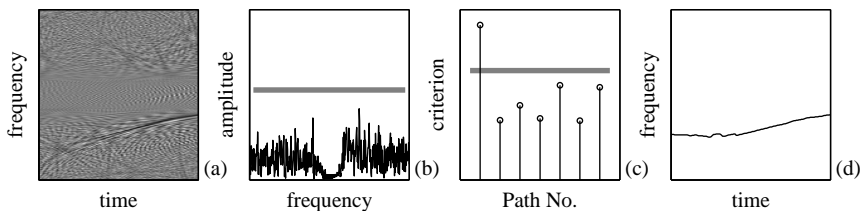


Figure 6.37 Signal 5 (nonstationary target velocity) with SNR = -8 dB. (a) Time-frequency representation; (b) Fourier transform with detection threshold; (c) sum over analyzed paths and detection threshold for time-frequency-based detector; and (d) optimal path in time-frequency plane.

spherical waves and thin lenses. The Wigner distribution (with ambiguity function and fractional Fourier transform as related transforms) relates in optics diverse fields, such as geometrical optics, ray optics, matrix optics, and radiometry. A significant contribution to this area has been made by researchers from the signal processing community.

Recently, it was shown that the analysis of the Wigner distribution in the light field in geometric optics is analogous to the analysis of the Wigner distribution

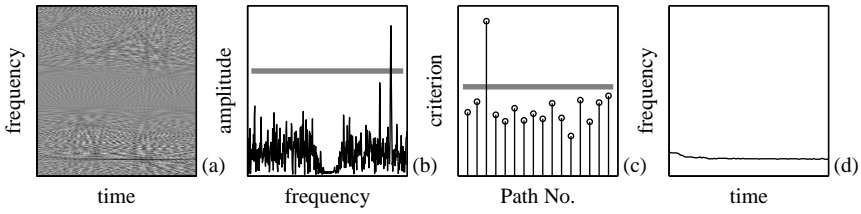


Figure 6.38 Signal 6 (stationary target velocity) with $\text{SNR} = -8 \text{ dB}$. (a) Time-frequency representation; (b) Fourier transform with detection threshold; (c) sum over analyzed paths and detection threshold for time-frequency-based detector; and (d) optimal path in time-frequency plane.

in wave optics, with some interesting practical applications in geometric optics. We will shortly review their approach to introduce a two-dimensional Wigner distribution form and present one of its possible interpretations. As it is known, the light propagates through three-dimensional space as a wave. Thus, the information about the light propagation may be obtained by measuring the scalar field of the wave at a plane. Then for a fixed plane, a two-dimensional scalar field is obtained. The Wigner distribution of a two-dimensional function $s(x, y)$ is a four-dimensional function

$$WD(x, y, \Omega_x, \Omega_y) = \int_{-\infty}^{\infty} \int_{-\infty}^{\infty} J(x, y, \alpha, \beta) e^{-j(\alpha\Omega_x + \beta\Omega_y)} d\alpha d\beta \quad (6.100)$$

$$J(x, y, \alpha, \beta) = s(x + \frac{\alpha}{2}, y + \frac{\beta}{2}) s^*(x - \frac{\alpha}{2}, y - \frac{\beta}{2})$$

It relates the field value at a point (x, y) with the corresponding frequencies. In the case of narrowband polychromatic light, the wave function is a description of oscillations in the electric and magnetic fields. It can be written in form of a time-varying phasor $s_3(x, y, z, t)$ of a scalar field. Suppose that values of scalar field are known at a plane $z = z_1$. Denote it by $s_2(x, y, t)$. The aim is to derive the intensity $I(x, y)$ at some other plane $z = z_2$ with optical elements in between. Instead of the standard method based on the Fresnel diffraction integral, they have derived the output image using the input scalar field's four-dimensional Wigner distribution. The local auto-correlation function $J(x, y, \alpha, \beta)$ presents mutual intensity function, since it describes how coherent are two points $(x + \alpha/2, y + \beta/2)$ and $(x - \alpha/2, y - \beta/2)$ in the scalar field. In general, the local auto-correlation function is additionally averaged over time for each (x, y, α, β) , so there is no time coordinate in the definition

(6.100). Averaging is not done for a fully coherent light, when $J(x, y, \alpha, \beta)$ is time invariant and $s(x, y)$ could be used. We used this description to introduce and to show the importance of two-dimensional space-spatial/frequency representations. Next we will restrict to the short description, within the signal processing framework, of a space/spatial frequency analysis, hoping that specialists from other fields can benefit from the processing tools presented in this book.

Consider an n -dimensional signal

$$x(\vec{r}) = g(\vec{r})e^{j\Phi(\vec{r})} \quad (6.101)$$

with $\vec{r} = (r_1, r_2, \dots, r_n) \in R^n$ and $g(\vec{r})$ being n -dimensional function.

In the case of slow-varying $g(\vec{r})$, the associated local frequency, at a point, is defined as $\vec{\Omega} = \nabla\Phi(\vec{r})$, with $\vec{\Omega} = (\Omega_1, \Omega_2, \dots, \Omega_n)$, while ∇ denotes the Hamiltonian operator.

6.6.1 Multidimensional Short-Time Fourier Transform

The short-time (space) Fourier transform of the signal $x(\vec{r})$ is defined by

$$STFT(\vec{r}, \vec{\Omega}) = \int_{R^n} x(\vec{r} + \vec{v})w^*(\vec{v})e^{-j\vec{\Omega}\vec{v}}dV_{\vec{v}} \quad (6.102)$$

where $w^*(\vec{r})$ denotes an n -dimensional, usually even and real-valued, window function and $dV_{\vec{v}} = dv_1dv_2 \cdots dv_n$. It will be assumed that $w(\vec{r}) = 0$ holds outside the bounded n -dimensional region $D \subset R^n$.

Substituting signal (6.101) into (6.102) and expanding $\Phi(\vec{r} + \vec{v})$ into a Taylor series around \vec{r} , we obtain

$$STFT(\vec{r}, \vec{\Omega}) = (2\pi)^n g(\vec{r})e^{j\Phi(\vec{r})} \delta[\vec{\Omega} - \nabla\Phi(\vec{r})] *_{\vec{\Omega}} W(\vec{\Omega}) *_{\vec{\Omega}} FT \left\{ e^{j\frac{(\vec{v}\nabla)^2}{2!}\Phi(\vec{r}_1)} \right\} \quad (6.103)$$

where $*_{\vec{\Omega}}$ denotes an n -dimensional convolution with respect to $\Omega_1, \Omega_2, \dots, \Omega_n$, and $g(\vec{r})$ is treated as a constant inside the window $w(\vec{r})$, that is, $g(\vec{r} + \vec{v})w(\vec{v}) \cong g(\vec{r})w(\vec{v})$.

If the second- and higher-order partial derivatives of $\Phi(\vec{r})$ may be neglected, then the associated spectrogram becomes

$$SPEC(\vec{r}, \vec{\Omega}) = |STFT(\vec{r}, \vec{\Omega})|^2 = |g(\vec{r})|^2 W^2[\vec{\Omega} - \nabla\Phi(\vec{r})]. \quad (6.104)$$

6.6.2 Multidimensional Wigner Distribution

The pseudo Wigner distribution of an n -dimensional signal is defined by

$$\begin{aligned} PWD(\vec{r}, \vec{\Omega}) &= \int_{R^n} x(\vec{r} + \vec{v}/2)x^*(\vec{r} - \vec{v}/2)w_s(\vec{v})e^{-j\vec{\Omega}\vec{v}}dV_{\vec{v}}, \\ \text{with } w_s(\vec{v}) &= w(\vec{v}/2)w^*(-\vec{v}/2). \end{aligned} \quad (6.105)$$

For signals (6.101), upon substitution in (6.105) and expansion of $\Phi(\vec{r} + \vec{v}/2)$ and $\Phi(\vec{r} - \vec{v}/2)$ into Taylor series, the following expression for the pseudo Wigner distribution is obtained

$$PWD(\vec{r}, \vec{\Omega}) = (2\pi)^n |g(\vec{r})|^2 \delta[\vec{\Omega} - \nabla\Phi(\vec{r})] *_{\vec{\Omega}} W_s(\vec{\Omega}) *_{\vec{\Omega}} \text{FT} \left\{ e^{j\frac{[(\vec{v}/2)\nabla]^3}{3!} [\Phi(\vec{r}_1) + \Phi(\vec{r}_2)]} \right\}.$$

The pseudo Wigner distribution provides an ideal time-frequency representation if the third- and higher-order partial derivatives of $\Phi(\vec{r})$ are negligible. This is obviously a significant improvement over the STFT.

6.6.3 Cohen Class of Distributions

We have seen that the Wigner distribution of a signal whose phase does not contain third- and higher-order terms produces the ideal space-frequency representation. We may ask then whether there exists another distribution from the Cohen class with the same ideal representation for the above shape of signals. The Cohen formula, defining the associated class of distributions for n -dimensional signals, is

$$\begin{aligned} CD(\vec{r}, \vec{\Omega}) &= \frac{1}{(2\pi)^n} \int_{R^n} \int_{R^n} \int_{R^n} x(\vec{u} + \vec{v}/2) \\ &\times x^*(\vec{u} - \vec{v}/2) c(\vec{\theta}, \vec{v}) e^{j\vec{\theta}\vec{r} - j\vec{\Omega}\vec{v} - j\vec{\theta}\vec{u}} dV_{\vec{\theta}} dV_{\vec{v}} dV_{\vec{u}} \end{aligned} \quad (6.106)$$

with $\vec{u}, \vec{v}, \vec{\theta}, \vec{r}, \vec{\Omega} \in R^n$, while $c(\vec{\theta}, \vec{v})$ represents kernel function for an n -dimensional case. Assume now that the phase function $\Phi(\vec{r})$ is quadratic, that is, that it possesses the following property

$$\nabla^i \Phi(\vec{r}) = 0 \text{ for } i \geq 3, \quad \nabla\Phi(\vec{r}) = \mathbf{B}\vec{r} + \vec{d} \quad (6.107)$$

where $\mathbf{B} \in R^{n \times n}$ is a constant symmetric matrix, while \vec{d} is a vector.

Expanding the functions $\Phi(\vec{u} + \vec{v}/2)$ and $\Phi(\vec{u} - \vec{v}/2)$ into a Taylor series around \vec{u} , integration over $\vec{\theta}$ and \vec{u} produces

$$CD(\vec{r}, \vec{\Omega}) = |g(\vec{r})|^2 \int_{R^n} c(\mathbf{B}\vec{v}, \vec{v}) e^{-j[\vec{\Omega} - (\mathbf{B}\vec{r} + \vec{d})]\vec{v}} dV_{\vec{v}} \quad (6.108)$$

The ideal time-frequency representation of the considered signal will be obtained if $c(\mathbf{B}\vec{v}, \vec{v})$ is equal to unity. For a given signal, it means that the kernel $c(\vec{\theta}, \vec{v})$ should be equal to unity on the n -dimensional subspace $\Pi : \vec{\theta} = \mathbf{B}\vec{v}$ of the $(\vec{\theta}, \vec{v})$ space, while it may take any value outside Π . However, if one wants to use the signal-independent kernel, then $c(\mathbf{B}\vec{v}, \vec{v}) = 1$ should hold for any \mathbf{B} , that is, everywhere in $(\vec{\theta}, \vec{v})$ space. The distribution from the Cohen class, with the unity kernel, corresponds to the Wigner distribution.

6.6.4 Multicomponent n -Dimensional Signals

Let us consider now an n -dimensional multicomponent signal given by

$$x(\vec{r}) = \sum_{i=1}^p g_i(\vec{r}) e^{j\Phi_i(\vec{r})} \quad (6.109)$$

where the functions $g_i(\vec{r}), i = 1, \dots, p$, belong to the same class as $g(\vec{r})$ in (6.101).

In analogy with the previous considerations, the spectrogram for this signal may be shown to be

$$\begin{aligned} SPEC(\vec{r}, \vec{\Omega}) &= \sum_{i=1}^p \sum_{k=1}^p g_i(\vec{r}) g_k(\vec{r}) e^{j[\Phi_i(\vec{r}) - \Phi_k(\vec{r})]} \\ &\times W[\vec{\Omega} - \nabla\Phi_i(\vec{r})] W^*[\vec{\Omega} - \nabla\Phi_k(\vec{r})] \end{aligned} \quad (6.110)$$

where we have neglected the artifacts due to higher-order partial derivatives of $\Phi_i(\vec{r}), i = 1, 2, \dots, p$, that is, $\nabla\Phi_i(\vec{r})$ is treated as a constant vector inside $w(\vec{r})$.

Generally, the spectrogram contains the cross-terms, but they are absent, provided the condition

$$W[\vec{\Omega} - \nabla\Phi_i(\vec{r})] W^*[\vec{\Omega} - \nabla\Phi_k(\vec{r})] = 0$$

$$\text{for any } \vec{\Omega} \text{ and } i \neq k \quad \text{or } \| \nabla\Phi_i(\vec{r}) - \nabla\Phi_k(\vec{r}) \| > W_\ell \quad (6.111)$$

is satisfied; $\|\cdot\|$ denotes an appropriately defined norm in R^n . This means that cross-terms do not appear if the n -dimensional distance between local frequencies is greater than the maximal width of the $W(\vec{\Omega})$ along the direction $\vec{\ell} = \nabla\Phi_i(\vec{r}) - \nabla\Phi_k(\vec{r})$, connecting the i th and k th local frequency. In that case

$$SPEC(\vec{r}, \vec{\Omega}) = \sum_{i=1}^p |g_i(\vec{r})|^2 W^2[\vec{\Omega} - \nabla\Phi_i(\vec{r})]. \quad (6.112)$$

Observe that the Wigner distribution may be expressed as

$$PWD(\vec{r}, \vec{\Omega}) = \frac{1}{\pi^n} \int_{R^n} STFT(\vec{r}, \vec{\Omega} + \vec{\theta}) STFT^*(\vec{r}, \vec{\Omega} - \vec{\theta}) dV_{\vec{\theta}}. \quad (6.113)$$

We will now use the above expression to analyze cross-terms in the pseudo Wigner distribution for the n -dimensional multicomponent signals. The integrand in (6.113) is nonzero for

$$\vec{\Omega} + \vec{\theta} - \nabla\Phi_i(\vec{r}) \in D_w \text{ and } \vec{\Omega} - \vec{\theta} - \nabla\Phi_k(\vec{r}) \in D_w \quad (6.114)$$

resulting in

$$\begin{aligned} \vec{\Omega} &\in D_{\Omega}(i, k) : (\vec{\Omega} - \frac{\nabla\Phi_i(\vec{r}) + \nabla\Phi_k(\vec{r})}{2}) \in D_w \\ \vec{\theta} &\in D_{\theta}(i, k) : (\vec{\theta} - \frac{\nabla\Phi_i(\vec{r}) - \nabla\Phi_k(\vec{r})}{2}) \in D_w \end{aligned} \quad (6.115)$$

where the Fourier transform $W(\vec{\Omega})$ of $w(\vec{r})$ is assumed to be nonzero only inside a bounded region $D_w \subset R^n$, and D_w is convex and symmetric with respect to the origin (i.e., $w(\vec{r})$ is real).

This means that the auto-terms ($i = k$) are concentrated within the region centered at the local auto-frequencies of each component of signal (6.109), that is, at $\vec{\Omega}_i = \nabla\Phi_i(\vec{r})$, $i = 1, 2, \dots, p$, while the cross-terms are centered between the corresponding auto-frequencies. Relation (6.115) also implies that, along the axes of the n -dimensional convolution $\vec{\theta}$, all auto-terms are concentrated at $\vec{\theta} = 0$ and its neighborhoods. The cross-terms are dislocated from the $\vec{\theta}$ origin. Having this in mind, we conclude that the cross-terms may be removed from the pseudo Wigner distribution of a multicomponent signal, and at the same time the integration over auto-terms performed, if the convolution (6.113) is evaluated with an n -dimensional

window function $P(\vec{\theta})$, in the S-method form

$$SM(\vec{r}, \vec{\Omega}) = \frac{1}{\pi^n} \int_{R^n} P(\vec{\theta}) STFT(\vec{r}, \vec{\Omega} + \vec{\theta}) STFT^*(\vec{r}, \vec{\Omega} - \vec{\theta}) dV_{\vec{\theta}} \quad (6.116)$$

where the region of support D_p of the window function $P(\vec{\theta})$ must comply with the conditions defined in (6.115), that is, $D_p \supset D_w \equiv D_{\theta}(i, i)$ and $D_p \cap D_{\theta}(i, k) = \emptyset$ for $i \neq k$.

The distribution (6.116) is derived from the condition that its auto-terms are equal to the auto-terms in the Wigner distribution. However, in contrast to the Wigner distribution, this distribution is cross-terms-free (under the described conditions).

Distribution (6.116), besides its efficiency in cross-terms removal and the preservation of the auto-terms presentation quality as in the Wigner distribution, leads to a numerically more efficient method than the Wigner distribution realization itself.

The discrete two-dimensional pseudo Wigner distribution is of the form

$$WD(n_1, n_2, k_1, k_2) = 4 \sum_{m_1=-N}^{N-1} \sum_{m_2=-N}^{N-1} x(n_1 + m_1, n_2 + m_2) x^*(n_1 - m_1, n_2 - m_2) e^{-j \frac{4\pi}{2N} (k_1 m_1 + k_2 m_2)} \quad (6.117)$$

where N is the number of samples, determined according to the sampling theorem.

The distribution (6.116) may be expressed in the discrete form for a rectangular window $P_d(i_1, i_2)$, as the two-dimensional S-method

$$SM(n_1, n_2, k_1, k_2) = \sum_{i_1=-L}^L \sum_{i_2=-L}^L STFT(n_1, n_2, k_1 + i_1, k_2 + i_2) \times STFT^*(n_1, n_2, k_1 - i_1, k_2 - i_2) \quad (6.118)$$

with $L_1 = L_2 = L$, where $2L_1 + 1$ and $2L_2 + 1$ represent the widths of two-dimensional window $P_d(i_1, i_2)$. Sampling in the STFT is defined by sampling theorem, and so is in the modified Wigner distribution due to $P_d(i_1, i_2)$.

The computation time may be reduced using an iterative procedure for computation of the STFT

$$STFT(n_1, n_2 + 1, k_1, k_2) = [STFT(n_1, n_2, k_1, k_2) + FT_{n_1}\{x(n_1, n_2 + N)\} - FT_{n_1}\{x(n_1, n_2)\}] e^{j \frac{2\pi}{N} k_2}$$

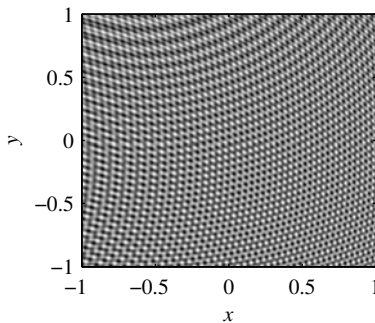


Figure 6.39 A two-dimensional signal inspired by interferograms in diffraction.

$$\begin{aligned} STFT(n_1 + 1, n_2, k_1, k_2) = & \quad (6.119) \\ [STFT(n_1, n_2, k_1, k_2) + FT_{n_2}\{x(n_1 + N, n_2)\} - FT_{n_2}\{x(n_1, n_2)\}]e^{j\frac{2\pi}{N}k_1} \end{aligned}$$

where FT_{n_1} and FT_{n_2} are one-dimensional Fourier transform, and the window $w(n)$ is rectangular. The STFT form which is used here is

$$STFT(n, k) = \sum_{m=0}^{N-1} x(n+m) \exp(-j2\pi mk/N)$$

Example 6.26. To illustrate the two-dimensional S-method, consider the two-dimensional signal

$$\begin{aligned} f(x, y) = & \cos(8\pi(x+0.6)^2 + 8\pi(y-2)^2) + \cos(8\pi(x+2.2)^2 + 8\pi(y+2.5)^2) \\ & + \cos(4\pi(x+6)^2 + 4\pi y^2) \end{aligned}$$

in the range: $|x| \leq -1, |y| \leq 1$ with discretization interval $\Delta x = \Delta y = 1/N$ and $N = 64$ (Fig. 6.39). The Hann(ing) two-dimensional window of the width $N \times N$ is used. The pseudo Wigner distribution is calculated without oversampling by using the S-method formulation over the whole frequency range. The STFT, the pseudo Wigner distribution, and the S-method are computed at the point $(x, y) = (0, 0)$, and the results are presented in Fig. 6.40. \square

By rotation of the Wigner distribution plane, we can apply the S-method form in other directions, choosing possibly the one with the simplest signal representation.

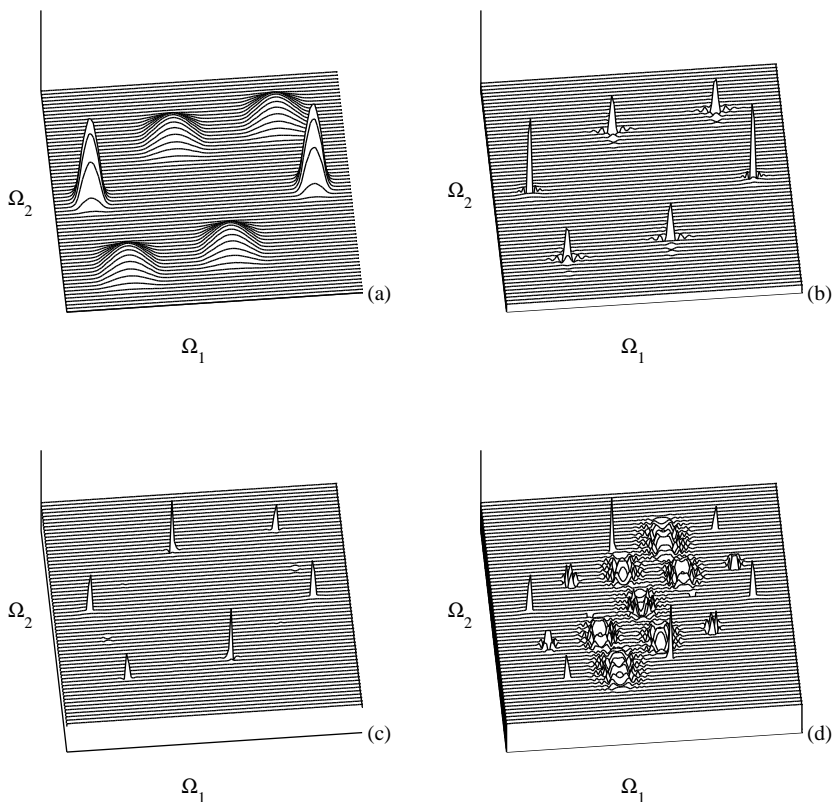


Figure 6.40 Local frequency representation of a two-dimensional signal at the point $(x, y) = (0, 0)$: (a) the spectrogram at this point, (b) the S-method-based representation with $L = 4$, (c) the S-method-based representation with $L = 11$, and (d) the pseudo Wigner Distribution.

6.7 ARRAY PROCESSING BASED ON TIME-FREQUENCY DISTRIBUTIONS

The spatial localization of sources by passive sensor array is an important problem in many areas, for example, in radars, sonars, and seismology. Direction of arrival (DOA) is the key parameter in this problem. Most of the DOA estimators are

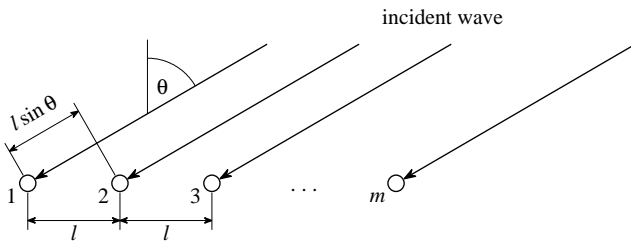


Figure 6.41 Antenna array illustration

based on the estimates of the data covariance matrix. In the case when phase of the input is not linear, then the time-frequency distributions may be used to analyze the data snapshots across the array. This kind of distribution is known as a spatial time-frequency distribution. It is able to spread the noise energy over the entire time-frequency plane, while localizing the energy of the input signals, in the cases of nonlinear phases. In this way spatial resolution and signal separation can be improved. Application of the spatial time-frequency distributions to the DOA estimation has been introduced by Amin et al. They also developed a time-frequency maximum likelihood method for the DOA estimation. These representations improve the DOA estimation by localizing the signal energy in the time-frequency domain. Better localization of signals permits the division of the time-frequency domain into smaller regions, each containing fewer signals than the input signal on the array. It relaxes the condition on the array aperture and simplifies optimization procedures.

Let us suppose that a planar array with m antennas, with distance l among them (illustrated in Fig. 6.41), receives a narrowband signal $d(t) \exp(j\Omega t - jkx)$ at an angle θ . Then the output from the antennas (demodulated received signal) is described by

$$s_1(t) = d(t) \quad (6.120)$$

$$s_2(t) = d(t) e^{j2\pi l \sin(\theta)/\lambda}$$

$$s_m(t) = d(t) e^{j2\pi l(m-1) \sin(\theta)/\lambda}$$

In a matrix notation

$$\mathbf{s}(t) = [1, e^{j2\pi l \sin(\theta)/\lambda}, \dots, e^{j2\pi(m-1)l \sin(\theta)/\lambda}]^T d(t) = \mathbf{a}(\theta) d(t). \quad (6.121)$$

For the case of n narrowband $d_i(t)$, $i = 1, 2, \dots, n$, signals

$$\mathbf{d}(t) = [d_1(t), d_2(t), \dots, d_n(t)]^T.$$

arriving at this antenna array from directions θ_i , we can write a linear data model

$$\mathbf{s}(t) = \mathbf{A}(\Theta)\mathbf{d}(t)$$

$$\mathbf{A}(\Theta) = \begin{bmatrix} 1 & 1 & \dots & 1 \\ e^{j2\pi l \sin(\theta_1)/\lambda} & e^{j2\pi l \sin(\theta_2)/\lambda} & \dots & e^{j2\pi l \sin(\theta_n)/\lambda} \\ \dots & \dots & \dots & \dots \\ e^{j2\pi(m-1)l \sin(\theta_1)/\lambda} & e^{j2\pi(m-1)l \sin(\theta_2)/\lambda} & \dots & e^{j2\pi(m-1)l \sin(\theta_n)/\lambda} \end{bmatrix}$$

where $\mathbf{A}(\Theta)$ is the mixing (steering) matrix $m \times n$ with steering vectors $\mathbf{a}(\theta_i)$ as its columns. It is assumed that each of the source signals $d_i(t)$ are monocomponent. Due to the mixing, data vector $\mathbf{s}(t)$ is multicomponent. For real scenarios, the noise should be added,

$$\mathbf{x}(t) = \mathbf{s}(t) + \mathbf{n}(t) = \mathbf{A}(\Theta)\mathbf{d}(t) + \mathbf{n}(t). \quad (6.122)$$

The vector of Gaussian zero-mean complex noise, with independent real and imaginary parts, of total variance σ^2 , is denoted by $\mathbf{n}(t)$. It is assumed that the number of sensors is larger than the number of sources $m > n$. Also, it is assumed that the vectors corresponding to n different angles of arrival are linearly independent.

The correlation matrix is defined by

$$\mathbf{R}_{xx} = \mathbb{E}\{\mathbf{x}(t)\mathbf{x}^*(t)\},$$

with its estimate, for $N > m$ snapshots in observation, of the form

$$\hat{\mathbf{R}}_{xx} = \frac{1}{N} \sum_{i=1}^N \mathbf{x}(i)\mathbf{x}^*(i). \quad (6.123)$$

Suppose that the auto-correlation matrix is nonsingular. Now it is possible to write

$$\mathbf{R}_{xx} = \mathbf{A}(\Theta)\mathbf{R}_{dd}\mathbf{A}^*(\Theta) + \sigma^2\mathbf{I}. \quad (6.124)$$

For the case of frequency-modulated signals

$$\mathbf{d}(t) = [d_1(t), d_2(t), \dots, d_n(t)]^T = [D_1 e^{j\phi_1(t)}, D_2 e^{j\phi_2(t)}, \dots, D_n e^{j\phi_n(t)}]^T$$

The spatial pseudo Wigner distribution matrix is defined by

$$\mathbf{D}_{xx}(t, \Omega) = \sum_{\tau=-(L-1)/2}^{(L-1)/2} \mathbf{x}(t + \tau) \mathbf{x}^*(t - \tau) e^{-j2\Omega\tau}. \quad (6.125)$$

For signal $\mathbf{x}(t) = \mathbf{s}(t) + \mathbf{n}(t)$, with uncorrelated signal and noise

$$\begin{aligned} E\{\mathbf{D}_{xx}(t, \Omega)\} &= E\{\mathbf{D}_{ss}(t, \Omega)\} + E\{\mathbf{D}_{nn}(t, \Omega)\} \\ &= \mathbf{A}(\Theta) \mathbf{D}_{dd}(t, \Omega) \mathbf{A}^*(\Theta) + E\{\mathbf{D}_{nn}(t, \Omega)\} \end{aligned} \quad (6.126)$$

This relation is of the form common for the DOA estimation. However, it is expressed in the form of spatial time-frequency matrices, being more appropriate for nonstationary signal cases.

In the case of a signal, when the third-order phase derivative can be neglected,

$$\phi_i(t + \tau) - \phi_i(t - \tau) = 2\Omega_i\tau$$

then for the i th source signal follows

$$D_{d_id_i}(t, \Omega) = \sum_{\tau=-(L-1)/2}^{(L-1)/2} D_i^2 e^{j2\Omega_i\tau} e^{-j2\Omega\tau}. \quad (6.127)$$

Along the instantaneous frequency points $\Omega = \Omega_i$, we get

$$D_{d_id_i}(t, \Omega_i) = \sum_{\tau=-(L-1)/2}^{(L-1)/2} D_i^2 = LD_i^2. \quad (6.128)$$

From the noise in the Wigner distribution analysis, we know that

$$E\{\mathbf{D}_{nn}(t, \Omega)\} = \sigma^2 \mathbf{I}$$

The pseudo Wigner distribution of each frequency-modulated source has a constant value over the observation period. It means that when we select time-frequency points along the instantaneous frequency, the SNR in (6.126) will be improved to LD_i^2/σ^2 with respect to the original one (6.124), when we get D_i^2/σ^2 . Taking into account that the ending points in the time-frequency representation, lower values will be obtained. The full sum in (6.125) can be calculated after first

$(L - 1)/2$ and before the last $(L - 1)/2$ points. Thus, the full sum is calculated over $N - L + 1$ values. If the time-frequency representation is calculated over n_0 signature of signals, then there are $n_0(N - L + 1)$ time-frequency points for calculation of (6.125). Then the overall improvement with respect to (6.124) will be achieved if $L > n_0$.

The spatial time-frequency distributions does not require simultaneous localization and extraction of all unknown signals received by the array. For signals that are localizable in the time-frequency domain, such as frequency-modulated signals, the signal-to-noise ratio (SNR) can be enhanced by utilizing time-frequency distributions, and subsequently improve the robustness of the signal and noise subspaces.

Note also the topic of DOA estimation by using the spatial time-frequency distributions has been reformulated in the sparse signal processing sense. Namely, as we have shown, an ideal representation for a one-component signal is

$$D_{d_i d_i}(t, \Omega) = 2\pi D_i^2 \delta(\Omega - \phi'_i(t))$$

However, that is not case for a given time-frequency distribution, except for Wigner distribution and the linear frequency-modulated. If we reformulate this problem within the sparse signal processing approach, then the compressive sensing-based approach will look for a perfectly localized solution that minimizes the total number of nonzero coefficients, that is, the l_0 norm of the time-frequency distribution (described in Chapter 2). Consider now $D_{d_i d_i}(t, \Omega)$ as a time-frequency distribution matrix defined over a finite region in (t, Ω) domain and $A(\theta, \tau)$ as its corresponding ambiguity function. Then the desired, localized time-frequency distribution is obtained as the solution of the following problem,

$$\min \sum_{k=1}^N \sum_{n=1}^N |D_{d_i d_i}(n, k)| \text{ subject to} \quad (6.129)$$

$$\frac{1}{N} \sum_{k=1}^N \sum_{n=1}^N D_{d_i d_i}(n, k) e^{-j2\pi(np-kl)/N} = AF(p, l), \text{ for } K \text{ selected points in } (p, l).$$

Norm l_1 is used here. It is described in Chapter 5, in section dealing with sparse signal processing.

6.8 HIGH-RESOLUTION TIME-FREQUENCY TECHNIQUES

High-resolution techniques are developed for efficient processing and separation of very close sinusoidal signals (in array signal processing, separation of sources with very close DOAs). Among these techniques the most widely used are Capon's method, MUSIC, and ESPRIT. The formulation of high-resolution techniques could be extended to the time-frequency representations. Here we will present a simple formulation of the STFT and the LPFT within Capon's method framework.

The simplest conventional way of estimating time-frequency content of a signal is in using the STFT. Here we will present its formulation in a common array signal-processing notation. The STFT of a discrete time signal $x(n)$ can be written as

$$\begin{aligned}\hat{s}(n) &= \mathbf{h}^* \mathbf{x}(n) = \frac{1}{N} \mathbf{a}^*(\omega) \mathbf{x}(n) = STFT(\omega, n) \\ \mathbf{a}^*(\omega) &= [1 \ e^{-i\omega} \ e^{-i\omega 2} \dots e^{-i\omega(N-1)}] \\ \mathbf{x}(n) &= [x(n) \ x(n+1) \ x(n+2) \dots x(n+N-1)]^T,\end{aligned}\quad (6.130)$$

where T denotes the transpose operation, and * denotes the conjugate and transpose operation. Normalization of the STFT with N is done, as in the robust signal analysis.

The average power of the output signal $\hat{s}(n)$, over M samples (ergodicity over M samples around n is assumed), for a frequency ω , is

$$P(\omega) = \frac{1}{M} \sum_n |\hat{s}(n)|^2 = \frac{1}{N^2} \mathbf{a}^*(\omega) \frac{1}{M} \sum_n [\mathbf{x}(n) \mathbf{x}^*(n)] \mathbf{a}^*(\omega) = \frac{1}{N^2} \mathbf{a}^*(\omega) \hat{\mathbf{R}}_x \mathbf{a}^*(\omega), \quad (6.131)$$

where $\hat{\mathbf{R}}_x$ is the matrix defined by

$$\hat{\mathbf{R}}_x = \frac{1}{M} \sum_n \mathbf{x}(n) \mathbf{x}^*(n).$$

The standard STFT (6.130) can be derived based on the following consideration. Find \mathbf{h} as a solution of the problem

$$\min_{\mathbf{h}} \{ \mathbf{h}^* \mathbf{h} \} \quad \text{subject to } \mathbf{h}^* \mathbf{a}(\omega) = 1. \quad (6.132)$$

This minimization problem will be explained through the next example.

Example 6.27. It will be shown that the previous minimization formulation means that the output power of the filter $s(n) = \mathbf{h}^* \mathbf{x}(n)$ is minimized for the input $\mathbf{x}(n) = A\mathbf{a}(\omega) + \boldsymbol{\varepsilon}(n)$, with respect the input white noise $\boldsymbol{\varepsilon}(n)$, whose auto-correlation function is $\hat{\mathbf{R}}_{\boldsymbol{\varepsilon}} = \rho \mathbf{I}$.

The output for the noise only is $s_{\boldsymbol{\varepsilon}}(n) = \mathbf{h}^* \boldsymbol{\varepsilon}(n)$, while its average power is

$$\frac{1}{M} \sum_n |\mathbf{h}^* \boldsymbol{\varepsilon}(n)|^2 = \frac{1}{M} \sum_n \mathbf{h}^* \boldsymbol{\varepsilon}(n) \boldsymbol{\varepsilon}^*(n) \mathbf{h} = \mathbf{h}^* \left(\frac{1}{M} \sum_n \boldsymbol{\varepsilon}(n) \boldsymbol{\varepsilon}^*(n) \right) \mathbf{h} = \rho \mathbf{h}^* \mathbf{h}.$$

Minimization of $\mathbf{h}^* \mathbf{h}$ is therefore equivalent to the output white noise power minimization.

The condition $\mathbf{h}^* \mathbf{a}(\omega) = 1$ means that the input in form of a sinusoid $A\mathbf{a}(\omega)$, at frequency ω , should not be changed, that is, if $\mathbf{x}(n) = A\mathbf{a}(\omega)$, then

$$\mathbf{h}^* \mathbf{x}(n) = \mathbf{h}^* A\mathbf{a}(\omega) = A.$$

Thus, the condition $\mathbf{h}^* \mathbf{a}(\omega) = 1$ means that the estimate is unbiased with respect to input sinusoidal signal amplitude A . \square

The solution of minimization problem (6.132) is

$$\begin{aligned} \frac{\partial}{\partial \mathbf{h}^*} \{ \mathbf{h}^* \mathbf{h} + \lambda (\mathbf{h}^* \mathbf{a}(\omega) - 1) \} &= 0 \quad \text{subject to } \mathbf{h}^* \mathbf{a}(\omega) = 1, \\ 2\mathbf{h} &= -\lambda \mathbf{a}(\omega) \quad \text{subject to } \mathbf{h}^* \mathbf{a}(\omega) = 1 \end{aligned}$$

resulting in

$$\mathbf{h} = \frac{\mathbf{a}(\omega)}{\mathbf{a}^*(\omega) \mathbf{a}(\omega)} = \frac{1}{N} \mathbf{a}(\omega) \quad (6.133)$$

and the estimate (6.130), which is the standard STFT, follows.

Consider now a different optimization problem, defined by

$$\min_{\mathbf{h}} \left\{ \frac{1}{M} \sum_n |\mathbf{h}^* \mathbf{x}(n)|^2 \right\} \quad \text{subject to } \mathbf{h}^* \mathbf{a}(\omega) = 1. \quad (6.134)$$

Two points are emphasized in this optimization problem. First, the weights are selected to minimize the average power $\frac{1}{M} \sum_n |\mathbf{h}^* \mathbf{x}(n)|^2$ of the output signal of the filter. It means that the filter should give the best possible suppression of all components of signals-plus-noise components of the observations as well as a suppression of the components of the desired signal for all time-instants (minimization of the power of $y(n)$). Second, by setting the condition $\mathbf{h}^* \mathbf{a}(\omega) = 1$, in the considered time instant n the signal amplitude is preserved at the output.

The optimization problem can be rewritten in the form

$$\min_{\mathbf{h}} \left\{ \frac{1}{M} \sum_n \mathbf{h}^* \mathbf{x}(n) \mathbf{x}^*(n) \mathbf{h} \right\} \quad \text{subject to } \mathbf{h}^* \mathbf{a}(\omega) = 1.$$

By denoting

$$\hat{\mathbf{R}}_x = \frac{1}{M} \sum_n \mathbf{x}(n) \mathbf{x}^*(n),$$

we get

$$\min_{\mathbf{h}} \left\{ \mathbf{h}^* \hat{\mathbf{R}}_x \mathbf{h} \right\} \quad \text{subject to } \mathbf{h}^* \mathbf{a}(\omega) = 1.$$

The constrained minimization

$$\frac{\partial}{\partial \mathbf{h}^*} \left\{ \mathbf{h}^* \hat{\mathbf{R}}_x \mathbf{h} + \lambda (\mathbf{h}^* \mathbf{a}(\omega) - 1) \right\} = 0 \quad \text{subject to } \mathbf{h}^* \mathbf{a}(\omega) = 1.$$

gives the solution

$$\mathbf{h} = -\hat{\mathbf{R}}_x^{-1} \frac{\lambda \mathbf{a}(\omega)}{2} \quad \text{subject to } \mathbf{h}^* \mathbf{a}(\omega) = 1. \quad (6.135)$$

The solution can be written in the form

$$\hat{\mathbf{h}} = \frac{\hat{\mathbf{R}}_x^{-1} \mathbf{a}(\omega)}{\mathbf{a}^*(\omega) \hat{\mathbf{R}}_x^{-1} \mathbf{a}(\omega)}, \quad (6.136)$$

where

$$\hat{\mathbf{R}}_x = \frac{1}{M} \sum_n \mathbf{x}(n) \mathbf{x}^*(n). \quad (6.137)$$

The output signal power, in these cases, corresponds to Capon's form of the STFT, defined by

$$S_{\text{Capon}}(n, \omega) = |\hat{s}(n)|^2 = |\hat{\mathbf{h}} \mathbf{x}(n)|^2 = \left| \frac{\mathbf{a}^*(\omega) \hat{\mathbf{R}}_x^{-1} \mathbf{x}(n)}{\mathbf{a}^*(\omega) \hat{\mathbf{R}}_x^{-1} \mathbf{a}(\omega)} \right|^2. \quad (6.138)$$

Along with (6.137), we can use a sliding window estimate of the auto-correlation matrix in the form

$$\hat{\mathbf{R}}_{\mathbf{x}}(n, K) = \frac{1}{K+1} \sum_{p=n-K/2}^{n+K/2} \mathbf{x}(p)\mathbf{x}^*(p), \quad (6.139)$$

where K is a parameter defining a size of the symmetric sliding window, that is, K is a number of observation-vectors in the window. Inserting $\hat{\mathbf{R}}_{\mathbf{x}}(n, K)$ instead of $\hat{\mathbf{R}}_{\mathbf{x}}$ in (6.138) gives the STFT with weights minimizing the output power in (6.134), for the observations in the neighborhood of the time instant of interest n .

The mean value of this power function, calculated in the neighborhood of the time n over the window used in (6.139), gives an averaged Capon's STFT as follows

$$S_{\text{Capon } K}^{\text{average}}(n, \omega) = \frac{1}{\mathbf{a}^*(\omega)\hat{\mathbf{R}}_{\mathbf{x}}^{-1}(n, K)\mathbf{a}(\omega)}. \quad (6.140)$$

where n indicates the time instant of the interest and the mean is calculated over the observations $\mathbf{y}(n)$ in the corresponding window.

In the realization the auto-correlation function is regularized by a unity matrix \mathbf{I} thus, we use

$$\hat{\mathbf{R}}_{\mathbf{y}}(n, K) = \frac{1}{K+1} \sum_{p=n-K/2}^{n+K/2} \mathbf{x}(p)\mathbf{x}^*(p) + \rho\mathbf{I}. \quad (6.141)$$

instead of $\hat{\mathbf{R}}_{\mathbf{x}}(n, K)$ for the inverse calculation in (6.140) and (6.138).

In what follows, we use this localized version of the correlation matrix estimate as being more general. It is clear that $\hat{\mathbf{R}}_{\mathbf{y}}(n, K) \rightarrow \mathbf{R}_{\mathbf{x}}$ as $K \rightarrow \infty$ and $\rho \rightarrow 0$, while for $\rho \rightarrow \infty$ the standard STFT form follows from the above formulas.

In order to relate Capon's STFT and the standard STFT, we will use the inversion formula

$$(\mathbf{Q}\mathbf{Q}^* + \rho\mathbf{I})^{-1} = \frac{1}{\rho} [\mathbf{I} - \mathbf{Q} \left(\mathbf{I} + \frac{\mathbf{Q}^*\mathbf{Q}}{\rho} \right)^{-1} \mathbf{Q}^*/\rho], \quad (6.142)$$

where \mathbf{Q} is the matrix whose columns are signal vectors $\mathbf{x}(n+p)$, $p = 0, 1, \dots, K-1$, and zero for other p .

Then, we get

$$\begin{aligned} S_{\text{Capon}}^{\text{average}}(n, \omega) &= \frac{1}{\mathbf{a}^*(\omega) \frac{1}{\rho} [\mathbf{I} - \mathbf{Q} \left(\mathbf{I} + \frac{\mathbf{Q}^*\mathbf{Q}}{\rho} \right)^{-1} \mathbf{Q}^*/\rho] \mathbf{a}(\omega)} \\ &= \frac{\rho}{N - \text{STFT}(\omega, n) (\rho\mathbf{I} + \mathbf{Q}^*\mathbf{Q})^{-1} \text{STFT}^*(\omega, n)} \end{aligned}$$

where

$$\text{STFT}(\omega, n) = \mathbf{a}^*(\omega) \mathbf{Q}$$

is a vector whose elements are

$$STFT(\omega, n+p) = \mathbf{a}^*(\omega) \mathbf{x}(n+p)$$

for $p = 0, 1, \dots, K - 1$. For $K = 1$ when $\mathbf{Q} = \mathbf{x}(n)$, we get

$$S_{\text{Capon}}^{\text{average}}(n, \omega) = \frac{\rho}{N - (E_x + \rho)^{-1} |STFT(\omega, n)|^2}, \quad (6.143)$$

where $E_x = \sum_{p=0}^{N-1} |x(n)|^2$ is the energy of $x(n)$ and $STFT(\omega, n) = \mathbf{a}^*(\omega) \mathbf{x}(n)$ is the standard STFT, while $|STFT(\omega, n)|^2$ is the standard spectrogram. Thus, in the case of one signal component the high-resolution representation just emphasizes the maximal value in the STFT.

For a complex sinusoidal signal of amplitude A and frequency ω_0 , we get

$$(E_x + \rho)^{-1} |STFT(\omega, n)|^2 = \frac{A^2 N^2}{(A^2 N + \rho)} \rightarrow N,$$

so, as expected, we get

$$S_{\text{Capon}}^{\text{average}}(n, \omega) \rightarrow \infty \text{ at } \omega = \omega_0 \quad (6.144)$$

$$\frac{S_{\text{Capon}}^{\text{average}}(n, \omega)}{S_{\text{Capon}}^{\text{average}}(n, \omega_0)} \rightarrow 0 \text{ at } \omega \neq \omega_0$$

The standard spectrogram would, in this case, produce

$$|STFT(n, \omega)|^2 = \left| \sum_{n=0}^{N-1} A e^{-j(\omega - \omega_0)n} \right|^2 = \left| A \frac{\sin((\omega - \omega_0)N/2)}{\sin((\omega - \omega_0)N/2)} \right|^2. \quad (6.145)$$

Note that concentration improvement is here rather mathematical than substitutional improvement, since just the maximal value in the STFT is emphasized. The same conclusion holds for well-separated signal components in the time-frequency plane. The illustration is presented in Fig. 6.42.

This example is not presented as a distribution that should be used, but to show how a simple mathematical procedure can make that distribution (6.143) look

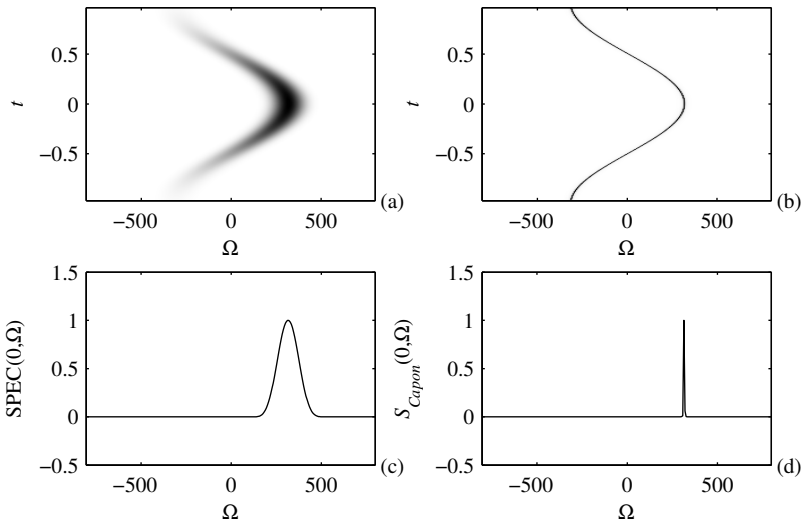


Figure 6.42 (a) Standard spectrogram and (b) Capon's spectrogram with (c, d) the values along line $t = 0$.

much better than the spectrogram, although it does not represent anything else but the maximal values of the spectrogram for each time instant t scaled to infinity. This procedure can be done locally for multicomponent signals as well. If maxima of the spectrogram are on biased (wrong) position, then this delta function will be at the same wrong positions. Thus, we always should ask ourselves (and others), when looking at two representations, whether there is a crucial improvement in comparing them or just is a different mathematical presentation of the same information.

However, the concentration improvement and the resolution enhancement in Capon's STFT is substitutional in the case of very close components. Thus, this kind of transform is to be used for resolution of very close components.

In a similar way, a high-resolution Wigner distribution may be defined with vector $\mathbf{a}^*(\omega)$ and signal vector appropriately adjusted to the Wigner definition. With varying coefficients or appropriate signal multiplication, before the STFT calculation, a local polynomial version of Capon's transform could be defined. For example, for a linear frequency-modulated signal of the form

$$x(n) = A e^{j(\alpha_0 n^2 + \omega_0 n + \varphi_0)}$$

we should use (6.140) or (6.138) with a signal of the form

$$\hat{\mathbf{R}}_{\mathbf{x}}(n, K, \alpha) = \frac{1}{K+1} \sum_{p=n-K/2}^{n+K/2} \mathbf{x}_{\alpha}(p) \mathbf{x}_{\alpha}^*(p)$$

with $\mathbf{x}_{\alpha}(p) = \mathbf{x}(p) e^{-j\alpha p^2}$,

with α as a parameter. It is easy to show that relation (6.144), in this case, has the form

$$\begin{aligned} SLP_{\text{Capon}}^{\text{average}}(n, \omega, \alpha) &\rightarrow \infty \text{ at } (\omega = \omega_0 \text{ and } \alpha = \alpha_0) \\ \frac{SLP_{\text{Capon}}^{\text{average}}(n, \omega, \alpha)}{SLP_{\text{Capon}}^{\text{average}}(n, \omega_0, \alpha_0)} &\rightarrow 0 \text{ at } (\omega \neq \omega_0 \text{ or } \alpha \neq \alpha_0). \end{aligned} \quad (6.146)$$

The high-resolution form of the LPFT can be used for efficient processing of close linear frequency-modulated signals, with the same rate within the considered interval.

Example 6.28. The Capon LPFT form is illustrated on an example with a signal with two close components

$$x(t) = \exp(j128\pi t(0.55 - t/2) + j5\pi t^3) + \exp(j128\pi t(0.45 - t/2) + j5\pi t^3),$$

that in addition to the linear frequency-modulated contained a small disturbing cubic phase term. The considered time interval was $-1 \leq t \leq 1 - \Delta t$ with $\Delta t = 2/512$, $\rho = 0.5$, $K = 30$, and the frequency domain is interpolated eight times. The standard STFT, LPFT, Capon's STFT, and Capon's LPFT-based representations are presented in Fig. 6.43. \square

In general, higher-order polynomial or any other nonstationary parametrized signal form can be analyzed in the same way.

Other high-resolution forms of the STFT, like MUSIC and ESPRIT, can be derived in a similar way.

6.9 WATERMARKING IN THE SPACE/SPATIAL-FREQUENCY DOMAIN

Digital watermarking has been rapidly developing in the last decade due to the widespread use of multimedia contents. It can provide an image (music, video)

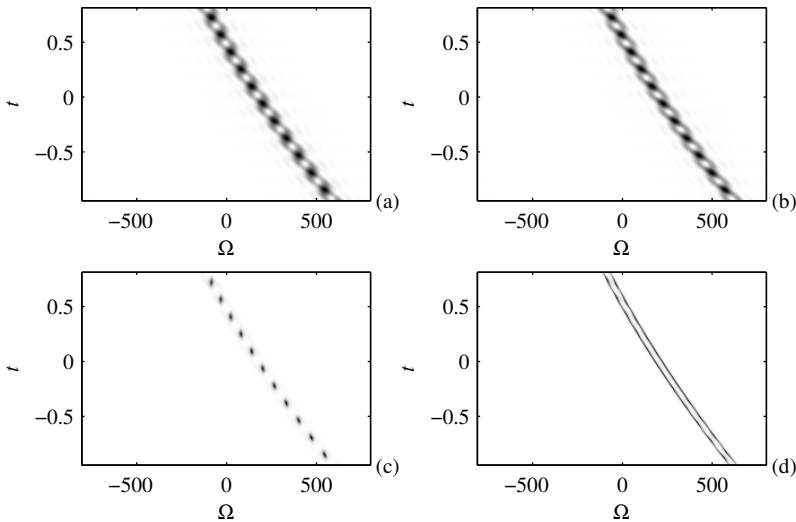


Figure 6.43 (a) The standard STFT, (b) the LPFT, (c) Capon’s STFT, and (d) Capon’s LPFT-based representations of two close almost linear frequency-modulated signals.

copyright protection, that is, identification of its owner and authorized distributor. The most commonly used approaches for image watermarking are either by embedding the watermark signal in the spatial domain or in the transformation (frequency) domain. Regardless, the watermarking approach, it is desirable to ensure that image watermarking satisfies the following important properties: (1) it is perceptually invisible; (2) watermark must be robust to the various attacks that consists of image processing algorithms, such as common geometric distortion (rotation, translation, cropping), resampling, filtering, and compression; (3) detection of the watermark by copyright owner should be possible without the original image.

A watermarking scheme in the space/spatial-frequency domain is introduced by Stanković, Djurović, and Pitas. Two-dimensional chirp signals are used as watermarks, due to their geometrical symmetry and robustness to stationary filtering. An ideal space/spatial-frequency representation for this type of signals is achieved by using the two-dimensional Wigner distribution. In order to additionally emphasize the watermark, with respect to the Wigner distribution of the original image, the Wigner distribution projections (two-dimensional Radon Wigner distribution) are

used. In this way the maximum watermark projection will be dominant, as compared to the projections of the Wigner distribution of the original image. It results in an efficient watermark detection procedure.

Consider an image $I(x,y)$. The Fourier domain watermark is implemented in the spatial domain as

$$W_F(x,y) = \sum_{i=1}^M A_i \exp[j(xa_i + yb_i)] = \sum_{i=1}^M A_i S_{Fi}(x,y) \quad (6.147)$$

where A_i is the watermark key (randomly generated amplitudes) and a_i, b_i determine location of transformation coefficients in the Fourier domain. The analytic part of an image is considered, for notation simplicity. The detection of watermark can be performed based on the value d of the two-dimensional Fourier transform of the watermarked image $I^w(x,y) = I(x,y) + W_F(x,y)$ at the points determined by a_i, b_i ,

$$d = \sum_{i=1}^M A_i \text{FT}_{2D}\{I^w(x,y)\}|_{(\Omega_x, \Omega_y) = (a_i, b_i)}$$

This concept of watermarking can be extended using a sum of two-dimensional linear frequency-modulated signals

$$W_W(x,y) = \sum_{i=1}^M A_i e^{j(a_{i1}x^2/2 + a_{i2}y^2/2 + a_{i3}xy)} e^{j(a_{i4}x + a_{i5}y)} = \sum_{i=1}^M A_i S_{Li}(x,y) S_{Fi}(x,y) \quad (6.148)$$

Since the Wigner distribution is an appropriate tool for two-dimensional linear frequency-modulated signal processing, it is used in this analysis. For signal (6.148), the Wigner distribution is

$$WD_w(x,y, \Omega_x, \Omega_y) = \sum_{i=1}^M A_i^2 \delta(\Omega_x - a_{i1}x - a_{i3}y - a_{i4}, \Omega_y - a_{i2}y - a_{i3}x - a_{i5}) \\ + \text{cross-terms} \quad (6.149)$$

Although the Wigner distribution of chirp signal is already completely concentrated along hyperplanes $\Omega_x = a_{i1}x + a_{i3}y + a_{i4}$, $\Omega_y = a_{i2}y + a_{i3}x + a_{i5}$, its application to watermark detection is simplified and detection performance is improved by using its projections, the Radon-Wigner distribution, along the planes defined by a_{i1}, a_{i2}, a_{i3} . In this way, a summing over delta pulses, along the projection planes, is performed. The cross-terms are eliminated at the same time. The projection of the

Wigner distribution of a chirp signal, along these projection planes, will be dominant over the Wigner distribution of the image, because the second is dispersed in different projection planes. The modulus of the Radon-Wigner distribution (RWD_i) can be easily calculated by multiplying the watermarked image by $A_i S_{Li}^*(x, y)$, and then calculating the Fourier transform of this product. Let $I_a(x, y)$ be the watermarked and, possibly, modified (attacked) image. The relation for watermark detection, according to the previous consideration and (6.102), is given by the correlation output

$$d = \sum_{i=1}^M RWD_i = \sum_{i=1}^M \text{AFT}_{2D}\{I_a(x, y)S_{Li}^*(x, y)\} \Big|_{\text{at } (\Omega_x, \Omega_y) = (a_{i4}, a_{i5})} \quad (6.150)$$

d should be greater than a reference detection threshold. The watermark key can be chosen in a form of Gaussian zero mean distributed amplitudes. The variance of amplitude A_i should be taken by a trade-off between the watermark detection possibility and the visual imperceptibility. The location of region where the transformation coefficients a_{ij} , $i = 1, 2, \dots, M$, $j = 1, \dots, 5$ are embedded is determined according to the criteria of visual imperceptibility as well.

Watermarking in the space/spatial-frequency domain implemented in this way is more flexible and reliable in protection than the standard watermarking in the Fourier domain. This algorithm, in a combination with the method of blind watermark detection of one stronger chirp signal embedded in an image, increases robustness to the very complex image transformations, as the rotation and scaling. A further generalization may be achieved by applying and detecting watermark in the generalized linear coordinate transformation domains. Watermarking of sound signals in the fractional Fourier domain is a one-dimensional form of the presented method.

6.10 HARDWARE DESIGN FOR TIME-FREQUENCY ANALYSIS

The time-frequency representation-based on the recursive STFT implementation, with additional transformation to the S-method, could be implemented as a hardware architecture shown in Fig. 6.44. It consists of two blocks. The first block is used for the STFT implementation, and the second block is used to modify the STFT in order to obtain the improved distribution concentration, according to the S-method relations. The STFT can be implemented using available FFT chips or the approaches based on the recursive algorithms. The design presented here is based on the recursive algorithm, presented in Chapter 2. It is suitable for VLSI

implementation, due to reduced hardware complexity. Assuming a rectangular lag window, the STFT of the form

$$STFT(n, k) = \sum_{m=-N/2+1}^{N/2} x(n+m) e^{-j2\pi mk/N}$$

can be written as

$$STFT(n, k) = [x(n+N/2) - x(n-N/2)](-1)^k + STFT(n-1, k)e^{j2\pi k/N}. \quad (6.151)$$

The STFT definition is shifted for one sample, with respect the one in Chapter 2. A complete system consists of N channels with $k = 0, 1, 2, \dots, N-1$. For the cases of Hann(ing) or Hamming lag window, the STFT is obtained by modifying $STFT(n, k)$ in (6.151) as follows

$$STFT_H(n, k) = a_{-1}STFT(n, k-1) + a_0STFT(n, k) + a_1STFT(n, k+1),$$

where the coefficients a_{-1}, a_0, a_1 are: $(0.25, 0.5, 0.25)$ and $(0.23, 0.54, 0.23)$ for the Hann(ing) and the Hamming window, respectively. Each channel described by (6.151) involves complex multiplication and can be separated in two subchannels involving only real computations. In order to describe these channels, (6.151) is modified, using

$$STFT(n, k) = STFT_{Re}(n, k) + jSTFT_{Im}(n, k)$$

where $STFT_{Re}(n, k)$ and $STFT_{Im}(n, k)$ are the real and imaginary parts of the STFT, respectively. The equations describing these two subchannels for a real-valued signals are

$$\begin{aligned} STFT_{Re}(n, k) &= [x(n+N/2) - x(n-N/2)](-1)^k \\ &\quad + c(k)STFT_{Re}(n-1, k) - s(k)STFT_{Im}(n-1, k) \\ STFT_{Im}(n, k) &= c(k)STFT_{Im}(n-1, k) + s(k)STFT_{Re}(n-1, k). \end{aligned} \quad (6.152)$$

where

$$\begin{aligned} c(k) &= \cos(2\pi k/N), \\ s(k) &= \sin(2\pi k/N). \end{aligned}$$

Now the S-method can be written as

$$\begin{aligned} SM(n, k) = & |STFT(n, k)|^2 + 2 \sum_{i=1}^{L_d} STFT_{Re}(n, k+i) STFT_{Re}(n, k-i) + \\ & 2 \sum_{i=1}^{L_d} STFT_{Im}(n, k+i) STFT_{Im}(n, k-i), \end{aligned} \quad (6.153)$$

which is the equation used to modify the outputs of the STFT block in order to obtain the S-method-based distribution.

The hardware necessary for one channel implementation and for $L_d = 2$ is presented in Fig. 6.44. It has been designed for a 16-bit fixed point arithmetic. The total number of multipliers is $2(L_d + 3)$ and the total number of adders is $2(L_d + 2)$. The multiplication operation results in a two-sign bit and, assuming Q15 format (15 fractional bit), the product must be shifted left by 1 bit to obtain correct results. This shifter is included as a part of multiplier. The throughput of the system is N . The longest path is one that connects the register storing $STFT(n - 1, k \pm L_d)$, through two multipliers and $L_d + 3$ adders, with the output $SM(n, k)$. This path determines the highest sampling rate. It can be observed that the S-method implementation introduces only an additional delay of L_d adders compared to the spectrogram implementation. Thus, the fastest sampling rate is essentially the same for both implementations (spectrogram and S-method).

The same hardware can be used for the L-Wigner distribution, according to the order-recursive L-Wigner distribution relation

$$LWD_L(n, k) = \sum_{i=-L_d}^{L_d} LWD_{L/2}(n, k+i) LWD_{L/2}(n, k-i).$$

In order to share the existing hardware (Block 2 in Fig. 6.44) for the realization with $L = 2$, we have to introduce the multiplexers at the input of block 2. The multiplexer's control signal determines whether the system processes $STFT(n, k)$ or $SM(n, k)$. In the latter case only half of Block 2 is used, since the S-method is always real. During the first part of the sampling period (T_{STFT}), Block 1 realizes $STFT(n, k)$, while Block 2 calculates $LWD_2(n - 1, k)$. In the second part of the sampling period (T_{SM}), control signal resets to zero, and $SM(n, k)$ is produced. Thus, for the L-Wigner distribution realization we did not use any extra time, that is, with the same hardware, within the same time period, system produces two outputs: the S-method and the L-Wigner distribution with $L = 2$. Note that for $LWD_2(n - 1, k)$ calculation only a half of the Block 2 hardware is used, thus

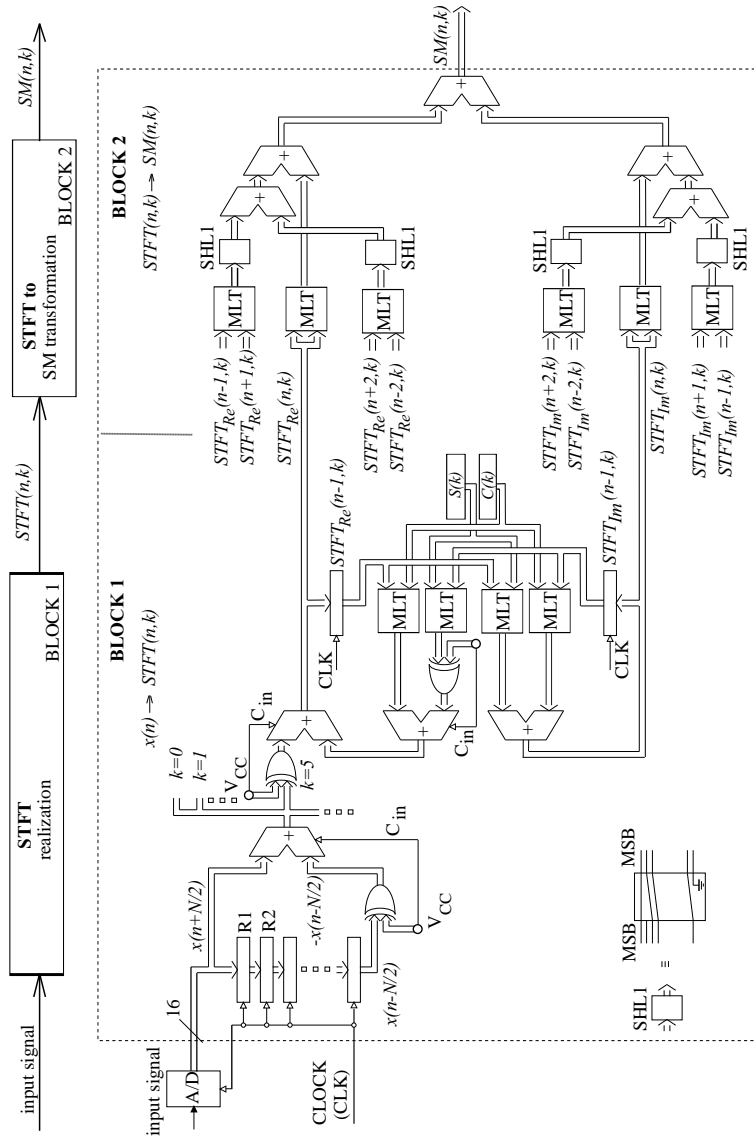


Figure 6.44 Architecture for the signal independent S-method realization (one channel with $L_d = 2$).

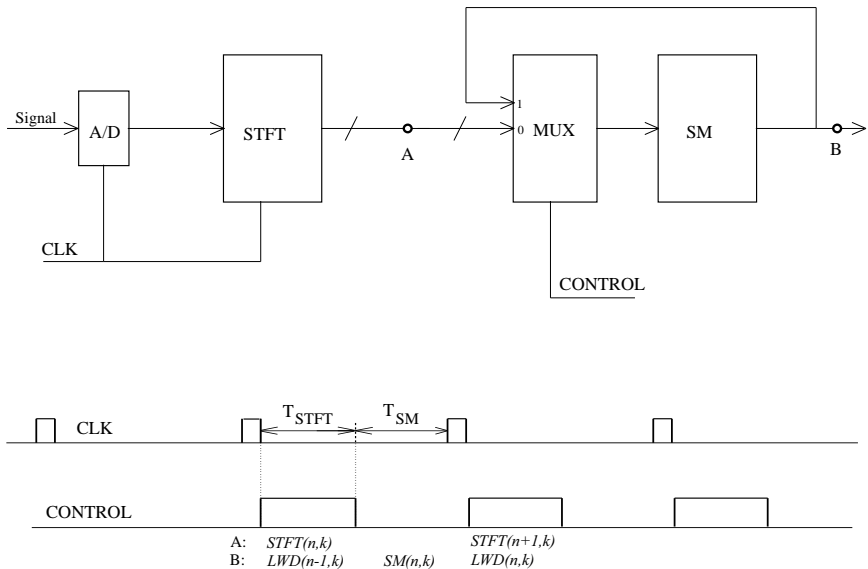


Figure 6.45 Block scheme for the L-Wigner realization, along with control signals.

the other half may be used in order to simultaneously compute $LWD_4(n - 2, k)$ for $L = 4$. The complete block diagram of the modified hardware, together with timing signals for multiplexer's control is presented in Fig. 6.45.

Here a simple the signal independent S-method-based parallel architecture of a time-frequency system is presented. Other designs for signal adaptive form of the S-method as well as the ones based on the multiple-clock-cycle architectures may be found in the literature.

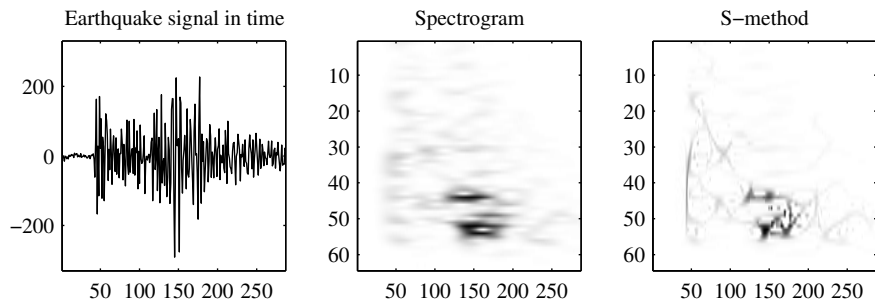


Figure 6.46 Representation of an earthquake signal in Montenegro in the time and time-frequency domain.

6.11 SEISMIC SIGNAL ANALYSIS

Earthquake analysis is very important because earthquakes cause many catastrophes all over the world. One of the applications in the analysis of seismic signals is in their reliable detection. Due to the high probability of false earthquake alarms when the seismometers detect nonseismic signals, the time-frequency analysis can be used for seismic signal separation and detection (Fig. 6.46). It is based on the instantaneous frequency analysis. Analyzing the energy of seismic signal, it is possible to make detection and send an earthquake alarm if the energy is above a specific level.

Seismic signals are also used in the analysis of propagation media, with application, for example, in gas and oil detection. A seismic wave is a periodic wave that can transmit energy through the media without causing their permanent deformation. The p-waves and s-waves are the waves used for the time-frequency analysis. Seismic reflection patterns can provide information of subsurface imaging by using the time-frequency tools (seismic stratigraphy). Analyzing the received reflected signal and its energy at the surface, it is possible to observe the characteristics of subsurfaces where the signal propagated. The subsurface imaging is widely used in gas and oil detection. A quantitative analysis in seismic reflection patterns, in order to get more information of geology by seismic reflection pattern, is possible by using the time-frequency analysis.

6.12 BIOMEDICAL SIGNAL ANALYSIS

Biomedical signals usually contain interferences of different nature. The separation of undesirable content from the considered signal is easier in the joint-time-frequency domain. In some cases the detection of frequency content changes and irregularities carry the most important information about the underlying process. Thus, analysis of highly nonstationary signals in biomedicine could benefit from using time-frequency tools. Such examples are EEG analysis in epilepsy patients, ECG analysis of cardiac abnormalities, identification of genetic abnormalities in brain tumors, early detection of multiple sclerosis lesions, study of pediatric disorders, or analysis of respiration sounds in asthmatic patients.

6.13 TIME-FREQUENCY ANALYSIS OF SPEECH SIGNALS

Speech signals are highly nonstationary, with a wide dynamic range of multiple frequency components in the short-time spectra. Time-frequency distributions have been introduced for the analysis of frequency components as a function of time of nonstationary signals. The most common time-frequency representation, the spectrogram, is characterized by a trade-off between time and frequency resolutions. Consequently, the development of other quadratic time-frequency distributions for representation and processing of nonstationary signals is an interesting challenge. For example, a possible application is the Wiener optimum filtering of speech signals corrupted by noise. A more accurate estimation of the signal spectrum yields higher suppression of noise components.

Because of the nonstationary nature of speech signals, statistically optimum filtering requires time-variant filtering methods. Filtering in the time-frequency domain could be advantageous compared to separate filtering in the time or frequency domain. Since there exists no unique definition of time-frequency spectra, many approaches for time-variant filtering have been proposed. Zadeh suggested using the Rihaczek distribution. However, this time-frequency spectrum is complex valued and badly concentrated in time. Therefore, filtering in the time-frequency domain has been redefined using the Wigner distribution, using the Weyl correspondence. The time-variant transfer function has been defined as the Weyl symbol mapping of the impulse response into the time-frequency plane. The Wigner spectrum is used in order to average out the cross-terms. For single-realization cases, reduced interference distributions are used.

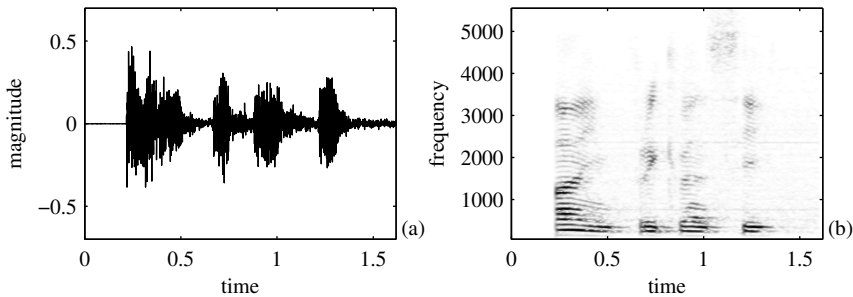


Figure 6.47 Speech signal of the word “time-frequency” in time (left) and in time-frequency, as the absolute STFT value, (right).

Let us conclude this presentation where we could start this book, by presenting a time-frequency distribution of a speech signal with the words “time-frequency” (Fig. 6.47). Such a time-frequency representation of speech is already a trade-mark not only for time-frequency analysis, but also for signal processing as a whole. Signal processing in speech recognition is the topic with many open problems. We are far from efficiently communicating with computers by using speech. The role of the time-frequency analysis is crucial in future research in this and many other areas.

Bibliography

- [1] M. Abed, A. Belouchrani, M. Cheriet, and B. Boashash, “Time-frequency distributions based on compact support Kernels: Properties and Performance Evaluation,” *IEEE Transactions on Signal Processing*, Vol. 60, No. 6, June 2012, pp. 2814-2827.
- [2] A. Abutaleb, “Instantaneous frequency estimation using stochastic calculus and bootstrapping,” *EURASIP Journal on Applied Signal Processing*, Vol. 2005, Jan. 2005, pp. 1886-1901.
- [3] M. H. Ackroyd, “Short-time spectra and time-frequency energy distribution,” *J. Acoust. Soc. Am.*, Vol. 50, 1970, pp. 1229-1231.
- [4] A. Akan and L. F. Chaparro, “Multiresolution Gabor expansion for evolutionary spectral analysis,” *Signal Processing*, Vol. 63, No. 3, Mar. 1998.
- [5] T. Alieva, M. J. Bastiaans, and LJ. Stanković, “Signal reconstruction from two close fractional Fourier power spectra,” *IEEE Transactions on Signal Processing*, Vol. 51, No. 1, Jan. 2003, pp. 112-123.
- [6] L. B. Almeida, “The fractional Fourier transform and time-frequency representations,” *IEEE Transactions on Signal Processing*, Vol. 42, No. 11, Nov. 1994, pp. 3084-3091.
- [7] L. B. Almeida, “Product and convolution theorems for the fractional Fourier transform,” *IEEE Signal Processing Letters*, Vol. 4, No. 1, Jan. 1997, pp. 15-17. Vol. 53, No. 1, Jan. 1997.
- [8] M. G. Amin, “A new approach to recursive Fourier transform,” *Proc. IEEE*, Vol. 75, 1987, pp. 1357-1358.
- [9] M. G. Amin, “Spectral smoothing and recursion based on the nonstationarity of the autocorrelation function,” *IEEE Transactions on Signal Processing*, Vol. 41, No. 2, Feb. 1993, pp. 930-934.
- [10] M. G. Amin, “Spectral decomposition of time-frequency distribution kernels,” *IEEE Transactions on Signal Processing*, Vol. 42, No. 5, May 1994, pp. 1156-1165.
- [11] M. G. Amin, “Minimum variance time-frequency distribution kernels for signals in additive noise,” *IEEE Transactions on Signal Processing*, Vol. 44, No. 9, Sep. 1996, pp. 2352-2356.
- [12] M. G. Amin, “Recursive kernels for time-frequency signal representations,” *IEEE Signal Processing Letters*, Vol. 3, No. 1, Jan. 1996, pp. 16-18.

- [13] M. G. Amin and K. D. Feng, "Short-time Fourier transform using cascade filter structures," *IEEE Transactions on Circuits and Systems*, Vol. 42, No. 10, Oct. 1995, pp. 631-641.
- [14] M. G. Amin, G. T. Venkatesan, and J. F. Carroll, "A constrained weighted least squares approach for time-frequency distribution kernel design," *IEEE Transactions on Signal Processing*, Vol. 44, No. 5, May 1996, pp. 1111-1124.
- [15] M. G. Amin and W. J. Williams, "High spectral resolution time-frequency distribution kernels," *IEEE Transactions on Signal Processing*, Vol. 46, No. 10, Oct. 1998, pp. 2796-2804.
- [16] M. G. Amin, "Time-frequency distributions in statistical signal and array processing," *Signal Processing Magazine*, Sept. 1998, pp. 32-42.
- [17] M. G. Amin, A. Belouchrani, and Y. Zhang, "The spatial ambiguity function and its applications," *IEEE Signal Processing Letters*, Vol. 7, pp. 138-140, June 2000.
- [18] G. Andria, M. Savino, and A. Trotta, "Application of the Wigner-Ville distribution to measurement of transient signals," *IEEE Transactions on Instrumentation and Measurements*, Vol. 43, No. 2, April 1994, pp. 187-193.
- [19] G. R. Arce and S. R Hasan, "Elimination of interference terms of the discrete Wigner distribution using nonlinear filtering," *IEEE Transactions on Signal Processing*, Vol. 48, No. 8, Aug. 2000, pp. 2321-2331.
- [20] J. T. Astola, et al., "Application of bispectrum estimation for time-frequency analysis of ground surveillance Doppler radar echo signals," *IEEE Transactions on Instrumentation and Measurement*, Vol. 57, No. 9, Sept. 2008, pp. 1949-1957.
- [21] L. E. Atlas, G. D. Benard, and S. B. Narayanan, "Applications of time-frequency analysis to signals from manufacturing and machine monitoring sensors," *Proc. IEEE*, Vol. 84, No. 9, Sept. 1996, pp. 1319-1329.
- [22] L. E. Atlas, Y. Zhao, and R. J. Marks II, "The use of cone shape kernels for generalized time-frequency representations of nonstationary signals," *IEEE Transactions Acoust., Speech, Signal Processing*, Vol. 38, 1990, pp. 1084-1091.
- [23] F. Auger, "Some simple parameter determination rules for the generalized Choi-Williams and Butterworth distributions," *IEEE Signal Processing Letters*, Vol. 1, No. 1, Jan. 1994, pp. 9-11.
- [24] F. Auger and P. Flandrin, "Improving the readability of time-frequency and time-scale representations by the reassignment method," *IEEE Transactions on Signal Processing*, Vol. 43, No. 5, May 1995, pp. 1068-1089.
- [25] F. Auger and F. Hlawatsch, *Time-Frequency Analysis*, Wiley-ISTE, Nov. 2008
- [26] L. Auslander, I. Gertner, and R. Tolimieri, "The discrete Zak transform application time-frequency analysis and synthesis of nonstationary signals," *IEEE Transactions on Signal Processing*, Vol. 39, No. 4, Apr. 1991, pp. 825-835.
- [27] Y. Avargel and I. Cohen, "Modeling and identification of nonlinear systems in the short-time Fourier transform domain," *IEEE Transactions on Signal Processing*, Vol. 58, No. 1, Jan. 2010, pp. 291-304.
- [28] Y. Avargel and I. Cohen, "Undermodeling-error quantification for quadratically nonlinear system identification in the short-time Fourier transform domain," *IEEE Transactions on Signal Processing*, Vol. 58, No. 12, Dec. 2010, pp. 6052-6065.

- [29] S. Aviyente and A. Y. Mutlu, "A time-frequency-based approach to phase and phase synchrony estimation," *IEEE Transactions on Signal Processing*, Vol. 59, No. 7, July 2011, pp. 3086-3098.
- [30] R. G. Baraniuk, M. Coates, and P. Steeghs, "Hybrid linear/quadratic time-frequency attributes," *IEEE Transactions on Signal Processing*, Vol. 49, No. 4, April 2001, pp. 760-766.
- [31] R. G. Baraniuk, P. Flandrin, A. J. E. M. Janssen, and O. J. J. Michel, "Measuring time-frequency information content using the Renyi entropies," *IEEE Transactions on Information Theory*, Vol. 47, No. 4, May 2001, pp. 1391-1409.
- [32] R. G. Baraniuk, "A limitation of the kernel method for joint distributions of arbitrary variables," *IEEE Signal Processing Letters*, Vol. 3, No. 2, Feb. 1996, pp. 51-53.
- [33] R. G. Baraniuk, "Covariant time-frequency representations through unitary equivalence," *IEEE Signal Processing Letters*, Vol. 3, No. 3, Mar. 1996, pp. 79-81.
- [34] R. G. Baraniuk, "Beyond time-frequency analysis: Energy densities in one and many dimensions," *IEEE Transactions on Signal Processing*, Vol. 46, No. 9, Sept. 1998, pp. 2305-2315.
- [35] R. G. Baraniuk and L. Cohen, "On joint distributions for arbitrary variables," *IEEE Signal Processing Letters*, Vol. 2, No. 1, Jan. 1995, pp. 10-12.
- [36] R. G. Baraniuk and D. L. Jones, "Signal-dependent time-frequency analysis using radially-gaussian kernel," *IEEE Transactions on Signal Processing*, Vol. 41, No. 3, 1993, pp. 263-284.
- [37] R. G. Baraniuk and D. L. Jones, "A signal dependent time-frequency representation: Fast algorithm for optimal kernel design," *IEEE Transactions on Signal Processing*, Vol. 42, No. 1, Jan. 1994, pp. 134-146.
- [38] R. G. Baraniuk, "Compressive sensing," *IEEE Signal Processing Magazine*, Vol. 24, No. 4, pp. 118-121, 2007
- [39] R. G. Baraniuk and D. L. Jones, "Wigner-based formulation of the chirplet transform," *IEEE Transactions on Signal Processing*, Vol. 44, No. 12, Dec. 1996, pp. 3129-3135.
- [40] S. Barbarossa, "Analysis of multicomponent LFM signals by a combined Wigner-Hough transform," *IEEE Transactions on Signal Processing*, Vol. 43, No. 6, June 1995, pp. 1511-1515.
- [41] S. Barbarossa and O. Lemoine, "Analysis of nonlinear FM signals by pattern recognition of their time-frequency representation," *IEEE Signal Processing Letters*, Vol. 3, No. 4, Apr. 1996, pp. 112-115.
- [42] S. Barbarossa and V. Petrone, "Analysis of polynomial-phase signals by the integrated generalized ambiguity functions," *IEEE Transactions on Signal Processing*, Vol. 45, No. 2, Feb. 1997, pp. 316-328.
- [43] S. Barbarossa, A. Scaglione, and G. B. Giannakis, "Product high-order ambiguity function for multicomponent polynomial-phase signal modeling," *IEEE Transactions on Signal Processing*, Vol. 46, No. 3, Mar. 1998, pp. 691-709.
- [44] S. Barbarossa and J. L. Krolok, "Adaptive time-varying cancellation of wideband interferences in spread-spectrum communications based on time-frequency distributions," *IEEE Transactions on Signal Processing*, Vol. 47, No. 4, Apr. 1999, pp. 957-965.
- [45] B. Barkat, "Instantaneous frequency estimation of nonlinear frequency-modulated signals in the presence of multiplicative and additive noise," *IEEE Transactions on Signal Processing*, Vol. 49, No. 10, Oct. 2001, pp. 2214-2222.

- [46] B. Barkat and B. Boashash, "A high-resolution quadratic time-frequency distribution for multicomponent signals analysis," *IEEE Transactions on Signal Processing*, Vol. 49, No. 10, Oct. 2001, pp. 2232-2239.
- [47] M. J. Bastiaans, "Application of the Wigner distribution function in optics," in Eds. W. F. G. Mecklenbrauker, F. Hlawatsch, *The Wigner distributions - theory and applications in signal processing*, Elsevier, 1997.
- [48] M. J. Bastiaans, "Application of the Wigner distribution function to partially coherent light," *J. Opt. Soc. Am.*, A3, pp. 1227-1238, 1986.
- [49] M. J. Bastiaans, "Comment on "The T-class of time–frequency distributions: Time-only kernels with amplitude estimation","*Journal of the Franklin Institute*, Vol. 348, No. 9, Nov. 2011, pp. 2670–2673.
- [50] M. J. Bastiaans and A. J. van Leest, "From the rectangular to the quincunx Gabor lattice via fractional Fourier transformation," *IEEE Signal Processing Letters*, Vol. 5, No. 8, Aug. 1998, pp. 203-205.
- [51] M. J. Bastiaans, T. Alieva, and LJ. Stanković, "On rotated time-frequency kernels," *IEEE Signal Processing Letters*, Vol. 9, No. 11, Nov. 2002, pp. 378-381.
- [52] I. Bayram and I. W. Selesnick, "A dual-tree rational-dilation complex wavelet transform," *IEEE Transactions on Signal Processing*, Vol. 59, No. 12, Dec. 2011, pp. 6251-6256.
- [53] I. Bayram and I. W. Selesnick, "Frequency-domain design of overcomplete rational-dilation wavelet transforms," *IEEE Transactions on Signal Processing*, Vol. 57, No. 8, Aug. 2009, pp. 2957-2972.
- [54] M. Benidir, "Characterization of polynomial functions and application to time-frequency analysis," *IEEE Transactions on Signal Processing*, Vol. 45, No. 5, May 1997, pp. 1351-1355.
- [55] R. Bernardini and J. Kovačević, "Arbitrary tilings of the time–frequency plane using local bases," *IEEE Transactions on Signal Processing*, Vol. 47, No. 8, Aug. 1999, pp. 2293-2304.
- [56] J. Bertrand and P. Bertrand, "Affine time-frequency distributions," in *Time-frequency analysis - Methods and Applications*, B. Boashash ed., Longman-Cheshire, Melbourne, 1991.
- [57] G. Bi, "New split-radix algorithm for the discrete Hartley transform," *IEEE Transactions on Signal Processing*, Vol. 45, No. 2, Feb. 1997, pp. 297-303.
- [58] G. Bi, Y. Ju and X. Li, "Fast algorithms for polynomial time-frequency transforms of real-valued sequences," *IEEE Transactions on Signal Processing*, Vol. 56, No. 5, May 2008, pp. 1905-1915.
- [59] G. Bi, Y. Wei, G. Li, and C. Wan, "Radix-2 DIF fast algorithms for polynomial time-frequency transforms," *IEEE Transactions on Aerospace and Electronic Systems*, Vol. 42, No. 4, Oct. 2006, pp. 1540-1546.
- [60] B. Boashash, "Estimating and interpreting the instantaneous frequency of a signal Part 1," *IEEE Proc.*, Vol. 80, No. 4, April 1992, pp. 519-538.
- [61] B. Boashash, "Estimating and interpreting the instantaneous frequency of a signal Part 2," *IEEE Proc.*, Vol. 80, No. 4, April 1992, pp. 519-538.
- [62] B. Boashash and J. B. Black, "An efficient real time implementation of the Wigner-Ville distribution," *IEEE Transactions on Acoustics, Speech and Signal Processing*, vol ASSP-35, no 11, Nov 1987. pp. 1611-1618.

- [63] B. Boashash and P. O'Shea, "Polynomial Wigner-Ville distributions and their relationship to time-varying higher order spectra," *IEEE Transactions on Signal Processing*, Vol. 42, No. 1, Jan. 1994, pp. 216-220.
- [64] B. Boashash and B. Ristić, "Polynomial WVDs and time-varying polyspectra," in *Higher Order Statistical Signal Processing*, B. Boashash et al, eds., Longman Cheshire, 1993.
- [65] B. Boashash and B. Ristić, "Polynomial time-frequency distributions and time-varying higher order spectra: Applications to analysis of multicomponent FM signals and to treatment of multiplicative noise," *Signal Processing*, Vol. 67, No. 1, May 1998, pp. 1-23.
- [66] B. Boashash and V. Sucic, "Resolution measure criteria for the objective assessment of the performance of quadratic time-frequency distributions," *IEEE Transactions on Signal Processing*, Vol. 51, No. 5, May 2003, pp. 1253-1263.
- [67] G. F. Bourdeaux-Bartels and T. W. Parks, "Time-varying filtering and signal estimation using the Wigner distribution," *IEEE Transactions on Acoustics, Speech and Signal Processing*, Vol. ASSP-34, No. 6, June 1986, pp. 442-451.
- [68] G. F. Bourdeaux-Bartels, "Time-varying signal processing using Wigner distribution synthesis techniques," in *The Wigner Distribution-Theory and Applications in Signal Processing*, W. Mecklenbrauker, Ed, Amsterdam, Elsevier 1997.
- [69] R. A. Brown, M. L. Lauzon, and R. Frayne, "A general description of linear time-frequency transforms and formulation of a fast, invertible transform that samples the continuous S-transform spectrum nonredundantly," *IEEE Transactions on Signal Processing*, Vol. 58, No. 1, Jan. 2010, pp. 281-290.
- [70] F. Cakrak and P. J. Loughlin, "Multiwindow time-varying spectrum with instantaneous bandwidth and frequency constraints," *IEEE Transactions on Signal Processing*, Vol. 49, No. 8, Aug. 2001, pp. 1656-1666.
- [71] F. Cakrak and P. J. Loughlin, "Multiple window time-varying spectral analysis," *IEEE Transactions on Signal Processing*, Vol. 49, No. 2, Feb. 2001, pp. 448-453. E.
- [72] Candès, J. Romberg J, and T. Tao, "Robust uncertainty principles: Exact signal reconstruction from highly incomplete frequency information," *IEEE Transactions on Information Theory*, Vol. 52, No. 2, 489-509.
- [73] R. A. Carmona, W. L. Hwang, and B. Torresani, "Multiridge detection and time-frequency reconstruction," *IEEE Transactions on Signal Processing*, Vol. 47, No. 2, Feb. 1999, pp. 480-492.
- [74] S. Chandra Sekhar and T. V. Sreenivas, "Adaptive spectrogram vs. adaptive pseudo-Wigner–Ville distribution for instantaneous frequency estimation," *Signal Processing*, Vol. 83, No. 7, July 2003, pp. 1529–1543.
- [75] S. Chandra Sekhar and T. V. Sreenivas, "Adaptive window zero-crossing-based instantaneous frequency estimation," *EURASIP Journal on Applied Signal Processing*, Vol. 2004, Jan. 2004, pp. 1791-1806.
- [76] S. Chandra Sekhar and T. V. Sreenivas, "Signal-to-noise ratio estimation using higher-order moments," *Signal Processing*, Vol. 86, No. 4, April 2006, pp. 716–732.

- [77] L. -W. Chang, "Roundoff error problem of the Systolic Array for DFT," *IEEE Transactions on Signal Processing*, Vol. 41, No. 1, Jan. 1993, pp. 395-398.
- [78] É. Chassande-Mottin and A. Pai, "Discrete Time and Frequency Wigner–Ville Distribution: Moyal's Formula and Aliasing," *IEEE Signal Processing Letters*, Vol. 12, No. 7, July 2005, pp. 508-511.
- [79] V. C. Chen, *The Micro-Doppler Effect in Radar*, Artech House, Jan. 2011
- [80] V. C. Chen, "Micro-Doppler effect in radar: Part I: Phenomenon, physics, mathematics, and simulation study," *IEEE Transactions on Aerosp. Electron. Syst.*, Vol. 42, No. 1 Jan 2006.
- [81] H. C. Chiang and J. C. Liu, "High resolution time-frequency representations at arbitrary frequencies," *Signal Processing*, Vol. 68, No. 3, Mar. 1997.
- [82] S. -H. Cho, G. Jang, and S. -H. Kwon, "Time-frequency analysis of power-quality disturbances via the Gabor–Wigner transform," *IEEE Transactions on Power Delivery*, Vol. 25, No. 1, Jan. 2010, pp. 494-499.
- [83] H. Choi and W. J. Williams, "Improved time-frequency representation of multicomponent signals using exponential kernels," *IEEE Transactions on Acoustics, Speech and Signal Processing*, Vol. ASSP-37, No. 6, June 1989, pp. 862-871.
- [84] L. Cirillo, A. Zoubir, and M. G. Amin, "Parameter estimation for locally linear FM signals using a time-frequency Hough transform," *IEEE Transactions on Signal Processing*, Vol. 56, No. 9, Sept. 2008, pp. 4162-4175.
- [85] T. A. C. M. Claasen and W. F. G. Mecklenbrauker, "The Wigner distribution-a tool for time frequency signal analysis, Part I," *Phillips J. Res.*, Vol. 35, No. 3, March 1980, pp. 217-250.
- [86] T. A. C. M. Claasen and W. F. G. Mecklenbrauker, "The Wigner distribution-a tool for time frequency signal analysis, Part II," *Phillips J. Res.*, Vol. 35, No. 4/5., April/May 1980, pp. 276-300.
- [87] T. A. C. M. Claasen and W. F. G. Mecklenbrauker, "The Wigner distribution-a tool for time frequency signal analysis, Part III," *Phillips J. Res.*, Vol. 35, No. 6, Jun 1980, pp. 372-389.
- [88] T. A. C. M. Claasen and W. F. G. Mecklenbrauker, "The aliasing problem in discrete time Wigner distributions," *IEEE Transactions on Acoustics, Speech and Signal Processing*, Vol. ASSP-31, No. 5, Oct. 1983, pp. 1067-1072.
- [89] L. Cohen, "Generalized phase-space distribution functions," *Journal of Math. Phys.*, Vol. 7, 1966, pp. 781-786.
- [90] L. Cohen, "Time-frequency distributions-a review," *Proc. IEEE*, Vol. 77, No. 7, July 1989, pp. 941-981.
- [91] L. Cohen, *Time-frequency analysis*, Prentice-Hall, 1995.
- [92] L. Cohen and C. Lee, "Instantaneous bandwidth," in *Time-frequency signal analysis*, B. Boashash ed., Longman Cheshire,1992.
- [93] L. Cohen, "A general approach for obtaining joint representations in signal analysis - Part I: Characteristic function operator method," *IEEE Transactions on Signal Processing*, Vol. 44, No. 5, May 1996, pp. 1080-1091.

- [94] L. Cohen, "A general approach for obtaining joint representations in signal analysis - Part II: General class, mean and local values, and bandwidth," *IEEE Transactions on Signal Processing*, Vol. 44, No. 5, May 1996, pp. 1091-1099.
- [95] L. Cohen, "Time-frequency analysis," *Signal Processing Magazine*, Jan. 1999, pp. 22-28.
- [96] L. Cohen, "Time-frequency approach to radar, sonar and seismic wave propagation with dispersion and attenuation" *IET Signal Processing*, Vol. 4, No. 4, Aug. 2010, pp. 421-427.
- [97] E. T. Copson, "Asymptotic expansions," *Cambridge University Press*, New York, 1967.
- [98] C. Cornu, et al., "Generalized representation of phase derivatives for regular signals," *IEEE Transactions on Signal Processing*, Vol. 55, No. 10, Oct. 2007, pp. 4831-4838.
- [99] A. H. Costa and G. F. Boudreux-Bartels, "Design of time-frequency representations using a multiform, tilttable exponential kernel," *IEEE Transactions on Signal Processing*, Vol. 43, No. 10, Oct. 1995, pp. 2283-2302.
- [100] G. Cristobal, J. Bescos, and J. Santamaría, "Image analysis through the Wigner distribution function," *Appl. Opt.*, Vol. 28, No. 2, 1989, pp. 262-271.
- [101] G. Cristobal, C. Gonzalo, and J. Bescos, "Image filtering and analysis through the Wigner distribution function," in *Advances in Electronics and Electron Physics*, ed. P. W. Haekes, AcademicPress, Boston, MA, 1991.
- [102] G. S. Cunningham and W. J. Williams, "Vector-valued time-frequency representations," *IEEE Transactions on Signal Processing*, Vol. 44, No. 7, July 1996, pp. 1642-1657.
- [103] Z. Cvetković, "On discrete short-time Fourier analysis," *IEEE Transactions on Signal Processing*, Vol. 48, No. 9, Sept. 2000, pp. 2628-2640.
- [104] R. N. Czerwinski and D. L. Jones, "Adaptive cone-kernel time-frequency analysis," *IEEE Transactions on Signal Processing*, Vol. 43, No. 7, July 1995, pp. 1715-1719.
- [105] R. N. Czerwinski, D. L. Jones, "Adaptive short-time Fourier analysis," *IEEE Signal Processing Letters*, Vol. 4, No. 2, Feb. 1997, pp. 42-45.
- [106] M. Daković, T. Thayaparan, and LJ. Stanković, "Time-frequency-based detection of fast manoeuvring targets," *IET Signal Processing*, Vol. 4, No. 3, June 2010, pp. 287-297
- [107] M. Daković, T. Thayaparan, S. Djukanović, and LJ. Stanković, "Time-frequency-based non-stationary interference suppression for noise radar systems," *IET Radar, Sonar & Navigation*, Vol. 2, No. 4, Aug. 2008, pp. 306-314.
- [108] I. Daubechies, "Ten lecture on wavelets," SIAM, Philadelphia, Pennsylvania, 1992.
- [109] M. Davy, C. Doncarli, and G. F. Boudreux-Bartels, "Improved optimization of time-frequency-based signal classifiers," *IEEE Signal Processing Letters*, Vol. 8, No. 2, Feb. 2001, pp. 52-57.
- [110] M. Davy and A. Doucet, "Copulas: a new insight into positive time-frequency distributions," *IEEE Signal Processing Letters*, Vol. 10, No. 7, July 2003, pp. 215-218.
- [111] A. DeBrunner, M. Ozaydin, and T. Przebinda, "Resolution in time-frequency," *IEEE Transactions on Signal Processing*, Vol. 47, No. 3, Mar. 1999, pp. 783-788.
- [112] N. Delpart, et al., "Asymptotic wavelet and Gabor analysis: Extraction of instantaneous frequency," *IEEE Transactions on Information Theory*, Vol. 38, No. 2, Feb. /Mar. 1992, pp. 644-661.

- [113] C. De Luigi and E. Moreau, "An iterative algorithm for estimation of linear frequency modulated signal parameters," *IEEE Signal Processing Letters* . , Vol. 9, No. 4, April 2002, pp. 127-129.
- [114] E. J. Diethorn, "The generalized exponential time-frequency distribution," *IEEE Transactions on Signal Processing*, Vol. 42, No. 5, May 1994, pp. 1028-1037.
- [115] S. Djukanović, M. Daković, and LJ. Stanković, "Local polynomial Fourier transform receiver for nonstationary interference excision in DSSS communications," *IEEE Transactions on Signal Processing*, Vol. 56, No. 4, April 2008, pp. 1627-1636.
- [116] S. Djukanović and I. Djurović, "Aliasing detection and resolving in the estimation of polynomial-phase signal parameters," *Signal Processing*, Vol. 92, No. 1, pp. 235-239, Jan. 2012.
- [117] I. Djurović and LJ. Stanković, "Virtual instrument for time-frequency analysis," *IEEE Transactions on Instrumentation and Measurements*, Vol. 48, No. 6, Dec. 1999, pp. 1086-1092.
- [118] I. Djurović and LJ. Stanković, "Time-frequency representation based on the reassigned S-method," *Signal Processing*, Vol. 77, No. 1, Aug. 1999, pp. 115-120.
- [119] I. Djurović and LJ. Stanković, "Influence of high noise on the instantaneous frequency estimation using quadratic time-frequency distributions," *IEEE Signal Processing Letters*, Vol. 7, No. 11, Nov. 2000, pp. 317-319.
- [120] I. Djurović and LJ. Stanković, "Robust Wigner distribution with application to the instantaneous frequency estimation," *IEEE Transactions on Signal Processing*, Vol. 49, No. 12, Dec. 2001 , pp. 2985-2993.
- [121] I. Djurović, LJ. Stanković, and J. F. Böhme, "Robust L-estimation based forms of signal transforms and time-frequency representations," *IEEE Transactions on Signal Processing*, Vol. 51, No. 7, July 2003, pp. 1753-1761.
- [122] I. Djurović and LJ. Stanković, "Realization of robust filters in the frequency domain," *IEEE Signal Processing Letters*, Vol. 9, No. 10, Oct. 2002, pp. 333-335.
- [123] I. Djurović, LJ. Stanković, and J. F. Böhme, "Robust L-estimation based forms of signal transforms and time-frequency representations," *IEEE Transactions on Signal Processing*, Vol. 51, No. 7, July 2003, pp. 1753-1761.
- [124] I. Djurović and S. Stanković, "Estimation of time-varying velocities of moving objects by time-frequency representations," *IEEE Transactions on Image Processing*, Vol. 12, No. 5, May 2003, pp. 550-562.
- [125] I. Djurović, T. Thayaparan, and LJ. Stanković, "SAR imaging of moving targets using polynomial Fourier transform," *IET Signal Processing*, Vol. 2, No. 3, Sep. 2008, pp. 237-246.
- [126] I. Djurović, M. Simeunović, S. Djukanović, and P. Wang, "A hybrid CPF-HAF estimation of polynomial-phase signals: Detailed statistical analysis," *IEEE Transactions on Signal Processing*, Vol. 60, No. 10, Oct. 2012, pp. 5010-5023.
- [127] I. Djurović, et al., "Cubic-phase function evaluation for multicomponent signals with application to SAR imaging," *IET Signal Processing*, Vol. 4, No. 4, Aug. 2010, pp. 371-381.
- [128] I. Djurović, et al., "An efficient joint estimation of wideband polynomial-phase signal parameters and direction-of-arrival in sensor array," *EURASIP Journal on Advances in Signal Processing*, Vol. 2012, No. 1, Feb. 2012, pp. 43.

- [129] I. Djurović, “Viterbi algorithm for chirp-rate and instantaneous frequency estimation,” *Signal Processing*, Vol. 91, No. 5, May 2011, pp. 1308-1314.
- [130] D. Donoho, “Compressed sensing,” *IEEE Transactions on Information Theory*, 52(4), pp. 1289 - 1306, 2006
- [131] P. J. Durka, D. Ircha, and K. J. Blinowska, “Stochastic time-frequency dictionaries for matching pursuit,” *IEEE Transactions on Signal Processing*, Vol. 49, No. 3, March 2001, pp. 507-510.
- [132] P. Duvaut and D. Declerq, “Statistical properties of the pseudo Wigner-Ville representation of normal random processes,” *Signal Processing*, Vol. 75, No. 1, May 1999.
- [133] M. K. Emresoy and A. El-Jaroudi, “Iterative instantaneous frequency estimation and adaptive matched spectrogram,” *Signal Processing*, Vol. 64, No. 2, Feb. 1997.
- [134] M. K. Emresoy and P. J. Loughlin, “Weighted least squares implementation of Cohen-Posh time-frequency distributions,” *IEEE Transactions on Signal Processing*, Vol. 46, No. 3, Mar. 1998, pp. 753-758.
- [135] F. Zhang, G. Bi, and Y. Chen, “Tomography time-frequency transform,” *IEEE Transactions on Signal Processing*, Vol. 50, No. 6, June 2002, pp. 1289-1297.
- [136] P. Flandrin and B. Escudie, “Time and frequency representation of finite energy signals: a physical property as a result of a Hilbertian condition,” *Signal Processing*, Vol. 2, 1980, pp. 93-100.
- [137] P. Flandrin and F. Hlawatsch, “Signal representation geometry and catastrophes in the time-frequency plane,” in *Mathematics in Signal Processing*, T. Durrani et all eds. , Oxford, U. K. , Clarendon, 1987, pp. 3-14.
- [138] P. Flandrin and W. Martin, “The Wigner-Ville spectrum of nonstationary random signals,” in *The Wigner distribution: Theory and applications in signal processing*, Eds. W. Mecklenbrauker, F. Hlawatsch, pp. 211-267.
- [139] P. Flandrin and P. Borgnat, “Time-frequency energy distributions meet compressed sensing,” *IEEE Transactions on Signal Processing*, Vol. 58, No. 6, June 2010, pp. 2974-2982.
- [140] J. R. Fonollosa, “Positive time-frequency distributions based on joint marginal constraints,” *IEEE Transactions on Signal Processing*, Vol. 44, No. 8, Aug. 1996, pp. 2086-2092.
- [141] J. R. Fonollosa and C. L. Nikias, “Wigner higher order moment spectra: Definitions, properties, computation and application to transient signal analysis,” *IEEE Transactions on Signal Processing*, Vol. SP-41, pp. 245-266, Jan. 1993.
- [142] A. Francos and M. Porat, “Analysis and synthesis of multicomponent signals using positive time-frequency distributions,” *IEEE Transactions on Signal Processing*, Vol. 47, No. 2, Feb. 1999, pp. 493-504.
- [143] B. Friedlander and J. M. Francos, “Estimation of amplitude and phase parameters of multicomponent signals,” *IEEE Transactions on Signal Processing*, Vol. 43, No. 4, April 1995, pp. 917-927.
- [144] J. M. Francos and B. Friedlander, “Bounds for estimation of complex exponentials in unknown colored noise,” *IEEE Transactions on Signal Processing*, Vol. 43, No. 9, Sept. 1995, pp. 2176-2186.
- [145] S. Gabarda and G. Cristóbal, “Detection of events in seismic time series by time-frequency methods,” *IET Signal Processing*, Aug. 2010.

- [146] S. Gabarda and G. Cristóbal, "Speckle denoising through local Rényi entropy smoothing," *Computer Analysis of Images and Patterns Lecture Notes, in Computer Science*, Vol. 6855, 2011, pp 340-347.
- [147] D. Gabor, "Theory of communications," *Journal Inst. Elect. Eng.*, Vol. 93, 1946, pp. 423-457.
- [148] A. B. Gershman and M. G. Amin, "Wideband direction-of-arrival estimation of multiple chirp signals using spatial time-frequency distributions," *IEEE Signal Processing Letters*, Vol. 7, No. 6, June 2000, pp. 152-155.
- [149] B. W. Gillespie and L. E. Atlas, "Optimizing time-frequency kernels for classification," *IEEE Transactions on Signal Processing*, Vol. 49, No. 3, March 2001, pp. 485-496.
- [150] J. -M. Girault and D. Kouame, "Length and frequency of band-limited signals," *IEEE Signal Processing Letters*, Vol. 9, No. 11, Nov. 2002, pp. 371-374.
- [151] E. Giusti and M. Martorella, "Range Doppler and image autofocusing for FMCW inverse synthetic aperture radar," *IEEE Transactions on Aerospace and Electronic Systems*, Vol. 47, No. 4, Oct. 2011, pp. 2807-2823.
- [152] S. Golden and B. Friedlander, "A modification of the discrete polynomial transform," *IEEE Transactions on Signal Processing*, Vol. 46, No. 5, May 1998, pp. 1452–1456.
- [153] P. Goncalves and R. G. Baraniuk, "A pseudo Bertrand distribution for time-scale analysis," *IEEE Signal Processing Letters*, Vol. 3, No. 3, Mar. 1996, pp. 82-84.
- [154] P. Goncalves and R. G. Baraniuk, "Pseudo affine Wigner distributions: Definition and kernel formulation," *IEEE Transactions on Signal Processing*, Vol. 46, No. 6, June 1998, pp. 1505-1517.
- [155] J. Gosme, C. Richard, and P. Goncalves, "Adaptive diffusion as a versatile tool for time-frequency and time-scale representations processing: a review," *IEEE Transactions on Signal Processing*, Vol. 53, No. 11, Nov. 2005, pp. 4136- 4146.
- [156] E. Grall-Maes and P. Beauseroy, "Mutual information-based feature extraction on the time-frequency plane," *IEEE Transactions on Signal Processing*, Vol. 50, No. 4, April 2002, pp. 779-790.
- [157] R. M. Gray and J. W. Goodman, *Fourier transforms*, Kluwer Academic Publishers, 1995.
- [158] D. Groutage, "A fast algorithm for computing minimum cross-entropy positive time-frequency distributions," *IEEE Transactions on Signal Processing*, Vol. 45, No. 8, Aug. 1997, pp. 1954-1971.
- [159] D. Groutage and D. Bennink, "Feature sets for nonstationary signals derived from moments of the singular value decomposition of Cohen-Posch, (positive time-frequency) distributions," *IEEE Transactions on Signal Processing*, Vol. 48, No. 5, May 2000, pp. 1498-1503.
- [160] H. Gu, "Ambiguity function and Cramer-Rao bound in the multisignal case," *IEE Proceedings: Radar, Sonar and Navigation*, Vol. 143, No. 4, Mar. 1997.
- [161] I. B. Gwan, A. Papandreou-Suppappola, and G. F. Boudreux-Bartels, "Wideband Weyl symbols for dispersive time-varying processing of systems and random signals," *IEEE Transactions on Signal Processing*, Vol. 50, No. 5, May 2002, pp. 1077-1090.
- [162] A. Hanssen and L. L. Scharf, "A theory of polyspectra for nonstationary stochastic processes," *IEEE Transactions on Signal Processing*, Vol. 51, No. 5, May 2003, pp. 1243-1252.

- [163] S. B. Hearon and M. G. Amin, "Minimum-variance time-frequency distribution kernels," *IEEE Transactions on Signal Processing*, Vol. 43, No. 5, May 1995, pp. 1258-1262.
- [164] C. Herley, J. Kovačević, K. Ramchandran, and M. Vetterli, "Tilings of the time-frequency plane: Construction of arbitrary orthogonal bases and fast tiling algorithms," *IEEE Transactions on Signal Processing*, Vol. 41, No. 12, Dec. 1993, pp. 3341-3359.
- [165] M. J. Hinich and H. Messer, "On the principal domain of the discrete bispectrum of a stationary signal," *IEEE Transactions on Signal Processing*, Vol. 43, No. 9, Sept. 1995, pp. 2130-2135.
- [166] F. Hlawatsch, "Duality and classification of bilinear time-frequency signal representation," *IEEE Transactions on Signal Processing*, Vol. 39, July 1991, pp. 1564-1574.
- [167] F. Hlawatsch and H. Bolcskei, "Covariant time-frequency distributions on conjugate operators," *IEEE Signal Processing Letters*, Vol. 3, No. 2, Feb. 1996, pp. 44-46.
- [168] F. Hlawatsch and G. F. Boudreux-Bartels, "Linear and quadratic time-frequency signal representations," *IEEE Signal Processing Magazine*, April 1992, pp. 21-67.
- [169] F. Hlawatsch and P. Flandrin, "The interference structure of Wigner distribution and related time-frequency signal representations," in *The Wigner Distribution-Theory and Applications in Signal Processing*, W. Mecklenbrauker, Ed, Amsterdam: Elsevier Science 1992.
- [170] F. Hlawatsch and W. Kozek, "Time-frequency projection filters and time-frequency signal expansions," *IEEE Transactions on Signal Processing*, Vol. 42, No. 12, Dec. 1994
- [171] F. Hlawatsch and W. Krattenthaler, "Phase matching algorithms for Wigner-distribution signal synthesis," *IEEE Transactions on Signal Processing*, Vol. 39, No. 3, Mar. 1991, pp. 612-619.
- [172] F. Hlawatsch and W. Krattenthaler, "Bilinear signal synthesis," *IEEE Transactions on Signal Processing*, Vol. 40, No. 2, Feb. 1992, pp. 352-363.
- [173] F. Hlawatsch and W. Krattenthaler, "Signal synthesis algorithms for bilinear time-frequency signal representations," in *The Wigner Distribution-Theory and Applications in Signal Processing*, W. Mecklenbrauker, Ed, Amsterdam: Elsevier 1997.
- [174] F. Hlawatsch, A. Papandreou-Suppappola, and G. F. Boudreux-Bartels, "The hyperbolic class of quadratic time-frequency representations - Part II: Subclasses, intersection with the affine and power classes, regularity, and unitarity," *IEEE Transactions on Signal Processing*, Vol. 45, No. 2, Feb. 1997, pp. 303-316.
- [175] F. Hlawatsch, G. Matz, H. Kirchauer, and W. Kozek, "Time-frequency formulation, design, and implementation of time-varying optimal filters for signal estimation," *IEEE Transactions on Signal Processing*, Vol. 48, No. 5, May 2000, pp. 1417-1432.
- [176] T. K. Hon and A. Georgakis, "Enhancing the resolution of the spectrogram based on a simple adaptation procedure," *IEEE Transactions on Signal Processing*, Vol. 60, No. 10, Oct. 2012, pp. 5566 - 5571.
- [177] P. Honeine, C. Richard, and P. Flandrin, "Time-frequency learning machines," *IEEE Transactions on Signal Processing*, Vol. 55, No. 7, July 2007, pp. 3930-3936.
- [178] J. Hormigo and G. Cristobal, "High resolution spectral analysis of images using the pseudo-Wigner distribution," *IEEE Transactions on Signal Processing*, Vol. 46, No. 6, June 1998, pp. 1757-1763.

- [179] C. Hory, N. Martin, and A. Chehikian, "Spectrogram segmentation by means of statistical features for non-stationary signal interpretation," *IEEE Transactions on Signal Processing*, Vol. 50, No. 12, Dec. 2002, pp. 2915-2925.
- [180] P. J. Huber, *Robust Statistics*, John Wiley&Sons Inc., 1981.
- [181] Z. M. Hussain and B. Boashash, "Adaptive instantaneous frequency estimation of multicomponent FM signals using quadratic time-frequency distributions," *IEEE Transactions on Signal Processing*, Vol. 50, No. 8, Aug. 2002, pp. 1866-1876.
- [182] Q. Q. Huynh, L. N. Cooper, N. Intrator, and H. Shouval, "Classification of underwater mammals using feature extraction based on time-frequency analysis and BCM theory," *IEEE Transactions on Signal Processing*, Vol. 46, No. 5, May 1998, pp. 1202-1208.
- [183] B. G. Iem, A. Papandreou-Suppappola, and G. F. Boudreault-Bartels, "Classes of smoothed Weyl symbols," *IEEE Signal Processing Letters*, Vol. 7, No. 7, July 2000, pp. 186-188.
- [184] C. Ioana, A. Quinquis, and Y. Stephan, "Feature Extraction From Underwater Signals Using Time-Frequency Warping Operators," *IEEE Journal of Oceanic Engineering*, Vol. 31, No. 3, July 2006, pp. 628-645.
- [185] C. Ioana, et al., "Localization in underwater dispersive channels using the time-frequency-phase continuity of signals," *IEEE Transactions on Signal Processing*, Vol. 58, No. 8, Aug. 2010, pp. 4093-4107.
- [186] V. Ivanović, LJ. Stanković, and D. Petranović, "Finite word-length effects in implementation of distributions for time-frequency signal analysis," *IEEE Transactions on Signal Processing*, Vol. 46, No. 7, July 1998, pp. 2035-2041.
- [187] V. N. Ivanović, M. Daković, and LJ. Stanković, "Performance of quadratic time-frequency distributions as instantaneous frequency estimators," *IEEE Transactions on Signal Processing*, Vol. 51, No. 1, Jan. 2003, pp. 77-89.
- [188] V. N. Ivanović and S. Jovanovski, "Signal adaptive system for time-frequency analysis," *Electronics Letters*, Vol. 44, No. 21, Oct. 9 2008, pp. 1279-1280.
- [189] V. N. Ivanović, N. Radović, and S. Jovanovski, "Real-time design of space/spatial-frequency optimal filter," *Electronics Letters*, Vol. 46, No. 25, Dec. 2010, pp. 1696-1697.
- [190] V. N. Ivanović and R. Stojanović, "An efficient hardware design of the flexible 2-D system for space/spatial-frequency signal analysis," *IEEE Transactions on Signal Processing*, Vol. 55, No. 6, pp. 3116-3125, June 2007.
- [191] V. N. Ivanović, R. Stojanović, and LJ. Stanković, "Multiple clock cycle architecture for the VLSI design of a system for time-frequency analysis," *EURASIP Journal on Applied Signal Processing, Special Issue on Design Methods for DSP Systems*, Vol. 2006, pp. 1-18.
- [192] M. Jabloun, F. Leonard, M. Vieira, and N. Martin, "A new flexible approach to estimate the IA and IF of nonstationary signals of long-time duration," *IEEE Transactions on Signal Processing*, Vol. 55, No. 7, July 2007, pp. 3633-3644.
- [193] L. Jacobson and H. Wechsler, "Joint spatial/spatial-frequency representation," *Signal Processing*, Vol. 14, 1988, pp. 37-68.
- [194] A. J. E. M. Janssen, "On the locus and spread of pseudo density functions in the time-frequency plane," *Phillips Journal of Research*, Vol. 37, 1982, pp. 79-110.

- [195] A. J. E. M. Janssen, "The Zak transform: A signal transform for sampled time-continuous signals," *Philips Journal of Research*, Vol. 43, 1988, pp. 23-69.
- [196] A. J. E. M. Janssen, "Wigner weight functions and Weyl symbols of nonnegative definite linear operators," *Philips Journal of Research*, Vol. 44, 1989, pp. 7-42.
- [197] S. -W. Jee, C. -H. Lee, and K. -S. Lee, "Signal analysis methods to distinguish tracking process using time-frequency analysis," *IEEE Transactions on Dielectrics and Electrical Insulation*, Vol. 16, No. 1, Feb. 2009, pp. 99-106.
- [198] J. Jeong, G. S. Cunningham, W. and J. Williams, "The discrete-time phase derivative as a definition of discrete instantaneous frequency and its relation to discrete time-frequency distributions," *IEEE Transactions on Signal Processing*, Vol. 43, No. 1, Jan. 1995, pp. 341-344.
- [199] J. Jeong and W. J. Williams, "Kernel design for reduced interference distributions," *IEEE Transactions on Signal Processing*, Vol. 40, No. 2, Feb. 1992, pp. 402-412.
- [200] J. Jeong and W. J. Williams, "Mechanism of the cross-terms in spectrograms," *IEEE Transactions on Signal Processing*, Vol. 40, No. 10, Oct. 1992, pp. 2608-2613.
- [201] J. Jeong and W. J. Williams, "Alias-free generalized discrete-time time-frequency distributions," *IEEE Transactions on Signal Processing*, Vol. 40, No. 11, Nov. 1992, pp. 2757-2765.
- [202] J. A. Johnston, "Wigner distribution and FM radar signal design," *IEE Proc. Part F*, Vol. 136, No. 2, Apr. 1989, pp. 81-87.
- [203] D. L. Jones and R. G. Baraniuk, "An adaptive optimal-kernel time-frequency representation," *IEEE Transactions on Signal Processing*, Vol. 43, No. 10, Oct. 1995, pp. 2361-2372.
- [204] D. L. Jones and T. W. Parks, "A high resolution data-adaptive time-frequency representation," *IEEE Transactions on Signal Processing*, Vol. 38, No. 12, Dec. 1990, pp. 2127-2135.
- [205] S. Joshi and J. M. Morris, "On a novel critically-sampled discrete-time Gabor transform," *Signal Processing*, Vol. 61, No. 1, Jan. 1997.
- [206] S. Kadamb and G. F. Boudreux-Bartels, "A comparison of the existence of 'cross terms' in the Wigner distribution and the squared magnitude of the Wavelet transform and Short-time Fourier transform," *IEEE Transactions on Signal Processing*, Vol. 40, No. 10, Oct. 1992, pp. 2498-2517.
- [207] V. Katkovnik, "A new form of the Fourier transform for time-frequency estimation," *Signal Processing*, Vol. 47, No. 2, 1995, pp. 187-200.
- [208] V. Katkovnik, "Local polynomial approximation of the instantaneous frequency: Asymptotic accuracy," *Signal Processing*, Vol. 52, No. 3, Mar. 1996.
- [209] V. Katkovnik, "Nonparametric estimation of the instantaneous frequency," *IEEE Transactions on Information Theory*, Vol. 43, No. 1, Jan. 1997, pp. 183-189.
- [210] V. Katkovnik, "Discrete-time local polynomial approximation of the instantaneous frequency," *IEEE Transactions on Signal Processing*, Vol. 46, No. 10, Oct. 1998, pp. 2626-2638.
- [211] V. Katkovnik and LJ. Stanković, "Instantaneous frequency estimation using the Wigner distribution with varying and data-driven window length," *IEEE Transactions on Signal Processing*, Vol. 46, No. 9, Sept. 1998, pp. 2315-2326.
- [212] V. Katkovnik and LJ. Stanković, "Periodogram with varying and data-driven window length," *Signal Processing*, Vol. 67, N3, 1998, pp. 345-358.

- [213] A. S. Kayhan, "Difference equation representation of chirp signals and instantaneous frequency/amplitude estimation," *IEEE Transactions on Signal Processing*, Vol. 44, No. 12, Dec. 1996, pp. 2948-2959.
- [214] L. Knockaert, "A class of positive isentropic time-frequency distributions," *IEEE Signal Processing Letters*, Vol. 9, No. 1, Jan. 2002, pp. 22-25.
- [215] D. Konig and J. F. Böhme, "Wigner-Ville spectral analysis of automotive signals captured at knock," *Applied Signal Processing*, No. 3, 1996, pp. 54-64.
- [216] J. Kovačević and M. Vetterli, "Non-separable multidimensional perfect reconstruction filter banks and wavelet bases for R^n ," *IEEE Transactions on Information theory*, Vol. 38, Mar. 1992, pp. 533-555.
- [217] J. Kovačević and M. Vetterli, "Nonseparable two- and three-dimensional wavelets," *IEEE Transactions on Signal Processing*, Vol. 43, No. 5, pp. 1269-1273, May 1995.
- [218] W. Kozek, "Time-frequency signal processing based on the Wigner-Weyl framework," *Signal Processing*, Vol. 29, No. 1, Oct. 1992, pp. 77-92.
- [219] W. Krattenthaler and F. Hlawatsch, "Time-frequency design and processing of signals via smoother Wigner distributions," *IEEE Transactions on Signal Processing*, Vol. 41, No. 1, Jan. 1993, pp. 278-287.
- [220] P. K. Kumar and K. M. M. Prabhu, "Simulation studies of moving target detection: A new approach with Wigner-Ville distribution," *IEE Proceedings: Radar, Sonar, and Navigation*, Vol. 144, No. 5, May 1998.
- [221] R. Kumaresan and A. Rao, "On minimum/maximum/all-pass decompositions in time and frequency domains," *IEEE Transactions on Signal Processing*, Vol. 48, No. 10, Oct. 2000, pp. 2973-2976.
- [222] H. K. Kwok and D. L. Jones, "Improved instantaneous frequency estimation using an adaptive short-time Fourier transform," *IEEE Transactions on Signal Processing*, Vol. 48, No. 10, Oct. 2000, pp. 2964-2972.
- [223] H. Laurent and C. Doncarli, "Stationarity index for abrupt changes detection in the time-frequency plane," *IEEE Signal Processing Letters*, Vol. 5, No. 2, Feb. 1998, pp. 43-45.
- [224] J. C. Liu and H. C. Chiang, "Fast Computation of high resolution Hartley transform at arbitrary frequencies," *Signal Processing*, Vol. 44, No. 2, Feb. 1995.
- [225] T. Le, M. Glesner, "A flexible and approximate computing approach for time-frequency distributions," *IEEE Transactions on Signal Processing*, Vol. 48, No. 4, April 2000, pp. 1193-1196.
- [226] B. Leprettre, N. Martin, F. Glangeaud, and J. -P. Navarre, "Three-component signal recognition using time, time-frequency, and polarization information - Application to seismic detection of avalanches," *IEEE Transactions on Signal Processing*, Vol. 46, No. 1, Jan. 1998, pp. 83-103.
- [227] J. Lerga and V. Sucic, "Nonlinear IF Estimation Based on the Pseudo WVD Adapted Using the Improved Sliding Pairwise ICI Rule," *IEEE Signal Processing Letters*, Vol. 16, No. 11, Nov. 2009, pp. 953-956.
- [228] A. R. Leyman, Z. M. Kamran, and K. Abed-Meraim, "Higher-order time frequency-based blind source separation technique," *IEEE Signal Processing Letters*, Vol. 7, No. 7, July 2000, pp. 193-196.

- [229] W. Lin and M. Xiaofeng, "An adaptive Generalized S-transform for instantaneous frequency estimation," *Signal Processing*, Vol. 91, No. 8, Aug. 2011, pp. 1876–1886.
- [230] K. J. R. Liu, "Novel parallel architecture for short time Fourier transform," *IEEE Transactions on Circuits and Systems II*, Vol. 40, No. 12, Dec. 1993, pp. 786-789.
- [231] P. J. Loglino, "Comments on scale invariance of time-frequency distributions," *IEEE Signal Processing Letters*, Vol. 2, No. 12, Dec. 1995, pp. 217-218.
- [232] P. J. Loughlin, J. Pitton, and B. Hannaford, "Approximating time-frequency density functions via optimal combinations of spectrograms," *IEEE Signal Processing Letters*, Vol. 1, No. 12, Dec. 1994, pp. 199-202.
- [233] P. J. Loughlin and B. Tacer, "Comments on the interpretation of instantaneous frequency," *IEEE Signal Processing Letters*, Vol. 4, No. 5, May 1997, pp. 123-125.
- [234] P. J. Loughlin and K. L. Davidson, "Instantaneous kurtosis," *IEEE Signal Processing Letters*, Vol. 7, No. 6, June 2000, pp. 156-159.
- [235] P. J. Loughlin and K. L. Davidson, "Modified Cohen-Lee time-frequency distributions and instantaneous bandwidth of multicomponent signals," *IEEE Transactions on Signal Processing*, Vol. 49, No. 6, June 2001, pp. 1153-1165.
- [236] C. Lu, S. Joshi, and J. Morris, "Parallel lattice structure of bloc time-recursive generalized Gabor transforms," *Signal Processing*, Vol. 57, No. 2, Feb. 1997.
- [237] S. Lu and P. C. Doerschuk, "Nonlinear modeling and processing of speech based on sums of AM-FM formant models," *IEEE Transactions on Signal Processing*, Vol. 44, No. 4, Apr. 1996, pp. 773-783.
- [238] Y. Lu and J. M. Morris, "Some results on discrete Gabor transforms for finite periodic sequences," *IEEE Transactions on Signal Processing*, Vol. 46, No. 6, June 1998, pp. 1703-1708.
- [239] Y. Lu, J. Morris, and H. G. Feichtinger, "On a complementary to derivation of discrete Gabor expansions," *IEEE Signal Processing Letters*, Vol. 4, No. 1, Jan. 1997, pp. 12-14.
- [240] X. Lv, G. Bi, C. Wan, and M. Xing, "Lv's distribution: Principle, implementation, properties, and performance," *IEEE Transactions on Signal Processing*, Vol. 59, No. 8, Aug. 2011, pp. 3576-3591.
- [241] N. Ma, D. Vray, Ph. Delacharte, and G. Gimenez, "Time-frequency representation of multicomponent chirp signals," *Signal Processing*, Vol. 56, No. 2, Feb. 1996.
- [242] N. H. Morgan and A. S. Gevins, "Wigner distributions of human event-related brain potentials," *IEEE Transactions on Biomedical engineering*, Vol. 33, No. 1, Jan 1986, pp. 66-70.
- [243] S. Mann and S. Haykin, "The chirplet transform: Physical considerations," Vol. 43, No. 11, Nov. 1995, pp. 2745-2761.
- [244] W. Martin and P. Flandrin, "Wigner-Will spectral analysis of nonstationary processes," *IEEE Transactions on Acoustics, Speech and Signal Processing*, Vol. 33, No. 6, Dec. 1985, pp. 1461-1470.
- [245] M. Martorella, "Novel approach for ISAR image cross-range scaling," *IEEE Transactions on Aerospace and Electronic Systems*, Vol. 44, No. 1, Jan. 2008, pp. 281-294.

- [246] G. Matz, F. Hlawatsch, and W. Kozek, "Generalized evolutionary spectral analysis and the Weyl spectrum of nonstationary random processes," *IEEE Transactions on Signal Processing*, Vol. 45, No. 6, June 1997, pp. 1520-1534.
- [247] W. F. G. Mecklenbrauker and F. Hlawatsch Eds, "The Wigner distributions - theory and applications in signal processing," Elsevier, 1997.
- [248] J. M. Mendel, "Tutorial on higher-order statistics (spectra) in signal processing and system theory: Theoretical results and some applications," *IEEE Proc.*, Vol. 79, No. 3, Mar. 1991, pp. 278-305.
- [249] F. Millioz and N. Martin, "Circularity of the STFT and spectral kurtosis for time-frequency segmentation in Gaussian environment," *IEEE Transactions on Signal Processing*, Vol. 59, No. 2, Feb. 2011, pp. 515-524.
- [250] S. K. Mitra, *Digital Signal Processing: A computer based approach*, McGraw-Hill, 1996.
- [251] J. M. Morris and D. Wu, "On alias-free formulations of discrete-time Cohen's class of distributions," *IEEE Transactions on Signal Processing*, Vol. 44, No. 6, June 1996, pp. 1355-1365.
- [252] W. Mu, M. G. Amin, and Y. Zhang, "Bilinear signal synthesis in array processing," *IEEE Transactions on Signal Processing*, Vol. 51, No. 1, Jan. 2003, pp. 90-100.
- [253] S. W. Nam and E. J. Powers, "Volterra series representation of time-frequency distributions," *IEEE Transactions on Signal Processing*, Vol. 51, No. 6, June 2003, pp. 1532-1537.
- [254] J. L. Navarro-Mesa, E. Lleida-Solano, and A. Moreno-Bilbao, "A new method for epoch detection based on the Cohen's class of time frequency representations," *IEEE Signal Processing Letters*, Vol. 8, No. 8, Aug. 2001, pp. 225-227.
- [255] S. R. Nelatury and B. G. Mobasseri, "Synthesis of discrete-time discrete-frequency Wigner distribution," *IEEE Signal Processing Letters*, Vol. 10, No. 8, Aug. 2003, pp. 221-224.
- [256] A. H. Nutall, "Signal Processing studies," *Technical report*, NUSC, New London, CT, 1989.
- [257] S. Oh and R. J. Marks II, "Some properties of generalized time-frequency representation with cone-shaped kernels," *IEEE Transactions on Signal Processing*, Vol. 40, No. 7, July 1992, pp. 1735-1745.
- [258] J. R. O'Hair and B. W. Suter, "The Zak transform and decimated time-frequency distributions," *IEEE Transactions on Signal Processing*, Vol. 44, No. 5, May 1996, pp. 1099-1111.
- [259] J. C. O'Neill and W. J. Williams, "Shift covariant time-frequency distributions of discrete signals," *IEEE Transactions on Signal Processing*, Vol. 47, No. 1, Jan. 1999, pp. 133-146.
- [260] J. C. O'Neill and W. J. Williams, "A function of time, frequency, lag and Doppler," *IEEE Transactions on Signal Processing*, Vol. 47, No. 3, Mar. 1999, pp. 1789-799.
- [261] J. C. O'Neill and P. Flandrin, "Virtues and vices of quartic time-frequency distributions," *IEEE Transactions on Signal Processing*, Vol. 48, No. 9, Sept. 2000, pp. 2641-2650.
- [262] J. C. O'Neill, P. Flandrin, and W. J. Williams, "On the existence of discrete Wigner distributions," *IEEE Signal Processing Letters*, Vol. 6, No. 12, Dec. 1999, pp. 304-307.
- [263] A. V. Oppenheim and R. W. Schafer, *Digital Signal Processing*, Prentice-Hall, New Jersey, 1975.
- [264] I. Orović, M. Orlandic, S. Stanković, and Z. Uskoković, "A Virtual Instrument for Time-Frequency Analysis of Signals With Highly Nonstationary Instantaneous Frequency," *IEEE Transactions on Instrumentation and Measurement*, Vol. 60, No. 3, March 2011, pp. 791-803.

- [265] I. Orovčić, S. Stanković, T. Thayaparan, and LJ. Stanković, “Multiwindow S-method for instantaneous frequency estimation and its application in radar signal analysis,” *IET Signal Processing*, Vol. 4, No. 4, Aug. 2010, pp. 363-370.
- [266] R. S. Orr, “The order of computation of finite discrete Gabor transform.” *IEEE Transactions on Signal Processing*, Vol. 41, No. 1, Jan. 1993, pp. 122-130.
- [267] P. O’Shea, “A new technique for instantaneous frequency rate estimation,” *IEEE Signal Processing Letters*, Vol. 9, No. 8, Aug. 2002, pp. 251-252.
- [268] J. M. O’Toole, M. Mesbah, and B. Boashash, “Accurate and efficient implementation of the time-frequency matched filter,” *IET Signal Processing*, Vol. 4, No. 4, Aug. 2010, pp. 428-437.
- [269] J. M. O’Toole, M. Mesbah, and B. Boashash, “A new discrete analytic signal for reducing aliasing in the discrete Wigner-Ville distribution ,” *IEEE Transactions on Signal Processing*, Vol. 56, No. 11, Nov. 2008, pp. 5427-5434.
- [270] X. Ouyang and M. G. Amin, “Short-time Fourier transform receiver for nonstationary interference excision in direct sequence spread spectrum communications,” *IEEE Transactions on Signal Processing*, Vol. 49, No. 4, April 2001, pp. 851-863.
- [271] H. M. Ozaktas, O. Arikan, M. A. Kutay, and G. Bozdagi, “Digital computation of the fractional Fourier transform,” *IEEE Transactions on Signal Processing*, Vol. 44, No. 9, Sept. 1996, pp. 2141-2151.
- [272] H. M. Ozaktas, N. Erkaya, and M. A. Kutay, “Effect of fractional Fourier transformation on time-frequency distributions belonging to the Cohen class,” *IEEE Signal Processing Letters*, Vol. 3, No. 2, Feb. 1996, pp. 40-41.
- [273] A. K. Ozdemir and O. Arikan, “Fast computation of the ambiguity function and the Wigner distribution on arbitrary line segments,” *IEEE Transactions on Signal Processing*, Vol. 49, No. 2, Feb. 2001, pp. 381-393.
- [274] C. H. Page, “Instantaneous power spectra,” *Journal Appl. Phys.*, Vol. 23, 1952, pp. 103-106.
- [275] A. Papandreou and G. F. Boudreux-Bartels, “Generalization of the Choi-Williams distribution and the Butterworth distribution for time-frequency analysis,” *IEEE Transactions on Signal Processing*, Vol. 41, No. 1, jan. 1993, pp. 463-472.
- [276] A. Papandreou-Suppappola, R. L. Murray, I. Byeong-Gwan, and G. F. Boudreux-Bartels, “Group delay shift covariant quadratic time-frequency representations,” *IEEE Transactions on Signal Processing*, Vol. 49, No. 11, Nov. 2001, pp. 2549-2564.
- [277] A. Papandreou-Suppappola and S. B. Suppappola, “Analysis and classification of time-varying signals with multiple time-frequency structures,” *IEEE Signal Processing Letters*, Vol. 9, No. 3, March 2002, pp. 92-95.
- [278] A. Papoulis, *Signal analysis*, McGraw Hill Book Company, New York, 1977.
- [279] M. Pasquier, P. Gonclaves, and R. Baraniuk, “Hybrid linear/bilinear time-scale analysis,” *IEEE Transactions on Signal Processing*, Vol. 47, No. 1, Jan. 1999, pp. 254-260.
- [280] S. C. Pei and E. J. Tsai, “Cross-terms analysis in the modified instantaneous power spectrum,” *IEEE Transactions on Signal Processing*, Vol. 41, No. 1, Jan. 1993, pp. 477-480.
- [281] S. C. Pei and E. J. Tsai, “New time-frequency distribution,” *Circuits, Systems, and Signal Processing*, Vol. 14, No. 4, Apr. 1998.

- [282] S. C. Pei and I. I. Yang, "High resolution Wigner distribution using chirp z-transform analysis," *IEEE Transactions on Signal Processing*, Vol. 39, No. 7, July 1991, pp. 1699-1702.
- [283] S. C. Pei and I. I. Yang, "Computing pseudo Wigner distribution by the fast Hartley transform," *IEEE Transactions on Signal Processing*, Vol. 40, No. 9, Sep. 1992, pp. 2346-2349.
- [284] S. C. Pei and M. H. Yeh, "Time frequency split Zak transform for finite Gabor expansion," *Signal Processing*, Vol. 52, No. 3, Mar. 1996.
- [285] S. C. Pei, "Two-dimensional affine generalized fractional Fourier transform," *IEEE Transactions on Signal Processing*, Vol. 49, No. 4, April 2001, pp. 878-897.
- [286] S. C. Pei and Jian-Jiun Ding, "Relations between fractional operations and time-frequency distributions, and their applications," *IEEE Transactions on Signal Processing*, Vol. 49, No. 8, Aug. 2001, pp. 1638-1655.
- [287] S. Peleg and B. Friedlander, "The discrete polynomial-phase transform," *IEEE Transactions on Signal Processing*, Vol. 43, No. 8, Aug. 1995, pp. 1901-1915.
- [288] S. Peleg and B. Porat, "Estimation and classification of polynomial phase signals," *IEEE Transactions on Information Theory*, No. 3, Mar. 1991, pp. 422-430.
- [289] S. Peleg, B. Porat, and B. Friedlander, "The achievable accuracy in estimating the instantaneous phase and frequency of a constant amplitude signal," *IEEE Transactions Signal Processing*, Vol. 41, pp. 2216-2223, June 1993.
- [290] D. Petranović, S. Stanković, and LJ. Stanković, "Special purpose hardware for time-frequency analysis," *Electronics Letters*, Vol. 33, No. 6, Mar. 1997, pp. 464-466.
- [291] F. Peyrin and R. Prost, "A unified definition for the discrete-time, discrete frequency, and discrete time/frequency Wigner distributions," *IEEE Transactions on Acoustics, Speech and Signal Processing*, Vol. 34, No. 4, Aug. 1986, pp. 858-867.
- [292] W. J. Pielemeir, G. H. Wakefield, and M. H. Simoni, "Time-frequency analysis of musical signals," *Proc. IEEE*, Vol. 84, No. 9, Sept, pp. 1216-1230.
- [293] J. W. Pitton and L. E. Atlas, "Discrete-time implementation of the cone-kernel time-frequency representation," *IEEE Transactions on Signal Processing*, Vol. 43, No. 8, Aug. 1995, pp. 1996-1998.
- [294] J. W. Pitton, K. Wang, and B. H. Juang, "Time-frequency analysis of auditory modeling for automatic recognition of speech," *Proc. IEEE*, Vol. 84, No. 9, Sept, pp. 1199-1215.
- [295] B. Porat, "*Digital processing of random signals*," Prentice Hall, 1994.
- [296] B. Porat and B. Friedlander, "Asymptotic analysis of the high-order ambiguity function for parameter estimation of the polynomial-phase signal," *IEEE Transactions on Information theory*, Vol. 42, pp. 995-1001, May 1996.
- [297] W. A. Porter, "Computational aspects of quadratic signal processing," *IEEE Transactions on Acoustics, Speech and Signal Processing*, Vol. 38, No. 1, Jan. 1990, pp. 137-144.
- [298] K. M. M. Prabhu and R. S. Sundaram, "Fixed-point error analysis of discrete Wigner-Ville distribution," *IEEE Transactions on Signal Processing*, Vol. 45, No. 10, Oct. 1997, pp. 2579-2582.

- [299] S. A. Qazi and L. K. Stergioulas, "Higher-order nested Wigner distributions: Properties and applications," *IEEE Transactions on Signal Processing*, Vol. 54, No. 12, Dec. 2006, pp. 4662-4674.
- [300] S. Qazi, A. Georgakis, L. K. Stergioulas, and M. Shikh-Bahaei, "Interference suppression in the Wigner distribution using fractional Fourier transformation and signal synthesis," *IEEE Transactions on Signal Processing*, Vol. 55, No. 6, June 2007, pp. 3150-3154. .
- [301] L. Qui, H. Yang, and S. N. Koh, "Fundamental frequency determination based on wavelet transform and instantaneous frequency estimation," *Signal Processing*, Vol. 44, No. 2, Feb. 1995.
- [302] S. Qui, "The undersampled discrete Gabor transform," *IEEE Transactions on Signal Processing*, Vol. 46, No. 5, May 1998, pp. 1221-1229.
- [303] S. Qian and D. Chen, "Joint Time-Frequency Analysis," Englewood Cliffs, NJ, Prentice Hall, 1996.
- [304] S. Qian: *Introduction to Time-Frequency and Wavelet Transforms*, Prentice Hall, Dec. 2001
- [305] *Proceedings of the IEEE*, special issue on Time-Frequency Analysis, Vol. 84, No. 9, Sep. 1996.
- [306] L. Rankine, M. Mesbah, and B. Boashash, "IF estimation for multicomponent signals using image processing techniques in the time-frequency domain," *Signal Processing*, Vol. 87, No. 6, June 2007, pp. 1234-1250.
- [307] P. Rao and F. J. Taylor, "Estimation of IF using the discrete Wigner-Ville distribution," *Electronic Letters*, Vol. 26, pp. 246-248, 1990.
- [308] T. Reed and H. Wechsler, "Segmentation of textured images and Gestalt organization using spatial/spatial-frequency representations," *IEEE Transactions Pattern Analysis, Mach. Intell.*, Vol. 12, No. 1, 1990, pp. 1-12.
- [309] D. C. Reid, A. M. Zoubir, and B. Boashash, "Aircraft flight parameter estimation based on passive acoustic techniques using the polynomial Wigner-Ville distribution, *J. Acoust. Soc. Am.*, Vol. 102, No. 1, pp. 207-223, 1997.
- [310] C. Richard, "Linear redundancy of information carried by the discrete Wigner distribution," *IEEE Transactions on Signal Processing*, Vol. 49, No. 11, Nov. 2001, pp. 2536-2544.
- [311] C. Richard, "Time-frequency-based detection using discrete-time discrete-frequency Wigner distributions," *IEEE Transactions on Signal Processing*, Vol. 50, No. 9, Sept. 2002, pp. 2170-2176.
- [312] C. Richard and R. Lengelle, "Joint recursive implementation of time-frequency representations and their modified version by the reassignment method," *Signal Processing*, Vol. 60, No. 2, pp. 163-179, 1997.
- [313] C. Richard and R. Lengelle, "On the linear relations connecting the components of the discrete Wigner distribution in the case of real-valued signals," *Proc. IEEE ICASSP*, Vol. 1, pp. 85-88 Vol. 1, 2000.
- [314] M. S. Richman, T. W. Parks, and R. G. Shenoy, "Discrete-time, discrete-frequency, time-frequency analysis," *IEEE Transactions on Signal Processing*, Vol. 46, No. 6, June 1998, pp. 1517-1528.
- [315] A. W. Rihaczek, "Signal energy distribution in time and frequency," *IEEE Transactions on Information Theory*, Vol. 14, 1968, pp. 369-374.

- [316] G. Rilling and P. Flandrin, "One or two Frequencies? The Empirical mode decomposition answers," *IEEE Transactions on Signal Processing*, Vol. 56, No. 1, Jan. 2008, pp. 85-95.
- [317] B. Ristic and B. Boashash, "Kernel design for time-frequency signal analysis using the Radon transform," *IEEE Transactions on Signal Processing*, Vol. 41, No. 5, May 1993, pp. 1996-2008.
- [318] B. Ristic and B. Boashash, "Relationship between the polynomial and higher-order Wigner-Ville distribution," *IEEE Signal Processing Letters*, Vol. 2, No. 12, Dec. 1995, pp. 227-229.
- [319] B. Ristic and B. Boashash, "Instantaneous frequency estimation of quadratic and cubic FM signals using the cross polynomial Wigner-Ville distribution," *IEEE Transactions on Signal Processing*, Vol. 44, No. 6, June 1996, pp. 1549-1553.
- [320] O. Rioul and P. Flandrin, "Time-scale energy distributions: A general class extending wavelet transforms," *IEEE Transactions on Signal Processing*, No. 7, July 1992, pp. 1746-1757.
- [321] O. Rioul and M. Vetterli, "Wavelets and signal processing," *IEEE Signal Processing Magazine*, Oct. 1991, pp. 14-38.
- [322] D. Rudoy, P. Basu, and P. J. Wolfe, "Superposition frames for adaptive time-frequency analysis and fast reconstruction," *IEEE Transactions on Signal Processing*, Vol. 58, No. 5, May 2010, pp. 2581-2596.
- [323] B. Santhanam and J. H. McClellan, "The discrete rotational Fourier transform," *IEEE Transactions on Signal Processing*, Vol. 44, No. 4, Apr. 1996, pp. 994-998.
- [324] A. M. Sayeed, "On the equivalence of the operator and kernel methods for joint distributions of arbitrary variables," *IEEE Transactions on Signal Processing*, Vol. 45, No. 4, Apr. 1997, pp. 1067-1070.
- [325] A. M. Sayeed and D. L. Jones, "Optimal detection using bilinear time-frequency and time-scale representations," *IEEE Transactions on Signal Processing*, Vol. 43, No. 12, Dec. 1995, pp. 2872-2884.
- [326] A. M. Sayeed and D. L. Jones, "Integral transforms covariant to unitary operators and their implications for joint signal representations," *IEEE Transactions on Signal Processing*, Vol. 44, No. 6, June 1996, pp. 1365-1378.
- [327] A. M. Sayeed and D. L. Jones, "Equivalence of generalized joint signal representations of arbitrary variables," *IEEE Transactions on Signal Processing*, Vol. 44, No. 12, Dec. 1996, pp. 2959-2971.
- [328] A. M. Sayeed and D. L. Jones, "A canonical covariance-based method for generalized joint signal representation," *IEEE Signal Processing Letters*, Vol. 3, No. 4, Apr. 1996, pp. 121-123.
- [329] A. Scaglione and S. Barbarossa, "On the spectral properties of polynomial-phase signals," *IEEE Signal Processing Letters*, Vol. 5, No. 9, Sep. 1998, pp. 237-240.
- [330] L. L. Scharf and B. Friedlander, "Toeplitz and Hankel kernels for estimating time-varying spectra of discrete-time random processes," *IEEE Transactions on Signal Processing*, Vol. 49, No. 1, Jan. 2001, pp. 179-189.
- [331] R. A. Schepers and A. Teolis, "Cramer-Rao bounds for wavelet transform-based instantaneous frequency estimates," *IEEE Transactions on Signal Processing*, Vol. 51, No. 6, June 2003, pp. 1593-1603.

- [332] M. Schimmel and J. Gallart, "The inverse S-transform in filters with time-frequency localization," *IEEE Transactions on Signal Processing*, Vol. 53, No. 11, Nov. 2005, pp. 4417- 4422.
- [333] E. Sejdic, L.J. Stanković, M. Daković, and J. Jiang, "Instantaneous Frequency Estimation Using the S-Transform," *IEEE Signal Processing Letters*, Vol. 15, No. , 2008, pp. 309-312.
- [334] E. Sejdic, I. Djurović, J. Jiang, and L.J. Stanković, "Time-Frequency Based Feature Extraction and Classification," VDM Verlag, Dec. 2009.
- [335] E. Sejdic, I. Djurović, and L.J. Stanković, "Quantitative Performance Analysis of Scalogram as Instantaneous Frequency Estimator," *IEEE Transactions on Signal Processing*, Vol. 56, No. 8, Aug. 2008, pp. 3837-3845.
- [336] E. Sejdic and I. Djurović, "Robust S-transform based on L-DFT," *Electronics Letters* , Vol. 46, No. 4, Feb. 2010, pp. 304-306.
- [337] E. Sejdic, I. Djurović, and L.J. Stanković, "Fractional Fourier transform as a signal processing tool: An overview of recent developments," *Signal Processing*, Special issue on the Fourier related transforms, Vol. 91, No. 6, June 2011, pp. 1351-1369.
- [338] I. W. Selesnick, "A higher density discrete wavelet transform," *IEEE Transactions on Signal Processing*, Vol. 54, No. 8, Aug. 2006, pp. 3039-3048.
- [339] I. Shafi, J. Ahmad, S. I. Shah, and F. M. Kashif, "Techniques to obtain good resolution and concentrated time-frequency distributions: a review" *EURASIP Journal on Advances in Signal Processing archive*, Vol. 2009, Jan. 2009, Article No. 27.
- [340] S. I. Shah, P. J. Loughlin, L. F. Chaparro, and A. El-Jaroudi, "Informative priors for minimum cross-entropy positive time-frequency distributions," *IEEE Signal Processing Letters*, Vol. 4, No. 6, Jun. 1997, pp. 176-177.
- [341] H. Shen and A. Papandreou-Suppappola, "Diversity and channel estimation using time-varying signals and time-frequency techniques," *IEEE Transactions on Signal Processing*, Vol. 54, No. 9, Sept. 2006, pp. 3400-3413.
- [342] R. G. Shenoy and T. W. Parks, "The Weyl correspondence and time-frequency analysis," *IEEE Transactions on Signal Processing*, Vol. 42, No. 2, Feb. 1994, pp. 318-331.
- [343] R. G. Shenoy and T. W. Parks, "Wide-band ambiguity functions and affine Wigner distributions," *Signal Processing*, Vol. 41, No. 3, Mar. 1996.
- [344] S. Shinde and V. M. Gadre, "An uncertainty principle for real signals in the fractional Fourier transform domain," *IEEE Transactions on Signal Processing*, Vol. 49, No. 11, Nov. 2001, pp. 2545-2548.
- [345] L. H. Sibul, L. G. Weiss, and R. K. Young, "Weighted time-frequency and time-scale transforms in reproducing kernel Hilbert spaces," *IEEE Signal Processing Letters*, Vol. 4, No. 1, Jan. 1997, pp. 21-22.
- [346] L. Sk, "Application of the L-Wigner distribution to the diagnosis of local defects of gear tooth," *KSME International Journal*, Vol. 13, No. 2, Feb. 1999, pp. 144-157.
- [347] L.J. Stanković, "A method for time-frequency analysis," *IEEE Transactions on Signal Processing*, Vol. 42, No. 1, Jan. 1994, pp. 225-229.
- [348] L.J. Stanković, "An analysis of Wigner higher order spectra of multicomponent signals," *Annales des telecommunications*, No. 3/4, Mar. /Apr. , 1994, pp. 132-136.

- [349] LJ. Stanković, “A multitime definition of the Wigner higher order distribution: L-Wigner distribution,” *IEEE Signal Processing Letters*, Vol. 1, No. 7, July 1994, pp. 106-109.
- [350] LJ. Stanković, “An analysis of some time-frequency and time-scale distributions,” *Annales des Telecommunications*, Vol. 49, No. 9/10, Sep. /Oct. 1994, pp. 505-517.
- [351] LJ. Stanković, “A method for improved distribution concentration in the time-frequency analysis of the multicomponent signals using the L-Wigner distribution,” *IEEE Transactions on Signal Processing*, Vol. 43, No. 5, May 1995, pp. 1262-1268.
- [352] LJ. Stanković, “L-class of time-frequency distributions,” *IEEE Signal Processing Letters*, Vol. 3, No. 1, Jan. 1996, pp. 22-25.
- [353] LJ. Stanković, “A time-frequency distribution concentrated along the instantaneous frequency,” *IEEE Signal Processing Letters*, Vol. 3, No. 3, Mar. 1996, pp. 89-91.
- [354] LJ. Stanković, “The auto-term representation by the reduced interference distributions; The procedure for a kernel design,” *IEEE Transactions on Signal Processing*, Vol. 44, No. 6, June 1996, pp. 1557-1564.
- [355] LJ. Stanković, “Highly concentrated time-frequency distributions: Pseudo quantum signal representation,” *IEEE Transactions on Signal Processing*, Vol. 45, No. 3, Mar. 1997, pp. 543-552.
- [356] LJ. Stanković, “S class of distributions,” *IEE Proc. Vision, Image and Signal Processing*, Vol. 144, No. 2, April 1997, pp. 57-64.
- [357] LJ. Stanković, “Local polynomial Wigner distribution,” *Signal Processing*, Vol. 59, No. 1, May 1997, pp. 123-128.
- [358] LJ. Stanković, “On the realization of the polynomial Wigner-Ville distribution for multicomponent signals,” *IEEE Signal Processing Letters*, Vol. 5, No. 7, July 1998, pp. 157-159.
- [359] LJ. Stanković and I. Djurović, “Relationship between ambiguity function coordinate transformations and fractional Fourier transform,” *Annales des Telecommunications*, Vol. 53, No. 7/8, July-Aug. 1998, pp. 316-319.
- [360] LJ. Stanković and V. Ivanović, “Further results on the minimum variance time-frequency distribution kernels,” *IEEE Transactions on Signal Processing*, Vol. 45, No. 6, June 1997, pp. 1650-1655.
- [361] LJ. Stanković, V. Ivanović, and Z. Petrović, “Unified approach to the noise analysis in the Wigner distribution and Spectrogram using the S-method,” *Annales des Telecommunication*, No. 11/12, Nov. /Dec. 1996, pp. 585-594.
- [362] LJ. Stanković and V. Katkovnik, “Algorithm for the instantaneous frequency estimation using time-frequency distributions with variable window width,” *IEEE Sign. Proc. Letters*, Vol. 5, No. 9, Sept. 1998, pp. 224-227.
- [363] LJ. Stanković and S. Stanković, “Wigner distribution of noisy signals,” *IEEE Transactions on Signal Processing*, Vol. 41, No. 2, Feb. 1993, pp. 956-960.
- [364] LJ. Stanković and S. Stanković, “On the Wigner distribution of the discrete-time noisy signals with application to the study of quantization effects,” *IEEE Transactions on Signal Processing*, Vol. 42, No. 7, July 1994, pp. 1863-1867.
- [365] LJ. Stanković and S. Stanković, “An analysis of the instantaneous frequency representation by some time-frequency distributions -Generalized Wigner distribution,” *IEEE Transactions on Signal Processing*, Vol. 43, No. 2, Feb. 1995, pp. 549-552.

- [366] LJ. Stanković and V. Katkovnik, "The Wigner distribution of noisy signals with adaptive time-frequency varying window," *IEEE Transactions on Signal Processing*, vol-47, No. 4, April 1999, pp. 1099-1108.
- [367] LJ. Stanković and J. F. Böhme, "Time-frequency analysis of multiple resonances in combustion engine signals," *Signal Processing*, Vol. 79, No. 1, Nov. 1999, pp. 15-28.
- [368] LJ. Stanković, S. Stanković, and Z. Uskoković, *Time-frequency signal analysis, research monograph*, Epsilon-Montenegropian, 1994.
- [369] LJ. Stanković, T. Alieva, and M. J. Bastiaans, "Time-frequency signal analysis based on the windowed fractional Fourier transform," *Signal Processing*, Vol. 83, No. 11, Nov. 2003, pp. 2459-2468
- [370] LJ. Stanković, T. Thayaparan, and M. Daković, "Signal Decomposition by Using the S-Method With Application to the Analysis of HF Radar Signals in Sea-Clutter," *IEEE Transactions on Signal Processing*, Vol. 54, No. 11, Nov. 2006, pp. 4332-4342
- [371] LJ. Stanković, "Time-frequency distributions with complex argument," *IEEE Transactions on Signal Processing*, Vol. 50, No. 3, March 2002, pp. 475-486.
- [372] LJ. Stanković and I. Djurović, "A note on "An overview of aliasing errors in discrete-time formulations of time-frequency representations," *IEEE Transactions on Signal Processing*, Vol. 49, No. 1, Jan. 2001, pp. 257-259.
- [373] LJ. Stanković, I. Djurović, and T. Thayaparan, "Separation of target rigid body and micro-doppler effects in ISAR imaging," *IEEE Transactions on Aerospace and Electronic Systems*, Vol. 42, No. 4, Oct. 2006, pp. 1496-1506.
- [374] LJ. Stanković and V. Katkovnik, "Instantaneous frequency estimation using higher order L-Wigner distributions with data-driven order and window length," *IEEE Transactions on Information Theory*, Vol. 46, No. 1, Jan. 2000, pp. 302-311.
- [375] LJ. Stanković, "Analysis of noise in time-frequency distributions," *IEEE Signal Processing Letters*, Vol. 9, No. 9, Sept. 2002 , pp. 286-289.
- [376] LJ. Stanković, M. Daković, and V. Ivanović, "Performance of spectrogram as IF estimator," *Electronics Letters*, Vol. 37, No. 12, Jun 2001, pp. 797-799.
- [377] LJ. Stanković, S. Stanković, and I. Djurović, "Space/spatial-frequency analysis based filtering," *IEEE Transactions on Signal Processing*, Vol. 48, No. 8, Aug. 2000, pp. 2343-2352.
- [378] LJ. Stanković, "A measure of some time-frequency distributions concentration," *Signal Processing*, Vol. 81, No. 3, Mar . 2001, pp. 621-631.
- [379] LJ. Stanković, "Performance analysis of the adaptive algorithm for bias-to-variance trade-off," *IEEE Transactions on Signal Processing*, Vol. 52, No. 5, May . 2004, pp. 1228-1234
- [380] LJ. Stanković, T. Thayaparan, and M. Daković, "Signal decomposition by using the S-Method with application to the analysis of HF radar signals in sea-clutter," *IEEE Transactions on Signal Processing*, Vol. 54, No. 11, Nov. 2006, pp. 4332- 4342.
- [381] LJ. Stanković and S. Djukanović, "Order adaptive local polynomial FT based interference rejection in spread spectrum communication systems,"*IEEE Transactions on Instrumentation and Measurements*, Vol. 54, No. 6, Dec. 2005, pp. 2156- 2162.

- [382] LJ. Stanković, T. Thayaparan, M. Daković, and V. Popović-Bugarin, "Micro-Doppler removal in the radar imaging analysis," *IEEE Transactions Aerosp. Electron. Systems*, 2013.
- [383] LJ. Stanković, I. Orović, S. Stanković, and M. Amin, "Robust time-frequency analysis based on the L-estimation and compressive sensing," submitted to the *IEEE Signal Processing Letters*.
- [384] LJ. Stanković, I. Orović, S. Stanković, and M. Amin, "Compressive sensing based separation of nonstationary and stationary signals overlapping in time-frequency," submitted to the *IEEE Transactions on Signal Processing*.
- [385] S. Stanković, I. Djurović, and V. Vuković, "System architecture for space-frequency image analysis," *Electronics Letters*, Vol. 34, No. 23, Nov. 1998, pp. 2224-2225.
- [386] S. Stanković, I. Djurović, and I. Pitas, "Watermarking in the space/spatial-frequency domain using two-dimensional Radon-Wigner distribution," *IEEE Transactions on Image Processing*, Vol. 10, No. 4, April 2001, pp. 650-658.
- [387] S. Stanković and LJ. Stanković, "An architecture for the realization of a system for time-frequency signal analysis," *IEEE Transactions on Circuits and Systems II*, Vol. 44, No. 2, Feb. 1997, pp. 600-604.
- [388] S. Stanković and LJ. Stanković, "Introducing time-frequency distributions with a "complex-time" argument," *Electronics Letters*, Vol. 32, No. 14, July 1996, pp. 1265-1267.
- [389] S. Stanković, LJ. Stanković, and Z. Uskoković, "On the local frequency, group shift and cross-terms in some multidimensional time-frequency distributions; A method for multidimensional time-frequency analysis," *IEEE Transactions on Signal Processing*, Vol. 43, No. 7, July 1995, pp. 1719-1725.
- [390] S. Stanković, LJ. Stanković, and Z. Uskoković, "Modified Wigner bispectrum and its generalizations," *Circuits, Systems and Signal Processing*, Vol. 16, No. 1, Jan. 1997, pp. 27-40.
- [391] S. Stanković and J. Tilp, "Time-varying filtering of speech signals using linear prediction," *Electronics Letters*, Vol. 36, No. 8, April 2000, pp. 763-764.
- [392] S. Stanković, LJ. Stanković, V. N. Ivanović, and R. Stojanović, "An architecture for the VLSI design of systems for time-frequency analysis and time-varying filtering," *Annales des Telecommunications*, Vol. 57, No. 9/10, Sept. /Oct. 2002, pp. 974-995.
- [393] S. Stanković, I. Orović, and N. Zarić, "An application of multidimensional time-frequency analysis as a base for the unified watermarking approach," *IEEE Transactions on Image Processing*, Vol. 19, No. 3, March 2010, pp. 736-745.
- [394] S. Stanković, N. Zarić, and C. Ioana, "General form of time-frequency distribution with complex-lag argument," *Electronics Letters*, Vol. 44, No. 11, May 22 2008, pp. 699-701.
- [395] S. Stanković, I. Orović, and C. Ioana, "Effects of Cauchy integral formula discretization on the precision of IF estimation: Unified approach to complex-lag distribution and its counterpart L-form," *IEEE Signal Processing Letters*, Vol. 16, No. 4, April 2009, pp. 327-330.
- [396] E. V. Stansfield, "Accuracy of an interferometer in noise," *IEE Proceedings: Radar, Sonar and Navigation*, Vol. 143, No. 4, Mar. 1997.
- [397] N. J. Stevenson, M. Mesbah, and B. Boashash, "Multiple-view time-frequency distribution based on the empirical mode decomposition," *IET Signal Processing*, Vol. 4, No. 4, Aug. 2010, pp. 447-456,

- [398] P. Stoica and T. Soderstrom, "On the convergence properties of a time-varying recursion," *IEEE Signal Processing Letters*, Vol. 2, No. 5, May 1995, pp. 95-96.
- [399] S. R. Subramaniam, B. W. -K. Ling, and A. Georgakis, "Filtering in rotated time-frequency domains with unknown noise statistics," *IEEE Transactions on Signal Processing*, Vol. 60, No. 1, Jan. 2012, pp. 489-493.
- [400] M. Sun, C. C. Li, L. N. Sekhar, and R. J. Scelbassi, "Efficient computation of the discrete pseudo Wigner distribution," *IEEE Transactions on Acoustics, Speech and Signal Processing*, Vol. 37, No. 11, Nov. 1989, pp. 1735-1741.
- [401] M. Sun, et al., "Localizing functional activity in the brain through time-frequency analysis and synthesis of the EEG," *Proc. IEEE*, Vol. 84, No. 9, Sept. 1996, pp. 1302-1311..
- [402] H. Suzuki and F. Kobayashi, "A method of two-dimensional spectral analysis using the Wigner distribution," *Electronics and Communications in Japan*, Vol. 75, No. 1, 1992, pp. 1006-1013.
- [403] J. L. Tan, A. Z. bin and Sha'ameri, "Adaptive optimal kernel smooth-windowed Wigner-Ville bispectrum for digital communication signals," *Signal Processing*, Vol. 91, No. 4, April 2011, pp. 931-937.
- [404] B. Tacer and P. Loughlin, "Time-scale energy density functions," *IEEE Transactions on Signal Processing*, Vol. 44, No. 5, May 1996, pp. 1310-1314.
- [405] V. I. Tatarski, "Wigner representations in quantum mechanics," in Russian, *Uspehi Fiziceskikh Nauk*, Vol. 139, No. 4, April 1993, pp. 587-619.
- [406] T. Thayaparan, LJ. Stanković, C. Wernik, and M. Daković, "Real-time motion compensation, image formation and image enhancement of moving targets in ISAR and SAR using S-method based approach," *IET Signal Processing*, Vol. 2, No. 3, Sep. 2008, pp. 247-264.
- [407] T. Thayaparan, et al., "Analysis of radar micro-Doppler signatures from experimental helicopter and human data," *IET Radar, Sonar & Navigation*, Vol. 1, No. 4, Aug. 2007, pp. 289-299.
- [408] T. Thayaparan, M. Daković, and LJ. Stanković, "Mutual interference and low probability of interception capabilities of noise radar," *IET Radar, Sonar & Navigation*, Vol. 2, No. 4, Aug. 2008, pp. 294-305.
- [409] F. Totir, et. al, "Systemic approach explored in the context of passive target tracking," *IET Signal Processing*, Vol. 4, No. 3, June 2010, pp. 314-323.
- [410] F. Totir and E. Radoi, "Superresolution algorithms for spatial extended scattering centers",*Digital Signal Processing* ", Vol. 19, No. 5, pp. 780-792, Sept. 2009.
- [411] M. Unser, "Fast Gabor-like windowed Fourier and continuous Wavelet transform," *IEEE Signal Processing Letters*, Vol. 1, No. 5, May 1994, pp. 76-79.
- [412] H. L. Van Trees, *Detection, Estimation, and Modulation Theory*, New York, Wiley, 1968.
- [413] G. T. Venkatesan and M. G. Amin, "Time-frequency distribution kernels using FIR filter design techniques," *IEEE Transactions on Signal Processing*, Vol. 45, No. 6, June 1997, pp. 1645-1650.
- [414] G. T. Venkatesan and M. G. Amin, "Time-frequency distribution kernel design over a discrete powers-of-two space," *IEEE Signal Processing Letters*, Vol. 3, No. 12, Dec. 1996, pp. 305-306.
- [415] M. Vetterli and J. Kovačević, *Wavelets and subband coding*, Prentice Hall, 1994.

- [416] J. Ville, "Theorie et applications de la notion de signal analytique," *Cables et Transmission*, Vol. 2, No. 1, 1946, pp. 61-74.
- [417] B. -H. Wang and J. -G. Huang, "Instantaneous frequency estimation of multi-component Chirp signals in noisy environments," *Journal of Marine Science and Application*, Dec. 2007, Vol. 6, No. 4, pp 13-17.
- [418] C. Wang and M. G. Amin, "Performance analysis of instantaneous frequency-based interference excision techniques in spread spectrum communications," *IEEE Transactions on Signal Processing*, Vol. 46, No. 1, Jan. 1998, pp. 70-83.
- [419] M. Wang, A. K. Chan, and C. K. Chui, "Linear frequency-modulated signal detection using Radon-ambiguity transform," *IEEE Transactions on Signal Processing*, Vol. 46, No. 3, Mar. 1998, pp. 571-587.
- [420] P. Wang, I. Djurović, and J. Yang, "Generalized high-order phase function for parameter estimation of polynomial phase signal," *IEEE Transactions on Signal Processing*, Vol. 56, No. 7, July 2008, pp. 3023-3028.
- [421] P. Wang, H. Li; I. Djurović, and B. Himed, "Performance of Instantaneous Frequency Rate Estimation Using High-Order Phase Function," *IEEE Transactions on Signal Processing*, Vol. 58, No. 4, April 2010, pp. 2415-2421.
- [422] P. Wang, H. Li, I. Djurović, and B. Himed, "Integrated cubic phase function for linear FM signal analysis," *IEEE Transactions on Aerospace and Electronic Systems*, Vol. 46, No. 3, July 2010, pp. 963-977.
- [423] Y. Wang and Y. Jiang, "ISAR imaging of maneuvering target based on the L-class of fourth-order complex-lag PWVD", *IEEE Transactions on Geoscience and Remote Sensing*, Vol. 48, No. 3, March 2010, pp. 1518 - 1527
- [424] Y. Wang and Y. C. Jiang, "New time-frequency distribution based on the polynomial Wigner-Ville distribution and L class of Wigner-Ville distribution" *IET Signal Processing*, Vol. 4, No. 2, April 2010, pp. 130 - 136.
- [425] Y. -C. Jiang, "Generalized time-frequency distributions for multicomponent polynomial phase signals," *Signal Processing*, Vol. 88, No. 4, April 2008, pp. 984–1001.
- [426] D. Wei and A. C. Bovik, "On the instantaneous frequencies of multicomponent AM-FM signals," *IEEE Signal Processing Letters*, Vol. 5, No. 4, Apr. 1998, pp. 84-86.
- [427] Y. S. Wei and S. S. Tan, "Signal decomposition of HF radar maneuvering targets by using S2-method with clutter rejection," *Journal of Systems Engineering and Electronics*, Vol. 23, No. 2, April 2012, pp. 167 - 172.
- [428] Y. S. Wei and S. S. Tan, "Signal decomposition by the S-method with general window functions," *Signal Processing*, Vol. 92, No. 1, Jan. 2012, pp. 288–293
- [429] P. E. Wigner, "On the quantum correction for thermodynamic equilibrium," *Phys. Rev.*, 1932, Vol. 40, pp. 246-254.
- [430] W. J. Williams, "Reduced interference distributions: Biological applications and interpretations," *Proc. IEEE*, Vol. 84, No. 9, Sept. 1996, pp. 1264-1280.
- [431] J. C. Wood and D. T. Barry, "Linear signal synthesis using the Radon-Wigner distribution," *IEEE Transactions on Signal Processing*, Vol. 42, No. 8, Aug. 1994, pp. 2105-2111.

- [432] J. C. Wood and D. T. Barry, "Radon transform of time-frequency distributions for analysis of multicomponent signals," *IEEE Transactions on Signal Processing*, Vol. 42, No. 11, Nov. 1994, pp. 3166-3177.
- [433] J. C. Wood and D. T. Barry, "Time-frequency analysis of skeletal muscle and cardiac vibrations," *Proc. IEEE*, Vol. 84, No. 9, Sept. 1996, pp. 1281-1294.
- [434] X. G. Xia, "On characterization of the optimal biorthogonal window functions for Gabor transforms," *IEEE Transactions on Signal Processing*, Vol. 44, No. 1, Jan. 1996, pp. 133-136.
- [435] X. G. Xia, "System identification using chirp signals and time-variant filters in the joint time-frequency domain," *IEEE Transactions on Signal Processing*, Vol. 45, No. 8, Aug. 1997, pp. 2072-2085.
- [436] X. G. Xia, "A quantitative analysis of SNR in the short-time Fourier transform domain for multicomponent signals," *IEEE Transactions on Signal Processing*, Vol. 46, No. 1, Jan. 1998, pp. 200-203.
- [437] X. G. Xia, "On bandlimited signals with fractional Fourier transform," *IEEE Signal Processing Letters*, Vol. 3, No. 3, Mar. 1996, pp. 72-74.
- [438] X. G. Xia, Y. Owechko, B. H. Soffer, and R. M. Matic, "On generalized-marginal time-frequency distributions," *IEEE Transactions on Signal Processing*, Vol. 44, No. 11, Nov. 1996, pp. 2882-2887.
- [439] J. Xiao and P. Flandrin, "Multitaper time-frequency reassignment for nonstationary spectrum estimation and chirp enhancement," *IEEE Transactions on Signal Processing*, Vol. 55, No. 6, June 2007, pp. 2851-2860.
- [440] G. Yu; S. Mallat, and E. Bacry, "Audio denoising by time-frequency block thresholding," *IEEE Transactions on Signal Processing*, Vol. 56, No. 5, May 2008, pp. 1830-1839.
- [441] L. A. Zadeh, "Frequency analysis of variable networks," *Proc. IRE*, Vol. 67, March 1950, pp. 291-299.
- [442] E. J. Zalubas and M. G. Amin, "Time-frequency kernel design by the two-dimensional frequency transformation method," *IEEE Transactions on Signal Processing*, Vol. 43, No. 9, Sept. 1995, pp. 2198-2203.
- [443] N. Zarić, N. Lekic, and S. Stanković, "An implementation of the L-estimate distributions for analysis of signals in heavy-tailed noise," *IEEE Transactions on Circuits and Systems II*, Vol. 58, No. 7, July 2011, pp. 427-431.
- [444] P. Zavarsky and N. Fuji, "Introduction of cross ambiguity function for elimination of crossterms in Wigner distribution of the third order," *Electronics Letters*, Vol. 32, No. 2, pp. 94-95, Jan 1996.
- [445] A. I. Zayed, "On the relationship between the Fourier and fractional Fourier transforms," *IEEE Signal Processing Letters*, Vol. 3, No. 12, Dec. 1996, pp. 310-311.
- [446] A. I. Zayed, "A convolution and product theorem for the fractional Fourier transform," *IEEE Signal Processing Letters*, Vol. 5, No. 4, Apr. 1998, pp. 101-103.
- [447] B. Zhang and S. Sato, "A time-frequency distribution of Cohen's class with a compound kernel and its application to speech signal processing," *IEEE Transactions on Signal Processing*, Vol. 42, No. 1, Jan. 1994, pp. 54-64.

- [448] Y. Zhang and M. G. Amin, "Array processing for nonstationary interference suppression in DS/SS communications using subspace projection techniques," *IEEE Transactions on Signal Processing*, Vol. 49, No. 12, Dec. 2001, pp. 3005-3014.
- [449] Y. Zhang and M. G. Amin, "Spatial averaging of time-frequency distributions for signal recovery in uniform linear arrays," *IEEE Transactions on Signal Processing*, Vol. 48, No. 10, Oct. 2000, pp. 2892-2902.
- [450] Y. Zhang, W. Mu, and M. G. Amin, "Subspace analysis of spatial time-frequency distribution matrices," *IEEE Transactions on Signal Processing*, Vol. 49, No. 4, April 2001, pp. 747-759.
- [451] J. J. Zhang, A. Papandreou-Suppappola, B. Gottin, and C. Ioana, "Time-frequency characterization and receiver waveform design for shallow water environments," *IEEE Transactions on Signal Processing*, Vol. 57, No. 8, Aug. 2009, pp. 2973-2985.
- [452] Y. Zhao, "Spectrum estimation of short-time stationary signals in additive noise and channel distortion," *IEEE Transactions on Signal Processing*, Vol. 49, No. 7, July 2001, pp. 1409-1420.
- [453] H. Zou, Q. Dai, R. Wang, and Y. Li, "Parametric TFR via windowed exponential frequency modulated atoms," *IEEE Signal Processing Letters*, Vol. 8, No. 5, May 2001, pp. 140-142.
- [454] G. T. Zhou and Y. Wang, "Exploring lag diversity in the higher order ambiguity function for polynomial phase signals," *IEEE Signal Processing Letters*, Vol. 4, No. 8, Aug. 1997, pp. 240-242.
- [455] Y. M. Zhu, R. Goutte, and M. Amiel, "On the use of a two-dimensional Wigner-Ville distribution for texture segmentation," *Signal Processing*, Vol. 30, 1993, pp. 329-354.
- [456] Y. M. Zhu, R. Goutte, and F. Peyrin, "The use of a two-dimensional Wigner-Ville distribution for texture segmentation," *Signal Processing*, Vol. 19, No. 3, 1990, pp. 205-222.
- [457] Y. M. Zhu, F. Peyrin, and R. Goutte, "Transformation de Wigner-Ville: description d'un nouvel outil de traitement du signal et des images," *Annales des telecommunication*, Vol. 42, No. 3/4, Mar./Apr. 1987, pp. 105-117.
- [458] Y. M. Zhu, F. Peyrin, and R. Goutte, "Sur la transformation de pseudo Wigner-Ville discrete en temps et en fréquence," *Annales des telecommunications*, Vol. 46, No. 5-6, 1991, pp. 301-309.

About the Authors

Ljubiša Stanković was born in Montenegro on June 1, 1960. He received a B.S. in electrical engineering from the University of Montenegro in 1982, with the award as the best student at the University. In 1984, he received an M.S. in communications from the University of Belgrade, and a Ph.D. in theory of electromagnetic waves from the University of Montenegro in 1988. As a Fulbright grantee, he spent the 1984–1985 academic year at the Worcester Polytechnic Institute in Worcester, MA. Since 1982, he has been on the faculty at the University of Montenegro, where he has been a full professor since 1995. In 1997–1999, he was on leave at the Ruhr University Bochum in Germany, supported by the Alexander von Humboldt Foundation. At the beginning of 2001, he was at the Technische Universiteit Eindhoven in the Netherlands as a visiting professor. During 2003–2008, he was the Rector of the University of Montenegro. He is the Ambassador of Montenegro to the United Kingdom, Ireland, and Iceland. His current interests are in signal processing. He published about 350 technical papers, more than 120 of them in the leading journals, mainly the IEEE editions. Dr. Stanković received the highest state award of Montenegro in 1997 for scientific achievements. He was a member the IEEE Signal Processing Society's Technical Committee on Theory and Methods, an associate editor of the IEEE Transactions on Image Processing, and an associate editor of the IEEE Signal Processing Letters. Dr. Stanković is an associate editor of the IEEE Transactions on Signal Processing. He has been a member of the National Academy of Science and Arts of Montenegro (CANU) since 1996 and a member of the European Academy of Sciences and Arts. Dr. Stanković is a Fellow of the IEEE for contributions to time-frequency signal analysis.

Miloš Daković was born in 1970 in Nikšić, Montenegro. He received a B.S. in 1996, an M.S. in 2001, and a Ph.D. in 2005, all in electrical engineering from the University of Montenegro. He is an associate professor at the University of Montenegro. His research interests are in signal processing, time-frequency signal analysis, and radar signal processing. He is a member of the Time-Frequency Signal Analysis Group (www.tfsa.ac.me) at the University of Montenegro, where he is involved in several research projects.

Thayananthan Thayaparan earned a B.S. (Hons.) in physics at the University of Jaffna, Sri-Lanka, an M.S. in physics at the University of Oslo, Norway in 1991, and a Ph.D. in atmospheric physics at the University of Western Ontario, Canada in 1996. From 1996 to 1997, he was employed as a postdoctoral fellow at the University of Western Ontario. In 1997, he joined the Defence Research and Development Canada-Ottawa, Department of National Defence, Canada, as a defence scientist. His research interests include advanced radar signal and image processing methodologies and techniques against SAR/ISAR and HFSWR problems, such as detection, classification, recognition, and identification. His current research includes synthetic aperture radar imaging algorithms, time-frequency analysis for radar imaging and signal analysis, radar micro-Doppler analysis, and noise radar technology. Thayaparan is a Fellow of the IET (Institute of Engineering & Technology). Currently, he is an adjunct professor at McMaster University. Dr. Thayaparan received IET Premium Award for Signal Processing for the best paper published in 2009–2010. Dr. Thayaparan is currently serving in the editorial board of IET Signal Processing. He has authored or coauthored over 174 publications in journals, proceedings, and internal distribution reports.

Index

- Adaptive algorithm, 410, 487
 - instantaneous frequency estimation, 420
 - signal smoothing, 416
- Adaptive analysis, 151
- Affine distributions, 285
- Affine transforms, 139
- Ambiguity function, 232, 239
 - generalized, 239
- Analytic extension of a function, 352
- Analytic part, 16
- Auto-correlation function, 51
- Auto-term function, 252
- Auto-terms, 229, 234, 247, 248, 252, 259, 265
- Auto-terms and cross-terms
 - higher-order spectra, 335
- Bandpass filtering, 103
- Biomedical signals, 623
- Bispectrum, 321
- Bit error rate (BER), 562
- Blackman window, 91, 102
- Born-Jordan distribution, 243
- Butterworth distribution, 243
- Capon's method, 608
 - local polynomial Fourier transform (LPFT), 613
 - short-time Fourier transform (STFT), 611
- Car engine signals, 562
- Central limit theorem, 54
- Chirplet transform, 144, 147
- Cohen class of distributions, 240, 311
 - affine, 285
 - auto-terms form, 251
 - discrete form, 245
 - kernel decomposition, 253
 - kernel design, 252
 - multidimensional, 598
 - noisy signals, 429
 - optimal kernel design, 247
 - positivity, 255
 - properties, 242
 - reassigned, 281
 - robust, 450
- Coherent integration time, 513
- Complex argument distribution, 348
- Complex lag distribution, 348, 373
- Complex sinusoidal signal, 3
- Complex time distribution, 346, 351
- Compressive sensing, 453
- Compressive sensing, 455
 - L-statistics, 465
 - short-time Fourier transform, 477
 - time-frequency domain, 469
- Concentration measure, 148
- Constant false alarm rate (CFAR), 581
- Continuous signals, 2
- Convolution, 11
 - circular, 38
 - in the frequency domain, 15, 27
- Coordinate rotation, 62
- Crank angle, 568
- Cross-range
 - resolution, 524
- Cross-terms, 229, 234, 243, 247, 248, 259, 265
 - in spectrogram, 96

- Decomposition, 270, 291
- Derivative approximation, 343
 - backward, 343
 - backward, second-order, 347
 - complex argument function, 346
 - symmetric, 344
- Detection, 579
 - target detection in radar signals, 591
- Direction of arrival (DOA), 603
- Discrete Fourier transform (DFT), 33, 39
- Discrete pseudo Wigner distribution, 218
- Discrete system, 25
- Discrete-time signals (discrete signals), 22
- Displacement bin, 44
- Doppler shift, 515
 - resolution, 518
- Duration measure, 96
- Empirical mode decomposition (EMD), 274
- Energy, 5, 25
- Energy property, 178
- Error function, 54
- Fast time, 517
- Filtering
 - jammer, 556
- First-order statistics, 49
- Fourier series, 6, 22, 39
- Fourier transform, 11, 22, 39
 - matrix, 36
 - of discrete-time signals, 26, 39
 - properties, 14
 - two-dimensional, 60
- Fractional Fourier transform, 135, 196
 - relation to the LPFT, 136
 - windowed, 136
- Frequency estimation, 44
- Frequency marginal property, 178
- Gabor transform, 121
- Group delay, 191
- Haar transform, 142
- Hadamard transform, 109
- Hamming window, 89, 102
- Hann(ing) window, 17, 29, 87, 102
- Hardware Design, 618
- Higher-order time-varying spectra, 317
- Hilbert transform, 17
- Hybrid time-frequency grid, 117
- Ideal representation, 85
- Impulse signal
 - continuous (delta function), 2
 - discrete-time, 23
- Inner interferences, 231
- Instantaneous (conditional) moments, 209
- Instantaneous bandwidth, 207
- Instantaneous frequency, 125, 190, 329, 345
 - bias, 407
 - estimation error, 401
 - estimation in high noise, 422
 - estimation variance, 408
 - Wigner distribution-based estimation, 399
- Instantaneous rate estimation, 348
- Interpolation, 39
- Inverse synthetic aperture radar (ISAR), 521
- Iterative procedure
 - robust transforms, 447
- Kernel function, 239
 - design, 252
 - in reduced interference distributions, 243
 - of positive distributions, 255
 - optimal, 247
 - properties, 242
- L-estimation, 451
- L-statistics, 451
 - radar signals, 540
 - robust short-time Fourier transform, 485
- L-Wigner distribution, 290, 337
 - higher-order spectra projection, 372
 - recursive realization, 354
- Laplacian noise, 455
- Laplace transform, 46
- Lattice in time-frequency plane, 104
- Linear coordinate transformation, 194
- Linear system, 9
- Local auto-correlation function, 181, 320
 - generalized, 241

- Local polynomial Fourier transform (LPFT),
 130, 147
 filtering, 132
 moments, 133
 relation to fractional Fourier transform, 136
- Local polynomial Wigner-Ville distribution,
 362
- Loss function, 445
- Margenau-Hill distribution, 297
- Marginal conditions (properties), 177
- Maximum likelihood (ML), 442
- Measure of concentration, 148
- Median, 51
 robust transforms, 448
- Micro-Doppler effect, 531
- Moments
 LPFT, 134
 Wigner distribution, 237
- Moyal property, 193
- Multicomponent signal, 95
- Multilag higher-order ambiguity function, 364
- Multilag instantaneous moments, 364
- Multitime Wigner higher-order distribution, 333
- Noise, 53
 Gaussian, 54
 Laplacian, 56
 uniform, 54
- Noise in Cohen class
 analytic, 433
 colored, 431
 nonstationary, 431
 real-valued, 433
- Noisy signal, 391
 Fourier transform, 57
 in Cohen class, 434
 Wigner distribution, 394
- Norm, 150
- Optimization, 150
- Parseval's theorem, 27
 two-dimensional, 61
- Pendulum, 290
- Period of a discrete signal, 24
- Polynomial higher-order ambiguity function
 (PHAF), 368
- Polynomial Wigner-Ville distribution, 341, 345
 realization, 360
- Power, 5, 25
- Probability density function, 50
- Projection, 61
- Pseudo quantum signal representation, 206,
 290
- Pseudo Wigner distribution, 215
- Q-factor, 139
- Radar signals, 511
- Radon transform, 62, 197, 238
- Random signals, 49
- Range, 513
- Real-time causal distribution, 356
- Reassignment method, 277
- Rectangular window, 18, 28
- Reduced interference distributions, 243
- Resolution, 88
- Rihaczek distribution, 180, 288
- Robust Fourier transform, 443
- Robust short-time Fourier transform, 446
- Robust transforms
 iterative procedure, 447
 loss function, 445
 vector approach, 448
- Rotation of the time-frequency plane, 196
- S-distribution, 309
- S-method, 256, 311
 adaptive, 264
 discrete form, 260
 in affine distributions, 287
 matrix form, 264
 recursive realization, 261
 two-dimensional, 601
- S-transform (the Stockwell transform), 143
- Sampling theorem
 in the frequency domain, 21
 in the time domain, 31
 two-dimensional, 61
- Scalogram, 140
- Second-order statistics, 51

- Seismic signals, 622
 Short-time Fourier transform (STFT), 83, 146
 discrete form, 99
 frequency-varying window, 115
 inversion, 93
 lattice, 111
 MATLAB code, 174
 noisy signals, 392
 optimal window, 127, 150, 175
 recursive, 102
 relation to continuous wavelet transform, 137
 robust, 446
 time-varying window, 113
 with overlapping, 118
 Sinc distribution, 243
 SLIDE algorithm, 572
 Slow time, 517
 Smoothed Wigner distribution, 216
 Sparse signals, 455, 486
 Spectral power density, 52
 Spectral power density function, 319
 Spectrogram, 94
 in Cohen class, 253
 multidimensional, 597
 Spread factor, 204
 Spread spectrum, 553
 Standard deviation, 52
 Stationary signals, 52
 Stationary-phase method, 123, 279
 Synthesis, 291
 Wigner distribution, 227
 Synthetic aperture radar (SAR), 529

 Target motion, 518
 Third-order moment, 320
 Time marginal property, 178
 Trispectrum, 327
 Two-dimensional signal, 60

 Uncertainty principle, 96, 204
 Unit step signal
 continuous (Heaviside function), 2
 discrete-time, 24

 Variance, 52

 Video surveillance systems
 motion detection, 572

 Watermarking, 615
 Radon Wigner distribution, 615
 Wavelet transform
 continuous, 137
 Morlet wavelet, 138
 scalogram, 140
 Wide sense stationary signals, 52
 Wiener filter, 480
 Wigner bispectrum, 324
 Wigner distribution, 182, 344
 alias-free, 263
 and spectrogram, 217
 array signal processing, 606
 auto-terms and cross-terms, 229
 bias, 396
 coordinate rotation, 196, 213
 coordinate transformation, 194
 cubic phase signal, 214
 discrete form, 218
 generalized, 183
 instantaneous bandwidth (moments), 207
 inversion, 183, 188
 joint moments, 236
 median, 450
 multidimensional, 598
 noisy signals, 394
 optics, 594
 optimal window, 399
 properties, 189
 pseudo form, 215
 quantum mechanics, 201
 Radon transform of, 198
 reassigned, 282
 reconstruction from two projections, 304
 robust, 450
 second-order moments relation, 237
 smoothed form, 216
 sparse processing, 461
 spread factor (quantum correction factor), 204
 synthesis, 227
 two-dimensional, 596
 uncertainty principle, 204

- variance, 397
- Wigner higher-order spectra, 328
- Wigner spectrum, 478
- Wigner trispectrum, 332, 334
- Window, 83, 85
 - Bartlet (triangular), 87
 - Blackman, 91
 - Gaussian, 90
 - Hamming, 89
 - Hann (Hanning), 87
 - Kaiser, 91
 - rectangular, 86
- z-transform, 48
- Zao-Atlas-Marks distribution, 243
- Zero-padding, 39